Fissures and fountains: magma dynamics in basaltic conduits

JONES, THOMAS,JAMES

Fissures and fountains: magma dynamics in basaltic conduits

Thomas James Jones

A thesis submitted in fulfilment of the requirements for the degree of Doctor of Philosophy

Department of Earth Sciences, University of Durham

2018

Abstract

Basaltic volcanoes are responsible for the bulk of the planet's magma output. Their eruptions are often spectacular and can have serious impacts on a local scale (through lava flows) and regional scale (through emission of ash and toxic gases). However, hazard planning and mitigation is challenging because these eruptions can be highly variable both temporally, lasting from hours to months, and spatially, localizing from a long, linear fissure to a discrete vent. In this thesis, I will explore the role that magma transport and eruption dynamics play in controlling the evolution of basaltic fissure eruptions in time and space. Firstly, I present results from a detailed field investigation of the proximal deposits from episode 1 of the 1969 fissure eruption of Mauna Ulu, Kīlauea, Hawai'i. Exceptional preservation of the deposits allows for the reconstruction of vent-proximal lava drainage patterns and the assessment of the role that drainage played in controlling vent localization. Secondly, I provide the first in-depth textural classification of low Hawaiian fountaining (< 100 m) products. Using spatter from the Mauna Ulu fissure eruption, I describe how the magma matured and produced late-stage spatter during the waning stages of the eruption. Furthermore, a new type of spatter is identified and interpreted to form by the disruption of lava flows above tectonic ground cracks; presenting a potential for misinterpretation of eruptive vents. Thirdly, through a series of scaled analogue experiments, I explore how the simultaneous drainage of dense, degassed, viscous magma and upwelling of less dense, less viscous magma can influence flow processes in the volcanic conduit. This convective system is characterized via the dimensionless Grashof number (Gr), which is a ratio of viscous to buoyancy forces. At low Gr ($\lesssim 0.1$), efficient laminar flow is observed with narrow, well-defined fingers of upwelling fluid separated by broad regions of downwelling fluid. As Gr increases (to ~ 100), the flow becomes increasingly chaotic and exchange becomes inefficient – no stable fingers or regions of coherent flow are established. Furthermore, the intrinsic properties of the fissure system (Gr) are related to the extrinsic properties (Reynolds number, Re – a ratio of inertial to viscous forces) to give the empirical relationship: $Re = 0.0401Gr^{0.767}$. Together, these field and lab data suggest that "top-down" lava drainage processes and "bottom-up" convective processes in basaltic fissure eruptions conspire together to control their localization and longevity. This new knowledge advances our understanding of how magma dynamics can influence key, hazard-relevant eruption parameters, such as: mass eruption rate, dynamics of proximal lava flow emplacement, lava fountain vigour, and eruption evolution. This work highlights the importance of understanding the central role that magma dynamics have in shaping volcanic eruptions in order to develop more robust conceptual and physical models of eruptive behaviour.

Table of Contents

List of Tables

List of Figures

Declaration

I declare that this thesis, which I submit for the degree of Doctor of Philosophy at Durham University, is my own work and not substantially the same as any which has previously been submitted at this or any other university.

Statement of Copyright

Acknowledgments

I would like to thank all of my supervisors – Ed, Bruce, Rich and Charlotte – who provided excellent guidance during my time at Durham and during fieldwork on Kīlauea. Particular thanks go to Ed, who provided encouragement throughout and imparted a great deal of knowledge. I may now love scaled analogue experiments as much as you!

The laboratory aspects of this thesis have been a collaborative effort and many members of Durham University have contributed their expertise – I am grateful to all of you. Ian Chaplin prepared thin sections from extremely delicate spatter clasts. Leon Bowen provided training and guidance on the SEM with great humour. Stephen Lishman and Andrew Crosby of the Physics workshop manufactured the tank (and several earlier versions) used for the analogue experiments in this thesis. Laura Höltgen helped with the experiments during a summer internship in 2016 and Veronica Becker assisted with subsequent image analysis during a summer internship in 2017.

The collaboration and interaction with other researchers has been an important part of my time as a PhD student, stretching my mind to other aspects of volcanology and beyond. Kelly, Amy and the rest of the UBC VPL group thank you for all your encouragement and friendship. Ste, Carl, Richard and the rest of the lab group, thanks for adopting me as an honorary material chemist and listening to me talk about “rocks” over drinks. The IAPETUS cohort are also thanked for the laughs and good spirit on our training courses and occasional holiday.

I would like to thank all my close friends and family members who probably feel like they have done parts of this thesis too. Paul and Duncan, thanks for continually pointing me in the direction of the nearest pub. Tim, Dave, Kate et al. our attendance at variations college events and bars was always a welcome refreshment. To all my cycling friends and past colleagues, thanks for getting me out of the office and refreshing my love for the sport. Last but not least, my family, including those that only experienced part of this journey, have provided continual love and support throughout – I could not have done it without you.

This work was funded by a Natural Environment Research Council PhD studentship (NE/L002590/1) and a British Geological Survey CASE award.

Dedication

For my family.

Chapter 1

Introduction

1.1 Background and motivation

Basaltic volcanoes are the most common type of continental volcano and are responsible for the bulk of the planet's magma output (Sigurdsson 2000; Valentine and Gregg 2008). Recent basaltic eruptions in Iceland – which are of particular relevance to UK and European risks – have included: the 2014–2015 Holuhraun eruption (e.g. Pedersen et al. 2017); the 2011 Grímsvötn eruption (e.g. Gudmundsson et al. 2012; Tesche et al. 2012) and the 2010 eruption of Eyjafjallajökull (e.g. Gudmundsson et al. 2010). These eruptions emitted large volumes of toxic gases and particulate matter that had adverse effects on agriculture, livestock and public health (Ilyinskaya et al. 2017; Stefánsson et al. 2017); generated abundant volcanic ash, particularly in the case of Eyjafjallajökull, that caused major disruption to air traffic through the closure of European air space (Sveinbjörnsson 2001; Schumann et al. 2011; Stohl et al. 2011); and outpoured large volumes of lava, leading to long term public exclusion zones and community disruption (e.g. Pedersen et al. 2017). Historic Icelandic eruptions include the 1783–1784 CE eruption of Laki which has been linked to a ~20% reduction in Iceland's population and an increased mortality rate across the UK and mainland Europe (Thordarson and Self 2003; Witham and Oppenheimer 2004; Schmidt et al. 2011; Ilyinskaya et al. 2017). Furthermore, in 2012 Icelandic basaltic fissure eruptions, were added to, and became one of the top three risks, on the UK National Risk Register of Civil Emergencies. This emphasises our aspiration as a community to fully understand these eruptions and the hazards that they pose.

Basaltic volcanism can produce a wide range of eruptive products and occurs within many tectonic environments (Valentine and Gregg 2008). Effusive behaviour is common, typically producing long-lived, often voluminous lava flows (e.g. Swanson 1973; Swanson et al. 1979; Tilling et al. 1987; Poland et al. 2016; Pedersen et al. 2017). Explosive behaviour at basaltic volcanoes is largely limited to Hawaiian and Strombolian type activity (Walker 1973), although a continuous spectrum exists with cases of Plinian style activity also reported (Walker et al. 1984; Houghton et al. 2004; Sable et al. 2006). Hawaiian type activity is characterized by sustained fountaining, with the type locality being Kīlauea, Hawaii. An example includes the 1969 Mauna Ulu eruption of Kīlauea which, in its first stage was characterized by 12 episodes of high or sustained fountaining lasting from a few hours to about 3 days (Swanson et al. 1979). Fountaining heights varied between 50 and 540 m, although they are not steady and feature pulsatory behavior (Swanson et al. 1979; Houghton et al. 2016). The most recent, and accepted method to distinguish between Hawaiian and Strombolian type activity is based on the ejection duration, with Hawaiian activity > 300 s and Strombolian < 300 s (Houghton et al. 2016). Although these eruption styles are described in discrete categories, (e.g. effusive vs. explosive or Hawaiian vs. Strombolian) in reality a continuum exists. For example, lava fountains may produce clastogenic lava flows if clasts remain hot enough and the accumulation rate is high (Karhunen 1988; Head and Wilson 1989; Sumner 1998; Heliker et al. 2003; Parcheta et al. 2012). Clastogenic lava flows therefore represent the interface between “explosive” and “effusive” activity.

In this study I will focus on basaltic fissure eruptions, and refer to stage 1, episode 1 of the 1969-75 Mauna Ulu eruption of Kīlauea, Hawaii as a case study. To illustrate the eruptive style and size of basaltic fissure eruptions a selection of photographs is presented in Figure 1.1. However, note that although I will only discuss eruptions of basaltic composition in this thesis, fissure eruptions are not exclusive to basaltic magmas – fissure

systems have erupted compositions ranging from low-viscosity “kimberlite” (Brown et al. 2012) to higher viscosity rhyolite (Lara et al. 2006).

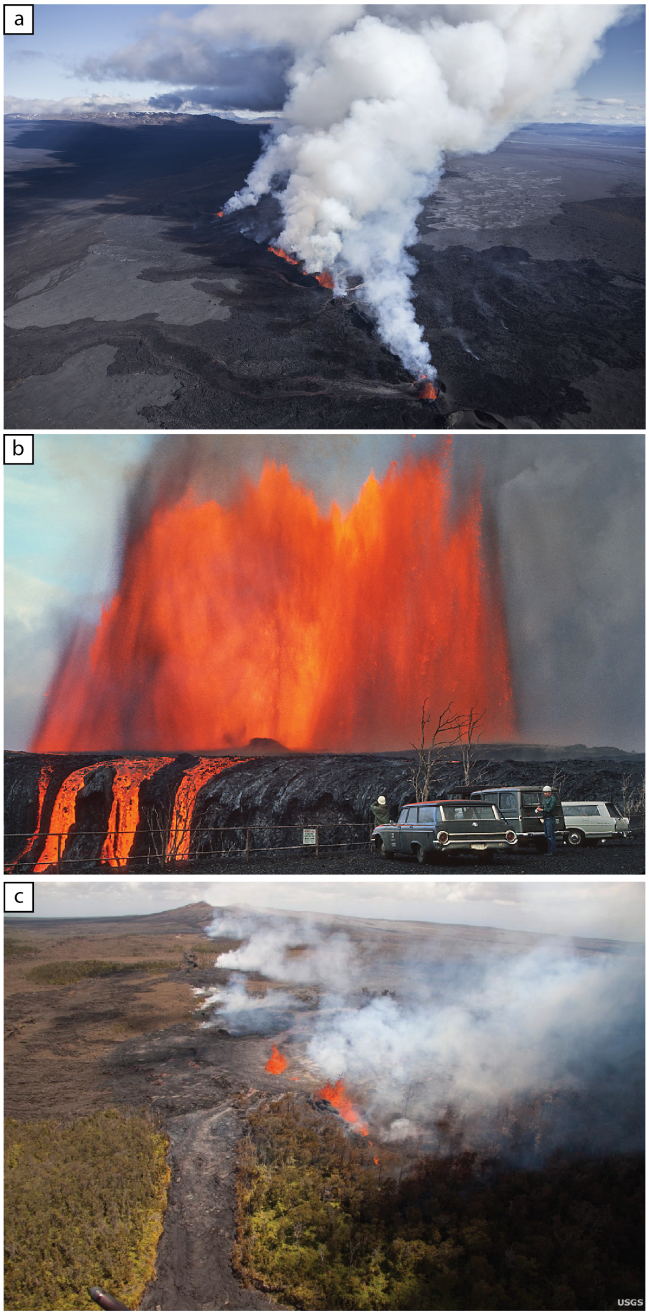

***Figure 1.1**: Photographs of basaltic fissure eruptions. **(a)** The ~ 3 km long opening fissure of the 2014 Holuhraun eruption, Iceland. Image from: www.guidetoiceland.is **(b)** 300 m high fountaining during episode 12 of the 1969 Mauna Ulu eruption, Hawaii image taken on 30th December 1969 by the United States Geological Survey (USGS). **(c)** The 2011 Kamoamoa fissure eruption, Hawaii, looking northeast toward Pu'u 'Ō 'ō, in the background. Image taken on the 8th of March by the USGS.*

In general, fissure eruptions initiate as curtains of fountaining spatter, bombs, and lapilli with heights of 10–500 m (Fig. 1.2). The eruptive geometries are initially of high aspect ratio with crack widths varying from ~ 2 m to 10's of m and have lengths ranging from several hundred metres to several kilometres (Gudmundsson 1987; Opheim and Gudmundsson 1989; Keating et al. 2008; Parcheta et al. 2015). Over the order of hours to days, the curtain focuses to a few point sources along the fissure (Richter et al. 1970; Thorarinsson et al. 1973; Swanson et al. 1979).

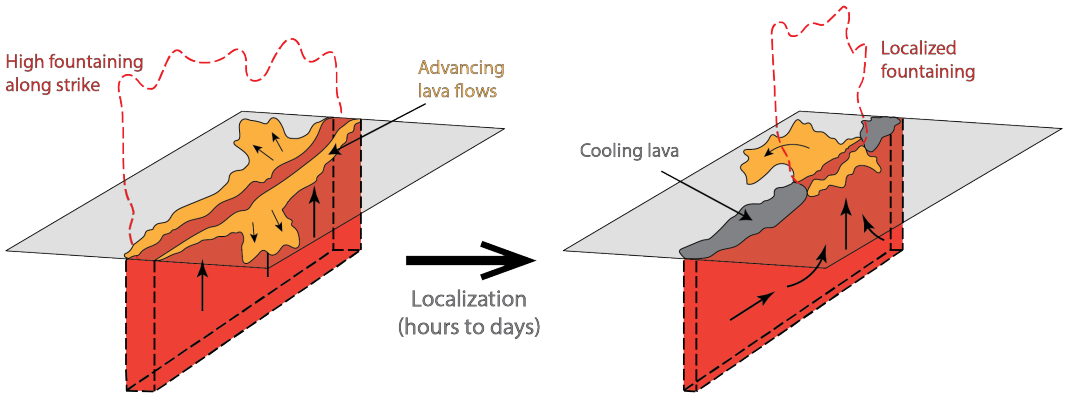

***Figure 1.2**: Schematic of a basaltic fissure eruption that initially produces high fountaining all along its strike, feeding lava flows that advance downslope. Then, through time the eruptive activity localizes and eventually focusses to a singular vent.*

Despite the prominent array of hazards that these eruptions pose and their high eruption frequency, the evolution of basaltic fissure systems is poorly understood and is considered to be a key future goal of the volcanology community (e.g. Valentine and Gregg 2008). In order for hazard management officials to better mitigate against the effects of these eruptions, we want to know: how the intensity of fountaining will evolve through time; how long eruptions will last; where the sites of ongoing magma discharge will be; and how the subsurface plumbing system influences surface behaviour. Although pioneering early work in the 1980's and 1990's (e.g. Bruce and Huppert 1989) addressed the thermo-rheological control on basaltic fissure localization to partly answer these questions (discussed further in Chapter 2) no work, until now, has been done to

investigate the effects of the magma dynamics (i.e. magma convection and eruption processes).

1.2 Thesis structure

This thesis will address many aspects of a basaltic fissure system; from subaerial fragmentation behaviours, to within conduit convection dynamics (Fig. 1.3). In this short sub-section, I will briefly set the context for each chapter.

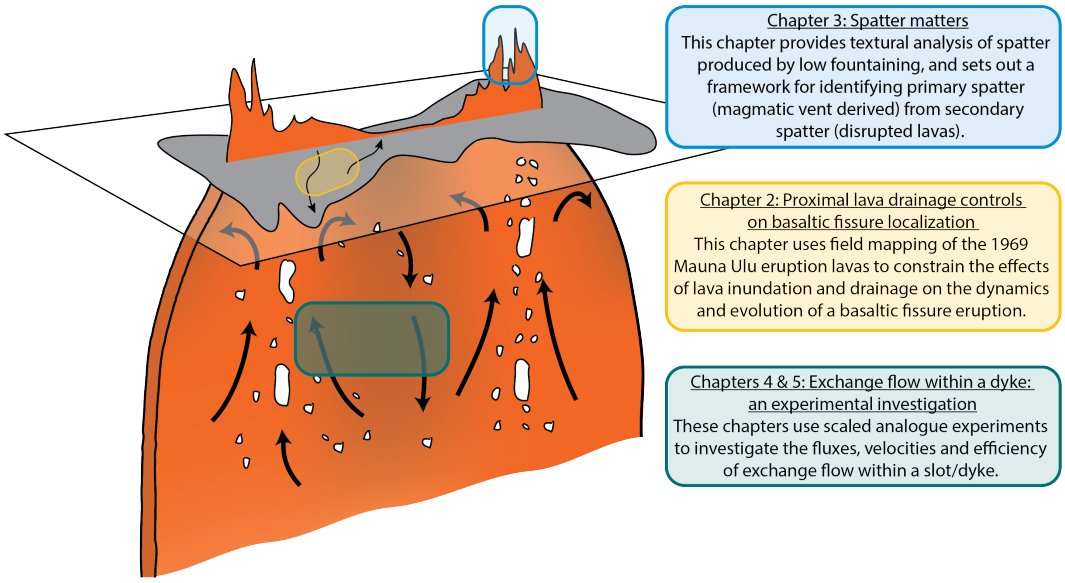

***Figure 1.3**: Schematic of a fissure eruption and its plumbing system. The coloured boxes highlight the spatial focus of each of the main data chapters.*

Chapter 2 introduces a novel mapping technique, using tree moulds, allowing for the reconstruction of pre-eruption, during eruption and post-eruption topographic maps. This technique is used to interpret the proximal deposits of episode 1 of the Mauna Ulu 1969 basaltic fissure eruption. Through interpretation of interactions between the erupting fissure and the proximal lava flow field I evaluate the role that surface or "top-down" processes have in controlling the evolution of fissure segments. Then, still using Mauna Ulu as a case example, in Chapter 3 I investigate how fountaining behaviour changes through an eruption. Detailed textural analysis on a large number of spatter clasts reveal

the textural changes in low fountaining activity as the eruption wanes. Furthermore, using the textural properties of pyroclasts a framework is set out to distinguish between primary fissures that formed through magma ascent and secondary or "non-eruptive" fissures that did not act as a magma pathway and just disrupted overlying lava flows. This is an important distinction that must be made when mapping sites of previous fissure eruptions – a crucial input parameter for probabilistic hazard distribution models.

These two field-based chapters show that surface processes and shallow conduit dynamics can control the eruption style and evolution. In Chapter 2 the high aspect ratio geometry of a fissure system is described, and it is shown that lava can drain-back down the conduit after it has been erupted. In Chapter 3 the textural properties of the dense, relatively outgassed lava/magma thought to descend back down the conduit are described. Therefore, to better understand the magma dynamics within a fissure system the simultaneous drainage and upwelling of magma within the conduit or feeder dyke must be investigated. However, this can be problematic since, direct, field-based observations are largely limited to surface activity and geophysical imaging on the short length scales of interest proves extremely difficult. Therefore, in this thesis, I use scaled analogue experiments to investigate the subsurface magma dynamics. Chapter 4 evaluates the use of analogue experiments in volcanology and presents a fundamental approach for scaling laboratory experiments to a natural system of interest. I also provide a scaling analysis for my analogue experiments (Chapter 5) and describe the physical properties of the fluids used. Then, Chapter 5 presents a series of analogue experiments designed to investigate the simultaneous drainage of dense, degassed, viscous magma (as evidenced in Chapters 2 & 3) and upwelling of less dense, less viscous magma within a dyke-like geometry. Then, the experimental results and semi-empirical models are used to evaluate the subsurface behaviour during episode 1 of the 1969 Mauna Ulu eruption. Lastly, in Chapter 6 I synthesize all of the scientific advances provided by this thesis and suggest key future steps for the volcanology community.

1.3 Author Contributions

Unless explicitly stated in the following section, all work in this thesis is my own.

Chapter 2 is based around the published paper: Jones, T.J., Llewellin, E.W., Houghton, B.F., Brown, R.J., and Vye-Brown, C. Proximal lava drainage controls on basaltic fissure eruption dynamics. *Bull Volcanol* (2017) 79: 81. https://doi.org/10.1007/s00445-017-1164-2. This sub-project was designed with assistance from all of my supervisors. I conducted all of the fieldwork and subsequent data processing with the exception of the raw GPS conversions, which were performed by Mike Poland (at the Hawaiian Volcano Observatory). The text presented in Chapter 2 represents a version, written by myself, before direct edits were made by co-authors. The paper in its published form can be found in Appendix A.

Chapter 3 is based around the accepted, in press, paper: Jones, T.J., Houghton, B.F., Llewellin, E.W., Parcheta, C.E., and Höltgen, L. Spatter matters – distinguishing primary (eruptive) and secondary (non-eruptive) spatter deposits**.** Nature Scientific Reports. *In press.* https://doi.org/10.1038/s41598-018-27065-1. This sub-project was designed with assistance from Bruce Houghton and Ed Llewellin. I performed the bulk vesicularity measurements and imaged all of the samples. With the assistance of Laura Höltgen (German academic exchange service intern, hosted by me), who manually traced five thin sections, I performed the image analysis and subsequent data analysis. The text presented in Chapter 3 represents a version, written by myself, before direct edits were made by co-authors. The paper in its accepted form can be found in Appendix B.

Chapter 4 contains material characterisation and analysis and is not intended to be submitted as a journal manuscript. After initial training on the rheometer by Stephen Boothroyd in Materials Chemistry, Durham University, I performed all of the rheology and density measurements independently.

Chapter 5 is based around a series of analogue experiments that were originally designed by Ed Llewellin when writing the PhD project proposal. Significant modifications to the original apparatus design were calculated by Ed and myself and carried out by the Physics workshop, Durham University. I conducted the experiments with practical support from Laura Höltgen. I then performed the image analysis with support from Veronica Becker (German academic exchange service intern, hosted by me). Like all other chapters, Chapter 5 represents a version, written by myself, before direct edits were made by supervisors.

Chapter 2

Proximal lava drainage controls on basaltic fissure localization

2.1 Introduction

The bulk of the planet's magma output is through basaltic fissure eruptions (Sigurdsson 2000), however despite being relatively common, their deposits can be challenging to investigate and interpret. Vent structures change and migrate throughout eruptions (Richter et al. 1970; Thorarinsson et al. 1973; Swanson et al. 1979; Bruce and Huppert 1989), however evidence of these dynamic processes is commonly buried beneath later syn-eruptive material, including spatter, tephra fall or re-surfacing by subsequently emplaced lava flows (Brown et al. 2015). Furthermore, evidence of clastogenic eruption processes, such as spattering and fountaining, can be lost if pyroclastic material becomes agglutinated and/or forms rheomorphic lava flows (Sumner et al. 2005; Valentine and Gregg 2008; Parcheta et al. 2012).

Fissure eruptions typically initiate as curtains of fountaining basaltic spatter, bombs, and lapilli, with heights of 10's to 100's of meters (e.g. Richter et al. 1970; Swanson et al. 1979; Wolfe et al. 1988; Alparone et al. 2003). The vents are initially of high aspect ratio, with crack widths varying from ~ 2 m to tens of meters, and lengths ranging from several hundred metres to several kilometres (e.g. Gudmundsson 1987; Opheim and Gudmundsson 1989; Keating et al. 2008; Parcheta et al. 2015). Over the order of hours, the curtain generally focuses to a few point sources along the fissure (e.g. Richter et al. 1970; Thorarinsson et al. 1973; Swanson et al. 1979), however controls on the temporal and spatial evolution of such systems are poorly understood (Bruce and Huppert 1989).

Progressive localization causes a change in the eruption parameters, such as an increase in fountain height (Wilson et al. 1995), restricted spatial distributions of lava discharge (Pedersen et al. 2017), and release of hazardous gases and aerosols (Walker et al. 1984; Stothers et al. 1986; Woods 1993) from a point, rather than a line, source. To track, and thus effectively manage, this dynamic situation, a better understanding of factors modulating fissure localization is required.

Vents along fissures are conduits for upwelling magma, but they also can act as locations for downwelling, relatively degassed lava. This phenomenon has been documented in several lava lakes (e.g., Halema‘uma‘u Crater, Kīlauea, Hawai’i (Patrick et al. 2015); Mt Erebus, Antarctica (e.g., Oppenheimer and Kyle 2008); Kīlauea Iki, Hawai’i (Stovall et al. 2009) and Erta Ale, Ethiopia (Oppenheimer and Francis 1997). Fluctuations in the lava lake height are commonly related to pressure changes within the magma plumbing system (e.g., Witham and Llewellin 2006). However, observations of drainage in a dyke or fissure vents are much less abundant. In rare cases lava has been observed to drain back down the fissure system (2002 eruption of Nyiragongo; Allard et al. 2002; Wunderman 2002; 1974 eruption of Kīlauea; Wilson et al. 1995), although it is very difficult to quantify. Additionally, previous studies in old dyke feeder systems have used anisotropy of magnetic susceptibility (AMS) and vesicle textures to record regions of upwards and downwards flow within a single dyke (Philpotts and Philpotts 2007). Further textural evidence from the 1809 Mt Etna eruption in the form of partially-filled cavities within the feeder system has suggested rapid drain-back of magma leading to the termination of the eruption (Geshi and Neri 2014). Finally, kinematic indicators such as draining flow lobes and surface folds have been interpreted as periods of magma ascent and drainage at Tongariro volcano, New Zealand (Wadsworth et al. 2015). In this study I present quantitative field evidence of drainage within a fissure vent geometry.

The descent, of relatively degassed, dense magma in a conduit has implications for sub-surface fluid dynamics (Stevenson and Blake 1998; Beckett et al. 2011; Palma et al. 2011) and may affect fissure localization. Previous studies of vent localization and termination of basaltic fissure eruptions have focused on the feedback between thermo-rheological effects of heat advection rates and magma movement in dykes. Delaney and Pollard (1982) showed that magma flowing at 1 ms^{-1} in a 2 m-wide dyke rapidly cooled and solidified inwards from conduit margins causing the dyke to close within a few hours. They inferred that, for eruptions to last longer than a few hours, as observed in Iceland (Thorarinsson et al. 1973) and Hawai'i (Swanson et al. 1979), the width of the ascending dyke must be larger than 2 m. Bruce and Huppert (1989) investigated the role of thermo-rheological effects in vent-localization. They showed that the balance between heat transfer by advection and conduction governs whether conduit walls are melted back, widening the conduit, or magma solidifies against the walls, narrowing and eventually blocking the conduit (Bruce and Huppert 1989; Bruce and Huppert 1990). More recent work has shown that, as the magma cools against the wall rock, local regions of relatively cooler, higher viscosity magma are formed (Wylie and Lister 1995; Wylie et al. 1999). The fresh, hotter upwelling magma will tend to minimize energy loss by flowing through the regions of lowest viscosity, forming fingers of localized upwelling (Whitehead and Helfrich 1991; Helfrich 1995; Wylie and Lister 1995; Wylie et al. 1999).

The role that drain-back plays in the evolution of magma flow organization within, and out of, a dyke is currently an open research question. In this Chapter, I use field evidence to investigate the inundation and drainage of basaltic lava during episode 1 of the 1969-74 eruption of Mauna Ulu, Hawai'i, USA, and assess its influence on shallow conduit dynamics and the spatio-temporal evolution of the fissure system.

2.2 Background

2.2.1 The Mauna Ulu 1969-74 eruption

Mauna Ulu is a small lava shield located on the East Rift Zone (ERZ) of Kīlauea volcano, Hawai‘i (Fig. 2.1a). The 1969–74 Mauna Ulu eruption that built this shield was characterized by two phases: Phase I began on May 24th 1969 and ended on October 15th 1971 during which 185 × 10^{6} m^{3} of lava were erupted (Swanson et al. 1979); and Phase II lasted from February 3rd 1972 to July 22nd 1974 (Tilling et al. 1987). These two phases were documented by Swanson et al. (1979) and Tilling et al. (1987) respectively. Phase 1 of the eruption (the focus here) can be split into several stages. Stages 1 to 4 (1969–71), consisted of 12 episodes of sustained fountaining, lava flows and overflows from the main Mauna Ulu shield vent (Swanson et al. 1979). This was followed by 3.5 months of quiescence, during which scientists concluded that the eruption was over. However, in February 1972 the eruptive activity restarted and continued until 1974. During this latter period eruptive activity was largely confined to Mauna Ulu and to a satellite shield located at the former site of the ‘Alae crater. In this thesis I solely focus on the first episode of stage 1 following the narrative of Swanson et al. (1979) and enhanced timings of Parcheta et al. (2012). Observation of this episode was limited to eye-witness accounts by Hawaiian Volcano Observatory (HVO) scientists (Swanson et al. 1979) and two aerial photographs from Sandia Labs (now held at the United States Geological Survey HVO; Fig. 2.2) taken one hour after the fissure system reached its full length (Swanson et al. 1979; Parcheta et al. 2012).

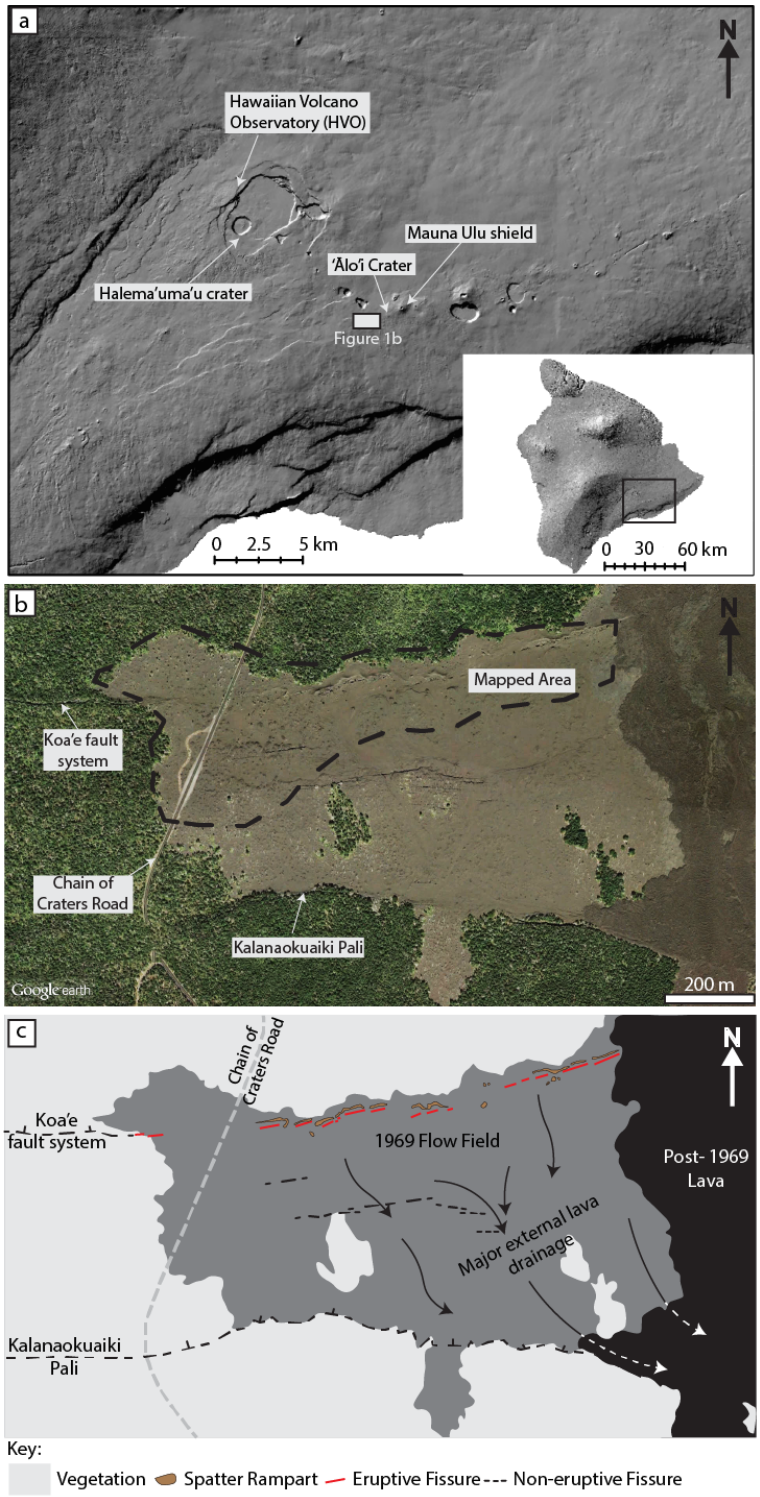

Figure 2.1: *Location map of Mauna Ulu on the Island of Hawai'i. (a) The location of the field area is shown in the black box. (b) Google Earth™ aerial image of the Mauna Ulu lava field, for reference the centre of the of view is at 19°21'39.43"N, 155°13'5.68"W. (c) Interpreted diagram of the image in (b) showing the surface features of the episode 1 Mauna Ulu eruption.*

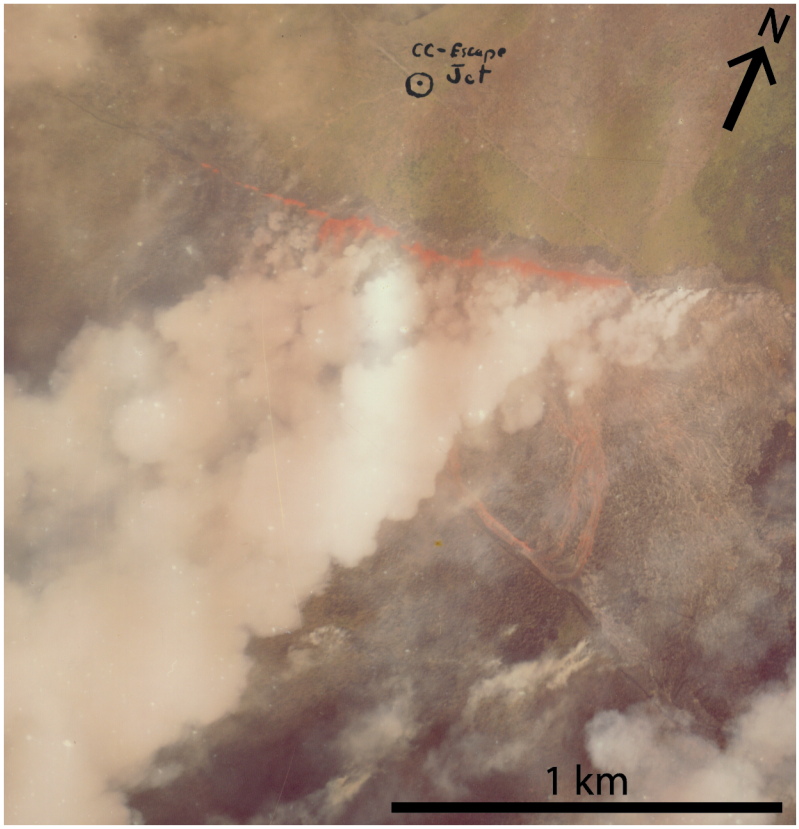

Figure 2.2: *Aerial photograph taken by Sandia Labs at 0940 HST; approximately 1 hour after the fissure reached its full length.*

Stage 1, episode 1 of the Mauna Ulu eruption initiated on May 24th 1969 with an earthquake swarm that could be felt in the nearby village of Volcano. Then at 0445 Hawaiian Standard Time (HST) fountaining began from a newly formed fissure system close to Aloi Crater. This fissure rapidly propagated westwards crossing the old Chain of Craters Road by 0500 HST. Propagation continued westward to cross Ainahou Road (the current Chain of Craters Road; Fig. 2.1) at 0830 HST and then extended ~ 150m west exploiting the Koa'e fault system (Swanson et al. 1979) to the edge of the study area (Fig. 2.1). Then steady fountaining and lava ponding occurred until 1200 – 1300 HST (Parcheta et al. 2012). During this time the pāhoehoe lava flow field advanced southward, down slope and ponded 1.2 km from the vent at the base of the north facing Kalanaokuaiki Pali (Swanson et al. 1979). Steady fountaining was followed by a period of waning fountaining activity and lava drain back ending at 2200 HST (Parcheta et al.

2012). This marks the end of episode 1, and the end of eruptive activity in the western segment of the Mauna Ulu fissure system. All subsequent activity occurred further to the east developing what became the Mauna Ulu shield. Most importantly a voluminous lava flow originating from the Mauna Ulu shield covered large sections of the originally 4.5 km fissure only to leave the 880 m western section available to study today (Figs. 2.1b, c). Therefore, this study solely focuses on the early stage development of a linear fissure system rather than the later stages that were confined to the Mauna Ulu shield to the east; all discussions of lava re-surfacing refer to the 1969 stage 1, episode 1 eruption.

2.2.2 Previous mapping of the episode 1 fissure system

The exceptional preservation of the episode 1 fissure system offers a unique opportunity to investigate shallow conduit geometries and processes. Parcheta et al., (2015) used ground-based light detection and ranging (LiDAR) to measure the geometry of the shallow conduit (< 15 m depth) and vent. They mapped 54 vents or segments along the surviving 880 m of fissure and document several distinct geometric features including: (1) five en echelon steps caused by the rotation of a rectilinear dyke to a near-shear stress orientation upon ascent; (2) sinuous individual fissure segments most likely related to stress field interactions between the ERZ and the Koa'e fault system and fissure irregularity; and (3) irregularity in the internal dyke wall surface, thought to represent pre-existing cooling joints within the pre-1969 lava flow wall rock (Parcheta et al. 2015). 3D imaging of the subsurface vent structures shows that the primary conduit wall consists of jigsaw-like fits between either sides of the conduit (Parcheta et al. 2016), indicating that the conduit walls have not been modified since the eruption.

The vent geometries range from sub-circular to linear in plan-view, and from parallel-sided to flared in cross-section. The degree of vent flaring was characterised quantitatively through the LiDAR point cloud for three vents (Parcheta et al. 2015). No clear relationship between fountain height and vent flaring was found, although fountain

height during the eruption was poorly quantified. Parcheta et al. (2015) suggested that the flaring was caused by either syn-eruptive erosion or late-stage drain-back of ponded lava.

2.3 Methodology

2.3.1 Fieldwork

This chapter focuses on the near-fissure products of the episode 1 flow field (Fig. 2.1c). Prior to the eruption this area was densely forested, and lava flows quenched against the trees. As the flows inflated the quench extended further up the trees, forming a cast up to 5 m high; this lava high-stand surface represents the maximum local inundation depth (Parcheta et al., 2015). During the waning stage of the eruption, lava drained to leave solidified lava quenched against the tree to form a tree mould (Finch 1931; Moore and Richter 1962; Lockwood and Williams 1978; Lockwood and Lipman 1980). The difference in height between the lava high-stand surface and final, post-eruption ground surface represents the extent of drainage from the maximum inundation depth, termed the lava drainage depth (Finch 1931; Moore and Richter 1962; Lockwood and Williams 1978; Parcheta et al. 2015). Prior to the eruption the entire area was densely forested, hence tree moulds provide a consistent dataset for inundation depth across the proximal lava flow field fed by the episode 1 fissure.

Elevation measurements of the lava high-stand (syn-eruption) surface and post-eruption ground surface (i.e. the present day surface) were taken using a Leica SR520 kinematic GPS (kGPS) on > 200 tree moulds (Fig. 2.3). The following measurements were made for each tree mould, where possible: (1) internal depth of the tree mould (by lowering a plumb-bob into the mould); (2) elevation of the uppermost crust level (lava high-stand); (3) elevation of the post-eruption surface around the tree mould (i.e. the level of the surface following drainage); (4) height of the top of the tree mould above the surrounding lava surface. Note this final measurement is the same as the difference between measurements 2 and 3 and is therefore redundant in some locations. Measurements are

summarized in Figure 2.3. Note that a tree mould's internal depth is subject to error if debris has fallen down the cast, therefore measurements are only reported where a soil horizon was hit by the plumb bob. In the field, the soil horizon was identified either by visual inspection if the tree mould was shallow, from the sound heard upon contact, or from the presence of soil on the plumb bob. Estimated accuracy of the tree mould depth measurement is ± 2 cm. The location of a specific point within the field area was re-measured seven times using the standard kGPS protocol, enabling quantification of uncertainty in the measured position associated with data acquisition and processing. A standard deviation of 0.012 m, 0.017 m and 0.018 m, was obtained for the E–W, N–S and vertical positions, respectively.

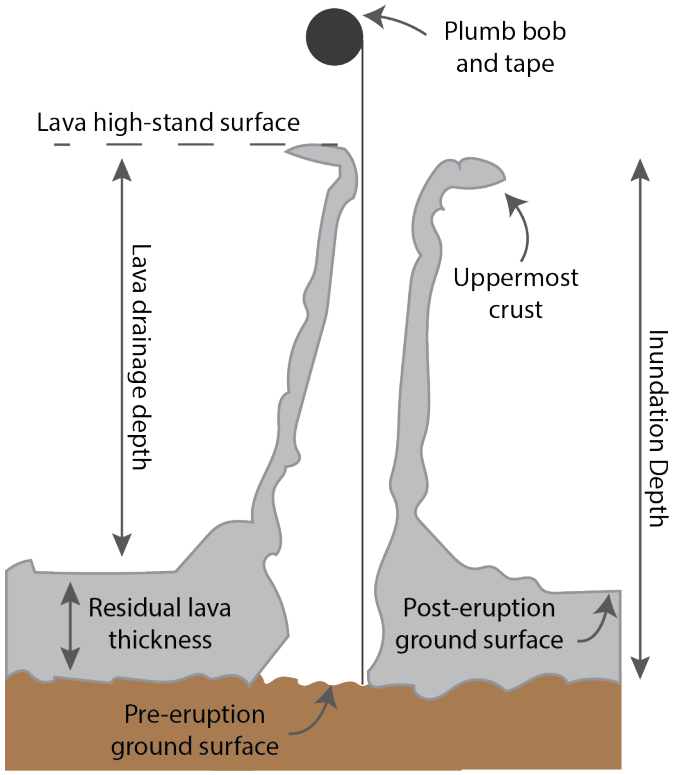

Figure 2.3: *Schematic tree mould showing the measured features, where the uppermost crust is interpreted to be the lava high-stand surface. The distance from the top of the tree mould to the pre-eruption ground surface – i.e. the inundation depth – was measured using a plumb-bob, dropped down the inside of the mould. The position of the lava high-stand surface and post-eruption ground surface were measured using kinematic GPS. Other quantities were determined by difference.*

2.3.2 Map production

A geo-referenced database relating all attributes (tree mould height and depth) to their associated kGPS location was created. These data were then imported into the geographic information systems program, ArcGIS™, for all further analyses. There are many different interpolation routines available within the ArcGIS™ platform (e.g. kriging, spline, natural neighbours and inverse distance weighting). For this work I used the spline interpolation method because, unlike the other techniques, it fits the interpolated surface through the input kGPS data points which are known to a high degree of accuracy. The spline interpolation has two variants – the tension spline and the regularized spline. Here, I used the tension spline because unlike the regularized spline the fitted surface remains within the input kGPS elevation limits (Franke 1982). Specifically, the tension spline interpolation routine bends a surface through the known input data points whilst trying to minimize the total curvature of the surface. In a *tension* spline both first and second derivatives terms are used to minimize the curvature of the surface (Franke 1982; Mitáš and Mitášová 1988).

When interpolating the kGPS data points to a raster using the tension spline function the number of points per region and φ must be chosen, where φ refers to the weight given to the first derivative term and can be thought of as the surface stiffness (Franke 1982). Through visual comparison with a National Oceanographic and Atmospheric Administration digital elevation model of the post-eruption ground surface (Fig. 2.4; 2005 IfSAR DEM), a tension spline interpolation of the post-eruption ground surface using 10 points per region and a φ of 1 gave the best agreement. This approach was used to create topographic maps for: (1) the pre-eruption ground surface, (2) the lava high stand surface and (3) the post eruption ground surface. In terms of field data (Fig. 2.3) these maps where produced from: (1) the kGPS positions of the top bench crust minus the measured tree mould depth, (2) the kGPS positions of the top bench crust and (3) the kGPS positions of the ground surface today.

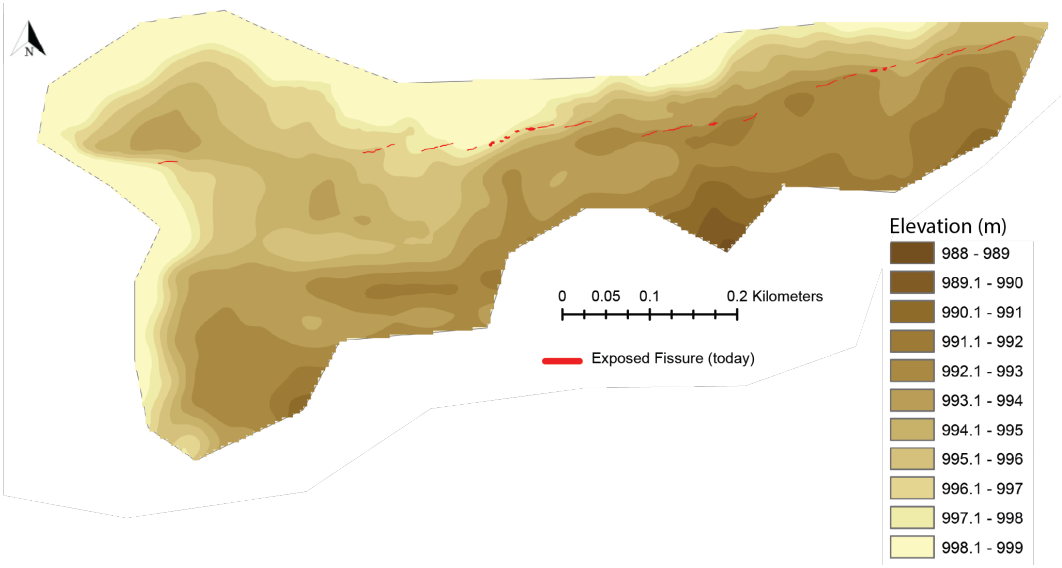

Figure 2.4: *National Oceanographic and Atmospheric Administration digital elevation model of the post-eruption ground surface (i.e. the present-day topography), produced using Interferometric Synthetic Aperture Radar mounted to an aircraft (2005 IfSAR DEM).*

After these three topographic maps were created, their surfaces were manipulated to to create two further maps: (1) a map of lava inundation depth during eruption, and (2) a map of lava drainage depth. Firstly, to map lava inundation, the pre-eruption ground surface raster was subtracted from the lava high-stand surface raster using the ArcMap™ 3D Analyst minus tool. Secondly, to map lava drainage depth the post-eruption ground surface raster was subtracted from the lava high-stand surface raster. It is possible that lava may have compacted slightly post-emplacement, however because these data do not allow for quantification of this process, it must be considered as a potential source of additional uncertainty on lava drainage. Note that, for completeness, a map of residual lava thickness is appended as Fig. 2.14 at the end of this chapter. This was created by subtracting the pre-eruption ground surface raster from the post-eruption surface raster. The distribution of residual lava thickness is not discussed further in this work.

2.3.3 Profile production

Variability in parameters (e.g. inundation depth) along strike have been calculated using a continuous profile across the entire length of the fissure. The various eruptive segments, commonly separated by en echelon steps, have been joined (Fig. 2.5). This allows for the investigation of any trends that occur along the entire eruptive fissure. Firstly, the aerial photograph taken by Sandia Labs (Fig. 2.2) was geo-referenced and the fissure segments that erupted material were marked onto the topographic maps. Next, to link all the discontinuous en echelon segments an overall trend line was superimposed at 79.365°. From the end of each segment, a tie-line was drawn perpendicular to the overall trend line, then the midpoint between the tie-lines, on the overall trend line, was located. Lastly, the segment trend lines were extended within each gap until they met at the midpoint. Parameters were then projected onto the overall trend line to create a continuous profile along strike, allowing for the investigation of trends that occur along the entire eruptive fissure.

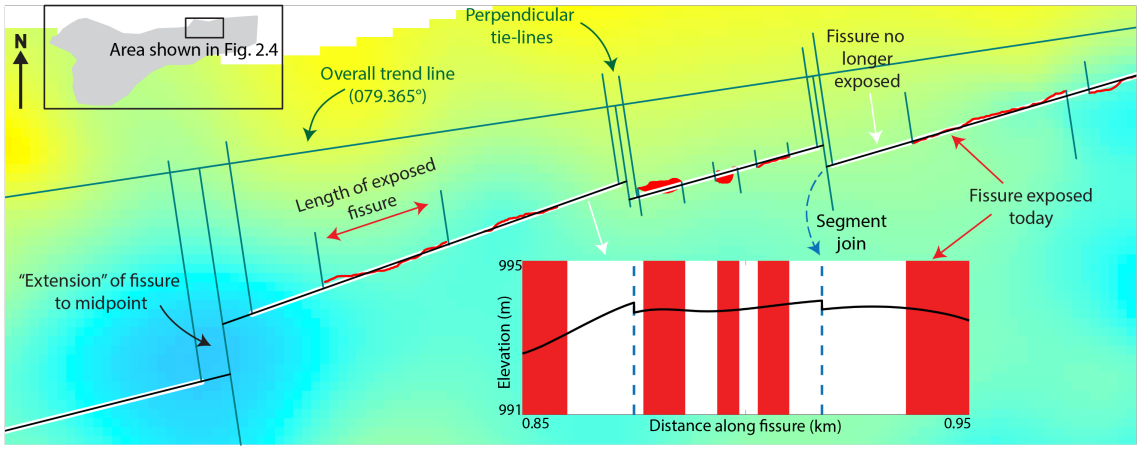

Figure 2.5: *A labelled portion of the fissure system showing how a continuous profile was constructed from discontinuous fissure segments, using the example of the post-eruption ground surface. The post-eruption ground surface base map used here is presented in full in Fig. 2.6c.*

2.4 Results

2.4.1 Topographic maps

Figure 2.6a shows a map of the pre-eruption ground surface prior to the 1969 Mauna Ulu eruption, reconstructed from tree mould depths. Overall the ground elevation slopes to the south, as expected for the southern flank of the basaltic Kīlauea shield. The 6.1 m vertical resolution pre-eruption map produced by the United States Geological Survey supports this general south sloping trend (Plate 1; Swanson et al. 1979). Although the absolute elevation values presented here differ to those of Swanson et al., (1979): this is explained by the vertical reference datum. Swanson et al., (1979) use a vertical reference of mean sea level whereas here the WGS 84 reference ellipsoid is used. In detail, the pre-eruption ground surface has two broad depressions to the east, starting close to the fissure and sloping southward. Close to the fissure these depressions are approximately 60 m wide and 1 m deep. Away from the fissure, these depressions broaden to > 170 m and deepen to 4 m. Furthermore, there is a shallow elongate depression, approximately 70 m wide, in the northwest section of the field area. The depression strikes roughly NW–SE and crosses the fissure (but note that there is no exposure of the fissure presently observable in this region). At a smaller scale, below the resolution of this measurement technique, the pre-eruption ground surface is expected to have had decimetre- and centimetre-scale variations caused by lava surface folding, changes in substrate (e.g., road vs. vegetation) and varying pre-existing lava type (e.g. shelly pāhoehoe vs. ropy pāhoehoe etc.).

Figure 2.6b shows the lava high-stand (HS) surface, which also slopes to the south. By visual inspection of the contour spacing, this surface in general shows less topographic relief than the pre-eruption ground surface. The north-west region of the field area has the highest elevation (~998 m) and there is no clear evidence of the topographic depression observed in the north-west section of the pre-eruption map. The two eastern, south-trending depressions observed in the pre-eruption map can also be detected on the lava high-stand surface.

Figure 2.6c represents the post-eruption ground surface (i.e. present day topography) and is the most robust dataset with the highest density of kGPS points (black circles) and it has been validated by the National Oceanographic and Atmospheric Administration digital elevation model shown in Figure 2.4 (2005 IfSAR DEM). The post-eruption ground surface also has an overall southward slope. In the west, a large, closed basin is present between fissure segments, and in the central and eastern sections several isolated depressions and topographic highs result in a more variable and steeper relief than that seen in Figures 2.6a and 2.6b.

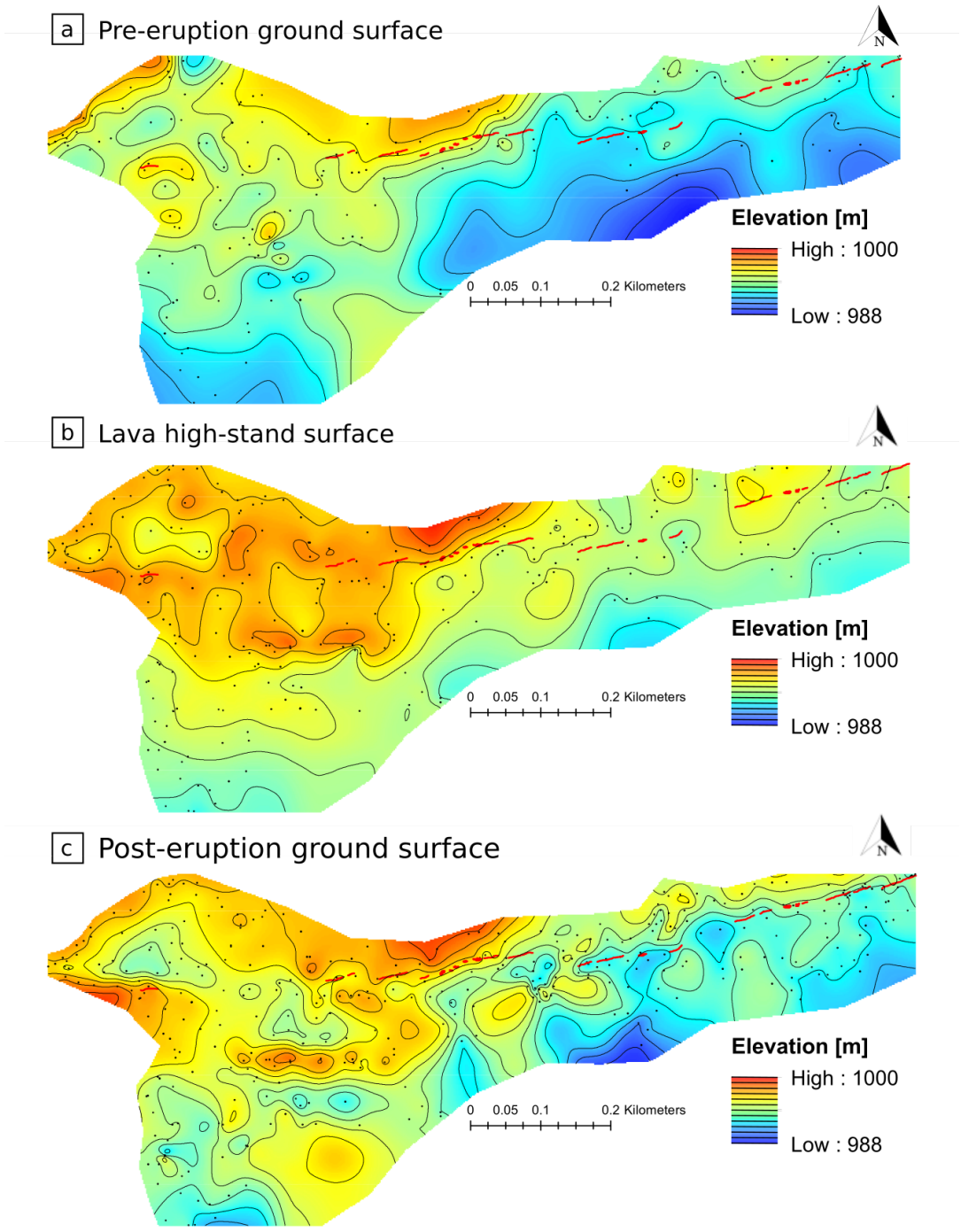

Figure 2.6: *Topographic maps, contoured at 1 m intervals, of the* ***(a)*** *pre-eruption ground surface topography prior to the 1969 Mauna Ulu eruption, reconstructed from tree mould depths (195 measurements; black dots),* ***(b)*** *lava high-stand surface (269 measurements) and* ***(c)*** *the post-eruption ground surface (383 measurements) produced within ArcMap from kGPS measurements. Not all data points appear in every map, because some tree moulds were broken and had no high-stand crust, and because measurements of the post-eruption ground surface were not restricted to locations with tree moulds. The fissure vents exposed at the surface today are marked in red. Elevations are ellipsoid heights (WGS 84) and not geoid corrected.*

2.4.2 Lava inundation

Figure 2.7 shows the lava inundation depth over the mapped area (i.e. the difference between the high-stand surface and pre-eruption ground surface). Much of the proximal flow field was inundated with 1 to 3 m thickness of lava during peak flow. Isolated regions of > 4 m-thick lava are commonly associated with depressions in the pre-eruption topography (Fig. 2.6a). Gaps where the eruptive fissure is no longer exposed at the surface (Fig. 2.7) occur within regions of relatively deep lava ponding/inundation. This is particularly evident in the west and at the central en-echelon step, and at the prominent en echelon step just east of the centre of the fissure system (arrows; Fig. 2.7).

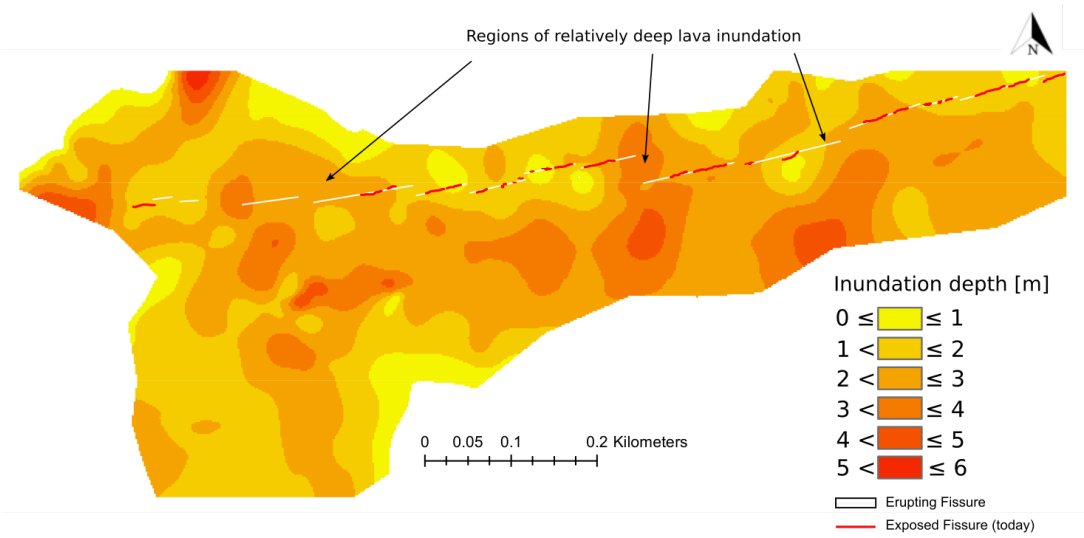

Figure 2.7: *Map of lava inundation depth during lava high-stand. The map is produced by subtracting the pre-eruption ground surface (Fig. 2.6a) from the lava high-stand surface (Fig. 2.6b). The fissure vents that can be observed in the field today are marked in red. Segments of the fissure known to be active during the eruption, identified from the Sandia Labs aerial imagery, are traced in white.*

2.4.3 Drainage

Figure 2.8 shows the amount of lava drainage that occurred after maximum inundation within the mapped area, i.e., the difference between the high-stand surface and post-eruption ground surface. Drainage varies between 0 – 4 m (Fig. 2.8) and is focused within the western basin between the exposed fissure segments, removing a maximum of 3.0 m

at its centre. East of the Chain of Craters Road, several drainage regions are centred along fissure segments. Some of these link southward to drainage channels (see Figs. 2.6a and c) and others form closed basins that are similar to, but smaller than, the western basin removing a maximum thickness of ~3.5 m.

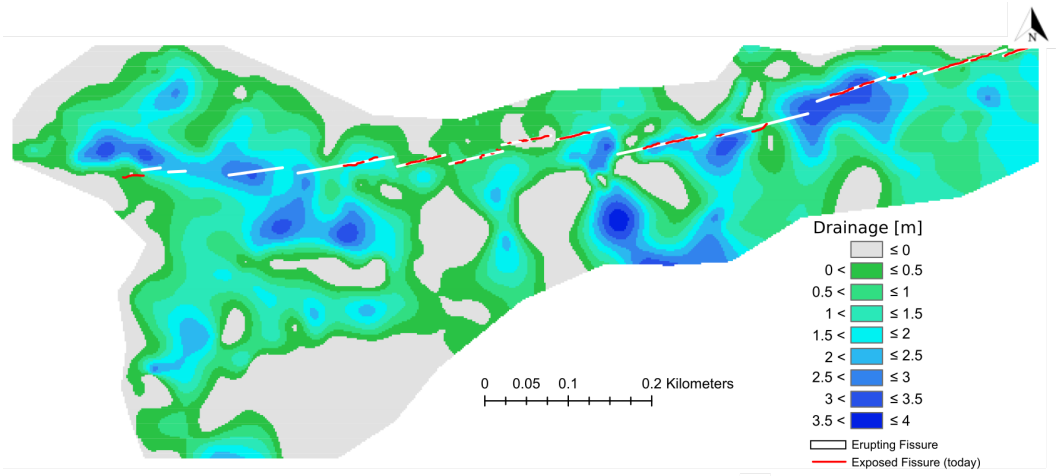

Figure 2.8: *Map of lava drainage depth. The map is produced by subtracting the post-eruption ground surface (Fig. 2.6c) from the lava high-stand surface (Fig. 2.6b). The fissure vents that can be observed in the field today are marked in red. Segments of the fissure known to be active during the eruption, identified from the Sandia Labs aerial imagery, are traced in white.*

2.5 Interpretations

To set the context for the interpretation of the results previously presented (Figs. 2.6–2.8) two hypothetical end-member scenarios are now introduced: (1) If a region were completely confined, with no pathway for the lava to drain away, then the lava would simply form a pond, and the high-stand surface would be flat and horizontal, with only minor perturbations that correspond to surface ropes and folding. (2) If all lava could freely drain either down slope, externally away from the fissure (outflow), or internally back down the conduit (drain-back), then the lava high-stand surface would reflect only dynamic ponding. These two end-member scenarios, of either widespread ponding or widespread drainage, constitute hypotheses against which the field data can be evaluated.

The situation during the 1969 Mauna Ulu eruption was much more complex than these end-member scenarios. The high stand surface was not flat but displayed a broad south-sloping trend with smaller scale topographic depressions and highs (Fig. 2.6b). Additionally, lava inundation was not consistent along strike (Fig. 2.7): certain fissure segments and the surrounding proximal flow field experienced a deeper inundation above the vent than others. This suggests that, during the eruption, the proximal flow field was characterized by a complex and spatially variable inundation, including elements of both static and dynamic ponding. To explore these complexities in detail, two regions within the proximal flow field will now be compared (Section 2.5.1). The first region is in the west of the field area (Box 1 in Fig. 2.9a) and has a lava high stand surface that is relatively flat and horizontal. It contains an unexposed eruptive fissure (Fig. 2.9b), and forms part of an isolated, closed basin in the pre-eruption ground surface. The second region is located in the east of the field area (Box 2 in Fig. 2.9a) and has a lava high-stand surface that consistently slopes to the south. It includes a prominent south-orientated channel in the pre-eruption ground surface.

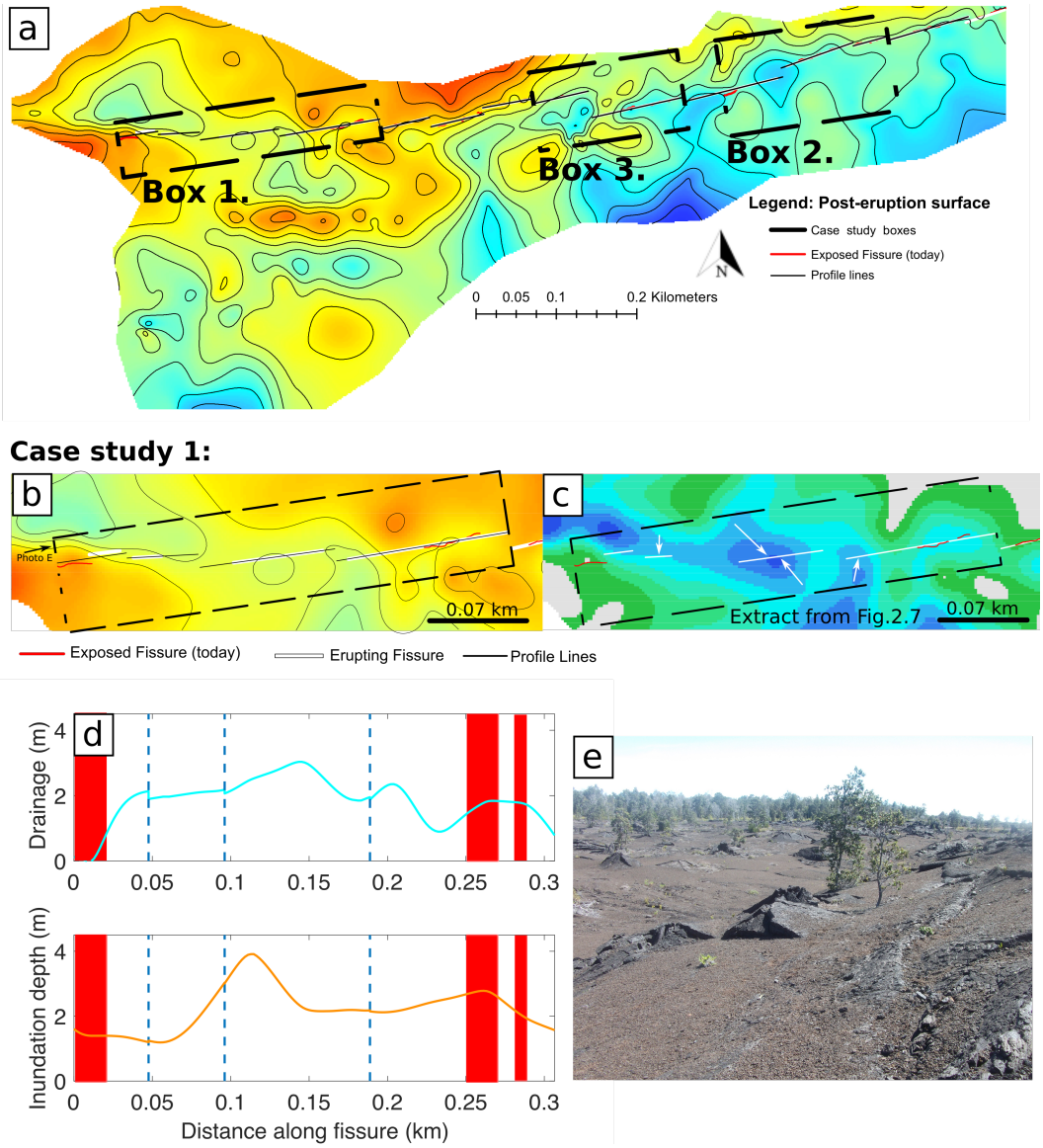

Figure 2.9: (a) *Post-eruption ground surface (i.e. present day topographic map) highlighting the three case study areas discussed in this study.* ***(b)*** *Detail of the area considered in case study 1 (Box 1 in (a)). The red lines show the fissure exposed at the surface today, the white lines show segments of fissure that were active during the eruption, and the black lines represent the analysed profiles, constructed according to the methodology presented in "Methods: Profile Production" and Figure 2.5.* ***(c)*** *An extract from Figure 2.8 with arrows showing areas where drainage focused into and around segments of now-buried fissure.* ***(d)*** *Profiles for drainage (blue) and inundation depth (orange) across Box 1. Blue vertical dashed lines represent a step from one fissure segment to another, red shaded regions mark fissure segments left exposed at the surface today, and white regions mark areas where the fissure is no longer exposed.* ***(e)*** *A field photograph of case study 1 (looking east; direction shown by arrow in part (b)) showing the large western basin depression.*

2.5.1 Case study 1: Isolated western basin

The first case study represents an isolated basin in the west of the field area. It comprises four fissure segments (Fig. 2.9b), all of which erupted material, but that are now either completely covered with no surface expression or are only partially exposed at the modern day surface. Drainage is at a local maximum on and near the fissure (Fig. 2.9c). The drainage regions are isolated and do not continue downslope and therefore drainage must have occurred down the fissure along segments that are no longer exposed at the surface. The topographic profile taken from the drainage map along the fissure in box 1 (Fig. 2.9d) reveals a maximum of 3 m of drainage (i.e. a 3 m reduction in ground elevation) in the central portion of the fissure, declining in both directions along fissure. The inundation profile across the same region (Fig. 2.9d) shows that the entire fissure segment had material ponded over the vent whilst it was erupting. The lava inundation reached a maximum of 3.9 m in the centre and it plateaus at ~ 2.2 m to the east. These high lava inundation values correspond to a valley in the pre-eruption ground surface. The inundation depths along the profile are roughly inversely correlated with the palaeo-depression's topography, which has its axis, and therefore deepest inundation, centred ~ 0.12 km from the western end of the fissure.

I infer that, as the 1969 lava flow field developed, it flooded the isolated western paleo-valley and led to high levels of inundation above the eruptive vent. During the waning stages of the eruption, lava drained back down the conduit (Fig. 2.9c). The amount of drainage fluctuated across the western basin but reaches a maximum between 0.1 and 0.15 km along strike. I hypothesise that this could be because: (1) this was the deepest part of the paleo-valley and the lava inundation was greatest and created the largest pressure head. Or, (2) the thick section of lava retained more heat and therefore maintained a lower viscosity than that in the surrounding flow field so it could drain faster or for longer. Lastly, the lava cooled to leave an isolated depression recording the loci of drainage in the post-eruption ground surface (Fig. 2.9e).

2.5.2 Case study 2: External and internal drainage

In the second case study, an area in the east of the field area is examined (Fig. 2.10a and Box 2; Fig. 2.9a). In this area, the Sandia Labs aerial imagery shows lava flows moving south, away from the fissure vent, following pre-existing topographic channels. Drainage mapping indicates that the amount of drainage peaks twice along the fissure (Fig. 2.10b), which correspond to two loci of drainage (Fig. 2.8). Unlike the previous case study, there is no correlation between the location of elevated drainage and the position of deep lava inundation (Fig. 2.10b); therefore, the same mechanism described in case study 1 cannot be invoked as the dominant process here. To investigate further, I constructed two profiles that cross-cut the fissure: (1) where it is now covered by lava, and hidden (A-A'), and: (2) where it remains exposed at the surface (B-B'). The pre-eruption ground surface across these two profile lines has a different slope (Fig. 2.10c): profile A-A' has a shallower proximal gradient than profile B-B'. I infer that, during the eruption, lava was more effectively drained away from the vent-proximal region at fissure location B-B' because of the greater slope. In this area, lava drainage mainly occurred down-slope away from the fissure (outflow), rather than internally back into the fissure (drain-back). By contrast, the shallower slope at A-A' inhibited external, down-slope outflow, hence lava either became dynamically ponded above the vent (when magma supply exceeded outflow) or drained back down fissure.

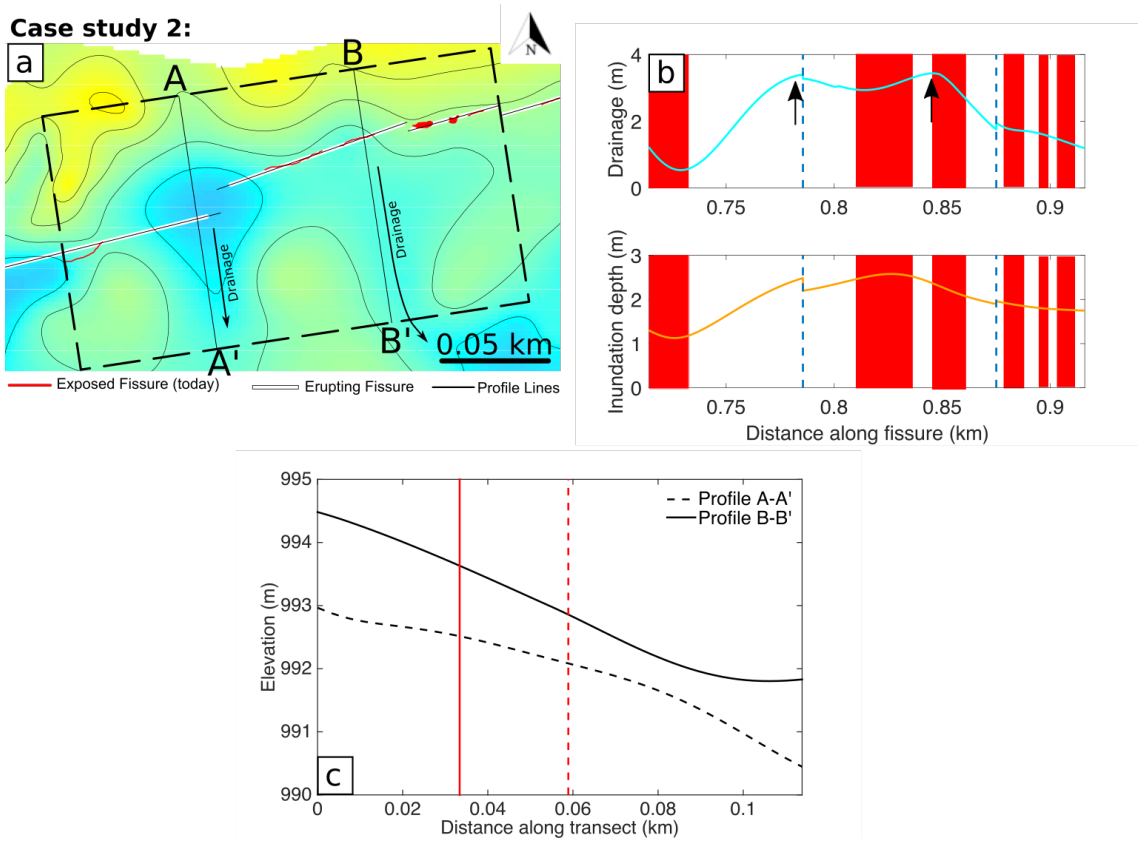

Figure 2.10: (a) *Detail of the area considered in case study 2 (Box 2 in Fig. 2.9a). The red lines show the fissure exposed at the surface today, the white lines show segments of fissure that were active during the eruption, and the black lines represent the analysed profiles.* ***(b)*** *Profiles for drainage (blue) and inundation depth (orange) across Box 2; arrows mark two maxima in the drainage profile.* ***(c)*** *Profiles A-A' (dashed) and B-B' (solid) of the pre-eruption ground surface. Vertical red lines mark the intersection between: (i) the A-A' profile (dashed red); (ii) the B-B' profile (solid red) and the fissure.*

2.6 Discussion

Tree mould mapping provides spatial information on lava drainage that allows us to reconstruct missing (i.e. buried) fissure segments. The region discussed in case study 1 (Fig. 2.9e) shows no indication of a vent and it has been completely covered by 1969 lava. This mapping technique, and the subsequent production of a drainage map, provides a way to constrain the location of the eruptive system in the absence of direct observations. It also demonstrates that calculations based on the aerial eruptive volume and thicknesses should be treated as a minimum, because they do not consider erupted material that has drained back down a vent during waning stages.

Both case studies indicate that lava ponded, at a variable inundation depth, over segments of the fissure. This was achieved either statically, as a result of topographic confinement within an isolated basin (case study 1), or dynamically, because magma supply temporarily exceeded outflow/ external drainage (section cut by line A-A', case study 2). In both cases, deep ponding is associated with no exposure of the fissure post-eruption. This suggests that the extent of the lava cover over an erupting vent, in turn a function of pre-eruption topography and the local eruption and outflow fluxes, may influence whether or not it will be preserved post-eruption, with deeply flooded vents less likely to be preserved. To understand the physical rationale for this interpretation, the effect that ponding has on eruption through an inundated linear vent must be discussed.

2.6.1 Eruption through ponded lava

The eruption of spatter through a perched lava pond occurred during the March 2011 Kamoamoa fissure eruption at Kīlauea (Lundgren et al. 2013; Orr et al. 2015). Ponding drowned the fissure and suppressed eruptive activity. Slow-moving magma in a fissure loses its heat to the country rock more effectively than fast-flowing magma, hence its viscosity increases, leading to a positive feedback that promotes stagnation and blocking of the most sluggish portions of a fissure (Bruce and Huppert 1989). This supports a hypothesis that ponding acts to suppress the eruption in that location indirectly by reducing mass flux and causing magma within the underlying section of fissure to slow its ascent. Here, it is further contended that fissure eruptions are likely to be particularly susceptible to flow perturbations induced by ponding, because ascending magma can flow laterally to bypass regions of stagnant or down-welling magma more easily than is the case for a circular conduit/vent geometry.

Wilson et al. (1995) present an analysis of the eruption of basaltic magma from a linear fissure vent, through a lava pond. They consider only the effect of the additional energy

required to eject entrained lava into the fountain, and do not consider thermo-rheological effects, nor along-fissure migration of flow in response to along-strike variations in pressure gradients. Nonetheless, an analysis of the episode 1 eruption, following their approach, is instructive. Figure 2.11 shows estimates of fountain height expected for the exsolved water contents and episode 1 mass eruption rates estimated for the Mauna Ulu eruption, for different ponding depths. Specifically, Swanson et al. (1979) report bulk volumetric eruption rates of 1.30×10^5 m^3 h^{-1} for episode 1 based on the aerial extent and thickness of new lava flows. This was then converted to a mass eruption rate of 6.31×10^4 kg s^{-1} using an average lava flow interior bulk density (1747 kg m^{-3}) measured from field samples. Then, to normalize the mass eruption rate to a unit length of fissure the length of incandescent fissure (assumed to be erupting) in the Sandia images was measured. This showed that ~ 1250 m of the original 4.5 km fissure was erupting thereby yielding a mass eruption rate per unit length of 50.5 kg s^{-1} m^{-1}. However, this bulk value should be taken as a minimum as it does not consider lateral variability along strike. For this reason and the data availability in Wilson et al. (1995) mass eruption rates are modelled as 10^2 kg $s^{-1}m^{-1}$. I estimate the water loss to be ~ 0.4 wt. %, calculated as the difference between the assumed water content of basaltic melt at Kīlauea's shallow (1–3 km) summit reservoir (0.5 wt.%; Moore 1970) and the water content of spatter from low fountains from Mauna Ulu (0.07 wt %; Swanson and Fabbi 1973).

The results show that an increase in lava depth over a fissure strongly influences fountain height (Fig. 2.11) – a ponding depth of 0.5 m above the vent reduces the fountain height by approximately two orders of magnitude (Fig. 2.11). Furthermore, at ponding depths ≥ 2 m the fountaining height tends to zero. Note however, that at shallow ponding depths (≤ 0.3 m) the absolute heights of the lava fountains calculated using the Wilson et al. (1995) approach are much greater than indicated by contemporary field observations. Swanson et al. (1979) report observed maximum fountain heights of 50 m; furthermore Parcheta et al. (2012) have subsequently calibrated field photographs taken at the time of the eruption

and suggest that fountain heights range between 13 and 32 m. One interpretation of the discrepancy between the theoretical calculations and the visual accounts is that all the vents were inundated to some degree. Another possibility is that this discrepancy arises because the model calculations do not account for lateral migration of magma along strike. If flow were to focus laterally, the mass eruption rate would increase at the localization points, resulting in higher fountaining. An increase in ponding depth at one location might therefore lead to an increase in mass eruption rate (and increasing fountain height) in adjacent parts of the fissure.

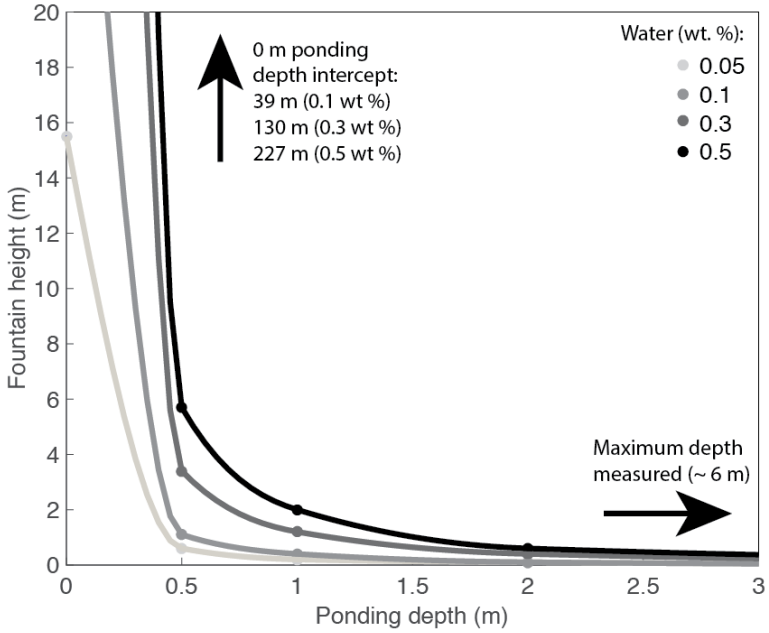

Figure 2.11: *Fountain height from a linear vent as a function of ponding depth above the vent (data taken from Table 3 of Wilson et al., 1995). The eruption is modelled to have a mass flux of 10^2 kg s^{-1} per meter of fissure with variable exsolved water contents (represented by sequential grey lines). The curves have no physical meaning and are included to guide the eye. For the ponding depths reported in this study (0 to 6 m), it is clear that a dramatic reduction in fountain height would have occurred as ponding depth increased.*

The contention, presented here, that magma can migrate laterally in response to ponding is supported by analysis of episode 1 rampart material (Parcheta et al. 2012) and visual observations at the time of eruption (Swanson et al. 1979), which indicate that

fountaining intensity varied laterally along strike and temporally throughout the eruption. For instance, at a single time, variations of 10 –15 m in fountain height were observed over short (4 – 15 m) distances along strike (Swanson et al. 1979; Parcheta et al. 2012). These variations are a result of the progressive vent localization process. To illustrate the effect that variable inundation can have on vent localization, a third case study is considered within the central portion of the field area (Box 3; Fig. 2.9a). Here there are vents on two segments of fissure (X-Y and Y-Z) that initially erupted along their entire lateral extent (interpreted from Sandia Labs aerial imagery; Figure 2.2) but are today only preserved in limited sections (Fig. 2.12a). An extract from the lava inundation map (Fig. 2.12b) shows that the maximum thickness of lava above the vent is highly variable along strike. In this area the pre-eruption ground surface reaches a local minimum between the two fissure segments (Fig. 2.12c). The lava inundation profile across the region of interest (Fig. 2.12d) shows that ponding depth varies between 0.5 m and 3.5 m and reaches a maximum in the centre where the fissure is no longer exposed at the surface. This ponding depth range (0.5–3.5 m) is sufficient to result in a large reduction in fountain height (Wilson et al. 1995). I suggest that deeper regions of lava ponding caused by palaeo-topography at the east of fissure X-Y and the west of fissure Y-Z suppressed fountaining in these regions, leading to blocking of the shallow conduit. This is consistent with the observation that the vents are no longer visible and are covered by 1969 lava. It is also possible that proximity to the end of the fissure segments in this region contributed to blocking of the conduit in this region.

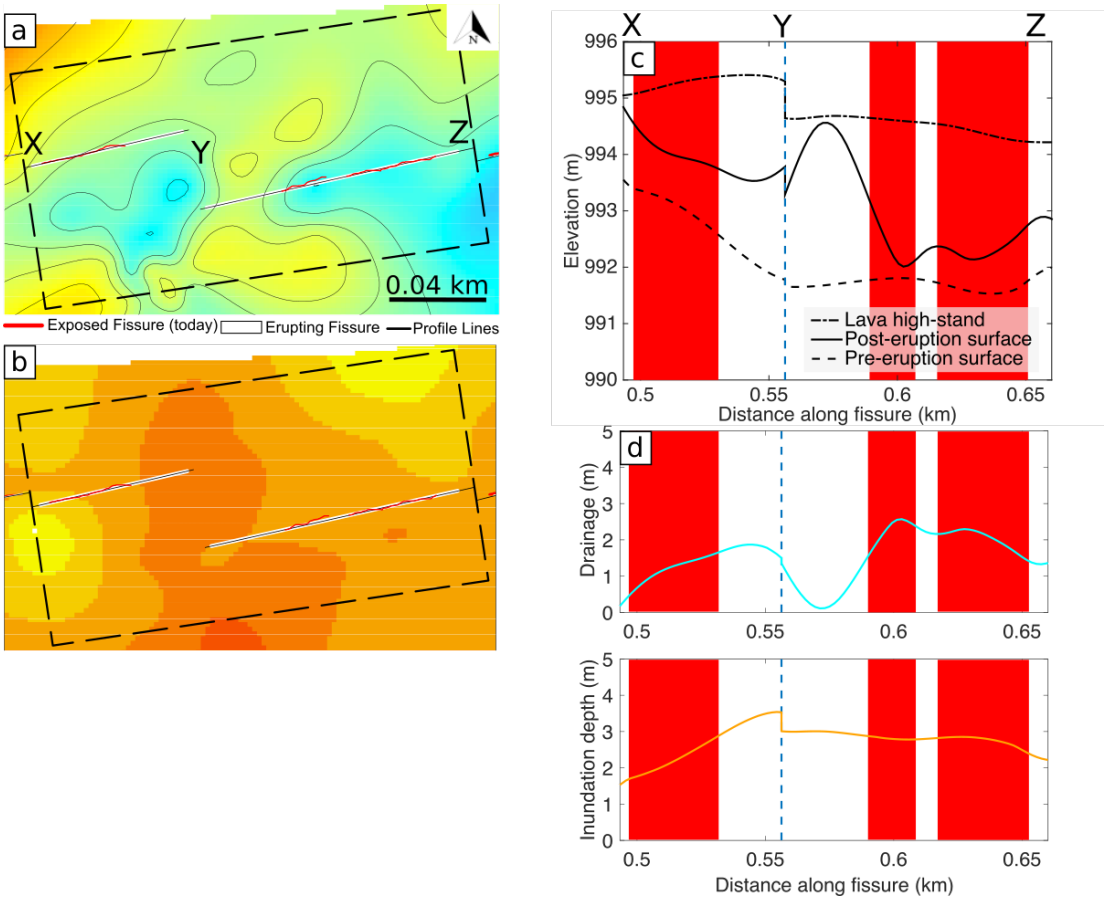

Figure 2.12: (a) *Detail of the area considered in case study 3 (Box 3 in Fig. 2.9a). The red lines show the fissure exposed at the surface today, the white lines show segments of fissure that were active during the eruption, and the black lines represent the analysed profiles.* ***(b)*** *Lava inundation map of the same area in box 3. The colour scale is the same as for Figure 2.7, hotter colours representing greater lava inundation depths (5 m maximum, 0 m minimum in inset).* ***(c)*** *Elevation profiles of the lava high-stand surface, and pre-eruption and post-eruption ground surface.* ***(d)*** *Profiles for drainage (blue) and inundation depth (orange) across Box 3.*

The observations and interpretations presented in this chapter support the idea that ponding over the vent may influence local eruption intensity and the longevity of an eruptive segment. In this model, summarized in Figure 2.13, suppression of fountaining by deep ponding is followed by stagnation of the eruption at that location, and/or drain-back of erupted lava into the conduit. In either case, the viscosity of the magma in that part of the conduit increases, resulting in early shut-down of the eruption at that fissure segment and decreasing the likelihood of it being preserved as an open vent post-

eruption. As a corollary, the location of pre-eruption topographic highs intersected by the eruptive fissure appears to correspond with preserved eruptive vents. These palaeo-topographic highs, along fissure from palaeo-lows, have relatively shallow lava ponding depths, and are often associated with sub-circular vent geometries. It is inferred that these parts of the fissure became focal points for ongoing magma ascent and discharge, and that consequent mechanical erosion transformed the fissure to a more circular geometry (Delaney and Pollard 1981; Wylie et al. 1999; Mitchell 2005).

2.7 Conclusions

Tree mould mapping allows the reconstruction of topographic maps before, during and after an eruption. These data can be combined to estimate: (1) the depth of lava inundation above the eruptive vent and (2) the amount of drainage that occurred since the lava high-stand and is particularly useful where syn-eruptive observations are limited or non-existent. This technique has been used to aid our understanding of how the fissure system that was active during episode 1 of the 1969 Mauna Ulu eruption of Kīlauea, Hawai'i, evolved from laterally continuous hawaiian fountaining to more discrete vents as fissure segments narrowed and closed. The pre-eruption ground surface topography is an important control on this evolution (Fig. 2.13): paleo-valleys dynamically ponded large volumes of lava and led to the reduction of upwelling magma and the migration of fountaining to other sites along the fissure. Also, significant volumes of lava were capable of draining back down the vent as the eruption progressed. Here, I proposed that internal drainage (drain-back into the vent) can cause an eruption within a segment to shut down and can leave the fissure vent completely covered by lava. This suggest that, in addition to thermal-rheological controls, surface effects (lava inundation, pre-eruption topography and drainage) play an important role in the evolution of a basaltic fissure system.

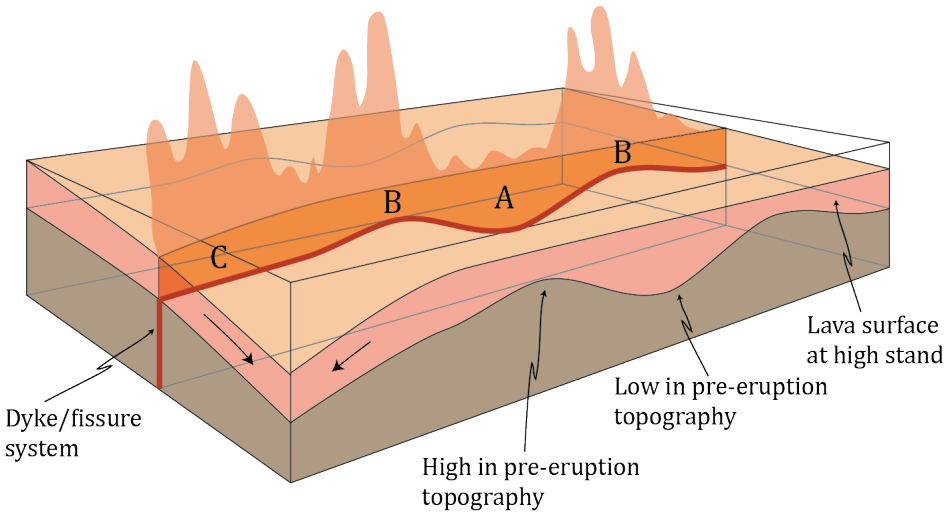

Figure 2.13: *A simplified schematic of the interaction between the surface and subsurface processes operating during a fissure eruption. In areas where there was a pre-eruption topographic low (A), the lava is able to inundate and cause deep ponding over the vent. Ponding supresses the subsurface upwelling flux and focuses flow along strike to areas of shallow inundation; these are palaeo- topographic high points (B) and regions with good external drainage (C). These localization regions are often preserved as open 'vents' post-eruption.*

Additional Figure:

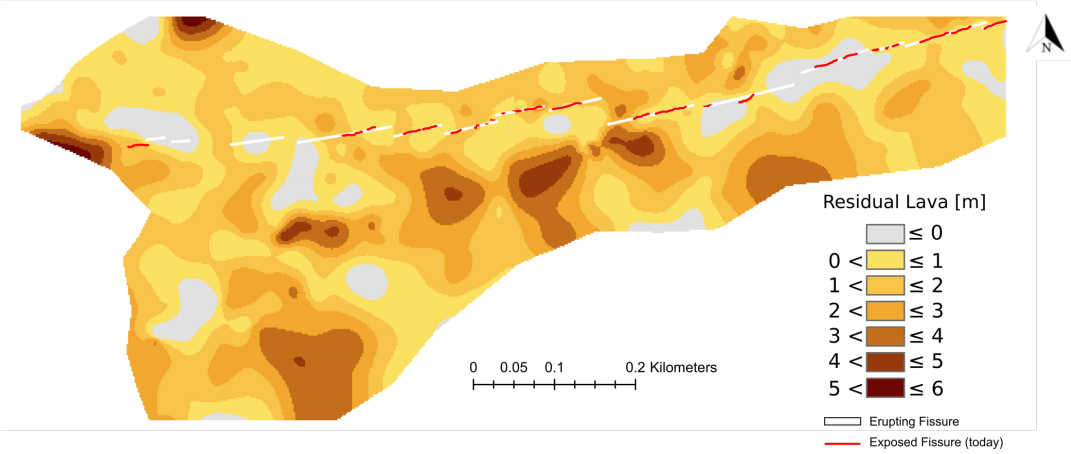

Figure 2.14: *Map of residual lava thickness. The map is produced by subtracting the post-eruption ground surface (Fig. 2.6c) from the pre-eruption ground surface (Fig. 2.6a).*

Chapter 3

Spatter matters – textural characteristics of spatter inform on the mechanisms of formation

---

3.1 Introduction

Basaltic hawaiian fountaining can produce a range of pyroclastic products that are defined by the efficiency of cooling experienced within the parent fountain (Head and Wilson, 1989; Sumner et al., 2005). The spectrum is continuous but ranges from brittle basaltic scoria and spindle bombs, which have experienced substantial cooling, to hot fluidal clasts – termed spatter – that agglutinate (flatten and/or adhere; Sumner et al., 2005) on landing because they remain predominantly above the glass transition temperature (T_g) (Rader and Geist, 2015). Ultimately, the characteristics of the final spatter deposit depend on both the accumulation rate and the amount of clast cooling. When both rates are low (~ < 10 m h^{-1} and ~ < 7°C min^{-1} respectively; Rader and Geist, 2015), molten clasts break-up and heavily deform on landing (type 4/5; Sumner et al., 2005), producing spatter deposits that are partially coalesed and deformed. Sumner et al. (2005) suggest that "liquid" break-up is very common for near-vent products. If the accumulation rate is increased (> 10 m h^{-1}; Rader and Geist, 2015; Sumner, 1998) but the degree of clast cooling remains low, then spatter becomes rheomorphic and may feed a clastogenic lava flow (Head and Wilson, 1989; Heliker et al., 2003; Karhunen, 1988; Sumner, 1998; Thordarson et al., 2001; Thordarson and Self, 1998). For a moderate cooling rate and/or low accumulation rate, the spatter forms agglutinated cones and ramparts as summarized by the classification scheme in Sumner et al. (2005).

During formation, spatter ramparts can be modified in two ways: (1) if the ramparts become thick enough and remain hot, then compactional welding can occur (Capaccioni and Cuccoli, 2005; Parcheta et al., 2012; Quane et al., 2009); and (2) if the clast cooling rate increases, ramparts are subject to slumping and failure (Head and Wilson, 1989; Rader and Geist, 2015; Sumner et al., 2005). This phenomenon was observed during both the 1986 eruption of Izu-Oshima volcano, Japan (Sumner, 1998) and the 1983-86 eruption of Pu'u'Ō'ō, Hawaii (Wolfe et al., 1988).

The location of eruptive products, such as cinder cones and spatter, observed in the field and in remotely sensed imagery, are commonly used to identify the sites of previous eruption (Becerril et al., 2013; Bonali et al., 2011; Cappello et al., 2012; Neri et al., 2011). Mapping of previous eruption sites has been performed on basaltic fissure systems, like Etna volcano, Italy, to produce a spatial probability map for the location of future volcanic eruptions (e.g. Cappello et al., 2012). Additionally, the identification of volcanic landforms, has been used to infer volcanic activity on other planets (e.g. Wilson and Head, 1994, 1983). However, most of this work relies on the assumption that spatter, or other pyroclastic material, is produced by a primary magma pathway transporting material to the surface. Rootless cones break this assumption and are secondary in nature; they are not erupted from a primary magma conduit. They form through explosive interactions as lava propagates over a water-saturated, unconsolidated sediment (Hamilton et al., 2010; Thorarinsson, 1953). During these interactions initial, high energy explosions can generate sediment-rich tephra fallout and pyroclastic density currents. Then, later, weaker explosions generate spatter-rich mounds (Reynolds et al., 2015). Littoral cones are another example of a vent-like structure that forms through secondary disruption as lava enters the sea (Moore and Ault, 1965). In this study, I will explore an enigmatic type of secondary spatter pyroclastic deposit that, to my knowledge has never been described before.

The quantification and analysis of vesicle size distributions (VSD) and vesicle number densities (VND) in eruptive products is commonly used to inform on ascent and decompression processes (Cashman and Mangan, 1994; Mangan et al., 1993; Toramaru, 1995), conduit dynamics (Janebo et al., 2016), and bubble nucleation and growth (Klug et al., 2002; Lautze and Houghton, 2007; Polacci et al., 2003; Shea et al., 2010). Importantly for this study, the vesicle size or volume distribution preserved within a pyroclast is not simply a function of nucleation rate or volatile concentration, rather, it is continually modified through time by expansion, coalescence, and collapse processes (Klug and Cashman, 1994; Shea et al., 2010; Stovall et al., 2012). Hence, the quantitative textural analysis of the vesicle population can provide information on shallow conduit recycling (i.e. upper 10's of m) and surface residence time (e.g., Janebo et al., 2016; Lautze and Houghton, 2005).

Previously, vesicularity studies of pyroclasts from hawaiian fountains have been largely confined to high fountaining (Cashman and Mangan, 1994; Mangan et al., 1993; Mangan and Cashman, 1996; Stovall et al., 2012, 2011), with only Parcheta et al. (2013) analysing low-fountaining activity (defined as a fountain with height < 100 m; Houghton et al., 2016). In this chapter I expand the quantification of vesicle textures for low fountaining hawaiian eruptions and set out a framework for distinguishing primary from secondary spatter. Furthermore, following the evidence for internal, down conduit drainage presented in Chapter 2, in this chapter I will document how the magma textures evolved during the eruption. This will provide insight into the contrasting physical properties of the magma both upwelling and descending within the shallow conduit.

3.2 Field evidence for a new type of spatter

Field investigation of the episode 1 deposits of Mauna Ulu identified spatter that is not associated with a primary volcanic vent. This subsection will briefly review the field context that underpins this inference.

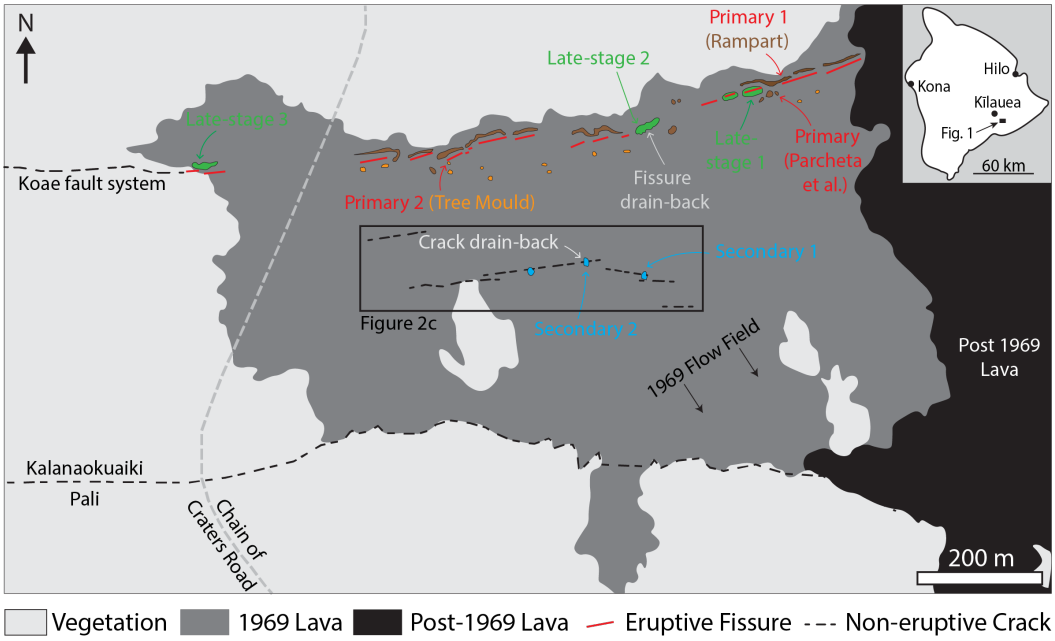

***Figure 3.1**: Interpretative map of the Mauna Ulu 1969 episode 1 fissure vents and associated products. Colour-coded arrows indicate locations where spatter and lava samples were taken. The central black box marks the field of view in Figure 3.2c. Numbering only distinguishes different sampling locations and has no temporal meaning.*

3.2.1 The 1969-74 Mauna Ulu eruption

Mauna Ulu is located on the ERZ of Kīlauea volcano, Hawai'i (Fig. 3.1). On May 24th 1969, episode 1 of the 1969-74 eruption initiated with an earthquake swarm. At 0445 Hawaiian Standard Time (HST) fountaining began from a newly formed fissure system, close to Aloi Crater (Swanson et al., 1979). The fissure rapidly propagated 1 km eastwards and 3 km westwards, crossing the old Chain of Craters Road by 0500 HST and crossing the Ainahou Road (the current Chain of Craters Road; Fig. 3.1) at 0830 HST (Swanson et al., 1979). Steady fountaining and lava ponding occurred until 1200 – 1300 HST (Parcheta et al., 2012) and fed a southward advancing pāhoehoe field. The steady fountaining was followed by a period of waning fountaining and lava drain-back ending at 2200 HST (Jones et al., 2017; Parcheta et al., 2012). This was the end of episode 1 fountaining in the field area (Fig. 3.1), and subsequent episodes occurred to the east, where weak episode 1 fountaining continued until ~1500 HST on May 25. For a complete

narrative of the 1969–74 Mauna Ulu eruption readers are directed to Swanson et al. (1979) and (Tilling et al., 1987).

3.2.2 Tectonic ground cracks: field evidence and eyewitness accounts

In addition to the eruptive fissure vents at Mauna Ulu, there are several large tectonic ground cracks approximately 100–200 m to the south, oriented roughly parallel to the fissure (marked in a black box in Fig. 3.1). Based on their location and orientation, the cracks are likely associated with the tensional opening of the ERZ caused by the seaward movement of Kīlauea's southern flank (Moore and Krivoy, 1964). Swanson et al., (1979) reported that these ground cracks opened during the morning of April 9th 1970 *"accompanied by the emission of fume"* and propagated westwards to reach the current Chain of Craters Road by 1000 HST April 10th. Importantly for this study, Swanson et al., (1979) describe and map these cracks as purely tectonic in nature and therefore did not act as a magma conduit. They also document that these cracks widened through time, growing to widths of ~ 1 m. However, following the field evidence of Parcheta et al. (2012) it is now known that this 1970 event was, in part, a reactivation of older tectonic cracks.

To establish a relative timing of crack opening and emplacement of the 1969 lava the morphological characteristics of the ground cracks were mapped. Two distinct morphologies were observed: firstly, simple saw-tooth edges where complementary 'jigsaw-fit' shapes can be observed at the either side of the crack (Fig. 3.2a); secondly, a mantle of draping lava, indicating drainage of 1969 surface lava into the crack (Fig. 3.2b). The well-developed 1969 lava channels are cross cut by the ground cracks that show crack-drainage (Fig. 3.2b) and in some cases the cracks have small (< 3 m) vertical offsets that displace the lava high-stand surface. Thus, the relative timing of crack opening can be interpreted: cracks associated with simple saw-tooth morphology formed after the 1969 lava had cooled, most likely in April of 1970 (blue; Fig. 3.2c); whereas

segments with lava drainage drapery opened during the waning stages or immediately after the May 1969 eruption (orange; Fig. 3.2c).

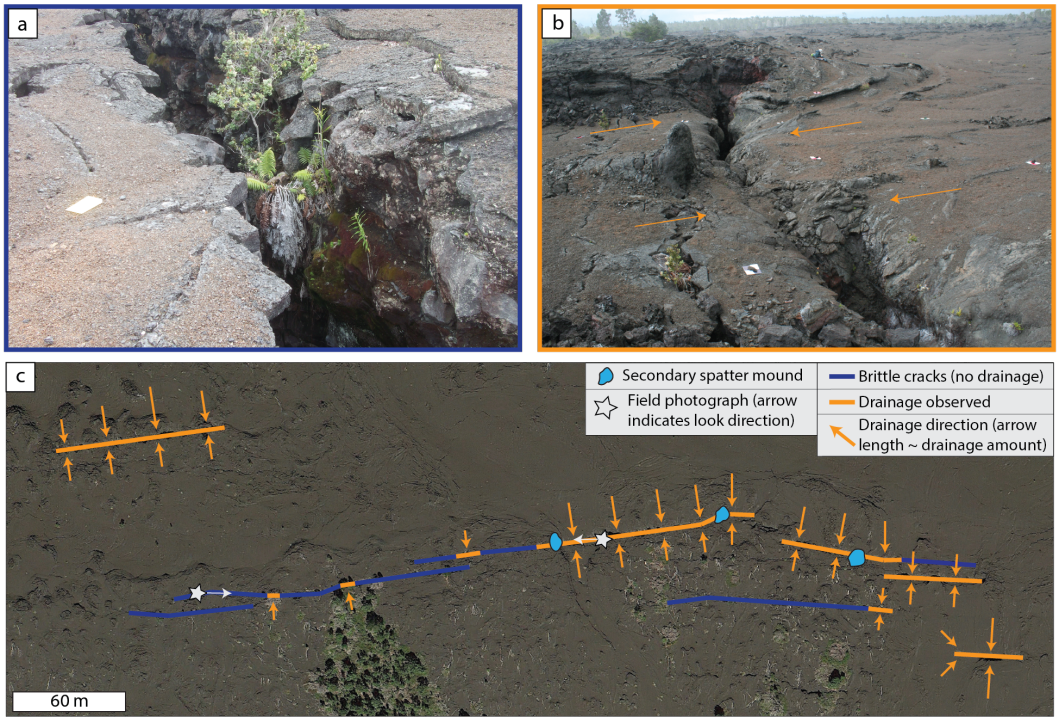

***Figure 3.2**: Field photographs and aerial images of the ground cracks: **(a)** Complementary jigsaw-fit ground cracks cross-cutting the 1969 surface lava (and older lavas at depth). There is no evidence here that the surface 1969 lava was mobile when the crack opened. For scale, the white rectangle in the photograph measures 24 cm by 13 cm. **(b)** Prominent southward draining lava channel cut by a ground crack. Lava can be observed draping down into the crack. Ground squares measure 30.5 cm by 30.5 cm. **(c)** Annotated Google Earth™ image showing regions of the southern ground cracks where either simple brittle ground cracking is observed (marked in blue) or where drainage of the surface lava down into the cracks is observed (marked in orange). The length of the orange arrows indicates the relative amount and direction of drainage.*

3.2.3 Episode 1 spatter deposits

Episode 1 of the Mauna Ulu eruption produced three distinctly different types of spatter deposit. Firstly, to the north and intermittently to the south of the eruptive fissure, a discontinuous series of spatter ramparts is preserved (Fig. 3.3a). The ramparts can be found along 80% of the fissure length on the northern side, they vary considerably in

height from 0.7 m to 7.1 m and are typically set back by ~ 10 m from the eruptive vent (Parcheta et al., 2012). Clasts within the ramparts are highly agglutinated (especially towards the deposit base) and have an elongate morphology (Fig. 3.3b). South of the eruptive fissure isolated spatter mounds can be found on the top of tree moulds (Parcheta et al., 2012). Clasts preserved by the tree moulds show less agglutination and are more fluidal in shape relative to those observed in the rampart interior (Fig. 3.3d). Both the spatter found within the ramparts and on top of tree moulds are the products of episode 1 fountaining deposited proximally to the vent (Swanson et al., 1979). Therefore, in this work, this type of spatter is termed 'primary spatter'.

Secondly, it is known from field studies that, during the waning stages of episode 1, the lava drained back into the fissure vent (Jones et al., 2017; Parcheta et al., 2012; Swanson et al., 1979). In some locations, and only within ~ 5 m of the eruptive vents, clasts of spatter are found on top of the back-draining 1969 lava carapace (Fig. 3.3e). This spatter does not form mounds or ramparts because the deposit is rarely greater than a single clast thick. The clasts are highly fluidal in morphology, varying from highly elongate strands and droplets to more circular disc shapes (Fig. 3.3f). It is likely that the larger clasts broke up upon impact forming adjacent smaller droplets (Sumner et al., 2005). Many of these spatter clasts have a dark green/blue surface colour. The field relations indicate that this spatter was emplaced following lava drain-back into the fissure vent, hence, here it is termed 'late-stage spatter'.

Thirdly, rare spatter mounds are observed associated with the southern ground cracks (Fig. 3.2). As previously described, these fissures are known not to have erupted any magma during the eruption, yet prominent spatter mounds (Fig. 3.3g) occur at three locations along these cracks (Fig. 3.2). Without previous eye-witness accounts from the Hawaiian Volcano Observatory, it would be extremely difficult to distinguish these ground cracks from the main 1969 eruptive vents to the north. The spatter is concentrated

very close (< 1 m) to the cracks (Fig. 3.3g), however, rare individual clasts can be located up to ~ 6 m either side of the crack. The mounds are only found on relative topographic highs and/or at an en echelon step. The clasts themselves (Fig. 3.3h), are highly variable in physical appearance; many isolated clasts (i.e. those not forming mounds) are thin discs and sheets whereas clasts forming mounds are slightly rheomorphic. Many clasts are cracked, and have a green/blue outer colour, similar to the late-stage spatter. Given the association of this type of spatter with cracks that were non-eruptive, I term this material 'secondary spatter'.

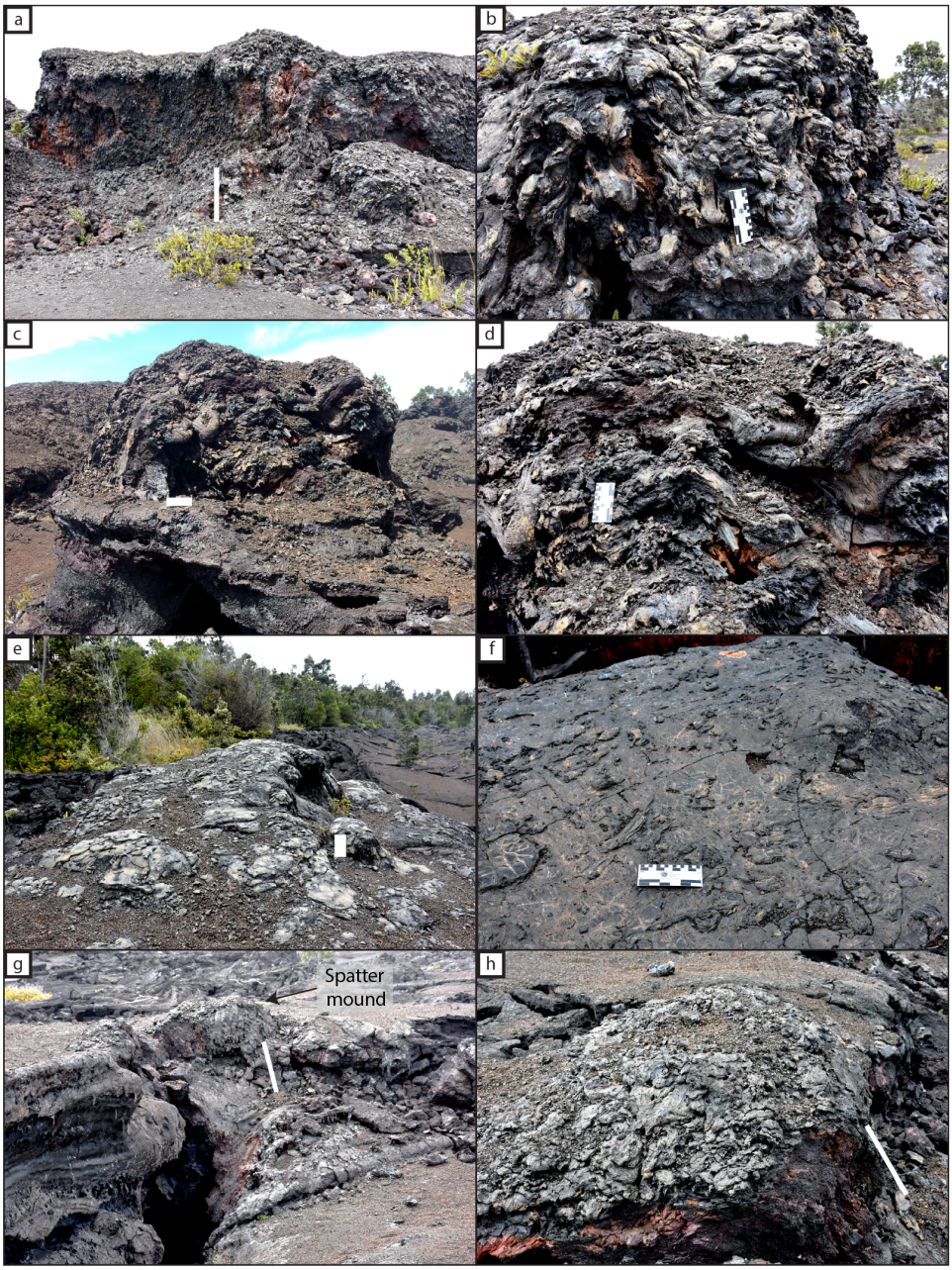

***Figure 3.3**: Field photographs of the three different spatter types described in this study: primary **(a – d)**; late-stage **(e & f)** and secondary **(g & h)**. **(a)** A spatter rampart that formed on the northern side of the 1969 Mauna Ulu eruptive fissure; **(b)** Agglutinated rampart interior with many clasts showing post depositional flow; **(c)** primary spatter located on top of a tree mould south of the eruptive fissure; **(d)** interior of tree mould spatter mound, clasts are less welded compared to the north rampart deposits; **(e)** green/blue vent proximal late-stage spatter forming a thin deposit on top of the erupted lava; **(f)** typical late-stage spatter clasts showing a wide range of fluidal shapes; **(g)** a secondary spatter mound formed over a ground crack to the south and **(h)** a close up view of a secondary spatter mound. Scales (marked in white if unclear) measure 16 cm for all images except in a, g and h where the scale is 1.2 m.*

3.3 Methods

3.3.1 Field sampling

Around 100 clasts of each spatter type were collected during March 2015 and May 2017. During sampling, clasts were chosen at random from a small area and where the deposits were thick, samples were taken from approximately the same stratigraphic horizon. Figure 3.1 marks the exact sample locations. The primary spatter was collected from the interior of one of the northern ramparts, towards the eastern end of the eruptive fissure, and from the top of a tree mould located 4.2 m south of the vent. The spatter from the rampart and tree mould collectively provide the primary spatter dataset. The late-stage spatter was sampled in three locations along the eruptive fissure: firstly, at the western end of the eruptive fissure, where it joins the Koae fault system; secondly, in the middle of the episode 1 fissure where the vent is completely covered in lava, and thirdly, at a flared, circular vent segment, towards the eastern end of the eruptive fissure as currently exposed. The secondary spatter was collected from two prominent mounds (Secondary spatter 1 and 2; Fig. 3.1) adjacent to the southern ground cracks. For bulk vesicularity comparisons, samples of lava crust that were obviously in-situ were broken up and sub-samples collected at random. This was done at two localities: directly above the, now covered, eruptive fissure labelled as "Fissure drain-back" and adjacent to the ground cracks labelled as "Crack drain-back" (Fig. 3.1).

3.3.2 Bulk vesicularity

A minimum of 95 clasts from each sample type were measured for bulk density using the Archimedes techniques outlined in Houghton and Wilson, (1989). The bulk vesicularity was calculated using a dense rock equivalent density (2873 ± 5 kg m^{-3}) measured independently by He pycnometry. From five repeat measurements on the same spatter clast I report a maximum absolute uncertainty associated with each clast bulk vesicularity

determination of ± 1 % vesicularity. The variation in vesicularity among different spatter types is considered later.

3.3.3 Quantitative vesicle analysis

From the spatter samples measured for bulk density, 14 were selected for quantitative vesicle analysis; samples were chosen to cover a range of spatter types and bulk vesicularity. In instances where a clast had a quenched rim and a micro-crystalline core, the two parts were separated and only the quenched rim was analysed. A nested image analysis approach (Shea et al., 2010) was adopted using: (1) full thin section scans taken at 4800 dpi on a flatbed scanner; and, (2) large back-scattered electron (BSE) image grids taken at 130x magnification on a Hitachi SU-70 scanning electron microscope (SEM). The SEM operating conditions were: a 15 kV accelerating voltage, a 45 μA beam current, a 15 mm sample working distance, and a 32 μs dwell time during image acquisition. All the images were then manually traced using a graphics package to create binary masks of vesicles and phenocrysts (Fig. 3.4). We note that, during tracing, vesicles were not heavily de-coalesced; only undeformed vesicles with thin (~ ≤ 50 μm) joining septa were de-coalesced. Quantification of the binary masks was performed with ImageJ software (http://rsbweb.nih.gov/ij/) to obtain vesicles areas and ultimately the 2D areal vesicle number density (N_A). N_A was then corrected for phenocrysts and converted to a volumetric (3D) vesicle number density (N_V) following the method of Proussevitch and Sahagian (1998). In samples where only the quenched rim was analyzed (denoted by a "q" in the sample names) I normalized to the image vesicularity, rather than the bulk vesicularity, after Stovall et al. (2011). Lastly, N_V was referenced to the melt volume to account for the volume occupied by the vesicles themselves (Klug et al., 2002). This forms the final metric, N_{Vm} that will be used throughout this study.

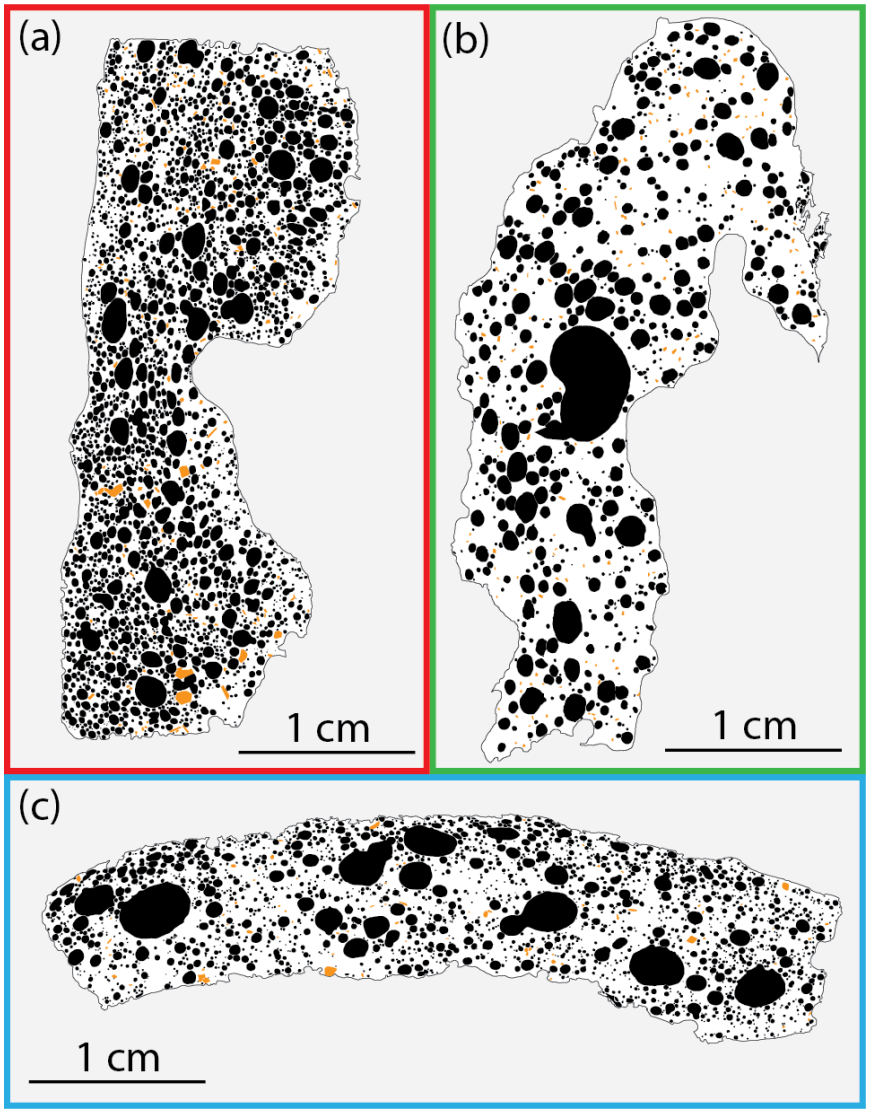

***Figure 3.4**: A representative binary thin section image for: **(a)** primary spatter; **(b)** late-stage spatter and **(c)** secondary spatter. Large vesicles and phenocrysts are shaded black and orange respectively.*

3.4 Results

3.4.1 Bulk clast vesicularity

Figure 3.5 shows the bulk vesicularity histograms for the primary (red), late-stage (green) and secondary (blue) spatter with median bulk vesicularity values of 63%, 49% and 68 % respectively. The primary spatter (rampart and tree mould deposits) displays a normal, unimodal distribution. The late-stage spatter is also unimodal but has a broader peak. However, the secondary spatter shows a slight bimodality with two modes at 50-55% and

65-70%. As indicated by the box-plots in Fig. 3.5, the secondary spatter samples are tightly distributed with the smallest inter-quartile range of all the sample types.

Samples of lava preserved proximally to the eruptive fissure show a bimodal distribution with modes at 50-55% and 70-75% vesicularity. These two modes reflect vesicle poor and vesicle rich domains in the lava respectively. Lava samples close to the southern ground cracks again show a bimodal distribution with similar subpopulation modes at 50-55% and 65-70% vesicularity. Note that the relative proportion of these subpopulations change between the two lava types; the crack drain-back lava is relatively enriched in the denser subpopulation and depleted in the more vesicular subpopulation.

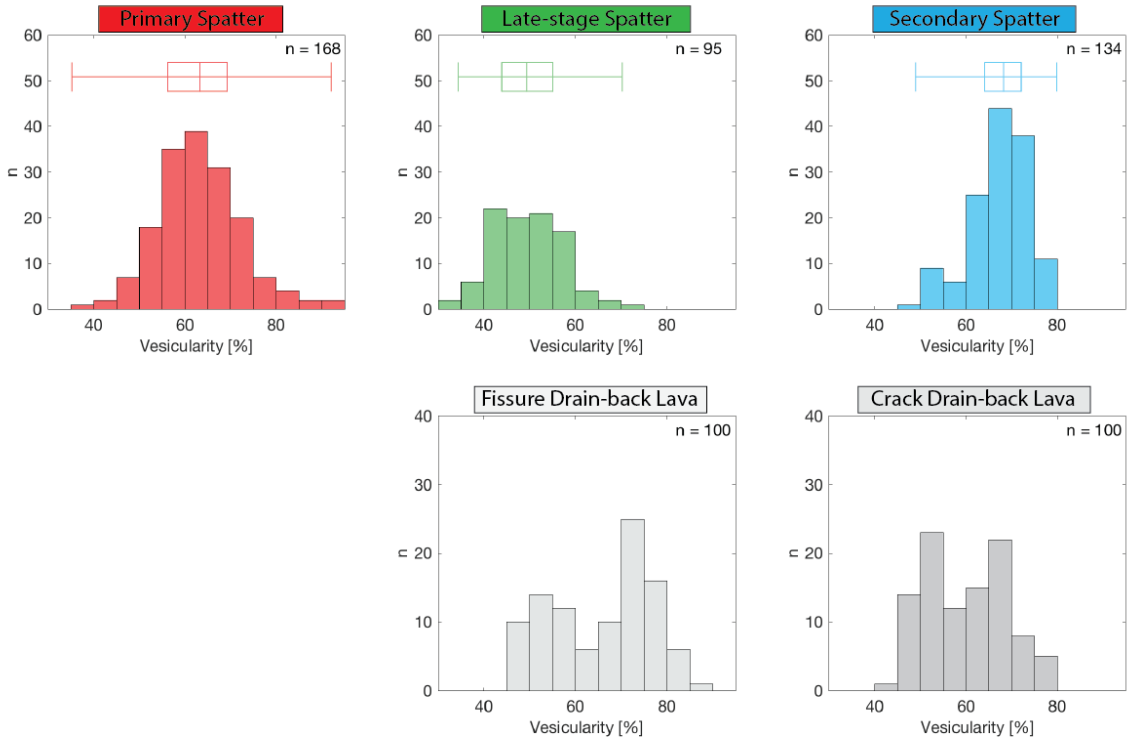

Figure 3.5*: Bulk vesicularity histograms for all spatter types, the lava sampled close to the fissure vent and to the southern ground cracks. The number of samples (n) measured for bulk density is reported for each dataset. The box and whisker plots display the data range (whiskers) and the first quartile, median and third quartile (box). Box and whisker plots were not calculated for the lavas, as these data are clearly bimodal.*

3.4.2 Qualitative textural observations

The three spatter types appear texturally distinct on visual inspection. The primary spatter contains abundant small-sized vesicles and they are mainly spherical, although in some cases, especially close to the clast margins, the vesicles are elongated (Fig. 3.4a). In contrast, the late-stage spatter has the much coarser vesicles, and very few small vesicles. The vesicles themselves are spherical, except where coalescence is evident (Fig. 3.4b). In many cases, microlites are observed in the late-stage groundmass. The secondary spatter vesicle population qualitatively lies between the late-stage and primary spatter; it still has a large number of small, spherical vesicles, but also has some larger vesicles and coalescence textures (Fig. 3.4c). No systematic changes in phenocryst content are observed among sample types; all samples have a plagioclase and olivine phenocryst abundance $\leq$ 2.5 %.

3.4.3 Quantitative textural observations

3.4.3.1 Vesicle number densities

The melt-referenced vesicle number densities range from 1.42×10^4 to 2.50×10^6 vesicles per cm^3 across all the sample types (Table 3.1). Primary spatter has the highest vesicle number density with a mean of 1.67×10^6 cm^{-3}. In contrast, the late-stage spatter has the lowest mean vesicle number density (3.87×10^5 cm^{-3}) and the largest range in N_{Vm} with values varying from 1.42×10^4 to 7.54×10^5 cm^{-3}. Secondary spatter has an intermediate N_{Vm} (mean: 5.77×10^5 cm^{-3}). The range of vesicle number densities for secondary spatter is also very small compared to the other sample types (Table 3.1).

3.4.3.2 Vesicle size distributions

Similar to the vesicle number density data, the vesicle size distributions (VSD), expressed as a volume fraction, vary according to spatter type. Figure 3.6 shows VSD histograms binned for equivalent spherical diameter. Primary spatter (red; Fig. 3.6) displays a variably unimodal, near normal distribution with a relatively high volume fraction; a

consequence of the high bulk vesicularity of primary spatter. A small secondary mode at 3 to 8 mm in some samples is due to coalescence of the largest vesicles. The late-stage spatter (green; Fig. 3.6) has a lower volume fraction (due to its lower bulk vesicularity), distributions that are slightly negatively skewed, and are mainly unimodal with the exceptions of samples 1C and 1A that have an additional coalescence-driven coarse mode at 8 mm and 5 mm equivalent diameter bins respectively. The secondary spatter volume fractions are comparable to the primary spatter, as expected from their similar bulk density (cf. Fig. 3.5), however, the size distributions are distinctly different. The secondary spatter (blue; Fig. 3.6) VSD histograms are broad and generally bimodal with a fine mode at 0.5 mm and a coarse mode at 3.15 mm. An outlier, 12Ni, still shows a bimodal distribution but has fine and coarse modes at 1.98 mm and 7.92 mm respectively.

Sample type	Clast name	Vesicularity [vol. %]	N_A[a] [#/cm^2]	N_V[b] [#/cm^3]	N_{Vm}[c] [#/cm^3]	V_g/V_m[d]	Median D[e] [mm]	n[f]
Primary	8B	57.7	2.77E+3	1.05E+6	2.47E+6	1.37	0.74	2949
Primary	8Ei	62.6	1.48E+3	4.96E+5	1.33E+6	1.69	0.61	1590
Primary	4Q	59.7	1.23E+3	2.67E+5	6.61E+5	1.49	0.47	1128
Primary	4A	52.3	1.83E+3	6.52E+5	1.37E+6	1.10	0.63	2067
Primary*	1t C05	65.0	3.94E+3	8.90E+5	2.50E+6	1.88	0.50	635
Late-stage	1D q	27.1[g]	3.54E+2	7.59E+4	1.04E+5	0.37	1.07	260
Late-stage	5K	55.6	6.49E+2	1.44E+5	3.24E+5	1.27	0.78	1218
Late-stage	6A q	32.3[g]	1.63E+3	4.99E+5	7.37E+5	0.48	0.50	723
Late-stage	1A q	31.9[g]	1.41E+2	9.64E+3	1.42E+4	0.47	0.91	371
Late-stage	1C q	53.7[g]	1.30E+3	3.50E+5	7.54E+5	1.16	1.36	933
Secondary	12H	49.0	9.56E+2	2.34E+5	4.58E+5	0.96	0.70	989
Secondary	12G	50.0	1.30E+3	3.72E+5	7.45E+5	1.00	0.49	1165
Secondary	12Ni	73.4	5.70E+2	1.09E+5	4.10E+5	2.77	1.50	786
Secondary	12B q	43.3[g]	1.17E+3	4.73E+5	8.36E+5	0.77	0.71	810
Secondary	15Mii q	43.2[g]	1.14E+3	2.49E+5	4.38E+5	0.77	0.61	751

[a] Number of vesicles per unit area
[b] Number of vesicles per unit volume of clast matrix, volume of phenocrysts subtracted
[c] Number of vesicles per unit volume, referenced to melt only
[d] Ratio of gas to melt volume
[e] Median equivalent diameter, assuming a circular cross-section
[f] Total number of bubbles traced
[g] Sample comprises a quenched rim and interior, the quench image vesicularity is used/reported
*Tephra sample also described in Parcheta et al. (2013)

Table 3.1: *Quantitative vesicle data from micro-textural analysis.*

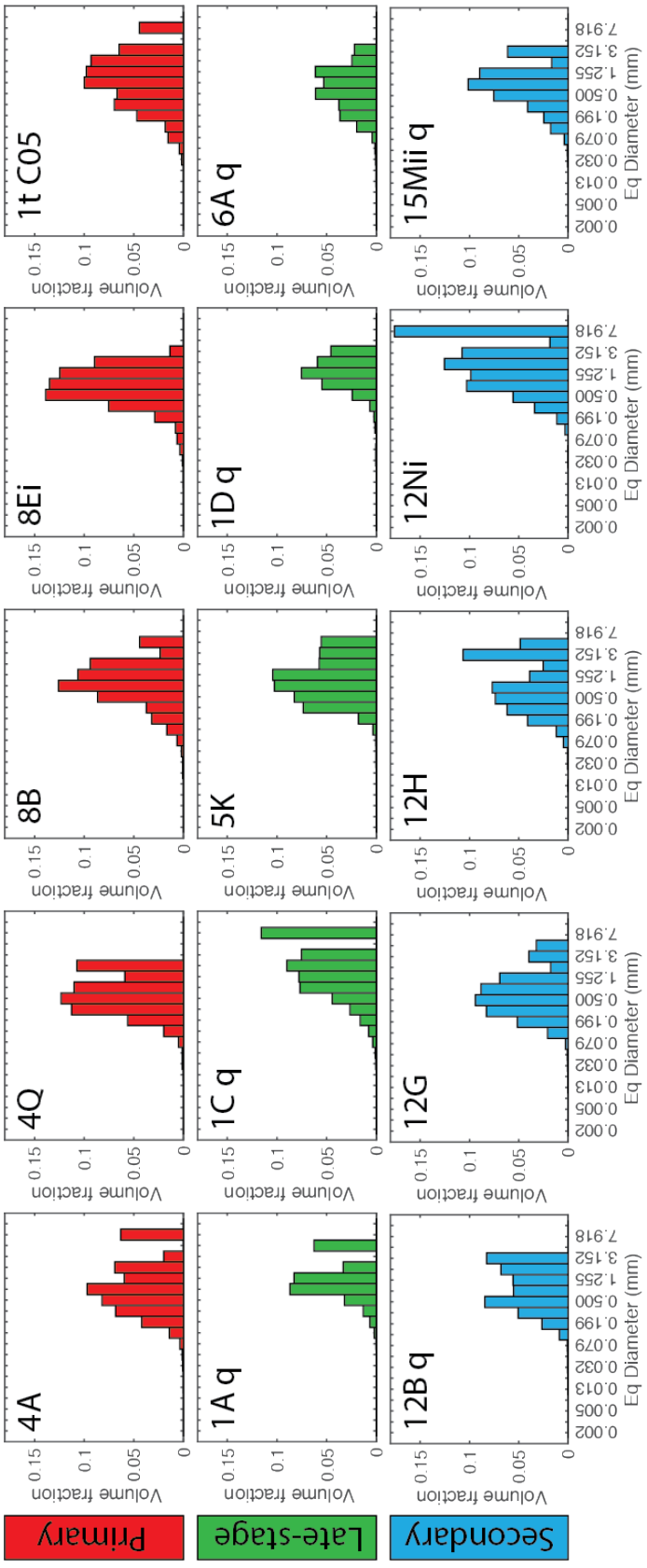

***Figure 3.6**: Vesicle size distribution histograms for primary (red), late-stage (green) and secondary spatter (blue). The equivalent (Eq) diameter is calculated from the traced vesicle area, assuming a circular cross-section.*

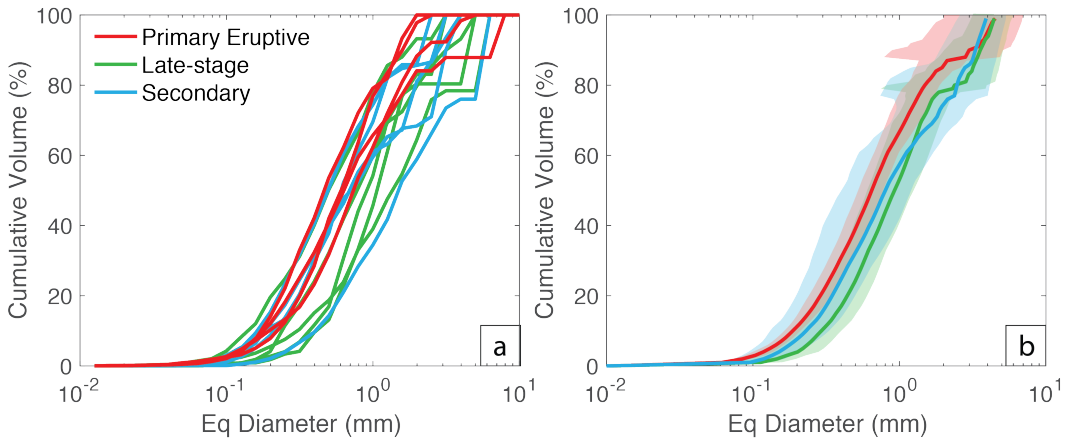

***Figure 3.7**: Cumulative vesicle volume % curves colour coded for sample type. **(a)** All samples, where each line represents an individual clast and **(b)** mean cumulative curves produced by calculating the average equivalent diameter for each percent from 0 to 100%. Shaded regions denote 1 standard deviation.*

VSD data is also presented in terms of cumulative volume % (Fig. 3.7a). To aid comparison among spatter types the mean average cumulative distribution curves for each sample type were calculated (Fig. 3.7b); specifically, I calculated the mean equivalent diameter for each cumulative volume from 1 to 100%. This plot clearly shows the contrast between the three spatter types both in terms of the size of the dominant subpopulation and the relative significance of a coarse, coalescence-related subpopulation. The primary spatter has the finest VSD with a median (50%) equivalent diameter of 0.65 mm. In comparison, both the secondary and late-stage spatter have coarsened distributions with median diameters of 0.80 and 0.93 mm respectively. Also worthy of note is that the late-stage spatter is extremely depleted in small vesicles but shares a similar secondary mode to the secondary spatter at high (> 80%) cumulative volume fractions. The ln(number density) vs. Equivalent bubble diameter form of data representation was not used in this thesis because bubble nucleation rates and kinetics are not the focus here. Instead I suggest that volume fraction histograms binned for bubble diameter (Fig. 3.6) facilitate the easiest comparison among the sample types.

3.5 Discussion

3.5.1 Eruptive or co-eruptive spatter?

The eruption of spatter is commonly associated with primary magmatic fragmentation where magma is disrupted and subsequently entrained by a rising gas jet as hot, incandescent pyroclasts (Wolff and Sumner, 2000). This eruption style is typical of hawaiian fountaining and produces spatter cones/mounds, ramparts and/or clastogenic lava flows (e.g., Karhunen, 1988; Sumner, 1998; Sumner et al., 2005); although it is not limited to mafic volcanism – similar deposits have been associated with felsic magmas (e.g. Duffield, 1990; Turbeville, 1992). However, in all these cases spatter mounds and ramparts are located next to the vent system, such that the presence of spatter may be taken as indicative of proximity to an eruptive vent. Spatter deposits have been found to occur along tectonic ground cracks, but only where those cracks have been occupied as magma ascent pathways during eruption. For example, in the case of Gjástykki, Iceland, magma used the pre-existing ground cracks as an ascent pathway, leading to the formation of spatter cones (Opheim and Gudmundsson, 1989).

In this work, it has been shown that spatter mounds can also be associated with ground cracks that did not act as primary eruptive vents or magma ascent pathways. In the absence of previous knowledge of the field site and its eruption history, these ground cracks could easily be mistaken for primary eruptive vents. Secondary spatter (as spatter mounds) associated with the ground cracks is difficult to distinguish from primary spatter in the field since both deposits have comparably high bulk vesicularity, are located proximally to the "vent" and lie on top of co-existing lavas. Therefore, field observations alone are not enough to identify the difference between primary and secondary spatter, and a more detailed micro-textural analysis is required.

3.5.2 Micro-textural interpretations

In hawaiian pyroclasts, vesicle number densities and size distributions can reveal information on bubble nucleation, coalescence, the timescales of magma ascent and the influence of post-fragmentation expansion within the thermally insulated fountain interior (Cashman and Mangan, 1994; Gonnermann and Houghton, 2012; Mangan and Cashman, 1996; Shea et al., 2010; Stovall et al., 2012, 2011; Wilson and Head, 1981). However, the micro-textural study of mafic melts proves challenging. Their high temperature and low viscosity promotes post-eruption bubble expansion and coalescence which can overprint original shallow conduit textures (Parcheta et al., 2013). In our case, however, this is advantageous; the textures we wish to contrast are those at final deposition and not necessarily the vesicle textures at primary fragmentation. To aid comparison between the spatter types (Fig. 3.8) the melt-referenced vesicle densities (N_{Vm}) have been plotted as a function of the ratio of the volume of gas V_g to volume of melt V_m after Stovall et al. (2011). Specifically, $V_g/V_m = \phi_v(1+\phi_p)/(1-\phi_v)$, where, ϕ_v is the volume fraction of vesicles and ϕ_p is the modal proportion of phenocrysts (Gardner et al., 1996). On this plot, different trends mark different physical processes (Fig. 3.8; top-left sub panel), for example, a decrease in the gas to melt volume ratio without changing the vesicle number density would indicate pure outgassing (the loss of gas from the system).

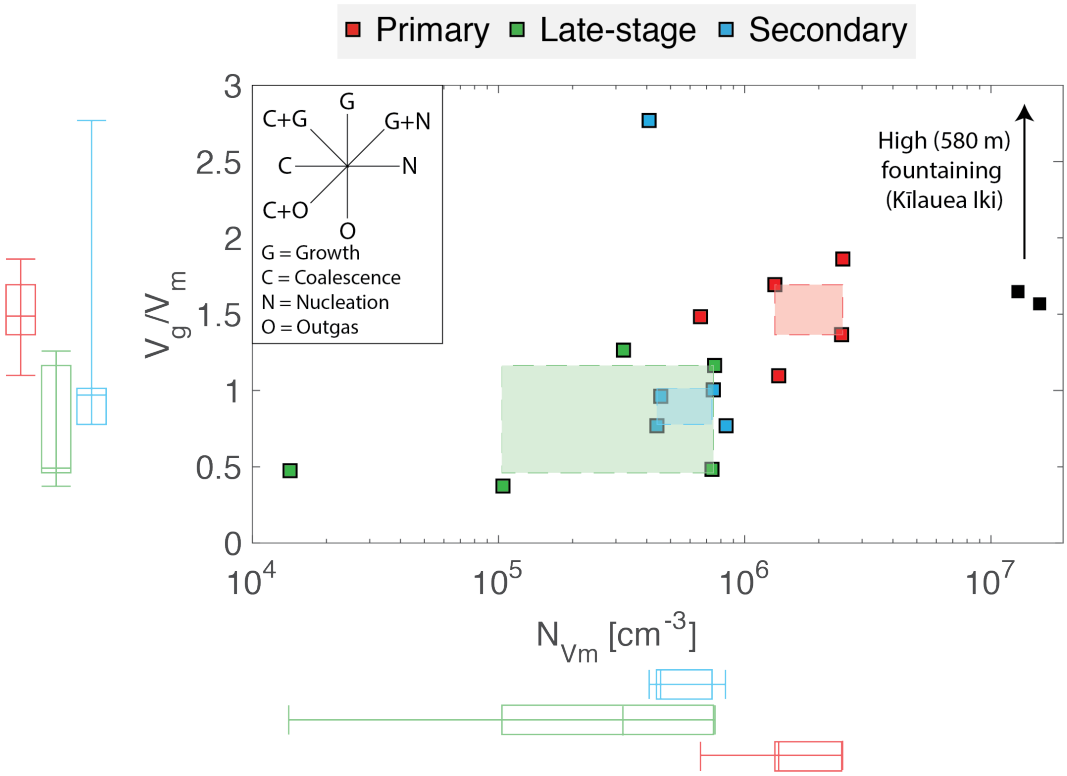

***Figure 3.8**: Volume ratio of gas (V_g) to melt (V_m) plotted against the melt-referenced vesicle number density (N_{Vm}) for all spatter types after Stovall et al. (2011). The box and whisker plots display the data range (whiskers) and the first quartile, median and third quartile, collectively forming the inter-quartile range (IQR; box). Shaded fields represent the overlapping IQR of both V_g/V_m and N_{Vm}. Primary spatter can be distinguished from the secondary and late-stage spatter based on vesicle number density (N_{Vm}). The black data points are from episode 15 of the 1959 Kīlauea Iki eruption which produced primary lava fountains 580 m in height (Stovall et al., 2012). These high fountaining data are provided for context and span a total V_g/V_m range of 1.5 to 15.4 and a total N_{Vm} range of 3.9 x10^6 to 1.8 x10^7 cm^{-3}.*

The primary spatter has the highest vesicle number densities and gas to melt volume ratios recorded in this study. The VSD of the primary spatter sampled is unimodal reflecting one period of nucleation and growth followed by minor coalescence. However, if a range of primary spatter were to be sampled systematically from fountains of different height and/or from different positions within a fountain, we would expect to see a range of vesicle textures resulting from different degrees of overprinting by coalescence. This has been previously observed at Mauna Ulu (Parcheta et al., 2013) and

Kīlauea Iki (Stovall et al., 2012, 2011) where increased coalescence was interpreted to be a result of longer residence time in the hot interior of the fountain (10's of seconds available for coalescence).

The late-stage spatter has much lower vesicle number densities and slightly lower gas to melt volume ratios compared to the primary spatter (Fig. 3.8; Table 3.1). The change from the primary spatter to the late-stage spatter indicates an evolution involving both outgassing and coalescence after nucleation of new bubbles had ceased (Fig. 3.8). Furthermore, this is supported by the VSDs (Fig 3.7) that show a coarsening and increased bimodality resulting from the reduced abundance of small vesicles as early, nucleated bubbles had expanded and coalesced. Also, the bulk vesicularity of the late-stage spatter is on average 13.5 % lower than the primary spatter (Fig. 3.5) supporting the interpretation that the magma that produced these late-stage clasts was relatively outgassed.

The micro-textural data from the secondary spatter reveals a bimodal VSD (Fig. 3.6) and a reduced vesicle number density relative to the primary spatter (Fig. 3.8) interpreted to have formed by bubble coalescence. The secondary VSD is coarser than the primary spatter but finer than the late-stage spatter at equivalent vesicle diameters < 63 μm and becomes coarser or comparable to the late-stage spatter at equivalent vesicle diameters > 63 μm. This suggests that the secondary spatter underwent less coalescence than the later-stage spatter and was able to retain (not outgas) more of its larger bubbles.

In this study, it has been shown that it is difficult to identify spatter types based on bulk density and field relationships alone. Now, the hypothesis that the three spatter types (primary, late-stage and secondary) can be separated based upon their vesicle number density (N_{Vm}) is tested quantitatively using a two-way analysis of variance (ANOVA). The ANOVA test results are shown in Table 3.2. The null hypothesis (the two sample

types are drawn from the same distribution) can be rejected at the 0.05% level (P-vales >0.05) for Primary – Late-stage and Secondary – Primary comparison. This means that, based on vesicle number density (N_{Vm}), primary spatter can be distinguished from both late-stage and secondary spatter. However, secondary and late-stage cannot be distinguished using this approach. An ANOVA test was also performed using V_g/V_m but this produced less statistically significant separations between sample types. Therefore, N_{Vm} is suggested to be the best metric to distinguish between the spatter types.

Spatter types compared	P-value	Outcome (based on N_{Vm})
Primary – Late-stage	0.0053781	Statistically different
Secondary – Primary	0.0152794	Statistically different
Secondary – Late-stage	0.8311387	Cannot be distinguished

Table 3.2: *ANOVA test results based on N_{Vm} distributed normally in linear space.*

3.5.3 Spatter formation re-visited

Spatter is commonly described in association with (primary) magmatic fountaining driven by the expansion and exsolution of volatiles in the upper conduit (e.g., Sumner et al., 2005; Wolff and Sumner, 2000). Here, I have shown that spatter deposits can form along ground cracks that did not act as pathways for ascending magma. This novel finding indicates a need for a more complete description of the formation conditions of the different spatter types. The formation of primary spatter has already been covered in great detail by many other studies (e.g., Capaccioni and Cuccoli, 2005; Head and Wilson, 1989; Rader and Geist, 2015; Sumner et al., 2005). In the case of Mauna Ulu, the primary spatter deposits were formed during episode 1 of the 1969 eruption by sustained fountaining reaching maximum heights of 50 m (Parcheta et al., 2012; Swanson et al., 1979). Primary spatter falling proximally (< 20 m) downslope, downwind of vent became incorporated into rheomorphic lava flows whereas material falling > 20 m downslope was rafted away by lava flows (Parcheta et al., 2012). In a few instances, primary spatter was preserved on top of tree moulds, which acted as local high points, and local barriers to

flow (Fig. 3.1; Fig 3.3c). To the north (upwind and upslope) a near-continuous spatter rampart was formed (Fig. 3.1; Fig. 3.3a). For a complete description of primary spatter formation during episode one of the 1969 Mauna Ulu eruption readers are referred to Parcheta et al. (2013, 2012).

As the eruption and associated primary fountaining started to wane, vent-proximal ponded lava began to drain back down into the conduit (Jones et al., 2017; Parcheta et al., 2012). Over time, the draining material and magma left stalled in the conduit matured by bubble coalescence and outgassing, causing the bulk magma vesicularity, the vesicle number density, and the gas to melt volume ratio to decrease (Fig. 3.8b; 3.9b). It is hypothesised that this maturing magma was ejected as late-stage spatter by the bursting of large gas bubbles (Fig. 3.9c), which may form by two mechanisms: (1) As the dense lava that was ponded over the vent drained back down the conduit (Jones et al., 2017), it trapped gas pockets. (2) Within the stagnant shallow conduit, continued coalescence led to the formation of large gas pockets. This process is envisaged to be similar to the dynamic coalescence, gas bubble rise and subsequent spattering that was inferred to occur when magma was relatively stagnant beneath Pu`u`Ō`ō during the 2004-2005 activity (Edmonds and Gerlach, 2007). Furthermore, the late-stage spatter is only found extremely proximal to the fissure (< 10 m), on top of the solidified drained lava surface, suggesting that the energy associated with gas pockets bursting was small. Lastly, the mismatch between the bulk vesicularity of the fissure drain-back lava and the late-stage spatter (Fig. 3.5) supports our interpretations about the parent magma/lava. If the late-stage spatter had formed directly from the proximal lava their bulk vesicularity would be the same; instead we observe that the late-stage spatter is much denser.

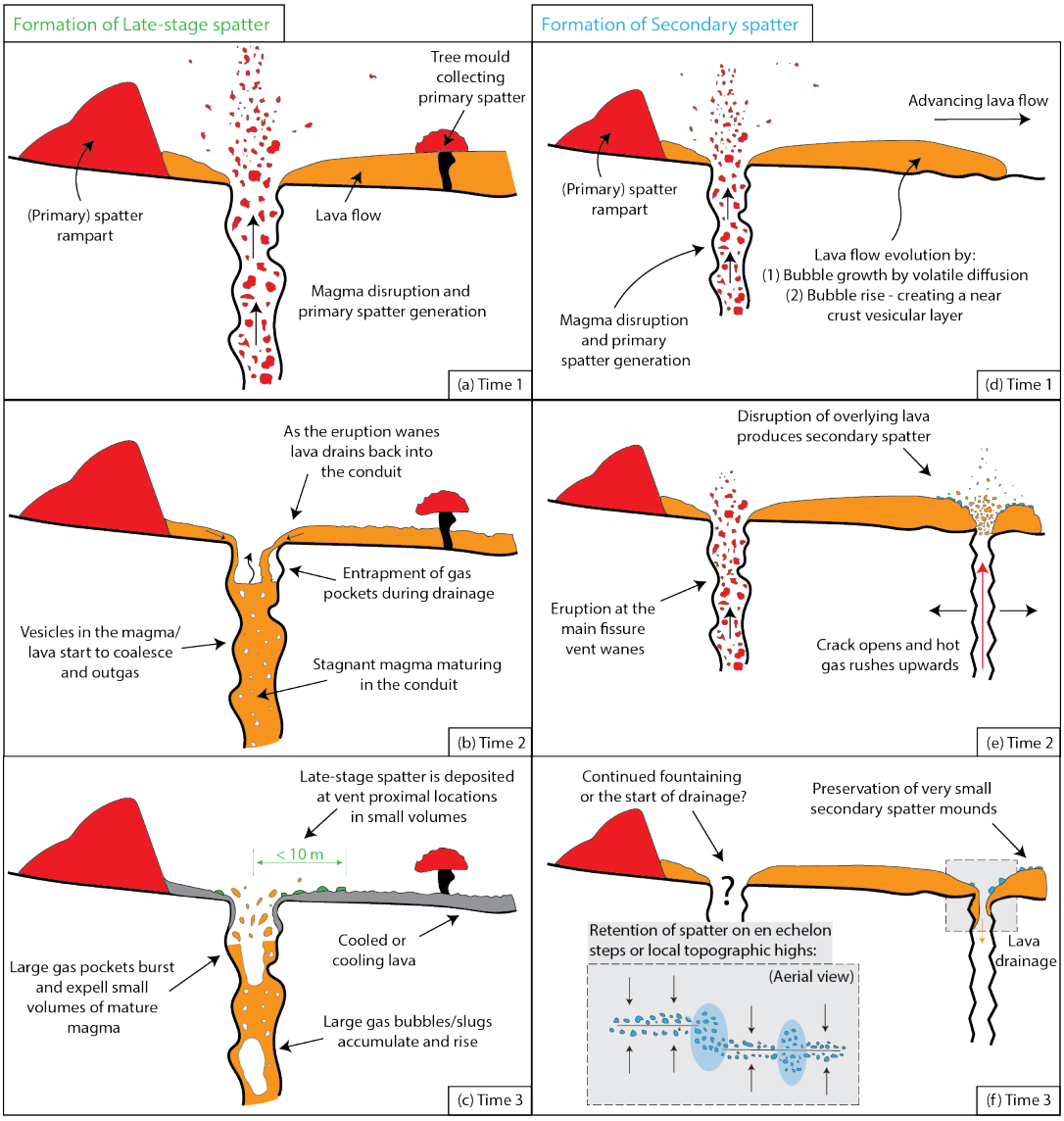

***Figure 3.9**: Schematic of the formation of the spatter types described in this study. Diagrams are not to scale. The view is to the east, along strike of the Mauna Ulu fissure.*

During the formation of the primary spatter deposits (northern ramparts and tree mould covers) spatter-fed rheomorphic lava flows propagated to the south (Swanson et al., 1979; Parcheta et al., 2012; Jones et al., 2017). During lava flow advance I suggest that the vesicularity of the flow evolved via a combination of two processes (Fig. 3.9d). Firstly, as lava flows advance, gas bubbles rise to create a stratified flow with a gas rich upper zone (e.g., Cashman and Kauahikaua, 1997; Sahagian, 1985; Thornber et al., 2004). Secondly, when material is erupted on short times scales (seconds) the volatiles are not likely to be in equilibrium with the co-existing silicate melt; hence, during lava flow advance

(minutes) volatiles diffuse out of the melt and cause bubble growth, thereby increasing the lava bulk vesicularity. My field evidence (cross-cutting relationships; Section 3.2.2), indicates that, after well-established southward trending drainage channels had developed in the flow field, tectonic ground cracks opened beneath the lava flow whilst it was still mobile (Fig. 3.2). I hypothesise that crack opening was accompanied by upward rushing hot gas from depth (similar to the April 1970 event) which disrupted the overlying mobile, draining lava flow and created secondary spatter (Fig. 3.9e). I suggest that the secondary spatter would have been distributed in very small volumes, at vent-proximal locations, where the flow was most mobile (orange; Fig. 3.2c). Furthermore, the bulk vesicularity data (Fig. 3.5) suggests that the lava disruption preferentially mobilised the less dense, near crust vesicular portion of the overlying stratified lava to form secondary spatter with modal bulk vesicularity of 65 to 70%, similar to the primary spatter, but with a larger modal vesicle size. Finally, once the uprising gas had ceased, small amounts of lava continued to drain down the ground crack carrying most of the secondary spatter with it (Fig. 3.9f), only to leave small mounds on local topographic highs or en echelon jogs as observed in the field today (Fig. 3.1).

3.6. Conclusions

In this study, I have identified and described the formation mechanisms of three different types of spatter associated with hawaiian low fountaining using field observations, bulk density measurements and micro-textural analysis. Using a N_{Vm} *versus* gas to melt volume ratio plot (Fig. 3.8), I classified different low fountaining products based on their micro-textural properties. Furthermore, I have shown that it is possible to find spatter deposits adjacent to ground cracks that did not act as magma conduits and purely act as sites of lava disruption to form a secondary pyroclastic deposit. Field relationships and macro-scale observations (e.g. bulk density) were not enough alone to distinguish these deposits as different from primary fissure-fed pyroclastic deposits. Consequently, this may lead to vent and eruption misinterpretation, incorrectly informing hazards and

probabilistic assessments. However, through a micro-vesicularity study it has been shown that based upon vesicle number density (N_{Vm}) secondary deposits can be distinguished from the primary spatter generated by typical hawaiian fountaining.

Chapter 4

Experimental scaling and fluid properties

4.1 Introduction

Field observations and measurements at volcanoes, such as those presented in earlier chapters provide direct data on the natural system, which form the foundation of our understanding of macroscopic volcanic processes. There are, however, several confounding factors that restrict the data that can be collected. Firstly, direct observations of eruptive processes are limited to the subaerial part of the system, and subsurface processes can only be inferred indirectly. Secondly, the volcanic system is extremely complex and behaviour that can be observed or inferred at the surface is a manifestation of many interacting processes; consequently, it is challenging for the observer to isolate and characterize the fundamental constituent processes, yet this is essential if a complete physical or numerical model of the system is to be developed. Furthermore, each eruption is different, so repeat observations are not usually possible, and variables cannot be controlled in a systematic way. Finally, risks associated with working on active volcanoes may limit observations, particularly of vent-proximal processes.

Experimental laboratory investigation offers a way to observe and measure volcanologically relevant processes in a systematic, controlled manner. Experiments on both natural and analogue materials are common, and both approaches have advantages and disadvantages. Natural materials (or synthetic materials with the same composition) have the advantage that their behaviour under given physical conditions is expected to

replicate directly their behaviour under the same conditions in the volcanic system. However, such experiments can be technically demanding because they commonly require extremely high operating pressures and temperatures. This usually restricts experiments to small sample sizes, which can complicate scaling, and makes accurate and precise measurement challenging. Furthermore, since the physical properties of natural materials themselves cannot be scaled, experiments at natural, volcanic conditions can only be performed at the same length scale as the natural system. If you want to reduce the length scale, other physical properties of the system must be changed to maintain the correct values of the dimensionless numbers. Analogue experimental approaches overcome many of these drawbacks. They are particularly useful when: 1) a specific physical property is required to facilitate measurements (e.g. transparency for optical measurements); 2) it is desirable to change the scale (typically length-scale or time-scale) of the phenomenon of interest; 3) it is desirable to isolate a single process from a more complex system of interacting processes. However, care must be taken to ensure that the system is not simplified so much that the experiments constitute a weak and uninformative analogy. For an analogue experiment to accurately describe the natural system, firstly, the material must have the same physical properties (e.g. shear thinning rheology) over the parameter space of interest, and secondly, the experimental conditions must lead to the same mode of behaviour observed in the volcanic system (e.g. laminar vs. turbulent, ductile vs. brittle, or viscous-dominated vs. surface-tension-dominated).

By using analogue experiments to isolate behaviours and remove multi-component complexity, many fundamental insights have been made to several areas of volcanology. Examples focusing on magma or lava dynamics include lava flow emplacement (Blake and Bruno 2000); the rheology of crystal bearing magmas (Cimarelli et al. 2011); basaltic magma degassing (Palma et al. 2011) and Strombolian eruption dynamics (Del Bello et al. 2015).

4.2 Scaling of analogue experiments

Despite all the advantages of performing analogue experiments to investigate volcanic processes, difficulties can arise when making links between experiments and the natural volcanic system. For direct links to be made between experimental observations and the volcanic system they must be analogous in some way. If quantitative results are desired, the experiments must be correctly scaled, otherwise they cannot inform on the natural volcanic phenomena.

4.2.1 The Buckingham Pi Theorem

For experiments to be scaled, firstly, they must operate within the same regime or display the same mode of behaviour as the system the experimentalist is attempting to replicate. For example, if the natural case under investigation was the flow of bubbly lava, the experimentalist would want to make sure the fluid chosen had a shear-thinning rheology. Similarly, if the natural case was Stokes settling of crystals within a magma chamber the user would want to make sure that the experiments were conducted under laminar (not turbulent) flow conditions. After this condition has been met, a dimensional analysis can be performed to identify the relevant dimensionless groups. The dimensional analysis technique used here is the Buckingham Pi Theorem; a well-established method that identifies the dimensionless groups important to a scientific problem (Bertrand 1878; Buckingham 1914; Tibaldi 1995; Merle and Borgia 1996; Merle 2015).

A full scaling analysis, following the Buckingham Pi Theorem, will now be performed with reference to the analogue experiments presented in this study (full description in Chapter 5). These analogue experiments investigate the exchange flow between two different fluids within a slot, aimed at investigating flow within a dyke, the subsurface expression of a fissure. To scale these experiments to nature, firstly, the important variables (j) relevant to the experimental question are identified (Table 4.1):

Variable	Symbol	Units	Dimensions
Slot width	D	m	L
Descending fluid density	ρ_d	kg m^{-3}	ML^{-3}
Upwelling fluid density	ρ_u	kg m^{-3}	ML^{-3}
Descending fluid viscosity	μ_d	Pa s	ML^{-1}T^{-1}
Upwelling fluid viscosity	μ_u	Pa s	ML^{-1}T^{-1}
Fluid velocity	U	m s^{-1}	LT^{-1}
Reduced gravity	g'	m s^{-2}	LT^{-2}

Table 4.1: *Important variables identified for an analogue experiment investigating buoyancy driven exchange flow between two Newtonian fluids. The reduced gravity is defined as:* $g' = g\,\Delta\rho/\rho_d$ *where* g *is the acceleration due to gravity and* $\Delta\rho$ *is the density difference between the two fluids.*

As shown in Table 4.1, the variables in this problem include three primary dimensions: mass [M], length [L] and time [T]. Hence, from the Buckingham Pi Theorem the number of repeating variables represented by this problem is: n =3, therefore, $j - n$ = 4, meaning that four independent Pi (dimensionless) groups can be formed (Buckingham 1914). Now that the number of repeating variables has been calculated they need to be chosen from the list of important variables in Table 4.1. The selection of repeating variables does not follow a set of well-defined rules and can be somewhat arbitrary, however the following conditions should be met where possible: the dependent variable (U in this example) should not be selected; they must not form a dimensionless Pi group by themselves; all of the primary dimensions should appear at least once in the total selection; variables that are already dimensionless should not be chosen; variables that have the same dimension or only slightly differ should be avoided and basic variables (e.g. a length) should be prioritized for selection (Buckingham 1914; Merle 2015). Following these guidelines, the variables D, μ_d and ρ_d are chosen as repeating variables for the exchange flow experiments (Chapter 5).

Now the first Pi group can be formed. This is done by listing all of the repeating variables and one of the other variables from Table 4.1, raising each parameter to a successive exponent a, b, c, etc. Following this approach the first Pi group becomes:

$$\pi_1 = D^a \rho_d^b \mu_d^c g'^d \quad [4.1]$$

Then, this Pi group can be expressed in terms of its base dimensions:

$$\pi_1 = L^a [ML^{-3}]^b [ML^{-1}T^{-1}]^c [LT^{-2}]^d \quad [4.2]$$

Now the exponents for each dimension are grouped and evaluated to give a set of three simultaneous equations that reduce each dimension to zero:

$$\text{For M: } 0 = b + c \quad [4.3]$$

$$\text{For L: } 0 = a - 3b - c + d \quad [4.4]$$

$$\text{For T: } 0 = -c - 2d \quad [4.5]$$

These three simultaneous equations (Eqns. 4.3 – 4.5) can then be solved to give $a = \frac{-3c}{2};\ b = -c;\ d = \frac{-c}{2}$ and allows for simplification of the Pi group to:

$$\pi_1 = D^{\frac{-3c}{2}} \rho_d^{-c} \mu_d^c g'^{\frac{-c}{2}} \quad [4.6]$$

Finally, now that every term has a common exponent (*c* in this case), this exponent can be set to any value to form a dimensionless group; in this example, for simplicity, I choose *c* = -2, which gives:

$$\pi_1 = \left(\frac{\rho_d}{\mu_d}\right)^2 g' D^3 \quad [4.7]$$

To form the second Pi group the method is repeated by changing the important variable listed at the end of the three repeating variables, this gives:

$$\pi_2 = D^a \rho_d^b \mu_d^c \mu_u^d = L^a [ML^{-3}]^b [ML^{-1}T^{-1}]^c [ML^{-1}T^{-1}]^d \quad [4.8]$$

Evaluating the exponents gives $a = 0;\ b = 0;\ c = -d$ and allows for simplification of the Pi group to:

$$\pi_2 = D^0 \rho_d^0 \mu_d^c \mu_u^{-c} \quad [4.9]$$

$$= \frac{\mu_d}{\mu_u}$$

Again, by changing the important variable listed at the end of the three repeating variables the third Pi group becomes:

$$\pi_3 = D^a \rho_d^b \mu_d^c U^d = L^a [ML^{-3}]^b [ML^{-1}T^{-1}]^c [LT^{-1}]^d \quad [4.10]$$

Evaluating the exponents gives $a = -c;\ b = -c;\ d = -c$ and allows for simplification of the Pi group to:

$$\pi_3 = D^{-c} \rho_d^{-c} \mu_d^c U^{-c} \quad [4.11]$$

$$= \frac{\mu_d}{DU\rho_d}$$

Lastly, by changing the important variable to ρ_u forms the fourth, and final, Pi group:

$$\pi_4 = D^a \rho_d^b \mu_d^c \rho_u^d = L^a [ML^{-3}]^b [ML^{-1}T^{-1}]^c [ML^{-3}]^d \quad [4.12]$$

Evaluating the exponents gives $a = 0;\ b = -d;\ c = 0$ and allows for simplification of the Pi group to:

$$\pi_4 = D^0 \rho_d^b \mu_d^0 \rho_u^{-b} \quad [4.13]$$

$$= \frac{\rho_d}{\rho_u}$$

4.2.2 Interpretation of the dimensionless groups

Each of the Pi groups will now be interpreted and related to common dimensionless groups previously described within the literature. The first Pi group, π_1, is identical to the Grashof number (Gr) in the form of Palma et al. (2011). By using the relationship $g' = g\,\Delta\rho/\rho_d$, π_1 can be recast to give:

$$\mathrm{Gr} = \frac{\rho_d\,\Delta\rho g D^3}{\mu_d^2} \quad [4.14]$$

This form of Gr will be used later in this thesis when interpreting experimental data. Gr can be conceptualised as the ratio of the buoyancy stress ($\Delta\rho g D$) against the viscous stress ($\mu_d^2/\rho_d D^2$). Therefore, at high Gr, buoyancy forces dominate, and flow is strongly driven by the density contrast between the two fluids. Whereas at low Gr, viscous forces dominate and hinder flow. Previously, Gr has been used to identify transitions in flow

behaviours within buoyancy-driven flows/ convection (e.g. Bratsun et al., 2003; Huang and Lin, 1994; Jin and Chen, 1996; Nandakumar et al., 1985).

Additionally, the first Pi group can be manipulated to form other dimensionless groups common to the fluid dynamics literature. For example, $\sqrt{\pi_1} = \mathrm{N_f}$, the dimensionless inverse viscosity, (Wallis 1969; Llewellin et al. 2011). This emphasises the point that there are only four *independent* dimensionless groups represented by this problem, but many other groups can be formed by the manipulation and combination of the Pi groups. Furthermore, any Pi group can be multiplied by a factor (a constant with no units) and remain dimensionless thus the regime transition described by a dimensionless group may not always occur at unity.

The second Pi group is identified as the viscosity ratio, β:

$$\beta = \frac{\mu_d}{\mu_u} \qquad [4.15]$$

a simple dimensionless group used in many previous works on exchange flow (e.g. Beckett et al., 2011; Huppert and Hallworth, 2007; Palma et al., 2011).

Taking the reciprocal of the third Pi group yields the Reynolds number, Re;

$$\mathrm{Re} = \frac{1}{\pi_3} = \frac{DU\rho_d}{\mu_d} \qquad [4.16]$$

a well-known dimensionless group that describes the ratio of inertial stresses ($\rho_d U^2$) to viscous stresses ($\mu_d(U/D)$). Note the Re defined here uses the slot or crack width, *D*, rather than the hydraulic diameter, D_H, where for high aspect ratio slots $D_H = 2D$. The hydraulic diameter is commonly used to relate the Re for a pipe to that of a duct within the inertial regime; since all the experiments presented here are performed within a duct/slot *D*, the slot width is used.

Given that in natural eruptions it is extremely difficult to measure a subsurface magma velocity, *U*, and in the experiments the fluid velocity can be difficult to directly measure so here, Re is redefined utilising the bulk volumetric flow rate of the system, *Q*:

$$\mathrm{Re} = \frac{Q\rho_d}{\mu_d L} \qquad [4.17]$$

Using the relationship, $U = Q/DL$, where L is the length of the slot, or along-strike fissure length. Furthermore, in this form, Equations 4.14 and 4.17 can be manipulated to give the Froude number:

$$\mathrm{Fr} = \frac{\mathrm{Re}}{\sqrt{\mathrm{Gr}}} = \frac{Q\sqrt{\rho_d}}{\sqrt{(g\Delta\rho)}D^{3/2}L} \qquad [4.18]$$

Lastly, the fourth Pi group is the dimensionless density ratio. This Pi group is not used any further in this study. However, it could be used to manipulate any of the dimensionless numbers already defined in order to change the specific density used (i.e. upwelling vs. downwelling).

4.2.3 Designing the analogue experiments

Now the dimensionless groups relevant to exchange flow between two liquids in a slot (or dyke) have been identified, the experimental analogue fluids are chosen so that the dimensionless numbers from the experiments are comparable to those in nature. Specifically, here, the Reynolds number (Re) and Grashof number (Gr) need to be the same in the experiments as those estimated for the volcanic system. These two dimensionless groups have been chosen for several reasons. Firstly, and most importantly, Gr is the independent variable with all the intrinsic properties of the system, set by the experimentalist, included. Whereas Re is a dependant variable – the volumetric flow rate is measured, both in the experiments and the natural system. Secondly, previous studies (e.g. Palma et al., 2011) have used both Re and Gr to identify changes in flow regime during their exchange flow experiments. Thirdly, from first principles you cannot

determine what dimensionless group(s) control(s) the regime. For instance, it is well known that the Re is the most important parameter when accessing turbulence within a pipe (Reynolds 1884). This dependence on Re was found experimentally by Osborne Reynolds, however, it still cannot be derived from first principles. Lastly, the other two dimensionless groups (viscosity and density ratio) can be incorporated into Gr and Re by the manipulation of the Pi groups.

To calculate Gr and Re, values for the important parameters in the natural case are sourced from published literature (Table 4.2). Where appropriate, a range of values is reported to account for natural variability, for instance the volumetric flow rate varies between different basaltic fissure eruptions and indeed during the course of an individual eruption. From these literature values (Table 4.2) a Re range of 10^{-5} to 10^{1} and a Gr range of 10^{-3} to 10^{4} is calculated. However, it should be stressed that for this study the volumetric *exchange* flow rate is the important parameter and not the volumetric *eruption* rate. Although these two rates are linked, and all extremes are possible. For instance, in the case of a stable lava lake the volumetric eruption rate is zero but the volumetric exchange rate is >> 0. Given that there are no direct measurements of exchange flow rates for basaltic fissure eruptions I use volumetric eruption rates as an approximation in Table 4.2.

Now the ranges of Gr and Re have been calculated for the natural system the experiments can be designed from a set of criteria. As previously described in Chapter 2 fissures are of high aspect ratio, and at Mauna Ulu eruptive segments had lengths of ~ 100 m and widths of ~ 1 m. For the experiments to have a similar aspect ratio and be a practical size for lab use, I decided to design a fluid tank 2 m in length with a slot gap width of 0.02 m. Furthermore, to easily measure exchange flow, the flow rates should be of a sensible magnitude. The flow should not be too fast such that the experiment is over within fractions of a second and not be too slow such that experiments take days to complete.

Therefore, a suitable range of volume flow rates would be 10^{-5} to 10^{-4} m^3 s^{-1}. Given these practical restrictions, fluids with densities between ~ 1 and 1500 kg m^{-3} and viscosities between ~ 1 and 100 Pa s should be used to maintain the appropriate range of Gr and Re. Fluids that match these criteria and are readily available in large quantities include: air at standard atmospheric conditions; glycerol; rapeseed (vegetable) oil; Tate and Lyle's Golden Syrup and dilutions thereof. Now, the rheology and density of these analogue fluids will be described along with a comparison to the values observed in the natural system.

	Units	Symbol	Nature	Experiment
Descending fluid density	kg m^{-3}	ρ_d	2200	?
Upwelling fluid density	kg m^{-3}	ρ_u	900	?
Density difference	kg m^{-3}	$\Delta\rho$	1300	?
Crack/slot length	m	L	40 to 6000	2
Crack/slot width	m	D	0.5 to 3	0.02
Descending fluid viscosity	Pa s	μ_d	10^3 to 10^1	?
Gravity	m^2 s^{-1}	g	9.81	9.81
Volumetric flow rate	m^3 s^{-1}	Q	10^{-2} to 10^3	10^{-5} to 10^{-4}
Grashof Number		Gr	10^{-3} to 10^4	?
Reynolds Number		Re	10^{-5} to 10^1	?

Table 4.2: *Important parameter values for both natural eruptions (gathered from the literature) and experimental conditions. Natural density estimates for basaltic melt assume a pure liquid density of 2700 kg m^{-3} (Murase and McBirney 1973) and a gas volume fraction of 0.19 and 0.85 for the descending and upwelling fluid respectively. Natural dyke width and length estimates derive from (Parcheta et al. 2015; Thorarinsson & Sigvaldason 1962). Basaltic viscosity estimates derive from (Giordano and Dingwell 2003; Giordano et al. 2008). Natural volumetric flow rate estimates derive from a range of basaltic fissure eruptions (Thorarinsson and Sigvaldason 1962; Swanson et al. 1979; Rhodes 1988; Orr et al. 2015).*

4.3 Rheology

4.3.1 Magma rheology

Magma rheology is one of the most important controls on eruptive style. It plays a central role in many volcanic processes, such as magma ascent through the plumbing system, magma fragmentation and degassing, and lava flow emplacement. Pure silicate

melts are Newtonian for strain rates $\dot{\gamma} \ll 1/\lambda_r$, where λ_r is the structural relaxation time of the melt (e.g. Giordano et al., 2008; Giordano and Dingwell, 2003; Hess and Dingwell, 1996). A Newtonian liquid deforms with strain rate proportional to the applied stress, τ; the constant of proportionality is the viscosity, μ:

$$\tau = \mu\dot{\gamma} \qquad [4.19]$$

The viscosity of natural silicate melts spans a huge range, from around 10^{-1}-10^{14} Pa s (Dingwell et al. 1996; Giordano et al. 2004; Giordano et al. 2008). Silica-poor melts, such as basalt typically fall in the range 10^{1}-10^{3} Pa s, whilst silica-rich melts, such as rhyolite typically fall in the range 10^{7}-10^{14} Pa s (Friedman et al. 1963; Shaw et al. 1968; Giordano and Dingwell 2003; Giordano et al. 2008). Temperature and dissolved water content exert a strong control on melt viscosity – an increase in either leads to a decrease in viscosity. The viscosity of silicate melts is comprehensively reviewed by (Giordano et al. 2008)

In volcanic systems pure melts are rare, and magma is usually a three-phase suspension composed of a melt (liquid) phase suspending bubbles (gas) and /or crystals (solid). The addition of bubbles and/or crystals changes the viscosity to give an apparent viscosity (η_a), this factor change is termed the relative viscosity ($\eta_r = \eta_a/\mu_l$). Bubbles introduce shear-thinning rheology that can be characterized by the dimensionless capillary number Ca.

$$\mathrm{Ca} = \frac{\mu_l a \dot{\gamma}}{\Gamma} \qquad [4.20]$$

where μ_l is the liquid viscosity, a the undeformed spherical bubble radius, $\dot{\gamma}$ the shear strain-rate and Γ is the surface tension. At low Ca, the surface tension stress dominates so the bubbles remain close to spherical in shape and act to increase the suspension viscosity. Conversely, at high Ca, viscous stress dominates so the bubbles become deformed and act to decrease the suspension viscosity (Llewellin et al. 2002a; Rust and Manga 2002). The addition of crystals to a silicate melt always acts to increase the

viscosity of the suspension, however the exact increase is highly dependent on the particle aspect ratio and volume fraction (Mader et al. 2013).

4.3.2 Method of measurement

Rotational rheometry was used to characterize the steady state viscosity and Newtonian rheology of all the fluid types used in this study. The rheological characterization was performed on a TA instruments Discovery Hybrid HR2 rheometer at Durham University, using a cone and plate measuring geometry with temperature control (peltier plate; Fig. 4.1). In all experiments a solvent trap, filled with deionised water, was used to prevent the solutions dehydrating during measurement. Using TA instruments' Trios software, the rheometer and sensor system were calibrated for internal friction, thermal expansion and inertia at the start of this experimental campaign. Then, for each successive measurement the measuring geometry was calibrated for any precession upon rotation. Each time a new aliquot of sample was loaded, it was left for 10 minutes to reach thermal equilibrium with the peltier plate.

During the rotational rheometry a shear stress was measured (through the observable torque; Fig. 4.1) at strain rates (related to the angular velocity by a geometric form factor) from $0.01 s^{-1}$ to $100\ s^{-1}$ with 10 measurement points per decade distributed logarithmically. Using this experimental approach viscosities were determined for golden syrup, dilutions of golden syrup, glycerol, rapeseed oil and a sample of each fluid type taken directly from the fluid tank after an experiment. Characterisation was performed at temperatures: 10°C, 14°C, 18°C, 20°C, 22°C, 26°C and 30°C in order to bracket the variations in lab temperature. Under some circumstances an additional set of measurements were taken at 21°C to improve the data quality. To quantify the measurement error, the most variable fluid (oil) was measured three times, across the full temperature range. After the viscosity calculation from the flow curve, the maximum deviation from the mean recorded was 8.14 %. Therefore, the maximum percentage

uncertainty for a given measurement incorporating machine errors, slight sample under and over filling is 8 %. This value is displayed by error bars on all rheology figures.

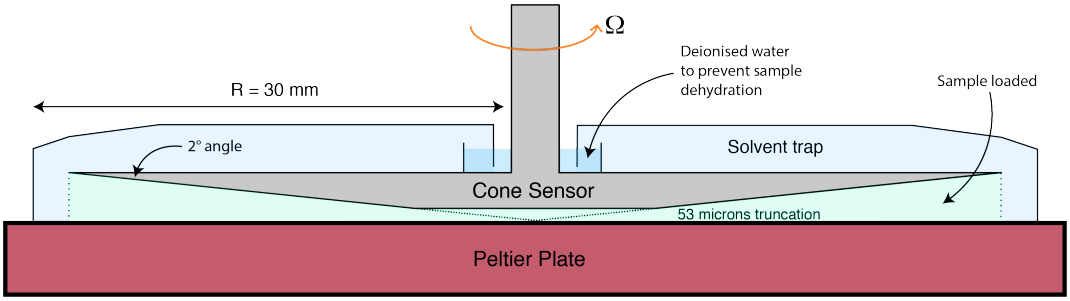

Figure 4.1: *Cone and peltier plate measuring geometry used with the TA instruments Discovery Hybrid HR2 rotational rheometer. After the sample was loaded the solvent trap was filled with deionised water during each experiment to prevent sample dehydration upon heating.*

4.3.3 Results and analysis

4.3.3.1 Pure golden syrup viscosity

At all temperatures, the stress is found to be proportional to the strain rate suggesting that pure golden syrup has a Newtonian rheology. In some cases, if a large strain rate (1000 s^{-1}) was applied the syrup was observed to decrease in viscosity, giving an apparent shear-thinning behaviour. This is caused by viscous heating at high rotation speeds and is not a property I expect to encounter in this study. Here, experiments were conducted at a lower strain rate to avoid viscous heating and if an apparent viscosity decreased was observed these data were excluded from the viscosity determination. The viscosity of pure golden syrup is highly temperature dependent (Fig. 4.2). The best-fit line follows the general form:

$$\mu = \mu_0 e^{-kT} \qquad [4.21]$$

where μ_0 (the 0°C viscosity) = 1641.7 Pa s and k = 0.166 $°C^{-1}$. Similarly, golden syrup sampled directly from an experiment follows the same functional form with constants: where μ_0 = 1859.2 Pa s and k = 0.168$°C^{-1}$. This indicates that the experimental fluid is slightly more viscous than "fresh" golden syrup taken directly from the manufacturers

container. This increase in viscosity is likely to originate from slight dehydration when transferring larger volumes of syrup into the experimental apparatus.

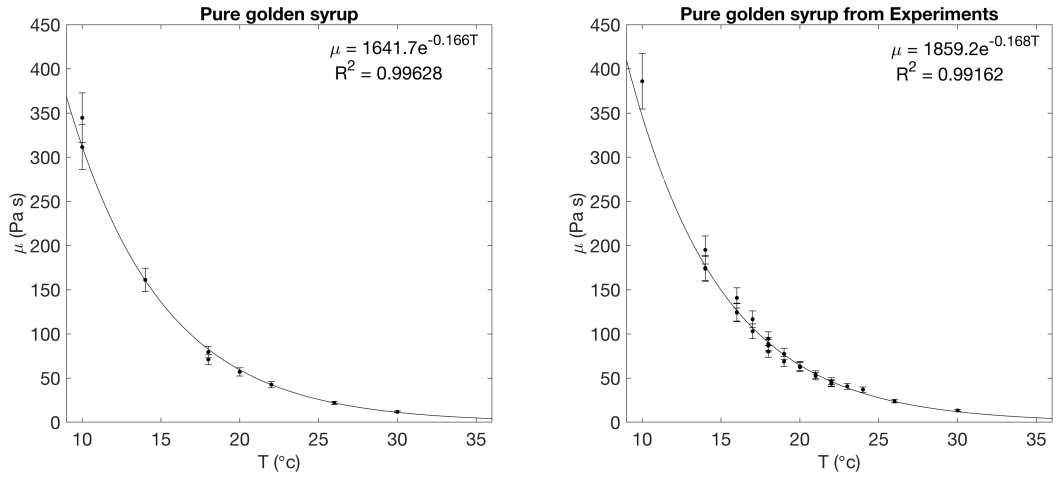

Figure 4.2: *Viscosity of pure golden syrup as a function of temperature. Best-fit lines are in the general form:* $\mu = \mu_0 e^{-kT}$.

4.3.3.2 Diluted golden syrup viscosity

The viscosity of golden syrup is also found to vary as a function of concentration or water dilution. Here, X_{water} is defined as the fraction of water added to the golden syrup by mass. For example, a 100 g sample containing 90 g of golden syrup and 10 g of water would be referred to as $X_{water} = 0.1$. Each dilution of golden syrup is temperature dependent such that the best-fit line follows: the general form: $\mu = \mu_0 e^{-kT}$. A full list of fitting parameters for each dilution is presented in Table 4.3.

X_{water} [wt. %]	μ_0 [Pa s]	k [°C^{-1}]	R^2
0	1641.7	0.166	0.99628
0.005	1123.5	0.158	0.9967
0.01	914.42	0.153	0.99829
0.02	552.42	0.15	0.99611
0.05	107.4	0.131	0.9969
0.1	14.467	0.11	0.99495
0.2	0.8654	0.078	0.99288

Table 4.3: *Fitting parameters for the range of golden syrup dilutions investigated.*

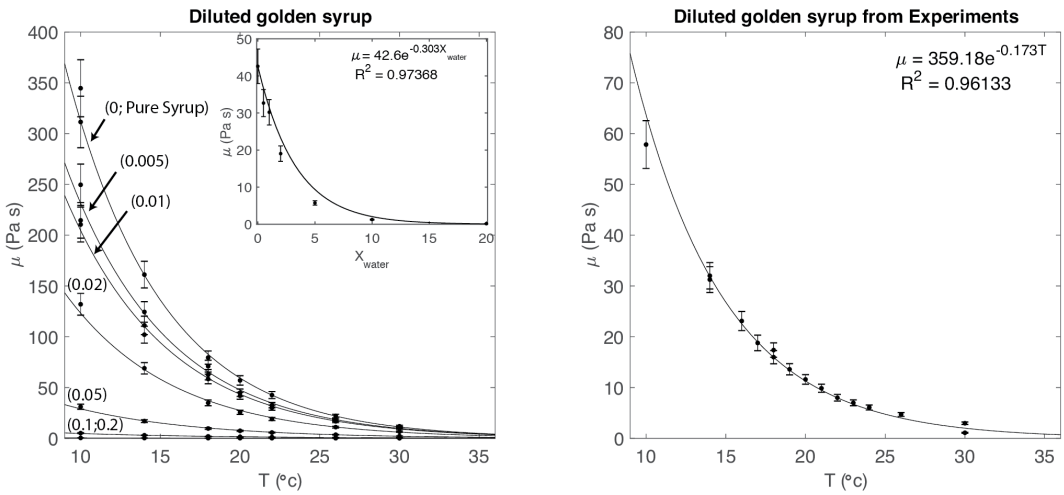

Figure 4.3: *Viscosity of golden syrup dilutions as a function of temperature. Best-fit lines are in the general form:* $\mu = \mu_0 e^{-kT}$. *Inset shows the syrup viscosity as a function of dilution (*X_{water}*) at 22°C, again the best-fit line takes an exponential general form:* $\mu = \mu_{X0} e^{-kT}$, *where* μ_{X0} *is the pure golden syrup viscosity (at 22°C in this case).*

Finally, combining both the dilution (concentration) and temperature effect on golden syrup viscosity a general, purely empirical equation can be formed:

$$\mu = \mu_0(X_{water}) e^{-k(X_{water})T} \qquad [4.22]$$

where, $\mu_0(X_{water}) = 1641.7e^{-40.52X_{water}}$ and $k\ (X_{water}) = 0.1609e^{-3.679X_{water}}$.

These model fits for μ_0 and k are shown in Figure 4.4 below.

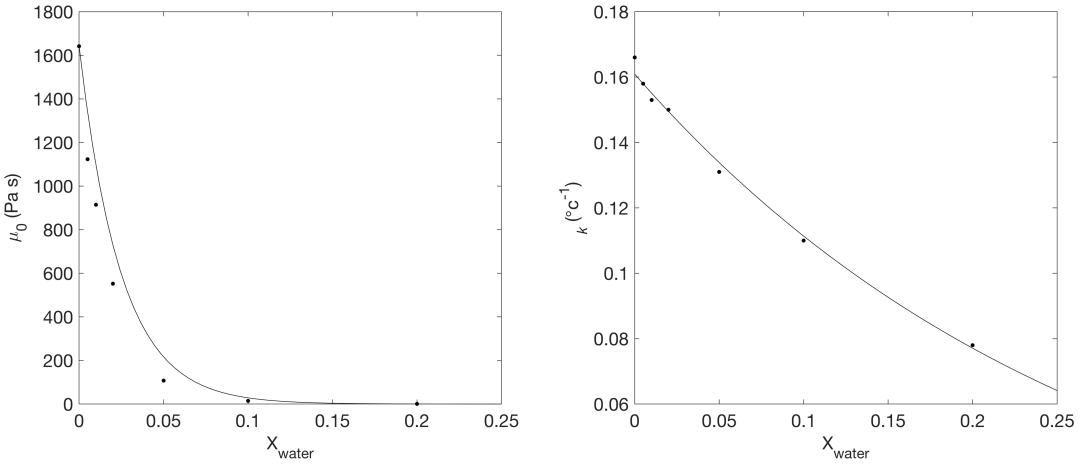

Figure 4.4: *Fits of* μ_0 *[Pa s] and* k *[°C-1] as a function of golden syrup dilution.*

However, where possible dilution specific fits should be used (Table 4.3) as Equation 4.22 compounds all the errors associated with the fits previously presented. All further analysis reported in this thesis uses the specific best-fit achieved from the actual experimental fluid used (i.e. right panel in Figure 4.3). Also note that, given the large ~ 65 litre volume of diluted golden syrup used in the experiment an aliquot of the actual fluid was taken and measured for its physical properties.

4.3.3.3 Glycerol viscosity

Glycerol viscosity was found to be Newtonian and highly dependent on temperature. Like golden syrup and its dilutions, the viscosity of glycerol as a function of temperature is best expressed in an exponential form (Equation 4.21), with constants: μ_0 (the 0°C viscosity) = 10.13 Pa s and k = 0.102°C^{-1}. Similarly, glycerol sampled directly from an experiment follows the same functional form with constants: where μ_0 = 14.993 Pa s and k = 0.133°C^{-1}. The fluid sampled from the experiment has a higher viscosity than fluid measured straight from the storage container (Fig. 4.5). Like golden syrup, glycerol is prone to dehydration and subsequent viscosity increase. This suggests that upon transfer to, and storage within, the experimental apparatus dehydration occurred.

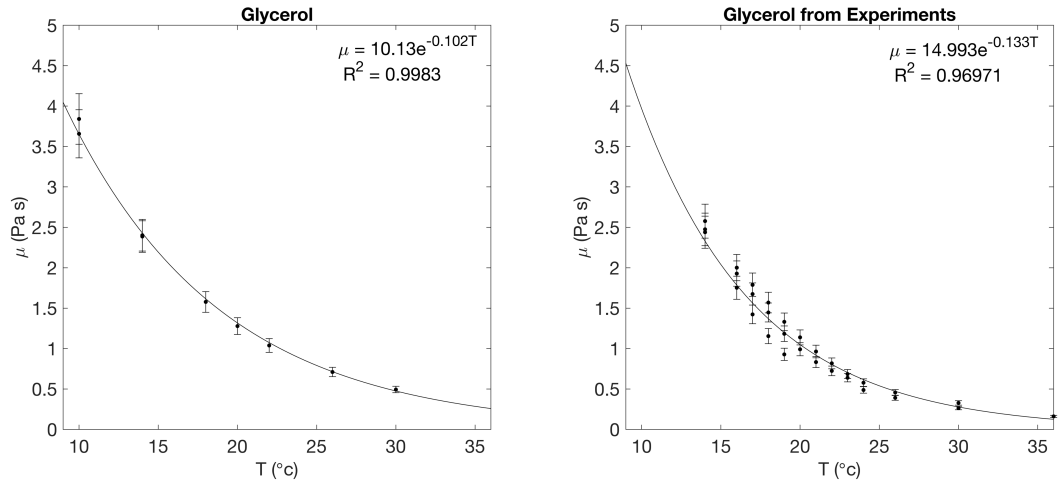

Figure 4.5: *Viscosity of glycerol as a function of temperature. Best-fit lines are in the general form:* $\mu = \mu_0 e^{-kT}$.

4.3.3.4 Rapeseed oil viscosity

The viscosity of rapeseed oil was found to be Newtonian and dependent on temperature (Fig. 4.6). Like all the other fluids previously described, the viscosity of rapeseed oil as a function of temperature is best expressed in an exponential form (Equation 4.21). Where μ_0 (the 0°C viscosity) = 0.2024 Pa s and k = 0.048°C^{-1}. Similarly, rapeseed oil sampled directly from an experiment follows the same functional form with constants: μ_0 = 0.1905 Pa s and k = 0.046°C^{-1}. The fits of the reference fluid and the experimental fluid are in good agreement with one another. This is because oil is much more stable when left at lab conditions compared to the other fluids; given that it is not aqueous dehydration does not occur.

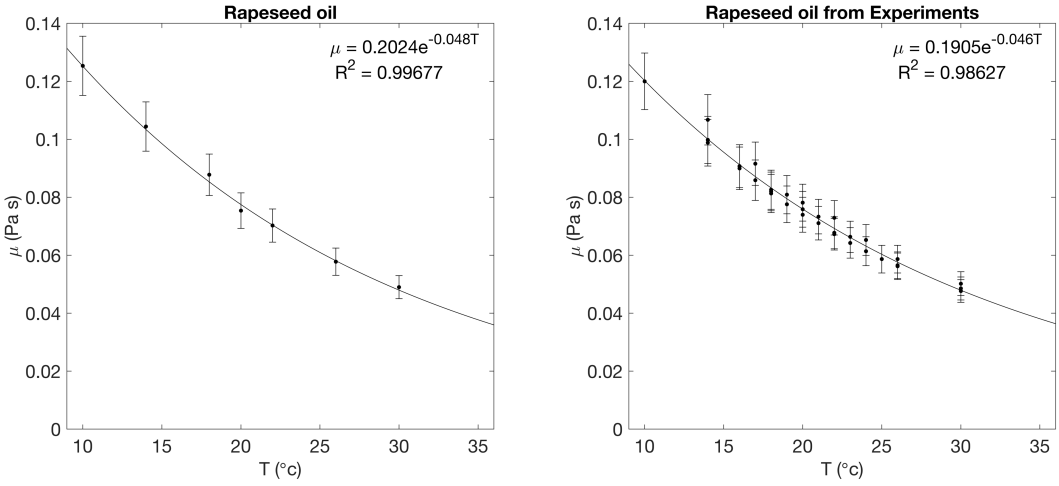

Figure 4.6: *Viscosity of rapeseed oil as a function of temperature. Best-fit lines are in the general form:* $\mu = \mu_0 e^{-kT}$.

4.4 Density

4.4.1 Background and magmatic properties

Measurements on multi-component silicate liquids have shown that their density is linearly dependent on temperature and oxide concentration, with the exception of TiO_2 (Lange and Carmichael 1987), where the addition of low density oxides (e.g., K_2O and Al_2O_3) act to lower the silicate liquid density and the addition of high density oxides (e.g.,

MgO and FeO) act to raise the liquid silicate density (Lange and Carmichael 1987). It is also known that small amounts of dissolved water and carbon dioxide have a large effect on reducing the silicate melt density (Lange and Carmichael 1990). For example, adding 1 wt. % water to a dry basaltic melt reduces its density by ~70 kg m^{-3} (Lange and Carmichael 1987; Lesher and Spera 2015). The density difference between a silicate melt and the country rock through which it moves is a key driver for magma ascent. Increasing the density contrast between the magma (typically achieved through decompression-driven vesiculation) and the country rock can lead to rapid ascent (Sparks 1978). Density is a parameter that often enters into dimensionless groups relevant to fluid dynamic studies. One example is the Reynolds number (Eqn. 4.17), which is defined as the ratio of inertial to viscous forces and commonly used in volcanology to classify a system's flow regime (laminar or turbulent). In analogue experiments we often wish to match the Re of our experiments to the natural system. For a given experimental set-up the fluid viscosity and density can be altered to give an appropriate Re, however in most cases is it much easier to change the viscosity than change the fluid density.

4.4.2 Method of measurement

Density values for the range of analogue fluids were measured using a calibrated 50 ml pycnometer flask. Fluids were added to the flask and left to equilibrate at 10, 12, 14, 16, 18, 20, 22, 24, 26, 28 and 30°C within a temperature controlled water bath. Once equilibrated, the flask exterior was dried and then its mass measured on a $\pm$ 500 μg desktop balance. This procedure was performed on: rapeseed oil; glycerol; pure golden syrup; aqueous dilutions of golden syrup (0.5, 1, 2, 5, 10, 20 wt.% H_2O) and a sample of each fluid used in the analogue experiments (Chapter 5).

4.4.3 Results and analysis

4.4.3.1 Golden syrup density

The density of golden syrup is found to vary both as a function of temperature and dilution (X_{water}; Fig. 4.7). Over the temperature range investigated (10 - 30°C) the density of a particular dilution follows the purely empirical general expression:

$$\rho = AT + B \quad [4.23]$$

where T [°C^{-1}] is the temperature and A [kg m^{-3} °C^{-1}] and B [kg m^{-3}] are constants, full fitting parameters for each dilution are shown in Table 4.4. The density measurements shown in Figure 4.7 have a maximum compound uncertainty of 0.231 kg m^{-3}, derived from the uncertainty on the contributing volume and mass measurements. Further analysis of the dataset identified that the concentration dependence enters through the constant B, such that, at any given T, concentration dependence follows the empirical form $\rho = CX_{water} + D$. Combining these, a general empirical equation is found for density as a function of both temperature and concentration:

$$\rho = -0.58724T - 5.3542X_{water} + 1450.5 \quad [4.24]$$

Fitting the same functional form as shown in Equation 4.23 to the experimental fluids yields:

$$\rho = -0.5593T + 1450.1 \quad [4.25]$$

with a regression coefficient of $R^2 = 0.9799$, for the experiments that used pure golden syrup and:

$$\rho = -0.58724T + 1420.0 \quad [4.26]$$

with a regression coefficient of $R^2 = 0.9898$, for the experiments that used a dilution of golden syrup. From this density fitting the fluid used in the experiments is calculated to have a dilution $X_{water} = 0.057$. This regression was performed to give the reader a sense of the dilution used. Given that the experiments used ~ 80 litres of diluted golden syrup it was practically challenging to directly measure the mass of pure golden syrup and mass of water when mixing. Instead an aliquot of the diluted syrup was taken, and its density and viscosity subsequently determined.

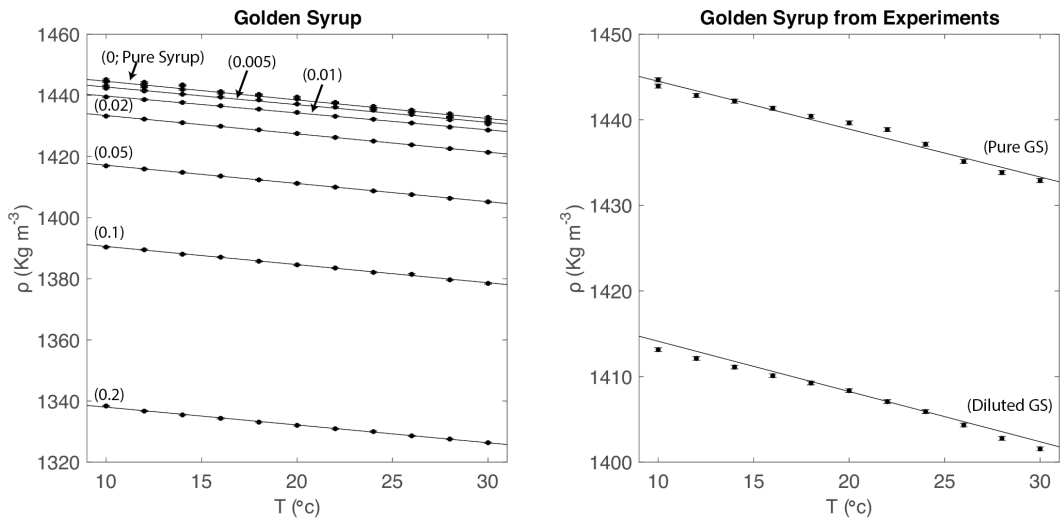

Figure 4.7: *Density of pure golden syrup and dilutions as a function of temperature. Error bars represent measurement error associated with each data point.*

X_{water}	A [kg m^{-3} °C^{-1}]	B [kg m^{-3}]	R^2
0	-0.6094	1450.7	0.97309
0.005	-0.5773	1448.5	0.99146
0.01	-0.5527	1445.3	0.99829
0.02	-0.5996	1439.4	0.99955
0.05	-0.5965	1423.1	0.99968
0.1	-0.5935	1396.5	0.99775
0.2	-0.5817	1343.8	0.99784

Table 4.4: *Density fitting parameters and regression coefficients for golden syrup dilutions.*

4.4.3.2 Glycerol density

The density of glycerol is found to vary as a function of temperature. Over the temperature range investigated (10 - 30°C) the density of glycerol follows the purely empirical general expression:

$$\rho = -0.6029T + 1272 \qquad [4.27]$$

with a regression coefficient of $R^2 = 0.9980$. Similarly, the density of a sample of glycerol used in an analogue experiment was found to be temperature dependent:

$$\rho = -0.6104T + 1272 \qquad [4.28]$$

with a regression coefficient of $R^2 = 0.9980$ (Fig. 4.8). The density measurements shown in Figure 4.8 have a maximum compound uncertainty of 0.203 kg m^{-3}, derived from the uncertainty on the contributing volume and mass measurements.

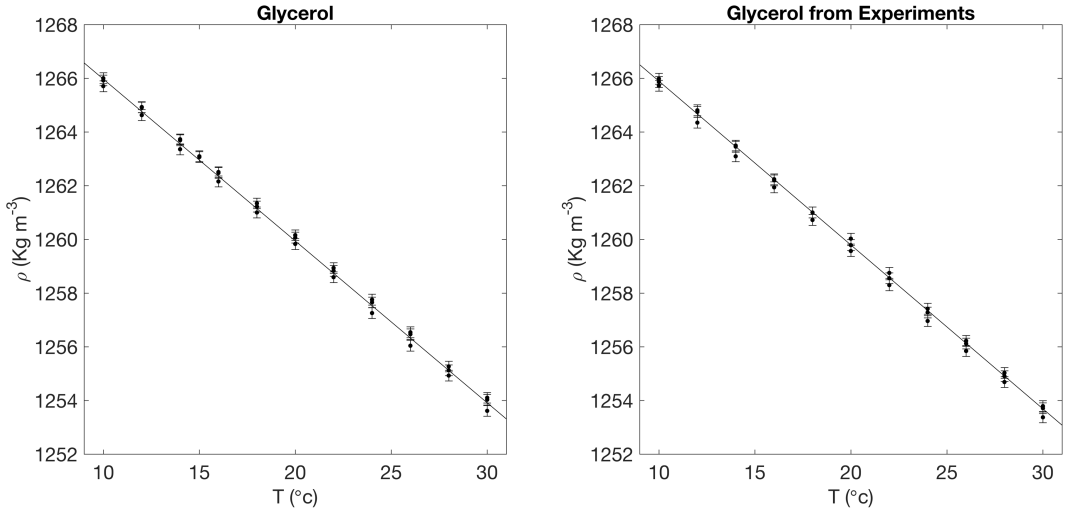

Figure 4.8: *Density of glycerol as a function of temperature. Error bars represent measurement error associated with each data point.*

4.4.3.3 Rapeseed oil density

The density of rapeseed oil is found to vary as a function of temperature. Over the temperature range investigated (10 - 30°C) the density of rapeseed oil follows the purely empirical general expression:

$$\rho = -0.6813T + 929.76 \qquad [4.29]$$

with a regression coefficient of $R^2 = 0.9996$. Similarly, the density of a sample of rapeseed oil used in an analogue experiment was found to be temperature dependent:

$$\rho = -0.6699T + 929.48 \qquad [4.30]$$

with a regression coefficient of $R^2 = 0.9992$ (Fig. 4.9). The density measurements shown in Figure 4.9 have a maximum compound uncertainty of 0.148 kg m^{-3}, derived from the uncertainty on the contributing volume and mass measurements.

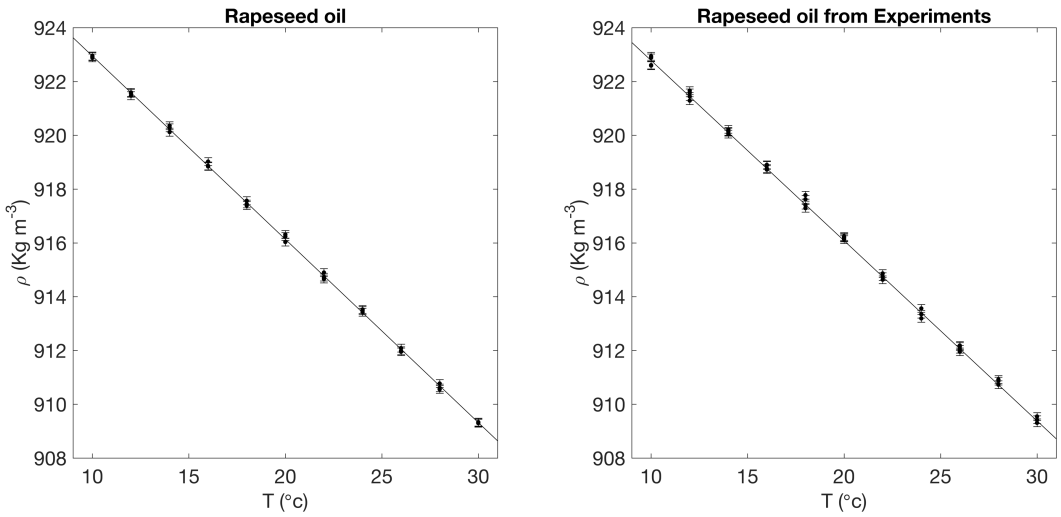

Figure 4.9: *Density of rapeseed oil as a function of temperature. Error bars represent measurement error associated with each data point.*

4.5 Scaling a slot/duct to a dyke

Now that the physical properties of the proposed experimental fluids have been characterised the scaling analysis presented in Section 2.3 can be re-visited. The parameter table can now be completed (Table 4.5) and the range of Grashof and Reynolds numbers covered by the analogue experiments are calculated as 10^{-2} to 10^{1} and 10^{-3} to 10^{0} respectively. A graphical representation (Fig. 4.10) of the Re – Gr space covered by natural basaltic fissure eruptions and by the analogue experiments (Chapter 5) conducted as part of this study shows clear overlap. Therefore, any fluid flow patterns, volume flow rate relationships and quantification of the exchange efficiency can be related to the natural system, through these dimensionless numbers.

	Units	Symbol	Nature	Experiment
Descending fluid density	kgm^{-3}	ρ_d	2200	1440 (cold golden syrup) to 1260 (glycerol)
Upwelling fluid density	kgm^{-3}	ρ_u	900	1.2 (air) to 914 (oil)
Density difference	kgm^{-3}	$\Delta\rho$	1300	1440 (cold golden syrup – air) to 345 (glycerol – oil)
Crack/slot length	m	L	40 to 6000	2
Crack/slot width	m	D	0.5 to 3	0.02
Descending fluid viscosity	Pas	μ_d	10^3 to 10^1	95 (cold golden syrup) to 0.7 (oil)
Gravity	m^2s^{-1}	g	9.81	9.81
Volumetric flow rate	m^3s^{-1}	Q	10^{-2} to 10^3	10^{-5} (cold golden syrup – air) to 10^{-4} (glycerol – oil)
Grashof Number		Gr	10^{-3} to 10^4	10^{-2} to 10^1
Reynolds Number		Re	10^{-5} to 10^1	10^{-3} to 10^0

Table 4.5: *Important parameter values for both natural eruptions (gathered from the literature) and experimental conditions (gathered from laboratory experiments described earlier in this chapter and from volumetric flow rates measured in Chapter 5). Natural density estimates for basaltic melt derive from (Murase and McBirney 1973). Natural dyke width and length estimates derive from (Parcheta et al. 2015; Thorarinsson & Sigvaldason 1962). Basaltic viscosity estimates derive from (Giordano and Dingwell 2003; Giordano et al. 2008). Natural volumetric flow rate estimates derive from a range of basaltic fissure eruptions (Thorarinsson and Sigvaldason 1962; Swanson et al. 1979; Rhodes 1988; Orr et al. 2015).*

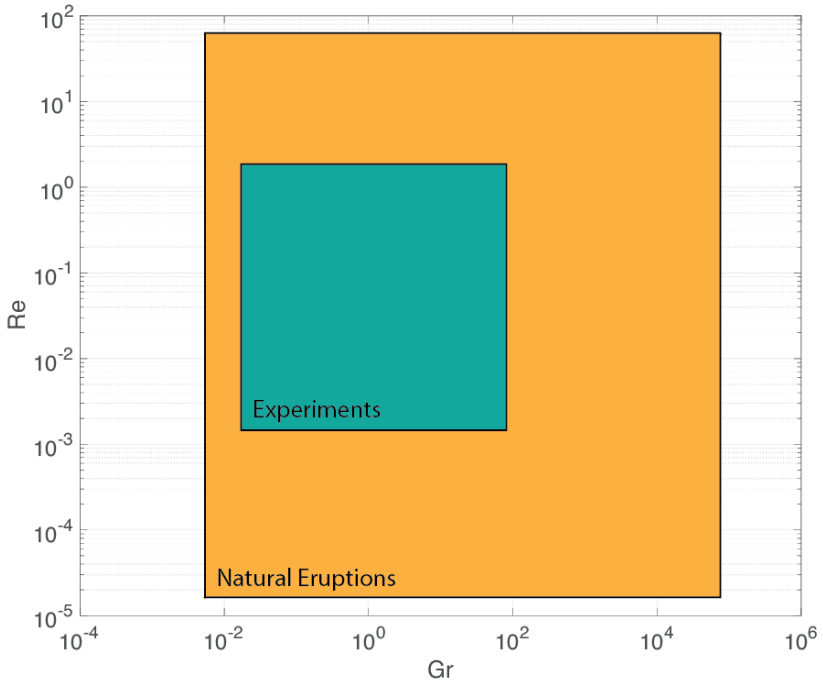

Figure 4.10: *A graphical representation of the Re-Gr dimensionless space covered by both natural volcanic eruptions and the experiments conducted as part of this study.*

One final consideration is the effect that interfacial tension plays. While, in the natural system the two exchanging magmas will be completely miscible, here, I use immiscible fluids for the experiments. This choice was made for a number of reasons: firstly, it allows for the simplest investigation of the fundamental behaviour; secondly, large quantities of fluid can be reused and thirdly, it allows for repeat experiments to be performed with relative ease. Therefore, as a final check, before the experiments can be conducted and interpreted, buoyancy forces must be shown to be dominant over interfacial tension forces. The dimensionless Eötvös number (Eo) describes this force balance: $Eo = \Delta\rho g D^2/\sigma$, where σ is the interfacial tension, $\Delta\rho$ is the density difference and D is the slot width. It has been shown that interfacial tension plays a negligible role in controlling behaviour at Eo > 40 (Viana et al. 2003; Llewellin et al. 2011). To calculate the Eötvös number for the experiments I use an interfacial tension of 0.08 N m^{-1} for the golden syrup – air experiments (Llewellin et al. 2002b) and, due to limited data availability, an approximate interfacial tension of 0.03 N m^{-1} (measured for oil against water) for the experiments that use oil as the low viscosity fluid (Fisher et al. 1985; Gaonkar 1989). For all the experiments conducted (see Chapter 5), Eo ranges from 45 (glycerol – oil) to 71 (cold golden syrup – air), therefore interfacial tension can be considered to have a negligible control.

Finally, it is important to note that even if a rigorous scaling analysis has been performed it does not guarantee that experimentally derived relationships hold true for the natural system. Many other factors are at work in the natural system, often such factors have been intentionally ignored when designing experiments to both simplify analysis and to understand the basic physics operating. For example, preliminary or early, pioneering studies often assume absence of bubbles and crystals and use a Newtonian rheology for simplicity (e.g. Del Bello et al. 2015). Given that the experiments performed here (Chapter 5) were the first of their kind, Newtonian fluids were chosen to investigate the fundamental physical behaviour.

Chapter 5

Exchange flow within a dyke: an experimental investigation

5.1 Introduction

5.1.1. Exchange flow in conduits

In previous chapters I have shown that the fluid dynamics within the volcanic conduit can, in part, explain changes in eruptive vigour, duration and style. The field evidence presented in Chapter 2 showed that lava can internally, drain-back into the fissure vent after it has been erupted. Then, in Chapter 3, I showed that the drain-back material was significantly denser and more outgassed than its primary lava fountain counterpart. Supported with data from these field studies I now experimentally investigate the simultaneous upwelling of low density magma and drainage of relatively dense lava/magma within a fissure geometry.

Density driven convection within the conduit is a process invoked at many basaltic volcanoes. This subsurface convection system is driven by differences in magma volatile contents at depth; regions with high volatile contents are lower in density (Lesher and Spera 2015); hence, become relatively buoyant and rise to develop a convection cell. Within the upper part of the conduit, above the saturation depth, volatiles are able to exsolve to form bubbles, generating a larger density contrast between the volatile poor and volatile rich magma. This further drives the exchange flow between upwelling, volatile-rich magma, and downwelling, volatile poor magma. Such conditions correspond to upwelling magma that is of relatively low viscosity and density and coexisting

descending magma of relatively high viscosity and density. In this section, I will give an overview of the evidence that supports the hypothesis that there is a convective system within the volcanic plumbing system.

The first line of evidence for this convective system comes from SO_2 measurements at persistently active basaltic volcanoes (e.g. Stromboli, Erta ‘Ale, Villarrica). At these volcanoes, the high SO_2 flux recorded cannot be explained by exclusive degassing of the erupted lava – much more gas is erupted than could have been generated by the erupted melt (Francis et al. 1993; Kazahaya et al. 1994; Allard et al. 1994; Harris and Stevenson 1997; Oppenheimer et al. 2004; Burton et al. 2007; Palma et al. 2008). The excess gas has been interpreted to indicate that a substantial fraction of the magma involved outgassed, subsequently became dense and then descended in the shallow conduit without being erupted (e.g. Kazahaya et al. 1994; Stevenson and Blake 1998). Further evidence comes from crystals found in the eruptive products. Plagioclase crystals show core to rim oscillatory zoning with sharp and large variations in anorthite content, indicating that repeated, rapid and efficient mixing between two magma compositions occurred (e.g. Landi et al. 2004; Bai et al. 2011). Landi et al. (2004) suggested that one possible mechanism to invoke mixing was convection; providing repeated cycles of ascent and descent of basaltic magma within the plumbing system (e.g. Kazahaya et al. 1994).

As demonstrated in Chapter 2 of this thesis, the flow organisation within erupting basaltic systems can also be influenced by concurrent draining of dense, degassed magma back into the conduit (Jones et al. 2017). Lava drainage has been documented at several lava lakes e.g., Halema‘uma‘u Crater, Kilauea, Hawai’i (Patrick et al. 2015); Mt Erebus, Antarctica (Oppenheimer and Kyle 2008); Kilauea Iki, Hawaii (Stovall et al. 2009) and Erta Ale, Ethiopia (Oppenheimer and Francis 1997), where fluctuations in the height of a lava lake are commonly related to pressure changes within the magma plumbing system (e.g., Witham and Llewellin 2006; Patrick et al. 2015). Additionally, in some cases, lava

has been directly observed to drain back down a fissure system geometry, examples include the 2002 eruption of Nyiragongo (Allard et al. 2002; Wunderman 2002); the 1974 eruption of Kīlauea (Tilling et al. 1987; Wilson et al. 1995), and the 2011 Kamoamoa eruption of Kīlauea (Orr et al. 2015). Drainage has also been inferred from studies of exposed vent deposits and dyke feeder systems at a range of depths (Lefebvre et al. 2012; Geshi and Neri 2014; Wadsworth et al. 2015; Jones et al. 2017).

5.1.2. Previous experimental work

Through scaled analogue experiments, exchange flow in a conduit has been investigated extensively for the case of a vertical, cylindrical conduit geometry (Stevenson and Blake 1998; Huppert and Hallworth 2007; Beckett et al. 2011; Palma et al. 2011). The upwelling and downwelling components have been found to organise either as core-annular flow, or side-by-side flow, depending on the viscosity ratio (Beckett et al. 2011). However, basaltic fissure systems, the surface expression of a dyke, are of high aspect ratio, with crack widths varying from ~ 2 m to 10's of m, and lengths ranging from several hundred metres to several kilometres (Gudmundsson 1987; Opheim and Gudmundsson 1989; Keating et al. 2008; Parcheta et al. 2015). Given that previous work has been entirely restricted to cylindrical geometries it is not possible to infer the subsurface processes operating during exchange flow within a dyke-like geometry.

To my knowledge, no experimental work has been conducted to explore exchange flow within a slot (or high aspect ratio duct) for the conditions relevant to the volcanic system. The only contribution exists in the appendix of Palma et al. (2011), in which the authors extend their analysis of core-annular flow within a pipe to co-axial, symmetric flow within a slot. Although this analysis is instructive, it cannot explain along strike variations and flow patterns observed in natural fissure eruptions and in the analogue experiments presented later in this thesis. This chapter aims to bridge this knowledge gap through a series of scaled analogue exchange flow experiments. The flow behaviour, flow

rate and transport efficiency are quantified for a convective system consisting of an upwelling fluid of low density and viscosity ($\rho_u; \mu_u$), and downwelling fluid of high density and viscosity ($\rho_d; \mu_d$) within a slot (dyke) of width, D and of length, L (Fig. 5.1).

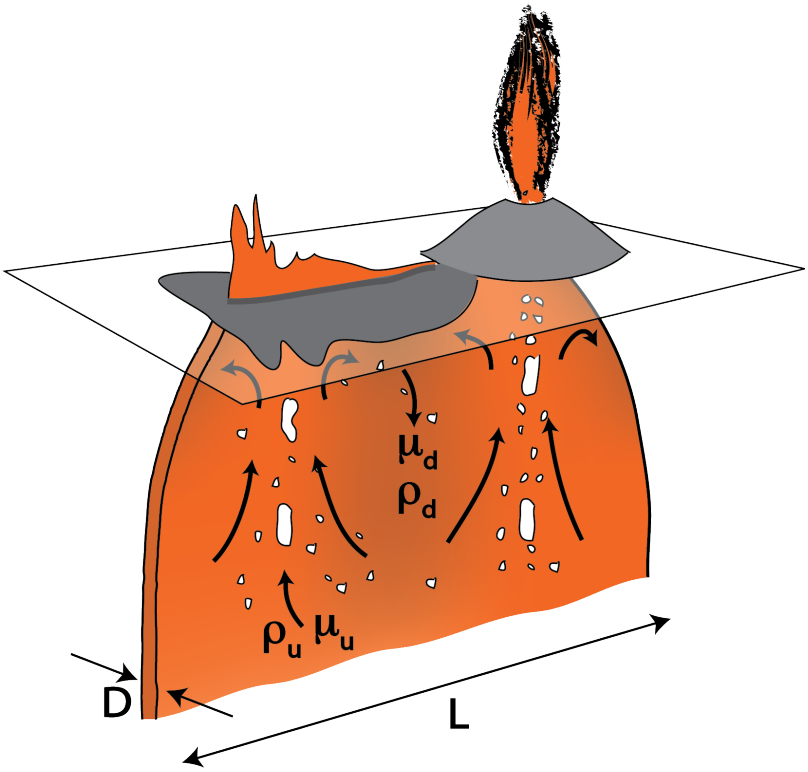

Figure 5.1: *Schematic of a basaltic fissure system wherein upwelling, fresh, magma of relatively low density (ρ_u) and viscosity (μ_u) co-exists alongside downwelling magma of relatively high density (ρ_d) and viscosity (μ_d). The magma filled crack, or dyke, at depth has a width, D, and an along strike length, L.*

5.2 Methodology

5.2.1 Experimental methods

The experimental apparatus used in this study consisted of two cuboidal reservoirs (~ 0.03 m^3 each) connected by a 2 m long, 1 m high slot with an internal gap width (D) of 0.02 m. The tank was made from transparent 15 mm thick acrylic to allow observation of flow patterns. Several metal support braces were added to prevent the slot from deforming once fluid was added. This large tank was suspended above the ground by a metal frame allowing for a full 360° rotation about its long axis (Fig. 5.2). In each

experiment, the tank was initially half filled with the dense, more viscous fluid and left to settle (allowing bubbles introduced by filling time to escape). Then, the second fluid was slowly added until the tank was full. Next, it was sealed, whilst checking for leaks and/or trapped gas pockets. The apparatus was then left for a few minutes until, by visual inspection, the interface between the two fluids was undisturbed and horizontal. A Nikon D7200 DSLR camera was positioned 2.7 m away from the fluid tank and set to acquire 2 images every 2 seconds. The specific camera settings that yielded the best images under our laboratory conditions were: 2000 ISO; 0 ev exposure; 1/250 shutter speed and a f-stop of 4. After all these preparations were complete, the camera was set to record, a timer was placed in the field of view and the kit was inverted by 180° to initiate overturn. The first image after overturn was defined as the experiment start time (t_0). The end of the experiment (t_{end}) was defined as the time at which the low density, low viscosity fluid began to fill the slot from the upper reservoir (i.e. when parts of the upper reservoir became full). Lastly, the apparatus was inverted again, back to its original position and the internal fluid was measured for temperature using a calibrated probe. This temperature was used to calculate the density and viscosity of both fluids using the empirical equations presented in Chapter 4.

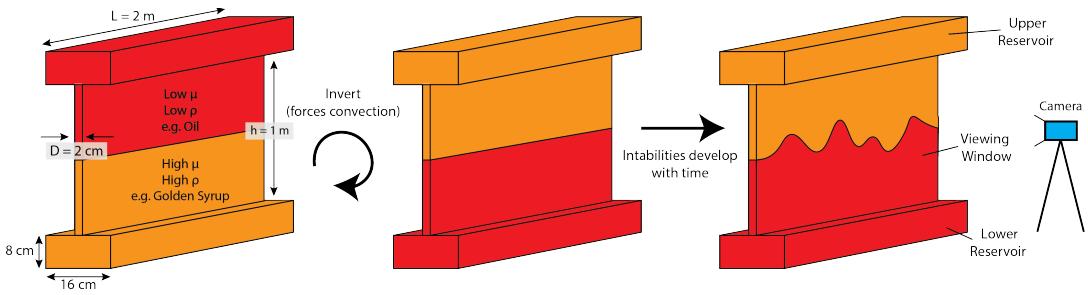

Figure 5.2: *The experimental apparatus used in this study and an abbreviated methodology.*

This methodology was conducted at least five times for each of the following fluid combinations: cold pure golden syrup (cPGS) and air; pure golden syrup (PGS) and air; PGS and oil; diluted golden syrup (DGS) and oil; glycerol (Gly) and oil. After the

experiments using a specific fluid pairing were completed an aliquot of each was taken and measured for viscosity and density using the techniques presented in Chapter 4. As a guide, Table 5.1 lists the values of density and viscosity for the experimental fluids at a specified temperature, however, note that for all calculations in this thesis the specific viscosity and density values were calculated using the measured temperature and the corresponding equations presented in Chapter 4.

Fluid	Temp. [°C]	Density [kg m^{-3}]	Viscosity [Pa s]
Air	21	1.200	$2.00x10^{-5}$
Oil	21	915.5	$7.25x10^{-2}$
cPGS	17.5	1440	$9.83x10^{1}$
PGS	21	1438	$5.46x10^{1}$
DGS	21	1408	$9.50x10^{0}$
Glycerol	21	1259	$9.18x10^{-1}$

Table 5.1: *The viscosity and density of the experimental fluids. Values are calculated using the equation in Chapter 4 for the temperature specified.*

To quantify any deformation of the slot, the apparatus was filled with water and the window deflection measured at six places across the tank at 10 cm vertical intervals. The slot retains a 2 cm width at the very top and bottom of the apparatus where it is connected to the reservoirs but, due to the weight of the fluid, deforms at all other positions (Fig. 5.3). The average deformation of each window was 0.3 cm at 10 cm depth, 0.6 cm at 20 cm depth and ~ 1 cm ($\pm$ 0.2 cm) thereafter. These gap width variations may alter the flow patterns, especially at early experiment times when the fluid is confined to the slot. However, given that the apparatus has a fixed volume with a constant slot to reservoir connection of 2 cm, the important, restricting length scale, D, remains at 2 cm for all experiments. One further source of uncertainty in D arises from the presence of a thin film of the more viscous fluid that coats the slot, thereby reducing D. From visual inspection during the experiments I expect this film to be $\leq$ 1 mm. These gap width errors are systematic and remain near constant for all experiments. The random error

associated with tracing, material characterisation and experimental variability is reported as error bars on all figures in this chapter.

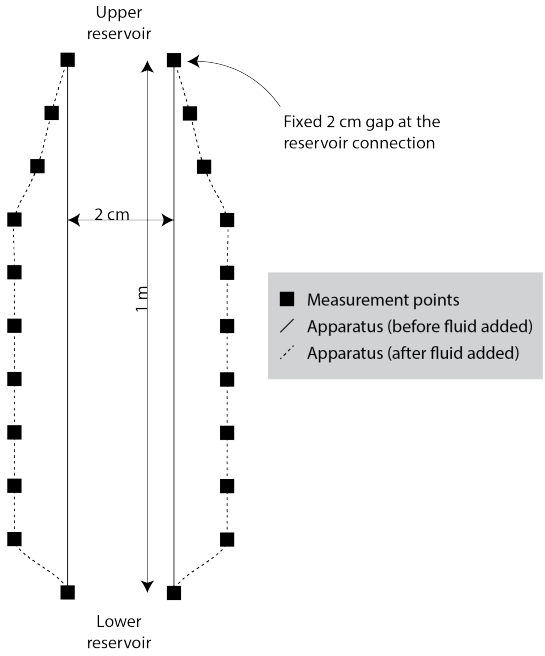

Figure 5.3: *A scaled cross -section of the slot deformation when a fluid is added (water in this case). The view is parallel to the long axis of the apparatus. Measurement points are represented by the black squares. Each window reaches a maximum deformation of 1 cm.*

5.2.2 Image Analysis methods

The fluid flow patterns observed during the experiments commonly feature the following series of events: (1) the initial development of an instability at the interface; (2) the growth and/or decay of upwelling fingers, and (3) steady state exchange flow. In order to describe these processes, various image analysis techniques using a graphics package (Inkscape or Adobe Illustrator) were performed to extract quantitative measurements from the imagery.

Firstly, the volume of low viscosity, low density fluid above the initial interface line was measured. To do this, the starting image at t_0 (with the horizontal interface line) was

overlain on the image to be measured. Then, a reference interface line was drawn and all upwelling fluid within the slot, (Fig. 5.2) above this reference line, was traced to produce a binary mask. The area of the binary mask was then measured in imageJ and, by assuming the fluid occupied the entire slot width (2 cm), converted to a volume of upwelling fluid. For images at longer times, after the upwelling fluid had reached the upper reservoir, an additional step was required to account for the volume held within the upper reservoir. The fluid area within the upper reservoir was measured in imageJ and converted to a volume using the known reservoir dimensions. The sum of the slot volume and the upper reservoir volume provided the volume of low viscosity fluid above the initial interface at a specific time within an experiment. This methodology was performed on three experiments from each fluid combination at several (11 – 13) times between t_0 and t_{end}, to track the exchanged volume over time (these data will be presented later in Fig. 5.6).

Secondly, the time-averaged volumetric flow rate, Q, for every experiment was determined. For each experiment, the final image (i.e. the image at t_{end}) was selected and any remaining dense, high viscosity fluid area in the upper reservoir was measured using imageJ. The area was then converted to a volume using the known reservoir dimensions. This volume was then subtracted from the total upper reservoir volume to give a volume change. Then, the time-averaged volumetric flow rate was calculated by simply dividing this volume change (i.e. the emptying of the reservoir) by the time taken. Specifically, the time taken was calculated as $t_{end} - t_{up}$, where t_{up} is the time at which the upwelling fluid reaches the top reservoir. Furthermore, t_{up} is the time at which the flow dynamics are no longer confined to the slot, after this time the fluid exchanges between the reservoirs.

Thirdly, once the exchange flow had reached the upper reservoir the velocity of both the upwelling and downwelling fluid was quantified. For a given image the area of each fluid occupying the slot was traced, exported as a binary and measured using imageJ. The fractional area of the window that the upwelling, and separately, the downwelling fluid occupied was calculated. Then, it was assumed that the fractional area in the window is representative of the fractional area occupied by each fluid in the cross-sectional area of the slot. Under this assumption, the cross-sectional area [m^2] perpendicular to flow, for each fluid was calculated and used to divide the time-averaged volumetric flow rate [$m^3\ s^{-1}$] to give an approximate mean velocity [$m\ s^{-1}$] at a specific time within an experiment. This method was performed on one experiment from each fluid combination at 25, 45, 65 and 85 % durations for the Gly – Oil experiments and at 45, 65 and 85 % durations for all other experiments.

Lastly, to quantify flow organisation, the interface length between the two fluids was measured as a function of time. For each selected image the contact between all the upwelling and the co-existing downwelling fluid observed through the viewing window was traced. Then, the contact line was exported at a 1 pixel thickness and measured for area using imageJ. Since, the line was 1 pixel thick, the line area is equal to its length. Finally, using the scale bar, the distance in pixels was converted to meters. This method was performed on one experiment (the same experiment quantified for velocity) from each fluid combination at 0, 5, 25, 45, 65 and 85 % durations.

5.3 Results

5.3.1 Description of flow

Upon changing the fluid properties, a large range of exchange flow patterns developed and were observed in the viewing window (Figs. 5.4 and 5.5; Appendix E). However, certain features are common to all experiments; after overturn an instability develops due to the density difference between the two fluids, this can occur instantaneously or over

the course of several seconds and is recorded by the instability growth timescale. Then, upwelling fingers grow until a limited number are selected for continued growth, leaving the remaining fingers to decay. During this finger growth and selection process the fluid dynamics are governed by fluid instabilities and confined to overturn within the slot. Lastly, after the upwelling fluid reaches the upper reservoir a steady state exchange flow is set up between the two reservoirs. This steady-state exchange flow is most relevant for the volcanic case and is therefore the focus of this thesis chapter.

In the cPGS – air experiments, the instability develops after ~ 13 s (the instability growth timescale; t_{inst}) and initially forms $\gtrsim 17$ upwelling fingers. Then, after approximately 40 s of growth between 5 and 9 fingers are selected for continued growth and outgrow the others. Continued growth of these selected fingers occurs until one or two reach the upper reservoir and support the exchange flow. After this point the unsuccessful fingers are carried downward by the dense descending liquid. This is then the stable configuration and all of the upward flow occurs within the one (or in rare cases two) narrow, well-defined, finger(s) until overturn is complete.

The PGS – air experiments display a very similar exchange flow pattern to the cPGS – air experiments. After the apparatus is overturned the instability develops after ~ 7.6 s and initially forms many ($\gtrsim 20$) upwelling fingers. Then, after ~ 20 s of growth between 4 and 6 fingers are selected for continued growth and outgrow the others. Continued growth of these selected fingers occurs until one or two reach the upper reservoir and support the exchange flow. After this point the unsuccessful fingers are carried downward by the dense descending liquid. This is then the stable configuration and all of the upward flow occurs within the one (or in rare cases two) narrow, well-defined, finger(s) until overturn is complete.

The PGS – oil experiments show increased complexity during exchange flow. After the apparatus is overturned the instability develops after ~ 8 s and initially forms ≳ 25 upwelling fingers. Then, after ~ 40 s of growth between 3 and 6 fingers are selected for continued growth and outgrow the others. However, in these experiments, during ascent some fingers start to bifurcate, forming multi-lobed heads. Continued growth occurs until one or, less commonly, two of these bifurcated fingers reaches the upper reservoir. After this point the unsuccessful fingers are carried downward by the dense descending liquid. This is then the stable configuration and all of the upward flow occurs within the narrow, well-defined, finger(s) until overturn is complete.

The DGS – oil exchange flow experiments are much more dynamic than the experiments previously described; they exhibit shorter length scales and common bifurcations. After the apparatus is overturned the instability develops after ~ 0.7 s and within 2 s, forms ≳ 30 upwelling fingers. Then, after ~ 10 s of growth between 4 and 7 fingers are selected for continued growth and outgrow the others. However, the growth is very dynamic; as the fingers grow they coalesce, bifurcate and re-join. Despite this complexity, continued growth occurs until, the bifurcating fingers (commonly three at a singular time) reach the upper reservoir and sustain the exchange flow. Although these DGS – oil experiments feature multiple upwelling fingers that readily bifurcate and change location through time, well-defined regions of ascending and descending fluid still exist.

Lastly, the Gly – oil experiments display turbulent, unorganised exchange flow. After the apparatus is overturned the instability develops immediately (by the time overturn is complete) and within < 1 s, fingers break into separate packets and thin (often sub-cm) strands. For the entire exchange, the flow comprises disconnected packets of rapidly moving upwelling and downwelling fluid; unlike in all of the other experiments there are no persistent loci of upwelling or downwelling – the flow is chaotic.

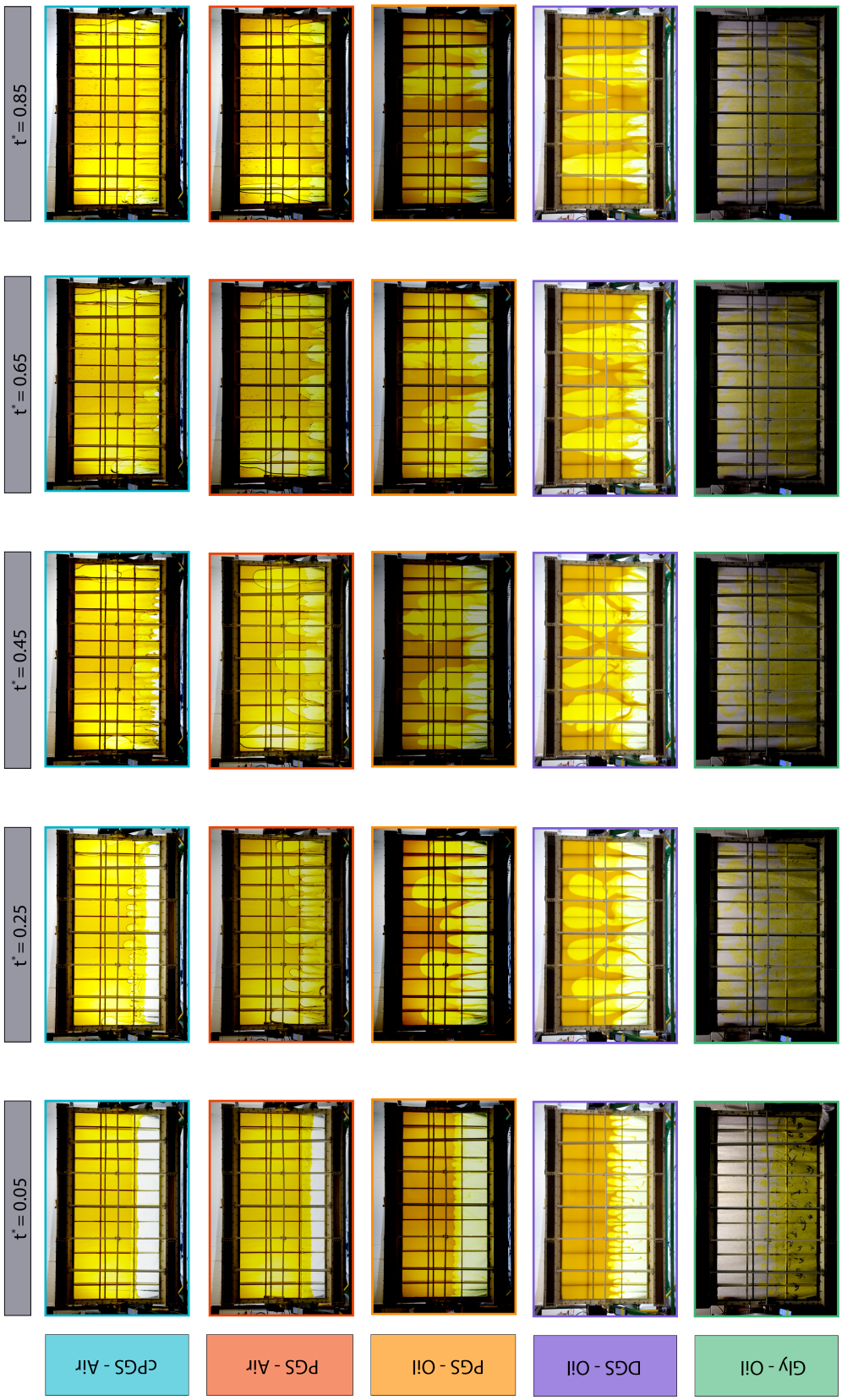

Figure 5.4: *Unprocessed images from exchange flow experiments: cold PGS – air (blue); PGS –air (red); PGS – oil (orange); DGS – oil (purple) and Gly –oil (green) experiments at 5, 25, 45, 65 and 85 % time durations, where* $t^* = 0$ *and* $t^* = 1$ *mark the start and end of an experiment respectively.*

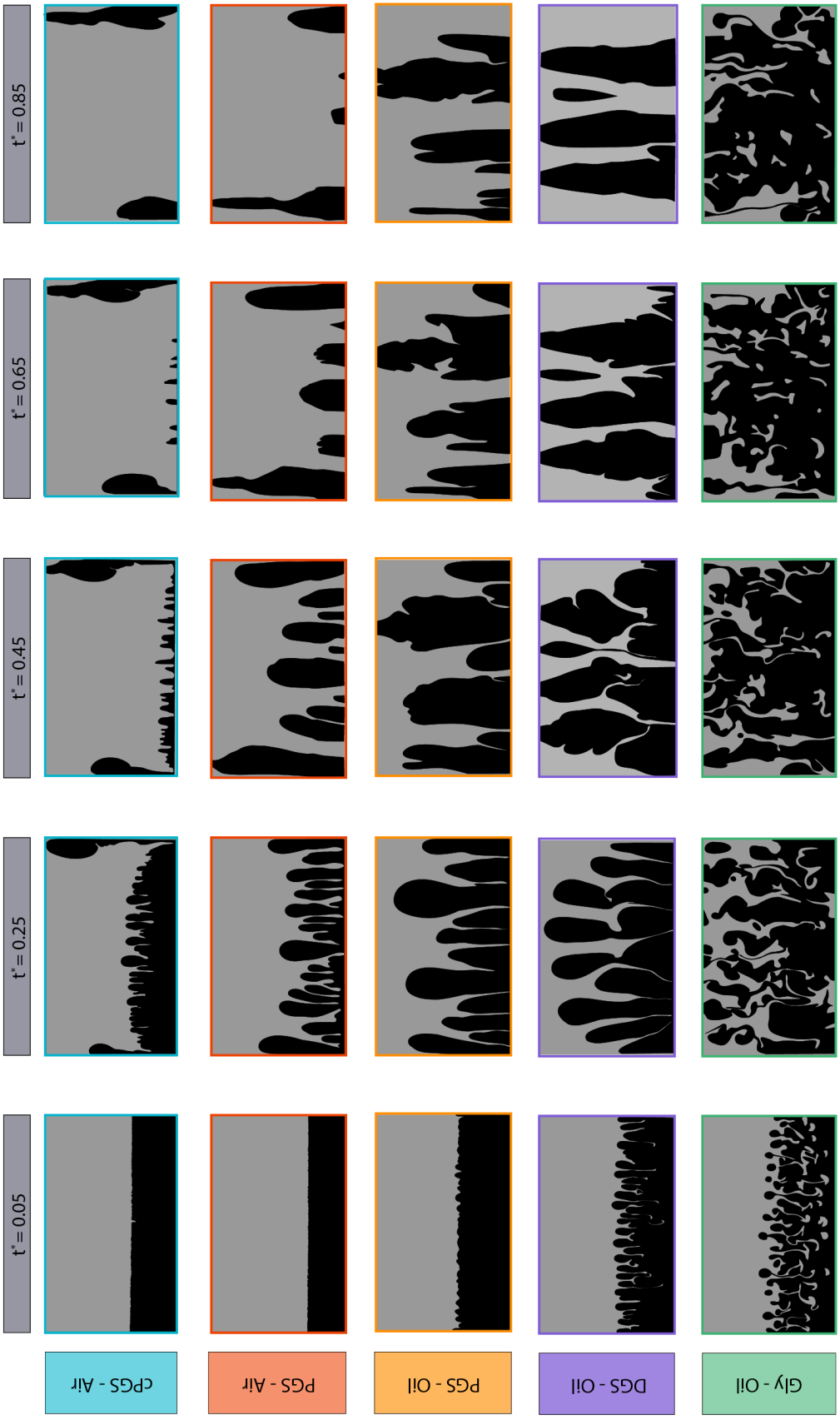

Figure 5.5: *Binarized images shown in Figure 5.4. Colour coding and time intervals remain in accordance with Fig. 5.4.*

5.3.2 Progressive flow rate

By plotting the volume of upwelling fluid above the initial interface line as a function of time into an experiment it can be seen that the increase in volume is linear with respect to time (Fig. 5.6). This is useful as a singular time-averaged volumetric flow rate value, which is much easier to determine, can be used as an accurate representation of the flow rate throughout an experiment. Furthermore, the flow rate systematically changes with each fluid combination. To quantify this, for each fluid combination, the experiment that was measured for velocity and interface length had a linear regression fitted (Fig. 5.6b). The gradient of this line is the progressive flow rate, Q_p and the x-axis intercept is the instability growth timescale. In order of increasing progressive volumetric flow rate, Q_p: the PGS – oil experiments have the lowest ($Q_p = 0.000153$ m^3 s^{-1}); followed by the cPGS – air ($Q_p = 0.000215$ m^3 s^{-1}); then the PGS – air ($Q_p = 0.000312$ m^3 s^{-1}); then the DGS – oil ($Q_p = 0.000539$ m^3 s^{-1}) and finally the Gly – oil experiments have the highest volumetric flow rate with $Q_p = 0.00105$ m^3 s^{-1}.

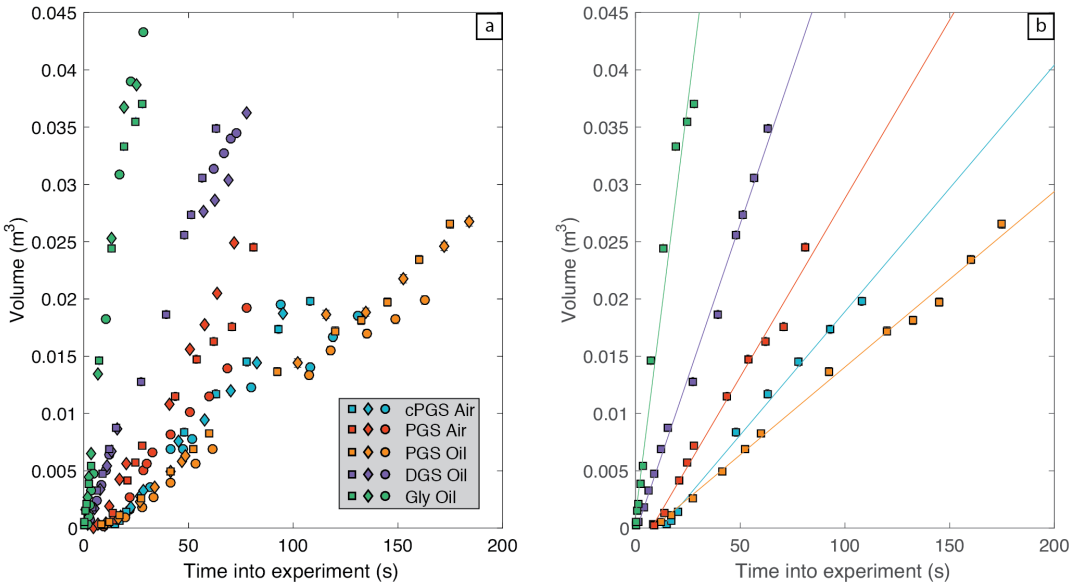

Figure 5.6: *The volume of the upwelling fluid above the initial interface line shown as a function of time into the experiment.* ***(a)*** *All results from three different experiments (denoted by the various symbols) at different fluid combinations (denoted by the symbol colour).* ***(b)*** *One experiment for each fluid pairing is re-plotted and a linear regression fitted; the gradient presents Q_p, the progressive volumetric flow rate [m^3 s^{-1}]. 1σ error bars are smaller than the data points.*

5.3.3 Time-averaged flow rate

The time-averaged volumetric flow rates, Q, for all experiments are reported in Table 5.2 along with other key experimental data. They are in good agreement with the flow rate values calculated from regression to the time series data (Q_p) plotted in Fig. 5.6b; further supporting the interpretation that Q_p is constant throughout an experiment. As previously observed Q increases for different pairs of fluids in the following order: PGS – oil; cPGS – air; PGS – air; DGS – oil and Gly – oil.

Table 5.2 *(overleaf): Key measurements taken during the exchange flow experiments. t_0 denotes the experiment start time, t_{inst} is the instability growth timescale, t_{up} and t_{down} are the times at which the fluid enters the upper and lower reservoir respectively and t_{end} is the time at which the upper reservoir is emptied. Lastly, the time-averaged volume flow rate, Q, is reported for all exchange flow experiments with a mean average and one standard deviation (1σ) for each fluid combination.*

Exp. name	Descending fluid	ρ_d [kg m^{-3}]	μ_d [Pa s]	Upwelling fluid	ρ_u [kg m^{-3}]	μ_u [Pa s]	t_0 [s]	t_{inst} [s]	t_{up} [s]	t_{down} [s]	t_{end} [s]	Q [m^3 s^{-1}]
280616a	cPGS	1440.1	91.9	Air	1.2000	2.00E-5	13.98	13	36.21	41.25	110.3	1.98E-04
280616b	cPGS	1440.1	93.5	Air	1.2000	2.00E-5	13.04	-	69.03	53.11	150.3	1.98E-04
280616c	cPGS	1440.1	93.5	Air	1.2000	2.00E-5	26.7	-	58.78	65.81	131.74	2.09E-04
280616d	cPGS	1440.3	98.3	Air	1.2000	2.00E-5	12.22	-	77.21	51.63	198.27	1.91E-04
280616e	cPGS	1440.3	98.3	Air	1.2000	2.00E-5	13.42	-	77.52	54.46	189.44	1.95E-04
Mean												1.98E-04
1σ												6.77E-06
010716a	PGS	1437.6	43.2	Air	1.2000	2.00E-5	26.84	7.2	55.86	39.80	104.56	3.46E-04
040716a	PGS	1437.8	46.2	Air	1.2000	2.00E-5	28.82	-	62.46	45.85	117.79	3.05E-04
040716b	PGS	1437.8	46.2	Air	1.2000	2.00E-5	21.67	-	52.02	35.67	111.96	3.58E-04
040716c	PGS	1437.8	46.2	Air	1.2000	2.00E-5	38.64	-	61.96	50.63	108.69	3.59E-04
040716d	PGS	1437.8	46.2	Air	1.2000	2.00E-5	60.57	-	81.60	75.25	139.22	4.02E-04
270616a	PGS	1438.0	48.5	Air	1.2000	2.00E-5	30.68	-	61.61	44.37	199.72	3.71E-04
270616b	PGS	1438.0	48.5	Air	1.2000	2.00E-5	74.2	-	103.12	90.45	147.18	3.94E-04
270616c	PGS	1438.0	48.5	Air	1.2000	2.00E-5	59.47	-	81.55	76.26	122.18	4.62E-04
270616d	PGS	1438.0	48.5	Air	1.2000	2.00E-5	34.12	-	64.46	50.16	110.46	3.92E-04
270616e	PGS	1438.0	48.5	Air	1.2000	2.00E-5	13.20	-	40.20	29.84	81.16	4.20E-04
290616a	PGS	1438.6	59.4	Air	1.2000	2.00E-5	21.22	-	47.58	37.51	107.18	2.85E-04
290616c	PGS	1438.6	59.4	Air	1.2000	2.00E-5	31.12	-	67.72	45.30	145.66	4.06E-04
290616e	PGS	1437.4	40.4	Air	1.2000	2.00E-5	54.77	-	85.76	71.43	134.78	3.38E-04
Mean												3.72E-04
1σ												4.80E-05
130716b	PGS	1437.9	46.9	RS Oil	914.9	0.0696	10.04	-	73.70	30.05	206.07	1.40E-04
130716c	PGS	1438.5	56.5	RS Oil	915.6	0.0713	19.50	-	84.16	47.45	255.10	1.45E-04

140716a	PGS	1437.6	43.9	RS Oil	914.6	0.0683	15.03	-	52.98	26.37	172.28	1.95E-04
140716b	PGS	1437.1	37.1	RS Oil	913.9	0.0652	20.36	-	70.34	35.08	207.42	1.72E-04
140716c	PGS	1437.1	37.1	RS Oil	913.9	0.0652	7.88	-	53.18	21.90	200.92	1.72E-04
180716a	PGS	1437.5	41.7	RS Oil	914.4	0.0674	12.10	8.0	73.40	28.44	219.16	1.79E-04
Mean												1.67E-04
1σ												2.09E-05
200716a	DGS	1406.4	6.60	RS Oil	914.1	0.0658	40.63	0.7	52.01	48.00	109.91	4.31E-04
200716b	DGS	1407.1	8.13	RS Oil	914.9	0.0696	17.20	-	30.52	26.20	93.46	4.29E-04
200716c	DGS	1407.2	8.27	RS Oil	914.9	0.0699	18.12	-	34.75	25.73	87.84	5.15E-04
200716d	DGS	1407.2	8.27	RS Oil	914.9	0.0699	41.46	-	58.87	47.85	116.83	4.70E-04
200716e	DGS	1407.1	7.99	RS Oil	914.8	0.0692	10.16	-	23.24	17.22	80.61	4.20E-04
210716a	DGS	1406.7	7.08	RS Oil	914.3	0.0671	39.17	-	55.22	47.56	100.24	5.88E-04
210716c	DGS	1406.8	7.45	RS Oil	914.5	0.0680	33.86	-	50.57	43.92	112.58	4.06E-04
Mean												4.65E-04
1σ												6.52E-05
060916d	Gly	1258.0	0.713	RS Oil	914.2	0.0664	24.52	-	29.13	27.14	65.61	7.75E-04
060916e	Gly	1257.7	0.676	RS Oil	913.9	0.0652	5.40	-	7.45	10.11	41.43	9.12E-04
070916d	Gly	1258.4	0.783	RS Oil	914.7	0.0686	12.84	-	7.04	9.20	44.52	1.05E-03
080916a	Gly	1258.1	0.732	RS Oil	914.3	0.0670	8.64	< 1	8.06	5.78	37.84	1.10E-03
080916b	Gly	1258.2	0.742	RS Oil	914.4	0.0673	4.00	-	8.41	6.37	34.37	1.10E-03
090916a	Gly	1257.8	0.676	RS Oil	913.9	0.0652	6	-	10	8	35	1.18E-03
140916c	Gly	1257.4	0.616	RS Oil	913.5	0.0632	7	-	10	8	27	1.77E-03
140916d	Gly	1257.5	0.633	RS Oil	913.6	0.0637	7	-	11	8	39	1.02E-03
Mean												1.11E-03
1σ												2.94E-04

5.3.4 Fluid velocity

The downwelling (i.e. negative) fluid velocity (circular data markers; Fig. 5.7) varies systematically between experiments. They range from 0.006 m s^{-1} to 0.1 m s^{-1}, increasing in the following order: cPGS; PGS (when paired with oil); PGS (when paired with air); DGS and Gly. The upwelling fluid velocities (square data markers; Fig. 5.7) increase in the same order as the time-averaged volumetric flow rate; the oil in the PGS – oil experiment has the slowest upwelling velocity of 0.001 m s^{-1} and the oil in the Gly – oil experiment has the fastest velocity of 0.02 m s^{-1}. Additionally, with the exception of the Gly – oil experiment, the upwelling fluid velocities increase with time into the exchange. This can be related to the changes in fluid area occupying the slot; through time the area of the upwelling fluid is reduced as the upwelling channels organise themselves into well-defined regions; a feature that is not prominent in the Gly – oil experiments.

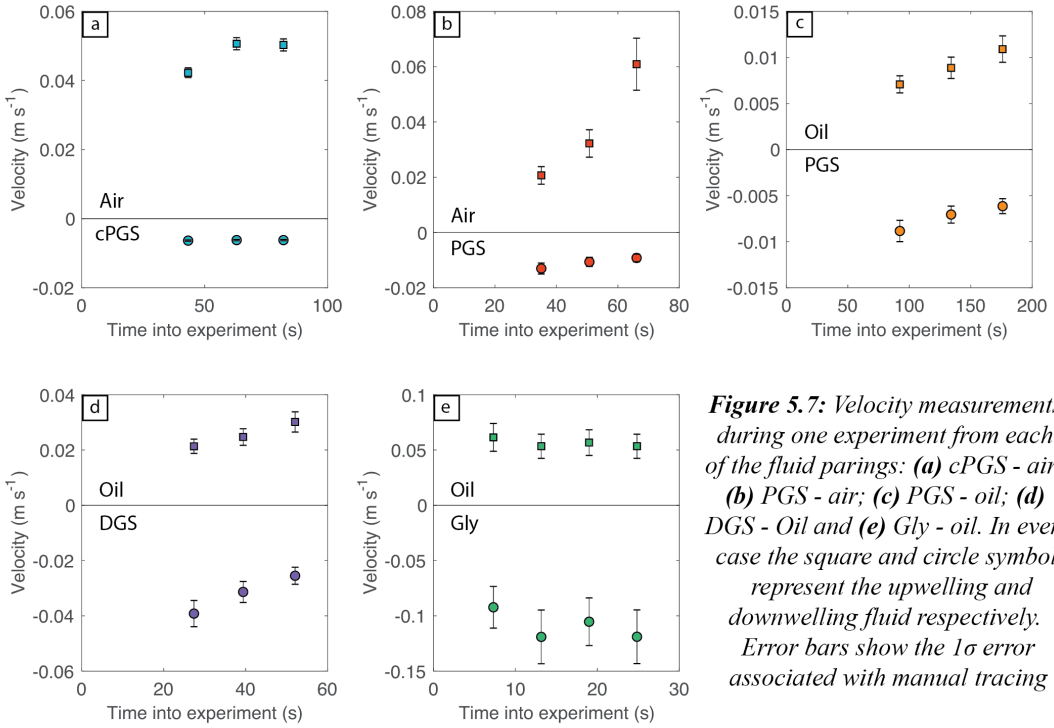

Figure 5.7: *Velocity measurements during one experiment from each of the fluid parings:* ***(a)*** *cPGS - air;* ***(b)*** *PGS - air;* ***(c)*** *PGS - oil;* ***(d)*** *DGS - Oil and* ***(e)*** *Gly - oil. In every case the square and circle symbols represent the upwelling and downwelling fluid respectively. Error bars show the 1σ error associated with manual tracing*

5.3.5 Interface length

Immediately after overturn of the apparatus, the interface length starts at 1.91 m (i.e. the length of the slot). Then, in all experiments, apart from the Gly –oil, as the instability

starts to develop, perturbations in the original, perfectly horizontal interface, cause the interface length to rapidly increase to distances typically > 10 m (Fig. 5.8). The time taken for the interface growth is controlled by the instability growth timescale (cf. Section 5.3.1). Then, as the exchange flow continues, certain fingers are selected for continued growth whilst others are suppressed until a stable configuration is reached (Figs. 5.4 and 5.5). This flow evolution is reflected in Figure 5.8; during continued exchange the interface length reduces to lower values with increased time into an experiment. The Gly – oil experiments do not show this rapid interface growth and subsequent reduction, rather, the interface rapidly reaches and then maintains a near constant value of ~ 8.3 m. This is because the flow rapidly becomes chaotic and remains unorganised throughout exchange.

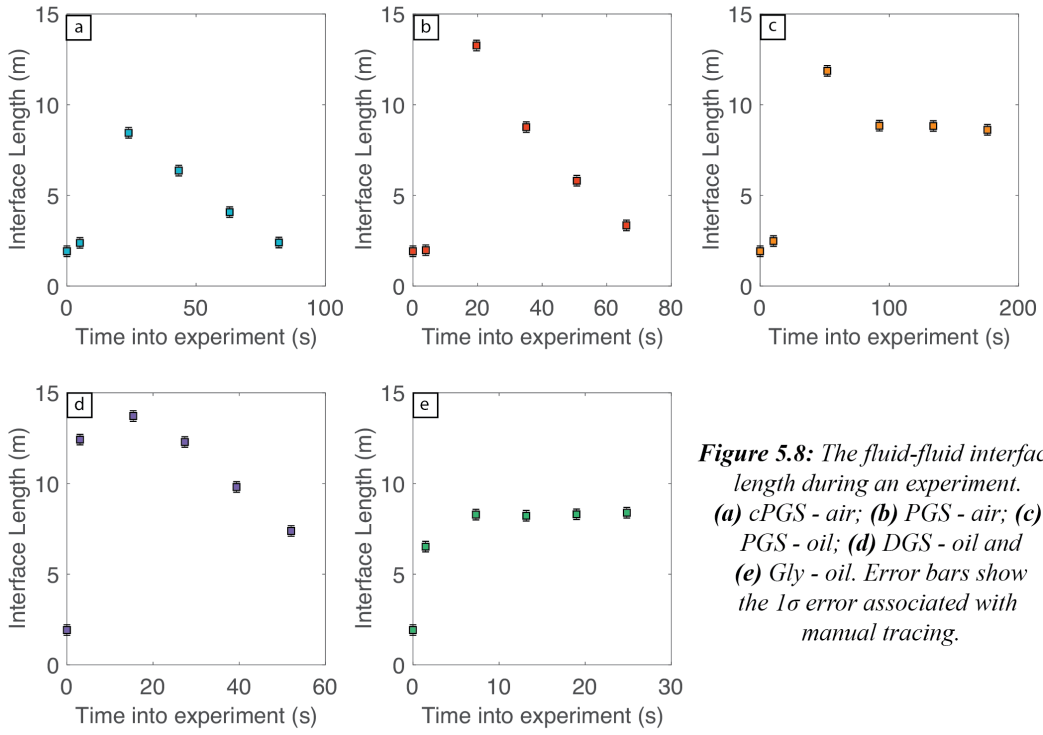

Figure 5.8: *The fluid-fluid interface length during an experiment.* ***(a)*** *cPGS - air;* ***(b)*** *PGS - air;* ***(c)*** *PGS - oil;* ***(d)*** *DGS - oil and* ***(e)*** *Gly - oil. Error bars show the 1σ error associated with manual tracing.*

5.4 Analysis and Discussion

5.4.1 Volumetric flow rate – a view into the subsurface

As discussed in Chapter 4, dimensional analysis and the representation of experimental data in terms of dimensionless groups can be a powerful tool when comparing analogue

experiments to the natural volcanic system. If the experiments are scaled correctly and exhibit the same mode of behaviour expected in the natural system (e.g. laminar vs. turbulent), then one can directly relate experimental observations to the natural system behaviour. Here, the experimental data will be presented in terms of the Grashof number (Gr; Eqn. 4.14) and the Reynolds number (Re; Eqn. 4.17), presented again below for convenience:

$$\mathrm{Gr} = \frac{\rho_d \, \Delta\rho g D^3}{\mu_d^2} \qquad [5.1]$$

$$\mathrm{Re} = \frac{Q\rho_d}{\mu_d L} \qquad [5.2]$$

Gr is an intrinsic property of the convection system, including no parameters that must be extracted from the experiments. It therefore represents the independent variable, where the measured fluid properties (Chapter 4) and system geometry are used to compute Gr for each experiment (Fig. 5.9).

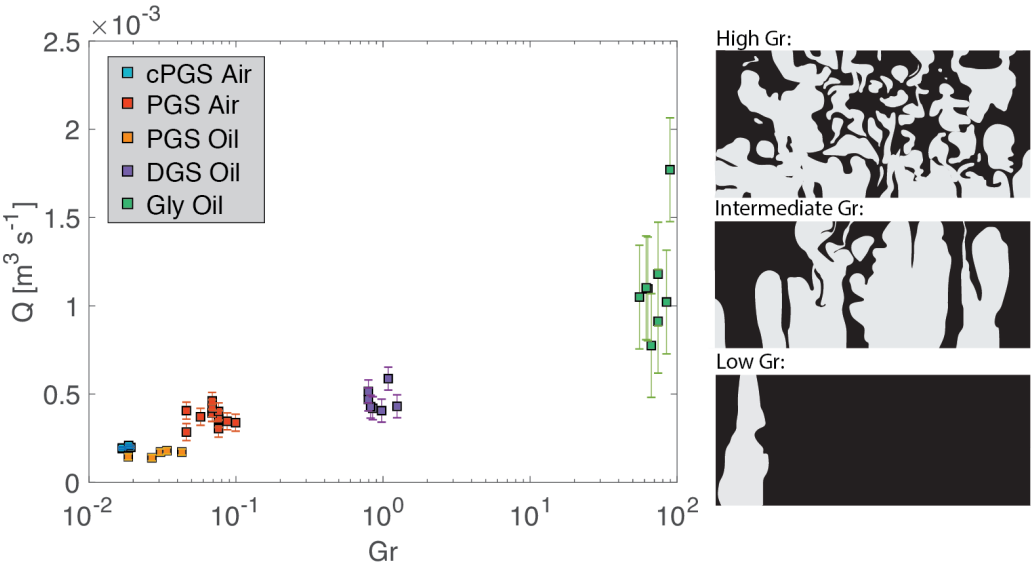

Figure 5.9: *Volumetric flow rate (Q) against Grashof number (Gr) plot for all experimental data. Binary traces represent typical flow patterns of the ascending, low density fluid (light grey) and the downwelling, dense fluid (black) for low, intermediate and high Gr investigated in this study. Error bars represent the 1σ compound error; note the Gr error bars are smaller than the data points.*

When plotting the volumetric flow rate, Q as a function of Gr, a systematic trend is observed (Fig. 5.9); increasing the Grashof number, increases the volumetric flow rate. This can be explained by the viscosity of the dense, most viscous fluid; experiments with high downwelling fluid viscosities exchange on the longest timescales. This shows that the viscosity of the most viscous fluid is the main factor controlling exchange rates. However, viscosity is not the only control. By comparing the PGS – air and PGS – oil experiments it can be seen that when PGS is exchanging with oil it has as slower volumetric flow rate (by ~ 0.00021 m^3 s^{-1} on average), suggesting that the density contrast between the exchanging fluids also plays a role. Higher density contrasts lead to faster velocities.

Every experiment started with an instability, interpreted here to be a Rayleigh–Taylor instability as it was formed by the density contrast between the two fluids (e.g. Sharp 1984). Then, as the fingering continued a large variety of fluid patterns emerged, which can be classified based on Gr (Fig. 5.9). At low Gr (~ 10^{-2} – 10^{-1}) all experiments exhibit well-organised exchange flow with one, or in rare cases, two, narrow finger(s) transporting the ascending low-density fluid at high velocity. At intermediate Gr (~ 1), exchange flow still consists of fingers of upwelling and downwelling fluid, however they are less stable, and are prone to bifurcate and change location throughout the exchange. At high Gr (~ 10^2), no sustained region of organised fingering is observed, instead high velocity ~ 0.1 m s^{-1} separated small packets of upwelling and downwelling fluid co-exist.

By contrast, the other important dimensionless group, Re is an extrinsic property of the system (Eqn. 5.2). It can be quantified in both the analogue experiments and in natural eruptions by measuring the volumetric flow rate, Q. As shown in Figure 5.6, the volumetric flow rate is linear throughout an experiment, therefore, here, the time-averaged volumetric flow rate for each experiment is used to compute Re. To provide a relationship between the measurable extrinsic properties and the system properties, Gr is

plotted against Re (Fig. 5.10). In logarithmic Re – Gr space all these experimental data collapse to a straight line given by:

$$\mathrm{Re} = 0.0401\mathrm{Gr}^{0.767} \quad [5.3]$$

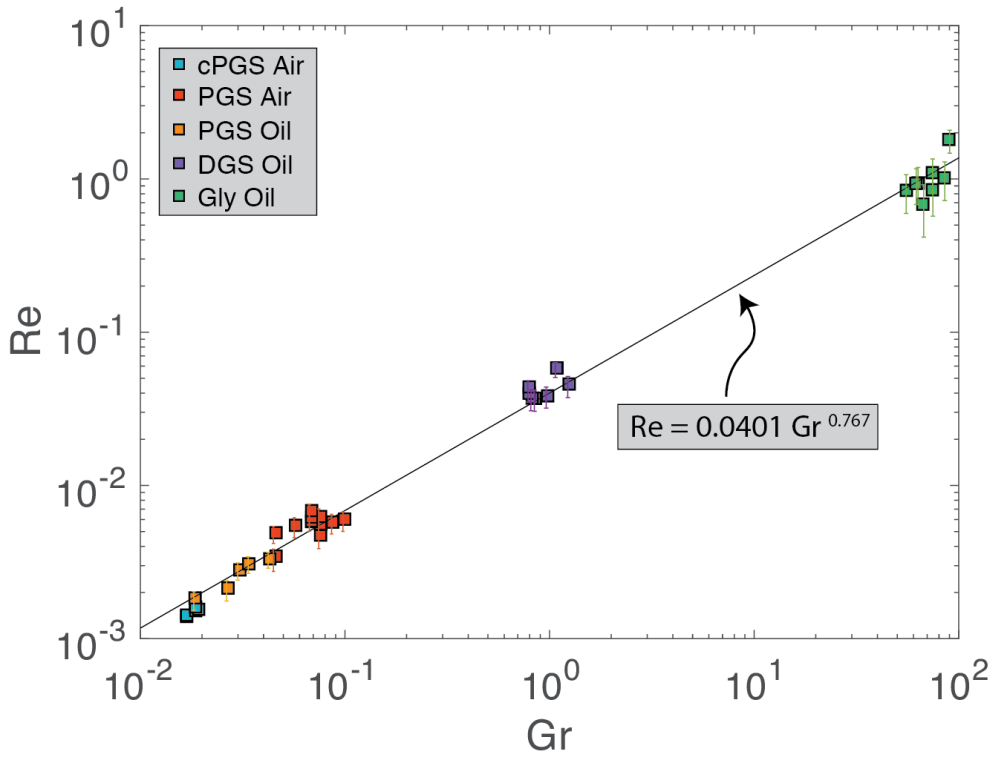

Figure 5.10: *Reynolds number (Re) against Grashof number (Gr) plot for all experimental data. Error bars represent the 1σ compound error.*

Furthermore, using the relationship presented in Equation 5.3, a model flow rate, Q_{model}, per unit length L can be calculated as:

$$\frac{Q_{model}}{L} = \frac{0.0401\mathrm{Gr}^{0.767}\mu_d}{\rho_d} \quad [5.4]$$

Note that the volumetric flow rate here, and in subsequent general equations, is presented as Q/L (i.e. flux per unit length of slot/fissure) to facilitate extrapolation to natural systems. Additionally, to visualise the quality of fit to the experimental data, Q_{model} is plotted against $Q_{exps,}$ wherein perfect solutions plot on the 1:1 line (Fig. 5.11).

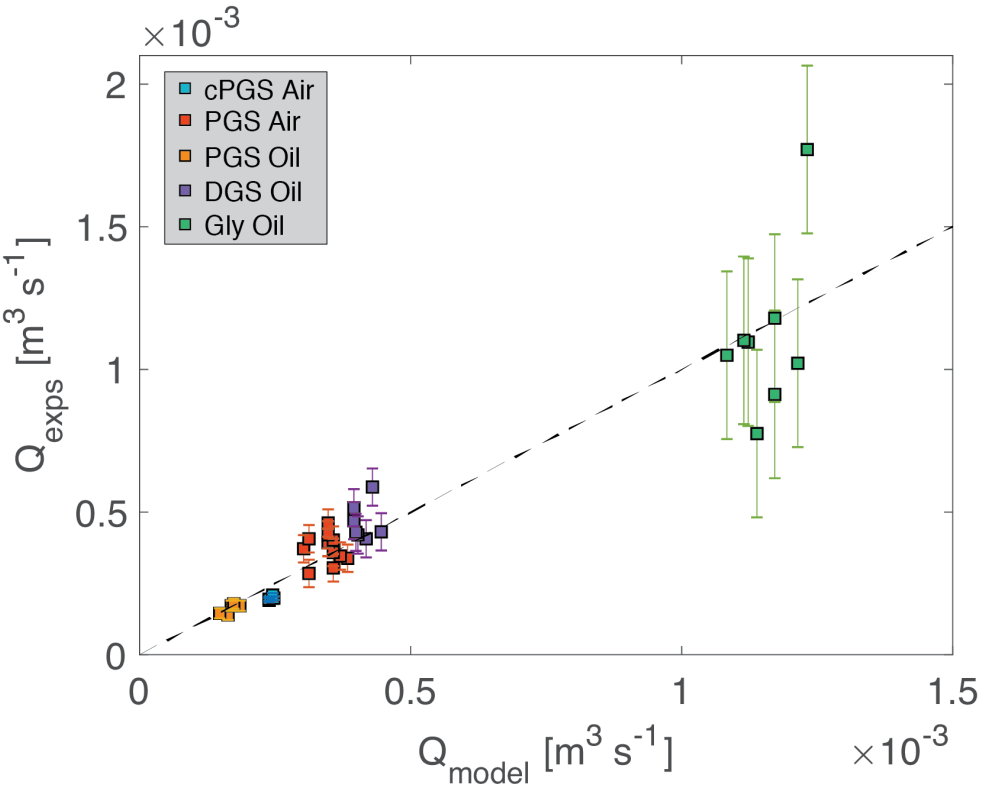

Figure 5.11: *Modelled volume flow rates (Q_{model}) plotted against the measured volume flow rates from the experiments (Q_{exps}). Error bars show the 1σ compound error.*

5.4.2 Quantifying exchange efficiency

The steady flow of an incompressible, Newtonian fluid under laminar flow conditions is a well-studied problem. From work in the Engineering Sciences, it has been shown that the Reynolds number (Eqn. 5.2) and the Fanning friction factor, f_F are two important dimensionless numbers that should be considered when describing this problem (e.g., Churchill 1988; Urbanek et al. 1993; Damean and Regtien 2001; Breyiannis et al. 2008; Dutkowski 2008; Hong et al. 2008). Specifically, the Fanning friction factor can be expressed as:

$$f_F = \frac{2\tau_w}{\rho_d U^2} \qquad [5.5]$$

where, τ_w is the wall shear stress given by $\tau_w = \Delta P\ D_h/4h$, D_h is the hydraulic diameter and $\Delta P = \Delta\rho g h$. These two dimensionless groups are often combined to produce a third dimensionless group:

$$\mathrm{Po} = f_F \mathrm{Re} = \frac{\Delta\rho g D^3 L}{Q\mu_d} \quad [5.6]$$

the Poiseuille number, Po, originally named in honour of the French physician Jean-Louis-Marie Poiseuille (Churchill 1988). Interestingly Po can also be formed by the combination of the Pi groups presented in Chapter 4, such that: $\mathrm{Po} = \mathrm{Gr}/\mathrm{Re}$. Po therefore represents a ratio of buoyancy forces to viscous and inertial forces.

Dimensionless number	Relationship to Po (Eqn. 5.6)	Modifications	Reference
$\mathrm{I} = {\mu_d U}/{\Delta\rho g R^2}$	${1}/{\mathrm{Po}}$	$U \rightarrow Q/DL$ and $R^2 \rightarrow D^2$	(Koyaguchi and Blake 1989)
$\mathrm{Ps} = {\mu_d U}/{\Delta\rho g R^2}$	${1}/{\mathrm{Po}}$	$U \rightarrow Q/DL$ and $R^2 \rightarrow D^2$	(Stevenson and Blake 1998)
$\mathrm{Te} = {\mu_d Q}/{\Delta\rho g R^4}$	${1}/{\mathrm{Po}}$	$Q \rightarrow UR^2$ and $R^2 \rightarrow D^2$	(Huppert and Hallworth 2007)
Po* =Ps	${1}/{\mathrm{Po}}$	-	(Palma et al. 2011)
$\mathrm{C}_Q = {\mu_d Q}/{\Delta\rho g R^4}$	${1}/{\mathrm{Po}}$	$Q \rightarrow UR^2$ and $R^2 \rightarrow D^2$	(Palma et al. 2011)

Table 5.3: *Previous dimensionless flow rate definitions for exchange flow within a pipe. Where R is the pipe radius. Po* is the Po number in the form of Palma et al. (2011).*

In volcanology, previous analogue experiments investigating exchange flow within a pipe, scaled for a cylindrical conduit, have used a dimensionless flow rate to interpret their data. These previous studies have used, and redefined, several dimensionless numbers that are all numerically related; such relationships and the modifications made to the original Po (Eqn. 5.6) are shown in Table 5.3. However, in this thesis I quantify the exchange efficiency by a slightly different approach with the goal of introducing a clearer physical underpinning. The Hagen–Poiseuille equation is a physical law that relates the volumetric flow rate to the driving pressure gradient, the container dimensions and the dynamic viscosity of the fluid. Again, it is valid for the flow of an incompressible, Newtonian fluid under laminar flow conditions. For a cylindrical pipe of constant circular cross-section, the Hagen–Poiseuille equation can be expressed as:

$$Q_{HP\,(pipe)} = \frac{\Delta P \pi R^4}{8\mu h} \quad [5.7]$$

Where $\Delta P/h$ is the driving pressure gradient, R is the pipe radius, μ is the dynamic viscosity of the fluid and $Q_{HP\,(pipe)}$ is the volumetric flow rate.

The Hagen–Poiseuille equation can also be written for a slot, a rectangular duct of high aspect ratio. For this geometry, the Hagen–Poiseuille equation takes the form:

$$Q_{HP\,(duct)} = \frac{\Delta P D^3 L}{12\mu h} \quad [5.8]$$

Where $\Delta P/h$ is the driving pressure gradient, D is the internal slot width and L is the slot length, such that the product of D and L gives the cross-sectional area perpendicular to flow.

Now, using Equations 5.7 and 5.8, two dimensionless numbers can be created to assess the efficiency of the experiments relative to ideal Hagen–Poiseuille flow. If we assume that, in the experiments, the driving pressure is solely driven by the density difference between the two exchanging fluids, such that: $\Delta P = \Delta \rho g h$ and that the viscous, downwelling fluid controls the timescale of overturn ($\mu = \mu_d$), since $\mu_d \gg \mu_u$, a volumetric flow rate predicted by Hagen–Poiseuille flow can be calculated (Q_{HP}). Hence, Q_{HP} represents the calculated flow rate for the high viscosity fluid draining within the slot under reduced gravity. Therefore, normalising the measured volumetric flow rate, Q_{exps} by the Hagen–Poiseuille equation gives:

$$Q_c^* = \frac{Q_{exps}}{Q_{HP\,(pipe)}} = \frac{8\mu_d Q_{exps}}{\Delta \rho g \pi R^4} \quad [5.9]$$

where Q_c^* is the dimensionless flow rate for a cylinder or cylindrical conduit, and:

$$Q_D^* = \frac{Q_{exps}}{Q_{HP\,(duct)}} = \frac{12\mu_d Q_{exps}}{\Delta \rho g D^3 L} \quad [5.10]$$

where Q_D^* is the dimensionless flow rate for a high aspect ratio duct or dyke. Note that Q_C^* and Q_D^* are simply related by a geometric factor and that $Q_D^* = 12/\mathrm{Po} = 12\,\mathrm{Re}/\mathrm{Gr}$.

Although this dimensionless number is similar to those presented in Table 5.3 and only varies by length scale definitions and a factor of 12, Q_D^* is preferred as it has an intuitive physical meaning. For $Q_D^* < 1$, the flow is less efficient than ideal Hagen–Poiseuille flow, for $Q_D^* > 1$, the flow is more efficient that ideal Hagen–Poiseuille flow and for $Q_D^* = 1$, exchange flow is equal to ideal Hagen–Poiseuille flow.

Using the empirical relationship (Eqn. 5.3), and the relationship $Q_D^* = 12\,\mathrm{Re}/\mathrm{Gr}$, a semi-empirical predictive model can be written for Q_D^*:

$$Q_D^* = 0.481\mathrm{Gr}^{-0.233} \qquad [5.11]$$

With increased Gr, the flow becomes less efficient at supporting exchange (Fig. 5.12). The data for the cPGS – air experiments are tightly grouped and have a mean $Q_D^* = 1.00$, showing that these experiments exchange at rate comparable to ideal Hagen–Poiseuille flow. The PGS – oil experiments have a more variable Q_D^*, ranging from 1.2 to 0.93 and a mean of 1.06. The PGS – air experiments range in Q_D^* from 1.3 to 0.72 and have a mean of 0.97. At higher Gr, the DGS – oil experiments have a mean dimensionless flow rate of 0.56; much less than the lower Gr experiments, indicating a decrease in exchange efficiency. Finally, at the highest Gr, the Gly – oil experiments have the lowest Q_D^* with a mean of 0.17 and therefore represent the least efficient exchange flow.

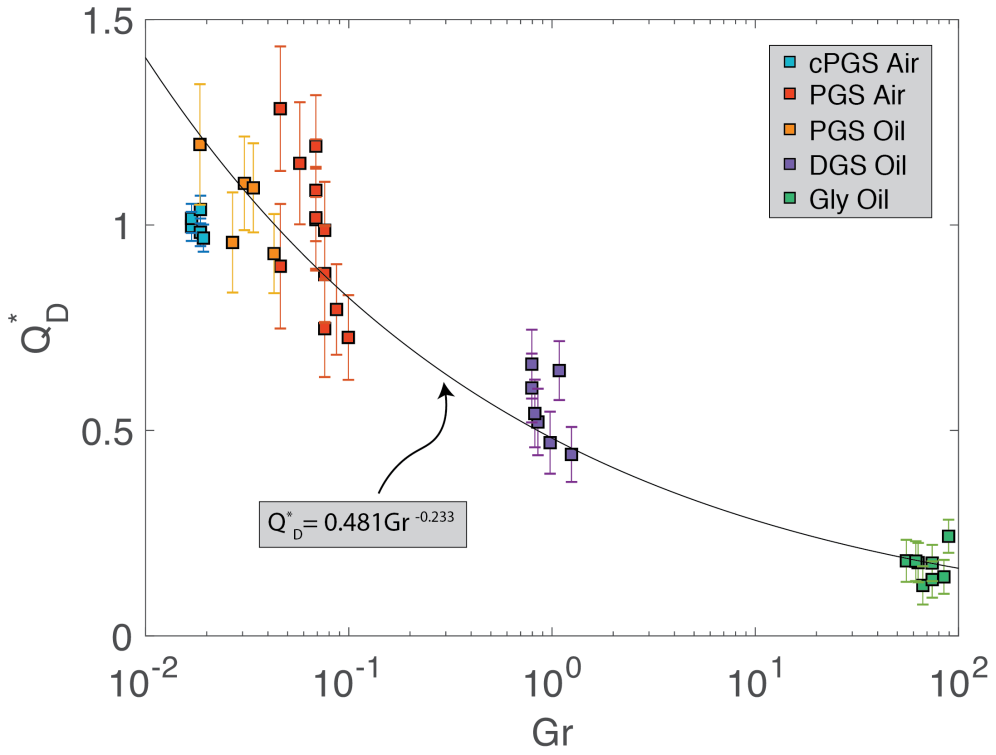

Figure 5.12: *The dimensionless flow rate for all experiments at a range of Gr. Equation 5.11 is shown by the solid black line. Error bars show the 1σ compound error.*

These data lead to the hypothesis that the observed decrease in dimensionless flow rate with increased Gr is a result of changing the exchange flow patterns. Experiments conducted at Gr $\lesssim$ 0.1 (i.e. all those with cold PGS or PGS as the dense, viscous fluid) exhibit well organised exchange flow, whereas as Gr is increased, the exchange flow becomes increasingly disorganised and the upwelling fingers readily bifurcate and break apart (cf. Section 5.3.1). I hypothesise that the reduction in dimensionless flow rate is a result of more complex, more disorganised, flow patterns. This increased complexity can be quantified by using the interface length (Fig. 5.8) as a metric.

To test this hypothesis and to provide an unbiased assessment of how the interface length changes between the various experiments, that all exchange on different timescales, Figure 5.8 is made non-dimensional. Specifically, the timestamp on the image measured (t_{mea}) is normalized to the experiment duration to produce a dimensionless time, t^*:

$$t^* = \frac{t_{mea} - t_{start}}{t_{end} - t_{start}} \quad [5.12]$$

and the measured interface length (x_{mea}) is normalized to the initial interface length before overturn (x_0) to produce a dimensionless interface length scale, x^*:

$$x^* = \frac{x_{mea}}{x_0} \quad [5.13]$$

This allows data from all the experiments to be compared (Fig. 5.13). During early ($t^* \leq 0.25$) Rayleigh-Taylor instability development and growth the interface length in all experiments increases to between 4 and 7 times its original length (Fig. 5.13a). Then, at $t^* > 0.3$, x^* is reduced for all experiments apart from Gly – Oil. This is because after the upwelling fluid enters the top reservoir all other "unsuccessful" fingers begin to descend in the slot carried by the downwelling fluid.

To assess the organisation of flow at steady-state conditions, taken to be at $t^* = 0.85$, the interface length of these unsuccessful fingers that are passively descending in the dense, viscous fluid must to be removed. I do this my modifying the x_{mea} term within x^* (Equation 5.13) to form x^*_{up} which only considers the interface length of fingers/regions actively moving the low density, low viscosity fluid upward at $t^* = 0.85$. This steady state value of x^*_{up}, can be correlated with Gr (Fig. 5.13b); experiments that exchange by discrete fingers at Gr $\lesssim$ 0.1 (cPGS – air; PGS – air; PGS – Oil) have short x^*_{up} lengths of ~ 1 at steady state. Whereas the DGS – Oil experiments have a much higher stable x^*_{up} of ~ 3.5, reflecting the higher number of stable fingers and common bifurcations. At the highest Gr, the Gly – Oil experiments have the largest steady state x^*_{up} of ~ 4.3; the flow is always chaotic and broken into several smaller packets. x^*_{up} therefore serves as an appropriate metric to quantify the degree of disorganisation.

By plotting x^*_{up} as a function of the dimensionless flow rate, the working hypothesis can be tested (Fig. 5.13c). This shows that increased disorganisation of the flow, quantified

by x^*_{up}, makes the exchange flow more inefficient (reducing Q_D^*). I interpret this to be caused by a higher contact surface between the exchanging fluids – the fluids will interact more during exchange and more energy will be dissipated. Palma et al. (2011) also note that dimensionless flow rate varies as a function of flow pattern and that the most efficient flow occurs when the liquids exchange under well organised stratified flow, but do not quantify interface length. By visual inspection of their images (Fig. 3; Palma et al. 2011), stratified flow appears to have the shortest interface length of all flow patterns which is consistent with my hypothesis.

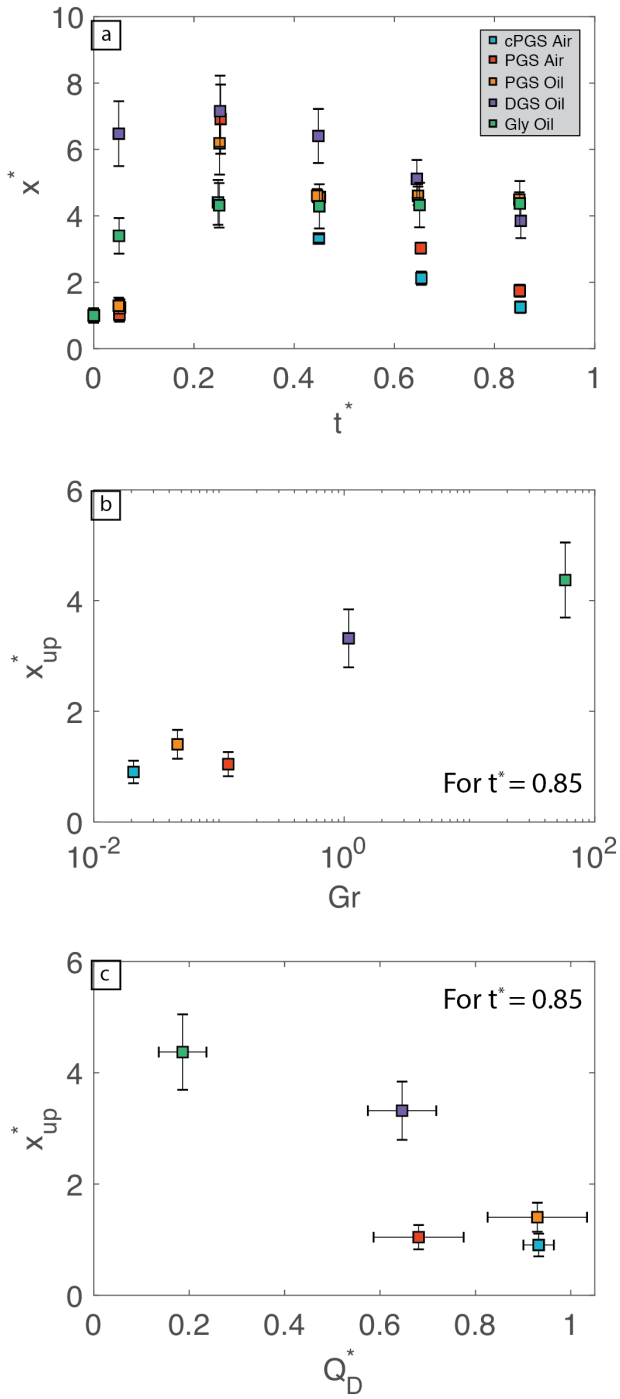

Figure 5.13: *The dimensionless interface length (x^*) as a function of* ***(a)*** *dimensionless times (t^*) 0, 0.25, 0.45, 0.65, 0.85. The dimensionless interface length of only the upwelling finger(s) (x^*_{up}) as a function of:* ***(b)*** *Grashof number at t^*=0.85 and* ***(c)*** *dimensionless flow rate t^*=0.85 for all experiments. Error bars show the compound 1σ error.*

5.4.3 The dependence on viscosity ratio

The dimensionless flow rates, Q_D^* calculated for the experiments presented in this chapter show no clear correlation with viscosity ratio (Fig. 5.14), defined here as: $\beta = \mu_d/\mu_u$ (Second Pi group; Chapter 4). Although a trend can be observed between ~10^1 and 10^3 β, this can be simply attributed to the reduction in the downwelling fluid viscosity. Furthermore, no trend is observed over the large 10^3 - 10^7 range in β; the reduction in Q_D^* between cPGS – air, PGS – oil and PGS – air is not clear, unlike Fig. 5.12. Based on the experiments performed in this study it is impossible to rule out the effect of β on Q_D^*; to do this a series of experiments would need to be performed at constant Gr whilst changing β. This is experimentally very challenging and beyond the scope of this study. However, based on the successful collapse of experimental data (Figs. 5.10 and 5.12) and the systematic change in flow patterns upon changing Gr, the Grashof number is suggested to be the dominant dimensionless parameter controlling the exchange flow rates and patterns.

In previous studies, the dimensionless flow rate or equivalent (Table 5.3) has been correlated with β. Both Huppert and Hallworth (2007) and Palma et al. (2011) show that the dimensionless flow rate decreases as $\beta < 10$ (i.e. the downwelling fluid has a lower or similar viscosity relative to the upwelling fluid). However, this can be explained by their choice of input parameters when calculating the dimensionless flow rate. In both of these previous studies authors use the downwelling fluid viscosity irrespective of its relative viscosity. Whereas, for sufficiently large viscosity ratios, it is the more viscous fluid that controls the exchange timescale, irrespective of whether it is upwelling or downwelling. In this study, unlike Huppert and Hallworth (2007) and Palma et al. (2011) all our experiments were performed at $\beta > 1$ and calculations always used the most viscous fluid.

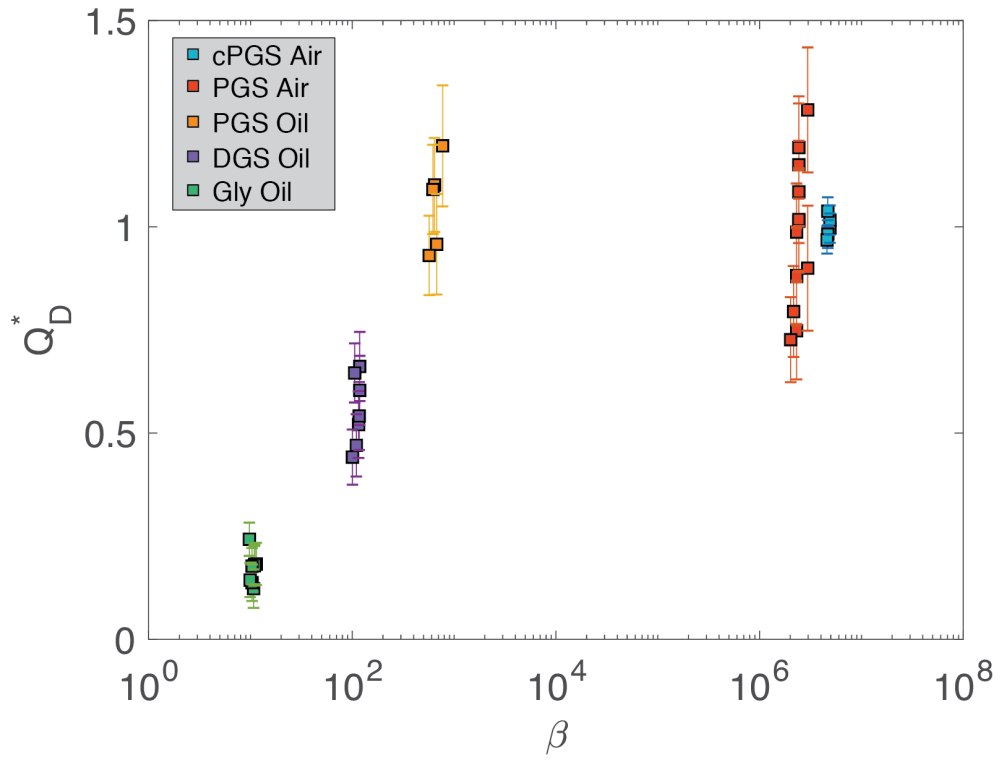

Figure 5.14: *The dimensionless flow rate as a function of viscosity ratio ($\beta = \mu_d/\mu_w$). Error bars show the 1σ compound error.*

5.5 Conclusions and Volcanological Implications

The scaled analogue experiments presented in this chapter have highlighted the variable exchange flow behaviour possible in natural basaltic fissure eruptions. By changing the Re or Gr, flow patterns within a dyke-like geometry can range from well organised, discrete fingers to chaotic, spatially variable, poorly organised flow. Dimensional analysis of the experimental results has yielded relationships that can be used to interrogate the natural system, firstly, the empirical relationship: $\mathrm{Re} = 0.0401\mathrm{Gr}^{0.767}$ (Eqn. 5.3), or re-arranged for the volumetric flow rate: $Q_{model}/L = 0.0401\mathrm{Gr}^{0.767}\mu_d/\rho_d$ (Eqn. 5.3) enables the measurable extrinsic properties of the volcanic system (e.g. Re, Q) to be linked to the intrinsic properties of the system (e.g. Gr, D, ρ, μ). Secondly, the efficiency of the exchange flow has been quantified through a dimensionless flow rate, Q_D^*, yielding a semi-empirical relationship: $Q_D^* = 0.481\mathrm{Gr}^{-0.233}$ (Eqn. 5.12). Where the reduction in Q_D^* upon increasing Gr can be linked to the changing

flow patterns; exchange flow with a longer interface between the two fluids has a slower Q_D^*. These empirical relationships have implications for interpreting exchange processes at erupting basaltic fissure volcanoes and could be used as predictive models. For example, either by measuring the time-averaged volumetric flow rate during an eruption or by measuring the system properties (ρ, D, μ) a volcanologist could quantify Gr or Re, and therefore estimate the subsurface flow behaviour (e.g. Figs. 5.9 and 5.10).

Now, to illustrate how these empirical and semi-empirical relationships can be useful for volcanic scenarios, the Gr, Re and dimensionless flow rate, Q_D^* are calculated for episode 1 of the 1969 Mauna Ulu basaltic fissure eruption (see Chapters 2 & 3). This requires estimation of several input parameters. The density values are obtained by bulk density measurements made in Chapter 3; where the primary spatter is the most juvenile material and is taken to represent the upwelling magma and the late-stage spatter is the most mature material and is taken to represent the downwelling magma. The temperature of the downwelling magma is assumed to be the same as the measured eruption temperature. This assumption is supported by contemporary measurements indicating that the proximal lava was the same temperature as the fountains (Swanson 1973). The downwelling viscosity, μ_d, was calculated as a two-phase suspension of melt and bubbles. The chemical composition of the episode 1 spatter measured by Wright et al. (1975) was used to calculate the pure melt viscosity, μ_l, using the model of Giordano et al. (2008). Then, using the mean bubble fraction of the late-stage spatter (ϕ_b), the viscosity of the downwelling bubble suspension was calculated by: $\mu_d = \mu_l(1 - \phi_b)^{-1}$ (e.g. Mader et al. 2013). A full list of input parameters and literature sources is provided in Table 5.4.

Parameter	Value	Units	Reference
D	1.1	m	Parcheta et al. (2015)
ρ_d $(\pm 2\sigma)$	1442 ± 15	kg m^{-3}	Late-stage spatter; Chapter 3
ρ_u $(\pm 2\sigma)$	1054 ± 19	kg m^{-3}	Primary spatter; Chapter 3
T	1165	°C	Eruption temperature from Swanson (1973)
X_{H20}	0.07	wt. %	Swanson and Fabbi (1973)
ϕ_b	0.40	-	Late-stage spatter; Chapter 3
μ_l	80.0	Pa s	Wright et al. (1975); Giordano et al. (2008)
μ_d	134	Pa s	$\mu_d = \mu_l(1-\phi_b)^{-1}$; Mader et al. (2013)

Table 5.4: *Model input parameters for episode 1 of the 1969 Mauna Ulu basaltic fissure eruption. Where, X_{H20} is the remaining water content after eruption and T_{melt} is the temperature of the downwelling melt.*

The calculated results for shallow exchange flow during episode 1 of Mauna Ulu are shown in Figure 5.15. The orange shaded regions show the range of possible values calculated using the 2σ variation in density observed in the natural products. Gr varies from 370 to 450 with a best estimate, denoted by the red dashed line (using mean ρ values) of 409. This "best estimate" of Gr corresponds to a Reynolds number of 4.0 and a dimensionless flow rate of 0.12. These data lie closest to the Gly – Oil experiments. This suggests that the exchange flow during the episode 1 Mauna Ulu eruption had a subsurface convective system that was chaotic, poorly organised and inefficient at bringing fresh material to the surface. However, it should be noted that the Gr may not be constant for a single eruption and could vary both spatially and temporally. For example, at greater depths (e.g. > 300 m) within the plumbing system, bubbles will not be exsolved; they will be present as dissolved volatiles within the melt. Therefore, the density difference between the upwelling and downwelling liquids will be substantially reduced; density differences of 400 kg m^{-3}, like those observed in the previous example will be reduced to ~ < 50 kg m^{-3} (Spera 2000; Lesher and Spera 2015) and thereby lower Gr.

As an example of how Gr can vary between different volcanic systems let us calculate the Grashof number for the well-studied basaltic system, Stromboli, where geophysical

signals suggest that the shallow conduit ~ < 1 km has a dyke-like geometry (Chouet et al. 2003; Chouet et al. 2008). Specifically, for the calculations, I use an upwelling density of 1300 kg m^{-3}, a downwelling density of 2600 kg m^{-3}, a downwelling density of 10^4 Pa s from Del Bello et al. (2012) and assume a dyke like geometry at depth with a gap-width of 1.1 m (same as Mauna Ulu). These input parameters result in a Gr of 0.44, a Re of 0.021 and a Q_D^* of 0.58 (blue dashed line; Fig. 5.15). This shows that subtle changes in the physical properties of the magma (density and viscosity) and/or changes in the plumbing system geometry can alter Gr, such that the exchange flow operates under a different regime. For the calculated case at Stromboli I would expect the subsurface system to constitute well-organised fingers of upwelling magma and discrete zones of downwelling magma (e.g. golden syrup experiments).

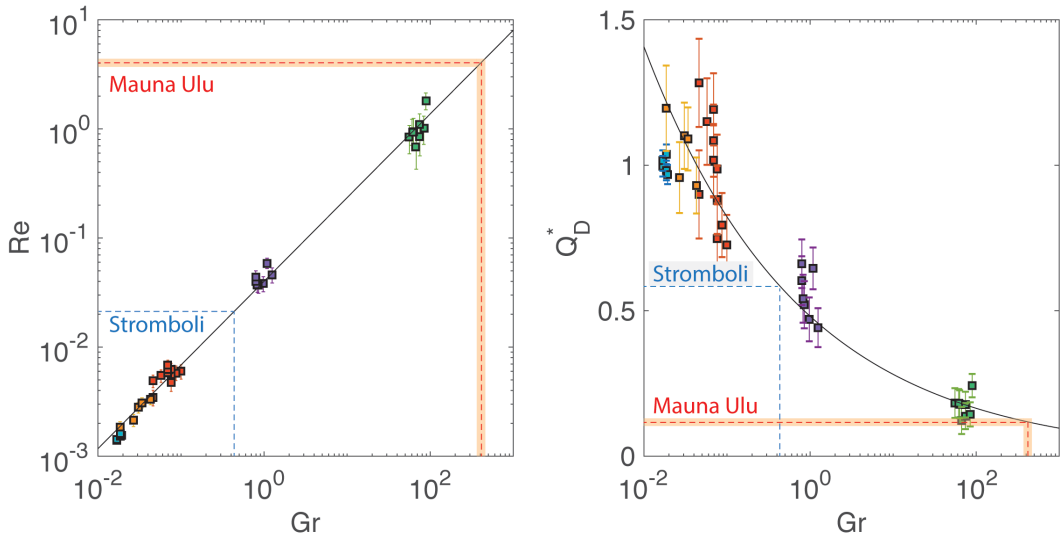

Figure 5.15: *Results of the Mauna Ulu and Stromboli example. The orange shaded field marks the range of values computed allowing for a 2σ error in the bulk density measurements. The dashed lines show the mean (Mauna Ulu), or best estimate (Stromboli) computed values. On both subplots error bars show the 1σ compound error.*

In this chapter I have shown that the dimensionless group termed the Grashof number controls the degree of flow organization. Experiments, or natural eruptions (inferred based on scaling) at low Gr, $\lesssim 0.1$, exhibit well-organised flow and efficient exchange.

Magma transported under these low Gr conditions would ascend easily with limited interaction with the co-existing downwelling magma. One of the implications of this is that the magma would remain relatively "unmodified" and retain its crystal cargo. Whereas, magma transport under higher Gr conditions (e.g. Gr ~ 100) would be less efficient and more energy would be dissipated due to the poor organization of the upwelling and downwelling magma components. Furthermore, these magmas would have a greater opportunity to mix and mingle during ascent allowing for: increased thermal advection within the dyke; easier crystal transfer between two compositionally different melts and increased hybridisation of melts reducing their compositional differences.

Chapter 6

Synthesis and Conclusions

6.1 Synthesis

This thesis has explored the various ways in which magma dynamics can affect the eruptive style, duration and localization of basaltic fissure eruptions. In this section I will synthesize the findings from the field and laboratory work and show how "top-down" surface processes and "bottom-up" subsurface processes may conspire together to control the evolution of these complex eruptions.

6.1.1 "Top-down" processes

The interaction between erupting vents and lava has been documented at numerous volcanoes. For example, during the 1969 eruption of Kīlauea Iki after the end of each high fountaining episode substantial volumes of lava (~ 10^6 m^3) drained back down into the vent (Richter et al., 1970; Stovall et al., 2009). Also, during the 1983-86 Pu'u 'Ō'ō-Kupaianaha eruption of Kīlauea, pyroclastic ejecta provided a topographic confinement around the vent, allowing for a perched lava pond to form, covering the vent for the first 19 episodes (Wolfe et al., 1988). These observations led to a series of studies that modelled the effect of lava entrainment, bubble coalescence and exsolved volatile content on fountain height (Head and Wilson, 1989, 1987; Parfitt et al., 1995; Wilson et al., 1995). In particular, Wilson et al. (1995) provide an analysis of fountain height reduction as a function of vent inundation for both circular and linear (fissure) vents (cf. Fig. 2.10). However, rather than just considering the extra energy involved in lava re-entrainment, in this thesis I suggest that, in the case of fissure eruptions vent inundation also provides differential pressure gradients along strike which can lead to lateral magma migration.

This interpretation is supported by field evidence (Chapter 2); fissure segments that experienced deep lava inundation stopped erupting early in the eruption episode and acted as a conduit for downwelling, degassed lava (Chapter 3).

I show that two pre-eruption topographic features often result in large inundation depths and subsequent localization. Firstly, topographically confined basins result in lava ponding and potential stagnation. Secondly, vent proximal areas with shallow topographic gradients are prone to dynamic ponding – where the eruption rate exceeds the local drainage (outflow) rate (cf. case studies in Chapter 2). These key findings could allow pre-eruptive topographic maps to be used as a predictive tool in the future. It is well known the dykes exploit pre-existing structural weaknesses (e.g. Cappello et al., 2012; Galindo and Gudmundsson, 2012). Therefore faults and ground cracks on basaltic shields could be identified as probable sites of future eruption (Becerril et al., 2013; Bonali et al., 2011; Cappello et al., 2012). Through the identification of relative topographic high points and low points along these ground cracks, the corresponding loci of on-going eruption and early segment closure could be estimated. These data would act to better inform hazard maps and lava flow models, allowing for greater spatial resolution in these highly variable systems.

The drainage of dense, degassed material into the conduit also has implications for the eruption style. As texturally mature material descends back down into the conduit it can potentially trap gas pockets which then rise, subsequently bursting to form a late-stage spatter deposit (Chapter 3). This activity is of extremely low energy and the ejecta are confined to vent proximal regions (< 10 m recorded in this study). Furthermore, I document a new type of "secondary" eruption whereby tectonic cracks open beneath active lava flows accompanied by upward rushing gas. This leads to lava disruption and the formation of spatter. This not only represents a further hazard associated with basaltic fissure systems but could lead to the misinterpretation of previous eruption sites. Care

must be taken when identifying fissure vents (on Earth and within remotely sensed data from other planets), so that accurate spatial probabilistic datasets, which inform hazard mapping, can be produced (e.g. Cappello et al., 2012).

6.1.2 "Bottom-up" processes

It is well known that magma ascent dynamics in the volcanic plumbing system play a key role in determining the eruptive behavior of a volcano (e.g. Scandone et al., 2007; Scandone and Malone, 1985; Woods and Koyaguchi, 1994). Previous work on basaltic fissure eruptions has shown the importance of the subsurface plumbing system in controlling the evolution of fissure eruptions. These subsurface factors include: a thermal control, whereby the rate of thermal advection is insufficient to keep the magma above its solidus so blocking occurs through solidification (Bruce and Huppert, 1989; Delaney and Pollard, 1982); viscosity variations, whereby slight along-strike temperature perturbations cause significant viscosity variations leading to focused flow within the region of lowest viscosity (e.g. Wylie et al., 1999); and conduit geometry, whereby along strike fissure width variations caused by geometrical or structural irregularities in the host rock are enhanced by mechanical and thermal erosion to ultimately form cylindrical conduits (Ida, 1992). Here, I identify and investigate a further subsurface control – convective flow processes in the conduit.

The experiments presented in Chapter 5 show that a wide range of convective fluid flow patterns can develop within the feeder system of basaltic fissure volcanoes. These patterns range from well organised, discrete fingers at low Re (~ 0.005) and Gr (~ 0.05) to poorly organised, highly disrupted fingers at high Re (~ 1) and Gr (~ 100). I propose that variation in the subsurface flow patterns in this manner will influence fissure localization and eruption style. To relate the subsurface processes governed by the volumetric *exchange* flow rate (Q) a connection must be made to the observable volumetric *eruption* rate. One possibility is to estimate the exchange flow rate from the

excess SO_2 gas. Specifically, a volcanologist could measure the SO_2 flux and the volume of lava erupting at an active volcano. Then, by using a gas budget principle, the total volume of magma rising, and outgassing can be calculated. This total volume of magma involved could then be subtracted by the measured erupting volume to calculate an exchange flux. As a first order approximation, the greater the eruption rate the greater the volumetric exchange flow rate.

As fissure systems open they erupt magma with a relatively low viscosity at a high eruption rate. Then, through time, the eruption rate is commonly observed to decrease due to pressure changes in the magma reservoir (Wylie et al., 1999). If we assume that the feeder dyke width remains constant, then these observations correspond to a Re reduction during the course of an eruption episode. This supports my experimental findings; I propose that as basaltic fissure systems open they experience high ($\gtrsim 1$) Re, unorganised, chaotic flow, which is manifest at the surface by an eruption along the entire fissure strike. Then, as the eruption proceeds the volumetric flow rate decreases and the downwelling magma becomes texturally mature (increasing its viscosity). Both of these system modifications lead to a lower Re and Gr, thereby shifting the subsurface flow pattern into a more organised state. With time, Re and Gr continue to decrease until the subsurface flow consists of one finger of upwelling magma. This is manifest on the surface by a singular point of eruption, building a pyroclastic edifice, along the original high-aspect ratio fissure – a typical end state of basaltic fissure eruptions.

These new subsurface controls on basaltic fissure localization proposed in this thesis can fully support, and work in conjunction with, the previous framework of thermo-rheological models. For instance, flow at high Re and Gr is chaotic and vigorous along the entire strike, this would lead to high rates of heat advection and act to maintain, and potentially thermally erode the active conduit. As the Re and Gr of the subsurface exchange flow rate decreases, fingers develop and lead to greater temperature (and

therefore viscosity) variations along strike. This lateral heterogeneity induced by convective processes may then be further compounded by the thermo-rheological effects demonstrated in previous works (e.g. Bruce and Huppert, 1989; Wylie et al., 1999).

6.2 Conclusions

This thesis has addressed many aspects of basaltic fissure systems; from subaerial fragmentation behaviours, to within conduit convection dynamics, delivering a more comprehensive physical view of basaltic fissure eruptions. In summary, this thesis has:

1. introduced a new mapping technique, using tree moulds, allowing for the reconstruction of pre-eruption, syn-eruption and post-eruption topographic maps;
2. provided unequivocal field evidence for concurrent lava drainage back down the conduit during a fissure eruption;
3. showed that vent-proximal lava flow dynamics and drainage can control fissure segment localization;
4. provided the first in-depth textural classification of products from low fountaining, hawaiian style eruptions;
5. identified a mechanism whereby lavas can be disrupted to form vent-like structures and secondary spatter deposits;
6. developed a classification scheme, based on bubble number density, to distinguish between primary (magmatic vent derived) and secondary (disrupted lava) spatter;
7. outlined a robust framework, based on dimensional analysis, for correctly scaling analogue experiments to natural systems;
8. shown that a wide variety of fluid flow patterns are possible during dyke transport and can be predicted based upon the Grashof number (Gr), and
9. derived an empirical equation (Eqn. 5.3; $\mathrm{Re} = 0.0401\mathrm{Gr}^{0.767}$) and a semi-empirical equation (Eqn. 5.12; $Q_D^* = 0.481\mathrm{Gr}^{-0.233}$) that relate fissure system parameters (Gr) to the eruption rate and exchange flow organisation, respectively.

6.3 Future work

Although the work presented here has provided further insight into how basaltic fissure eruptions localize through time, it has also raised further questions. We know that "top-down" processes such as vent inundation and "bottom-up" processes such as flow organisation must act together to evolve the eruptive system. However, we do not know the relative importance of such processes, nor the vertical depth in the plumbing system where below which surface processes become irrelevant. A future direction for the volcanology community should be to develop a conduit scale model for basaltic fissure eruptions that considers the factors presented in this thesis and the wealth of previous work on structural and thermo-rheological controls (Bruce and Huppert, 1990, 1989; Delaney and Pollard, 1982; Helfrich, 1995; Ida, 1992; Lister and Dellar, 1996; Whitehead and Helfrich, 1991; Wylie et al., 1999; Wylie and Lister, 1995). Ultimately, a conduit scale model could be used to predict sites of long lived magma discharge which would better inform lava flow hazard maps and source parameters for ash and gas dispersion models.

The experiments presented in Chapters 4 & 5 were the first of their kind and thereby set up a new field of experimental work that could be investigated. For example, magmas are miscible liquids, unlike my experiments which used immiscible fluids. Therefore, performing a series of experiments using miscible fluids (e.g. glycerol and water) would better inform on dynamic processes such as crystal exchange, mafic recharge and magma mixing within a dyke. If miscible liquids were to be used the Gr, and therefore the Re would change during the course of an experiment. This is also true of natural eruptions, Gr and Re are not fixed, instead they will vary as a function of depth into the plumbing system and eruption duration. In natural eruptions I hypothesize that exchange flow initially at high Gr would support substantial mixing between the upwelling and

downwelling magmas, thereby reducing the driving density difference and reduce the Gr and Re of the convection system.

Furthermore, although pure silicate melts are Newtonian (e.g. Giordano et al., 2008; Giordano and Dingwell, 2003; Hess and Dingwell, 1996), in volcanic systems pure melts are rare, and magma is usually a multiphase suspension composed of a melt (liquid) phase that suspends bubbles (gas) and /or crystals (solid). The addition of bubbles and/or crystals changes the viscosity to give an apparent viscosity and a non-Newtonian rheology (Cimarelli et al., 2011; Llewellin et al., 2002; Mader et al., 2013; Truby et al., 2015). Given that convective processes in the subsurface plumbing system are thought to be driven by density variations introduced by differing volatile contents, a series of experiments investigating the exchange of shear-thinning (i.e. bubbly) liquids would prove extremely useful. I hypothesize that experiments using shear-thinning liquids would show progressive localization, in terms of better organized fingers, with increased experiment/eruption duration. Within an upwelling finger the shear rate will be spatially variable – the shear rate will be approximately zero at the finger's centre and at a maximum along its edges. Thus, when the fluid has a shear-thinning rheology the viscosity will be relatively low at the finger's edges and highest in its centre. The low viscosity fluid at the finger edge will act to "lubricate" the flow such that the finger becomes the locus of easy, preferential, upward transport. All other upwelling flow would be suppressed and migrate to the location(s) of least resistance (i.e. the developed fingers).

The experiments presented here use a slot with perfectly planar walls. This is an obvious simplification of the natural case; conduit walls are highly irregular with perturbations on a range of scales (Parcheta et al., 2015). We know that the conduit shape can affect the eruption dynamics (e.g. Ida, 1992; Mitchell, 2005) and exert feedbacks on the thermo-rheological localization processes previously described (e.g. Bruce and Huppert, 1989). It

would therefore be useful to perform experiments with rough walls. Although scaling these experiments to the natural case would be challenging. With the recent advances in 3D printing, it may be possible to insert a printed geometry, taken from a natural conduit dataset (e.g. Parcheta et al., 2016), into an existing analogue tank set-up.

Lastly, to expand the range of parameter space investigated numerical models could be performed, benchmarked by the experiments in this thesis. This would allow for the investigation of scenarios which are experimentally demanding, or impossible (e.g. independently changing the density contrast without changing the fluid viscosity).

Bibliography

Allard, P., Baxter, P., Halbwachs, M., Komorowski, J.-C., 2002. The January 2002 eruption of Nyiragongo volcano (Dem. Repub. Congo) and related hazards: observations and recommendations. Final Report of the French-British Team: submitted to the Minsitry of Foreign Affairs, Paris, France, Foreign Office, London, United Kingdom and respective Embassies in Democratic Rebublic of Congo and Republic of Rwanda, p. 24.

Allard, P., Carbonnelle, J., Metrich, N., Loyer, H., Zettwoog, P., 1994. Sulphur output and magma degassing budget of Stromboli volcano. Nature 368, 326–330.

Alparone, S., Andronico, D., Lodato, L., Sgroi, T., 2003. Relationship between tremor and volcanic activity during the Southeast Crater eruption on Mount Etna in early 2000. J. Geophys. Res. Solid Earth 108 (B5), 2241– 2245. doi:10.1029/2002JB001866

Bai, L., Baker, D.R., Polacci, M., Hill, R.J., 2011. In-situ degassing study on crystal-bearing Stromboli basaltic magmas: Implications for Stromboli explosions. Geophys. Res. Lett. 38 (17). doi:10.1029/2011GL048540

Becerril, L., Cappello, A., Galindo, I., Neri, M., Del Negro, C., 2013. Spatial probability distribution of future volcanic eruptions at El Hierro Island (Canary Islands, Spain). J. Volcanol. Geotherm. Res. 257, 21–30. doi:10.1016/j.jvolgeores.2013.03.005

Beckett, F.M., Mader, H.M., Phillips, J.C., Rust, A.C., Witham, F., 2011. An experimental study of low-Reynolds-number exchange flow of two Newtonian fluids in a vertical pipe. J. Fluid Mech. 682, 652–670.

Bertrand, J., 1878. Sur l'homogénéité dans les formules de physique. Comptes rendus 86, 916–920.

Blake, S., Bruno, B.C., 2000. Modelling the emplacement of compound lava flows. Earth Planet. Sci. Lett. 184, 181–197.

Bonali, F.L., Corazzato, C., Tibaldi, A., 2011. Identifying rift zones on volcanoes: an example from La Réunion island, Indian Ocean. Bull. Volcanol. 73, 347–366. doi:10.1007/s00445-010-0416-1

Bratsun, D.A., Zyuzgin, A. V, Putin, G.F., 2003. Non-linear dynamics and pattern formation in a vertical fluid layer heated from the side. Int. J. heat fluid flow 24, 835–852.

Breyiannis, G., Varoutis, S., Valougeorgis, D., 2008. Rarefied gas flow in concentric annular tube: Estimation of the Poiseuille number and the exact hydraulic diameter. Eur. J. Mech. B/Fluids 27, 609–622. doi:10.1016/j.euromechflu.2007.10.002

Brown, R.J., Manya, S., Buisman, I., Fontana, G., Field, M., Mac Niocaill, C., Sparks, R.S.J., Stuart, F.M., 2012. Eruption of kimberlite magmas: physical volcanology, geomorphology and age of the youngest kimberlitic volcanoes known on earth (the Upper Pleistocene/Holocene Igwisi Hills volcanoes, Tanzania). Bull. Volcanol. 74, 1621–1643.

Brown, R.J., Thordarson, T., Self, S., Blake, S., 2015. Disruption of tephra fall deposits caused by lava flows during basaltic eruptions. Bull. Volcanol. 77 (90). doi:10.1007/s00445-015-0974-3

Bruce, P.M., Huppert, H.E., 1990. Solidification and melting along dykes by the laminar flow of basaltic magma, in: Ryan MP (Ed) Magma Transport and Storage. Wiley, Hoboken pp. 87–101.

Bruce, P.M., Huppert, H.E., 1989. Thermal control of basaltic fissure eruptions. Nature 342, 665–667.

Buckingham, E., 1914. On physically similar systems; illustrations of the use of dimensional equations. Phys. Rev. 4, 345-376. doi: 10.1029/TC004i007p00705

Burton, M.R., Mader, H.M., Polacci, M., 2007. The role of gas percolation in quiescent degassing of persistently active basaltic volcanoes. Earth Planet. Sci. Lett. 264, 46–60. doi:10.1016/j.epsl.2007.08.028

Capaccioni, B., Cuccoli, F., 2005. Spatter and welded air fall deposits generated by fire-

fountaining eruptions: cooling of pyroclasts during transport and deposition. J. Volcanol. Geotherm. Res. 145, 263–280.

Cappello, A., Neri, M., Acocella, V., Gallo, G., Vicari, A., Del Negro, C., 2012. Spatial vent opening probability map of Etna volcano (Sicily, Italy). Bull. Volcanol. 74, 2083–2094. doi:10.1007/s00445-012-0647-4

Cashman, K. V, Kauahikaua, J.P., 1997. Reevaluation of vesicle distributions in basaltic lava flows. Geology 25, 419–422.

Cashman, K. V, Mangan, M.T., 1994. Physical aspects of magmatic degassing; II, Constraints on vesiculation processes from textural studies of eruptive products. Rev. Mineral. Geochemistry 30, 447–478.

Chouet, B., Dawson, P., Martini, M., 2008. Shallow-conduit dynamics at Stromboli Volcano, Italy, imaged from waveform inversions. Geol. Soc. London, Spec. Publ. 307, 57–84.

Chouet, B., Dawson, P., Ohminato, T., Martini, M., Saccorotti, G., Giudicepietro, F., De Luca, G., Milana, G., Scarpa, R., 2003. Source mechanisms of explosions at Stromboli Volcano, Italy, determined from moment-tensor inversions of very-long-period data. J. Geophys. Res. Solid Earth 108 (B1). doi:10.1029/2002JB001919

Churchill, S.W., 1988. Chapter 1 - Identification of Geometries and Dimensionless Variables, in: Brenner, H. (Ed.) Viscous flows: the practical use of theory. Butterworth-Heinemann, Boston, pp. 3–16. doi:10.1016/B978-0-409-95185-1.50009-7

Cimarelli, C., Costa, A., Mueller, S., Mader, H.M., 2011. Rheology of magmas with bimodal crystal size and shape distributions: Insights from analog experiments. Geochemistry, Geophys. Geosystems 12 (7). doi:10.1029/2011GC003606.

Damean, N., Regtien, P.P.L., 2001. Poiseuille number for the fully developed laminar fow through hexagonal ducts etched in <1 0 0> silicon. Sensors Actuators A Phys. 90, 96–101.

Del Bello, E., Lane, S.J., James, M.R., Llewellin, E.W., Taddeucci, J., Scarlato, P.,

Capponi, A., 2015. Viscous plugging can enhance and modulate explosivity of strombolian eruptions. Earth Planet. Sci. Lett. 423, 210–218.

Del Bello, E., Llewellin, E.W., Taddeucci, J., Scarlato, P., Lane, S.J., 2012. An analytical model for gas overpressure in slug-driven explosions: Insights into Strombolian volcanic eruptions. J. Geophys. Res. Solid Earth 117 (B2). doi:10.1029/2011JB008747

Delaney, P.T., Pollard, D.D., 1982. Solidification of basaltic magma during flow in a dike. Am. J. Sci. 282, 856–885.

Delaney, P.T., Pollard, D.D., 1981. Deformation of host rocks and flow of magma during growth of minette dikes and breccia-bearing intrusions near Ship Rock, New Mexico, US Geological Survey professional paper 1202.

Dingwell, D.B., Romano, C., Hess, K.-U., 1996. The effect of water on the viscosity of a haplogranitic melt under PTX conditions relevant to silicic volcanism. Contrib. to Mineral. Petrol. 124, 19–28.

Duffield, W.A., 1990. Eruptive fountains of silicic magma and their possible effects on the tin content of fountain-fed lavas, Taylor Creek Rhyolite, New Mexico. Geol. Soc. Am. Spec. Pap. 246, 251–262.

Dutkowski, K., 2008. Experimental investigations of Poiseuille number laminar flow of water and air in minichannels. Int. J. Heat Mass Transf. 51, 5983–5990. doi:10.1016/j.ijheatmasstransfer.2008.04.070

Edmonds, M., Gerlach, T.M., 2007. Vapor segregation and loss in basaltic melts. Geology 35, 751–754.

Finch, R.H., 1931. Lava tree casts and tree molds. Volc Lett 316, 1–3.

Fisher, L.R., Mitchell, E.E., Parker, N.S., 1985. Interfacial tensions of commercial vegetable oils with water. J. Food Sci. 50, 1201–1202.

Francis, P., Oppenheimer, C., Stevenson, D., 1993. Endogenous growth of persistently active volcanoes. Nature 366, 554–557.

Franke, R., 1982. Smooth interpolation of scattered data by local thin plate splines.

Comput. Math. with Appl. 8, 273–281.

Friedman, I., Long, W., Smith, R.L., 1963. Viscosity and water content of rhyolite glass. J. Geophys. Res. 68, 6523–6535.

Galindo, I., Gudmundsson, A., 2012. Basaltic feeder dykes in rift zones: geometry, emplacement, and effusion rates. Nat. Hazards Earth Syst. Sci. 12, 3683–3700.

Gaonkar, A.G., 1989. Interfacial tensions of vegetable oil/water systems: effect of oil purification. J. Am. Oil Chem. Soc. 66, 1090–1092.

Gardner, J.E., Thomas, R.M.E., Jaupart, C., Tait, S., 1996. Fragmentation of magma during Plinian volcanic eruptions. Bull. Volcanol. 58, 144–162.

Geshi, N., Neri, M., 2014. Dynamic feeder dyke systems in basaltic volcanoes: the exceptional example of the 1809 Etna eruption (Italy). Front. Earth Sci. 2, 1–13. doi:10.3389/feart.2014.00013

Giordano, D., Dingwell, D., 2003. Viscosity of hydrous Etna basalt: implications for Plinian-style basaltic eruptions. Bull. Volcanol. 65, 8–14.

Giordano, D., Romano, C., Dingwell, D.B., Poe, B., Behrens, H., 2004. The combined effects of water and fluorine on the viscosity of silicic magmas. Geochim. Cosmochim. Acta 68, 5159–5168.

Giordano, D., Russell, J.K., Dingwell, D.B., 2008. Viscosity of magmatic liquids: a model. Earth Planet. Sci. Lett. 271, 123–134.

Gonnermann, H.M., Houghton, B.F., 2012. Magma degassing during the Plinian eruption of Novarupta, Alaska, 1912. Geochemistry, Geophys. Geosystems 13, Q10009. doi:10.1029/2012GC004273.

Gudmundsson, A., 1987. Tectonics of the Thingvellir fissure swarm, SW Iceland. J. Struct. Geol. 9, 61–69. doi:10.1016/0191-8141(87)90044-7

Gudmundsson, M.T., Höskuldsson, A., Larsen, G., Thordarson, T., Oladottir, B.A., Oddsson, B., Gudnason, J., Högnadottir, T., Stevenson, J.A., Houghton, B.F., McGarvie, D., Sigurdardottir, G.M., 2012. The may 2011 eruption of Grimsvötn, in: EGU General Assembly Conference Abstracts. 14, p. 12119.

Gudmundsson, M.T., Pedersen, R., Vogfjörd, K., Thorbjarnardóttir, B., Jakobsdóttir, S., Roberts, M.J., 2010. Eruptions of Eyjafjallajökull Volcano, Iceland. Eos, Trans. Am. Geophys. Union 91, 190–191.

Hamilton, C.W., Thordarson, T., Fagents, S.A., 2010. Explosive lava--water interactions I: architecture and emplacement chronology of volcanic rootless cone groups in the 1783-1784 Laki lava flow, Iceland. Bull. Volcanol. 72, 449–467.

Harris, A.J.L., Stevenson, D.S., 1997. Magma budgets and steady-state activity of Vulcano and Stromboli. Geophys. Res. Lett. 24, 1043–1046.

Head, J.W., Wilson, L., 1989. Basaltic pyroclastic eruptions: influence of gas-release patterns and volume fluxes on fountain structure, and the formation of cinder cones, spatter cones, rootless flows, lava ponds and lava flows. J. Volcanol. Geotherm. Res. 37, 261–271.

Head, J.W., Wilson, L., 1987. Lava fountain heights at Pu'u'O'o, Kilauea, Hawaii: Indicators of amount and variations of exsolved magma volatiles. J. Geophys. Res. Solid Earth 92, 13715–13719.

Helfrich, K.R., 1995. Thermo-viscous fingering of flow in a thin gap: a model of magma flow in dikes and fissures. J. Fluid Mech. 305, 219–238.

Heliker, C., Swanson, D.A., Takahashi, T.J., 2003. The Pu'u'O'o-Kupaianaha Eruption of Kilauea Volcano, Hawai'i: The First 20 Years. US Geological Survey professional paper 1676.

Hess, K.U., Dingwell, D.B., 1996. Viscosities of hydrous leucogranitic melts: A non-Arrhenian model. Am. Mineral. 81, 1297–1300.

Hong, C., Asako, Y., Lee, J.H., 2008. Poiseuille number correlation for high speed micro-flows. J. Phys. D. Appl. Phys. 41, 105111. doi:10.1088/0022-3727/41/10/105111

Houghton, B.F., Taddeucci, J., Andronico, D., Gonnermann, H.M., Pistolesi, M., Patrick, M.R., Orr, T.R., Swanson, D.A., Edmonds, M., Gaudin, D., Carey, R.J., Scarlato, P., 2016. Stronger or longer: Discriminating between Hawaiian and Strombolian eruption styles. Geology 44, 163–166.

Houghton, B.F., Wilson, C.J.N., 1989. A vesicularity index for pyroclastic deposits. Bull. Volcanol. 51, 451–462.

Houghton, B.F., Wilson, C.J.N., Del Carlo, P., Coltelli, M., Sable, J.E., Carey, R., 2004. The influence of conduit processes on changes in style of basaltic Plinian eruptions: Tarawera 1886 and Etna 122 BC. J. Volcanol. Geotherm. Res. 137, 1–14.

Huang, C.C., Lin, T.F., 1994. Buoyancy induced flow transition in mixed convective flow of air through a bottom heated horizontal rectangular duct. Int. J. Heat Mass Transf. 37, 1235–1255.

Huppert, H.E., Hallworth, M.A., 2007. Bi-directional flows in constrained systems. J. Fluid Mech. 578, 95–112.

Ida, Y., 1992. Width change of a planar magma path: implication for the evolution and style of volcanic eruptions. Phys. earth Planet. Inter. 74, 127–138.

Ilyinskaya, E., Schmidt, A., Mather, T.A., Pope, F.D., Witham, C., Baxter, P., Jóhannsson, T., Pfeffer, M., Barsotti, S., Singh, A., others, 2017. Understanding the environmental impacts of large fissure eruptions: Aerosol and gas emissions from the 2014-2015 Holuhraun eruption (Iceland). Earth Planet. Sci. Lett. 472, 309–322.

Janebo, M.H., Houghton, B.F., Thordarson, T., Larsen, G., 2016. Shallow conduit processes during the ad 1158 explosive eruption of Hekla volcano, Iceland. Bull. Volcanol. 10, 1–17.

Jin, Y.Y., Chen, C.F., 1996. Natural convection of high Prandtl number fluids with variable viscosity in a vertical slot. Int. J. Heat Mass Transf. 39, 2663–2670.

Jones, T.J., Llewellin, E.W., Houghton, B.F., Brown, R.J., Vye-Brown, C., 2017. Proximal lava drainage controls on basaltic fissure eruption dynamics. Bull. Volcanol. 79 (81). doi:10.1007/s00445-017-1164-2

Karhunen, R., 1988. Eruption mechanism and rheomorphism during the basaltic fissure eruption in Biskupsfell, Kverkfjöll, north-central Iceland. Lic Phil. Dissertation Abo Akademi, Finland (Thesis published by Nordic Volcanological Institute, Iceland, Report 8802).

Kazahaya, K., Shinohara, H., Saito, G., 1994. Excessive degassing of Izu-Oshima volcano: magma convection in a conduit. Bull. Volcanol. 56, 207–216.

Keating, G.N., Valentine, G.A., Krier, D.J., Perry, F. V., 2008. Shallow plumbing systems for small-volume basaltic volcanoes. Bull. Volcanol. 70, 563–582. doi:10.1007/s00445-007-0154-1

Klug, C., Cashman, K., Bacon, C., 2002. Structure and physical characteristics of pumice from the climactic eruption of Mount Mazama (Crater Lake), Oregon. Bull. Volcanol. 64, 486–501.

Klug, C., Cashman, K. V, 1994. Vesiculation of May 18, 1980, Mount St. Helens magma. Geology 22, 468–472.

Koyaguchi, T., Blake, S., 1989. The dynamics of magma mixing in a rising magma batch. Bull. Volcanol. 52, 127–137. doi:10.1007/BF00301552

Landi, P., Métrich, N., Bertagnini, A., Rosi, M., 2004. Dynamics of magma mixing and degassing recorded in plagioclase at Stromboli (Aeolian Archipelago, Italy). Contrib. to Mineral. Petrol. 147, 213–227. doi:10.1007/s00410-004-0555-5

Lange, R.A., Carmichael, I.S.E., 1987. Densities of Na_2O-K_2O-MgO-MgO-FeO-Fe_2O_3-Al_3O_3-TiO_2-SiO_2 liquids: New measurements and derived partial molar properties. Geochim. Cosmochim. Acta 51, 2931–2946.

Lange, R.L., Carmichael, I.S.E., 1990. Thermodynamic properties of silicate liquids with emphasis on density, thermal expansion and compressibility. Rev. Mineral. Geochemistry 24, 25–64.

Lara, L.E., Moreno, H., Naranjo, J.A., Matthews, S., de Arce, C.P., 2006. Magmatic evolution of the Puyehue--Cordón Caulle Volcanic Complex (40 S), Southern Andean Volcanic Zone: from shield to unusual rhyolitic fissure volcanism. J. Volcanol. Geotherm. Res. 157, 343–366.

Lautze, N.C., Houghton, B.F., 2007. Linking variable explosion style and magma textures during 2002 at Stromboli volcano, Italy. Bull. Volcanol. 69, 445–460.

Lautze, N.C., Houghton, B.F., 2005. Physical mingling of magma and complex eruption

dynamics in the shallow conduit at Stromboli volcano, Italy. Geology 33, 425–428.

Lefebvre, N.S., White, J.D.L., Kjarsgaard, B.A., 2012. Spatter-dike reveals subterranean magma diversions: Consequences for small multivent basaltic eruptions. Geology 40, 423–426.

Lesher, C.E., Spera, F.J., 2015. Chapter 5 - Thermodynamic and Transport Properties of Silicate Melts and Magma, in: Sigurdsson, H. (Ed.), The Encyclopedia of Volcanoes (Second Edition). Academic Press, Amsterdam, pp. 113–141. doi:10.1016/B978-0-12-385938-9.00005-5

Lister, J.R., Dellar, P.J., 1996. Solidification of pressure-driven flow in a finite rigid channel with application to volcanic eruptions. J. Fluid Mech. 323, 267–283.

Llewellin, E.W., Del Bello, E., Taddeucci, J., Scarlato, P., Lane, S.J., 2011. The thickness of the falling film of liquid around a Taylor bubble. Proc. R. Soc. A. 468, 1041–1064.

Llewellin, E.W., Mader, H.M., Wilson, S.D.R., 2002a. The constitutive equation and flow dynamics of bubbly magmas. Geophys. Res. Lett. 29 (24), 2170. doi:10.1029/2002GL015697

Llewellin, E.W., Mader, H.M., Wilson, S.D.R., 2002b. The rheology of a bubbly liquid. Proc. R. Soc. A. 458, 987–1016.

Lockwood, J.P., Lipman, P.W., 1980. Recovery of datable charcoal beneath young lavas: lessons from Hawaii. Bull. Volcanol. 43, 609–615.

Lockwood, J.P., Williams, I.S., 1978. Lava trees and tree moulds as indicators of lava flow direction. Geol. Mag. 115, 69–74.

Lundgren, P., Poland, M., Miklius, A., Orr, T., Yun, S.-H., Fielding, E., Liu, Z., Tanaka, A., Szeliga, W., Hensley, S., Owen, S., 2013. Evolution of dike opening during the March 2011 Kamoamoa fissure eruption, Kīlauea Volcano, Hawai`i. J. Geophys. Res. Solid Earth 118, 897–914. doi:10.1002/jgrb.50108

Mader, H.M., Llewellin, E.W., Mueller, S.P., 2013. The rheology of two-phase magmas: A review and analysis. J. Volcanol. Geotherm. Res. 257, 135–158.

Mangan, M.T., Cashman, K. V, 1996. The structure of basaltic scoria and reticulite and inferences for vesiculation, foam formation, and fragmentation in lava fountains. J. Volcanol. Geotherm. Res. 73, 1–18.

Mangan, M.T., Cashman, K. V, Newman, S., 1993. Vesiculation of basaltic magma during eruption. Geology 21, 157–160.

Merle, O., 2015. The scaling of experiments on volcanic systems. Front. Earth Sci. 3, 1–26. doi:10.3389/feart.2015.00026.

Merle, O., Borgia, A., 1996. Scaled experiments of volcanic spreading. J. Geophys. Res. Solid Earth 101, 13805–13817.

Mitáš, L., Mitášová, H., 1988. General variational approach to the interpolation problem. Comput. Math. with Appl. 16, 983–992.

Mitchell, K.L., 2005. Coupled conduit flow and shape in explosive volcanic eruptions. J. Volcanol. Geotherm. Res. 143, 187–203.

Moore, J.G., 1970. Water content of basalt erupted on the ocean floor. Contrib. to Mineral. Petrol. 28, 272–279.

Moore, J.G., Ault, W.U., 1965. Historic littoral cones in Hawaii. Pacific Sci. 19, 8–11.

Moore, J.G., Krivoy, H.L., 1964. The 1962 flank eruption of Kilauea Volcano and structure of the east rift zone. J. Geophys. Res. 69, 2033–2045.

Moore, J.G., Richter, D.H., 1962. Lava tree molds of the September 1961 eruption, Kilauea Volcano, Hawaii. Geol. Soc. Am. Bull. 73, 1153–1158.

Murase, T., McBirney, A.R., 1973. Properties of some common igneous rocks and their melts at high temperatures. Geol. Soc. Am. Bull. 84, 3563–3592.

Nandakumar, K., Masliyah, J.H., Law, H.-S., 1985. Bifurcation in steady laminar mixed convection flow in horizontal ducts. J. Fluid Mech. 152, 145–161.

Neri, M., Acocella, V., Behncke, B., Giammanco, S., Mazzarini, F., Rust, D., 2011. Structural analysis of the eruptive fissures at Mount Etna (Italy). Ann. Geophys. 54 (5), 464–479. doi:10.4401/ag-5332

Opheim, J.A., Gudmundsson, A., 1989. Formation and geometry of fractures, and related

volcanism, of the Krafla fissure swarm, northeast Iceland. Geol. Soc. Am. Bull. 101, 1608–1622. doi:10.1130/0016-7606(1989)101<1608:FAGOFA>2.3.CO;2

Oppenheimer, C., Francis, P., 1997. Remote sensing of heat, lava and fumarole emissions from Erta'Ale volcano, Ethiopia. Int. J. Remote Sens. 18, 1661–1692.

Oppenheimer, C., Kyle, P.R., 2008. Probing the magma plumbing of Erebus volcano, Antarctica, by open-path FTIR spectroscopy of gas emissions. J. Volcanol. Geotherm. Res. 177, 743–754.

Oppenheimer, C., McGonigle, A.J.S., Allard, P., Wooster, M.J., Tsanev, V., 2004. Sulfur, heat, and magma budget of Erta 'Ale lava lake, Ethiopia. Geology 32, 509–512.

Orr, T.R., Poland, M.P., Patrick, M.R., Thelen, W.A., Sutton, A.J., Elias, T., Thornber, C.R., Parcheta, C., Wooten, K.M., 2015. Kilauea's 5–9 March 2011 Kamoamoa fissure eruption and its relation to 30+ years of activity from Pu'u "O"o, in: Carey R, Poland M, Cayol V, Weis D (eds) Hawaiian Volcanoes: From Source to Surface, American Geophysical Union geophysical monograph, vol 208. John Wiley & Sons (2015), pp. 393–402.

Palma, J.L., Blake, S., Calder, E.S., 2011. Constraints on the rates of degassing and convection in basaltic open-vent volcanoes. Geochemistry, Geophys. Geosystems 12 (11). doi:10.1029/2011GC003715

Palma, J.L., Calder, E.S., Basualto, D., Blake, S., Rothery, D.A., 2008. Correlations between SO2 flux, seismicity, and outgassing activity at the open vent of Villarrica volcano, Chile. J. Geophys. Res. Solid Earth 113 (B10). doi:10.1029/2008JB005577

Parcheta, C., Fagents, S., Swanson, D.A., Houghton, B.F., Ericksen, T., 2015. Hawaiian Fissure Fountains: Quantifying Vent and Shallow Conduit Geometry, Episode1 of the 1969--1974 Mauna Ulu Eruption, in: Carey R, Poland M, Cayol V, Weis D (eds) Hawaiian Volcanoes: From Source to Surface, American Geophysical Union geophysical monograph, vol 208. John Wiley & Sons (2015), pp. 369–391.

Parcheta, C.E., Houghton, B.F., Swanson, D.A., 2013. Contrasting patterns of vesiculation in low, intermediate, and high Hawaiian fountains: a case study of the

1969 Mauna Ulu eruption. J. Volcanol. Geotherm. Res. 255, 79–89.

Parcheta, C.E., Houghton, B.F., Swanson, D.A., 2012. Hawaiian fissure fountains 1: decoding deposits—episode 1 of the 1969–1974 Mauna Ulu eruption. Bull. Volcanol. 74, 1729–1743.

Parcheta, C.E., Pavlov, C.A., Wiltsie, N., Carpenter, K.C., Nash, J., Parness, A., Mitchell, K.L., 2016. A robotic approach to mapping post-eruptive volcanic fissure conduits. J. Volcanol. Geotherm. Res. 320, 19–28.

Parfitt, E.A., Wilson, L., Neal, C.A., 1995. Factors influencing the height of Hawaiian lava fountains: implications for the use of fountain height as an indicator of magma gas content. Bull. Volcanol. 57, 440–450.

Patrick, M.R., Anderson, K.R., Poland, M.P., Orr, T.R., Swanson, D.A., 2015. Lava lake level as a gauge of magma reservoir pressure and eruptive hazard. Geology 43, 831–834.

Pedersen, G.B.M., Höskuldsson, A., Dürig, T., Thordarson, T., Jónsdóttir, I., Riishuus, M.S., Óskarsson, B. V, Dumont, S., Magnusson, E., Gudmundsson, M.T., others, 2017. Lava field evolution and emplacement dynamics of the 2014-2015 basaltic fissure eruption at Holuhraun, Iceland. J. Volcanol. Geotherm. Res. 340, 155–169.

Philpotts, A.R., Philpotts, D.E., 2007. Upward and downward flow in a camptonite dike as recorded by deformed vesicles and the anisotropy of magnetic susceptibility (AMS). J. Volcanol. Geotherm. Res. 161, 81–94. doi:10.1016/j.jvolgeores.2006.11.006

Polacci, M., Pioli, L., Rosi, M., 2003. The Plinian phase of the Campanian Ignimbrite eruption (Phlegrean Fields, Italy): evidence from density measurements and textural characterization of pumice. Bull. Volcanol. 65, 418–432.

Poland, M., Orr, T.R., Kauahikaua, J.P., Brantley, S.R., Babb, J.L., Patrick, M.R., Neal, C.A., Anderson, K.R., Antolik, L., Burgess, M., others, 2016. The 2014--2015 Pahoa lava flow crisis at Kilauea Volcano, Hawai'i: Disaster avoided and lessons learned. GSA Today 26, 4–10.

Proussevitch, A.A., Sahagian, D.L., 1998. Dynamics and energetics of bubble growth in magmas: analytical formulation and numerical modeling. J. Geophys. Res. Solid Earth 103, 18223–18251.

Quane, S.L., Russell, J.K., Friedlander, E.A., 2009. Time scales of compaction in volcanic systems. Geology 37, 471–474.

Rader, E., Geist, D., 2015. Eruption conditions of spatter deposits. J. Volcanol. Geotherm. Res. 304, 287–293.

Reynolds, O., 1884. XXIX. An experimental investigation of the circumstances which determine whether the motion of water shall he direct or sinuous, and of the law of resistance in parallel channels. Philos. Trans. R. Soc. London 174, 935–982.

Reynolds, P., Brown, R.J., Thordarson, T., Llewellin, E.W., Fielding, K., 2015. Rootless cone eruption processes informed by dissected tephra deposits and conduits. Bull. Volcanol. 77 (72). doi:10.1007/s00445-015-0958-3

Rhodes, J.M., 1988. Geochemistry of the 1984 Mauna Loa eruption: implications for magma storage and supply. J. Geophys. Res. Solid Earth 93, 4453–4466.

Richter, D.H., Eaton, J.P., Murata, K.J., Ault, W.U., Krivoy, H.L., 1970. Chronological narrative of the 1959-60 eruption of Kilauea volcano, Hawaii. US Geological Survey professional paper 537.

Rust, A.C., Manga, M., 2002. Effects of bubble deformation on the viscosity of dilute suspensions. J. Nonnewton. Fluid Mech. 104, 53–63.

Sable, J.E., Houghton, B.F., Del Carlo, P., Coltelli, M., 2006. Changing conditions of magma ascent and fragmentation during the Etna 122 BC basaltic Plinian eruption: Evidence from clast microtextures. J. Volcanol. Geotherm. Res. 158, 333–354.

Sahagian, D., 1985. Bubble migration and coalescence during the solidification of basaltic lava flows. J. Geol. 93, 205–211.

Scandone, R., Cashman, K. V., Malone, S.D., 2007. Magma supply, magma ascent and the style of volcanic eruptions. Earth Planet. Sci. Lett. 253, 513–529. doi:10.1016/j.epsl.2006.11.016

Scandone, R., Malone, S.D., 1985. Magma supply, magma discharge and readjustment of the feeding system of Mount St. Helens during 1980. J. Volcanol. Geotherm. Res. 23, 239–262.

Schmidt, A., Ostro, B., Carslaw, K.S., Wilson, M., Thordarson, T., Mann, G.W., Simmons, A.J., 2011. Excess mortality in Europe following a future Laki-style Icelandic eruption. Proc. Natl. Acad. Sci. 108, 15710–15715.

Schumann, U., Weinzierl, B., Reitebuch, O., Schlager, H., Minikin, A., Forster, C., Baumann, R., Sailer, T., Graf, K., Mannstein, H., others, 2011. Airborne observations of the Eyjafjalla volcano ash cloud over Europe during air space closure in April and May 2010. Atmos. Chem. Phys. 11, 2245–2279.

Sharp, D.H., 1984. An overview of Rayleigh-Taylor instability. Phys. D Nonlinear Phenom. 12, 3–18.

Shaw, H.R., Wright, T.L., Peck, D.L., Okamura, R., 1968. The viscosity of basaltic magma; an analysis of field measurements in Makaopuhi lava lake, Hawaii. Am. J. Sci. 266, 225–264.

Shea, T., Houghton, B.F., Gurioli, L., Cashman, K. V, Hammer, J.E., Hobden, B.J., 2010. Textural studies of vesicles in volcanic rocks: an integrated methodology. J. Volcanol. Geotherm. Res. 190, 271–289.

Sigurdsson, H., 2000. Volcanic episodes and rates of volcanism, in: Sigurduson H, Houghton B, Rymer H, Stix J, McNutt, S (eds) Encyclopedia of Volcanoes (1st Ed.). Academic Press San Diego, CA, pp. 271–279.

Sparks, R.S.J., 1978. The dynamics of bubble formation and growth in magmas: A review and analysis. J. Volcanol. Geotherm. Res. 3, 1–37. doi:10.1016/0377-0273(78)90002-1

Spera, F.J., 2000. Physical properties of magma, in: Sigurduson H, Houghton B, Rymer H, Stix J, McNutt, S (eds) Encyclopedia of Volcanoes (1st Ed.). Academic Press San Diego, CA, pp. 171–190.

Stefánsson, A., Stefánsson, G., Keller, N.S., Barsotti, S., Sigurdsson, Á., Thorláksdóttir,

S.B., Pfeffer, M.A., Eir'\iksdóttir, E.S., Jónasdóttir, E.B., Löwis, S., others, 2017. Major impact of volcanic gases on the chemical composition of precipitation in Iceland during the 2014--2015 Holuhraun eruption. J. Geophys. Res. Atmos. 122, 1971–1982.

Stevenson, D.S., Blake, S., 1998. Modelling the dynamics and thermodynamics of volcanic degassing. Bull. Volcanol. 60, 307–317.

Stohl, A., Prata, A.J., Eckhardt, S., Clarisse, L., Durant, A., Henne, S., Kristiansen, N.I., Minikin, A., Schumann, U., Seibert, P., others, 2011. Determination of time-and height-resolved volcanic ash emissions and their use for quantitative ash dispersion modeling: the 2010 Eyjafjallajökull eruption. Atmos. Chem. Phys. 11, 4333–4351.

Stothers, R.B., Wolff, J.A., Self, S., Rampino, M.R., 1986. Basaltic fissure eruptions, plume heights, and atmospheric aerosols. Geophys. Res. Lett. 13, 725–728.

Stovall, W.K., Houghton, B.F., Gonnermann, H., Fagents, S.A., Swanson, D.A., 2011. Eruption dynamics of Hawaiian-style fountains: the case study of episode 1 of the Kilauea Iki 1959 eruption. Bull. Volcanol. 73, 511–529.

Stovall, W.K., Houghton, B.F., Hammer, J.E., Fagents, S.A., Swanson, D.A., 2012. Vesiculation of high fountaining Hawaiian eruptions: episodes 15 and 16 of 1959 Kilauea Iki. Bull. Volcanol. 74, 441–455.

Stovall, W.K., Houghton, B.F., Harris, A.J.L., Swanson, D.A., 2009. Features of lava lake filling and draining and their implications for eruption dynamics. Bull. Volcanol. 71, 767–780.

Sumner, J.M., 1998. Formation of clastogenic lava flows during fissure eruption and scoria cone collapse: the 1986 eruption of Izu-Oshima Volcano, eastern Japan. Bull. Volcanol. 60, 195–212.

Sumner, J.M., Blake, S., Matela, R.J., Wolff, J.A., 2005. Spatter. J. Volcanol. Geotherm. Res. 142, 49–65.

Sveinbjörnsson, M., 2001. Volcanic eruptions in Iceland: potential hazards and aviation safety. Unpubl. MSc thesis, University of Iceland p. 71.

Swanson, D.A., 1973. Pahoehoe Flows from the 1969–1971 Mauna Ulu Eruption, Kilauea Volcano, Hawaii. GSA Bull. 84, 615–626.

Swanson, D.A., Duffield, W.A., Jackson, D.B., Peterson, D.W., 1979. Chronological narrative of the 1969-71 Mauna Ulu eruption of Kilauea Volcano, Hawaii, US Geological Survey professional paper 1056.

Swanson, D.A., Fabbi, B.P., 1973. Loss of volatiles during fountaining and flowage of basaltic lava at Kilauea volcano, Hawaii. J. Res. US Geol. Surv 1, 649–658.

Tesche, M., Glantz, P., Johansson, C., Norman, M., Hiebsch, A., Ansmann, A., Althausen, D., Engelmann, R., Seifert, P., 2012. Volcanic ash over Scandinavia originating from the Grimsvötn eruptions in May 2011. J. Geophys. Res. Atmos. 117 (D9). doi:10.1029/2011JD017090

Thorarinsson, S., 1953. The crater groups in Iceland. Bull. Volcanol. 14, 3–44.

Thorarinsson, S., Sigvaldason, G.E., 1962. The eruption in Askja, 1961; a preliminary report. Am. J. Sci. 260, 641–651.

Thorarinsson, S., Steinthorsson, S., Einarsson, T., Kristmannsdottir, H., Oskarsson, N., 1973. The eruption on Heimaey, Iceland. Nature 241, 372–375.

Thordarson, T., Miller, D.J., Larsen, G., Self, S., Sigurdsson, H., 2001. New estimates of sulfur degassing and atmospheric mass-loading by the 934 AD Eldgjá eruption, Iceland. J. Volcanol. Geotherm. Res. 108, 33–54.

Thordarson, T., Self, S., 2003. Atmospheric and environmental effects of the 1783--1784 Laki eruption: A review and reassessment. J. Geophys. Res. Atmos. 108 (D1). doi:10.1029/2001JD002042

Thordarson, T., Self, S., 1998. The Roza Member, Columbia River Basalt Group: A gigantic pahoehoe lava flow field formed by endogenous processes? J. Geophys. Res. Solid Earth 103, 27411–27445.

Thornber, C., Keszthelyi, L., Lewis-Kenedi, C., Cazeneuve, M., Goehring, D., 2004. Drilling an Active Pahoehoe Lava Flow, in: AGU Fall Meeting Abstracts. Abstr. V31D-09.

Tibaldi, A., 1995. Morphology of pyroclastic cones and tectonics. J. Geophys. Res. Solid Earth 100, 24521–24535.

Tilling, R.., Christian, R.., Duffield, W.A., Endo, E.., Holcomb, R.., Koyanagi, R.., Peterson, D.W., Unger, J.D., 1987. The 1972-1974 Mauna Ulu eruption, Kilauea Volcano: An example of quasi steady-state magma transfer. US Geological Survey professional paper 1350, 405–469.

Toramaru, A., 1995. Numerical study of nucleation and growth of bubbles in viscous magmas. J. Geophys. Res. Solid Earth 100, 1913–1931.

Truby, J.M., Mueller, S.P., Llewellin, E.W., Mader, H.M., 2015. The rheology of three-phase suspensions at low bubble capillary number. Proc. R. Soc. A. 471 (20140557). doi:10.1098/rspa.2014.0557

Turbeville, B.N., 1992. Tephra fountaining, rheomorphism, and spatter flow during emplacement of the Pitigliano Tuffs, Latera caldera, Italy. J. Volcanol. Geotherm. Res. 53, 309–327.

Urbanek, W., Zemel, J.N., Bau, H.H., 1993. An investigation of the temperature dependence of Poiseuille numbers in microchannel flow. J. Micromechanics Microengineering 3, 206–209. doi:10.1088/0960-1317/3/4/009

Valentine, G.A., Gregg, T.K.P., 2008. Continental basaltic volcanoes- processes and problems. J. Volcanol. Geotherm. Res. 177, 857–873.

Viana, F., Pardo, R., Yánez, R., Trallero, J.L., Joseph, D.D., 2003. Universal correlation for the rise velocity of long gas bubbles in round pipes. J. Fluid Mech. 494, 379–398.

Wadsworth, F.B., Kennedy, B.M., Branney, M.J., von Aulock, F.W., Lavallée, Y., Menendez, A., 2015. Exhumed conduit records magma ascent and drain-back during a Strombolian eruption at Tongariro volcano, New Zealand. Bull. Volcanol. 77, 1–10. doi:10.1007/s00445-015-0962-7

Walker, G.P.L., 1973. Explosive volcanic eruptions—a new classification scheme. Geol. Rundschau 62, 431–446.

Walker, G.P.L., Self, S., Wilson, L., 1984. Tarawera 1886, New Zealand a basaltic plinian fissure eruption. J. Volcanol. Geotherm. Res. 21, 61–78.

Wallis, G.B., 1969. One-dimensional two-phase flow. McGraw-Hill Book Company, New York. p. 431.

Whitehead, J.A., Helfrich, K.R., 1991. Instability of flow with temperature-dependent viscosity: A model of magma dynamics. J. Geophys. Res. Solid Earth 96, 4145–4155. doi:10.1029/90JB02342

Wilson, L., Head, J.W., 1994. Mars: Review and analysis of volcanic eruption theory and relationships to observed landforms. Rev. Geophys. 32, 221–263.

Wilson, L., Head, J.W., 1983. A comparison of volcanic eruption processes on Earth, Moon, Mars, lo and Venus. Nat. 302, 663–669.

Wilson, L., Head, J.W., 1981. Ascent and eruption of basaltic magma on the Earth and Moon. J. Geophys. Res. Solid Earth 86, 2971–3001.

Wilson, L., Parfitt, E.A., Head, J.W., 1995. Explosive volcanic eruptions—VIII. The role of magma recycling in controlling the behaviour of Hawaiian-style lava fountains. Geophys. J. Int. 121, 215–225. doi:10.1111/j.1365-246X.1995.tb03522.x

Witham, C.S., Oppenheimer, C., 2004. Mortality in England during the 1783-4 Laki Craters eruption. Bull. Volcanol. 67, 15–26.

Witham, F., Llewellin, E.W., 2006. Stability of lava lakes. J. Volcanol. Geotherm. Res. 158, 321–332.

Wolfe, E.W., Neal, C.., Bamks, N.., Duggan, T.., 1988. Puu Oo Eruption of Kilauea Volcano, Hawaii: Espisodes 1 Through 20, January 3, 1983, Through June 8, 1984. US Geological Survey professional paper 1463.

Wolff, J.A., Sumner, J.M., 2000. Lava fountains and their products, in: Sigurduson H, Houghton B, Rymer H, Stix J, McNutt, S (eds) Encyclopedia of Volcanoes (1st Ed.). Academic Press San Diego, CA, pp. 321–329.

Woods, A.W., 1993. A model of the plumes above basaltic fissure eruptions. Geophys. Res. Lett. 20, 1115–1118.

Woods, A.W., Koyaguchi, T., 1994. Transitions between explosive and effusive eruptions of silicic magmas. Nature 370, 641–644.

Wright, T.L., Swanson, D.A., Duffield, W.A., 1975. Chemical compositions of Kilauea east-rift lava, 1968-1971. J. Petrol. 16, 110–133.

Wunderman, R., 2002. Report on Nyiragongo (DR Congo). Bull. Glob. Volcanism Netw. 27. doi:10.5479/si.GVP.BGVN200204-223030

Wylie, J.J., Helfrich, K.R., Dade, B., Lister, J.R., Salzig, J.F., 1999. Flow localization in fissure eruptions. Bull. Volcanol. 60, 432–440. doi:10.1007/s004450050243

Wylie, J.J., Lister, J.R., 1995. The effects of temperature-dependent viscosity on flow in a cooled channel with application to basaltic fissure eruptions. J. Fluid Mech. 305, 239–261.

Appendix A

Published work

Bull Volcanol (2017) 79: 81
https://doi.org/10.1007/s00445-017-1164-2

RESEARCH ARTICLE

Proximal lava drainage controls on basaltic fissure eruption dynamics

T. J. Jones [1] · E. W. Llewellin [1] · B. F. Houghton [2] · R. J. Brown [1] · C. Vye-Brown [3]

Received: 10 June 2017 / Accepted: 3 October 2017 / Published online: 28 October 2017

Abstract Hawaiian basaltic eruptions commonly initiate as a fissure, producing fountains, spattering, and clastogenic lava flows. Most fissures rapidly localize to form a small number of eruptive vents, the location of which may influence the subsequent distribution of lava flows and associated hazards. We present results from a detailed field investigation of the proximal deposits of episode 1 of the 1969 fissure eruption of Mauna Ulu, Kīlauea, Hawai'i. Exceptional preservation of the deposits allows us to reconstruct vent-proximal lava drainage patterns and to assess the role that drainage played in constraining vent localization. Through detailed field mapping, including measurements of the height and internal depth of lava tree moulds, we reconstruct high-resolution topographic maps of the pre-eruption ground surface, the lava high-stand surface and the post-eruption ground surface. We calculate the difference in elevation between pairs of maps to estimate the lava inundation depth and lava drainage depth over the field area and along different segments of fissure. Aerial photographs collected during episode 1 of the eruption allow us to locate those parts of the fissure that are no longer exposed at the surface. By comparing with the inundation and drainage maps, we find that fissure segments that were inundated with lava to greater depths (typically 1–6 m) during the eruption later became foci of lava drainage back into the fissure (internal drain-back). We infer that, in these areas, lava ponding over the fissure suppressed discharge of magma, thereby favouring drain-back and stagnation. By contrast, segments with relatively shallow inundation (typically less than ~ 1 m), such as where the fissure intersects pre-eruptive topographic highs, or where flow away from the vent (outflow) was efficient, are often associated with sub-circular vent geometries in the post-eruption ground surface. We infer that these parts of the fissure became localization points for ongoing magma ascent and discharge. We conclude that lava inundation and drainage processes in basaltic fissure eruptions can play an important role in controlling their localization and longevity.

Keywords Mauna Ulu · Vent localization · Lava ponding · Lava tree moulds · Eruption longevity · Vent inundation

Editorial responsibility: J. Taddeucci

Electronic supplementary material The online version of this article (https://doi.org/10.1007/s00445-017-1164-2) contains supplementary material, which is available to authorized users.

✉ T. J. Jones
t.j.jones@durham.ac.uk

[1] Department of Earth Sciences, Durham University, South Road, Durham DH1 3LE, UK

[2] Department of Geology & Geophysics, SOEST, University of Hawai'i at Mānoa, Honolulu, HI 96822, USA

[3] British Geological Survey, The Lyell Centre, Research Avenue South, Edinburgh EH14 4AP, UK

Introduction

Basaltic fissure eruptions account for the bulk of the Earth's magma output (Sigurdsson 2000). Although relatively common, their deposits can nonetheless be challenging to investigate and interpret. Vent structures are known to evolve and migrate during eruptions (e.g. Richter et al. 1970; Thorarinsson et al. 1973; Swanson et al. 1979; Bruce and Huppert 1989); however, evidence of these dynamic processes is commonly buried beneath later syn-eruptive material, including spatter, tephra fall and subsequent lava flows (e.g. Thordarson and Self 1993; Larsen 2000; Brown et al. 2015; Reynolds et al. 2016). Furthermore, evidence of clastogenic

eruption processes, such as spattering and fountaining, can be lost if pyroclastic material becomes agglutinated and/or forms rheomorphic lava flows (Sumner et al. 2005; Valentine and Gregg 2008; Parcheta et al. 2012).

Basaltic fissure eruptions typically initiate as curtains of fountaining basaltic spatter, bombs and lapilli, with heights of 10s to 100s of meters (e.g. Richter et al. 1970; Swanson et al. 1979; Wolfe 1988; Alparone et al. 2003). The vents are initially of high aspect ratio, with crack widths varying from ~ 2 m to tens of meters and lengths ranging from several hundred metres to several kilometres (e.g. Gudmundsson 1987; Opheim and Gudmundsson 1989; Keating et al. 2008; Parcheta et al. 2015). Over the order of hours, the curtain generally focuses to a few point sources along the fissure (e.g. Richter et al. 1970; Thorarinsson et al. 1973; Swanson et al. 1979); however, controls on the temporal and spatial evolution of such systems are poorly understood (Bruce and Huppert 1989). Progressive localization causes a change in the eruption parameters, such as an increase in fountain height (Wilson et al. 1995), restricted spatial distributions of lava discharge (Pedersen et al. 2017) and release of hazardous gases and aerosols (Walker et al. 1984; Stothers et al. 1986; Woods 1993) from a point, rather than a line, source. To track, and thus effectively manage, this dynamic situation, a better understanding of factors modulating fissure localization is required.

Previous studies of vent localization and termination of basaltic fissure eruptions have focused on thermo-rheological effects and the solidification of magma in the feeder dyke. Delaney and Pollard (1982) calculated that magma flowing at 1 m s^{-1} in a 2-m-wide dyke should rapidly cool and solidify inwards from conduit margins to close the dyke within a few hours. They inferred that, for eruptions to last longer than a few hours, as observed in Iceland (Thorarinsson et al. 1973) and Hawai'i (Swanson et al. 1979), the width of the ascending dyke must be greater than 2 m. Bruce and Huppert (1989) investigated the role of thermo-rheological effects in vent-localization. They showed that the balance between heat transfer by advection and conduction governs whether conduit walls are melted back, widening the conduit, or magma solidifies against the walls, narrowing and eventually blocking the conduit (Bruce and Huppert 1989; Bruce and Huppert 1990). More recent work has shown that, as the magma cools against the wall rock, local regions of relatively cooler, and higher viscosity magma are formed (Wylie and Lister 1995; Wylie et al. 1999). The fresh, hotter upwelling magma will tend to minimize energy loss by flowing through the regions of lowest viscosity, forming fingers of localized upwelling (Whitehead and Helfrich 1991; Helfrich 1995; Wylie and Lister 1995; Wylie et al. 1999).

Flow organization within basaltic feeder systems must also be influenced by drain-back of dense, degassed magma into the conduit. Drain-back has been documented at several lava lakes, such as at Halema'uma'u Crater, Kīlauea Iki and Makaopuhi on Kīlauea, Hawai'i (Wright et al. 1968; Richter et al. 1970; Swanson et al. 1979; Stovall et al. 2009; Patrick et al. 2015), Mt. Erebus, Antarctica (e.g. Oppenheimer and Kyle 2008) and Erta Ale, Ethiopia (Oppenheimer and Francis 1997). At these systems, fluctuations in the height of a lava lake have been related to pressure changes, magma flux or gas flux within the magma plumbing system (e.g. Tilling 1987; Witham and Llewellin 2006; Patrick et al. 2015). Bidirectional flow induced by the descent of relatively degassed, dense magma in a conduit has been investigated for the case of a vertical, cylindrical conduit geometry, and the upwelling and downwelling components organized either as core-annular flow or side-by-side flow, depending on the viscosity ratio (Kazahaya et al. 1994; Stevenson and Blake 1998; Huppert and Hallworth 2007; Beckett et al. 2011; Palma et al. 2011; Beckett et al. 2014). Bidirectional flow has also been inferred from mass balance calculations at lava lakes; that is, to maintain a non-overflowing lake, supply into the lake must be balanced by flow back down the conduit (Tilling 1987; Harris et al. 1999; Witham and Llewellin 2006; Harris 2008).

In some cases, lava has been directly observed to drain back down a fissure system, such as the 2002 eruption of Nyiragongo (Allard et al. 2002; Wunderman 2002), 1974 eruption of Kīlauea (Tilling et al. 1987; Wilson et al. 1995) and the 2011 Kamoamoa eruption (Orr et al. 2015). Drainage has also been inferred from studies of exposed vent deposits and dyke feeder systems at a range of depths (Lefebvre et al. 2012; Geshi and Neri 2014; Wadsworth et al. 2015). At greater depths, regions of both upwards and downwards flow have been identified within a single camptonite dyke at Higby Mountain, Connecticut (Philpotts and Philpotts 2007).

The role that drain-back plays in the evolution of magma flow organization within, and out of, a dyke is currently an open research question. Here, we use field evidence to investigate the inundation and drainage of basaltic lava during episode 1 of the 1969–1974 eruption of Mauna Ulu, Hawai'i, USA, and assess its influence on shallow conduit dynamics and the spatio-temporal evolution of the fissure system.

Background

The Mauna Ulu 1969–1974 eruption

Mauna Ulu is a small lava shield, located on the East Rift Zone (ERZ) of Kīlauea volcano, Hawai'i (Fig. 1a). The 1969–1974 Mauna Ulu eruption that built this shield was characterized by two phases: Phase I began on May 24, 1969 and ended on October 15, 1971 during which 185 × 10^6 m^3 of lava were erupted (Swanson et al. 1979), and phase II lasted from February 3, 1972 to July 22, 1974 (Tilling et al. 1987). The

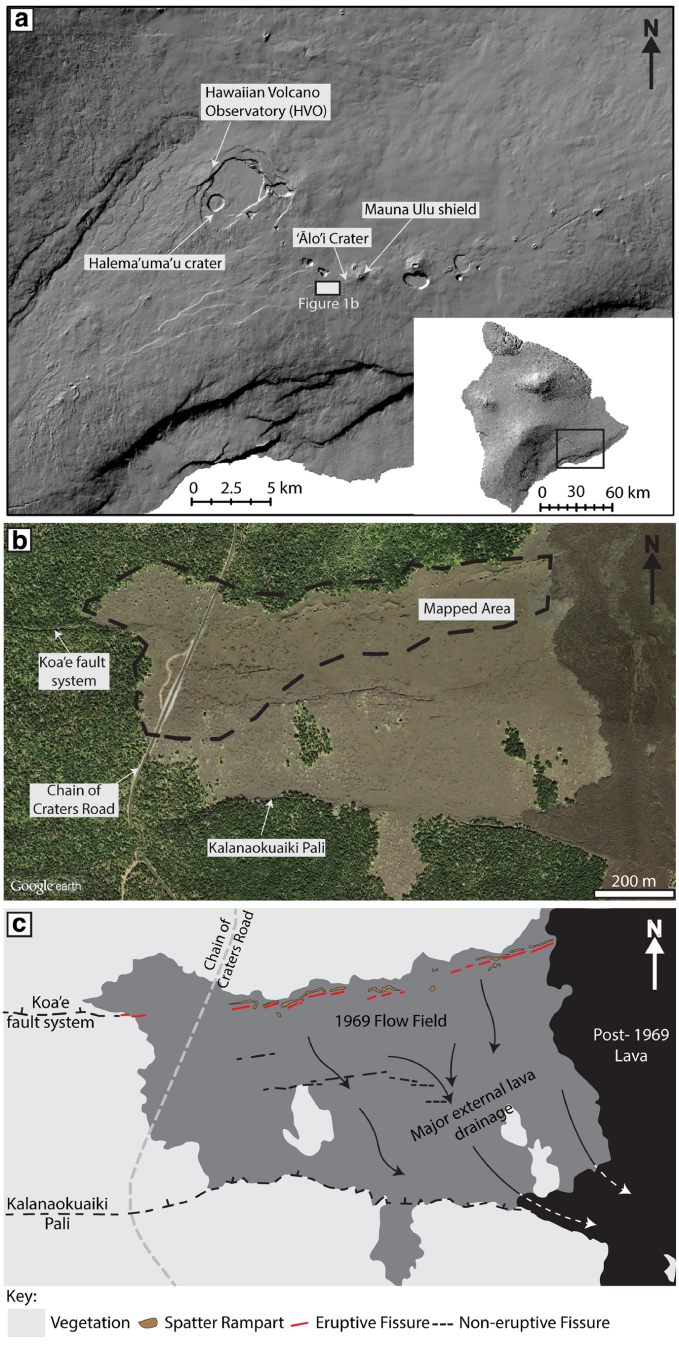

Fig. 1 Location map of Mauna Ulu on the Island of Hawai'i. **a** The location of the field area is shown in the black box. **b** Google Earth™ aerial image of the Mauna Ulu lava field; for reference, the centre of the of view is at 19° 21′ 39.43″ N, 155° 13′ 5.68″ W. **c** Interpreted diagram of the image in **b** showing the surface features of the episode 1 Mauna Ulu eruption

two phases were documented by Swanson et al. (1979) and Tilling et al. (1987), respectively. Here, we follow the narrative of Swanson et al. (1979) and enhanced timings of (Parcheta et al. 2012). Episode 1 of the eruption initiated on May 24, 1969 with an earthquake swarm that could be felt in the nearby village of Volcano. At 04:45 Hawaiian Standard Time (HST), fountaining began from a newly formed fissure system close to ʻĀloʻi Crater. This fissure rapidly propagated westwards, crossing the old Chain of Craters Road by 05:00 HST, and ʻĀinahou Road (the current Chain of Craters Road; Fig. 1) at 08:30 HST, beyond which it exploited the Koaʻe fault system and terminated ~ 150 m west of ʻĀinahou Road. Steady fountaining and lava ponding occurred until 12:00–13:00 HST. During this time, a pāhoehoe lava field advanced southward down slope from the fissure and ponded 1.2 km from the vent at the base of the north-facing Kalanaokuaiki Pali fault scarp (Fig. 1). Steady fountaining was followed by a period of waning activity and lava drain-back ending at 22:00 HST. This marked the end of episode 1 and the last eruptive activity in the western segment of the Mauna Ulu fissure system. All subsequent activity occurred further to the east, forming the Mauna Ulu shield and its associated lava flow field. Most significantly for this study, a voluminous lava flow in January–March 1974, originating from the Mauna Ulu shield, covered large sections of the originally 4.5-km-long fissure, leaving only the 880 m long western section exposed and available to study today (Fig. 1b, c). Therefore, this study solely focuses on the early development of the fissure system rather than the later phases that were confined to the Mauna Ulu shield to the east; all discussions of lava re-surfacing refer to the 1969 episode 1 eruption. Contemporary observation of episode 1 was limited to eyewitness accounts by Hawaiian Volcano Observatory (HVO) scientists (Swanson et al. 1979) and aerial photographs were taken serendipitously by a Sandia Labs aerial survey (now held at the US Geological Survey HVO; Fig. S1) taken 1 h after the fissure system reached its full length (Swanson et al. 1979; Parcheta et al. 2012).

Previous mapping of the episode 1 fissure system

The exceptional preservation of the episode 1 fissure system offers a unique opportunity to investigate shallow conduit geometries and processes. Parcheta et al. (2015) used ground-based light detection and ranging (LiDAR) to measure the geometry of parts of the shallow conduit (< 15 m depth) and vents associated with the episode 1 fissure system. They mapped 54 vents or fissure segments along the surviving 880 m of fissure and document several distinct geometric features including (1) five en echelon steps caused by the rotation of a rectilinear dyke to a near-shear stress orientation upon ascent; (2) sinuous individual fissure segments most likely related to stress field interactions between the ERZ and the Koaʻe fault system, as well as fissure irregularity; and (3) irregularity in the internal dyke wall surface, thought to represent pre-existing cooling joints within the pre-1969 lava flow through which the dyke cuts (Parcheta et al. 2015). Three-dimensional imaging of the sub-surface vent structures showed that the primary conduit wall consists of jigsaw-like fits between either side of the conduit (Parcheta et al. 2016), indicating that the conduit walls have not been modified since the eruption.

The vent geometries range from sub-circular to linear in plan view and from parallel-sided to flared in cross-section. The degree of vent flaring was characterized quantitatively through the LiDAR point cloud for three vents (Parcheta et al. 2015). No clear relationship between fountain height and vent flaring was found, although fountain height during the eruption was poorly quantified. Parcheta et al. (2015) suggested that the flaring was caused by either syn-eruptive erosion or late-stage drain-back of ponded lava.

Methods

Fieldwork

In this study, we focus on the near-fissure products of the episode 1 flow field (Fig. 1c). At the time of the eruption, this area was densely forested, and the episode 1 lava flows quenched against the trees. As the flows inflated, the quench surface extended higher up the trees, forming casts up to 5 m high; this lava high-stand surface represents the maximum local inundation depth (Parcheta et al. 2015). During the waning stage of the eruption, lava drained to leave solidified lava quenched against the tree to form a tree mould (Finch 1931; Moore and Richter 1962; Lockwood and Williams 1978; Lockwood and Lipman 1980). The difference in height between the lava high-stand surface and final, post-eruption ground surface represents the extent of drainage from the maximum inundation depth, termed the lava drainage depth (Finch 1931; Moore and Richter 1962; Lockwood and Williams 1978; Parcheta et al. 2015). The entire area was densely forested; hence, tree moulds provide a consistent dataset for inundation depth across the proximal lava flow field fed by the episode 1 fissure.

Measurements of elevation of the lava high-stand (syn-eruption) surface and post-eruption ground surface (i.e. the present day surface) were taken using a Leica SR520 kinematic GPS (kGPS) on > 200 tree moulds (Fig. 2). The following measurements were made for each tree mould, where possible: (1) internal depth of the tree mould (by lowering a plumb-bob into the mould), (2) elevation of the uppermost crust level (lava high-stand), (3) elevation of the post-eruption ground surface around the tree mould (i.e. the level of the surface following drainage) and (4) height of the top of the tree mould above the surrounding lava surface. Note that this final

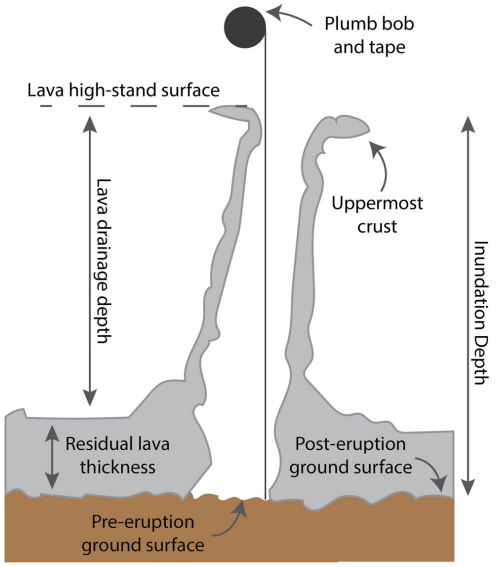

Fig. 2 Schematic tree mould showing the measured features, where the uppermost crust is interpreted to be the lava high-stand surface. The distance from the top of the tree mould to the pre-eruption ground surface—i.e. the inundation depth—was measured using a plumb-bob, dropped down the inside of the mould. The position of the lava high-stand surface and post-eruption ground surface was measured using kinematic GPS. Other quantities were determined by difference

measurement is the same as the difference between measurements 2 and 3 and is therefore redundant in some locations. Measurements are summarized in Fig. 2. We note that a tree mould's internal depth is subject to error if debris has fallen down the cast; therefore, measurements are only reported where a soil horizon was hit by the plumb bob. In the field, the soil horizon was identified by visual inspection if the tree mould was shallow, and if deep, either from the sound heard upon contact or from the presence of soil on the plumb bob. Estimated accuracy of the tree mould depth measurement is ± 2 cm. The location of a specific point within the field area was re-measured seven times using our standard kGPS protocol, enabling quantification of uncertainty in the measured position associated with data acquisition and processing. We obtained a standard deviation of 0.012, 0.017 and 0.018 m, for the E–W, N–S and vertical positions, respectively.

Map production

A geo-referenced database relating all attributes (tree mould height and depth) to their associated kGPS location was created. These data were then imported into a geographic information systems program (ArcGIS™) for all further analysis. Interpolation to produce a raster map was performed using the tension spline interpolation routine. This routine bends a surface through the known input data points whilst trying to minimize the total curvature of the surface. In a *tension* spline, both first and second derivative terms are used to minimize the curvature of the surface (Franke 1982; Mitáš and Mitášová 1988). We used the routine with 10 points per region and $\phi = 1$, where ϕ is the weight given to the first derivative term and can be thought of as the 'surface stiffness' (Franke 1982). This approach was used to create topographic maps for (1) the pre-eruption ground surface, (2) the lava high-stand surface and (3) the post-eruption ground surface. These maps were produced from the following data (Fig. 2): (1) the kGPS positions of the uppermost crust minus the measured tree mould depth, (2) the kGPS positions of the uppermost crust and (3) the kGPS positions of the post-eruption ground surface respectively.

The three topographic surface maps were used to create two further maps: (1) a map of lava inundation depth during eruption and (2) a map of lava drainage depth. The map of lava inundation was created by subtracting the pre-eruption ground surface raster map from the lava high-stand surface raster map using the ArcMap™ 3D Analyst minus tool. The map of lava drainage depth was created by subtracting the post-eruption ground surface raster map from the lava high-stand surface raster map. We note that it is possible that lava may have compacted slightly post-emplacement. Because our data do not allow us to quantify this process, it must be considered as a potential source of additional uncertainty on lava drainage. Note that, for completeness, we also produce a map of residual lava thickness, presented as Fig. S2 in the supplementary information, by subtracting the pre-eruption ground surface raster map from the post-eruption surface raster map. The distribution of residual lava thickness is not discussed further in this work.

Profile production

One of the goals of our study is to investigate how measured parameters, such as inundation depth, vary along the fissure. This is complicated by the fact that the fissure is discontinuous, and is divided into roughly parallel-trending segments that are offset from one another perpendicular to strike. To create a continuous profile along the entire length of the fissure system, we project each segment of the fissure onto a single line with the same overall trend as the fissure system, where the overall trend line is taken as the line connecting the locations of the western-most and eastern-most fissure exposures. The process is illustrated in Fig. 3. As part of the process, we first geo-referenced the aerial photograph taken by Sandia Labs (Fig. S1) and marked the active fissure segments onto the topographic maps. Next, to link all the discontinuous en echelon segments, we determined the overall trend line for the system, which has bearing 079.365°. From the end of each segment, a tie-line was drawn perpendicular to the overall

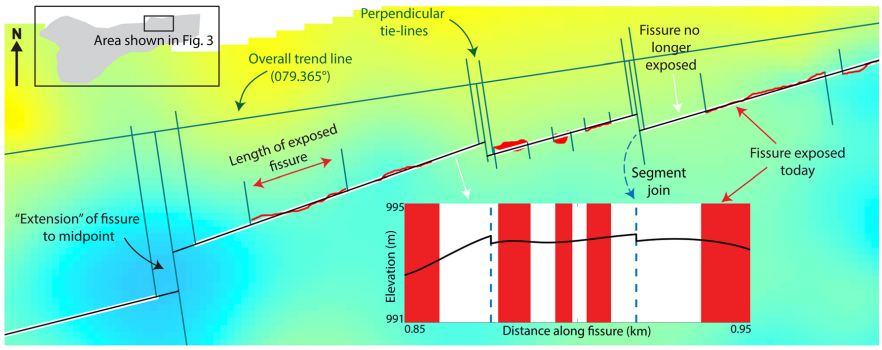

Fig. 3 A labelled portion of the fissure system showing how a continuous profile was constructed from discontinuous fissure segments, using the example of the post-eruption ground surface. The post-eruption ground surface base map used is presented in full in Fig. 4c

trend line, and then the midpoint between the tie-lines, on the overall trend line, was located. Lastly, the segment trend lines were extended within each gap until they met at the midpoint. Parameters were then projected onto the overall trend line to create a continuous profile along strike, allowing us to investigate trends that occur along the entire eruptive fissure.

Results

Topographic maps

Figure 4a shows a map of the pre-eruption ground surface topography prior to the 1969 Mauna Ulu eruption, reconstructed from tree mould depths. Overall, the ground elevation slopes to the south, consistent with the regional trend on the southern flank of the Kīlauea shield. The broad trends in the map are also consistent with the relatively low resolution topographic map (1:24,000 scale; 6.1 m vertical resolution) produced by the US Geological Survey before the 1969 eruption (Plate 1 of Swanson et al. 1979). Note that our absolute elevation values differ from those of Swanson et al. (1979) because we use a different vertical reference datum: Swanson et al. (1979) use a vertical reference of mean sea level whereas we use the WGS 84 reference ellipsoid. In detail, the pre-eruption topography has two broad depressions in the east of the mapped area, starting close to the fissure and sloping southward. Close to the fissure, these depressions are approximately 60 m wide and 1 m deep relative to surrounding topography. Away from the fissure, these depressions broaden to > 170 m and deepen to 4 m. There is a shallow elongate depression, approximately 70 m wide, in the northwest section of the field area. The depression strikes roughly NW–SE and crosses the fissure (but note that there is no exposure of the fissure presently observable in this region). At a smaller scale, below the resolution of this measurement technique, we expect the pre-eruption ground surface to have had decimetre- and centimetre-scale variations caused by lava surface folding, changes in substrate (e.g. road vs. vegetation) and varying pre-existing lava type (e.g. shelly pāhoehoe vs. ropy pāhoehoe).

The lava high-stand surface (Fig. 4b) also has an overall southward slope. By visual inspection of the contour spacing, this surface in general shows less topographic relief than the pre-eruption ground surface. The northwest region of the field area has the highest elevation (~ 998 m), and there is no clear evidence of the topographic depression observed in the northwest section of the pre-eruption map. The two eastern, south-trending depressions observed in the pre-eruption map can also be detected on this surface, though they are less prominent.

The post-eruption ground surface (i.e. the present day topography; Fig. 4c) is the most robust dataset because it has the highest density of kGPS points (black circles in Fig. 4c); it has been validated through visual comparison with a National Oceanic and Atmospheric Administration digital elevation model (2005 IfSAR DEM). The post-eruption ground surface also has an overall southward slope. In the west, a large, closed basin is present between exposed fissure segments, and in the central and eastern sections, several isolated depressions and topographic highs result in a more variable and steeper relief than that seen in Fig. 4a, b.

Lava inundation

Figure 5 shows the lava inundation depth over the mapped area (i.e. the difference between the lava high-stand and pre-eruption ground surface). Much of the proximal lava flow field was inundated with a 1- to 3-m thickness of lava at peak height. Isolated regions of > 4 m thick lava are commonly associated with depressions in the pre-eruption topography (Fig. 4a).

Also shown in Fig. 5 are segments of the fissure that are in eruption on the Sandia Labs aerial imagery. These segments

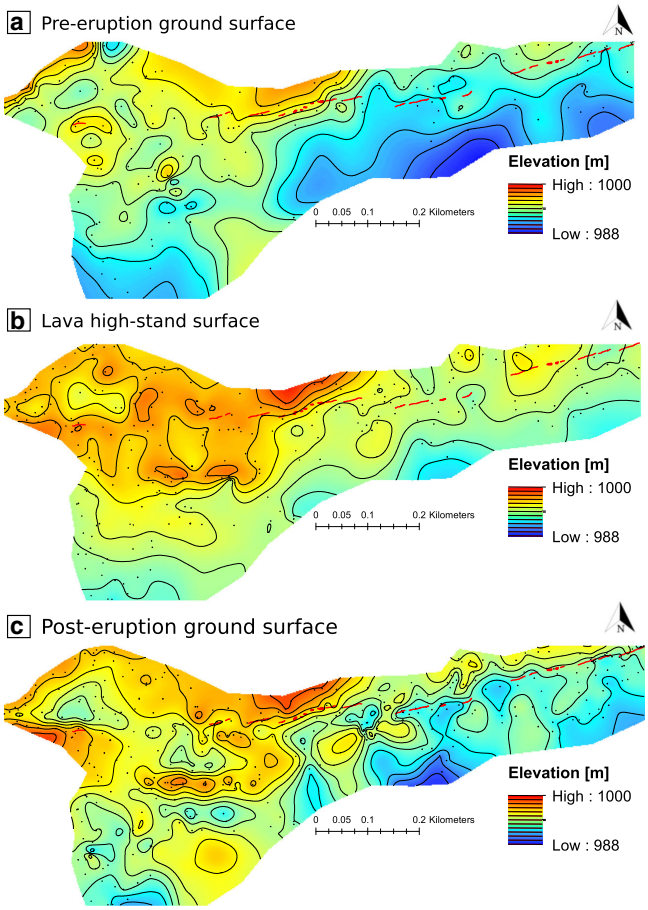

Fig. 4 Topographic maps, contoured at 1 m intervals, of the **a** pre-eruption ground surface topography prior to the 1969 Mauna Ulu eruption, reconstructed from tree mould depths (195 measurements; black dots), **b** lava high-stand surface (269 measurements) and **c** the post-eruption ground surface (383 measurements) produced within ArcMap from kGPS measurements. Not all data points appear in every map, because some tree moulds were broken and had no high-stand crust, and because measurements of the post-eruption ground surface were not restricted to locations with tree moulds. The fissure vents exposed at the surface today are marked in red. Elevations are ellipsoid heights (WGS 84) and not geoid corrected

appear as orange (incandescent) lines on the images. Segments were traced from the Sandia Labs aerial imagery and overlain onto our maps using Google Earth Pro™. Note that substantial parts of the fissure that were active in the images have no surface expression in the field today. Gaps in exposure of the fissure (Fig. 5) are generally associated with regions of relatively deep lava inundation. This is particularly evident in the western part of the fissure system and at the prominent en echelon step just east of the centre of the fissure system (Fig. 5).

Drainage

Drainage depth varies between 0 and 4 m (Fig. 6). In the western part of the fissure system, drainage is greatest in the basin along fissure segments that once erupted (but are no longer exposed at the surface), removing a maximum of 3.0 m of lava at its centre. In the eastern part of the fissure system, several drainage regions are centred directly along fissure segments and remove a maximum of ~ 3.5 m of lava. Some of these regions link southward into drainage channels

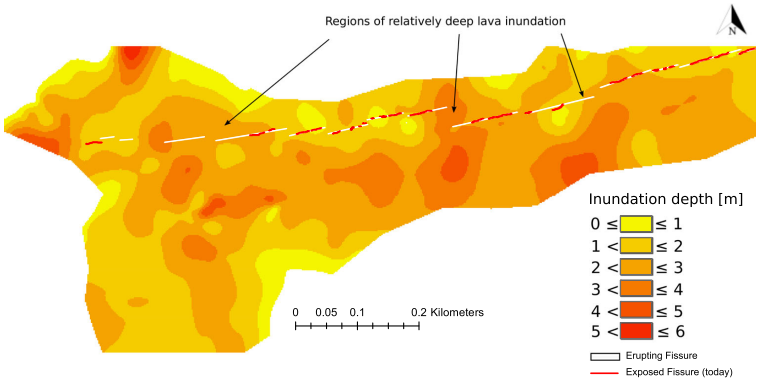

Fig. 5 Map of lava inundation depth during lava high stand. The map is produced by subtracting the pre-eruption ground surface (Fig. 4a) from the lava high-stand surface (Fig. 4b). The fissure vents that can be observed in the field today are marked in red. Segments of the fissure known to be active during the eruption, identified from the Sandia Labs aerial imagery, are traced in white

(see Fig. 4a, c) and others form closed basins that are similar to, but smaller than, the western basin.

Interpretations

One of our goals is to understand and interpret the lava drainage patterns evidenced by the Mauna Ulu episode 1 field data. We define two terms to describe drainage: 'outflow' is the drainage of lava away from the fissure; 'drain-back' is the drainage of lava back into the fissure. To set the context for our interpretation of the results previously presented (Figs. 4, 5 and 6), we introduce two hypothetical end-member scenarios. (1) If a region was completely confined, with no pathway for the lava to drain away, then the lava would simply form a pond, and the high-stand surface would be flat and horizontal, with only minor perturbations that correspond to surface ropes and folding. (2) If all lava could freely drain either down slope, away from the fissure (outflow) or back down the conduit (drain-back), then the lava high-stand surface would reflect only dynamic ponding. These two end-member scenarios, of either widespread ponding or widespread drainage, constitute hypotheses against which we can evaluate the field data.

The situation during episode 1 of the 1969 Mauna Ulu eruption was more complex than these simple end-member scenarios. Whilst the lava high-stand surface in the western part of the fissure system was fairly flat, the eastern part adopted a broad south-sloping trend with smaller scale topographic depressions and highs (Fig. 4b). Additionally, lava inundation depth was not consistent along the fissure (Fig. 5): certain fissure segments, and the adjacent proximal flow field, experienced a deeper inundation above the vent than others. This suggests that, during the eruption, the proximal flow field was characterized by a complex and

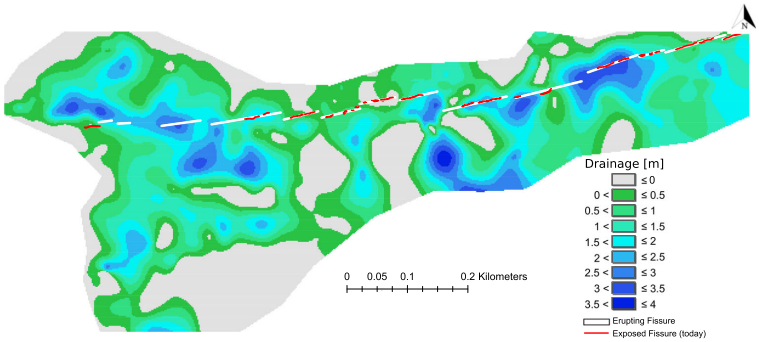

Fig. 6 Map of lava drainage depth. The map is produced by subtracting the post-eruption ground surface (Fig. 4c) from the lava high-stand surface (Fig. 4b). The fissure vents that can be observed in the field today are marked in red. Segments of the fissure known to be active during the eruption, identified from the Sandia Labs aerial imagery, are traced in white

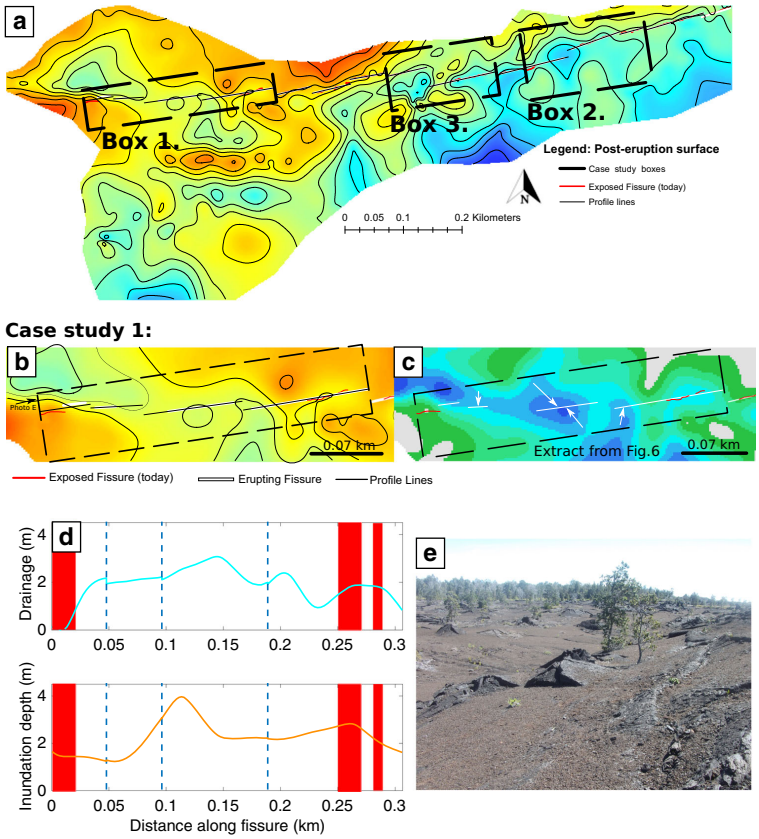

Fig. 7 **a** Post-eruption ground surface (i.e. present day topographic map) highlighting the three case study areas discussed in this study. **b** Detail of the area considered in case study 1 (box 1 in **a**). The red lines show the fissure exposed at the surface today, the white lines show segments of fissure that were active during the eruption and the black lines represent the analysed profiles, constructed according to the methodology presented in the 'Profile production' and Fig. 3. **c** An extract from Fig. 5 with arrows showing areas where drainage focused into and around segments of now-buried fissure. **d** Profiles for drainage (blue) and inundation depth (orange) across box 1. Blue vertical dashed lines represent a step from one fissure segment to another, red-shaded regions mark fissure segments left exposed at the surface today and white regions mark areas where the fissure is no longer exposed. **e** A field photograph of case study 1 (looking east; direction shown by arrow in part **b**) showing the large western basin depression

spatially variable inundation, including elements of both static and dynamic ponding. We explore these complexities in detail by comparing two regions of the proximal flow field. The first region is in the west of the field area (box 1 in Fig. 7a) and has a lava high-stand surface that is relatively flat and horizontal. It contains an unexposed eruptive fissure (Fig. 7b) and forms part of an isolated, closed basin in the pre-eruption topography. The second region is in the east of the field area (box 2 in Fig. 7a) and has a lava high-stand surface that consistently slopes to the south. It includes a prominent south-orientated channel in the pre-eruption topography.

Case study 1: isolated western basin

The first case study location includes four fissure segments (Fig. 7b), all of which erupted material, but which are now either completely covered, with no surface expression, or are only partially exposed. Drainage is at a local maximum on and near the fissure (Fig. 7c). The drainage regions are isolated and do not continue downslope away from the fissure; hence, drainage must have occurred as internal, drain-back into the fissure, along segments that are no longer exposed at the surface. The topographic profile taken from the drainage map along the fissure in box 1 (Fig. 7d)

reveals a maximum of 3 m of drainage (i.e. a 3-m reduction in ground elevation) in the central portion of the fissure, declining in both directions along fissure. The inundation profile along the same portion of the fissure (Fig. 7d) shows that the entire segment had material ponded over the fissure whilst it was erupting. The lava inundation reached a maximum of 3.9 m in the central portion of the fissure and plateaued at ~ 2.2 m to the east. This region of deep lava inundation corresponds to an elongate depression in the pre-eruption topography (Fig. 4a). The inundation depths along the profile are roughly inversely correlated with the palaeo-depression's topography, which has its axis, and therefore deepest inundation, centred ~ 0.12 km from the western end of the fissure.

We infer that, as the episode 1 lava flow field developed, it flooded the isolated western palaeo-depression leading to deep inundation above the erupting fissure. At present, there is a local, isolated depression in this area, indicating that, during the waning stages of the eruption, lava drained back down the fissure (Fig. 7c, e). The amount of drainage varies across the western basin but reaches a maximum between 0.1 and 0.16 km from the western end of the fissure. We hypothesize that this could be because (1) this was the deepest part of the palaeo-depression, where the greatest thickness was available to drain, and/or (2) the depth of the lava allowed it to retain more heat and maintain a lower viscosity than that in the surrounding flow field; hence, it could drain more easily or for longer.

Case study 2: external and internal drainages

For the second case study, we examine an area in the east of the field area, where the Sandia Labs aerial imagery shows lava flows moving south, following pre-existing topographic channels, away from the fissure vent (Fig. 8a and box 2 of Fig. 7a). The drainage map indicates that the drainage depth peaks twice along the fissure (Fig. 8b). Unlike case study 1, there is no correlation between the location of the drainage maxima and the location of areas of deepest lava inundation (Fig. 8b); therefore, we cannot invoke the same drainage mechanisms. To investigate further, we construct two profiles that crosscut the fissure: (1) where it is now covered by lava and hidden (A–A′) and (2) where it remains exposed at the surface (B–B′). The pre-eruption ground surface across these two profile lines has a different slope (Fig. 8c): profile A–A′ has a shallower proximal gradient than profile B–B′. We infer that, during the eruption, lava was more effectively drained away from the vent-proximal region at fissure location B–B′ because of the greater slope. In this area, lava drainage mainly occurred downslope away from the fissure (outflow), rather than internally back into the fissure (drain-back). By contrast, the shallower slope at A–A′ inhibited external, downslope outflow; hence, lava either became dynamically ponded above the vent (when magma supply exceeded outflow) or drained back down fissure.

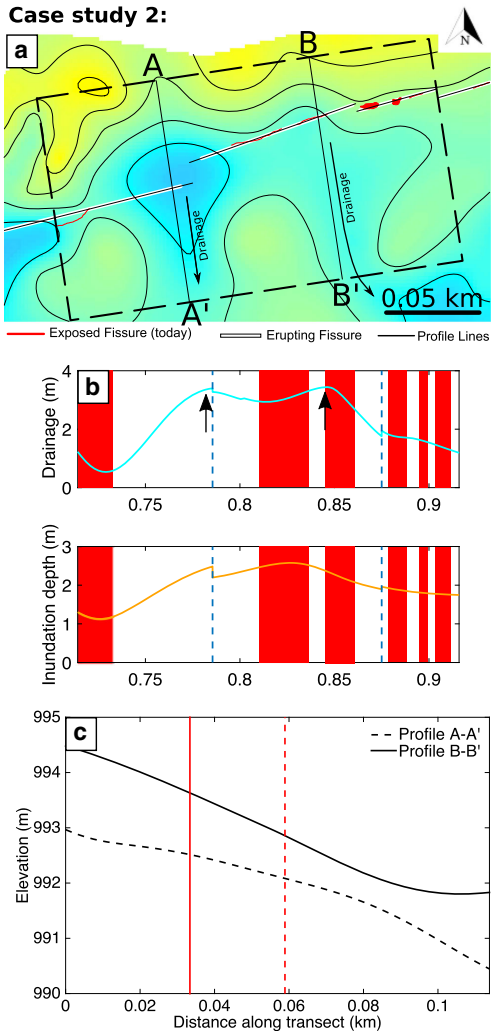

Fig. 8 **a** Detail of the area considered in case study 2 (box 2 in Fig. 7a). The red lines show the fissure exposed at the surface today, the white lines show segments of fissure that were active during the eruption and the black lines represent the analysed profiles. **b** Profiles for drainage (blue) and inundation depth (orange) across box 2; arrows mark two maxima in the drainage profile. **c** Profiles A–A′ (dashed) and B–B′ (solid) of the pre-eruption ground surface. Vertical red lines mark the intersection between (i) the A–A′ profile (dashed red), (ii) the B–B′ profile (solid red) and (iii) the fissure

Discussion

Tree mould mapping provides spatial information on lava drainage that allows us to reconstruct activity at and around missing (buried) fissure segments. The part of the fissure discussed in case study 1 (Fig. 7e) shows no indication of an eruptive vent and has been completely covered by episode 1 lava. Our mapping approach, and the subsequent production of a drainage map, provides a way to constrain the location of the eruptive fissure in the absence of direct observations. It also suggests that calculations of eruptive volume based on the present aerial extent and thickness of deposits are a minimum, because they do not consider erupted material that has drained back down a vent during waning stages.

The two case studies indicate that lava ponded over segments of the fissure either statically, as a result of topographic confinement (case study 1), or dynamically, because magma supply temporarily exceeded outflow (section cut by line A–A′, case study 2). In both cases, deep ponding is associated with no exposure of the fissure post-eruption. This suggests that the extent of the lava cover over an erupting vent, in turn a function of pre-eruption topography and the local eruption and outflow fluxes, may influence whether or not it will be preserved post-eruption, with deeply flooded vents less likely to be preserved. To understand the physical rationale for this interpretation, we must consider the effect that ponding has on eruption through an inundated linear vent.

The eruption of spatter through ponded lava was observed directly during the March 2011 Kamoamoa fissure eruption at Kīlauea (Lundgren et al. 2013; Orr et al. 2015). In this case, ponding 'drowned' the fissure and locally suppressed eruptive activity (Orr et al. 2015). Slow-moving magma in a fissure loses its heat to the country rock more effectively than fast-flowing magma; hence, its viscosity increases, leading to a positive feedback that promotes stagnation and blocking of the most sluggish portions of a fissure (Bruce and Huppert 1989). This supports a hypothesis that ponding acts to suppress the eruption in that location indirectly by reducing mass flux and causing magma within the underlying section of fissure to slow its ascent. We further contend that fissure eruptions are likely to be particularly susceptible to flow perturbations induced by ponding, because ascending magma can flow laterally to bypass regions of stagnant or down-welling magma more easily than is the case for a circular conduit/vent geometry.

Wilson et al. (1995) present an analysis of the eruption of basaltic magma from a linear fissure vent, through a lava pond, determining the height of lava fountaining as a function of pond depth, exsolved water content and mass eruption rate. They consider only the effect of the additional energy required to eject entrained lava into the fountain and do not consider thermo-rheological effects nor along-fissure migration of flow in response to along-strike variations in pressure gradients.

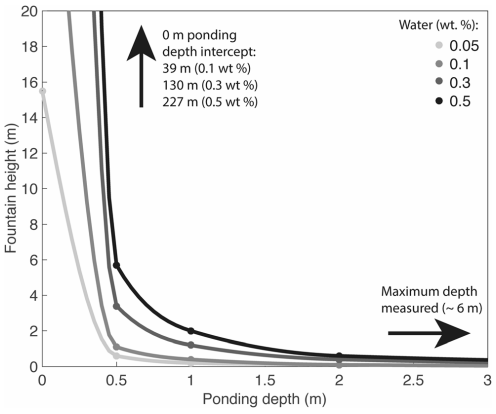

Fig. 9 Fountain height from a linear vent as a function of ponding depth above the vent (data taken from Table 3 of Wilson et al. 1995). The eruption is modelled to have a mass flux of 10^2 kg s^{-1} per meter of fissure with variable exsolved water contents (represented by sequential grey lines). The curves have no physical meaning and are included to guide the eye. For the ponding depths reported in this study (0 to 6 m), it is clear that a dramatic reduction in fountain height would have occurred as ponding depth increased

Nonetheless, an analysis of the episode 1 eruption, following their approach, is instructive. Figure 9 shows estimates of fountain height expected for the eruption as a function of ponding depth, based on data in Table 3 of Wilson et al. (1995). The episode 1 mass eruption rate is estimated from Swanson et al. (1979), who report bulk volumetric eruption rates of 1.30×10^5 m^3 h^{-1} for episode 1 based on the aerial extent and thickness of the lava flows it produced. Using an average lava flow interior bulk density (1750 kg m^{-3}) that we measure from field samples, this equates to an average mass eruption rate of 6.31×10^4 kg s^{-1}. To normalize the mass eruption rate to a unit length of fissure, we measured the length of incandescent fissure (assumed to be erupting) in the Sandia Labs aerial imagery, which were taken approximately 1 h after the fissure system had reached its full length. We found that ~ 1250 m of the original 4.5 km fissure was erupting, giving a mass eruption rate per unit length of 50.5 kg s^{-1} m^{-1}. This value represents an estimate of the average eruption rate through the whole of episode 1 and neglects temporal variations, for instance during the waxing and waning stages of the eruption; consequently, it should be taken as a minimum estimate of the typical eruption rate when the fissure was at full length. We therefore take 10^2 kg s^{-1} m^{-1} as an order of magnitude estimate for comparison with the model curves of Wilson et al. (1995). We estimate the water loss to be ~ 0.4 wt%, calculated as the difference between the assumed water content of basaltic melt at Kīlauea's shallow (1–3 km) summit reservoir (0.5 wt%; Moore 1970) and the

water content of spatter from low fountains at Mauna Ulu (0.07 wt%; Swanson and Fabbi 1973).

The results show that an increase in lava pond depth over a fissure strongly influences fountain height (Fig. 9). A ponding depth of 0.5 m above the vent reduces the fountain height by approximately two orders of magnitude compared with the pond-free case—from around 150 m to around 5 m. At ponding depths ≥ 2 m, the fountaining height tends to zero. We note, however, that at shallow ponding depths (≤ 0.3 m), the absolute heights of the lava fountains calculated using the Wilson et al. (1995) approach are much greater than indicated by contemporary field observations. Swanson et al. (1979) report observed maximum fountain heights of 50 m, whilst Parcheta et al. (2012) inferred that fountain heights ranged between 13 and 32 m, based on calibration of field photographs taken at the time of the eruption. One interpretation of the discrepancy between the theoretical calculations and the visual accounts is that all the vents were inundated to some degree. Another possibility is that this discrepancy arises because the model calculations do not account for lateral migration of magma along strike. If flow were to focus laterally, the mass eruption rate would increase at the localization points, resulting in higher fountaining. An increase in ponding depth at one location might therefore lead to an increase in mass eruption rate (and increasing fountain height) in adjacent parts of the fissure.

Our contention that magma can migrate laterally in response to ponding is supported by analysis of episode 1 rampart material (Parcheta et al. 2012) and visual observations at the time of eruption (Swanson et al. 1979), which indicate that fountaining intensity varied laterally along strike and temporally throughout the eruption. For instance, at a single time, variations of 10–15 m in fountain height were observed over short (4–15 m) distances along strike (Swanson et al. 1979; Parcheta et al. 2012). These variations are a result of the progressive vent localization process. To illustrate the effect that variable inundation can have on vent localization, we consider a third case study region within the central portion of the field area (box 3; Fig. 7a). Here, there are vents on two segments of fissure (X–Y and Y–Z) that initially erupted along their entire lateral extent (interpreted from Sandia Labs aerial imagery; Fig. S1) but are today only preserved in limited sections (Fig. 10a). An extract from our lava inundation map (Fig. 10b) shows that the maximum thickness of lava above the vent is highly variable along strike. In this area, the pre-eruption ground surface reaches a local minimum between the two fissure segments (Fig. 10c). The lava inundation profile across the region of interest (Fig. 10a) shows that ponding depth varies between 0.5 and 3.5 m and reaches a maximum in the centre where the fissure is no longer exposed at the surface. This ponding depth range (0.5–3.5 m) is sufficient to result in a large reduction in fountain height (Wilson et al. 1995). We suggest that deeper regions of lava ponding caused

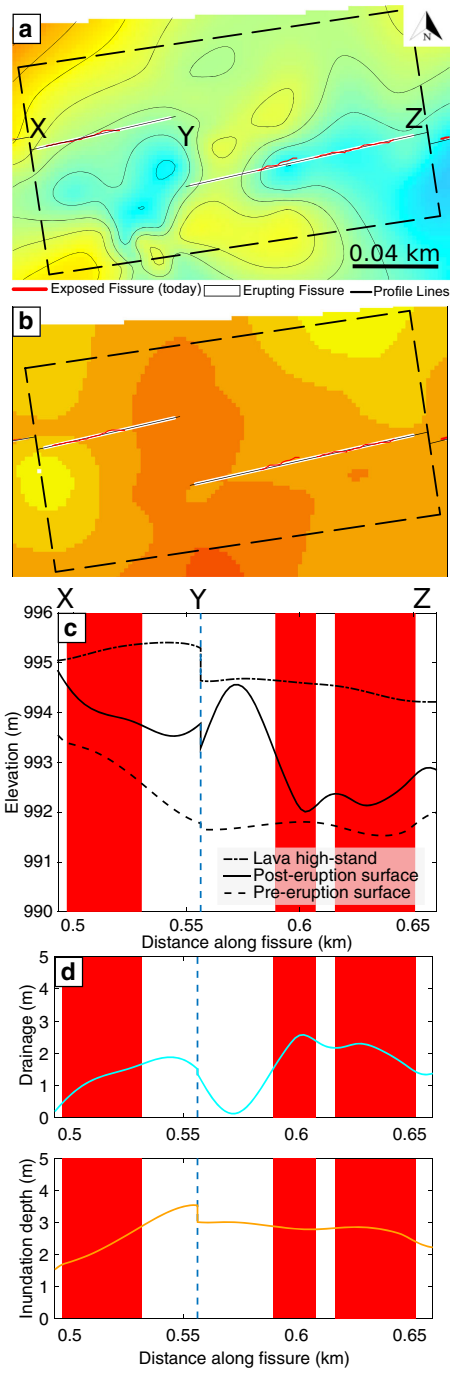

◀ **Fig. 10** **a** Detail of the area considered in case study 3 (box 3 in Fig. 7a). The red lines show the fissure exposed at the surface today, the white lines show segments of fissure that were active during the eruption and the black lines represent the analysed profiles. **b** Lava inundation map of the same area in box 3. The colour scale is the same as for Fig. 4, hotter colours representing greater lava inundation depths (5 m maximum, 0 m minimum in inset). **c** Elevation profiles of the lava high-stand surface and pre-eruption and post-eruption ground surfaces. **d** Profiles for drainage (blue) and inundation depth (orange) across box 3

by palaeo-topography at the east of fissure X–Y, and the west of fissure Y–Z suppressed fountaining in these regions, leading to blocking of the shallow conduit. This is consistent with the observation that the vents are no longer visible and are covered by 1969 lava. It is also possible that proximity to the end of the fissure segments in this region contributed to blocking of the conduit in this region.

Our observations and interpretations support the idea that ponding over the vent may influence local eruption intensity and the longevity of an eruptive segment. In this model, summarized in Fig. 11, suppression of fountaining by deep ponding is followed by stagnation of the eruption at that location and/or drain-back of erupted lava into the conduit. In either case, the viscosity of the magma in that part of the conduit increases, resulting in early shutdown of the eruption at that fissure segment and decreasing the likelihood of it being preserved as an open vent post-eruption. As a corollary, the location of pre-eruption topographic highs intersected by the eruptive fissure appears to correspond with preserved eruptive vents. These palaeo-topographic highs, along fissure from palaeo-lows, have relatively shallow lava ponding depths and are often associated with sub-circular vent geometries. We infer that these parts of the fissure became focal points for ongoing magma ascent and discharge and that consequent mechanical erosion transformed the fissure to a more circular geometry (Delaney and Pollard 1981; Wylie et al. 1999; Mitchell 2005).

We note that the topographic variation across the Mauna Ulu field site is fairly modest. The pre-eruption ground surface elevation varies along the eruptive fissure by just a few metres (Fig. 4). Furthermore, the mass eruption rates are low (~ 50 kg s^{-1} m^{-1}). Eruptions with more extreme (~ 100 m) topographic variations and much higher mass eruption rates may experience different controls on localization to those discussed in this study.

Conclusions

Tree mould mapping allows the reconstruction of topographic maps for the ground/lava surface before, during and after an eruption. These data can be combined to estimate (1) the depth of lava inundation above the eruptive vent and (2) the amount of drainage that occurred since the lava high-stand. This is particularly useful where syn-eruptive observations are limited or non-existent. We use this technique to investigate the episode 1 fissure system of the 1969 Mauna Ulu eruption of Kīlauea, Hawai'i, and analyse its evolution from laterally continuous Hawaiian fountaining to more discrete vents, as fissure segments narrowed and closed. Pre-eruption topography is an important control on the evolution of this eruption (Fig. 11): we have shown that the suppression of fountaining by deep ponding—either statically or dynamically—is followed by stagnation of the eruption at that location and/or drain-back of erupted lava into the conduit. In either case, the viscosity of the underlying magma is expected to increase, resulting in early shutdown of the eruption at that fissure segment and decreasing the likelihood of it being preserved as an open vent post-eruption. In contrast, we have shown that parts

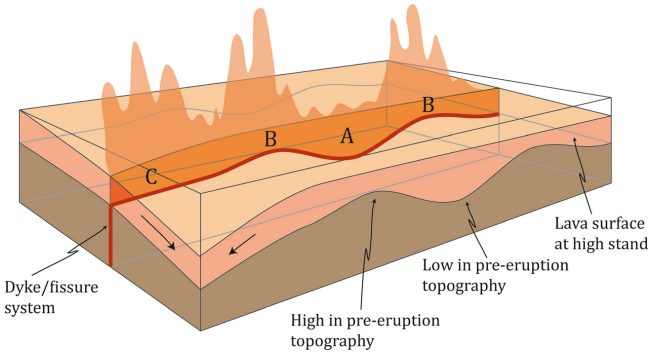

Fig. 11 A simplified schematic of the interaction between the surface and sub-surface processes operating during a fissure eruption. In areas where there was a pre-eruption topographic low (A), the lava is able to inundate and cause deep ponding over the vent. Ponding supresses the sub-surface upwelling flux and focuses flow along strike to areas of shallow inundation; these are palaeo-topographic high points (B) and regions with good external drainage/outflow (C). These localization regions are often preserved as open 'vents' post-eruption

of the fissure with shallow ponding, such as palaeo-highs and regions where external drainage (outflow) is effective (Fig. 11), are the focal points of continued magma discharge and eruption. We therefore conclude that, in addition to thermal-rheological controls, surface effects (lava inundation, pre-eruption topography, and drainage) can play an important role in the evolution of a basaltic fissure system. Finally, we propose that using the pre-eruption surface to predict the amount of internal (drain-back) and external (outflow) drainage could be a useful tool in hazard forecasting and assessment. For instance, knowing the relative proportion of drain-back and outflow along a fissure could support prediction of the variation in eruption longevity at specific locations along strike, allowing the vent localization pattern to be predicted. Prediction of, or early identification of, those parts of a fissure along which outflow localizes could, in turn, inform source parameters for consequent lava flow hazard modelling.

Acknowledgements Mike Poland is thanked for his support with the kGPS measurements and data processing. Tim Orr and Carolyn Parcheta are thanked for their discussions from which this work benefitted. CVB publishes with the permission of the Executive Director of the British Geological Survey. We thank Matt Patrick, Greg Valentine, the handling editor Jacopo Taddeucci and the executive editor Andrew Harris for their comments that improved the manuscript.

Funding information TJJ is funded by NERC grant NE/L0025901, part of the IAPETUS doctoral training partnership. EWL acknowledges support from NERC grant NE/N018443/1.

References

Allard P, Baxter P, Halbwachs M, Komorowski J-C (2002) The January 2002 eruption of Nyiragongo volcano (Dem. Repub. Congo) and related hazards: observations and recommendations. Final report of the French-British scientific team: submitted to the Ministry for Foreign Affairs, Paris, France, Foreign Office, London,United Kingdom and respective Embassies in Democratic Republic of Congo and Republic of Rwanda, Paris, p 24

Alparone S, Andronico D, Lodato L, Sgroi T (2003) Relationship between tremor and volcanic activity during the Southeast Crater eruption on Mount Etna in early 2000. J Geophys Res Solid Earth. https://doi.org/10.1029/2002JB001866

Beckett FM, Burton M, Mader HM et al (2014) Conduit convection driving persistent degassing at basaltic volcanoes. J Volcanol Geotherm Res 283:19–35

Beckett FM, Mader HM, Phillips JC et al (2011) An experimental study of low-Reynolds-number exchange flow of two Newtonian fluids in a vertical pipe. J Fluid Mech 682:652–670

Brown RJ, Thordarson T, Self S, Blake S (2015) Disruption of tephra fall deposits caused by lava flows during basaltic eruptions. Bull Volcanol 77:90. https://doi.org/10.1007/s00445-015-0974-3

Bruce PM, Huppert HE (1989) Thermal control of basaltic fissure eruptions. Nature 342:665–667

Bruce PM, Huppert HE (1990) Solidification and melting along dykes by the laminar flow of basaltic magma. In: Ryan MP (ed) Magma transport and storage. Wiley, Hoboken, pp 87–101

Delaney PT, Pollard DD (1982) Solidification of basaltic magma during flow in a dike. Am J Sci 282:856–885

Delaney PT, Pollard DD (1981) Deformation of host rocks and flow of magma during growth of minette dikes and breccia-bearing intrusions near Ship Rock, New Mexico. US Geol Surv Prof Pap 1202:61

Finch RH (1931) Lava tree casts and tree molds. Volc Lett 316:1–3

Franke R (1982) Smooth interpolation of scattered data by local thin plate splines. Comput Math Appl 8:273–281

Geshi N, Neri M (2014) Dynamic feeder dyke systems in basaltic volcanoes: the exceptional example of the 1809 Etna eruption (Italy). Front Earth Sci 2:13. https://doi.org/10.3389/feart.2014.00013

Gudmundsson A (1987) Tectonics of the Thingvellir fissure swarm, SW Iceland. J Struct Geol 9:61–69. https://doi.org/10.1016/0191-8141(87)90044-7

Harris AJL (2008) Modeling lava lake heat loss, rheology, and convection. Geophys Res Lett. https://doi.org/10.1029/2008GL033190

Harris AJL, Flynn LP, Rothery DA et al (1999) Mass flux measurements at active lava lakes: implications for magma recycling. J Geophys Res Solid Earth 104:7117–7136

Helfrich KR (1995) Thermo-viscous fingering of flow in a thin gap: a model of magma flow in dikes and fissures. J Fluid Mech 305:219–238

Huppert HE, Hallworth MA (2007) Bi-directional flows in constrained systems. J Fluid Mech 578:95–112

Kazahaya K, Shinohara H, Saito G (1994) Excessive degassing of Izu-Oshima volcano: magma convection in a conduit. Bull Volcanol 56:207–216

Keating GN, Valentine GA, Krier DJ, Perry FV (2008) Shallow plumbing systems for small-volume basaltic volcanoes. Bull Volcanol 70:563–582. https://doi.org/10.1007/s00445-007-0154-1

Larsen G (2000) Holocene eruptions within the Katla volcanic system, south Iceland: characteristics and environmental impact. Jökull 49:1–28

Lefebvre NS, White JDL, Kjarsgaard BA (2012) Spatter-dike reveals subterranean magma diversions: consequences for small multivent basaltic eruptions. Geology 40:423–426

Lockwood JP, Lipman PW (1980) Recovery of datable charcoal beneath young lavas: lessons from Hawaii. Bull Volcanol 43:609–615

Lockwood JP, Williams IS (1978) Lava trees and tree moulds as indicators of lava flow direction. Geol Mag 115:69–74

Lundgren P, Poland M, Miklius A et al (2013) Evolution of dike opening during the March 2011 Kamoamoa fissure eruption, Kīlauea Volcano, Hawai'i. J Geophys Res Solid Earth 118:897–914. https://doi.org/10.1002/jgrb.50108

Mitáš L, Mitášová H (1988) General variational approach to the interpolation problem. Comput Math Appl 16:983–992

Mitchell KL (2005) Coupled conduit flow and shape in explosive volcanic eruptions. J Volcanol Geotherm Res 143:187–203

Moore JG (1970) Water content of basalt erupted on the ocean floor. Contrib Mineral Petrol 28:272–279

Moore JG, Richter DH (1962) Lava tree molds of the September 1961 eruption, Kilauea Volcano, Hawaii. Geol Soc Am Bull 73:1153–1158

Opheim JA, Gudmundsson A (1989) Formation and geometry of fractures, and related volcanism, of the Krafla fissure swarm, northeast Iceland. Geol Soc Am Bull 101:1608–1622. https://doi.org/10.1130/0016-7606(1989)101<1608:FAGOFA>2.3.CO;2

Oppenheimer C, Francis P (1997) Remote sensing of heat, lava and fumarole emissions from Erta'Ale volcano, Ethiopia. Int J Remote Sens 18:1661–1692

Oppenheimer C, Kyle PR (2008) Probing the magma plumbing of Erebus volcano, Antarctica, by open-path FTIR spectroscopy of gas emissions. J Volcanol Geotherm Res 177:743–754

Orr TR, Poland MP, Patrick MR et al (2015) Kilauea's 5–9 March 2011 Kamoamoa fissure eruption and its relation to 30+ years of activity from Pu'u "O"o. In: Carey R, Poland M, Cayol V, Weis D (eds) Hawaiian volcanism: from source to surface, American Geophysical Union geophysical monograph, vol 208. Wiley, Hoboken (2015), pp 393–420

Palma JL, Blake S, Calder ES (2011) Constraints on the rates of degassing and convection in basaltic open-vent volcanoes. Geochem Geophys Geosyst. https://doi.org/10.1029/2011GC003715

Parcheta C, Fagents S, Swanson DA et al (2015) Hawaiian fissure fountains: quantifying vent and shallow conduit geometry, Episode 1 of the 1969–1974 Mauna Ulu Eruption. In: Carey R, Poland M, Cayol V, Weis D (eds) Hawaiian volcanism: from source to surface, American Geophysical Union geophysical monograph, vol 208. Wiley, Hoboken (2015, pp 369–391

Parcheta CE, Houghton BF, Swanson DA (2012) Hawaiian fissure fountains 1: decoding deposits—episode 1 of the 1969–1974 Mauna Ulu eruption. Bull Volcanol 74:1729–1743

Parcheta CE, Pavlov CA, Wiltsie N et al (2016) A robotic approach to mapping post-eruptive volcanic fissure conduits. J Volcanol Geotherm Res 320:19–28

Patrick MR, Anderson KR, Poland MP et al (2015) Lava lake level as a gauge of magma reservoir pressure and eruptive hazard. Geology 43:831–834

Pedersen GBM, Höskuldsson A, Dürig T et al (2017) Lava field evolution and emplacement dynamics of the 2014–2015 basaltic fissure eruption at Holuhraun, Iceland. J Volcanol Geotherm Res 340:155–169. https://doi.org/10.1016/j.jvolgeores.2017.02.027

Philpotts AR, Philpotts DE (2007) Upward and downward flow in a camptonite dike as recorded by deformed vesicles and the anisotropy of magnetic susceptibility (AMS). J Volcanol Geotherm Res 161: 81–94. https://doi.org/10.1016/j.jvolgeores.2006.11.006

Reynolds P, Brown RJ, Thordarson T, Llewellin EW (2016) The architecture and shallow conduits of Laki-type pyroclastic cones: insights into a basaltic fissure eruption. Bull Volcanol 78:1–18. https://doi.org/10.1007/s00445-016-1029-0

Richter DH, Eaton JP, Murata KJ et al (1970) Chronological narrative of the 1959-60 eruption of Kilauea volcano. Hawaii. US Geol. Surv. Prof. Paper:537

Sigurdsson H (2000) Volcanic episodes and rates of volcanism. In: Encyclopedia of volcanoes. Academic Press, San Diego, pp 271–279

Stevenson DS, Blake S (1998) Modelling the dynamics and thermodynamics of volcanic degassing. Bull Volcanol 60:307–317

Stothers RB, Wolff JA, Self S, Rampino MR (1986) Basaltic fissure eruptions, plume heights, and atmospheric aerosols. Geophys Res Lett 13:725–728

Stovall WK, Houghton BF, Harris AJL, Swanson DA (2009) Features of lava lake filling and draining and their implications for eruption dynamics. Bull Volcanol 71:767–780

Sumner JM, Blake S, Matela RJ, Wolff JA (2005) Spatter. J Volcanol Geotherm Res 142:49–65

Swanson DA, Duffield WA, Jackson DB et al (1979) Chronological narrative of the 1969-71 Mauna Ulu eruption of Kilauea Volcano. Hawaii US Geol Surv Prof Paper:1056

Swanson DA, Fabbi BP (1973) Loss of volatiles during fountaining and flowage of basaltic lava at Kilauea volcano, Hawaii. J Res US Geol Surv 1:649–658

Thorarinsson S, Steinthorsson S, Einarsson T et al (1973) The eruption on Heimaey, Iceland. Nature 241:372–375

Thordarson T, Self S (1993) The Laki (Skaftár Fires) and Grimsvötn eruptions in 1783-1785. Bull Volcanol 55:233–263

Tilling R, Christian R, Duffield WA et al (1987) The 1972-1974 Mauna Ulu eruption, Kilauea Volcano: an example of quasi steady-state magma transfer. US Geol Surv Prof Pap 1350:405–469

Tilling RI (1987) Fluctuations in surface height of active lava lakes during 1972-1974 Mauna Ulu eruption, Kilauea volcano, Hawaii. J Geophys Res Solid Earth 92:13721–13730

Valentine GA, Gregg TKP (2008) Continental basaltic volcanoes—processes and problems. J Volcanol Geotherm Res 177:857–873

Wadsworth FB, Kennedy BM, Branney MJ et al (2015) Exhumed conduit records magma ascent and drain-back during a Strombolian eruption at Tongariro volcano, New Zealand. Bull Volcanol 77:1–10. https://doi.org/10.1007/s00445-015-0962-7

Walker GPL, Self S, Wilson L (1984) Tarawera 1886, New Zealand a basaltic plinian fissure eruption. J Volcanol Geotherm Res 21:61–78

Whitehead JA, Helfrich KR (1991) Instability of flow with temperature-dependent viscosity: a model of magma dynamics. J Geophys Res Solid Earth 96:4145–4155. https://doi.org/10.1029/90JB02342

Wilson L, Parfitt EA, Head JW (1995) Explosive volcanic eruptions—VIII. The role of magma recycling in controlling the behaviour of Hawaiian-style lava fountains. Geophys J Int 121:215–225. https://doi.org/10.1111/j.1365-246X.1995.tb03522.x

Witham F, Llewellin EW (2006) Stability of lava lakes. J Volcanol Geotherm Res 158:321–332

Wolfe EW (ed) (1988) The Puu Oo eruption of Kilauea Volcano, Hawaii: episodes 1 through 20, January 3, 1983 through June 8, 1984. US Geol Surv Prof Pap 1463:251

Woods AW (1993) A model of the plumes above basaltic fissure eruptions. Geophys Res Lett 20:1115–1118

Wright TL, Kinoshita WT, Peck DL (1968) March 1965 eruption of Kilauea volcano and the formation of Makaopuhi lava lake. J Geophys Res 73:3181–3205

Wunderman R (2002) Report on Nyiragongo (DR Congo). Bull Glob Volcanism Netw. https://doi.org/10.5479/si.GVP.BGVN200204-223030

Wylie JJ, Helfrich KR, Dade B et al (1999) Flow localization in fissure eruptions. Bull Volcanol 60:432–440. https://doi.org/10.1007/s004450050243

Wylie JJ, Lister JR (1995) The effects of temperature-dependent viscosity on flow in a cooled channel with application to basaltic fissure eruptions. J Fluid Mech 305:239–261

Appendix B

Accepted work (in press)

SCIENTIFIC REPORTS

OPEN

Spatter matters – distinguishing primary (eruptive) and secondary (non-eruptive) spatter deposits

Received: 1 March 2018
Accepted: 29 May 2018
Published: xx xx xxxx

T. J. Jones[1], B. F. Houghton[2], E. W. Llewellin[1], C. E. Parcheta[3] & L. Höltgen[1,4]

Spatter is a common pyroclastic product of hawaiian fountaining, which typically forms vent-proximal ramparts or cones. Based on textural characteristics and field relations of spatter from the 1969 Mauna Ulu eruption of Kīlauea, Hawai'i, three spatter types were identified: (1) Primary spatter deposited as spatter ramparts and isolated cones during the peak of episode 1; (2) Late-stage spatter comprising dense, small volume, vent proximal deposits, formed at the end of episode 1; (3) Secondary spatter preserved in isolated mounds around tectonic ground cracks that we interpret to have formed by the disruption of overlying lava. We propose that not all spatter deposits are evidence of primary magmatic fountaining. Rather, deposits can be "secondary" in nature and associated with lava drain-back, disruption, and subsequent ejection from tectonic cracks. Importantly, these secondary pyroclastic deposits are difficult to distinguish from primary eruptive features based on field relations and bulk clast vesicularity alone, allowing for the potential misinterpretation of eruption vents, on Earth and in remotely sensed planetary data, thereby misinforming hazard maps and probabilistic assessments. Here, we show that vesicle number density provides a statistically-robust metric by which to discriminate primary and secondary spatter, supporting accurate identification of eruptive vents.

Basaltic hawaiian fountaining can produce a range of pyroclastic products defined by the cooling efficiency within the parent fountain[1,2]. The continuous spectrum ranges from brittle basaltic scoria and spindle bombs, which have experienced substantial cooling, to hot fluidal clasts – termed spatter – that agglutinate (flatten and/or adhere)[2] on landing because they remain predominantly above the glass transition temperature (T_g)[3]. The degree of spatter welding depends on the clasts' temperature upon impact and the accumulation rate. For a low cooling rate and/or high accumulation rate, spatter becomes rheomorphic, and may feed a clastogenic lava flow[1,4–8]. For a moderate cooling rate and/or low accumulation rate, the spatter forms agglutinated cones and ramparts as summarized by the classification scheme in Sumner *et al.*[2].

The locations of pyroclastic products, such as scoria cones and spatter, observed in the field and by remote sensing are commonly used to identify the sites of previous eruptions[9–12]. Mapping of eruption vents has been performed on basaltic fissure systems, such as on Etna volcano, Italy, to produce a spatial probability map for the location of future volcanic eruptions[12]. Similarly, the identification of volcanic landforms has been used to infer volcanic activity on other planets[13,14]. However, most of this work relies on the assumption that spatter, and/or other pyroclasts, is erupted from a primary magma pathway transporting material to the surface. We note that there are three counter-examples recognized in the literature: rootless cones, which form through explosive interactions as lava propagates over a water-saturated, unconsolidated substrata[15,16]; hornitos, which form on the top of lava, by pressurized ejection of lava through gaps in the lava crust[7]; and littoral cones, which form through secondary disruption as lava enters the sea[17]. In this study, we will explore another enigmatic type of secondary spatter pyroclastic deposit that, to our knowledge, has never been described before.

The quantification and analysis of vesicle size distributions (VSD) and vesicle number densities (VND) in eruptive products is commonly used to constrain ascent and decompression processes[18–20], conduit dynamics[21], and bubble nucleation and growth[22–25]. Importantly for this study, the vesicle size or volume distribution preserved within a pyroclast is not simply a function of nucleation rate or volatile concentration, but instead

[1]Department of Earth Sciences, Durham University, South Road, Durham, DH1 3LE, UK. [2]Department of Geology & Geophysics, SOEST, University of Hawai'i at Mānoa, Honolulu, HI, 96822, USA. [3]U.S. Geological Survey, Hawaiian Volcano Observatory, Hawaii Volcanoes National Park, HI, 96718, USA. [4]Department of Earth and Environmental Sciences, LMU Munich, Theresienstr. 41, 80333, Munich, Germany. Correspondence and requests for materials should be addressed to T.J.J. (email: t.j.jones@durham.ac.uk)

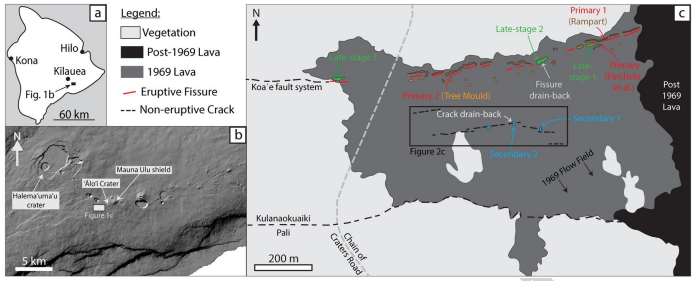

Figure 1. (**a**) Overview map of the Island of Hawai'i with the location of our field area marked. (**b**) The location of Mauna Ulu with reference to other landforms on the southern flank of Kilauea. Modified from Jones *et al.*[35] and reproduced under the Creative Commons Attribution 4.0 International License (http://creativecommons.org/licenses/by/4.0/). (**c**) Interpretative map of the Mauna Ulu 1969 episode 1 fissure vents and associated products. Colour-coded arrows indicate locations where spatter and lava samples were taken. The central black box marks the field of view in Fig. 2c. Numbering only distinguishes different sampling locations and has no temporal meaning. Note that the modern Chain of Craters Road labelled in this figure is in the same location as the old 'Āinahou Road described by Swanson *et al.*[33].

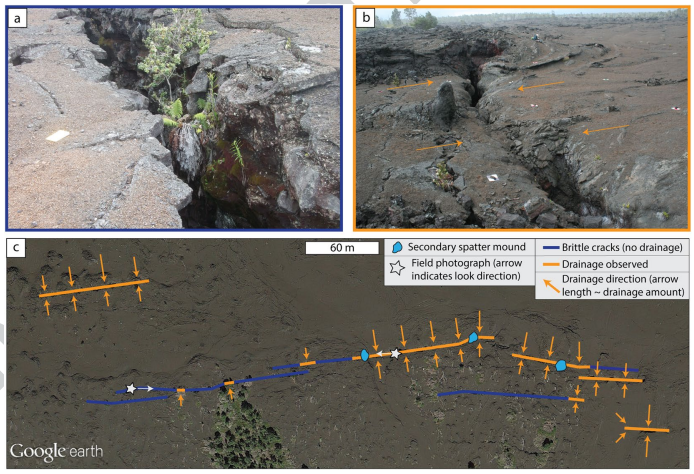

Figure 2. Field photographs and aerial images of the ground cracks. (**a**) Complementary jigsaw-fit ground cracks cross-cutting the 1969 surface lava (and older lavas at depth). There is no evidence here that the surface 1969 lava was mobile when the crack opened. For scale, the white rectangle in the photograph measures 24 cm by 13 cm. (**b**) Prominent southward-draining lava channel cut by a ground crack. Lava can be observed draping down into the crack. Ground squares measure 30.5 cm by 30.5 cm. (**c**) Annotated Google Earth image showing regions of the southern ground cracks where either simple brittle ground cracking is observed (marked in blue) or where drainage of the surface lava down into the cracks is observed (marked in orange). The length of the orange arrows indicates the relative amount and direction of drainage. The photograph locations and look directions are indicated by the white stars.

is modified through time by expansion, coalescence, and collapse processes[22,26,27]. Hence, the quantitative textural analysis of the vesicle population can provide information on the timing of magma fragmentation and the extent of shallow conduit recycling (i.e. upper 10's of m) and surface flow[21,28]. Previously, vesicularity studies of pyroclasts from hawaiian fountains have been largely confined to high fountaining episodes[19,20,27,29,30], with only Parcheta *et al.*[31] analysing low-fountaining activity (defined as a fountain with height <100 m)[32]. In this paper we expand the quantification of vesicle textures for low fountaining hawaiian eruptions and set out a framework for distinguishing primary from secondary spatter.

Field evidence for a new type of spatter

Field investigation of the episode 1 deposits of Mauna Ulu identified spatter that is not associated with a primary volcanic vent. In this section we briefly review the field context that underpins this inference.

The 1969-74 Mauna Ulu eruption. Mauna Ulu is located on the East Rift Zone (ERZ) of Kīlauea volcano, Hawai'i (Fig. 1). On May 24th, 1969, episode 1 of the 1969–74 eruption initiated with an earthquake swarm. At 04:45 Hawaiian Standard Time (HST) low fountaining began from a newly formed fissure system, east of 'Ālo'i Crater[33]. The fissure system rapidly propagated 1 km eastwards and 3 km westwards, crossing the old, now abandoned, Chain of Craters Road by 05:00 HST and crossing 'Āinahou Road (which has become the current Chain of Craters Road; Fig. 1) at 08:30 HST[33]. Steady fountaining and lava ponding around the fissure occurred until 1200–1300 HST[34] and fed a southward-advancing pāhoehoe field. The steady fountaining was followed by a period of waning fountaining and lava drain-back ending at 22:00 HST[34,35]. This was the end of episode 1 fountaining in our field area (Fig. 1), but subsequent episodes occurred to the east, where weak episode 1 fountaining continued until ~15:00 HST on May 25. All spatter described here is related to the episode 1 activity, however for a complete narrative of the 1969–74 Mauna Ulu eruption, readers are directed to Swanson *et al.*[33] and Tilling *et al.*[36].

Tectonic ground cracks: field evidence and eyewitness accounts. In addition to the fissure containing the eruptive vents at Mauna Ulu, there are several large tectonic ground cracks approximately 100–200 m to the south, oriented roughly parallel to the fissure (marked in a black box in Fig. 1). Based on their location and orientation, the cracks are likely associated with the ongoing tensional opening of the ERZ caused by the seaward movement of Kilauea's southern flank[37,38]. Swanson *et al.*[33] reported that ground cracks in this region opened during the morning of April 9th, 1970 *"accompanied by emission of fume"* and propagated westwards to reach the current Chain of Craters Road by 10:00 HST April 10th. Importantly for this study, Swanson *et al.*[33] describe that these cracks did not act as eruption sites. They also document that these cracks widened through time, growing to widths of ~1 m. However, following the field evidence of Parcheta *et al.*[34] we now know that this 1970 event was, probably a reactivation of older tectonic cracks and/or creation of new ground cracks.

To establish a relative timing of crack opening and emplacement of the 1969 lava, we mapped the morphological characteristics of the ground cracks. We observed two distinct features: firstly, piercing points, which are simple saw-tooth edges where complementary 'jigsaw-fit' shapes can be observed at either side of the crack (Fig. 2a); secondly, a mantle of draping lava, indicating drainage of 1969 surface lava into the crack (Fig. 2b). The well-developed 1969 lava channels are cross cut by the ground cracks that show crack-drainage (Fig. 2b) and in some cases the cracks have small (<3 m) vertical offsets that displace the lava high-stand surface. Thus, we can interpret the relative timing of crack opening: cracks associated with simple saw-tooth morphology formed after the 1969 lava had cooled, most likely in April of 1970 (blue; Fig. 2c); whereas segments with lava drainage drapery opened/widened during the waning stages or immediately after the May 1969 eruption (orange; Fig. 2c).

Episode 1 spatter deposits. Episode 1 of the Mauna Ulu eruption produced three distinctly different types of spatter deposit. The main primary deposit[34], is to the north and intermittently to the south of the eruptive fissure as a discontinuous series of asymmetrical spatter ramparts (Fig. 3a). The ramparts can be found along 80% of the fissure length on the northern side, they vary considerably in height from 0.7 m to 7.1 m, and are typically set back by ~10 m from the eruptive vent[34]. Clasts within the ramparts are highly agglutinated (especially towards the deposit base) and elongate (Fig. 3b). South of the eruptive fissure, isolated spatter mounds can be found on the top of tree moulds[34]. Clasts preserved on the tree moulds show less agglutination and are more fluidal in shape relative to those observed in the rampart interior (Fig. 3d). Both the spatter found within the ramparts and on top of tree moulds are the products of episode 1 fountaining deposited proximally to the vent[33]. Therefore, in this work, this type of spatter is termed 'primary spatter'.

A second type of spatter deposit is found overlying 'drain-back' lava at the primary fissure. Flow directions quantified in previous studies show that, during the waning stages of episode 1, some of the lava drained back into the fissure vents[33–35]. In some locations, and only within ~5 m of the eruptive vents, clasts of spatter are found on top of the back-draining 1969 lava carapace (Fig. 3e). This spatter does not form mounds or ramparts because the deposit is rarely greater than a single clast thick. The clasts are fluidal in morphology, varying from highly elongate strands and droplets to more circular discoidal shapes and have a dark green/blue surface colour (Fig. 3f). It is likely that the larger clasts broke up upon impact forming adjacent smaller droplets[2]. The field relations indicate that this spatter was emplaced following lava drain-back into the fissure vent, hence we term this 'late-stage spatter'.

A third, rare type of spatter deposit is observed associated with the southern tectonic ground cracks (Fig. 2). As previously described, these fissures are known not to have erupted any magma during the eruption, yet prominent spatter mounds (Fig. 3g) occur at three locations along these cracks (Fig. 1). Without eye-witness accounts, it would be extremely difficult to distinguish portions of these ground cracks from the main 1969 eruptive vents to the north. The spatter is concentrated very close (<1 m) to the cracks (Fig. 3g), although rare individual single clasts can be found up to ~6 m on either side of the crack. The discrete mounds are only found on relative

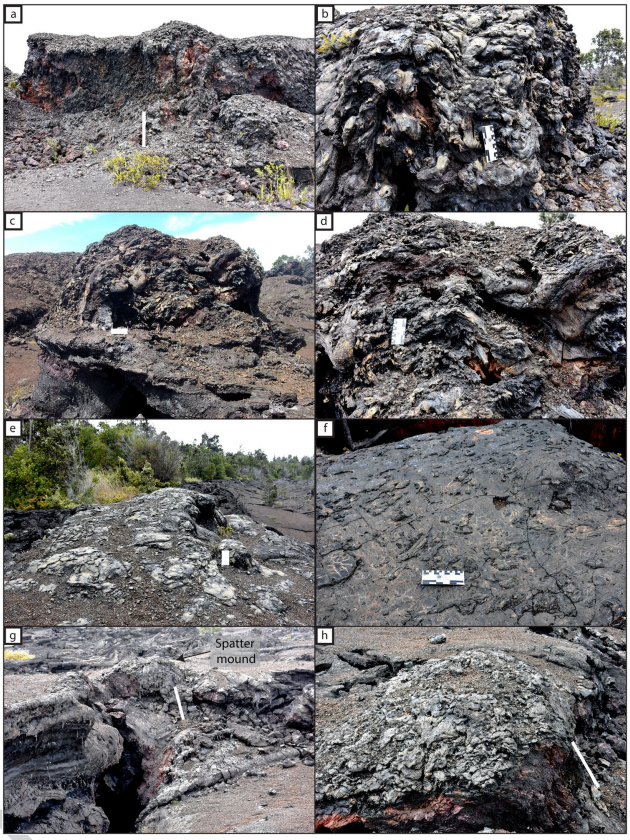

Figure 3. Field photographs of the three different spatter types described in this study: primary (**a–d**); late-stage (**e**,**f**) and secondary (**g**,**h**). (**a**) A spatter rampart that formed on the northern side of the 1969 Mauna Ulu eruptive fissure; (**b**) agglutinated rampart interior with many clasts showing post depositional flow; (**c**) primary spatter located on top of a tree mould south of the eruptive fissure; (**d**) interior of tree mould spatter mound, where clasts are less welded compared to those in the north rampart deposits; (**e**) green/blue vent proximal late-stage spatter forming a thin deposit on top of the drain-back lava; (**f**) typical late-stage spatter clasts showing a wide range of fluidal shapes; (**g**) a secondary spatter mound formed over a ground crack to the south and (**h**) a close up view of a secondary spatter mound. Scales (marked in white if unclear) measure 16 cm for all images except in a, g and h where the scale is 1.2 m.

topographic highs and/or at an en echelon step. The clasts themselves (Fig. 3h), are highly variable in physical appearance; many isolated clasts (i.e. those not forming mounds) are thin discs and sheets whereas clasts forming mounds are slightly rheomorphic. Many clasts are cracked, and have a green/blue outer colour, similar to the late-stage spatter. We term this type of spatter on the non-eruptive cracks as 'secondary spatter'.

Methods

Field sampling. Around 100 clasts of each sample type were collected during March 2015 and May 2017. During sampling, clasts were chosen at random from a small area and, where the deposits were thick, samples

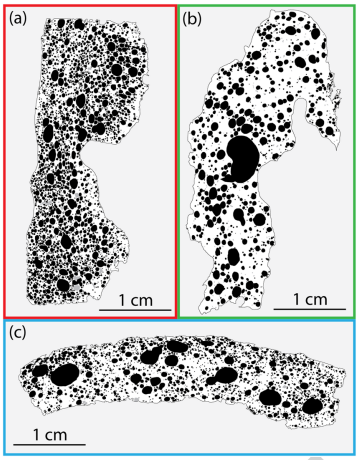

Figure 4. A representative binary thin section image for: (**a**) primary spatter; (**b**) late-stage spatter and (**c**) secondary spatter. Large vesicles and phenocrysts are shaded black and grey respectively.

were limited to single stratigraphic horizons. Figure 1 marks the exact sample locations. The primary spatter was collected from the interior of one of the northern ramparts, towards the eastern end of the eruptive fissure, and from the top of a tree mould located 4.2 m south of the vent. The spatter from the rampart and tree mould collectively provide the primary spatter dataset. The late-stage spatter was sampled in three locations along the eruptive fissure: at the western end of the eruptive fissure, where it joins the Koa'e fault system, in the low eastern section of the episode 1 fissure where the vent is completely covered in lava, and at a flared, circular vent segment, towards the eastern end of the eruptive fissure as currently exposed. The secondary spatter was collected from two prominent mounds (Secondary spatter 1 and 2; Fig. 1) adjacent to the southern ground cracks. For bulk vesicularity comparisons, samples of lava crust that were obviously *in-situ* were broken up and sub-samples collected at random. This was done at two localities: directly above the, now covered, eruptive fissure labelled as "Fissure drain-back" and adjacent to the ground cracks labelled as "Crack drain-back" (Fig. 1).

Bulk vesicularity. A minimum of 95 clasts from each sample type (spatter and lava) were measured for bulk density using the Archimedes techniques outlined in Houghton and Wilson, (1989)[39]. The bulk vesicularity was calculated using a dense rock equivalent density ($2873 \pm 5\,kg\,m^{-3}$) measured independently by He pycnometry. From five repeat measurements on the same spatter clast we report a maximum absolute uncertainty associated with each clast bulk vesicularity determination of $\pm 1\%$ vesicularity. The variation in vesicularity among different spatter types is considered later.

Quantitative vesicle analysis. From the samples measured for bulk density, 14 were selected for quantitative vesicle analysis; samples were chosen to cover a range of spatter types and bulk vesicularity. If a clast had a quenched rim and a micro-crystalline core, the two parts were separated and only the quenched rim was analysed as the bubbles in the core have been modified by crystallisation and inflation after deposition. The quenched rims, and therefore all our data, represent textures immediately following clast formation. A nested image analysis approach[22] was adopted to accurately capture all bubble sizes using: (1) full thin section scans taken at 4800 dpi on a flatbed scanner and, (2) large back-scattered electron (BSE) image grids taken at 130× magnification on a Hitachi SU-70 scanning electron microscope (SEM). The SEM operating conditions were: a 15 kV accelerating voltage, a 45 μA beam current, a 15 mm sample working distance, and a 32 μs dwell time during image acquisition. All the images were then manually traced using Inkscape or Adobe Illustrator to create binary masks of vesicles and phenocrysts (Fig. 4). We note that, during tracing, vesicles were not heavily de-coalesced; only undeformed vesicles with thin ($\sim \leq 50\,\mu m$) joining septa were de-coalesced. Quantification of the binary masks was performed with ImageJ software to obtain vesicle areas and ultimately the 2D areal vesicle number density (N_A). N_A was then corrected for phenocrysts and converted to a volumetric (3D) vesicle number density (N_V) following the method of Proussevitch and Sahagian (1998)[40]. In samples where only the quenched rim was analyzed (denoted by a "q" in the sample names) we normalized to the image vesicularity, rather than the bulk vesicularity, after Stovall *et al.*[29]. Lastly, N_V was referenced to the melt volume to account for the volume occupied by the vesicles themselves[25]. This forms the final metric, N_{Vm} that we use throughout this study.

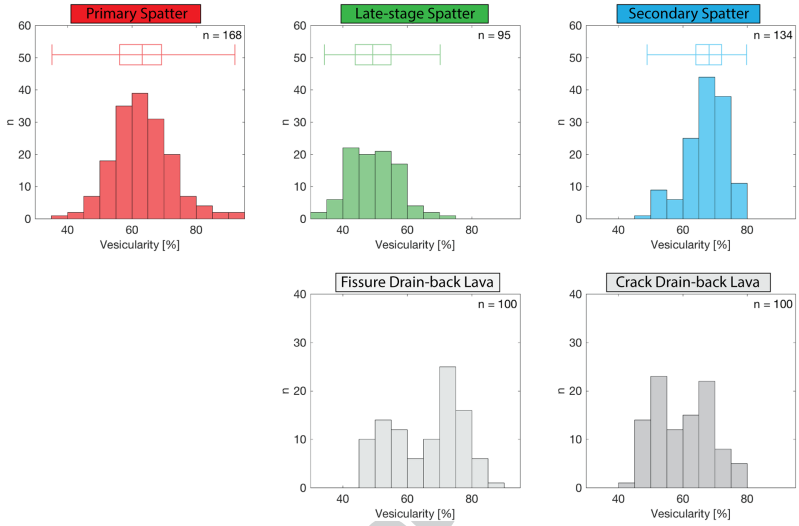

Figure 5. Bulk vesicularity histograms for all spatter types, the drain-back lava sampled close to the fissure vent, and the drain-back lava along the southern ground cracks. The number of samples (n) measured is reported for each dataset. The box and whisker plots display the data range (whiskers) and the first quartile, median and third quartile (box). Box and whisker plots were not calculated for the lavas, as these data are clearly bimodal.

Q2 **Data availability.** The datasets generated during and/or analysed during the current study are available from the corresponding author upon request.

Results

Bulk clast vesicularity. Figure 5 shows the bulk vesicularity histograms for the primary (red), late-stage (green) and secondary (blue) spatter with median bulk vesicularity values of 63%, 49% and 68% respectively. The primary spatter displays a normal, unimodal distribution. The late-stage spatter is also unimodal but has a broader peak. However, the secondary spatter shows a slight bimodality with modes at 50–55% and 65–70%. As indicated by the box-plots in Fig. 5, the secondary spatter samples are tightly distributed, with the smallest inter-quartile range of all the sample types.

Samples of lava preserved proximally to the eruptive fissure also show a bimodal distribution with modes at 50–55% and 70–75% vesicularity. These two modes reflect vesicle poor and vesicle rich domains in the lava respectively. Lava samples close to the southern ground cracks again show a bimodal distribution with similar subpopulation modes at 50–55% and 65–70% vesicularity. We note that the relative proportion of these subpopulations changes between the two lava types; the crack drain-back lava is relatively enriched in the denser subpopulation and depleted in the more vesicular subpopulation. Furthermore, although most of the lava is spatter-fed, it is extremely rare to find any remaining textural evidence of a rheomorphic origin.

Qualitative textural observations. The three spatter types are texturally distinct on visual inspection. The primary spatter contains abundant small vesicles that are mainly spherical, although, some vesicles are elongated, especially those close to a clast margin (Fig. 4a). In contrast, the late-stage spatter has much coarser vesicles and very few small vesicles. The vesicles themselves are spherical, except where coalescence is evident (Fig. 4b). Microlites are common in the late-stage groundmass. The secondary spatter vesicle population qualitatively lies between the late-stage and primary spatter; it has a large number of small, spherical vesicles but also some larger vesicles and coalescence textures (Fig. 4c). No systematic changes in phenocryst content are observed among sample types; all samples have plagioclase and olivine phenocryst abundance $\leq$2.5%.

Quantitative textural observations. *Vesicle number densities.* The melt-referenced vesicle number densities (N_{Vm}) range from 1.42×10^4 to 2.50×10^6 vesicles per cm^3 across all the sample types (Table S1). Primary spatter has the highest N_{Vm} with a mean of $1.67 \times 10^6\,cm^{-3}$. In contrast, the late-stage spatter has the lowest N_{Vm} ($3.87 \times 10^5\,cm^{-3}$) and the largest range in N_{Vm} with values varying from 1.42×10^4 to $7.54 \times 10^5\,cm^{-3}$. Secondary

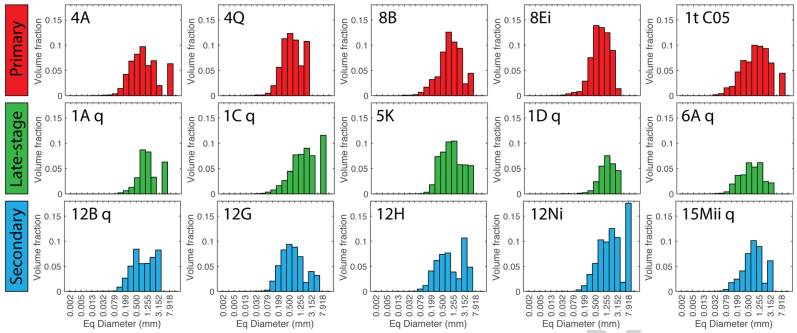

Figure 6. Vesicle size distribution histograms for primary (red), late-stage (green) and secondary (blue) spatter. The equivalent (Eq) diameter is calculated from the traced vesicle area, assuming a circular cross-section.

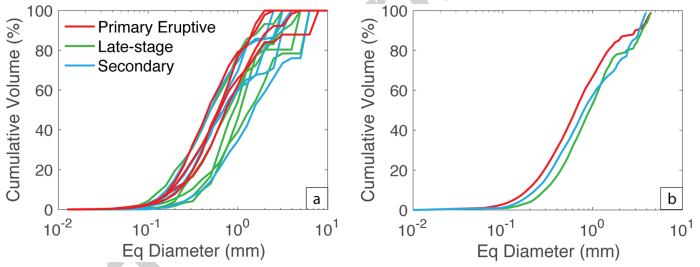

Figure 7. Cumulative vesicle volume % curves colour coded for sample type. (**a**) All samples, where each line represents an individual clast and (**b**) mean cumulative curves produced by calculating the average equivalent diameter for each percent from 0 to 100%.

spatter has an intermediate N_{Vm} (mean: $5.77 \times 10^5\,cm^{-3}$). The range of vesicle number densities for secondary spatter is also very small compared to the other sample types (Table S1).

Vesicle size distributions. The vesicle size distributions (VSD), expressed as a volume fraction, also vary according to spatter type. Figure 6 shows VSD histograms binned for equivalent spherical diameter. Primary spatter (red; Fig. 6) displays a variably unimodal, near normal distribution with a relatively high volume fraction; a consequence of the high bulk vesicularity of primary spatter. A small secondary mode at 3 to 8 mm in some samples is due to coalescence of the largest vesicles. The late-stage spatter (green; Fig. 6) has a lower volume fraction (due to its lower bulk vesicularity), distributions that are slightly negatively skewed, and are mainly unimodal with the exceptions of samples 1C and 1A that have an additional coalescence-driven coarse mode at 8 mm and 5 mm equivalent diameter bins respectively. The secondary spatter volume fractions are comparable to the primary spatter, as expected from their similar bulk density (Fig. 5), however, the size distributions are distinctly different. The secondary spatter (blue; Fig. 6) VSD histograms are broad and generally bimodal with a fine mode at 0.5 mm and a coarse mode at 3.15 mm. An outlier, 12Ni, still shows a bimodal distribution but has fine and coarse modes at 1.98 mm and 7.92 mm respectively.

Figure 7a presents all VSD data in terms of cumulative volume percent. To aid comparison among spatter types we calculate the mean average cumulative distribution curves for each sample type (Fig. 7b); specifically, we calculated the mean equivalent diameter for each cumulative volume from 1 to 100%. This plot clearly shows the contrast between the three spatter types both in terms of the size of the dominant subpopulation and the relative significance of a coarse, coalescence-related subpopulation. The primary spatter has the finest VSD with a median (50%) equivalent diameter of 0.65 mm. In comparison, both the secondary and late-stage spatter have coarsened distributions with median diameters of 0.80 and 0.93 mm respectively. Also worthy of note is that the late-stage

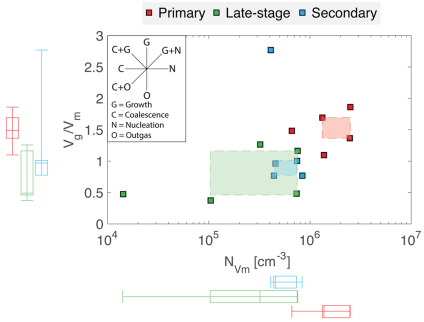

Figure 8. Volume ratio of gas (V_g) to melt (V_m) plotted against the melt-referenced vesicle number density (N_{Vm}) for all spatter types. The box and whisker plots display the data range (whiskers) and the first quartile, median and third quartile, collectively forming the inter-quartile range (IQR; box). Shaded fields represent the overlapping IQR of both V_g/V_m and N_{Vm}. Primary spatter can be distinguished from the secondary and late-stage spatter based on vesicle number density (N_{Vm}).

spatter is extremely depleted in small vesicles but shares a similar secondary mode to the secondary spatter at high (>80%) cumulative volume fractions.

Discussion

The production of spatter is most commonly attributed to primary magmatic fragmentation, where magma is disrupted and subsequently entrained by a rising gas jet as hot, incandescent pyroclasts[41]. This eruption style is typical of hawaiian fountaining and produces spatter cones/mounds, ramparts and/or clastogenic lava flows[2,6,8], although it is not limited to mafic volcanism – similar deposits are associated with felsic magmas[42,43]. However, in all these cases spatter mounds and ramparts are located proximally to the vent system, and the presence of spatter may be taken as indicative of proximity to an eruptive vent. Spatter deposits have been found to occur along tectonic ground cracks, but only where those cracks have been occupied as magma ascent pathways during eruption. For example, at Gjástykki, Iceland, magma rose along pre-existing ground cracks, leading to the formation of spatter cones[44].

In this work, we have shown that spatter mounds can also be associated with non-eruptive ground cracks into which lava drained. The clear spatial clustering of secondary spatter along the cracks removes the possibility that simple rafting of primary spatter on top of lava flows formed the deposits. Based on field observations alone, and in the absence of microtextural analysis of the pyroclasts, certain regions of these ground cracks could easily be mistaken for primary eruptive vents. Secondary spatter (as spatter mounds) associated with the ground cracks is difficult to distinguish from primary spatter in the field since both deposits have comparably high bulk vesicularity, are located along fissures/cracks and lie on top of co-existing lavas. Therefore, field observations alone are not enough to identify the difference between primary and secondary spatter, and a more detailed micro-textural analysis is required.

Micro-textural interpretations. In hawaiian pyroclasts, vesicle number densities and size distributions can reveal information on bubble nucleation, growth, coalescence, the timescales of magma ascent and the influence of post-fragmentation expansion, if present, within the thermally insulated fountain interior[20,22,27,29,30,45,46]. However, the micro-textural study of mafic melts provides challenges. Their high temperature and low viscosity promote post-eruption bubble expansion and coalescence, which can overprint original shallow conduit textures[31]. In our case, however, this is advantageous; the textures we wish to contrast are those at final deposition and not necessarily the vesicle textures at primary fragmentation. To aid comparison between the spatter types, we plot (Fig. 8) the melt-referenced vesicle densities (N_{Vm}) as a function of the ratio of the volume of gas V_g to volume of melt V_m after Stovall *et al.*[29]. Specifically, $V_g/V_m = \phi v(1+\phi_p)/(1-\phi_b)$, where ϕ_v is the volume fraction of vesicles and ϕ_p is the modal proportion of phenocrysts[47]. On this plot (Fig. 8; top-left sub panel), different trends denote different physical processes; for example, a decrease in the gas to melt volume ratio without changing the vesicle number density would indicate pure outgassing (the loss of gas from the system).

The primary spatter has the highest vesicle number densities and gas to melt volume ratios recorded in this study. The VSD of primary spatter sampled is unimodal reflecting one period of nucleation and growth followed by minor coalescence. However, if a range of primary pyroclasts were to be sampled systematically from fountains of different height and/or from different positions within a fountain, or for a wide range of particle sizes, we would expect to see a range of vesicle textures resulting from different degrees of overprinting by coalescence and/or expansion. This has been previously observed at Mauna Ulu[31] and Kīlauea Iki[27,29] where increased coalescence was interpreted to be a result of longer residence time in the hot interior of the fountain (10's of seconds available for coalescence).

The late-stage spatter has much lower vesicle number densities and slightly lower gas to melt volume ratios compared to the primary spatter (Fig. 8; Table S1). The change from the primary spatter to the late-stage spatter indicates an evolution involving both outgassing (escape of gas) and coalescence of new bubbles after nucleation had ceased (Fig. 8). Furthermore, this is supported by the VSDs (Fig. 7) that show a coarsening and increased bimodality resulting from the reduced abundance of small vesicles as early, nucleated bubbles had expanded and coalesced. Additionally, the bulk vesicularity of the late-stage spatter is on average 13.5% lower than the primary spatter (Fig. 5), supporting the interpretation that the magma producing these late-stage clasts was more outgassed.

The micro-textural data from the secondary spatter reveals a bimodal VSD (Fig. 6) and a reduced vesicle number density relative to the primary spatter (Fig. 8) interpreted to result from bubble coalescence. The secondary VSD is coarser than the primary spatter but finer than the late-stage spatter at equivalent vesicle diameters <63 μm but becomes coarser or comparable to the late-stage spatter at larger equivalent vesicle diameters. This suggests that the secondary spatter underwent less coalescence than the late-stage spatter and was able to retain (not outgas) more of its larger bubbles.

We have shown the difficulty in identifying spatter types based on bulk density and field relationships alone. Now, the hypothesis that the three spatter types (primary, late-stage and secondary) can be separated based upon their vesicle number density (N_{Vm}) is tested quantitatively using a two-way analysis of variance (ANOVA). The ANOVA test results are shown in Table S2. The null hypothesis (the two sample types are drawn from the same distribution) can be rejected at the 0.05% level (P-vales > 0.05) for Primary – Late-stage and Secondary – Primary comparison. This means that, based on vesicle number density (N_{Vm}), primary spatter can be distinguished from both late-stage and secondary spatter. However, secondary and late-stage cannot be distinguished using this approach. An ANOVA test was also performed using V_g/V_m, but this produced less statistically significant separations between sample types. Therefore, N_{Vm} is the best metric to distinguish primary spatter from the other types.

Spatter formation re-visited. Spatter is commonly described in association with (primary) magmatic fountaining driven by the expansion and exsolution of volatiles in the upper conduit[2,41]. Here, we have shown that some spatter deposits can form along ground cracks that did not act as pathways for ascending magma. This novel finding indicates a need for a more complete description of the formation conditions of the different spatter types. The formation of primary spatter has already been covered in great detail by many other studies[1–3,48]. In the case of Mauna Ulu, the primary spatter deposits were formed during episode 1 of the 1969 eruption by sustained weak fountaining reaching maximum heights of 50 m[33,34]. Primary spatter falling proximally (<20 m) downslope, downwind of the vent became incorporated into rheomorphic lava flows, whereas material falling >20 m downslope was rafted away on top of these lava flows[34]. Primary spatter was preserved locally on top of some tree moulds, which acted as high points, and local barriers to flow (Figs 1 and 3c). To the north (upwind and upslope) a near-continuous spatter rampart was formed (Figs 1 and 3a). For a complete description of primary spatter formation during episode one of the 1969 Mauna Ulu eruption, readers are referred to Parcheta *et al.*[31,34].

As the eruption and associated primary fountaining started to wane, vent-proximal ponded lava began to drain back down into the conduit locally[34,35]. Over time, the draining material and magma left stalled in the conduit matured by bubble coalescence and outgassing, causing the bulk magma vesicularity, the vesicle number density, and the gas to melt volume ratio to decrease (Figs 8 and 9b). We hypothesize that some parts of this maturing magma were ejected as late-stage spatter by the bursting of large, decoupled gas bubbles (Fig. 9c), which may have formed by two mechanisms: (1) As the dense lava that was ponded over the vent[35] drained back down the conduit, it trapped air pockets. (2) Within the stagnant shallow conduit, continued coalescence led to the formation of large gas pockets. We envisage this process to be similar to the dynamic coalescence, gas bubble rise and subsequent spattering that was inferred to occur when magma was relatively stagnant beneath Pu'u'Ō'ō during the 2004–2005 activity[49]. Furthermore, the late-stage spatter is only found extremely proximal to the fissure (<10 m), on top of the solidified drained lava surface, suggesting that the energy released by gas/air pockets bursting was small. Lastly, the mismatch between the bulk vesicularity of the fissure drain-back lava and the late-stage spatter (Fig. 5) supports our interpretations about the parent magma/lava. If the late-stage spatter had formed entirely from the proximal draining lava, their bulk vesicularity would be the same; instead we observe that the late-stage spatter is much denser because material in the conduit (either stalled magma or recycled lava) had an extended opportunity for bubble rise and escape.

During the formation of the primary spatter deposits (northern ramparts and tree mould caps), spatter-fed rheomorphic lava flows moved south[33–35]. During lava flow advance we suggest that the vesicularity of the flow evolved via a combination of two processes (Fig. 9d). Firstly, as lava flows advance, gas bubbles rise to create a stratified flow with a gas rich upper zone directly beneath the quenched surface crust[50–52]. Secondly, when material is erupted on short timescales (seconds) the volatiles are not likely to be in equilibrium with the co-existing silicate melt; hence, during lava flow advance (minutes) volatiles diffuse out of the melt and cause bubble growth, thereby increasing the lava bulk vesicularity. Our field evidence (cross-cutting relationships; Section 2.2), indicates that, after well-established southward trending drainage channels had developed in the flow field, tectonic ground cracks opened or widened beneath the lava flow whilst it was still mobile (Fig. 2). We hypothesise that crack opening was accompanied by upward rushing hot gas from depth (similar to the April 1970 event) which disrupted the overlying mobile, draining lava flow and created secondary spatter (Fig. 9e). Also, during drainage into the cracks air pockets may have become trapped and subsequently burst (as described for the late-stage spatter). Either of these mechanisms, or both in combination, could distribute secondary spatter, in very small volumes, at vent-proximal locations, where the flow was most mobile (orange; Fig. 2c). Furthermore, the bulk vesicularity data (Fig. 5) suggests that the lava disruption preferentially mobilised the less dense, vesicular portion of the stratified lava to form secondary spatter with modal bulk vesicularity of 65 to 70%, similar to that of the primary spatter, but with a larger modal vesicle size. Finally, small amounts of lava continued to drain down the

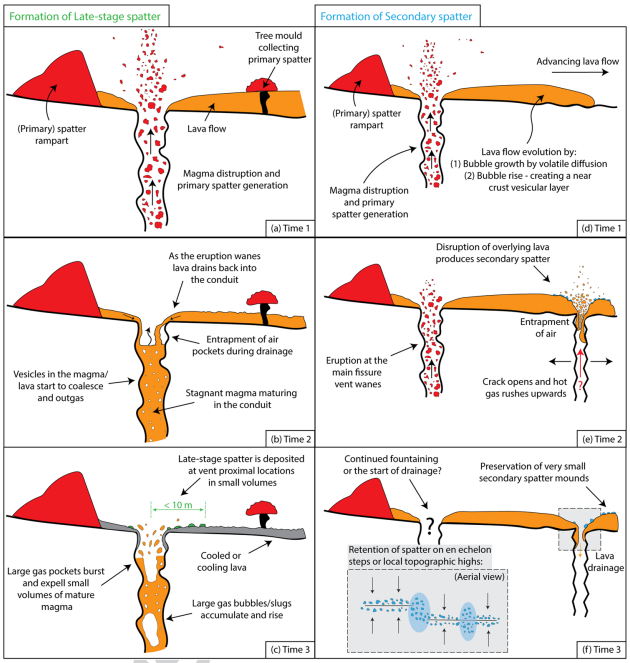

Figure 9. Schematic of the formation of the spatter types described in this study. Diagrams are not to scale. The view is to the east along strike of the Mauna Ulu fissure.

ground crack carrying most of the secondary spatter with it (Fig. 9f), only to leave small mounds on local topographic highs or en echelon jogs as observed in the field today (Fig. 1).

Conclusions

In this study, we have identified and described the formation mechanisms of three different types of spatter associated with hawaiian low fountaining using field observations, bulk density measurements and micro-textural analysis. Using a N_{Vm} *versus* gas to melt volume ratio plot (Fig. 8), a framework has been set out to help classify different low fountaining products based on their micro-textural properties. Furthermore, we have shown that it is possible to find spatter deposits adjacent to ground cracks that did not act as magma conduits and purely act as sites of lava drain-back and disruption to form a secondary pyroclastic deposit. Field relationships and macro-scale observations (e.g. bulk density) were not enough alone to distinguish these deposits as different from primary fissure-fed pyroclastic deposits. Consequently, this may lead to vent and eruption misinterpretation, incorrectly informing hazards and probabilistic assessments, and spatter landforms within remotely sensed (planetary) data may require further investigation before their origin can be ascribed. However, through a micro-vesicularity study it has been shown that, based upon vesicle number density (N_{Vm}), secondary deposits can be distinguished from the primary spatter generated by typical hawaiian fountaining. Therefore, N_{Vm} may be used as a classification metric to identity spatter types.

References

1. Head, J. W. & Wilson, L. Basaltic pyroclastic eruptions: influence of gas-release patterns and volume fluxes on fountain structure, and the formation of cinder cones, spatter cones, rootless flows, lava ponds and lava flows. *J. Volcanol. Geotherm. Res.* **37**, 261–271 (1989).
2. Sumner, J. M., Blake, S., Matela, R. J. & Wolff, J. A. Spatter. *J. Volcanol. Geotherm. Res.* **142**, 49–65 (2005).
3. Rader, E. & Geist, D. Eruption conditions of spatter deposits. *J. Volcanol. Geotherm. Res.* **304**, 287–293 (2015).
4. Thordarson, T. & Self, S. The Roza Member, Columbia River Basalt Group: A gigantic pahoehoe lava flow field formed by endogenous processes? *J. Geophys. Res. Solid Earth* **103**, 27411–27445 (1998).

5. Thordarson, T., Miller, D. J., Larsen, G., Self, S. & Sigurdsson, H. New estimates of sulfur degassing and atmospheric mass-loading by the 934 AD Eldgjá eruption, Iceland. *J. Volcanol. Geotherm. Res.* **108**, 33–54 (2001).
6. Karhunen, R. *Eruption mechanism and rheomorphism during the basaltic fissure eruption in Biskupsfell, Kverkfjöll, north-central Iceland*. (Thesis published by the Nordic Volcanological Institute, University of Iceland 1988).
7. Heliker, C., Swanson, D. A. & Takahashi, T. J. The Pu'u'O'o-Kupaianaha Eruption of Kilauea Volcano, Hawai'i: The First 20 Years. *US Geol. Surv. Prof. Pap.* **1676** (2003).
8. Sumner, J. M. Formation of clastogenic lava flows during fissure eruption and scoria cone collapse: the 1986 eruption of Izu-Oshima Volcano, eastern Japan. *Bull. Volcanol.* **60**, 195–212 (1998).
9. Bonali, F. L., Corazzato, C. & Tibaldi, A. Identifying rift zones on volcanoes: an example from La Réunion island, Indian Ocean. *Bull. Volcanol.* **73**, 347–366 (2011).
10. Becerril, L., Cappello, A., Galindo, I., Neri, M. & Del Negro, C. Spatial probability distribution of future volcanic eruptions at El Hierro Island (Canary Islands, Spain). *J. Volcanol. Geotherm. Res.* **257**, 21–30 (2013).
11. Neri, M. *et al*. Structural analysis of the eruptive fissures at Mount Etna (Italy). *Ann. Geophys.* **54**, 464–479 (2011).
12. Cappello, A. *et al*. Spatial vent opening probability map of Etna volcano (Sicily, Italy). *Bull. Volcanol.* **74**, 2083–2094 (2012).
13. Wilson, L. & Head, J. W. Mars: Review and analysis of volcanic eruption theory and relationships to observed landforms. *Rev. Geophys.* **32**, 221–263 (1994).
14. Wilson, L. & Head, J. W. A comparison of volcanic eruption processes on Earth, Moon, Mars, Io and Venus. *Nat.* **302**, 663–669 (1983).
15. Thorarinsson, S. The crater groups in Iceland. *Bull. Volcanol.* **14**, 3–44 (1953).
16. Hamilton, C. W., Thordarson, T. & Fagents, S. A. Explosive lava–water interactions I: architecture and emplacement chronology of volcanic rootless cone groups in the 1783-1784 Laki lava flow, Iceland. *Bull. Volcanol.* **72**, 449–467 (2010).
17. Moore, J. G. & Ault, W. U. Historic littoral cones in Hawaii. *Pacific Sci.* **19**, 8–11 (1965).
18. Toramaru, A. Numerical study of nucleation and growth of bubbles in viscous magmas. *J. Geophys. Res. Solid Earth* **100**, 1913–1931 (1995).
19. Mangan, M. T., Cashman, K. V. & Newman, S. Vesiculation of basaltic magma during eruption. *Geology* **21**, 157–160 (1993).
20. Cashman, K. V. & Mangan, M. T. Physical aspects of magmatic degassing; II, Constraints on vesiculation processes from textural studies of eruptive products. *Rev. Mineral. Geochemistry* **30**, 447–478 (1994).
21. Janebo, M. H., Houghton, B. F., Thordarson, T. & Larsen, G. Shallow conduit processes during the ad 1158 explosive eruption of Hekla volcano, Iceland. *Bull. Volcanol.* **10**, 1–17 (2016).
22. Shea, T. *et al*. Textural studies of vesicles in volcanic rocks: an integrated methodology. *J. Volcanol. Geotherm. Res.* **190**, 271–289 (2010).
23. Polacci, M., Pioli, L. & Rosi, M. The Plinian phase of the Campanian Ignimbrite eruption (Phlegrean Fields, Italy): evidence from density measurements and textural characterization of pumice. *Bull. Volcanol.* **65**, 418–432 (2003).
24. Lautze, N. C. & Houghton, B. F. Linking variable explosion style and magma textures during 2002 at Stromboli volcano, Italy. *Bull. Volcanol.* **69**, 445–460 (2007).
25. Klug, C., Cashman, K. & Bacon, C. Structure and physical characteristics of pumice from the climactic eruption of Mount Mazama (Crater Lake), Oregon. *Bull. Volcanol.* **64**, 486–501 (2002).
26. Klug, C. & Cashman, K. V. Vesiculation of May 18, 1980, Mount St. Helens magma. *Geology* **22**, 468–472 (1994).
27. Stovall, W. K., Houghton, B. F., Hammer, J. E., Fagents, S. A. & Swanson, D. A. Vesiculation of high fountaining Hawaiian eruptions: episodes 15 and 16 of 1959 Kilauea Iki. *Bull. Volcanol.* **74**, 441–455 (2012).
28. Lautze, N. C. & Houghton, B. F. Physical mingling of magma and complex eruption dynamics in the shallow conduit at Stromboli volcano, Italy. *Geology* **33**, 425–428 (2005).
29. Stovall, W. K., Houghton, B. F., Gonnermann, H., Fagents, S. A. & Swanson, D. A. Eruption dynamics of Hawaiian-style fountains: the case study of episode 1 of the Kilauea Iki 1959 eruption. *Bull. Volcanol.* **73**, 511–529 (2011).
30. Mangan, M. T. & Cashman, K. V. The structure of basaltic scoria and reticulite and inferences for vesiculation, foam formation, and fragmentation in lava fountains. *J. Volcanol. Geotherm. Res.* **73**, 1–18 (1996).
31. Parcheta, C. E., Houghton, B. F. & Swanson, D. A. Contrasting patterns of vesiculation in low, intermediate, and high Hawaiian fountains: a case study of the 1969 Mauna Ulu eruption. *J. Volcanol. Geotherm. Res.* **255**, 79–89 (2013).
32. Houghton, B. F. *et al*. Stronger or longer: Discriminating between Hawaiian and Strombolian eruption styles. *Geology* **44**, 163–166 (2016).
33. Swanson, D. A., Duffield, W. A., Jackson, D. B. & Peterson, D. W. Chronological narrative of the 1969–71 Mauna Ulu eruption of Kilauea Volcano, Hawaii. *US Geol. Surv. Prof. Pap.* **1056** (1979).
34. Parcheta, C. E., Houghton, B. F. & Swanson, D. A. Hawaiian fissure fountains 1: decoding deposits—episode 1 of the 1969–1974 Mauna Ulu eruption. *Bull. Volcanol.* **74**, 1729–1743 (2012).
35. Jones, T. J., Llewellin, E. W., Houghton, B. F., Brown, R. J. & Vye-Brown, C. Proximal lava drainage controls on basaltic fissure eruption dynamics. *Bull. Volcanol.* **79**, 81 (2017).
36. Tilling, R. *et al*. The 1972–1974 Mauna Ulu eruption, Kilauea Volcano: An example of quasi steady-state magma transfer. *US Geol. Surv. Prof. Pap.* **1350**, 405–469 (1987).
37. Lipman, P. W., Lockwood, J. P., Okamura, R. T., Swanson, D. A. & Yamashita, K. M. Ground deformation associated with the 1975 magnitude-7.2 earthquake and resulting changes in activity of Kilauea volcano, Hawaii. *US Geol. Surv. Prof. Pap.* **1276**, 45 (1985).
38. Moore, J. G. & Krivoy, H. L. The 1962 flank eruption of Kilauea Volcano and structure of the east rift zone. *J. Geophys. Res.* **69**, 2033–2045 (1964).
39. Houghton, B. F. & Wilson, C. J. N. A vesicularity index for pyroclastic deposits. *Bull. Volcanol.* **51**, 451–462 (1989).
40. Proussevitch, A. A. & Sahagian, D. L. Dynamics and energetics of bubble growth in magmas: analytical formulation and numerical modeling. *J. Geophys. Res. Solid Earth* **103**, 18223–18251 (1998).
41. Wolff, J. A. & Sumner, J. M. Lava fountains and their products. *Encycl. volcanoes* (ed. Sigurduson, H. *et al*.) 321–329 (2000).
42. Duffield, W. A. Eruptive fountains of silicic magma and their possible effects on the tin content of fountain-fed lavas, Taylor Creek Rhyolite, New Mexico. *Geol. Soc. Am. Spec. Pap.* **246**, 251–262 (1990).
43. Turbeville, B. N. Tephra fountaining, rheomorphism, and spatter flow during emplacement of the Pitigliano Tuffs, Latera caldera, Italy. *J. Volcanol. Geotherm. Res.* **53**, 309–327 (1992).
44. Opheim, J. A. & Gudmundsson, A. Formation and geometry of fractures, and related volcanism, of the Krafla fissure swarm, northeast Iceland. *Geol. Soc. Am. Bull.* **101**, 1608–1622 (1989).
45. Gonnermann, H. M. & Houghton, B. F. Magma degassing during the Plinian eruption of Novarupta, Alaska, 1912. *Geochemistry, Geophys. Geosystems* **13** (2012).
46. Wilson, L. & Head, J. W. Ascent and eruption of basaltic magma on the Earth andMoon. *J. Geophys. Res. Solid Earth* **86**, 2971–3001 (1981).
47. Gardner, J. E., Thomas, R. M. E., Jaupart, C. & Tait, S. Fragmentation of magma during Plinian volcanic eruptions. *Bull. Volcanol.* **58**, 144–162 (1996).
48. Capaccioni, B. & Cuccoli, F. Spatter and welded air fall deposits generated by fire-fountaining eruptions: cooling of pyroclasts during transport and deposition. *J. Volcanol. Geotherm. Res.* **145**, 263–280 (2005).
49. Edmonds, M. & Gerlach, T. M. Vapor segregation and loss in basaltic melts. *Geology* **35**, 751–754 (2007).

50. Cashman, K. V. & Kauahikaua, J. P. Reevaluation of vesicle distributions in basaltic lava flows. *Geology* **25**, 419–422 (1997).
51. Sahagian, D. Bubble migration and coalescence during the solidification of basaltic lava flows. *J. Geol.* **93**, 205–211 (1985).
52. Thornber, C., Keszthelyi, L., Lewis-Kenedi, C., Cazeneuve, M. & Goehring, D. Drilling an Active Pahoehoe Lava Flow. In *AGU Fall Meeting Abstracts* (2004).

Acknowledgements
TJJ was supported by NERC grant NE/L0025901. BFH and CEP were supported by NSF awards EAR-1145159 and EAR-1521855. EWL acknowledges support from NERC grant NE/N018443/1.

Author Contributions
T.J.J. designed the study with support from B.F.H. and E.W.J.; T.J.J. performed the textural analysis with the support of L.H. C.E.P contributed the textural analysis for sample 1t C05. All authors contributed to the editing of the manuscript after an initial draft was prepared by T.J.J.

Additional Information
Supplementary information accompanies this paper at https://doi.org/10.1038/s41598-018-27065-1.

Competing Interests: The authors declare no competing interests.

Publisher's note: Springer Nature remains neutral with regard to jurisdictional claims in published maps and institutional affiliations.

Supplementary Information (Tables S1 and S2)

to accompany:

Spatter matters – distinguishing primary (eruptive) and secondary (non-eruptive) spatter deposits

T.J. Jones[1*], B.F. Houghton[2], E.W. Llewellin[1], C.E. Parcheta[3] and L. Höltgen[1, 4]

[1] Department of Earth Sciences, Durham University, South Road, Durham, DH1 3LE, UK.

[2] Department of Geology & Geophysics, SOEST, University of Hawai‘i at Mānoa, Honolulu, HI 96822, USA.

[3] U.S. Geological Survey, Hawaiian Volcano Observatory, Hawaii Volcanoes National Park, HI, 96718, USA.

[4] Department of Earth and Environmental Sciences, LMU Munich, Theresienstr. 41, 80333 Munich, Germany.

Sample type	Clast name	Vesicularity [vol. %]	N_A[a] [#/cm^2]	N_V[b] [#/cm^3]	N_{Vm}[c] [#/cm^3]	V_g/V_m[d]	Median D[e] [mm]
Primary	8B	57.7	2.77E+3	1.05E+6	2.47E+6	1.37	0.74
Primary	8Ei	62.6	1.48E+3	4.96E+5	1.33E+6	1.69	0.61
Primary	4Q	59.7	1.23E+3	2.67E+5	6.61E+5	1.49	0.47
Primary	4A	52.3	1.83E+3	6.52E+5	1.37E+6	1.10	0.63
Primary*	1t C05	65.0	3.94E+3	8.90E+5	2.50E+6	1.88	0.50
Late-stage	1D q	27.1[f]	3.54E+2	7.59E+4	1.04E+5	0.37	1.07
Late-stage	5K	55.6	6.49E+2	1.44E+5	3.24E+5	1.27	0.78
Late-stage	6A q	32.3[f]	1.63E+3	4.99E+5	7.37E+5	0.48	0.50
Late-stage	1A q	31.9[f]	1.41E+2	9.64E+3	1.42E+4	0.47	0.91
Late-stage	1C q	53.7[f]	1.30E+3	3.50E+5	7.54E+5	1.16	1.36
Secondary	12H	49.0	9.56E+2	2.34E+5	4.58E+5	0.96	0.70
Secondary	12G	50.0	1.30E+3	3.72E+5	7.45E+5	1.00	0.49
Secondary	12Ni	73.4	5.70E+2	1.09E+5	4.10E+5	2.77	1.50
Secondary	12B q	43.3[f]	1.17E+3	4.73E+5	8.36E+5	0.77	0.71
Secondary	15Mii q	43.2[f]	1.14E+3	2.49E+5	4.38E+5	0.77	0.61

[a] Number of vesicles per unit area
[b] Number of vesicles per unit volume of clast matrix, volume of phenocrysts subtracted
[c] Number of vesicles per unit volume, referenced to melt only
[d] Ratio of gas to melt volume
[e] Median equivalent diameter, assuming a circular cross-section
[f] Sample comprises a quenched rim and interior, the quench image vesicularity is used/reported
*Tephra sample also described in Parcheta et al. (2013)

Table S1: Quantitative vesicle data from micro-textural analysis.

Spatter types compared	P-value
Primary – Late-stage	0.0053781
Secondary – Primary	0.0152794
Secondary – Late-stage	0.8311387

Table S2: ANOVA test results based on N_{Vm} distributed normally in linear space.

Appendix C

Field measurements from Chapter 2

The following data table reports all the raw field data corresponding to Chapter 2. The tree mould height measurements are the height (in meters) above the corresponding kinematic GPS measurement point. The tree mould depth measurements are the depth (in meters) below the corresponding kinematic GPS measurement point. All elevation values are ellipsoid heights (WGS 84) and not geoid corrected, consistent with Figure 2.6.

Measurement type	Value (m)	Latitude	Longitude	Elevation (m)
Tree Mould Height	2.35	19.36236152	-155.2231144	995.3476
Tree Mould Height	0	19.36160212	-155.2237422	996.6241
Tree Mould Height	0	19.36174667	-155.2238028	996.7515
Tree Mould Height	1.13	19.3621266	-155.2238621	996.917
Tree Mould Height	3.55	19.36259666	-155.2246491	994.9401
Tree Mould Height	0.94	19.36270021	-155.2247119	995.4594
Tree Mould Height	1.47	19.36259225	-155.2248281	995.5627
Tree Mould Height	1.1	19.36264747	-155.2250991	995.8856
Tree Mould Height	1.4	19.36267113	-155.22515	995.8569
Tree Mould Height	0.16	19.36270674	-155.2252757	996.8451
Tree Mould Height	0.22	19.36266883	-155.225363	996.6765
Tree Mould Height	0	19.36278628	-155.2251793	997.1669
Tree Mould Height	0.58	19.36274153	-155.2251241	996.7246
Tree Mould Height	0.81	19.36281974	-155.2249994	996.6965
Tree Mould Height	0.88	19.36305342	-155.2248189	996.8542
Tree Mould Height	1.04	19.36310255	-155.224417	995.8941
Tree Mould Height	1.65	19.36274195	-155.224535	995.0648
Tree Mould Height	1.53	19.36291925	-155.224045	993.7822
Tree Mould Height	1.52	19.36272153	-155.2238063	994.3398
Tree Mould Height	0.74	19.3626676	-155.2234361	994.7612
Tree Mould Height	0.17	19.36192167	-155.2231613	995.4916
Tree Mould Height	2.71	19.36325275	-155.2236197	995.4638
Tree Mould Height	0.97	19.36359945	-155.2237992	996.5957
Tree Mould Height	0	19.36339346	-155.2243058	997.3942
Tree Mould Height	0	19.36372814	-155.2238154	997.1541
Tree Mould Height	0	19.36320746	-155.2228929	997.1914
Tree Mould Height	0.62	19.36327416	-155.2227328	996.6242
Tree Mould Height	0.41	19.36330617	-155.2226183	996.7616
Tree Mould Height	0.96	19.36293512	-155.2226111	996.9258
Tree Mould Height	1.45	19.36269039	-155.2227756	996.4558
Tree Mould Height	1.55	19.36249534	-155.2222529	995.1306
Tree Mould Height	1.76	19.36168233	-155.2220988	994.5345
Tree Mould Height	0	19.36139246	-155.2224612	997.6425
Tree Mould Height	0	19.36146118	-155.2228588	997.3718
Tree Mould Height	0	19.359981	-155.2236479	993.6091
Tree Mould Height	0.87	19.3597598	-155.2236629	992.7127
Tree Mould Height	0.72	19.35935552	-155.2234809	991.6258
Tree Mould Height	1.14	19.36025013	-155.2238655	993.0672
Tree Mould Height	0.87	19.36064265	-155.2237728	994.0422
Tree Mould Height	0.37	19.36123691	-155.2239357	994.452
Tree Mould Height	1.2	19.36132146	-155.2235125	995.6833
Tree Mould Height	0.54	19.36157353	-155.2236766	996.3937
Tree Mould Height	1.30	19.36233001	-155.2236622	996.4744
Tree Mould Height	0.62	19.36248452	-155.2241962	996.0989
Tree Mould Height	1.35	19.36275674	-155.2230911	996.1362
Tree Mould Height	0.83	19.36279742	-155.2220444	997.4336
Tree Mould Height	1.8	19.36249756	-155.2222576	995.155
Tree Mould Height	1.39	19.36185491	-155.2222791	993.9506
Tree Mould Height	0.83	19.36064129	-155.2237703	994.067
Tree Mould Height	0.93	19.36112758	-155.2237634	994.1399

Tree Mould Height	0.4	19.3612362	-155.2239327	994.4621
Tree Mould Height	0.44	19.36101569	-155.224085	994.425
Tree Mould Height	1.19	19.36065646	-155.2237003	994.0268
Tree Mould Height	0.84	19.36044412	-155.2238307	993.8531
Tree Mould Height	1.21	19.36023826	-155.2238697	994.2543
Tree Mould Height	0.89	19.36004228	-155.2235639	993.1778
Tree Mould Height	0.39	19.35966371	-155.2234419	992.5671
Tree Mould Height	0.76	19.35944476	-155.2232207	991.3101
Tree Mould Height	0	19.35986211	-155.2228255	993.2824
Tree Mould Height	0.81	19.36025214	-155.2227916	993.5866
Tree Mould Height	1.25	19.36065116	-155.2225137	994.5187
Tree Mould Height	1.36	19.3611963	-155.2227234	994.6055
Tree Mould Height	1.24	19.36065624	-155.2231734	994.098
Tree Mould Height	1.66	19.36156235	-155.2227618	996.4397
Tree Mould Height	1.02	19.36124925	-155.2226891	994.9858
Tree Mould Height	0.95	19.36137408	-155.2230193	995.2001
Tree Mould Height	1.71	19.36202988	-155.2226939	995.4471
Tree Mould Height	0.66	19.36037617	-155.2228265	993.6309
Tree Mould Height	1.01	19.36064332	-155.2221346	994.5963
Tree Mould Height	1.88	19.36097393	-155.222188	992.7347
Tree Mould Height	1.43	19.36100704	-155.2225621	993.6254
Tree Mould Height	1.05	19.36135809	-155.2228037	995.6303
Tree Mould Height	0	19.36148258	-155.2214627	997.4523
Tree Mould Height	1.12	19.36185137	-155.2211682	995.9352
Tree Mould Height	0.73	19.36229783	-155.2214823	996.8951
Tree Mould Height	1.33	19.36292832	-155.2230176	996.4116
Tree Mould Height	1.032	19.36327247	-155.2145221	992.8169
Tree Mould Height	1.38	19.36324739	-155.2146157	992.4225
Tree Mould Height	1.37	19.3634997	-155.2146219	992.7215
Tree Mould Height	1.4	19.36343166	-155.2148754	992.5404
Tree Mould Height	1.12	19.36261148	-155.2149552	991.6046
Tree Mould Height	1.25	19.36290925	-155.2152429	992.2473
Tree Mould Height	1.24	19.36338599	-155.2154102	993.4084
Tree Mould Height	1.43	19.36322156	-155.2153915	993.0872
Tree Mould Height	0.83	19.36304237	-155.2153707	993.2714
Tree Mould Height	0.77	19.36256713	-155.2153686	992.1642
Tree Mould Height	0.9	19.36266285	-155.2155699	992.4239
Tree Mould Height	0.86	19.36272658	-155.215773	993.426
Tree Mould Height	0	19.36245178	-155.2160804	993.442
Tree Mould Height	1.51	19.36279083	-155.2161768	993.08
Tree Mould Height	0.96	19.36279419	-155.2164825	993.9041
Tree Mould Height	1.12	19.3626329	-155.2164674	993.336
Tree Mould Height	0	19.36262284	-155.2174677	993.0993
Tree Mould Height	0.88	19.3622642	-155.2173042	992.4733
Tree Mould Height	2.81	19.36264353	-155.2178192	991.3594
Tree Mould Height	1.36	19.36210133	-155.2175615	991.6007
Tree Mould Height	1.67	19.36185792	-155.2176747	990.7299
Tree Mould Height	0.73	19.36207011	-155.2179321	992.5095
Tree Mould Height	1.45	19.36240549	-155.217927	992.0995
Tree Mould Height	0.72	19.36299076	-155.218837	994.305
Tree Mould Height	0	19.3635762	-155.2152262	993.4583

Tree Mould Height	0.32	19.36367656	-155.2148781	992.8538
Tree Mould Height	0	19.36365958	-155.2146675	992.9695
Tree Mould Height	0	19.36379835	-155.2144442	993.641
Tree Mould Height	0.24	19.36371614	-155.2153551	994.818
Tree Mould Height	0.39	19.3637523	-155.2158931	995.5508
Tree Mould Height	0	19.36375146	-155.2160806	995.7078
Tree Mould Height	0	19.36372817	-155.2163025	995.1308
Tree Mould Height	0.86	19.36360314	-155.216465	995.5834
Tree Mould Height	0.54	19.36347679	-155.2166844	994.3884
Tree Mould Height	0.44	19.36351766	-155.2168236	993.8764
Tree Mould Height	0	19.36360846	-155.2170421	994.4334
Tree Mould Height	0.38	19.36359387	-155.2172579	995.93
Tree Mould Height	0.36	19.36357499	-155.2174063	995.5335
Tree Mould Height	0.71	19.36362688	-155.2174665	994.8427
Tree Mould Height	0	19.36346861	-155.2175423	995.1405
Tree Mould Height	0.4	19.36333994	-155.2175909	994.4407
Tree Mould Height	1.41	19.36321614	-155.2175646	993.2791
Tree Mould Height	1.44	19.36312767	-155.2176129	993.1374
Tree Mould Height	0	19.36303345	-155.2178951	993.9967
Tree Mould Height	0	19.36298439	-155.2179997	993.8556
Tree Mould Height	0.99	19.36301493	-155.2181922	993.4102
Tree Mould Height	0	19.36321569	-155.2182841	994.1197
Tree Mould Height	0.65	19.36302439	-155.2184104	994.9593
Tree Mould Height	1.15	19.36307099	-155.21858	994.3174
Tree Mould Height	1.14	19.36287357	-155.2187602	994.2184
Tree Mould Height	1.41	19.36308436	-155.2188598	994.0103
Tree Mould Height	0.78	19.36299321	-155.2195053	995.9602
Tree Mould Height	0.57	19.36309745	-155.2195909	997.169
Tree Mould Height	0	19.36311147	-155.2198386	998.8213
Tree Mould Height	0	19.36309038	-155.2199711	998.8034
Tree Mould Height	0.63	19.36270316	-155.2205982	997.4641
Tree Mould Height	0	19.36268836	-155.2209042	997.7385
Tree Mould Height	0	19.3629282	-155.2212707	997.2783
Tree Mould Height	0.96	19.36273368	-155.2217421	997.1343
Tree Mould Height	1.64	19.36229908	-155.2218232	995.3189
Tree Mould Height	0	19.36147753	-155.2225241	997.885
Tree Mould Height	0.8	19.36143609	-155.2215639	996.4816
Tree Mould Height	2.1	19.36143325	-155.2214483	996.7766
Tree Mould Height	0.84	19.36145448	-155.2213476	995.9533
Tree Mould Height	0.99	19.36137265	-155.2213582	996.0849
Tree Mould Height	0	19.36230571	-155.2213801	997.46
Tree Mould Height	1.15	19.36254747	-155.2214202	996.1081
Tree Mould Height	1.18	19.36234958	-155.2212717	996.8912
Tree Mould Height	0.76	19.3622287	-155.2210453	996.6823
Tree Mould Height	0.22	19.36254095	-155.2208841	996.715
Tree Mould Height	0.83	19.36235094	-155.2203137	994.0269
Tree Mould Height	0.49	19.36247947	-155.2205383	996.0023
Tree Mould Height	0.18	19.36268963	-155.2195339	994.4366
Tree Mould Height	1.56	19.36274499	-155.2179304	992.6877
Tree Mould Height	0	19.36278192	-155.2194878	994.7593
Tree Mould Height	0	19.36277988	-155.2198268	996.3887

Tree Mould Height		19.36260784	-155.2203125	996.5396
Tree Mould Height		19.36253398	-155.2216669	995.9596
Tree Mould Height	1.34	19.3635105	-155.2145867	992.8665
Tree Mould Height	0.86	19.36164245	-155.2232262	995.6265
Tree Mould Height	0	19.36373076	-155.2145189	994.1694
Tree Mould Height	0	19.3636802	-155.2148805	992.9258
Tree Mould Height	0.83	19.36210416	-155.2232022	995.7437
Tree Mould Height	0	19.36367973	-155.2149049	992.7676
Tree Mould Height	0	19.36369961	-155.2149201	993.2908
Tree Mould Height	0.84	19.36221055	-155.2235262	996.7086
Tree Mould Height	0.85	19.36373096	-155.2148901	993.7757
Tree Mould Height	0	19.36361733	-155.2151669	993.1872
Tree Mould Height	0.34	19.36233017	-155.224133	997.641
Tree Mould Height	0	19.36364761	-155.2151574	994.0237
Tree Mould Height	0.55	19.36355592	-155.2151097	993.0688
Tree Mould Height	0	19.3624132	-155.2240786	997.8296
Tree Mould Height	0	19.36357729	-155.2152261	993.6686
Tree Mould Height	0	19.36347211	-155.2152194	993.4207
Tree Mould Height	0.7	19.36314191	-155.2239877	994.6788
Tree Mould Height	0.59	19.36352172	-155.223818	996.3822
Tree Mould Height		19.36279525	-155.2180291	992.5447
Tree Mould Height	0.91	19.3637355	-155.2236261	996.8005
Tree Mould Height	0.5	19.36269064	-155.2181688	992.2363
Tree Mould Height	0.5	19.36273096	-155.2191354	993.1298
Tree Mould Height	0.53	19.36343693	-155.2231377	996.634
Tree Mould Height	0.48	19.36316534	-155.2228992	996.7073
Tree Mould Height	0	19.36280373	-155.2196493	996.2136
Tree Mould Height	0.5	19.36264209	-155.2195941	994.1808
Tree Mould Height	1.34	19.36294103	-155.223019	996.405
Tree Mould Height	1.32	19.36270102	-155.2233348	995.1351
Tree Mould Height	1.69	19.36296985	-155.2237804	994.7592
Tree Mould Height	0.91	19.36296719	-155.2236449	995.0706
Tree Mould Height	1.21	19.36246024	-155.2224005	994.8751
Tree Mould Height	0.93	19.36220181	-155.221923	996.2283
Tree Mould Height	0.77	19.36200972	-155.2219222	995.6375
Tree Mould Height	1.37	19.36175374	-155.2215394	995.2016
Tree Mould Height	2.03	19.36088725	-155.2221327	992.6574
Tree Mould Height	1.29	19.36118276	-155.2224008	995.0385
Tree Mould Height	0.38	19.36064208	-155.2221045	994.8016
Tree Mould Height	0	19.36079897	-155.2203323	993.0989
Tree Mould Height	0.35	19.36075112	-155.2203298	993.3985
Tree Mould Height	0.9	19.36089327	-155.2197906	991.7623
Tree Mould Height	1.25	19.36075332	-155.2197383	992.6994
Tree Mould Height	0.53	19.36085986	-155.2193354	991.7841
Tree Mould Height	0.91	19.36097559	-155.2180472	989.3288
Tree Mould Height	1.21	19.36084691	-155.2180268	989.9733
Tree Mould Height	0.64	19.36085918	-155.2183051	990.8949
Tree Mould Height	0.35	19.36074439	-155.2177296	989.8625
Tree Mould Height	0.77	19.36098185	-155.2176466	989.2327
Tree Mould Height	0.88	19.36246848	-155.2181608	993.2589
Tree Mould Height	1.38	19.36256967	-155.2184341	993.5819

Tree Mould Depth	3.9	19.36237167	-155.2231078	997.7691
Tree Mould Depth	0.9	19.36160212	-155.2237422	996.6241
Tree Mould Depth	0.45	19.36174667	-155.2238028	996.7515
Tree Mould Depth	2.55	19.3621266	-155.2238621	996.917
Tree Mould Depth	1.55	19.36270021	-155.2247119	996.3988
Tree Mould Depth	2.57	19.36259225	-155.2248281	996.3988
Tree Mould Depth	2.56	19.36264461	-155.2251144	996.9199
Tree Mould Depth	2.16	19.36268438	-155.2251501	996.9957
Tree Mould Depth	0.99	19.3627007	-155.2252748	997.0214
Tree Mould Depth	0.68	19.36266701	-155.2253623	996.8334
Tree Mould Depth	0.525	19.36278628	-155.2251793	997.1669
Tree Mould Depth	1.24	19.36274153	-155.2251241	996.9957
Tree Mould Depth	1.97	19.36281974	-155.2249994	997.1669
Tree Mould Depth	0	19.36299857	-155.2249114	997.4561
Tree Mould Depth	1.95	19.36303005	-155.224805	997.4378
Tree Mould Depth	1.42	19.36312544	-155.2244087	996.7689
Tree Mould Depth	2.96	19.36274094	-155.2245599	997.1368
Tree Mould Depth	2.28	19.36294774	-155.2240473	995.3283
Tree Mould Depth	1.67	19.36267686	-155.2234277	995.5756
Tree Mould Depth	2.17	19.36194568	-155.2231558	996.5989
Tree Mould Depth	3.34	19.36330524	-155.2236102	998.1695
Tree Mould Depth	1.36	19.36360136	-155.223825	997.5638
Tree Mould Depth	1.09	19.36339346	-155.2243058	997.3942
Tree Mould Depth	0.32	19.36372814	-155.2238154	997.1541
Tree Mould Depth	1.12	19.36320746	-155.2228929	997.1914
Tree Mould Depth	1.11	19.36328334	-155.2227349	997.2392
Tree Mould Depth	0.75	19.36329451	-155.2226221	997.1355
Tree Mould Depth	2.40	19.3629489	-155.2226173	997.798
Tree Mould Depth	2.59	19.36269134	-155.2228041	997.8528
Tree Mould Depth	2.72	19.36227113	-155.2228726	997.298
Tree Mould Depth	2.11	19.36251052	-155.2222468	996.7617
Tree Mould Depth	2.33	19.36225973	-155.2218563	996.9783
Tree Mould Depth	3.67	19.36166596	-155.2221029	996.3655
Tree Mould Depth	4.77	19.36139246	-155.2224612	997.6425
Tree Mould Depth	2.8	19.36146118	-155.2228588	997.3718
Tree Mould Depth	1.74	19.359981	-155.2236479	993.6091
Tree Mould Depth	2.14	19.35976528	-155.2236685	993.4304
Tree Mould Depth	1.26	19.35934633	-155.2234923	992.2852
Tree Mould Depth	1.8	19.36023815	-155.2238652	994.2543
Tree Mould Depth	1.75	19.36063289	-155.223763	994.8218
Tree Mould Depth	1.22	19.36123352	-155.2239348	994.86
Tree Mould Depth	2.87	19.36133907	-155.2234776	996.7647
Tree Mould Depth	1.23	19.36159087	-155.223682	996.9445
Tree Mould Depth	1.98	19.36221247	-155.2235141	997.7726
Tree Mould Depth	1.36	19.36234339	-155.2236466	997.7726
Tree Mould Depth	1.62	19.36249158	-155.2241989	996.6643
Tree Mould Depth	2.67	19.3627522	-155.2231088	997.8652
Tree Mould Depth	1.82	19.36279666	-155.2220251	997.7894
Tree Mould Depth	2.16	19.3625103	-155.2222459	996.8218
Tree Mould Depth	2.06	19.36181603	-155.2222594	996.3655
Tree Mould Depth	1.78	19.36063083	-155.2237583	994.8705

Tree Mould Depth	1.46	19.36113374	-155.2237689	994.9564
Tree Mould Depth	1.24	19.36123316	-155.223932	994.8867
Tree Mould Depth	1.41	19.36101915	-155.2240786	994.7211
Tree Mould Depth	1.86	19.36066505	-155.2237133	995.2044
Tree Mould Depth	1.22	19.36044386	-155.223842	994.6426
Tree Mould Depth	1.85	19.36023826	-155.2238697	994.2469
Tree Mould Depth	2.04	19.3600512	-155.2235711	994.0349
Tree Mould Depth	1.49	19.35967555	-155.2234426	992.9493
Tree Mould Depth	1.88	19.35944476	-155.2232207	993.0609
Tree Mould Depth	1.77	19.35986211	-155.2228255	993.2824
Tree Mould Depth	1.76	19.36025214	-155.2227916	994.3399
Tree Mould Depth	2.92	19.36065782	-155.222505	995.6851
Tree Mould Depth	2.235	19.36120488	-155.222713	996.1109
Tree Mould Depth	1.42	19.36065472	-155.2231785	995.3078
Tree Mould Depth	3.52	19.36157367	-155.2227441	997.9489
Tree Mould Depth	1.84	19.36123869	-155.2226696	996.0958
Tree Mould Depth	1.63	19.36133003	-155.2230374	996.4669
Tree Mould Depth	3.99	19.36202371	-155.2226539	997.298
Tree Mould Depth	2.26	19.36238243	-155.2227825	997.8528
Tree Mould Depth	1.87	19.36036566	-155.2228064	994.424
Tree Mould Depth	2.12	19.36066642	-155.2221347	995.5498
Tree Mould Depth	2.53	19.36095996	-155.2222243	994.5999
Tree Mould Depth	3.31	19.36099998	-155.2225382	995.1275
Tree Mould Depth	2.1	19.36137735	-155.222786	996.5784
Tree Mould Depth	3.32	19.36148258	-155.2214627	997.4523
Tree Mould Depth	2.31	19.36179992	-155.2224604	997.298
Tree Mould Depth	3.64	19.36166618	-155.2221038	996.3655
Tree Mould Depth	2.335	19.36188326	-155.2211691	997.0523
Tree Mould Depth	1.86	19.36230272	-155.2214703	997.4927
Tree Mould Depth	2.62	19.36294102	-155.2230011	997.7655
Tree Mould Depth	1.23	19.36328048	-155.2145269	993.8489
Tree Mould Depth	2.56	19.36265698	-155.2149482	992.721
Tree Mould Depth	2.55	19.36293536	-155.215234	993.7053
Tree Mould Depth	2.36	19.36324159	-155.2153997	994.4576
Tree Mould Depth	3.01	19.36303556	-155.2153186	993.8624
Tree Mould Depth	2.53	19.36258277	-155.2153434	992.8395
Tree Mould Depth	2.61	19.36265835	-155.2155549	993.2478
Tree Mould Depth	1.48	19.36245178	-155.2160804	993.442
Tree Mould Depth	3.38	19.36280223	-155.2164822	994.8217
Tree Mould Depth	3.52	19.36264811	-155.2164701	994.3215
Tree Mould Depth	1.59	19.36260989	-155.2174657	994.5317
Tree Mould Depth	2.58	19.3622642	-155.2173042	992.4733
Tree Mould Depth	2.81	19.3626055	-155.2178133	994.2066
Tree Mould Depth	2.73	19.36207631	-155.2179447	993.1892
Tree Mould Depth	2.19	19.36239717	-155.2178965	993.8466
Tree Mould Depth	3.08	19.36298897	-155.2188466	994.891
Tree Mould Depth	0.52	19.3635762	-155.2152262	993.4583
Tree Mould Depth	0.73	19.36368133	-155.2148775	993.2016
Tree Mould Depth	0.52	19.36365958	-155.2146675	992.9695
Tree Mould Depth	0.56	19.36379835	-155.2144442	993.641
Tree Mould Depth	1.59	19.36371753	-155.2153539	995.0548

Tree Mould Depth	1.58	19.36375449	-155.2158888	995.9689
Tree Mould Depth	0.88	19.36375146	-155.2160806	995.7078
Tree Mould Depth	0.92	19.36372817	-155.2163025	995.1308
Tree Mould Depth	2.49	19.36359375	-155.2164598	996.2787
Tree Mould Depth	1.64	19.36347164	-155.2166778	994.8683
Tree Mould Depth	1.45	19.36352228	-155.2168171	994.2476
Tree Mould Depth	1.03	19.36360846	-155.2170421	994.4334
Tree Mould Depth	2.34	19.3635886	-155.2172562	996.2544
Tree Mould Depth	1.65	19.36357046	-155.2174034	995.7495
Tree Mould Depth	1.76	19.36363294	-155.2174681	995.5048
Tree Mould Depth	2	19.36346861	-155.2175423	995.1405
Tree Mould Depth	1.54	19.36334062	-155.2175847	994.8698
Tree Mould Depth	2.71	19.36319807	-155.2175598	994.5892
Tree Mould Depth	2.55	19.36312659	-155.2176248	994.4843
Tree Mould Depth	1.82	19.36303345	-155.2178951	993.9967
Tree Mould Depth	1.09	19.36298439	-155.2179997	993.8556
Tree Mould Depth	1.99	19.36300802	-155.2181896	994.3389
Tree Mould Depth	0.95	19.36321569	-155.2182841	994.1197
Tree Mould Depth	2.29	19.36302123	-155.2184177	995.5063
Tree Mould Depth	2.42	19.36308838	-155.2185862	995.3662
Tree Mould Depth	3.22	19.36307487	-155.2188465	995.321
Tree Mould Depth	1.44	19.36300542	-155.2195129	996.6704
Tree Mould Depth	1.37	19.36309379	-155.2195941	997.6865
Tree Mould Depth	1.8	19.36311147	-155.2198386	998.8213
Tree Mould Depth	1.34	19.36309038	-155.2199711	998.8034
Tree Mould Depth	1.32	19.36270008	-155.2205938	998.0888
Tree Mould Depth	0.73	19.36268836	-155.2209042	997.7385
Tree Mould Depth	1.17	19.3629282	-155.2212707	997.2783
Tree Mould Depth	1.745	19.36271804	-155.2217629	997.9812
Tree Mould Depth	2.33	19.36232093	-155.2218333	996.9783
Tree Mould Depth	1.31	19.36147753	-155.2225241	997.885
Tree Mould Depth	2.98	19.36145688	-155.2215826	997.28
Tree Mould Depth	2.39	19.36146758	-155.2213407	996.9423
Tree Mould Depth	2.13	19.36137264	-155.2213583	996.1004
Tree Mould Depth	1.88	19.36230571	-155.2213801	997.46
Tree Mould Depth	1.88	19.36255584	-155.2214084	997.8357
Tree Mould Depth	2.08	19.3623338	-155.2212865	997.8357
Tree Mould Depth	3.19	19.3622282	-155.2210573	997.2671
Tree Mould Depth	0.87	19.36254244	-155.2208811	997.0025
Tree Mould Depth	1.57	19.3623556	-155.2203031	994.9201
Tree Mould Depth	0.96	19.36260631	-155.2199333	995.4648
Tree Mould Depth	2.55	19.36275546	-155.2179272	994.3096
Tree Mould Depth	1.33	19.36278192	-155.2194878	994.7593
Tree Mould Depth	1.01	19.36277988	-155.2198268	996.3887
Tree Mould Depth	2.65	19.36260784	-155.2203125	996.5396
Tree Mould Depth	0.9	19.36253398	-155.2216669	995.9596
Tree Mould Depth	2.63	19.36163493	-155.2232118	996.5373
Tree Mould Depth	1.41	19.36373076	-155.2145189	994.1694
Tree Mould Depth	0.54	19.3636802	-155.2148805	992.9258
Tree Mould Depth	0.81	19.36367973	-155.2149049	992.7676
Tree Mould Depth	1.7	19.36211488	-155.2231901	996.5891

Tree Mould Depth	0.7	19.36369961	-155.2149201	993.2908
Tree Mould Depth	1.45	19.36373096	-155.2148901	993.7757
Tree Mould Depth	2.01	19.36221104	-155.2235126	997.7726
Tree Mould Depth	0.86	19.36361733	-155.2151669	993.1872
Tree Mould Depth	1.65	19.36364761	-155.2151574	994.0237
Tree Mould Depth	1.63	19.36233133	-155.2241286	997.9982
Tree Mould Depth	1.43	19.3624132	-155.2240786	997.8296
Tree Mould Depth	1.2	19.36355346	-155.2151059	993.5633
Tree Mould Depth	0.65	19.36357729	-155.2152261	993.6686
Tree Mould Depth	1.15	19.36347211	-155.2152194	993.4207
Tree Mould Depth	1.61	19.36352852	-155.2238052	996.8512
Tree Mould Depth	0.95	19.36279525	-155.2180291	992.5447
Tree Mould Depth	4.96	19.3637339	-155.2236312	997.4433
Tree Mould Depth	1.3	19.36268936	-155.218179	992.6737
Tree Mould Depth	1.23	19.36272697	-155.21914	993.5767
Tree Mould Depth	2.95	19.36258159	-155.2191335	995.0947
Tree Mould Depth	1.55	19.36344613	-155.2231381	997.0685
Tree Mould Depth	1.3	19.36317439	-155.2229143	997.265
Tree Mould Depth	2.66	19.36280373	-155.2196493	996.2136
Tree Mould Depth	0.92	19.36264425	-155.2196001	994.6581
Tree Mould Depth	2.57	19.36294223	-155.2230045	997.6707
Tree Mould Depth	2.31	19.36268003	-155.2233325	995.5756
Tree Mould Depth	2.55	19.36298555	-155.2237858	996.2275
Tree Mould Depth	1.58	19.36297374	-155.2236556	996.2275
Tree Mould Depth	2.16	19.36247734	-155.2224091	996.8218
Tree Mould Depth	1.58	19.3622083	-155.2219078	996.9201
Tree Mould Depth	1.99	19.36201946	-155.2219254	996.4054
Tree Mould Depth	2.69	19.36175695	-155.221529	997.4523
Tree Mould Depth	2.93	19.36093742	-155.2221169	994.6889
Tree Mould Depth	1.56	19.36120163	-155.2223869	996.1555
Tree Mould Depth	2.03	19.36067024	-155.2221321	995.5946
Tree Mould Depth	1.07	19.36079897	-155.2203323	993.0989
Tree Mould Depth	0.95	19.36074917	-155.2203343	993.631
Tree Mould Depth	2.34	19.36091172	-155.2197668	992.7543
Tree Mould Depth	2.02	19.36077627	-155.2197292	993.5927
Tree Mould Depth	2.82	19.36087463	-155.2193311	992.9231
Tree Mould Depth	3.165	19.36098395	-155.2180545	990.1662
Tree Mould Depth	1.64	19.36084691	-155.2180268	989.9733
Tree Mould Depth	2.33	19.36087111	-155.2183047	991.4779
Tree Mould Depth	1.23	19.3607471	-155.2177256	990.1529
Tree Mould Depth	3.13	19.36098494	-155.2176816	990.0054
Lava High-stand Surface	997.7691	19.36237167	-155.2231078	997.7691
Lava High-stand Surface	996.6241	19.36160212	-155.2237422	996.6241
Lava High-stand Surface	996.7515	19.36174667	-155.2238028	996.7515
Lava High-stand Surface	996.917	19.3621266	-155.2238621	996.917
Lava High-stand Surface	997.2844	19.36257251	-155.2246669	997.2844
Lava High-stand Surface	996.3988	19.36270021	-155.2247119	996.3988
Lava High-stand Surface	996.3988	19.36259225	-155.2248281	996.3988
Lava High-stand Surface	996.9199	19.36264461	-155.2251144	996.9199
Lava High-stand Surface	996.9957	19.36268438	-155.2251501	996.9957
Lava High-stand Surface	997.0214	19.3627007	-155.2252748	997.0214

Lava High-stand Surface	996.8334	19.36266701	-155.2253623	996.8334
Lava High-stand Surface	997.1669	19.36278628	-155.2251793	997.1669
Lava High-stand Surface	996.9957	19.36274153	-155.2251241	996.9957
Lava High-stand Surface	997.1669	19.36281974	-155.2249994	997.1669
Lava High-stand Surface	997.4561	19.36299857	-155.2249114	997.4561
Lava High-stand Surface	997.4378	19.36303005	-155.224805	997.4378
Lava High-stand Surface	996.7689	19.36312544	-155.2244087	996.7689
Lava High-stand Surface	997.1368	19.36274094	-155.2245599	997.1368
Lava High-stand Surface	995.3283	19.36294774	-155.2240473	995.3283
Lava High-stand Surface	995.5756	19.36267686	-155.2234277	995.5756
Lava High-stand Surface	996.5989	19.36194568	-155.2231558	996.5989
Lava High-stand Surface	998.1695	19.36330524	-155.2236102	998.1695
Lava High-stand Surface	997.5638	19.36360136	-155.223825	997.5638
Lava High-stand Surface	997.3942	19.36339346	-155.2243058	997.3942
Lava High-stand Surface	997.1541	19.36372814	-155.2238154	997.1541
Lava High-stand Surface	997.1914	19.36320746	-155.2228929	997.1914
Lava High-stand Surface	997.2392	19.36328334	-155.2227349	997.2392
Lava High-stand Surface	997.1355	19.36329451	-155.2226221	997.1355
Lava High-stand Surface	997.798	19.3629489	-155.2226173	997.798
Lava High-stand Surface	997.8528	19.36269134	-155.2228041	997.8528
Lava High-stand Surface	997.298	19.36227113	-155.2228726	997.298
Lava High-stand Surface	996.7617	19.36251052	-155.2222468	996.7617
Lava High-stand Surface	996.9783	19.36225973	-155.2218563	996.9783
Lava High-stand Surface	996.3655	19.36166596	-155.2221029	996.3655
Lava High-stand Surface	997.6425	19.36139246	-155.2224612	997.6425
Lava High-stand Surface	997.3718	19.36146118	-155.2228588	997.3718
Lava High-stand Surface	993.6091	19.359981	-155.2236479	993.6091
Lava High-stand Surface	993.4304	19.35976528	-155.2236685	993.4304
Lava High-stand Surface	992.2852	19.35934633	-155.2234923	992.2852
Lava High-stand Surface	994.2543	19.36023815	-155.2238652	994.2543
Lava High-stand Surface	994.8218	19.36063289	-155.223763	994.8218
Lava High-stand Surface	994.86	19.36123352	-155.2239348	994.86
Lava High-stand Surface	996.7647	19.36133907	-155.2234776	996.7647
Lava High-stand Surface	996.9445	19.36159087	-155.223682	996.9445
Lava High-stand Surface	997.7726	19.36221247	-155.2235141	997.7726
Lava High-stand Surface	997.7726	19.36234339	-155.2236466	997.7726
Lava High-stand Surface	996.6643	19.36249158	-155.2241989	996.6643
Lava High-stand Surface	997.8652	19.3627522	-155.2231088	997.8652
Lava High-stand Surface	997.7894	19.36279666	-155.2220251	997.7894
Lava High-stand Surface	996.8218	19.3625103	-155.2222459	996.8218
Lava High-stand Surface	993.6633	19.35988392	-155.2239549	993.6633
Lava High-stand Surface	993.8178	19.36013632	-155.2239463	993.8178
Lava High-stand Surface	993.761	19.36013654	-155.2240815	993.761
Lava High-stand Surface	994.3517	19.36049965	-155.2239922	994.3517
Lava High-stand Surface	994.3959	19.36079744	-155.2240157	994.3959
Lava High-stand Surface	994.5115	19.3610072	-155.2241046	994.5115
Lava High-stand Surface	994.8787	19.36125878	-155.223962	994.8787
Lava High-stand Surface	996.3645	19.36150338	-155.2237304	996.3645
Lava High-stand Surface	996.8391	19.36180975	-155.2238895	996.8391
Lava High-stand Surface	997.4706	19.36203099	-155.224084	997.4706
Lava High-stand Surface	997.8082	19.36226543	-155.2241856	997.8082

Lava High-stand Surface	997.7664	19.36236403	-155.2242917	997.7664
Lava High-stand Surface	998.0892	19.36241485	-155.2244754	998.0892
Lava High-stand Surface	997.9741	19.36242983	-155.2247772	997.9741
Lava High-stand Surface	997.7543	19.36246815	-155.2249743	997.7543
Lava High-stand Surface	997.5639	19.36254029	-155.2251434	997.5639
Lava High-stand Surface	997.5865	19.36294602	-155.2249985	997.5865
Lava High-stand Surface	997.4101	19.3631705	-155.2248225	997.4101
Lava High-stand Surface	997.2516	19.36335939	-155.2245223	997.2516
Lava High-stand Surface	997.3353	19.36362718	-155.2241342	997.3353
Lava High-stand Surface	996.8012	19.36371972	-155.2239662	996.8012
Lava High-stand Surface	997.1716	19.36378109	-155.2237621	997.1716
Lava High-stand Surface	997.1503	19.36374619	-155.2234534	997.1503
Lava High-stand Surface	996.79	19.36354972	-155.223189	996.79
Lava High-stand Surface	996.9983	19.36334158	-155.2229335	996.9983
Lava High-stand Surface	996.9091	19.36338989	-155.2225811	996.9091
Lava High-stand Surface	997.043	19.36334256	-155.2223452	997.043
Lava High-stand Surface	997.0931	19.36312156	-155.2221219	997.0931
Lava High-stand Surface	997.5751	19.36279804	-155.2220084	997.5751
Lava High-stand Surface	998.1444	19.36261317	-155.2220051	998.1444
Lava High-stand Surface	997.5505	19.36229358	-155.2216239	997.5505
Lava High-stand Surface	997.4455	19.36226694	-155.2212517	997.4455
Lava High-stand Surface	996.6556	19.36174882	-155.2210026	996.6556
Lava High-stand Surface	996.7934	19.36154063	-155.2209305	996.7934
Lava High-stand Surface	994.4507	19.36112474	-155.2207836	994.4507
Lava High-stand Surface	994.3664	19.36087733	-155.2205693	994.3664
Lava High-stand Surface	994.0337	19.36070914	-155.2207333	994.0337
Lava High-stand Surface	994.6749	19.36063493	-155.2213737	994.6749
Lava High-stand Surface	995.298	19.36065168	-155.2219319	995.298
Lava High-stand Surface	995.6176	19.36077827	-155.2223218	995.6176
Lava High-stand Surface	995.8048	19.36096005	-155.2229753	995.8048
Lava High-stand Surface	995.4466	19.3606417	-155.2231209	995.4466
Lava High-stand Surface	994.5835	19.36022235	-155.2231271	994.5835
Lava High-stand Surface	993.2107	19.35973146	-155.2230471	993.2107
Lava High-stand Surface	993.0609	19.35962019	-155.2232914	993.0609
Lava High-stand Surface	992.5779	19.35935202	-155.2235641	992.5779
Lava High-stand Surface	992.7459	19.35941205	-155.2238533	992.7459
Lava High-stand Surface	994.8705	19.36063083	-155.2237583	994.8705
Lava High-stand Surface	994.9564	19.36113374	-155.2237689	994.9564
Lava High-stand Surface	994.8867	19.36123316	-155.223932	994.8867
Lava High-stand Surface	994.7211	19.36101915	-155.2240786	994.7211
Lava High-stand Surface	995.2044	19.36066505	-155.2237133	995.2044
Lava High-stand Surface	994.6426	19.36044386	-155.223842	994.6426
Lava High-stand Surface	994.2469	19.36023826	-155.2238697	994.2469
Lava High-stand Surface	994.0349	19.3600512	-155.2235711	994.0349
Lava High-stand Surface	992.9493	19.35967555	-155.2234426	992.9493
Lava High-stand Surface	993.0609	19.35944476	-155.2232207	993.0609
Lava High-stand Surface	993.2824	19.35986211	-155.2228255	993.2824
Lava High-stand Surface	994.3399	19.36025214	-155.2227916	994.3399
Lava High-stand Surface	995.6851	19.36065782	-155.222505	995.6851
Lava High-stand Surface	996.1109	19.36120488	-155.222713	996.1109
Lava High-stand Surface	995.3078	19.36065472	-155.2231785	995.3078

Lava High-stand Surface	997.9489	19.36157367	-155.2227441	997.9489
Lava High-stand Surface	996.0958	19.36123869	-155.2226696	996.0958
Lava High-stand Surface	996.4669	19.36133003	-155.2230374	996.4669
Lava High-stand Surface	997.298	19.36202371	-155.2226539	997.298
Lava High-stand Surface	997.8528	19.36238243	-155.2227825	997.8528
Lava High-stand Surface	994.424	19.36036566	-155.2228064	994.424
Lava High-stand Surface	995.5498	19.36066642	-155.2221347	995.5498
Lava High-stand Surface	994.5999	19.36095996	-155.2222243	994.5999
Lava High-stand Surface	995.1275	19.36099998	-155.2225382	995.1275
Lava High-stand Surface	996.5784	19.36137735	-155.222786	996.5784
Lava High-stand Surface	997.8734	19.36147179	-155.2225705	997.8734
Lava High-stand Surface	997.517	19.36143764	-155.2222586	997.517
Lava High-stand Surface	997.9233	19.36149069	-155.2218691	997.9233
Lava High-stand Surface	997.4523	19.36148258	-155.2214627	997.4523
Lava High-stand Surface	996.8767	19.36161044	-155.2209311	996.8767
Lava High-stand Surface	997.298	19.36179992	-155.2224604	997.298
Lava High-stand Surface	996.3655	19.36166618	-155.2221038	996.3655
Lava High-stand Surface	997.0523	19.36188326	-155.2211691	997.0523
Lava High-stand Surface	997.4927	19.36230272	-155.2214703	997.4927
Lava High-stand Surface	997.7655	19.36294102	-155.2230011	997.7655
Lava High-stand Surface	994.4966	19.36337834	-155.2143278	994.4966
Lava High-stand Surface	993.8489	19.36328048	-155.2145269	993.8489
Lava High-stand Surface	993.8096	19.36324195	-155.2146301	993.8096
Lava High-stand Surface	994.1265	19.36349896	-155.2146095	994.1265
Lava High-stand Surface	994.1265	19.36343166	-155.2148754	994.1265
Lava High-stand Surface	992.721	19.36265698	-155.2149482	992.721
Lava High-stand Surface	993.7053	19.36293536	-155.215234	993.7053
Lava High-stand Surface	994.4594	19.36336513	-155.2154282	994.4594
Lava High-stand Surface	994.4576	19.36324159	-155.2153997	994.4576
Lava High-stand Surface	993.8624	19.36303556	-155.2153186	993.8624
Lava High-stand Surface	992.8395	19.36258277	-155.2153434	992.8395
Lava High-stand Surface	992.7326	19.36252105	-155.2154633	992.7326
Lava High-stand Surface	993.2478	19.36265835	-155.2155549	993.2478
Lava High-stand Surface	994.2155	19.36271723	-155.2157973	994.2155
Lava High-stand Surface	994.9287	19.36330669	-155.2157342	994.9287
Lava High-stand Surface	993.6688	19.3623565	-155.215835	993.6688
Lava High-stand Surface	993.442	19.36245178	-155.2160804	993.442
Lava High-stand Surface	994.5828	19.36277291	-155.2161291	994.5828
Lava High-stand Surface	994.8217	19.36280223	-155.2164822	994.8217
Lava High-stand Surface	994.3215	19.36264811	-155.2164701	994.3215
Lava High-stand Surface	993.5449	19.36267379	-155.217225	993.5449
Lava High-stand Surface	994.5317	19.36260989	-155.2174657	994.5317
Lava High-stand Surface	993.8559	19.36273761	-155.2171791	993.8559
Lava High-stand Surface	994.2066	19.3626055	-155.2178133	994.2066
Lava High-stand Surface	992.9183	19.36208739	-155.2175593	992.9183
Lava High-stand Surface	992.1018	19.36182864	-155.2176644	992.1018
Lava High-stand Surface	993.1892	19.36207631	-155.2179447	993.1892
Lava High-stand Surface	993.8466	19.36239717	-155.2178965	993.8466
Lava High-stand Surface	994.6871	19.36257911	-155.2185709	994.6871
Lava High-stand Surface	994.8326	19.36277309	-155.2186437	994.8326
Lava High-stand Surface	994.891	19.36298897	-155.2188466	994.891

Lava High-stand Surface	993.4583	19.3635762	-155.2152262	993.4583
Lava High-stand Surface	993.2016	19.36368133	-155.2148775	993.2016
Lava High-stand Surface	995.0548	19.36371753	-155.2153539	995.0548
Lava High-stand Surface	995.9689	19.36375449	-155.2158888	995.9689
Lava High-stand Surface	995.7078	19.36375146	-155.2160806	995.7078
Lava High-stand Surface	995.1308	19.36372817	-155.2163025	995.1308
Lava High-stand Surface	996.2787	19.36359375	-155.2164598	996.2787
Lava High-stand Surface	994.8683	19.36347164	-155.2166778	994.8683
Lava High-stand Surface	994.2476	19.36352228	-155.2168171	994.2476
Lava High-stand Surface	994.4334	19.36360846	-155.2170421	994.4334
Lava High-stand Surface	996.2544	19.3635886	-155.2172562	996.2544
Lava High-stand Surface	995.7495	19.36357046	-155.2174034	995.7495
Lava High-stand Surface	995.5048	19.36363294	-155.2174681	995.5048
Lava High-stand Surface	995.1405	19.36346861	-155.2175423	995.1405
Lava High-stand Surface	994.8698	19.36334062	-155.2175847	994.8698
Lava High-stand Surface	994.5892	19.36319807	-155.2175598	994.5892
Lava High-stand Surface	994.4843	19.36312659	-155.2176248	994.4843
Lava High-stand Surface	993.9967	19.36303345	-155.2178951	993.9967
Lava High-stand Surface	993.8556	19.36298439	-155.2179997	993.8556
Lava High-stand Surface	994.3389	19.36300802	-155.2181896	994.3389
Lava High-stand Surface	994.1197	19.36321569	-155.2182841	994.1197
Lava High-stand Surface	995.5063	19.36302123	-155.2184177	995.5063
Lava High-stand Surface	995.3662	19.36308838	-155.2185862	995.3662
Lava High-stand Surface	995.3409	19.36287341	-155.2187453	995.3409
Lava High-stand Surface	995.3051	19.36291479	-155.2189223	995.3051
Lava High-stand Surface	995.321	19.36307487	-155.2188465	995.321
Lava High-stand Surface	996.6704	19.36300542	-155.2195129	996.6704
Lava High-stand Surface	997.6865	19.36309379	-155.2195941	997.6865
Lava High-stand Surface	998.8213	19.36311147	-155.2198386	998.8213
Lava High-stand Surface	998.8034	19.36309038	-155.2199711	998.8034
Lava High-stand Surface	998.9411	19.36275366	-155.2204763	998.9411
Lava High-stand Surface	998.0888	19.36270008	-155.2205938	998.0888
Lava High-stand Surface	997.7385	19.36268836	-155.2209042	997.7385
Lava High-stand Surface	997.2783	19.3629282	-155.2212707	997.2783
Lava High-stand Surface	997.9812	19.36271804	-155.2217629	997.9812
Lava High-stand Surface	996.9783	19.36232093	-155.2218333	996.9783
Lava High-stand Surface	997.885	19.36147753	-155.2225241	997.885
Lava High-stand Surface	998.3638	19.36146598	-155.2222598	998.3638
Lava High-stand Surface	997.28	19.36145688	-155.2215826	997.28
Lava High-stand Surface	994.5076	19.36141897	-155.221427	994.5076
Lava High-stand Surface	996.9423	19.36146758	-155.2213407	996.9423
Lava High-stand Surface	997.0758	19.36144005	-155.2210488	997.0758
Lava High-stand Surface	996.1004	19.36137264	-155.2213583	996.1004
Lava High-stand Surface	997.46	19.36230571	-155.2213801	997.46
Lava High-stand Surface	997.8357	19.36255584	-155.2214084	997.8357
Lava High-stand Surface	997.8357	19.3623338	-155.2212865	997.8357
Lava High-stand Surface	997.2671	19.3622282	-155.2210573	997.2671
Lava High-stand Surface	997.0025	19.36254244	-155.2208811	997.0025
Lava High-stand Surface	996.1482	19.36227241	-155.2207019	996.1482
Lava High-stand Surface	994.9201	19.3623556	-155.2203031	994.9201
Lava High-stand Surface	996.6117	19.36248547	-155.2205273	996.6117

Lava High-stand Surface	994.8003	19.36177093	-155.2202337	994.8003
Lava High-stand Surface	995.5241	19.36193076	-155.2202967	995.5241
Lava High-stand Surface	994.2813	19.36178382	-155.2198736	994.2813
Lava High-stand Surface	995.1204	19.36215949	-155.2199099	995.1204
Lava High-stand Surface	995.4648	19.36237308	-155.2200122	995.4648
Lava High-stand Surface	995.4648	19.36260631	-155.2199333	995.4648
Lava High-stand Surface	994.6581	19.3626899	-155.219538	994.6581
Lava High-stand Surface	994.6197	19.36253173	-155.2188574	994.6197
Lava High-stand Surface	995.3044	19.36241674	-155.2188809	995.3044
Lava High-stand Surface	995.1376	19.36228987	-155.2189754	995.1376
Lava High-stand Surface	994.8747	19.36227306	-155.2191427	994.8747
Lava High-stand Surface	994.6715	19.3624164	-155.2192142	994.6715
Lava High-stand Surface	994.6647	19.36237888	-155.2190666	994.6647
Lava High-stand Surface	995.0956	19.36278313	-155.2187547	995.0956
Lava High-stand Surface	994.9072	19.36286511	-155.2184714	994.9072
Lava High-stand Surface	994.3096	19.36275546	-155.2179272	994.3096
Lava High-stand Surface	996.5373	19.36163493	-155.2232118	996.5373
Lava High-stand Surface	996.5891	19.36211488	-155.2231901	996.5891
Lava High-stand Surface	997.7726	19.36221104	-155.2235126	997.7726
Lava High-stand Surface	997.9982	19.36233133	-155.2241286	997.9982
Lava High-stand Surface	997.8296	19.3624132	-155.2240786	997.8296
Lava High-stand Surface	993.5633	19.36355346	-155.2151059	993.5633
Lava High-stand Surface	997.6559	19.36225821	-155.224198	997.6559
Lava High-stand Surface	996.8512	19.36352852	-155.2238052	996.8512
Lava High-stand Surface	997.4433	19.3637339	-155.2236312	997.4433
Lava High-stand Surface	995.0947	19.36272697	-155.21914	995.0947
Lava High-stand Surface	995.0947	19.36258159	-155.2191335	995.0947
Lava High-stand Surface	997.0685	19.36344613	-155.2231381	997.0685
Lava High-stand Surface	997.265	19.36317439	-155.2229143	997.265
Lava High-stand Surface	994.6581	19.36264425	-155.2196001	994.6581
Lava High-stand Surface	997.6707	19.36294223	-155.2230045	997.6707
Lava High-stand Surface	995.5756	19.36268003	-155.2233325	995.5756
Lava High-stand Surface	996.2275	19.36298555	-155.2237858	996.2275
Lava High-stand Surface	996.2275	19.36297374	-155.2236556	996.2275
Lava High-stand Surface	996.8218	19.36247734	-155.2224091	996.8218
Lava High-stand Surface	996.9201	19.3622083	-155.2219078	996.9201
Lava High-stand Surface	996.9201	19.36201946	-155.2219254	996.9201
Lava High-stand Surface	997.4523	19.36175695	-155.221529	997.4523
Lava High-stand Surface	994.6889	19.36093742	-155.2221169	994.6889
Lava High-stand Surface	996.1555	19.36120163	-155.2223869	996.1555
Lava High-stand Surface	995.5946	19.36067024	-155.2221321	995.5946
Lava High-stand Surface	993.0989	19.36079897	-155.2203323	993.0989
Lava High-stand Surface	993.631	19.36074917	-155.2203343	993.631
Lava High-stand Surface	992.7543	19.36091172	-155.2197668	992.7543
Lava High-stand Surface	993.5927	19.36077627	-155.2197292	993.5927
Lava High-stand Surface	993.7652	19.36066447	-155.2202191	993.7652
Lava High-stand Surface	992.9231	19.36087463	-155.2193311	992.9231
Lava High-stand Surface	990.1662	19.36098395	-155.2180545	990.1662
Lava High-stand Surface	991.4779	19.36087111	-155.2183047	991.4779
Lava High-stand Surface	990.1529	19.3607471	-155.2177256	990.1529
Lava High-stand Surface	990.0054	19.36098494	-155.2176816	990.0054

Lava High-stand Surface	992.7479	19.36205831	-155.2180975	992.7479
Lava High-stand Surface	994.0743	19.36246409	-155.2181797	994.0743
Lava High-stand Surface	993.3676	19.36279695	-155.2172152	993.3676
Lava High-stand Surface	994.1936	19.3635047	-155.214597	994.1936
Post-eruption Ground Surface	995.3476	19.36236152	-155.2231144	995.3476
Post-eruption Ground Surface	996.6241	19.36160212	-155.2237422	996.6241
Post-eruption Ground Surface	996.7515	19.36174667	-155.2238028	996.7515
Post-eruption Ground Surface	996.917	19.3621266	-155.2238621	996.917
Post-eruption Ground Surface	994.9401	19.36259666	-155.2246491	994.9401
Post-eruption Ground Surface	995.4594	19.36270021	-155.2247119	995.4594
Post-eruption Ground Surface	995.8856	19.36264747	-155.2250991	995.8856
Post-eruption Ground Surface	995.8569	19.36267113	-155.22515	995.8569
Post-eruption Ground Surface	996.8451	19.36270674	-155.2252757	996.8451
Post-eruption Ground Surface	996.6765	19.36266883	-155.225363	996.6765
Post-eruption Ground Surface	997.1669	19.36278628	-155.2251793	997.1669
Post-eruption Ground Surface	996.7246	19.36274153	-155.2251241	996.7246
Post-eruption Ground Surface	996.6965	19.36281974	-155.2249994	996.6965
Post-eruption Ground Surface	997.4561	19.36299857	-155.2249114	997.4561
Post-eruption Ground Surface	996.8542	19.36305342	-155.2248189	996.8542
Post-eruption Ground Surface	995.8941	19.36310255	-155.224417	995.8941
Post-eruption Ground Surface	995.0648	19.36274195	-155.224535	995.0648
Post-eruption Ground Surface	993.7822	19.36291925	-155.224045	993.7822
Post-eruption Ground Surface	994.3398	19.36272153	-155.2238063	994.3398
Post-eruption Ground Surface	994.7612	19.3626676	-155.2234361	994.7612
Post-eruption Ground Surface	995.4916	19.36192167	-155.2231613	995.4916
Post-eruption Ground Surface	995.4638	19.36325275	-155.2236197	995.4638
Post-eruption Ground Surface	996.5957	19.36359945	-155.2237992	996.5957
Post-eruption Ground Surface	997.3942	19.36339346	-155.2243058	997.3942
Post-eruption Ground Surface	997.1541	19.36372814	-155.2238154	997.1541
Post-eruption Ground Surface	997.1914	19.36320746	-155.2228929	997.1914
Post-eruption Ground Surface	996.6242	19.36327416	-155.2227328	996.6242
Post-eruption Ground Surface	996.7616	19.36330617	-155.2226183	996.7616
Post-eruption Ground Surface	996.9258	19.36293512	-155.2226111	996.9258
Post-eruption Ground Surface	996.4558	19.36269039	-155.2227756	996.4558
Post-eruption Ground Surface	994.9248	19.36230342	-155.2228602	994.9248
Post-eruption Ground Surface	995.1306	19.36249534	-155.2222529	995.1306
Post-eruption Ground Surface	996.307	19.36226608	-155.2218752	996.307
Post-eruption Ground Surface	994.5345	19.36168233	-155.2220988	994.5345
Post-eruption Ground Surface	997.6425	19.36139246	-155.2224612	997.6425
Post-eruption Ground Surface	997.3718	19.36146118	-155.2228588	997.3718
Post-eruption Ground Surface	993.6091	19.359981	-155.2236479	993.6091
Post-eruption Ground Surface	992.7127	19.3597598	-155.2236629	992.7127
Post-eruption Ground Surface	991.6258	19.35935552	-155.2234809	991.6258
Post-eruption Ground Surface	993.0672	19.36025013	-155.2238655	993.0672
Post-eruption Ground Surface	994.0422	19.36064265	-155.2237728	994.0422
Post-eruption Ground Surface	994.452	19.36123691	-155.2239357	994.452
Post-eruption Ground Surface	995.6833	19.36132146	-155.2235125	995.6833
Post-eruption Ground Surface	996.3937	19.36157353	-155.2236766	996.3937
Post-eruption Ground Surface	996.6156	19.3622178	-155.2235207	996.6156
Post-eruption Ground Surface	996.4744	19.36233001	-155.2236622	996.4744
Post-eruption Ground Surface	996.0989	19.36248452	-155.2241962	996.0989

Post-eruption Ground Surface	996.1362	19.36275674	-155.2230911	996.1362
Post-eruption Ground Surface	997.4336	19.36279742	-155.2220444	997.4336
Post-eruption Ground Surface	995.155	19.36249756	-155.2222576	995.155
Post-eruption Ground Surface	993.9506	19.36185491	-155.2222791	993.9506
Post-eruption Ground Surface	993.6633	19.35988392	-155.2239549	993.6633
Post-eruption Ground Surface	993.8178	19.36013632	-155.2239463	993.8178
Post-eruption Ground Surface	993.761	19.36013654	-155.2240815	993.761
Post-eruption Ground Surface	994.3517	19.36049965	-155.2239922	994.3517
Post-eruption Ground Surface	994.3959	19.36079744	-155.2240157	994.3959
Post-eruption Ground Surface	994.5115	19.3610072	-155.2241046	994.5115
Post-eruption Ground Surface	994.8787	19.36125878	-155.223962	994.8787
Post-eruption Ground Surface	996.3645	19.36150338	-155.2237304	996.3645
Post-eruption Ground Surface	996.8391	19.36180975	-155.2238895	996.8391
Post-eruption Ground Surface	997.4706	19.36203099	-155.224084	997.4706
Post-eruption Ground Surface	997.8082	19.36226543	-155.2241856	997.8082
Post-eruption Ground Surface	997.7664	19.36236403	-155.2242917	997.7664
Post-eruption Ground Surface	998.0892	19.36241485	-155.2244754	998.0892
Post-eruption Ground Surface	997.9741	19.36242983	-155.2247772	997.9741
Post-eruption Ground Surface	997.7543	19.36246815	-155.2249743	997.7543
Post-eruption Ground Surface	997.5639	19.36254029	-155.2251434	997.5639
Post-eruption Ground Surface	997.5865	19.36294602	-155.2249985	997.5865
Post-eruption Ground Surface	997.4101	19.3631705	-155.2248225	997.4101
Post-eruption Ground Surface	997.2516	19.36335939	-155.2245223	997.2516
Post-eruption Ground Surface	997.3353	19.36362718	-155.2241342	997.3353
Post-eruption Ground Surface	996.8012	19.36371972	-155.2239662	996.8012
Post-eruption Ground Surface	997.1716	19.36378109	-155.2237621	997.1716
Post-eruption Ground Surface	997.1503	19.36374619	-155.2234534	997.1503
Post-eruption Ground Surface	996.79	19.36354972	-155.223189	996.79
Post-eruption Ground Surface	996.9983	19.36334158	-155.2229335	996.9983
Post-eruption Ground Surface	996.9091	19.36338989	-155.2225811	996.9091
Post-eruption Ground Surface	997.043	19.36334256	-155.2223452	997.043
Post-eruption Ground Surface	997.0931	19.36312156	-155.2221219	997.0931
Post-eruption Ground Surface	997.5751	19.36279804	-155.2220084	997.5751
Post-eruption Ground Surface	998.1444	19.36261317	-155.2220051	998.1444
Post-eruption Ground Surface	997.5505	19.36229358	-155.2216239	997.5505
Post-eruption Ground Surface	997.4455	19.36226694	-155.2212517	997.4455
Post-eruption Ground Surface	996.6556	19.36174882	-155.2210026	996.6556
Post-eruption Ground Surface	996.7934	19.36154063	-155.2209305	996.7934
Post-eruption Ground Surface	994.4507	19.36112474	-155.2207836	994.4507
Post-eruption Ground Surface	994.3664	19.36087733	-155.2205693	994.3664
Post-eruption Ground Surface	994.0337	19.36070914	-155.2207333	994.0337
Post-eruption Ground Surface	994.6749	19.36063493	-155.2213737	994.6749
Post-eruption Ground Surface	995.298	19.36065168	-155.2219319	995.298
Post-eruption Ground Surface	995.6176	19.36077827	-155.2223218	995.6176
Post-eruption Ground Surface	995.8048	19.36096005	-155.2229753	995.8048
Post-eruption Ground Surface	995.4466	19.3606417	-155.2231209	995.4466
Post-eruption Ground Surface	994.5835	19.36022235	-155.2231271	994.5835
Post-eruption Ground Surface	993.2107	19.35973146	-155.2230471	993.2107
Post-eruption Ground Surface	993.0609	19.35962019	-155.2232914	993.0609
Post-eruption Ground Surface	992.5779	19.35935202	-155.2235641	992.5779
Post-eruption Ground Surface	992.7459	19.35941205	-155.2238533	992.7459

Post-eruption Ground Surface	994.067	19.36064129	-155.2237703	994.067
Post-eruption Ground Surface	994.1399	19.36112758	-155.2237634	994.1399
Post-eruption Ground Surface	994.4621	19.3612362	-155.2239327	994.4621
Post-eruption Ground Surface	994.425	19.36101569	-155.224085	994.425
Post-eruption Ground Surface	994.0268	19.36065646	-155.2237003	994.0268
Post-eruption Ground Surface	993.8531	19.36044412	-155.2238307	993.8531
Post-eruption Ground Surface	994.2543	19.36023826	-155.2238697	994.2543
Post-eruption Ground Surface	993.1778	19.36004228	-155.2235639	993.1778
Post-eruption Ground Surface	992.5671	19.35966371	-155.2234419	992.5671
Post-eruption Ground Surface	991.3101	19.35944476	-155.2232207	991.3101
Post-eruption Ground Surface	993.2824	19.35986211	-155.2228255	993.2824
Post-eruption Ground Surface	994.5187	19.36065116	-155.2225137	994.5187
Post-eruption Ground Surface	994.6055	19.3611963	-155.2227234	994.6055
Post-eruption Ground Surface	994.098	19.36065624	-155.2231734	994.098
Post-eruption Ground Surface	996.4397	19.36156235	-155.2227618	996.4397
Post-eruption Ground Surface	994.9858	19.36124925	-155.2226891	994.9858
Post-eruption Ground Surface	995.2001	19.36137408	-155.2230193	995.2001
Post-eruption Ground Surface	995.4471	19.36202988	-155.2226939	995.4471
Post-eruption Ground Surface	994.7532	19.36238243	-155.2227825	994.7532
Post-eruption Ground Surface	993.6309	19.36037617	-155.2228265	993.6309
Post-eruption Ground Surface	994.424	19.36036566	-155.2228064	994.424
Post-eruption Ground Surface	992.2192	19.36093698	-155.2215538	992.2192
Post-eruption Ground Surface	993.2098	19.36092396	-155.2220198	993.2098
Post-eruption Ground Surface	992.7347	19.36097393	-155.222188	992.7347
Post-eruption Ground Surface	993.6254	19.36100704	-155.2225621	993.6254
Post-eruption Ground Surface	995.6303	19.36135809	-155.2228037	995.6303
Post-eruption Ground Surface	997.8734	19.36147179	-155.2225705	997.8734
Post-eruption Ground Surface	997.517	19.36143764	-155.2222586	997.517
Post-eruption Ground Surface	997.9233	19.36149069	-155.2218691	997.9233
Post-eruption Ground Surface	997.4523	19.36148258	-155.2214627	997.4523
Post-eruption Ground Surface	996.8767	19.36161044	-155.2209311	996.8767
Post-eruption Ground Surface	994.2257	19.36178828	-155.2224715	994.2257
Post-eruption Ground Surface	994.5546	19.36168311	-155.2220894	994.5546
Post-eruption Ground Surface	995.9352	19.36185137	-155.2211682	995.9352
Post-eruption Ground Surface	996.8951	19.36229783	-155.2214823	996.8951
Post-eruption Ground Surface	994.9464	19.36207346	-155.2217505	994.9464
Post-eruption Ground Surface	994.2238	19.36170598	-155.2218022	994.2238
Post-eruption Ground Surface	993.8009	19.36203598	-155.2222832	993.8009
Post-eruption Ground Surface	995.2652	19.36236983	-155.2224333	995.2652
Post-eruption Ground Surface	994.3581	19.36255611	-155.2233871	994.3581
Post-eruption Ground Surface	994.3239	19.36257901	-155.2237104	994.3239
Post-eruption Ground Surface	993.4355	19.36258745	-155.2239646	993.4355
Post-eruption Ground Surface	993.5478	19.36261267	-155.2243644	993.5478
Post-eruption Ground Surface	993.8106	19.36288425	-155.2240657	993.8106
Post-eruption Ground Surface	996.4116	19.36292832	-155.2230176	996.4116
Post-eruption Ground Surface	992.9137	19.363838	-155.2142899	992.9137
Post-eruption Ground Surface	993.0644	19.36383714	-155.2142895	993.0644
Post-eruption Ground Surface	993.1636	19.36383549	-155.2142888	993.1636
Post-eruption Ground Surface	993.2303	19.36383364	-155.2142881	993.2303
Post-eruption Ground Surface	993.2591	19.36383211	-155.214287	993.2591
Post-eruption Ground Surface	993.2463	19.36383034	-155.2142863	993.2463

Post-eruption Ground Surface	992.7898	19.36338983	-155.2143424	992.7898
Post-eruption Ground Surface	992.8169	19.36327247	-155.2145221	992.8169
Post-eruption Ground Surface	992.4225	19.36324739	-155.2146157	992.4225
Post-eruption Ground Surface	992.7215	19.3634997	-155.2146219	992.7215
Post-eruption Ground Surface	992.5404	19.36343166	-155.2148754	992.5404
Post-eruption Ground Surface	992.5353	19.3633429	-155.2150801	992.5353
Post-eruption Ground Surface	991.4885	19.36319836	-155.2148785	991.4885
Post-eruption Ground Surface	992.8328	19.36307292	-155.2149516	992.8328
Post-eruption Ground Surface	991.4539	19.36282193	-155.2148551	991.4539
Post-eruption Ground Surface	992.1739	19.36275213	-155.2150247	992.1739
Post-eruption Ground Surface	991.6046	19.36261148	-155.2149552	991.6046
Post-eruption Ground Surface	992.1246	19.36267339	-155.2151876	992.1246
Post-eruption Ground Surface	992.2473	19.36290925	-155.2152429	992.2473
Post-eruption Ground Surface	992.9387	19.36368726	-155.2144646	992.9387
Post-eruption Ground Surface	992.7486	19.36366921	-155.2147979	992.7486
Post-eruption Ground Surface	992.5998	19.36358242	-155.2150829	992.5998
Post-eruption Ground Surface	993.4084	19.36338599	-155.2154102	993.4084
Post-eruption Ground Surface	993.0872	19.36322156	-155.2153915	993.0872
Post-eruption Ground Surface	993.2714	19.36304237	-155.2153707	993.2714
Post-eruption Ground Surface	992.1642	19.36256713	-155.2153686	992.1642
Post-eruption Ground Surface	991.637	19.36256811	-155.2154762	991.637
Post-eruption Ground Surface	992.4239	19.36266285	-155.2155699	992.4239
Post-eruption Ground Surface	993.426	19.36272658	-155.215773	993.426
Post-eruption Ground Surface	993.0971	19.36336982	-155.2157479	993.0971
Post-eruption Ground Surface	992.6615	19.36329006	-155.216152	992.6615
Post-eruption Ground Surface	992.4089	19.36306486	-155.216026	992.4089
Post-eruption Ground Surface	992.3665	19.36277867	-155.2159484	992.3665
Post-eruption Ground Surface	992.0994	19.3625281	-155.2158271	992.0994
Post-eruption Ground Surface	992.0152	19.36224807	-155.2157162	992.0152
Post-eruption Ground Surface	992.7271	19.36236584	-155.2158292	992.7271
Post-eruption Ground Surface	993.442	19.36245178	-155.2160804	993.442
Post-eruption Ground Surface	993.08	19.36279083	-155.2161768	993.08
Post-eruption Ground Surface	993.9041	19.36279419	-155.2164825	993.9041
Post-eruption Ground Surface	993.336	19.3626329	-155.2164674	993.336
Post-eruption Ground Surface	992.5795	19.36251594	-155.2167044	992.5795
Post-eruption Ground Surface	992.1293	19.36264266	-155.2167155	992.1293
Post-eruption Ground Surface	991.9807	19.36285103	-155.2167006	991.9807
Post-eruption Ground Surface	991.2508	19.36314458	-155.2167471	991.2508
Post-eruption Ground Surface	992.4826	19.36316504	-155.2164393	992.4826
Post-eruption Ground Surface	993.1269	19.36339873	-155.2163235	993.1269
Post-eruption Ground Surface	991.6588	19.36310166	-155.2169928	991.6588
Post-eruption Ground Surface	993.5449	19.36267379	-155.217225	993.5449
Post-eruption Ground Surface	993.0993	19.36262284	-155.2174677	993.0993
Post-eruption Ground Surface	992.4733	19.3622642	-155.2173042	992.4733
Post-eruption Ground Surface	993.8559	19.36273761	-155.2171791	993.8559
Post-eruption Ground Surface	991.3785	19.36282394	-155.2174625	991.3785
Post-eruption Ground Surface	991.1059	19.3627499	-155.2176711	991.1059
Post-eruption Ground Surface	991.3594	19.36264353	-155.2178192	991.3594
Post-eruption Ground Surface	992.4575	19.36238715	-155.2175392	992.4575
Post-eruption Ground Surface	991.6007	19.36210133	-155.2175615	991.6007
Post-eruption Ground Surface	990.7299	19.36185792	-155.2176747	990.7299

Post-eruption Ground Surface	989.2142	19.36166518	-155.2177551	989.2142
Post-eruption Ground Surface	990.0492	19.36194328	-155.2177954	990.0492
Post-eruption Ground Surface	992.5095	19.36207011	-155.2179321	992.5095
Post-eruption Ground Surface	992.0995	19.36240549	-155.217927	992.0995
Post-eruption Ground Surface	992.6293	19.36266166	-155.2183248	992.6293
Post-eruption Ground Surface	993.3954	19.36258953	-155.2185621	993.3954
Post-eruption Ground Surface	994.8326	19.36277309	-155.2186437	994.8326
Post-eruption Ground Surface	994.305	19.36299076	-155.218837	994.305
Post-eruption Ground Surface	992.3713	19.36077594	-155.2200003	992.3713
Post-eruption Ground Surface	993.4583	19.3635762	-155.2152262	993.4583
Post-eruption Ground Surface	992.8538	19.36367656	-155.2148781	992.8538
Post-eruption Ground Surface	992.9695	19.36365958	-155.2146675	992.9695
Post-eruption Ground Surface	993.641	19.36379835	-155.2144442	993.641
Post-eruption Ground Surface	994.818	19.36371614	-155.2153551	994.818
Post-eruption Ground Surface	995.5508	19.3637523	-155.2158931	995.5508
Post-eruption Ground Surface	995.7078	19.36375146	-155.2160806	995.7078
Post-eruption Ground Surface	995.1308	19.36372817	-155.2163025	995.1308
Post-eruption Ground Surface	995.5834	19.36360314	-155.216465	995.5834
Post-eruption Ground Surface	994.3884	19.36347679	-155.2166844	994.3884
Post-eruption Ground Surface	993.8764	19.36351766	-155.2168236	993.8764
Post-eruption Ground Surface	994.4334	19.36360846	-155.2170421	994.4334
Post-eruption Ground Surface	996.0074	19.36349494	-155.2171539	996.0074
Post-eruption Ground Surface	993.6218	19.36325609	-155.2171731	993.6218
Post-eruption Ground Surface	994.5729	19.36338769	-155.2172057	994.5729
Post-eruption Ground Surface	995.93	19.36359387	-155.2172579	995.93
Post-eruption Ground Surface	995.5335	19.36357499	-155.2174063	995.5335
Post-eruption Ground Surface	994.8427	19.36362688	-155.2174665	994.8427
Post-eruption Ground Surface	995.1405	19.36346861	-155.2175423	995.1405
Post-eruption Ground Surface	994.4407	19.36333994	-155.2175909	994.4407
Post-eruption Ground Surface	993.2791	19.36321614	-155.2175646	993.2791
Post-eruption Ground Surface	993.1374	19.36312767	-155.2176129	993.1374
Post-eruption Ground Surface	993.9825	19.36302148	-155.2175411	993.9825
Post-eruption Ground Surface	994.4415	19.36316207	-155.2173229	994.4415
Post-eruption Ground Surface	995.9617	19.36318752	-155.2173834	995.9617
Post-eruption Ground Surface	995.1833	19.36335602	-155.2174053	995.1833
Post-eruption Ground Surface	993.8373	19.36339431	-155.2175097	993.8373
Post-eruption Ground Surface	993.3098	19.36325996	-155.2175	993.3098
Post-eruption Ground Surface	994.3052	19.36321452	-155.2176585	994.3052
Post-eruption Ground Surface	993.9967	19.36303345	-155.2178951	993.9967
Post-eruption Ground Surface	993.8556	19.36298439	-155.2179997	993.8556
Post-eruption Ground Surface	993.4102	19.36301493	-155.2181922	993.4102
Post-eruption Ground Surface	994.1197	19.36321569	-155.2182841	994.1197
Post-eruption Ground Surface	994.9593	19.36302439	-155.2184104	994.9593
Post-eruption Ground Surface	994.3174	19.36307099	-155.21858	994.3174
Post-eruption Ground Surface	994.2184	19.36287357	-155.2187602	994.2184
Post-eruption Ground Surface	994.0103	19.36308436	-155.2188598	994.0103
Post-eruption Ground Surface	995.0454	19.36312555	-155.2190476	995.0454
Post-eruption Ground Surface	995.9602	19.36299321	-155.2195053	995.9602
Post-eruption Ground Surface	997.169	19.36309745	-155.2195909	997.169
Post-eruption Ground Surface	998.8213	19.36311147	-155.2198386	998.8213
Post-eruption Ground Surface	998.8034	19.36309038	-155.2199711	998.8034

Post-eruption Ground Surface	998.9777	19.36289385	-155.2203761	998.9777
Post-eruption Ground Surface	998.9411	19.36275366	-155.2204763	998.9411
Post-eruption Ground Surface	997.4641	19.36270316	-155.2205982	997.4641
Post-eruption Ground Surface	997.7385	19.36268836	-155.2209042	997.7385
Post-eruption Ground Surface	997.2783	19.3629282	-155.2212707	997.2783
Post-eruption Ground Surface	997.1781	19.36277135	-155.2214717	997.1781
Post-eruption Ground Surface	997.1343	19.36273368	-155.2217421	997.1343
Post-eruption Ground Surface	995.3189	19.36229908	-155.2218232	995.3189
Post-eruption Ground Surface	997.885	19.36147753	-155.2225241	997.885
Post-eruption Ground Surface	998.3638	19.36146598	-155.2222598	998.3638
Post-eruption Ground Surface	996.4816	19.36143609	-155.2215639	996.4816
Post-eruption Ground Surface	996.7766	19.36143325	-155.2214483	996.7766
Post-eruption Ground Surface	995.9533	19.36145448	-155.2213476	995.9533
Post-eruption Ground Surface	997.0758	19.36144005	-155.2210488	997.0758
Post-eruption Ground Surface	996.0849	19.36137265	-155.2213582	996.0849
Post-eruption Ground Surface	997.46	19.36230571	-155.2213801	997.46
Post-eruption Ground Surface	996.1081	19.36254747	-155.2214202	996.1081
Post-eruption Ground Surface	996.8912	19.36234958	-155.2212717	996.8912
Post-eruption Ground Surface	996.6823	19.3622287	-155.2210453	996.6823
Post-eruption Ground Surface	995.0878	19.36237791	-155.2209397	995.0878
Post-eruption Ground Surface	996.715	19.36254095	-155.2208841	996.715
Post-eruption Ground Surface	996.1482	19.36227241	-155.2207019	996.1482
Post-eruption Ground Surface	994.0269	19.36235094	-155.2203137	994.0269
Post-eruption Ground Surface	996.0023	19.36247947	-155.2205383	996.0023
Post-eruption Ground Surface	994.4596	19.36228292	-155.2204675	994.4596
Post-eruption Ground Surface	992.9112	19.36220634	-155.2201969	992.9112
Post-eruption Ground Surface	993.3461	19.36206216	-155.2201462	993.3461
Post-eruption Ground Surface	992.2214	19.36171492	-155.2200619	992.2214
Post-eruption Ground Surface	994.8003	19.36177093	-155.2202337	994.8003
Post-eruption Ground Surface	995.5241	19.36193076	-155.2202967	995.5241
Post-eruption Ground Surface	994.2813	19.36178382	-155.2198736	994.2813
Post-eruption Ground Surface	995.1204	19.36215949	-155.2199099	995.1204
Post-eruption Ground Surface	993.6214	19.36237636	-155.219984	993.6214
Post-eruption Ground Surface	994.4627	19.3625999	-155.2199307	994.4627
Post-eruption Ground Surface	994.4366	19.36268963	-155.2195339	994.4366
Post-eruption Ground Surface	992.605	19.36256796	-155.2193539	992.605
Post-eruption Ground Surface	992.3139	19.36248334	-155.2191481	992.3139
Post-eruption Ground Surface	992.5998	19.36239306	-155.2191215	992.5998
Post-eruption Ground Surface	993.3317	19.36231888	-155.2190962	993.3317
Post-eruption Ground Surface	993.477	19.36221872	-155.2190633	993.477
Post-eruption Ground Surface	993.6771	19.36230301	-155.2189152	993.6771
Post-eruption Ground Surface	992.8736	19.36244257	-155.2189897	992.8736
Post-eruption Ground Surface	992.0643	19.36269619	-155.2189089	992.0643
Post-eruption Ground Surface	994.6197	19.36253173	-155.2188574	994.6197
Post-eruption Ground Surface	995.3044	19.36241674	-155.2188809	995.3044
Post-eruption Ground Surface	995.1376	19.36228987	-155.2189754	995.1376
Post-eruption Ground Surface	994.8747	19.36227306	-155.2191427	994.8747
Post-eruption Ground Surface	994.6715	19.3624164	-155.2192142	994.6715
Post-eruption Ground Surface	994.6647	19.36237888	-155.2190666	994.6647
Post-eruption Ground Surface	995.0956	19.36278313	-155.2187547	995.0956
Post-eruption Ground Surface	994.9072	19.36286511	-155.2184714	994.9072

Post-eruption Ground Surface	992.6877	19.36274499	-155.2179304	992.6877
Post-eruption Ground Surface	992.1439	19.36285125	-155.2177704	992.1439
Post-eruption Ground Surface	992.1563	19.36277001	-155.2182135	992.1563
Post-eruption Ground Surface	992.1043	19.36272583	-155.2184543	992.1043
Post-eruption Ground Surface	994.7593	19.36278192	-155.2194878	994.7593
Post-eruption Ground Surface	995.5474	19.36281494	-155.2197584	995.5474
Post-eruption Ground Surface	996.5449	19.3627565	-155.2198783	996.5449
Post-eruption Ground Surface	996.3887	19.36277988	-155.2198268	996.3887
Post-eruption Ground Surface	996.5396	19.36260784	-155.2203125	996.5396
Post-eruption Ground Surface	997.2035	19.36258151	-155.2208512	997.2035
Post-eruption Ground Surface	997.3835	19.36251073	-155.2211394	997.3835
Post-eruption Ground Surface	995.9596	19.36253398	-155.2216669	995.9596
Post-eruption Ground Surface	992.8665	19.3635105	-155.2145867	992.8665
Post-eruption Ground Surface	993.2129	19.36382645	-155.2143007	993.2129
Post-eruption Ground Surface	995.6265	19.36164245	-155.2232262	995.6265
Post-eruption Ground Surface	992.9868	19.36385524	-155.2142427	992.9868
Post-eruption Ground Surface	994.1694	19.36373076	-155.2145189	994.1694
Post-eruption Ground Surface	995.9578	19.36186821	-155.2234138	995.9578
Post-eruption Ground Surface	992.9567	19.36370223	-155.2146485	992.9567
Post-eruption Ground Surface	996.6592	19.36199229	-155.2236288	996.6592
Post-eruption Ground Surface	992.9258	19.3636802	-155.2148805	992.9258
Post-eruption Ground Surface	995.7437	19.36210416	-155.2232022	995.7437
Post-eruption Ground Surface	992.7676	19.36367973	-155.2149049	992.7676
Post-eruption Ground Surface	993.2908	19.36369961	-155.2149201	993.2908
Post-eruption Ground Surface	996.7086	19.36221055	-155.2235262	996.7086
Post-eruption Ground Surface	993.7757	19.36373096	-155.2148901	993.7757
Post-eruption Ground Surface	993.1872	19.36361733	-155.2151669	993.1872
Post-eruption Ground Surface	997.641	19.36233017	-155.224133	997.641
Post-eruption Ground Surface	994.0237	19.36364761	-155.2151574	994.0237
Post-eruption Ground Surface	993.0688	19.36355592	-155.2151097	993.0688
Post-eruption Ground Surface	997.8296	19.3624132	-155.2240786	997.8296
Post-eruption Ground Surface	997.6559	19.36225821	-155.224198	997.6559
Post-eruption Ground Surface	993.6686	19.36357729	-155.2152261	993.6686
Post-eruption Ground Surface	993.4207	19.36347211	-155.2152194	993.4207
Post-eruption Ground Surface	994.6788	19.36314191	-155.2239877	994.6788
Post-eruption Ground Surface	993.6733	19.3634534	-155.2158107	993.6733
Post-eruption Ground Surface	994.8073	19.36316627	-155.2237707	994.8073
Post-eruption Ground Surface	993.9976	19.36346196	-155.2159355	993.9976
Post-eruption Ground Surface	996.3822	19.36352172	-155.223818	996.3822
Post-eruption Ground Surface	992.5589	19.36337643	-155.2161928	992.5589
Post-eruption Ground Surface	992.5447	19.36279525	-155.2180291	992.5447
Post-eruption Ground Surface	996.8005	19.3637355	-155.2236261	996.8005
Post-eruption Ground Surface	992.2363	19.36269064	-155.2181688	992.2363
Post-eruption Ground Surface	996.264	19.36359165	-155.2234663	996.264
Post-eruption Ground Surface	993.1298	19.36273096	-155.2191354	993.1298
Post-eruption Ground Surface	996.4836	19.36332101	-155.2233017	996.4836
Post-eruption Ground Surface	996.634	19.36343693	-155.2231377	996.634
Post-eruption Ground Surface	992.9578	19.36261309	-155.2191451	992.9578
Post-eruption Ground Surface	996.7073	19.36316534	-155.2228992	996.7073
Post-eruption Ground Surface	996.2136	19.36280373	-155.2196493	996.2136
Post-eruption Ground Surface	994.1808	19.36264209	-155.2195941	994.1808

Post-eruption Ground Surface	996.405	19.36294103	-155.223019	996.405
Post-eruption Ground Surface	995.1351	19.36270102	-155.2233348	995.1351
Post-eruption Ground Surface	994.7592	19.36296985	-155.2237804	994.7592
Post-eruption Ground Surface	995.0706	19.36296719	-155.2236449	995.0706
Post-eruption Ground Surface	994.7825	19.36277359	-155.2236553	994.7825
Post-eruption Ground Surface	994.8751	19.36246024	-155.2224005	994.8751
Post-eruption Ground Surface	994.3338	19.36231296	-155.2221775	994.3338
Post-eruption Ground Surface	996.2283	19.36220181	-155.221923	996.2283
Post-eruption Ground Surface	995.6375	19.36200972	-155.2219222	995.6375
Post-eruption Ground Surface	995.2016	19.36175374	-155.2215394	995.2016
Post-eruption Ground Surface	992.6574	19.36088725	-155.2221327	992.6574
Post-eruption Ground Surface	995.0385	19.36118276	-155.2224008	995.0385
Post-eruption Ground Surface	994.8016	19.36064208	-155.2221045	994.8016
Post-eruption Ground Surface	993.0989	19.36079897	-155.2203323	993.0989
Post-eruption Ground Surface	993.3985	19.36075112	-155.2203298	993.3985
Post-eruption Ground Surface	991.7623	19.36089327	-155.2197906	991.7623
Post-eruption Ground Surface	992.6994	19.36075332	-155.2197383	992.6994
Post-eruption Ground Surface	993.7652	19.36066447	-155.2202191	993.7652
Post-eruption Ground Surface	991.7841	19.36085986	-155.2193354	991.7841
Post-eruption Ground Surface	990.3709	19.36098788	-155.2188079	990.3709
Post-eruption Ground Surface	989.9461	19.36101747	-155.2185662	989.9461
Post-eruption Ground Surface	989.3288	19.36097559	-155.2180472	989.3288
Post-eruption Ground Surface	989.9733	19.36084691	-155.2180268	989.9733
Post-eruption Ground Surface	990.8949	19.36085918	-155.2183051	990.8949
Post-eruption Ground Surface	989.8625	19.36074439	-155.2177296	989.8625
Post-eruption Ground Surface	989.2327	19.36098185	-155.2176466	989.2327
Post-eruption Ground Surface	992.7479	19.36205831	-155.2180975	992.7479
Post-eruption Ground Surface	993.2589	19.36246848	-155.2181608	993.2589
Post-eruption Ground Surface	993.5819	19.36256967	-155.2184341	993.5819
Post-eruption Ground Surface	994.8159	19.36252688	-155.2184391	994.8159

Appendix D

Binary images from Chapter 3

This appendix contains the manually traced thin section scans and large SEM image grids used in this thesis. Bubbles are shown in black and the phenocrysts are shown in blue. After the binary images, raw results tables are reported containing: (1) the traced bubble areas from the thin section scans; (2) the traced bubble areas from the SEM images; (3) the traced phenocryst areas from the thin section scans; the traced phenocryst areas from the SEM images and (4) the total thin section and SEM image area measured for each spatter sample.

Sample 8B (Primary):

Thin section scan (Scale bar = 25.67 mm)

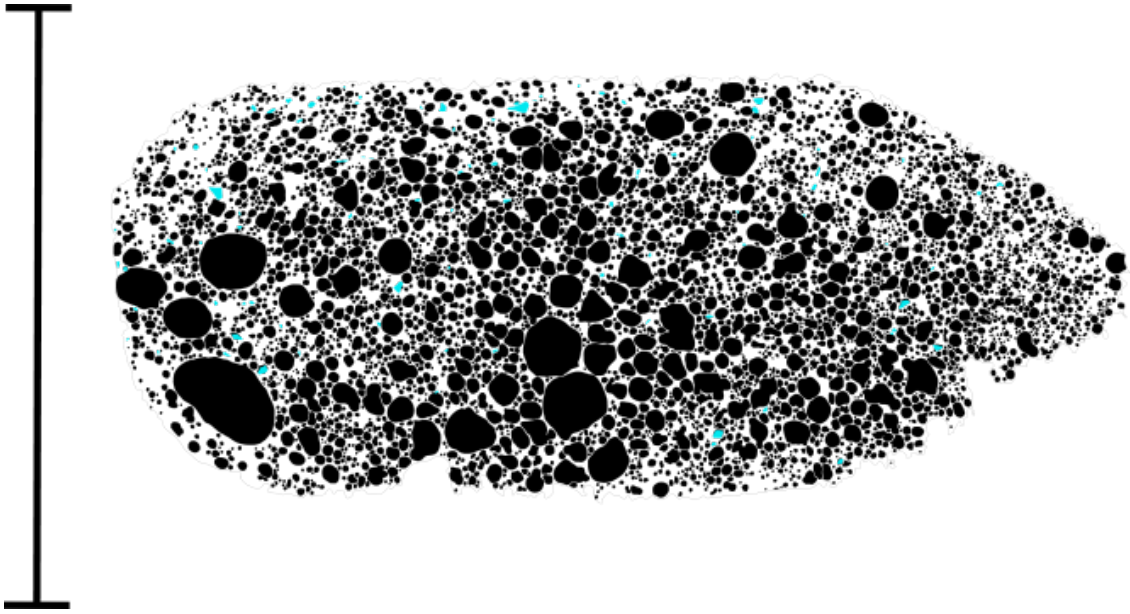

SEM images (Scale bar = 0.4 mm)

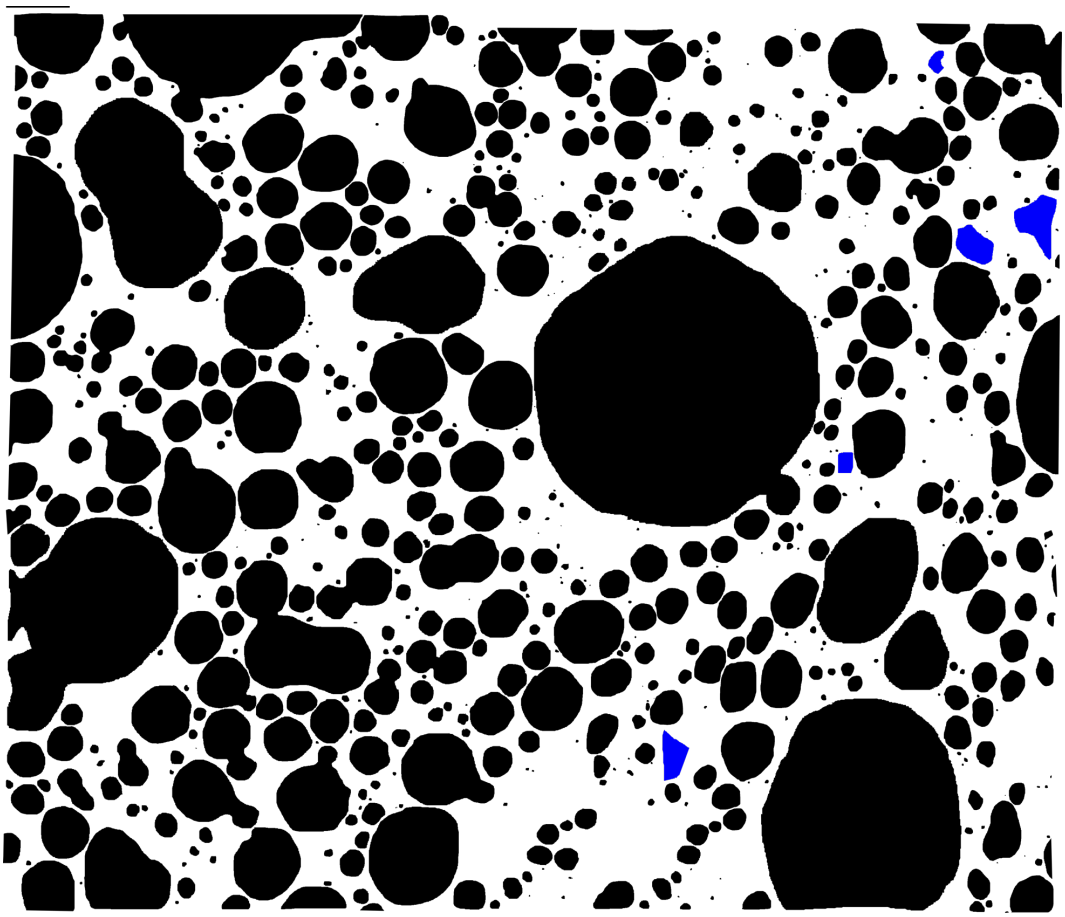

Sample 8Ei (Primary):

Thin section scan (Scale bar = 25.55 mm)

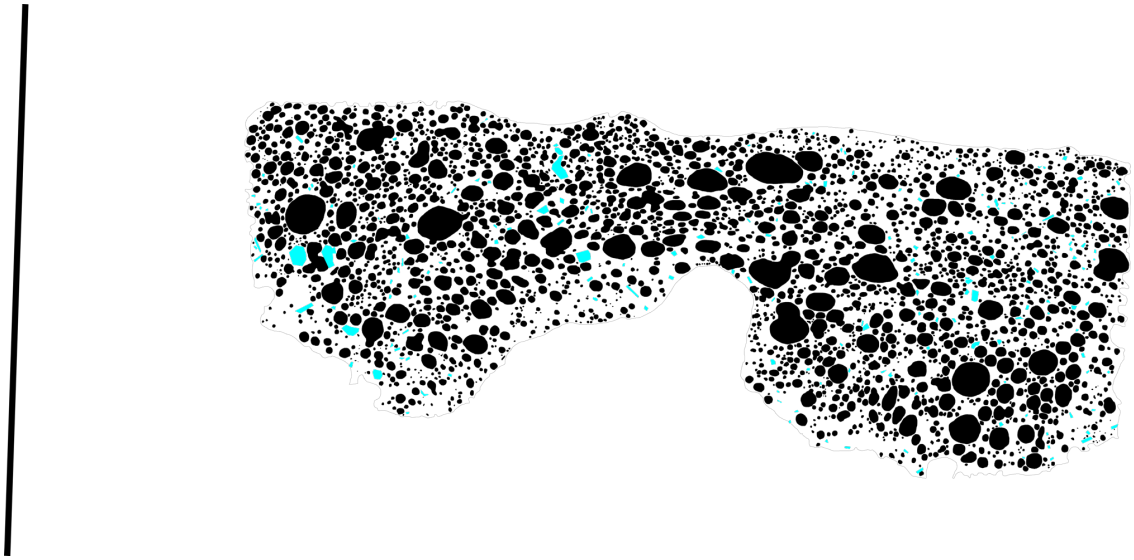

SEM images (Scale bars = 1 mm)

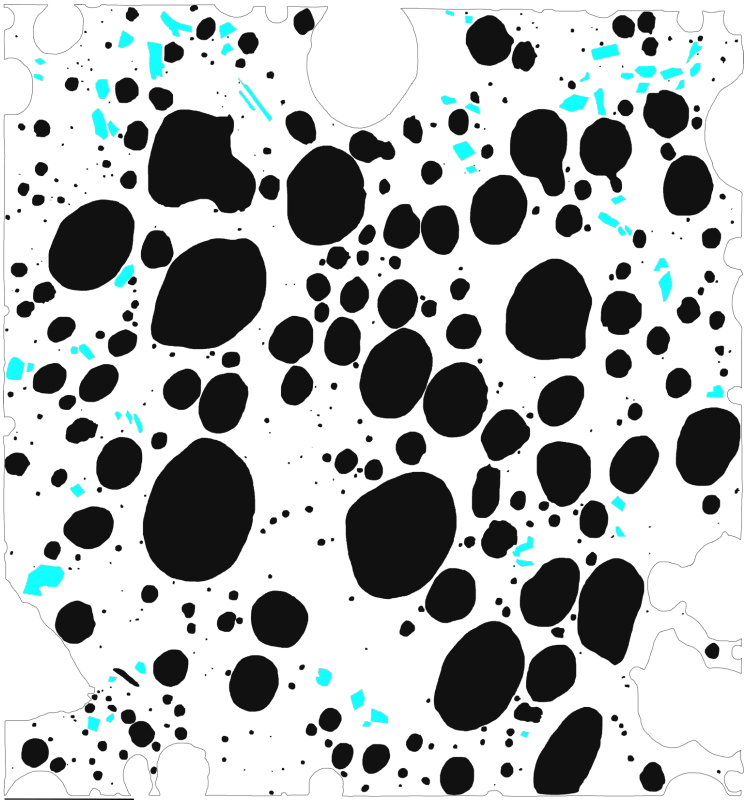

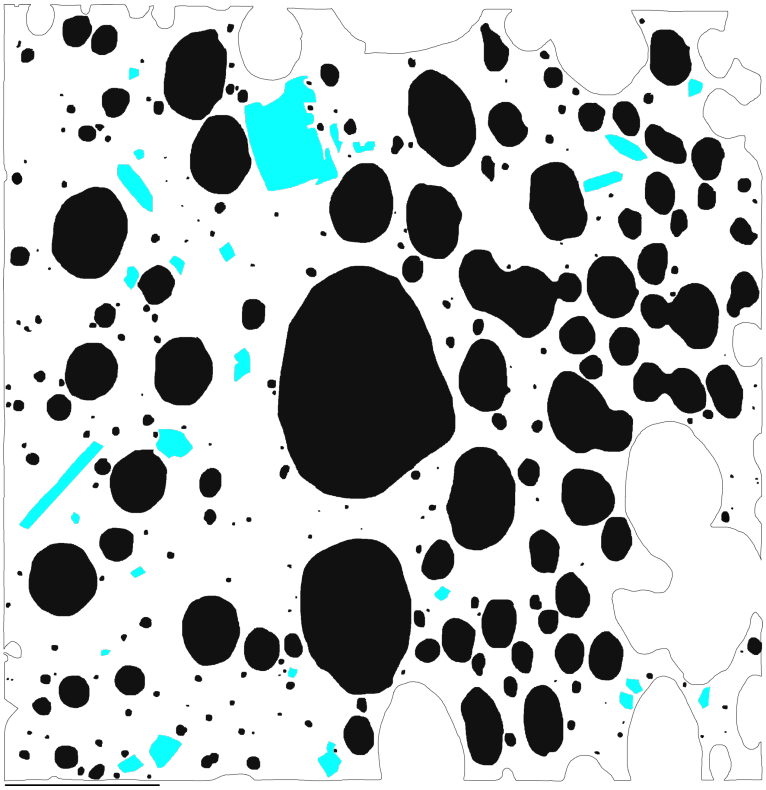

Sample 4Q (Primary):

Thin section scan (Scale bar = 25.30 mm)

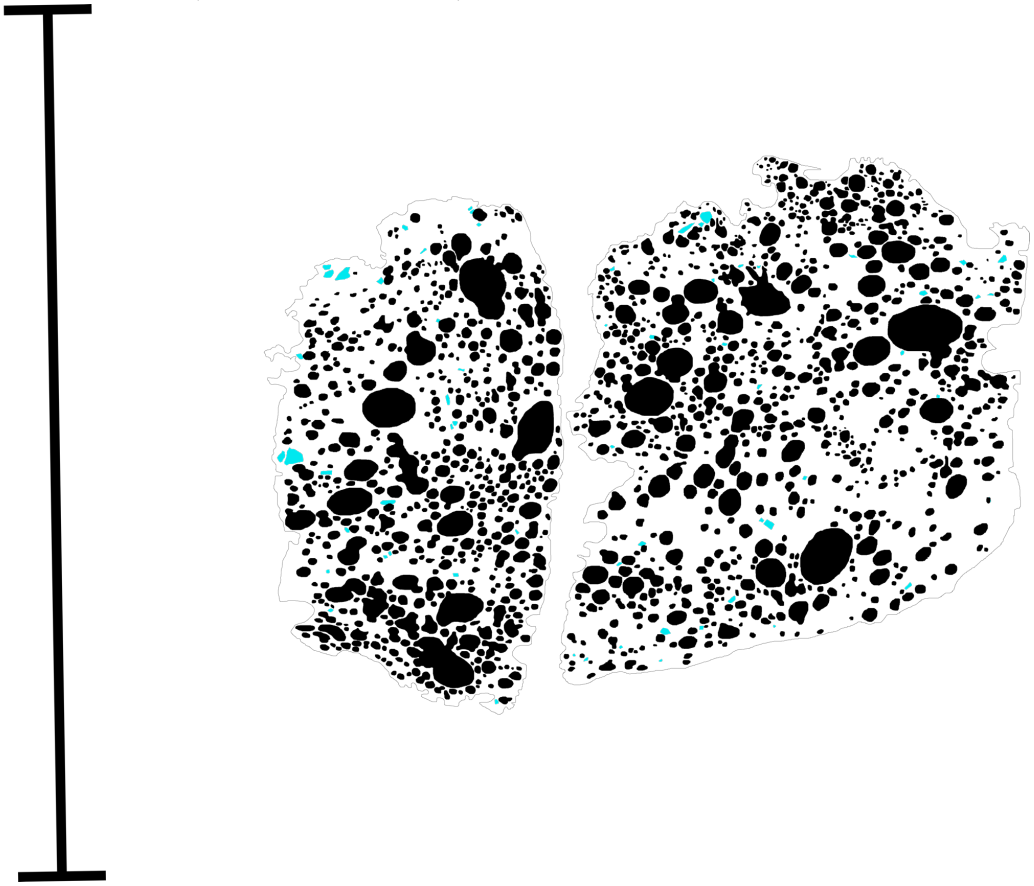

SEM images (Scale bars = 1 mm)

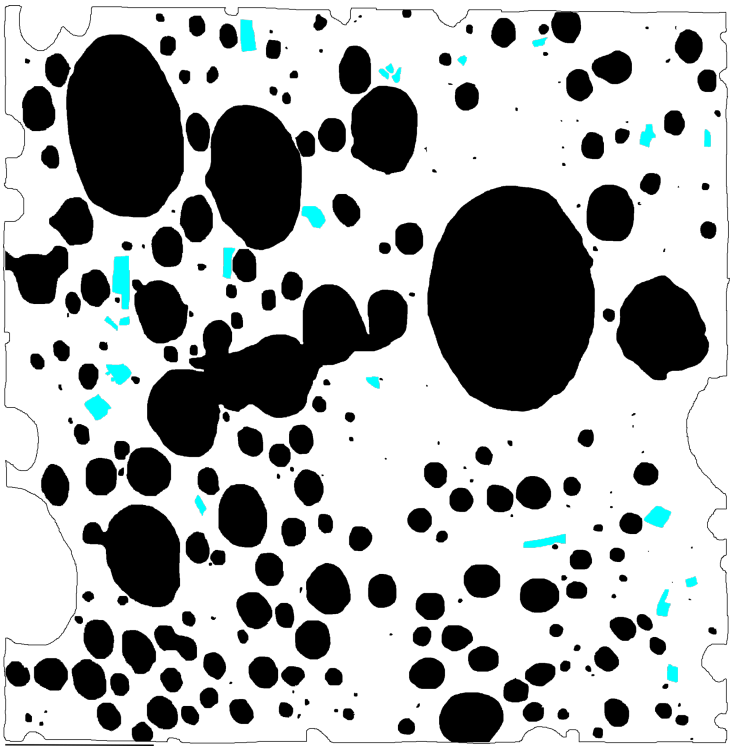

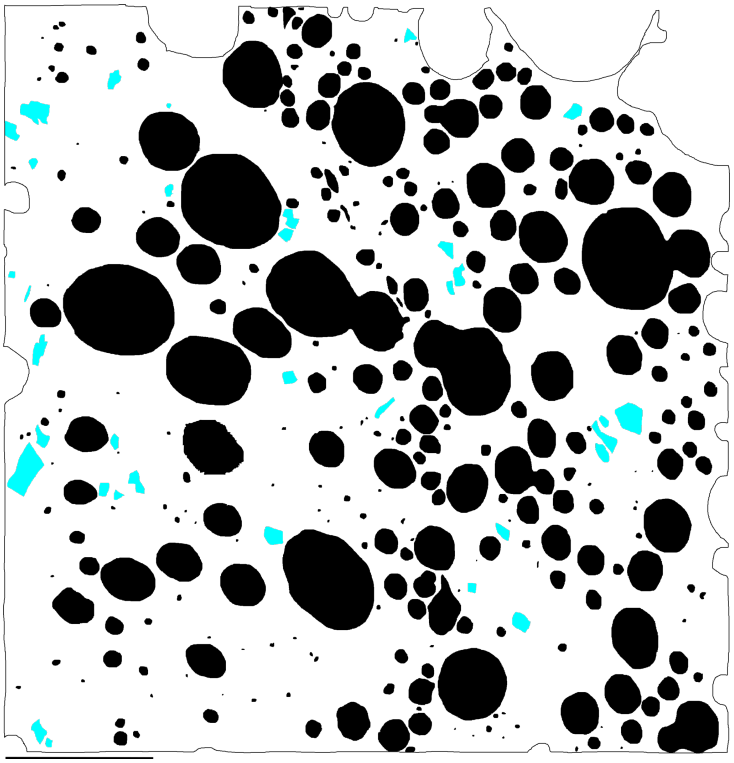

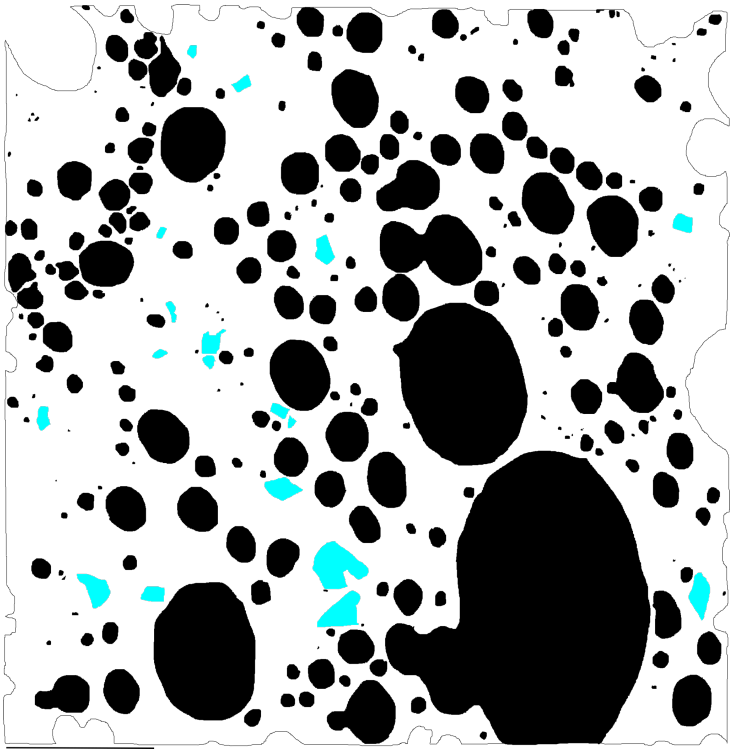

Sample 4A (Primary):

Thin section scan (Scale bar = 25.34 mm)

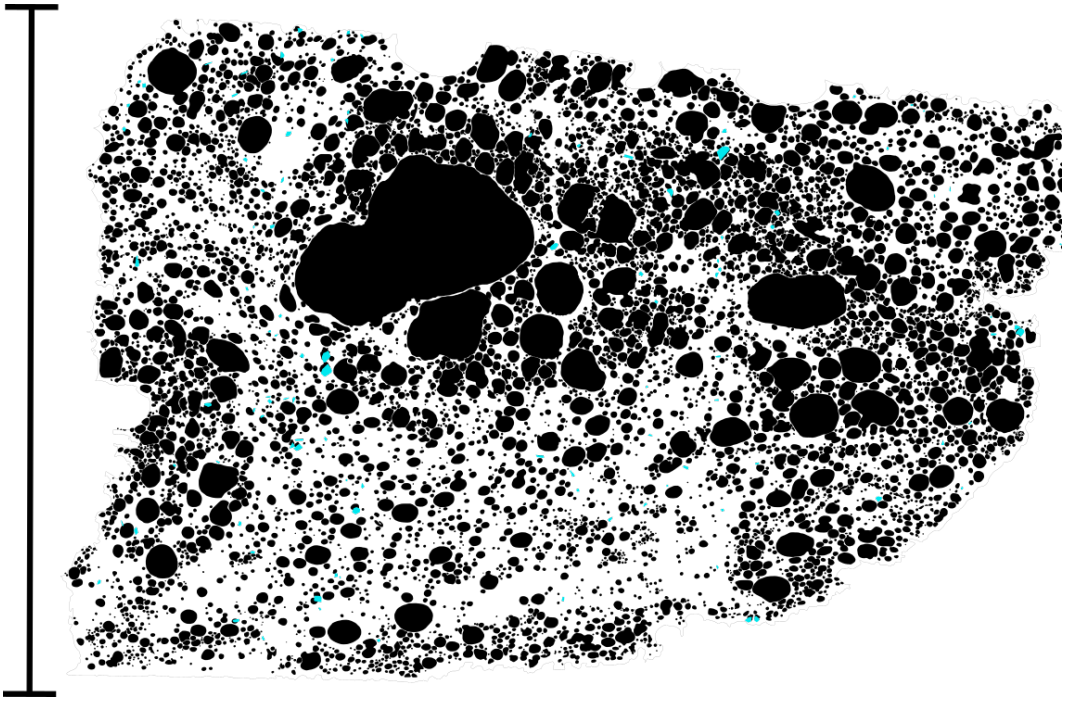

SEM images (Scale bar = 1 mm)

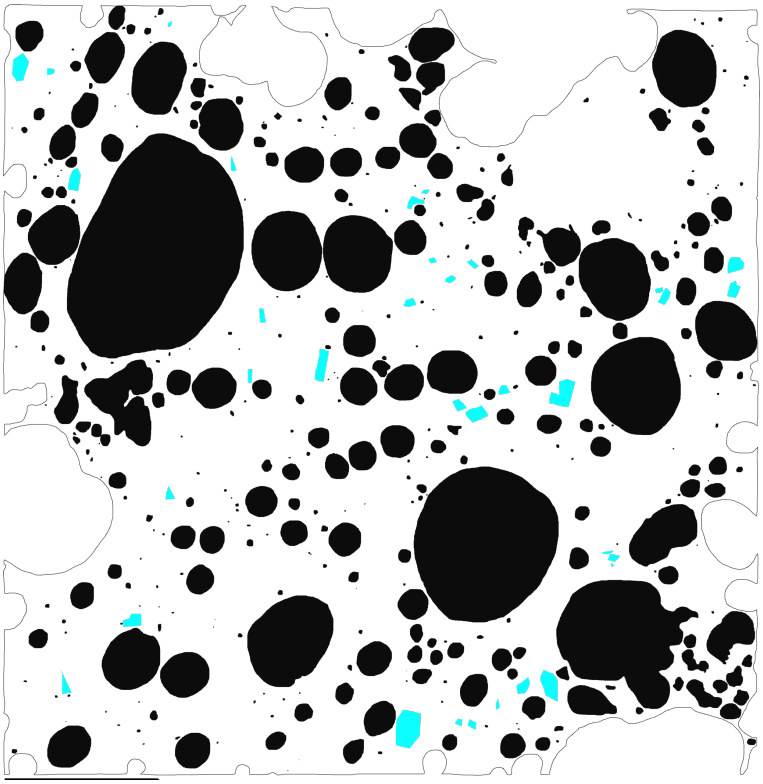

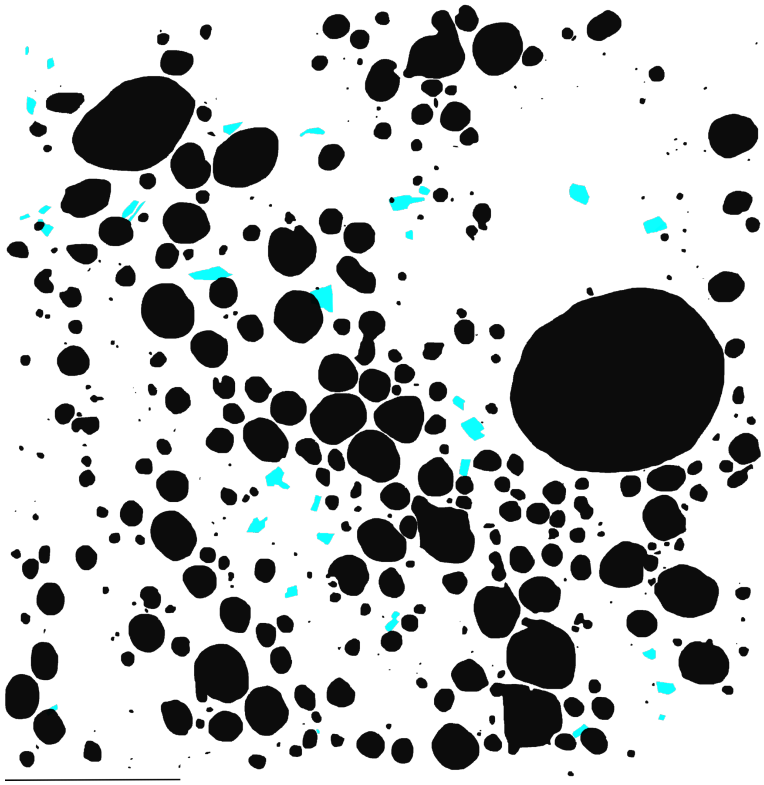

Sample 1Dq (Late-stage):

Thin section scan (Scale bar = 25.08 mm)

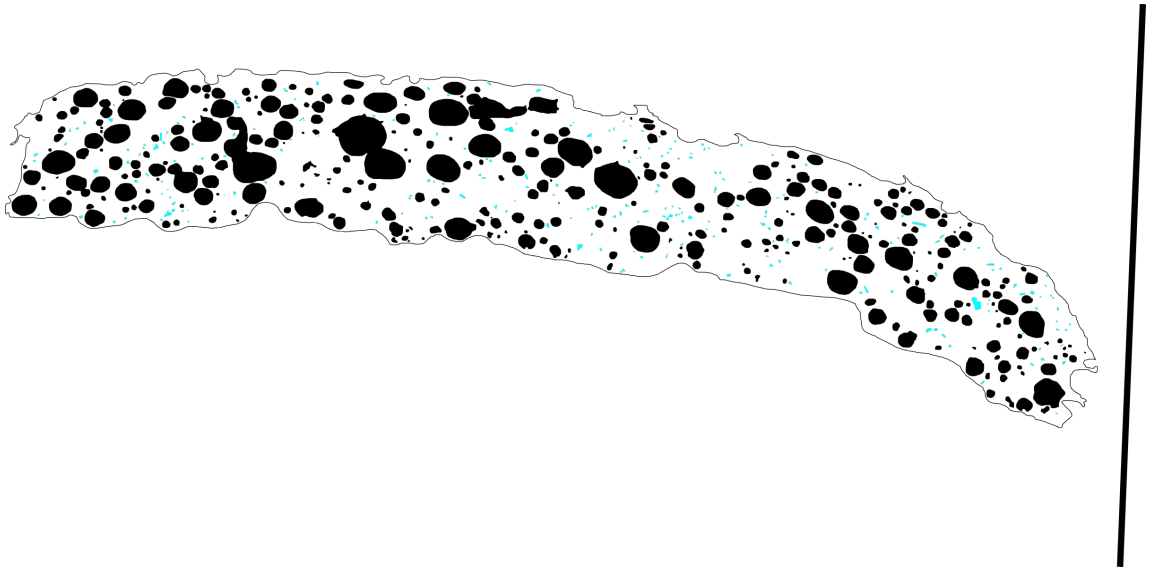

SEM images (Scale bar = 1 mm)

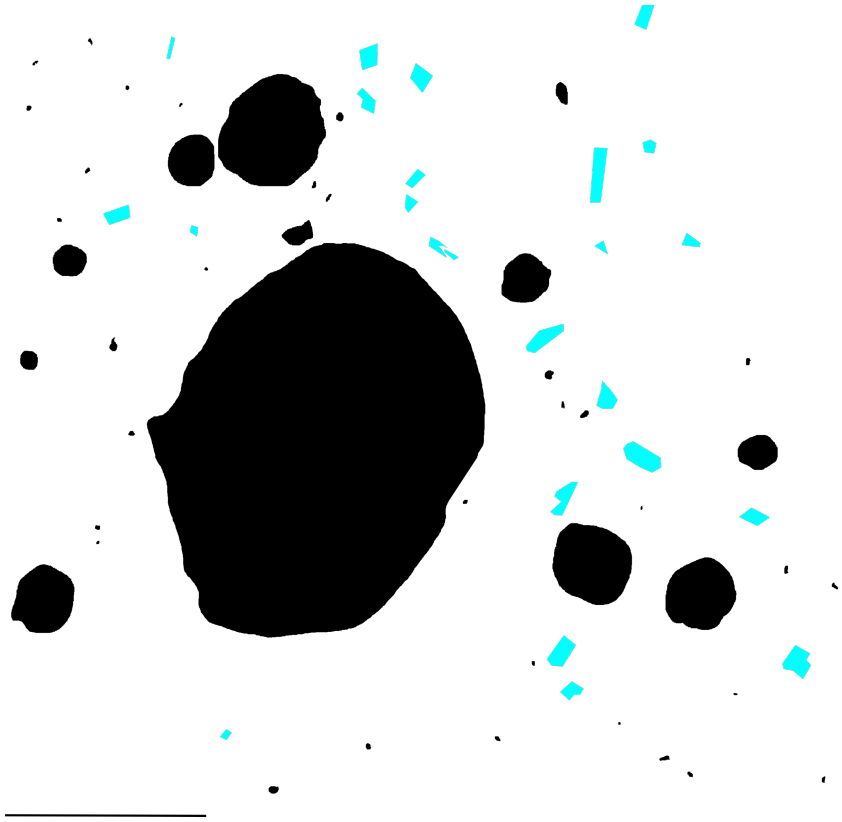

Sample 5K (Late-stage):

Thin section scan (Scale bar = 25.32 mm)

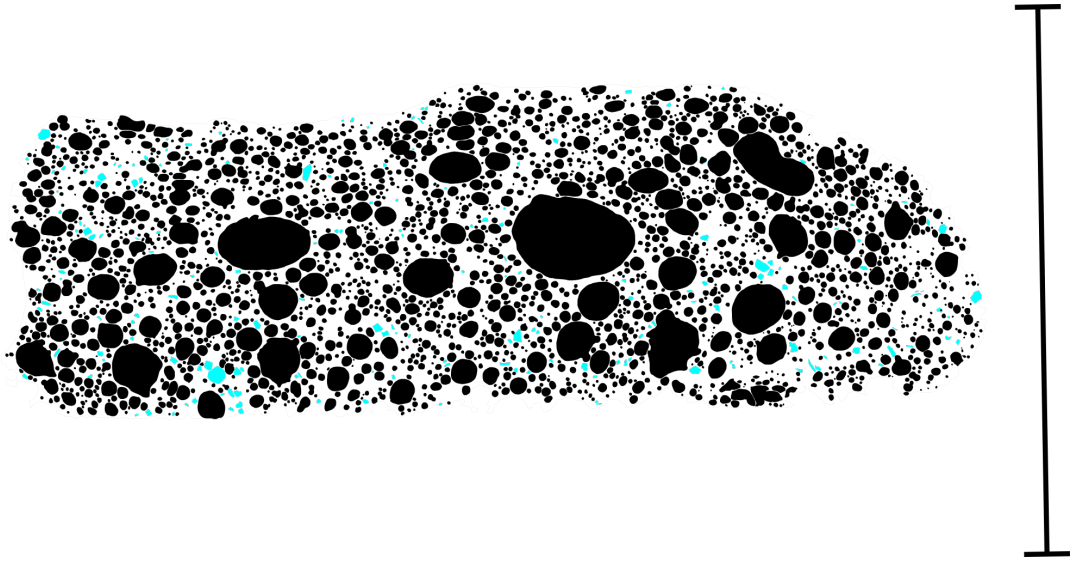

SEM images (Scale bar = 1 mm)

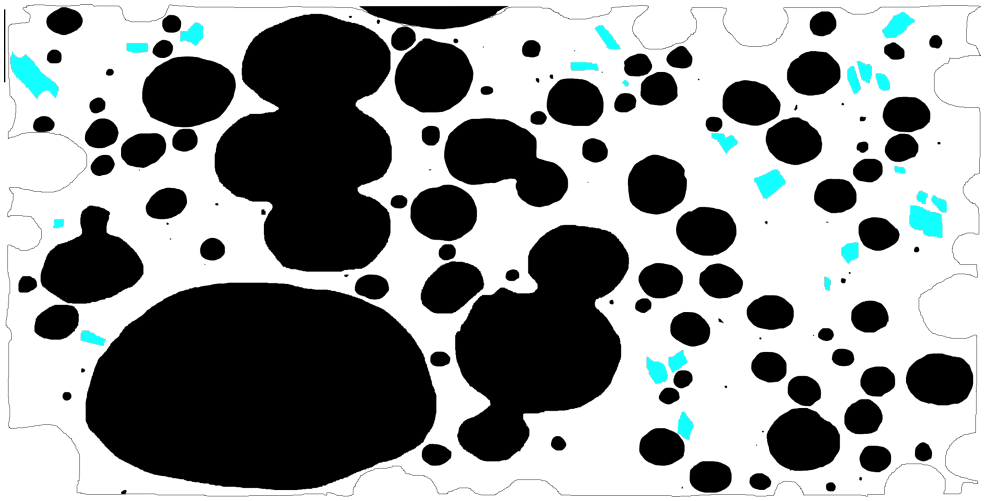

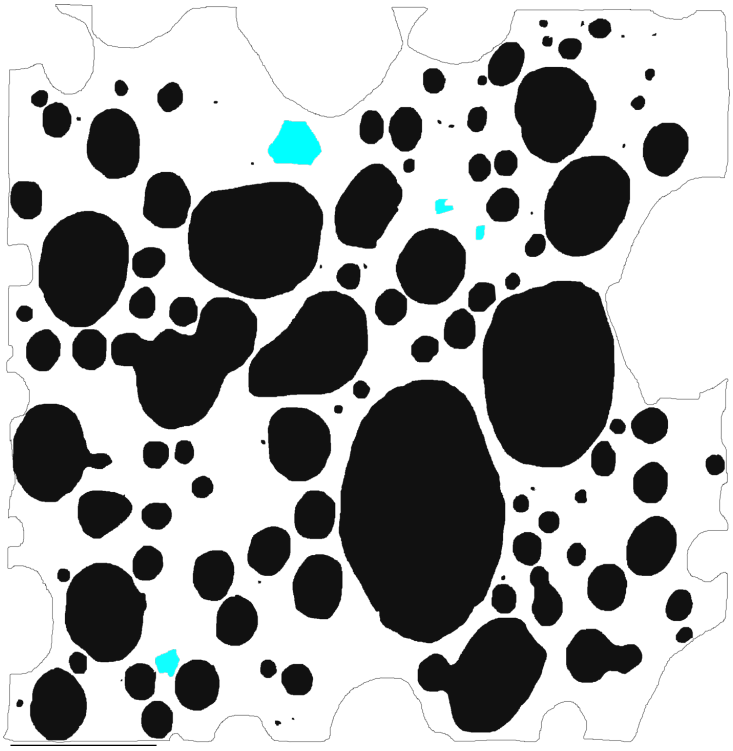

Sample 6Aq (Late-stage):

Thin section scan (Scale bar = 25.04 mm)

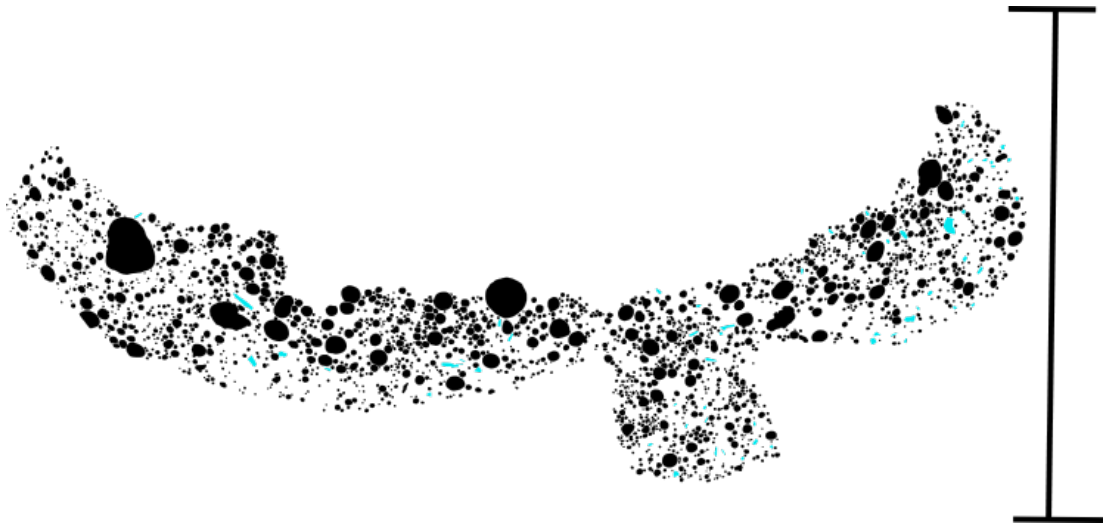

SEM images (Scale bar = 1 mm)

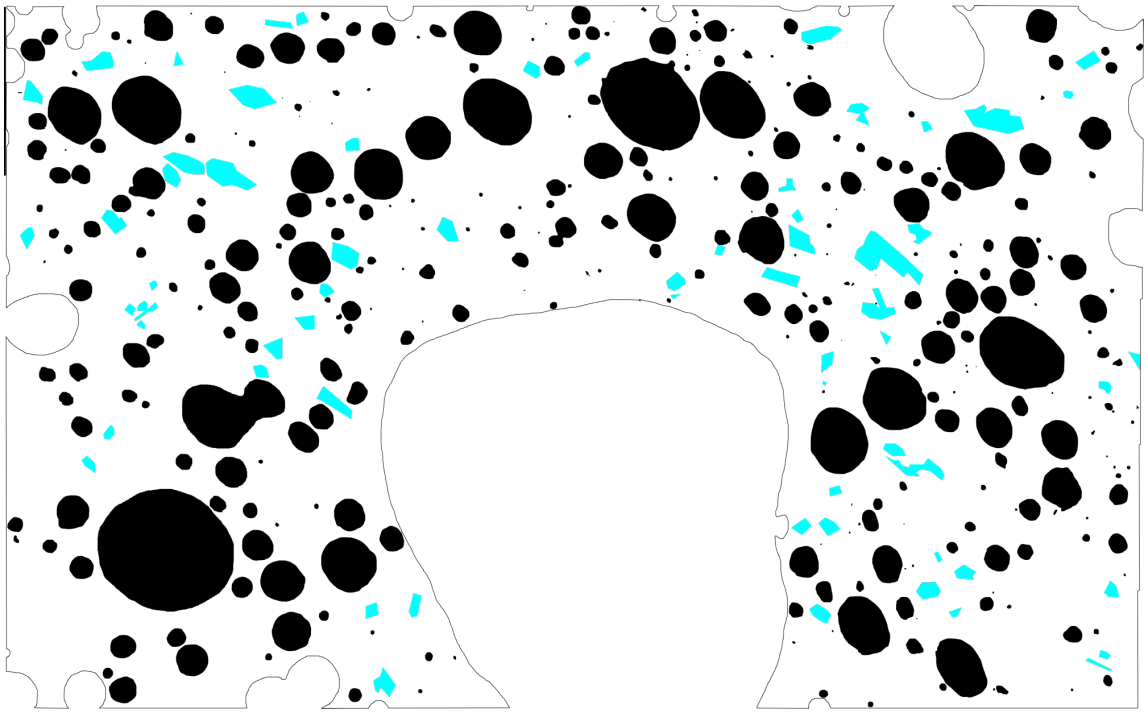

Sample 1Aq (Late-stage):

Thin section scan (Scale bar = 25.08 mm)

SEM images (Scale bar = 0.4 mm)

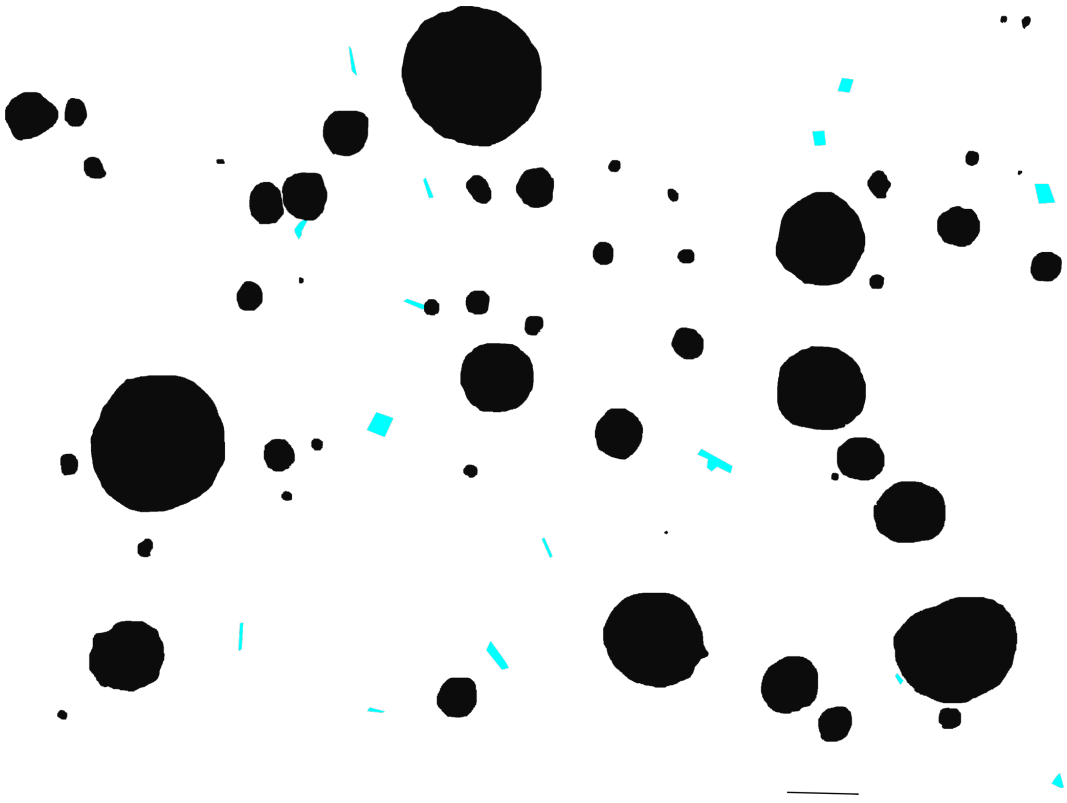

Sample 1Cq (Late-stage):

Thin section scan (Scale bar = 25.66 mm)

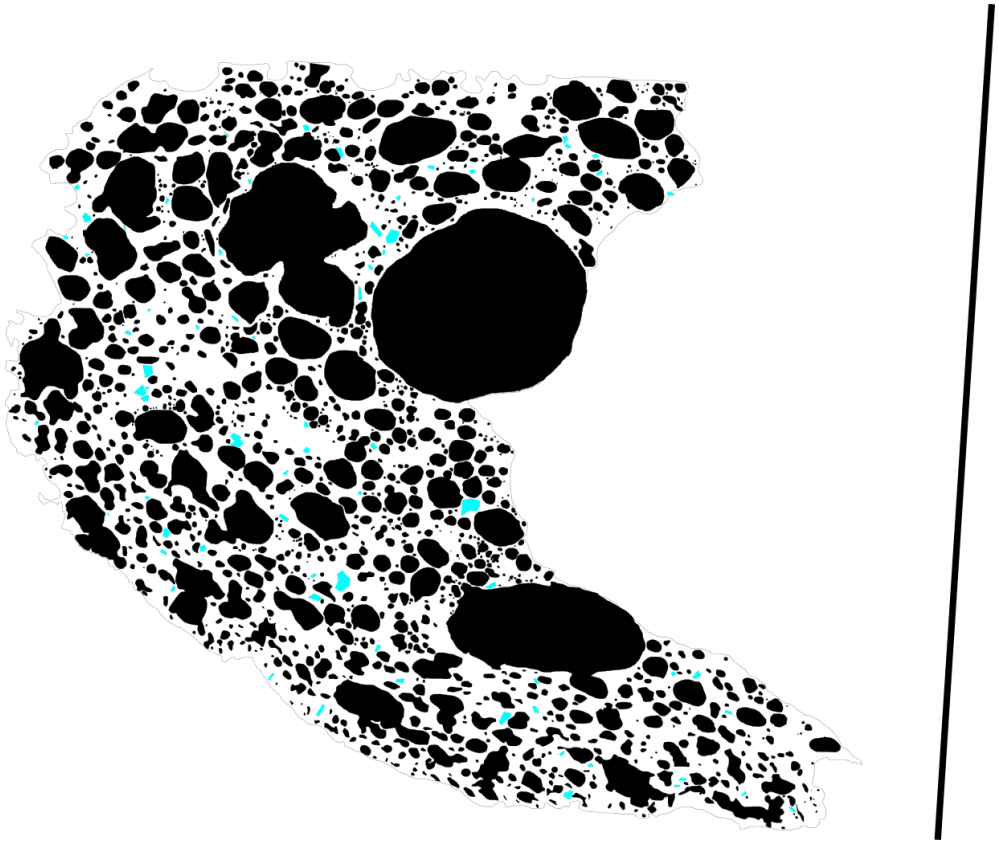

SEM images (Scale bar = 1 mm)

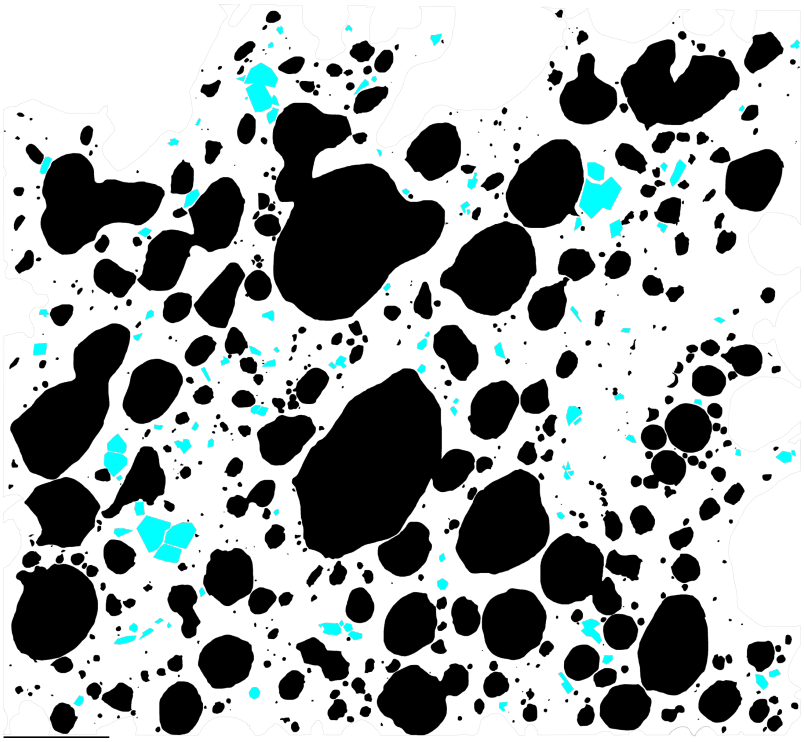

Sample 12H (Secondary):

Thin section scan (Scale bar = 25.55 mm)

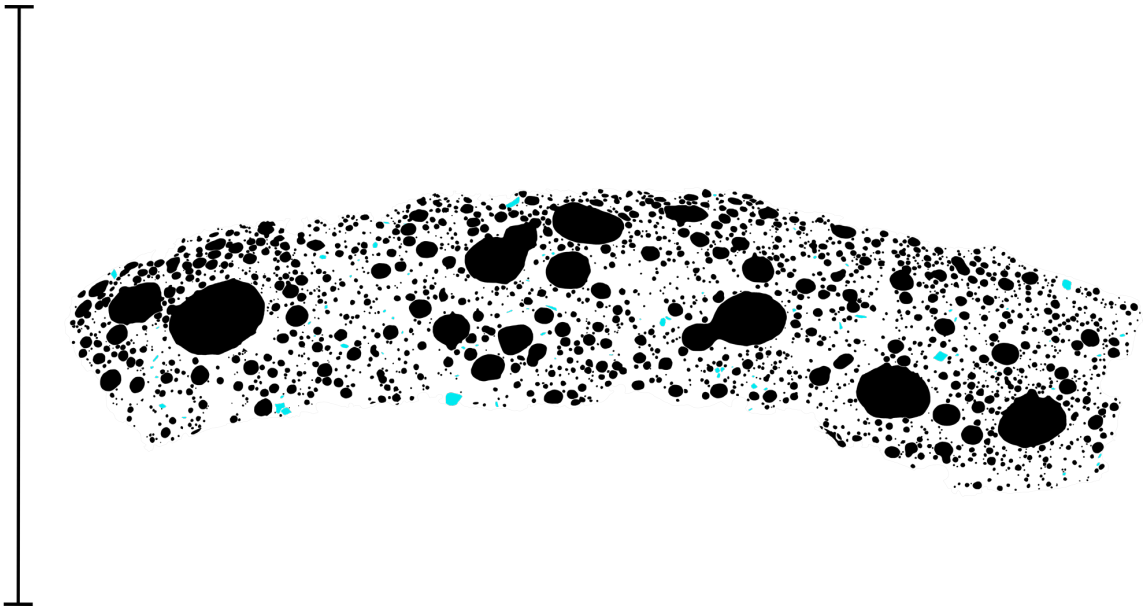

SEM images (Scale bar = 1 mm)

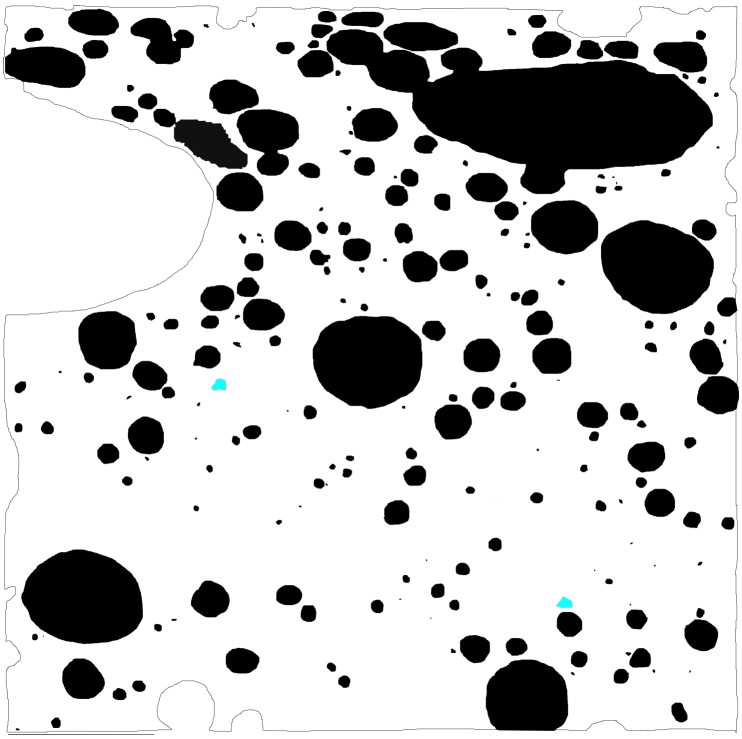

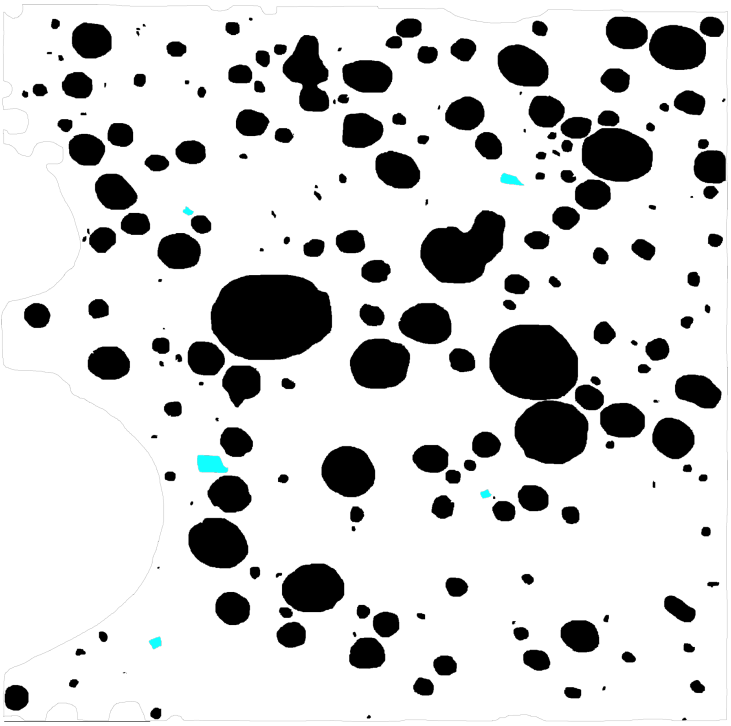

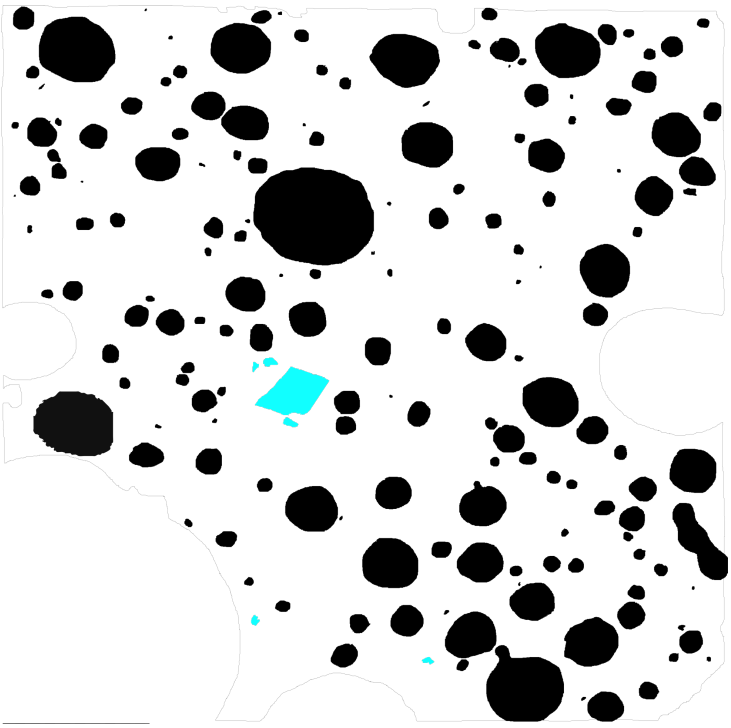

Sample 12G (Secondary):

Thin section scan (Scale bar = 25.42 mm)

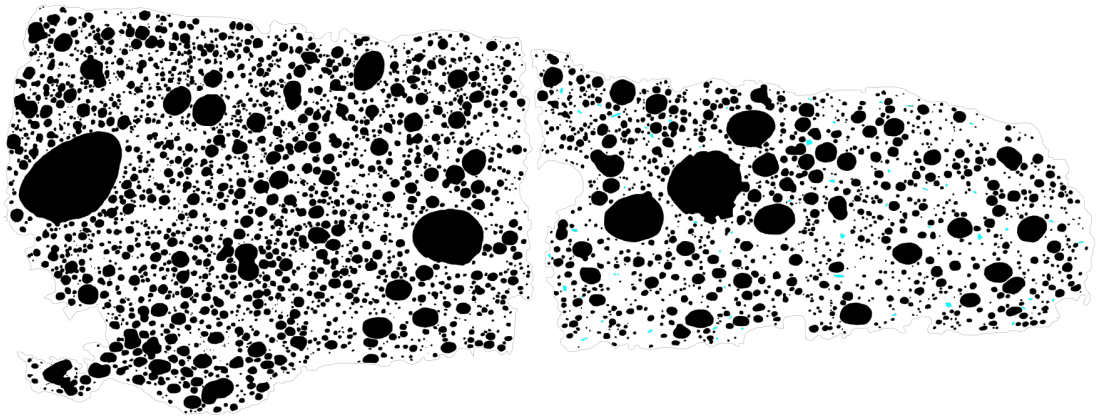

SEM images (Scale bar = 1 mm)

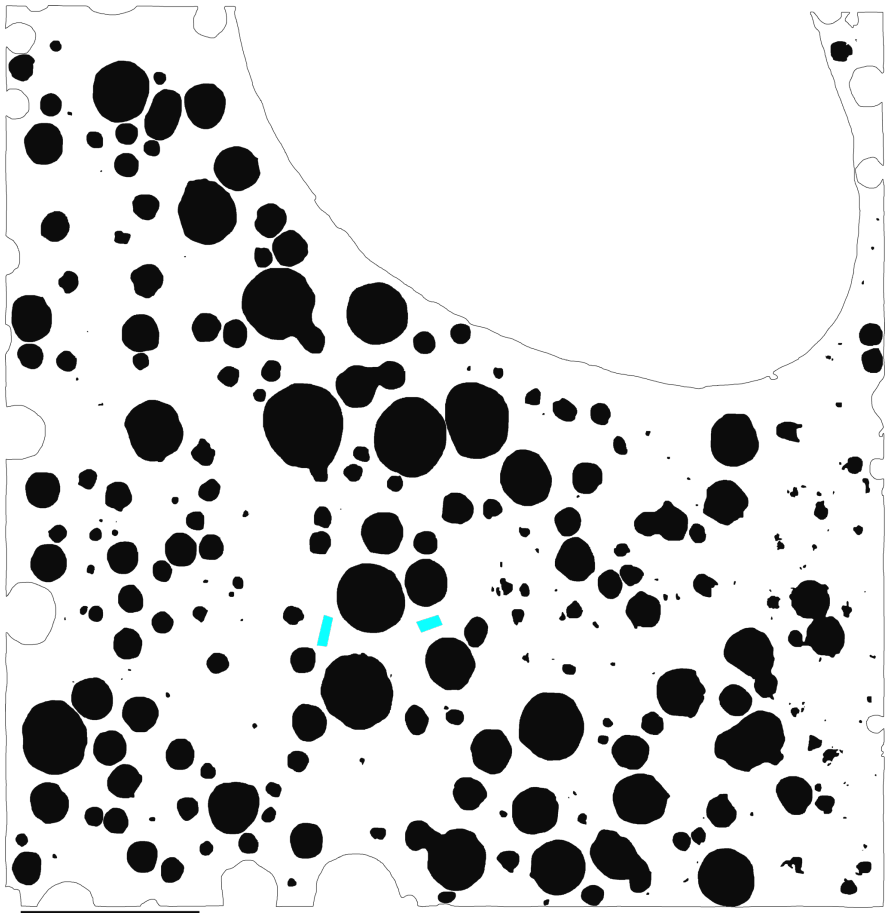

Sample 12Ni (Secondary):

Thin section scan (Scale bar = 25.56 mm)

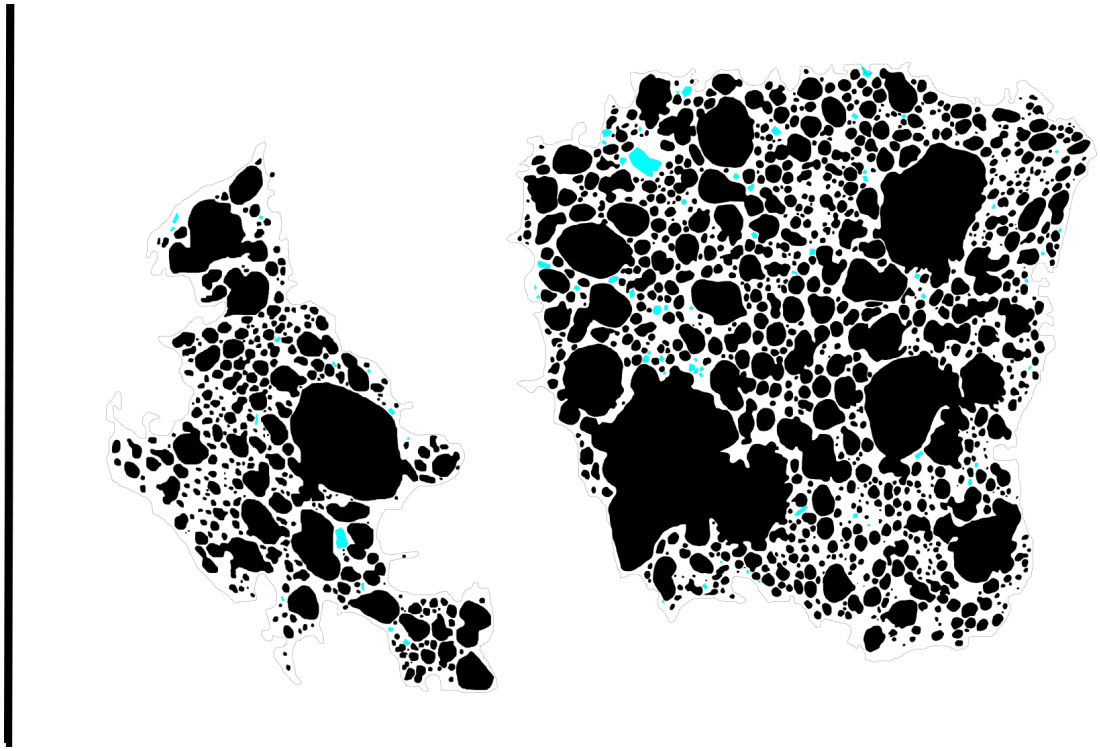

SEM images (Scale bar = 1 mm)

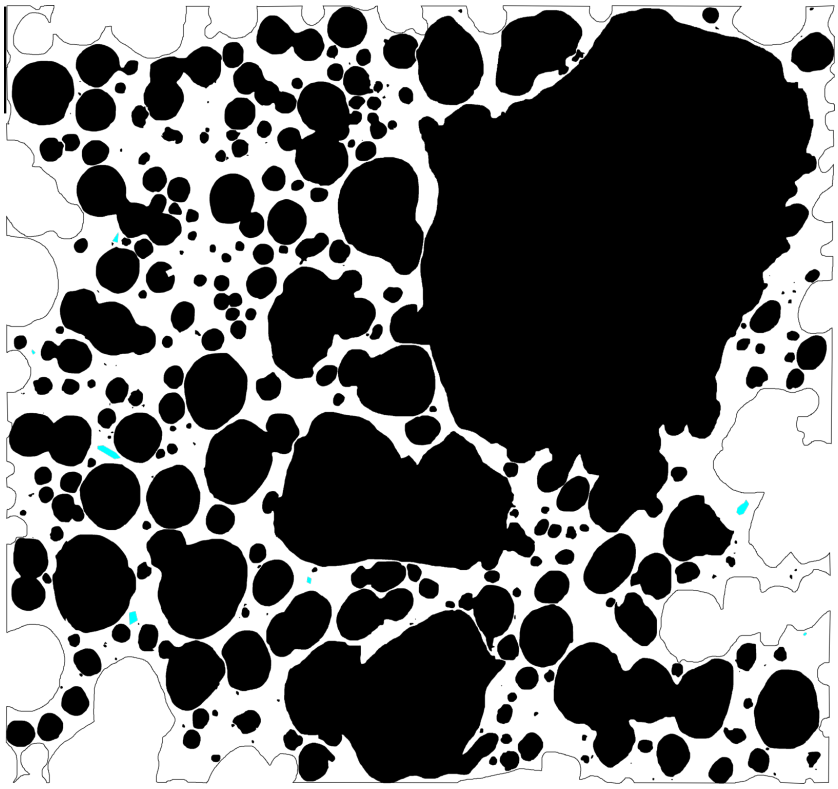

Sample 12Bq (Secondary):

Thin section scan (Scale bar = 25.36 mm)

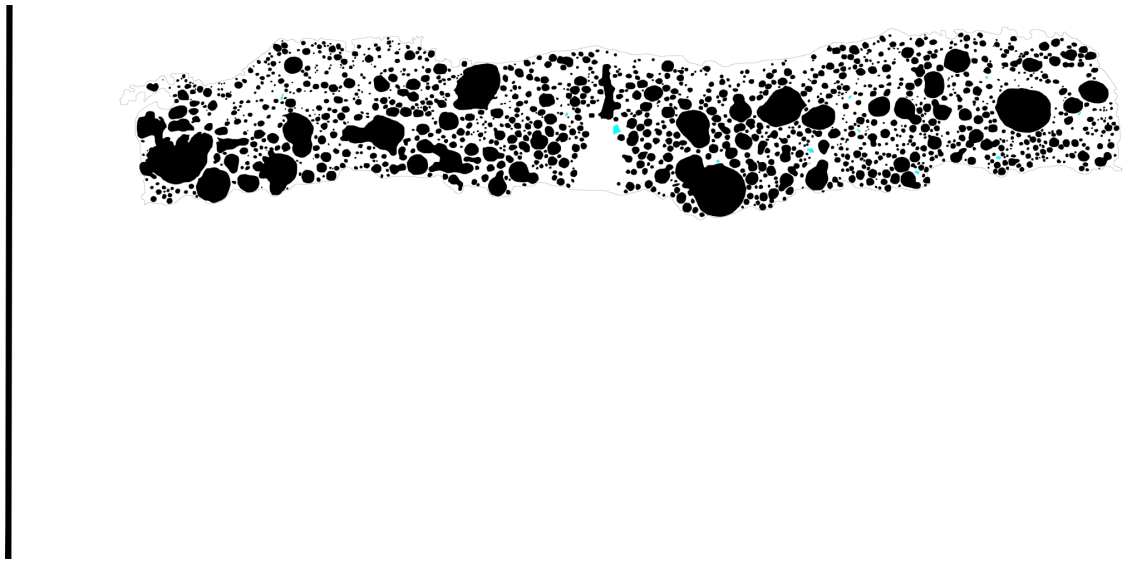

SEM images (Scale bar = 0.4 mm)

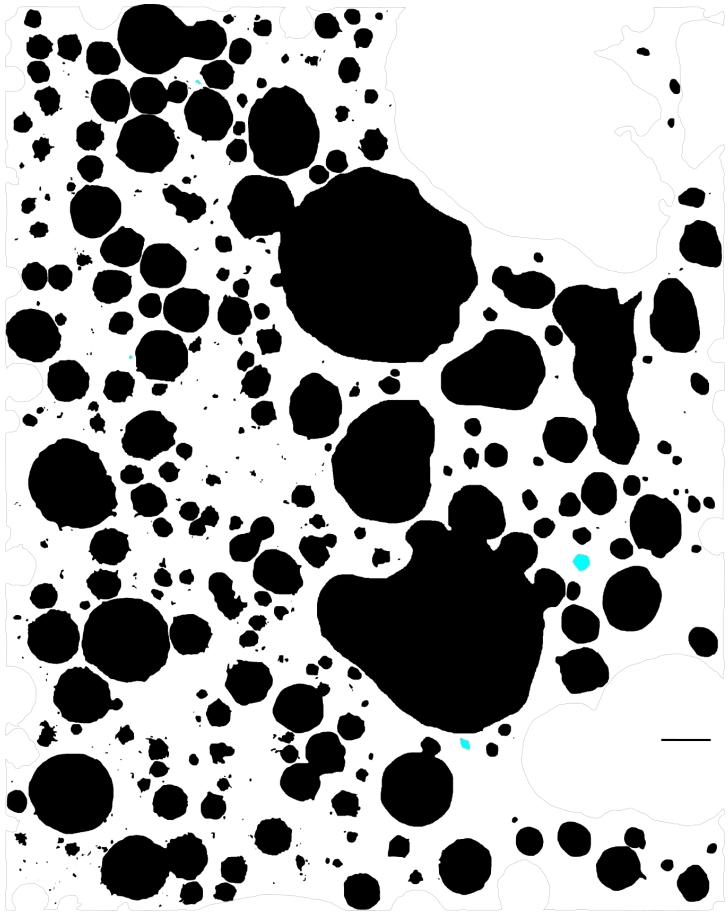

Sample 15Miiiq (Secondary):

Thin section scan (Scale bar = 25.45 mm)

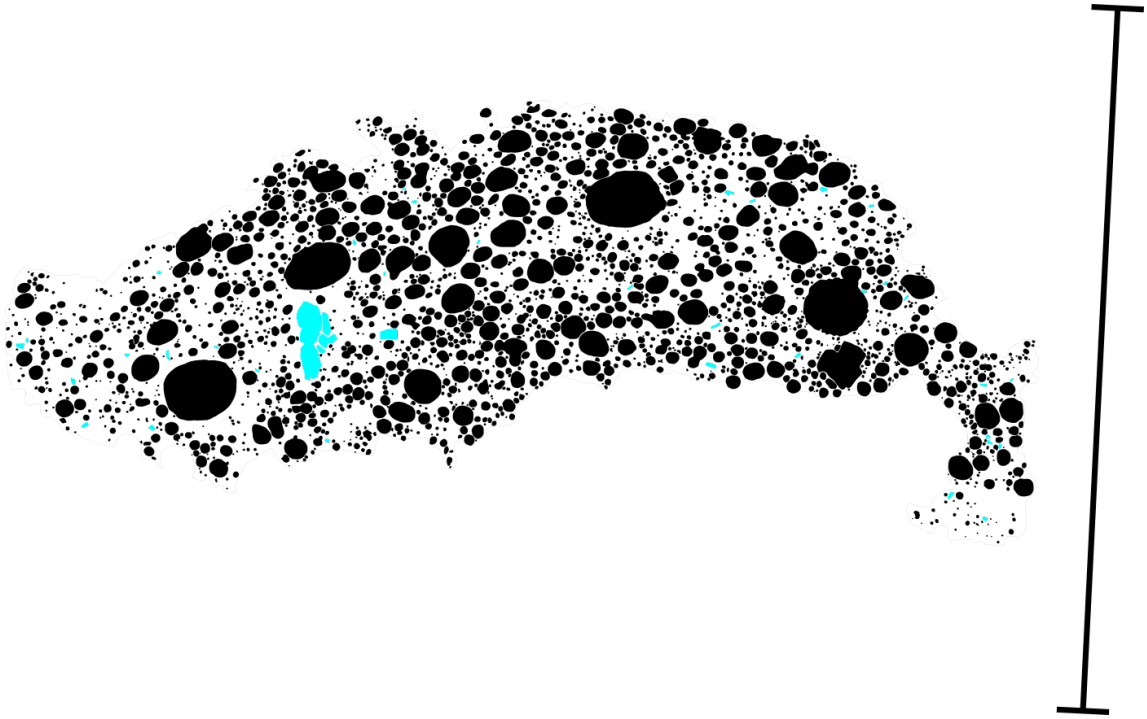

SEM images (Scale bar = 1 mm)

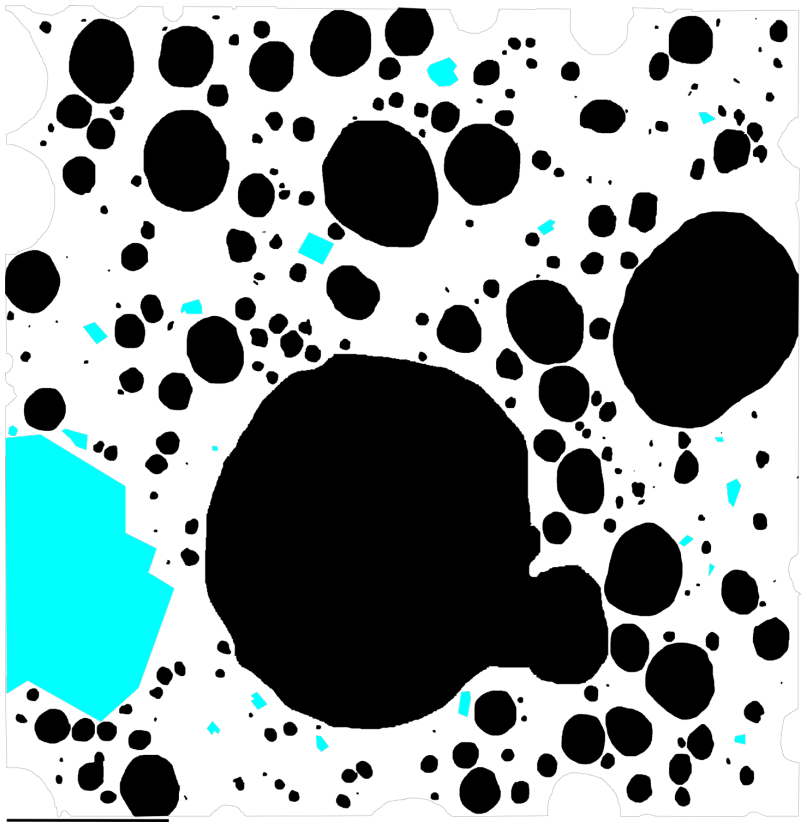

Sample	TS area measured (mm^2)	SEM area measured (mm^2)	Area of phenocrysts in TS (mm^2)	Area of phenocrysts in SEM (mm^2)
4A	737.900753	44.5881333	1.780492	0.39011471
4Q	248.669786	69.1380679	1.323542	0.81132713
8B	647.889	63.4974	2.778	0.33
8Ei	494.115333	52.255784	5.889011	1.075179
1A q	473.715957	39.376505	2.227132	0.5122
1C q	346.199423	46.1339432	2.104333	0.94519678
5K	571.159429	62.9220153	6.669051	0.73322171
1D q	316.163684	14.941633	2.203463	0.163315
6A q	327.266083	21.673836	2.643232	0.558756
12B q	275.859297	35.6817666	0.262025	0.0192614
12G	489.788934	38.87087	0.621252	0.070581
12H	384.104555	64.9374955	1.919435	0.16208945
12Ni	413.097663	50.126367	2.388067	0.031633
15Mii q	313.43755	22.247124	3.167439	1.43084

All raw bubble area data (mm^2) from the image analysis of the thin section binary images. Values correspond to the binary images presented in Appendix D.

Primary				Late-stage					Secondary				
4A	4Q	8B	8Ei	1A q	1C q	5K	1D q	6A q	12B q	12G	12H	12Ni	15Mii q
35.357149	2.543532	0.623	1.798946	23.944069	2.033119	16.885219	5.304002	5.214	6.640964	10.774183	9.778617	29.737346	4.592726
6.278595	2.122429	0.06	4.107085	3.251304	1.83414	8.429476	5.13175	3.039	5.930435	6.672177	7.092799	13.097542	4.550493
6.14017	1.838495	0.243	2.74654	2.967742	0.829208	6.257546	2.359913	2.209	4.089201	5.114989	5.807753	12.964534	4.133733
2.861788	1.737652	0.021	2.695301	2.567022	0.673278	5.288568	2.196863	1.954	3.50464	3.693517	5.470943	12.431389	3.11383
2.569103	1.421581	0.01	2.599732	2.379698	0.649806	4.584654	1.776537	1.524	2.999825	2.341699	5.126264	5.132975	1.858843
2.462109	1.395516	0.033	2.545965	2.081008	0.607075	4.031327	1.550068	1.058	2.739288	1.643324	4.169591	4.856444	1.645376
2.39032	1.353349	0.072	2.293138	1.836875	0.597536	3.340035	1.472845	1.029	2.505208	1.53268	3.165743	4.640466	1.331256
2.27144	1.245932	0.006	2.199423	1.824161	0.562789	3.284186	1.384418	1.003	2.135253	1.391187	2.458756	3.766521	1.222859
2.125757	0.974969	0.028	1.668487	1.779583	0.512249	2.776231	1.337004	1.003	2.00398	1.125317	1.770608	3.724104	1.197684
2.014327	0.948308	0.022	1.63208	1.727602	0.48385	2.748014	1.275785	0.871	1.983199	1.113344	1.508136	2.999253	1.158614
1.971554	0.822267	0.009	1.588594	1.591776	0.469957	2.708491	1.254779	0.849	1.919532	1.01256	1.302335	2.711518	1.144537
1.968439	0.804159	0.023	1.466058	1.590006	0.394766	2.690557	1.251178	0.816	1.322391	1.011504	1.296963	2.500452	1.037577
1.910089	0.729556	0.009	1.432347	1.558141	0.389474	2.549423	1.19256	0.798	1.256432	1.010447	1.168337	2.370883	0.99386
1.876704	0.648448	0.007	1.418189	1.476549	0.340088	2.383094	1.148347	0.765	1.10662	0.981642	0.890052	2.291651	0.974527
1.671018	0.607189	0.37	1.390884	1.399141	0.330921	2.317595	1.118338	0.749	1.062215	0.945652	0.878703	2.17515	0.96394
1.572793	0.603312	0.016	1.312002	1.298558	0.253909	2.170565	1.096331	0.729	1.032954	0.910931	0.793053	2.066106	0.858571
1.537847	0.572476	0.03	1.176824	1.290994	0.252178	1.77733	1.09113	0.694	0.949522	0.909381	0.690455	1.811417	0.834206
1.496486	0.553704	0.005	1.12727	1.286488	0.241867	1.650427	1.062121	0.685	0.939262	0.862616	0.642864	1.69123	0.823088
1.475672	0.545246	0.007	1.09238	1.28166	0.232356	1.586877	1.043715	0.664	0.9264	0.830712	0.622775	1.593605	0.803746
1.466033	0.52932	0.007	1.014172	1.266855	0.213764	1.464945	0.969893	0.64	0.91594	0.797751	0.613507	1.56958	0.801162
1.418875	0.517527	0.021	0.990912	1.171261	0.209285	1.434291	0.953688	0.621	0.736936	0.793948	0.611086	1.560673	0.793545
1.401402	0.515345	0.046	0.965292	1.165146	0.206386	1.319474	0.901472	0.62	0.718386	0.743943	0.597769	1.535113	0.790893
1.389341	0.489619	0.165	0.929222	1.156456	0.200081	1.3146	0.854458	0.593	0.683729	0.739506	0.590014	1.50873	0.774203
1.352072	0.465384	0.075	0.889107	1.134408	0.193316	1.128729	0.832451	0.586	0.662657	0.708095	0.53584	1.299816	0.773489
1.312457	0.430103	0.015	0.882702	1.115418	0.191203	1.128095	0.817047	0.565	0.657452	0.689149	0.523355	1.275121	0.76781
1.287642	0.426782	0.007	0.864836	1.078565	0.186161	1.125025	0.812045	0.561	0.632381	0.688868	0.519421	1.268726	0.762362
1.279181	0.413621	0.052	0.860453	1.074541	0.173646	1.124148	0.775434	0.56	0.567659	0.686473	0.509774	1.228523	0.738296
1.264623	0.408294	0.009	0.822361	1.059896	0.170888	1.120005	0.752827	0.541	0.533966	0.680698	0.506861	1.223086	0.6851
1.218434	0.402859	0.019	0.821181	0.997777	0.169753	1.095785	0.744425	0.522	0.531997	0.614776	0.491312	1.167116	0.681494
1.200359	0.400134	0.007	0.81427	0.982006	0.166069	1.091106	0.708414	0.514	0.52635	0.598296	0.475877	1.123134	0.67622
1.168436	0.364988	0.009	0.789493	0.976695	0.152621	1.078192	0.708414	0.513	0.524812	0.584492	0.472283	1.120992	0.668738
1.150796	0.345185	0.09	0.775335	0.976695	0.133138	1.049439	0.690809	0.495	0.49738	0.583083	0.470013	1.107862	0.649444
1.139645	0.3375	0.006	0.737917	0.955613	0.124596	1.038912	0.660399	0.474	0.492687	0.55963	0.458361	1.090891	0.618628
1.074463	0.331604	0.008	0.723421	0.947083	0.116454	0.984574	0.634392	0.453	0.478599	0.55139	0.456016	1.061624	0.609255
1.0685	0.330832	0.027	0.713308	0.932278	0.103716	0.958598	0.619387	0.447	0.475947	0.5416	0.443683	1.043263	0.583598
1.05121	0.330113	0.133	0.700667	0.924231	0.101451	0.957331	0.613385	0.429	0.474078	0.537375	0.442321	1.039875	0.561633
1.045606	0.328622	0.022	0.692914	0.821396	0.099077	0.948657	0.608384	0.424	0.461828	0.519133	0.412586	1.033068	0.54043
1.0248	0.328527	0.085	0.68634	0.752839	0.093163	0.907817	0.570172	0.421	0.460994	0.502442	0.406798	0.970941	0.540025
1.012021	0.328188	0.004	0.685329	0.751551	0.091459	0.901774	0.546565	0.416	0.438898	0.497512	0.402598	0.946473	0.530209
0.934694	0.325152	0.006	0.681789	0.726446	0.091419	0.900897	0.541564	0.407	0.428699	0.497441	0.400177	0.916681	0.507444
0.934552	0.323539	0.049	0.681284	0.71679	0.085339	0.863664	0.53136	0.38	0.424538	0.486666	0.398097	0.866911	0.501177
0.926592	0.317792	0.006	0.67589	0.706973	0.084412	0.862397	0.53036	0.378	0.420187	0.478284	0.396848	0.865995	0.490687
0.910455	0.314716	0.024	0.668474	0.704076	0.082087	0.835837	0.524158	0.373	0.391831	0.475749	0.3942	0.864666	0.486473
0.903848	0.311354	0.008	0.668305	0.703594	0.081252	0.82648	0.516956	0.371	0.370025	0.47427	0.392725	0.857653	0.483667
0.890201	0.285154	0.01	0.667462	0.677845	0.078297	0.820876	0.494349	0.367	0.350531	0.472932	0.372371	0.856109	0.477303
0.881355	0.284002	0.015	0.64336	0.672373	0.078193	0.812006	0.490548	0.366	0.335137	0.467298	0.371955	0.856016	0.459764
0.880002	0.282741	0.658	0.630718	0.668832	0.077456	0.808741	0.484346	0.366	0.333107	0.465255	0.363519	0.849456	0.445735
0.833688	0.265825	0.02	0.622628	0.647589	0.072249	0.783302	0.477544	0.362	0.327782	0.464128	0.361211	0.849106	0.444578
0.826589	0.265636	0.021	0.619931	0.625542	0.070056	0.778477	0.469542	0.352	0.323923	0.460677	0.350581	0.844297	0.442621
0.821168	0.264863	0.018	0.610492	0.623611	0.067886	0.739734	0.468341	0.349	0.303213	0.459832	0.348424	0.803136	0.434782
0.778203	0.264213	0.016	0.602739	0.613311	0.064602	0.723993	0.46374	0.341	0.301424	0.446169	0.344679	0.797987	0.432921
0.768046	0.262152	0.006	0.601559	0.609931	0.061675	0.712443	0.46374	0.336	0.299053	0.442718	0.342787	0.779245	0.426885
0.762041	0.257015	0.004	0.595154	0.594643	0.060496	0.712248	0.459939	0.331	0.296651	0.419335	0.339572	0.752027	0.415382
0.758466	0.252908	0.024	0.588918	0.593355	0.060352	0.709275	0.454137	0.324	0.296511	0.416659	0.3314	0.751811	0.401651
0.753964	0.252068	0.002	0.577288	0.579837	0.058543	0.708593	0.440333	0.322	0.291296	0.41518	0.329055	0.731401	0.40116
0.743758	0.249899	0.005	0.569534	0.572273	0.057775	0.704109	0.42953	0.312	0.28194	0.396657	0.328941	0.71789	0.399463
0.723729	0.241319	0.013	0.568354	0.565031	0.057775	0.699333	0.425529	0.311	0.279951	0.393488	0.318008	0.696367	0.394873
0.708001	0.235654	0.074	0.562118	0.560042	0.057621	0.691341	0.405723	0.308	0.27761	0.386445	0.313922	0.685966	0.383891
0.700308	0.234353	0.02	0.560432	0.552157	0.057127	0.689586	0.383516	0.305	0.273851	0.382219	0.309383	0.681744	0.378954
0.687696	0.233417	0.048	0.55605	0.547329	0.056587	0.686906	0.36451	0.302	0.267913	0.379331	0.306356	0.679128	0.377546
0.669087	0.232631	0.045	0.553185	0.54057	0.054329	0.667266	0.357908	0.3	0.266275	0.377571	0.29792	0.671611	0.36102
0.662539	0.231425	0.025	0.552679	0.538317	0.05141	0.662588	0.356508	0.298	0.262547	0.366725	0.296936	0.665772	0.352669
0.658596	0.228538	0.054	0.550994	0.53027	0.051338	0.661954	0.350706	0.297	0.261904	0.365598	0.284679	0.663455	0.352091
0.653167	0.226667	0.002	0.537847	0.519005	0.049635	0.659761	0.342904	0.289	0.260346	0.36264	0.284603	0.661045	0.337801
0.629012	0.223292	0.063	0.537172	0.517878	0.049001	0.656691	0.338302	0.28	0.259512	0.359048	0.284263	0.646185	0.333858
0.626406	0.222127	0.011	0.52234	0.506774	0.048024	0.642363	0.335701	0.278	0.256357	0.356865	0.283582	0.6398	0.326028
0.623483	0.220907	0.007	0.521666	0.502429	0.046863	0.638464	0.333501	0.277	0.255754	0.343553	0.278323	0.636042	0.325913
0.611054	0.219619	0.064	0.516272	0.499854	0.045027	0.622626	0.322898	0.277	0.245947	0.337426	0.270492	0.628493	0.32384
0.60555	0.218996	0.032	0.513238	0.496474	0.042136	0.621944	0.322097	0.265	0.245183	0.336088	0.268336	0.616362	0.321284
0.59298	0.218779	0.011	0.512058	0.492451	0.042048	0.61746	0.321297	0.262	0.236622	0.324185	0.266634	0.612912	0.320397
0.590775	0.213926	0.003	0.509024	0.488428	0.040366	0.607031	0.318696	0.258	0.235898	0.318199	0.265915	0.576653	0.318334
0.590374	0.206932	0.043	0.502788	0.47153	0.040161	0.601085	0.310494	0.257	0.232984	0.317776	0.261186	0.574934	0.318276
0.587492	0.203598	0.015	0.501945	0.467024	0.039455	0.59782	0.29869	0.249	0.230552	0.317002	0.259294	0.561176	0.311671
0.583867	0.200697	0.018	0.493349	0.458495	0.036359	0.596115	0.296289	0.247	0.217992	0.316157	0.259219	0.554029	0.310514
0.572441	0.199505	0.004	0.486944	0.454149	0.03477	0.586806	0.294289	0.246	0.217007	0.313269	0.255927	0.551166	0.307872
0.571063	0.198664	0.005	0.483405	0.444333	0.034413	0.57589	0.286887	0.246	0.21547	0.312987	0.255852	0.54231	0.305799
0.564289	0.198461	0.008	0.482225	0.437091	0.034327	0.574379	0.286286	0.246	0.208657	0.308057	0.249496	0.527852	0.304469
0.558802	0.195628	0.02	0.480539	0.432263	0.033936	0.569018	0.276884	0.246	0.206677	0.306649	0.247529	0.524113	0.302569
0.556513	0.195249	0.044	0.479022	0.426952	0.032609	0.561562	0.275283	0.244	0.205049	0.305733	0.247453	0.516472	0.29743
0.549614	0.194449	0.004	0.473629	0.418583	0.032271	0.544457	0.273082	0.244	0.202678	0.303902	0.243443	0.514876	0.296032
0.540694	0.194151	0.004	0.46992	0.41794	0.031578	0.544262	0.26628	0.244	0.200075	0.300733	0.24053	0.50878	0.295926
0.532809	0.192199	0.01	0.464527	0.412951	0.03132	0.542848	0.26468	0.24	0.200045	0.30038	0.226608	0.502807	0.293322
0.525242	0.191833	0.005	0.446323	0.412629	0.031169	0.525012	0.26468	0.229	0.199714	0.296507	0.221274	0.491654	0.291866
0.523914	0.188648	0.009	0.443121	0.408284	0.031087	0.524963	0.262479	0.226	0.197704	0.295098	0.218021	0.482983	0.289138
0.522427	0.183402	0.037	0.440761	0.407318	0.030159	0.524817	0.257878	0.226	0.196428	0.289041	0.216205	0.478154	0.288839
0.514826	0.182752	0.009	0.439581	0.4041	0.030077	0.524134	0.257278	0.224	0.194509	0.286717	0.216167	0.473859	0.287614
0.512822	0.18061	0.004	0.43503	0.402973	0.029722	0.51931	0.253877	0.223	0.192428	0.276716	0.216016	0.47251	0.285001
0.50467	0.180136	0.018	0.434188	0.398306	0.027575	0.510733	0.251276	0.221	0.191404	0.273054	0.210681	0.46663	0.281299
0.49879	0.178482	0.042	0.4293	0.397662	0.027442	0.495284	0.249675	0.22	0.188309	0.270025	0.210568	0.463438	0.280845
0.492492	0.177465	0.009	0.42576	0.393961	0.027018	0.49119	0.244874	0.216	0.187143	0.267772	0.209509	0.46109	0.277818
0.491164	0.176828	0.004	0.42576	0.3938	0.026857	0.489436	0.242073	0.215	0.187043	0.266574	0.208903	0.46039	0.276381
0.488942	0.176246	0.005	0.422726	0.391064	0.026301	0.488023	0.240673	0.21	0.186108	0.266363	0.204439	0.460071	0.275629
0.481759	0.175161	0.048	0.420704	0.389616	0.026236	0.486366	0.239872	0.21	0.185495	0.263828	0.20425	0.454674	0.27319
0.480991	0.172776	0.085	0.414973	0.388489	0.025414	0.484611	0.238672	0.21	0.185093	0.263546	0.203039	0.452769	0.267742
0.475954	0.17264	0.029	0.413456	0.386719	0.024062	0.482321	0.235071	0.208	0.184922	0.255869	0.202585	0.452028	0.265823
0.475804	0.171908	0.115	0.411939	0.383661	0.023728	0.482077	0.23187	0.207	0.18246	0.249953	0.198462	0.432997	0.264599
0.4742	0.171488	0.021	0.411096	0.383178	0.023633	0.48003	0.23147	0.192	0.181245	0.249953	0.196759	0.42687	0.262468
0.47202	0.169523	0.199	0.404691	0.377707	0.023569	0.479299	0.23087	0.192	0.180521	0.249601	0.196532	0.423286	0.259565
0.471552	0.169008	0.003	0.39205	0.37658	0.022787	0.477155	0.227469	0.192	0.17813	0.248967	0.195965	0.420938	0.258688
0.47146	0.16795	0.036	0.391376	0.372879	0.022047	0.476278	0.225268	0.191	0.176351	0.248474	0.194792	0.419857	0.256432
0.470158	0.167883	0.006	0.390196	0.372396	0.021621	0.470917	0.224868	0.188	0.175698	0.248263	0.190177	0.411269	0.252064
0.461346	0.162285	0.018	0.386825	0.369016	0.021563	0.470381	0.222667	0.187	0.175025	0.247981	0.188815	0.407427	0.251765
0.460995	0.161241	0.021	0.381431	0.365798	0.021525	0.466482	0.220467	0.185	0.174351	0.246925	0.183746	0.403247	0.247976
0.456209	0.159249	0.009	0.378229	0.364028	0.021493	0.450254	0.214865	0.183	0.174241	0.243121	0.183405	0.401383	0.247243
0.445735	0.157121	0.014	0.37806	0.363062	0.02139	0.448012	0.213865	0.178	0.173387	0.238191	0.183065	0.397634	0.247175
0.443597	0.156118	0.026	0.377892	0.36274	0.021049	0.446891	0.212264	0.177	0.171015	0.236924	0.182913	0.395018	0.245237
0.437825	0.155914	0.011	0.374352	0.360165	0.019691	0.440848	0.209863	0.176	0.169478	0.236783	0.182157	0.388737	0.244138
0.435862	0.152688	0.003	0.374352	0.358717	0.019592	0.432466	0.208663	0.175	0.169428	0.236219	0.181816	0.388541	0.243791
0.435637	0.152621	0.015	0.373509	0.355981	0.019447	0.423937	0.206862	0.174	0.164996	0.235093	0.180492	0.383124	0.242364
0.432354	0.152363	0.019	0.370981	0.348417	0.01895	0.419015	0.193058	0.173	0.164785	0.234881	0.180341	0.375277	0.239442

0.429448	0.151658	0.019	0.369801	0.343911	0.018907	0.411218	0.190858	0.172	0.16364	0.234247	0.180227	0.370767	0.238661
0.424821	0.151333	0.034	0.369801	0.339405	0.018838	0.405516	0.184456	0.171	0.162856	0.232487	0.180152	0.344394	0.23843
0.424002	0.144122	0.147	0.368958	0.338761	0.018665	0.404151	0.182655	0.171	0.161801	0.231571	0.179735	0.344003	0.234052
0.418531	0.143621	0.099	0.367104	0.336186	0.018481	0.40303	0.180254	0.169	0.158887	0.230796	0.177957	0.343735	0.232008
0.416978	0.140354	0.005	0.366599	0.335382	0.017654	0.402835	0.174453	0.169	0.157982	0.229599	0.177125	0.341871	0.229636
0.416735	0.140137	0.039	0.359688	0.333612	0.017093	0.397231	0.173452	0.167	0.157912	0.229177	0.176936	0.341562	0.226233
0.414748	0.139378	0.021	0.357328	0.329105	0.017074	0.397182	0.170852	0.167	0.157008	0.228261	0.176482	0.339379	0.224439
0.41271	0.138741	0.004	0.354463	0.328623	0.016955	0.397036	0.167251	0.167	0.155159	0.2265	0.17391	0.3332	0.221412
0.410012	0.138578	0.01	0.353452	0.320737	0.016883	0.394941	0.163249	0.166	0.154978	0.225655	0.172396	0.322634	0.219628
0.409795	0.138172	0.008	0.351429	0.318484	0.016485	0.39343	0.162249	0.165	0.152978	0.225092	0.17111	0.317434	0.217825
0.406621	0.137982	0.016	0.350586	0.317518	0.016339	0.391188	0.162049	0.165	0.152948	0.223894	0.168954	0.315004	0.216812
0.405359	0.137033	0.008	0.350249	0.317518	0.016241	0.388849	0.158448	0.164	0.152415	0.223331	0.168424	0.313727	0.215906
0.404992	0.135569	0.008	0.346204	0.316875	0.015706	0.383683	0.157448	0.163	0.150355	0.22326	0.164981	0.310668	0.21471
0.404875	0.135176	0.17	0.343339	0.315426	0.015403	0.380905	0.153246	0.161	0.150275	0.222627	0.164868	0.31004	0.212994
0.402912	0.134865	0.007	0.339293	0.313173	0.015248	0.37993	0.152446	0.16	0.149893	0.222556	0.163506	0.307157	0.211798
0.395479	0.133455	0.041	0.337271	0.301586	0.015227	0.379736	0.148245	0.16	0.148848	0.220514	0.163506	0.3021	0.211413
0.395186	0.133265	0.009	0.336091	0.301586	0.015151	0.375155	0.147244	0.16	0.148537	0.220443	0.162901	0.298465	0.210815
0.393198	0.133143	0.047	0.335248	0.30046	0.014783	0.362532	0.146444	0.16	0.148074	0.216922	0.162712	0.297734	0.210738
0.393148	0.132208	0.003	0.333057	0.298689	0.01471	0.361801	0.144244	0.158	0.147964	0.216358	0.162598	0.296117	0.210227
0.389348	0.13214	0.034	0.329686	0.295793	0.014674	0.358098	0.143043	0.156	0.147853	0.214316	0.162295	0.295293	0.209581
0.386483	0.1313	0.023	0.328506	0.295471	0.01448	0.357659	0.141043	0.153	0.146497	0.214175	0.158739	0.292472	0.209002
0.386015	0.130351	0.014	0.328	0.295149	0.013869	0.356636	0.141043	0.151	0.145522	0.213612	0.155524	0.292101	0.208626
0.38584	0.129958	0.004	0.32109	0.294022	0.013854	0.354248	0.140642	0.149	0.143442	0.212696	0.152497	0.291988	0.208626
0.385648	0.129375	0.006	0.319404	0.293379	0.013187	0.352834	0.135441	0.148	0.143	0.211217	0.150492	0.289207	0.207778
0.384495	0.12905	0.009	0.318562	0.291608	0.012962	0.349667	0.13384	0.147	0.142055	0.208118	0.150152	0.288857	0.207479
0.382992	0.128494	0.014	0.316708	0.287585	0.0127	0.349472	0.13264	0.147	0.141995	0.206921	0.149508	0.2886	0.204605
0.382081	0.127437	0.023	0.316202	0.287102	0.012537	0.34645	0.129239	0.145	0.141483	0.205583	0.149508	0.285521	0.204143
0.380411	0.127139	0.009	0.315359	0.28324	0.012399	0.345622	0.127839	0.145	0.140538	0.205583	0.14739	0.28203	0.204075
0.379049	0.126447	0.007	0.313505	0.282596	0.012348	0.345378	0.126038	0.142	0.13877	0.204526	0.147314	0.279929	0.202957
0.376051	0.126068	0.051	0.312831	0.281309	0.012049	0.344647	0.123237	0.142	0.138739	0.203681	0.14652	0.278147	0.20287
0.368993	0.125295	0.009	0.312662	0.281309	0.011788	0.342405	0.122837	0.138	0.136056	0.20347	0.146331	0.276963	0.202407
0.368793	0.123859	0.034	0.311651	0.278251	0.011418	0.340602	0.122237	0.138	0.135484	0.203188	0.145915	0.274522	0.20153
0.368751	0.123831	0.04	0.305583	0.26602	0.011311	0.334949	0.122037	0.136	0.135403	0.202273	0.14512	0.273729	0.200045
0.367891	0.122964	0.086	0.303898	0.259744	0.010962	0.334705	0.120836	0.136	0.133605	0.201709	0.144931	0.271464	0.199341
0.36617	0.12127	0.074	0.301875	0.251536	0.010948	0.330563	0.119636	0.136	0.133293	0.200934	0.144704	0.264358	0.198714
0.36455	0.12028	0.021	0.300527	0.243168	0.010786	0.328565	0.119236	0.135	0.131515	0.200089	0.143834	0.261774	0.197036
0.360515	0.119467	0.038	0.30019	0.243168	0.010596	0.327249	0.118836	0.134	0.131032	0.199596	0.143569	0.261722	0.196911
0.357684	0.119453	0.048	0.292605	0.240915	0.01057	0.326177	0.118236	0.134	0.130048	0.199385	0.143191	0.254091	0.196034
0.357375	0.119006	0.011	0.292268	0.240593	0.010452	0.325641	0.116635	0.134	0.129505	0.19854	0.143039	0.25335	0.189766
0.356498	0.117095	0.007	0.291593	0.240271	0.010401	0.321742	0.115835	0.133	0.128641	0.198399	0.142812	0.25127	0.18966
0.3538	0.11658	0.05	0.290414	0.237857	0.010329	0.318721	0.114435	0.133	0.128369	0.195934	0.142472	0.250672	0.188609
0.353407	0.116553	0.004	0.284346	0.23657	0.010315	0.314724	0.112634	0.133	0.127606	0.195371	0.141677	0.249375	0.18777
0.352781	0.115916	0.011	0.28266	0.234799	0.010036	0.313993	0.110033	0.132	0.12641	0.194032	0.141034	0.249128	0.18615
0.351411	0.115265	0.06	0.278278	0.233995	0.009966	0.30756	0.109233	0.13	0.126048	0.192131	0.140316	0.247748	0.178157
0.347811	0.113625	0.009	0.276592	0.231903	0.009866	0.306147	0.108033	0.13	0.126048	0.188398	0.139029	0.246769	0.177926
0.343084	0.113124	0.004	0.27575	0.231259	0.00979	0.30488	0.107833	0.129	0.125847	0.188116	0.136608	0.242424	0.176691
0.342733	0.11288	0.002	0.275581	0.229489	0.009598	0.302395	0.105432	0.129	0.125395	0.188046	0.135322	0.240405	0.175004
0.342407	0.112798	0.007	0.275413	0.22804	0.009589	0.30103	0.105232	0.129	0.125214	0.186989	0.135057	0.23917	0.173799
0.34128	0.112432	0.004	0.27339	0.227236	0.009502	0.300689	0.105032	0.128	0.124219	0.184806	0.133884	0.238933	0.173249
0.337797	0.112188	0.059	0.271873	0.224983	0.009488	0.299909	0.105032	0.127	0.123998	0.182834	0.132674	0.237234	0.17135
0.33611	0.111389	0.034	0.26985	0.224017	0.009361	0.296985	0.104832	0.127	0.122923	0.181778	0.132333	0.23366	0.170916
0.334489	0.110806	0.025	0.267659	0.223212	0.009353	0.296936	0.104432	0.127	0.122742	0.181355	0.132295	0.231106	0.170405
0.331758	0.110684	0.008	0.267322	0.221603	0.009322	0.296303	0.104231	0.126	0.121134	0.181285	0.129798	0.22917	0.170405
0.330622	0.110345	0.005	0.266985	0.210338	0.008611	0.293135	0.103831	0.125	0.12021	0.180862	0.129118	0.22883	0.168679
0.329762	0.11025	0.002	0.265637	0.208085	0.008288	0.292989	0.103231	0.125	0.120059	0.180299	0.128853	0.228151	0.16785
0.328818	0.109871	0.101	0.263782	0.202774	0.008169	0.292794	0.103231	0.125	0.119677	0.179947	0.12681	0.227265	0.16783
0.328684	0.109518	0.009	0.262771	0.201969	0.00807	0.291381	0.102831	0.125	0.119326	0.178397	0.124918	0.225061	0.167146
0.328058	0.109112	0.005	0.261928	0.199555	0.008016	0.286556	0.102031	0.125	0.118864	0.178256	0.124616	0.223939	0.166664
0.326412	0.108881	0.005	0.261591	0.199394	0.007981	0.286166	0.10023	0.124	0.117969	0.178186	0.12454	0.222961	0.166644
0.32597	0.108624	0.004	0.261423	0.197624	0.007913	0.284266	0.096629	0.123	0.117457	0.176425	0.123897	0.221931	0.16462
0.325961	0.107837	0.025	0.258557	0.192796	0.007889	0.283437	0.096229	0.122	0.117457	0.175862	0.123065	0.221158	0.164552
0.325343	0.106089	0.069	0.258557	0.186037	0.007876	0.28256	0.094829	0.122	0.117155	0.175439	0.122005	0.218883	0.163202
0.325126	0.104476	0.031	0.256366	0.185393	0.007747	0.281878	0.094228	0.121	0.11604	0.175228	0.121778	0.217564	0.162161
0.323339	0.104435	0.027	0.255523	0.184267	0.007565	0.281244	0.092828	0.12	0.11602	0.175016	0.121589	0.215649	0.161544
0.32262	0.10392	0.01	0.255186	0.183623	0.007463	0.280562	0.091628	0.118	0.115869	0.174805	0.119773	0.213898	0.16085
0.322161	0.10327	0.25	0.252321	0.182175	0.007246	0.280269	0.090627	0.118	0.115708	0.174664	0.119698	0.213507	0.159442
0.318494	0.103026	0.015	0.25013	0.181853	0.006965	0.278759	0.090027	0.118	0.115678	0.174171	0.119622	0.212766	0.159422
0.317241	0.102605	0.006	0.248613	0.175898	0.006818	0.273008	0.090027	0.117	0.115648	0.173397	0.119319	0.212385	0.159201
0.315655	0.101874	0.005	0.247433	0.175577	0.006773	0.272521	0.089227	0.116	0.115276	0.172974	0.118979	0.212261	0.157938
0.31502	0.100952	0.044	0.244568	0.175094	0.00674	0.271692	0.088427	0.116	0.115226	0.172692	0.117844	0.211087	0.157899
0.313266	0.100952	0.038	0.23968	0.173806	0.006473	0.269597	0.088027	0.115	0.113849	0.172411	0.117428	0.208595	0.15706
0.31218	0.100762	0.051	0.238837	0.172358	0.006411	0.26945	0.086626	0.115	0.112211	0.171918	0.117087	0.20841	0.156568
0.311846	0.10041	0.028	0.238163	0.170105	0.00641	0.266721	0.086226	0.114	0.111629	0.170439	0.114931	0.206412	0.156009
0.30919	0.100057	0.029	0.236814	0.168656	0.006363	0.266429	0.083825	0.113	0.110503	0.167058	0.114628	0.203055	0.155103
0.306793	0.09938	0.028	0.235634	0.166082	0.006305	0.265308	0.082425	0.113	0.110071	0.166706	0.113834	0.202169	0.153714
0.306158	0.099176	0.007	0.23496	0.165599	0.00628	0.265259	0.081825	0.112	0.109669	0.166635	0.113304	0.202076	0.153589
0.305272	0.097211	0.023	0.23378	0.163989	0.005944	0.264041	0.080824	0.112	0.109418	0.164945	0.112169	0.20185	0.153155
0.30478	0.096316	0.043	0.232601	0.163185	0.005814	0.261361	0.080624	0.111	0.109348	0.160085	0.111564	0.200717	0.15276
0.304771	0.096316	0.024	0.231589	0.162219	0.005687	0.260532	0.079624	0.111	0.109066	0.159733	0.111299	0.200099	0.152451
0.304287	0.096099	0.007	0.230746	0.161254	0.005678	0.259655	0.079624	0.111	0.108815	0.159522	0.111186	0.198503	0.151988
0.303092	0.09549	0.009	0.230746	0.160288	0.005629	0.258534	0.079424	0.11	0.108624	0.159522	0.110883	0.198266	0.151352
0.3026	0.09427	0.022	0.22923	0.159322	0.005542	0.257706	0.076223	0.11	0.108182	0.158747	0.11058	0.197576	0.150012
0.302508	0.094121	0.005	0.228724	0.157874	0.005502	0.255756	0.075423	0.11	0.108132	0.158043	0.110505	0.197102	0.147534
0.302383	0.094012	0.346	0.228555	0.157713	0.005483	0.255707	0.074823	0.11	0.108031	0.15755	0.110505	0.196794	0.146772
0.301881	0.093714	0.004	0.227544	0.156748	0.005452	0.253856	0.074422	0.11	0.106675	0.157409	0.109975	0.196526	0.14575
0.299927	0.092684	0.014	0.226364	0.153851	0.005379	0.252978	0.074422	0.109	0.106102	0.156423	0.109067	0.195867	0.145461
0.299643	0.092115	0.044	0.224679	0.153207	0.005372	0.251321	0.073622	0.108	0.106032	0.156353	0.108575	0.192592	0.145335
0.297179	0.091762	0.045	0.220802	0.151115	0.005268	0.250688	0.073222	0.108	0.105981	0.155578	0.10831	0.192468	0.144082
0.297054	0.091681	0.016	0.220465	0.151115	0.005255	0.250639	0.073022	0.107	0.105961	0.155085	0.108235	0.19183	0.143947
0.295041	0.091559	0.015	0.219959	0.150954	0.005251	0.249811	0.068021	0.107	0.104766	0.154803	0.107894	0.191737	0.142385
0.293445	0.091518	0.022	0.219285	0.14854	0.005213	0.2483	0.06742	0.106	0.104544	0.15431	0.107819	0.189472	0.141411
0.293086	0.091396	0.006	0.218779	0.147092	0.005188	0.247471	0.063619	0.106	0.104243	0.153113	0.107667	0.188524	0.13955
0.291608	0.09061	0.017	0.218779	0.146609	0.00515	0.245376	0.063619	0.106	0.104153	0.15255	0.106721	0.187412	0.138046
0.290915	0.090583	0.018	0.218274	0.146448	0.005121	0.244986	0.063219	0.105	0.10359	0.152127	0.106041	0.187299	0.137101
0.289503	0.089485	0.058	0.218105	0.145965	0.005107	0.244011	0.058218	0.105	0.103329	0.151845	0.104906	0.18701	0.136359
0.288843	0.089404	0.032	0.217768	0.144839	0.004985	0.243816	0.058018	0.105	0.103218	0.151564	0.104489	0.185383	0.136349
0.288509	0.08798	0.143	0.217431	0.143873	0.004969	0.243524	0.057417	0.105	0.102856	0.150507	0.104262	0.184879	0.134768
0.283723	0.086964	0.051	0.216925	0.142586	0.004954	0.243183	0.057217	0.103	0.102545	0.150437	0.103922	0.184148	0.13471
0.283122	0.086815	0.003	0.214734	0.140654	0.004897	0.239333	0.057017	0.103	0.100716	0.149803	0.103165	0.183396	0.134392
0.281819	0.086788	0.007	0.21406	0.139206	0.004834	0.238066	0.056417	0.103	0.099822	0.149239	0.102749	0.183314	0.134218
0.281343	0.086774	0.003	0.213723	0.138079	0.004801	0.238066	0.055817	0.103	0.098757	0.148958	0.101955	0.183066	0.133967
0.281025	0.086137	0.019	0.213386	0.137275	0.004722	0.235775	0.055417	0.102	0.098485	0.148746	0.101879	0.18217	0.133803
0.278102	0.085839	0.024	0.2117	0.137114	0.004704	0.235142	0.055217	0.102	0.098274	0.148535	0.101766	0.179071	0.133235
0.277918	0.085798	0.015	0.210352	0.136953	0.004657	0.234703	0.054817	0.102	0.098123	0.148465	0.101425	0.178504	0.133206
0.277484	0.085649	0.054	0.210183	0.133091	0.004569	0.233826	0.053016	0.101	0.097772	0.148394	0.100896	0.177639	0.132791
0.275212	0.085622	0.027	0.210015	0.131964	0.004511	0.233387	0.053016	0.101	0.097621	0.14769	0.100442	0.177248	0.130313
0.273249	0.085595	0.17	0.209846	0.131803	0.004463	0.232315	0.051215	0.1	0.097511	0.14762	0.10029	0.175127	0.13012
0.271746	0.085039	0.026	0.206138	0.129711	0.004386	0.231633	0.049615	0.1	0.09736	0.147479	0.100177	0.175055	0.129387
0.271687	0.084971	0.008	0.205969	0.12955	0.004339	0.230463	0.049015	0.1	0.096465	0.147408	0.099723	0.174478	0.129329
0.270869	0.084497	0.006	0.205632	0.128584	0.004333	0.229245	0.048015	0.1	0.096395	0.146986	0.099382	0.171986	0.128818
0.270735	0.084389	0.029	0.205127	0.126814	0.004309	0.228855	0.047614	0.099	0.096264	0.146774	0.099231	0.171492	0.127902
0.269474	0.083806	0.64	0.205127	0.126492	0.004282	0.225833	0.047614	0.099	0.096204	0.146563	0.098928	0.168392	0.127546
0.267177	0.083291	0.022	0.204284	0.12617	0.004276	0.225102	0.047214	0.098	0.095963	0.146281	0.098134	0.167259	0.127469
0.266876	0.083142	0.007	0.20361	0.125044	0.004263	0.224371	0.046214	0.098	0.094797	0.14607	0.097945	0.165405	0.127305

0.266718	0.083047	0.006	0.203441	0.124883	0.00423	0.22364	0.046214	0.097	0.094426	0.145577	0.097112	0.163315	0.12716
0.261097	0.082938	0.007	0.201587	0.124883	0.004205	0.223592	0.046214	0.096	0.094416	0.145577	0.094956	0.163284	0.126659
0.260437	0.082477	0.006	0.200913	0.122147	0.00417	0.223251	0.045614	0.096	0.094004	0.144802	0.094578	0.161811	0.126292
0.2591	0.081068	0.118	0.20007	0.121825	0.004085	0.222471	0.045014	0.096	0.09319	0.144098	0.093291	0.159834	0.125752
0.258599	0.080065	0.004	0.199227	0.119572	0.004074	0.222471	0.044613	0.095	0.092888	0.143464	0.092837	0.159536	0.124171
0.257864	0.079658	0.007	0.19889	0.11925	0.004059	0.221009	0.044613	0.094	0.092707	0.14283	0.092005	0.158475	0.12367
0.256879	0.079157	0.005	0.198385	0.118446	0.004015	0.220034	0.044213	0.094	0.092245	0.142478	0.091513	0.158176	0.122792
0.256678	0.078804	0.031	0.19771	0.113457	0.00401	0.219547	0.044013	0.093	0.090718	0.142126	0.091097	0.158012	0.122619
0.255642	0.078804	0.037	0.196699	0.112974	0.003929	0.219254	0.043413	0.092	0.090436	0.141915	0.091059	0.157981	0.122551
0.255617	0.078371	0.05	0.195351	0.111848	0.003901	0.218816	0.043013	0.092	0.089874	0.141563	0.090946	0.157888	0.122406
0.255459	0.077964	0.003	0.195182	0.111526	0.003866	0.218475	0.041212	0.092	0.089452	0.14114	0.090795	0.157744	0.121751
0.255049	0.076527	0.079	0.194677	0.110077	0.003809	0.216135	0.040612	0.092	0.089371	0.140647	0.090076	0.157404	0.121606
0.252945	0.076446	0.074	0.193665	0.109112	0.003765	0.215843	0.040012	0.091	0.088286	0.139943	0.089773	0.15692	0.121471
0.251241	0.076256	0.004	0.19316	0.108468	0.003716	0.215551	0.039812	0.09	0.087472	0.139027	0.089433	0.15659	0.121317
0.251099	0.076134	0.007	0.192822	0.104927	0.003708	0.214917	0.039012	0.089	0.08711	0.138464	0.089433	0.155705	0.120902
0.251032	0.07608	0.061	0.192485	0.104445	0.003626	0.21443	0.039012	0.089	0.087	0.136773	0.089168	0.155458	0.120777
0.250213	0.076026	0.006	0.191811	0.104284	0.00362	0.213796	0.039012	0.088	0.086909	0.136703	0.088676	0.154953	0.120709
0.249236	0.075944	0.005	0.1908	0.10364	0.003599	0.21326	0.037811	0.087	0.086648	0.136069	0.088487	0.154387	0.120112
0.248885	0.075524	0.057	0.189957	0.103479	0.003466	0.212919	0.037411	0.087	0.086397	0.135506	0.08826	0.154325	0.119678
0.247674	0.075483	0.034	0.189283	0.103318	0.003424	0.211457	0.036811	0.087	0.085613	0.133604	0.08826	0.1538	0.119321
0.247014	0.075443	0.009	0.189283	0.103318	0.003365	0.211262	0.036611	0.087	0.08489	0.133322	0.087844	0.152945	0.119003
0.245753	0.075063	0.008	0.189114	0.102353	0.003313	0.209946	0.036611	0.087	0.08488	0.133182	0.087465	0.152605	0.118231
0.244951	0.074996	0.006	0.188777	0.10187	0.003245	0.208338	0.036211	0.086	0.084307	0.133111	0.086671	0.152482	0.117788
0.244442	0.074752	0.005	0.188609	0.101709	0.003213	0.207753	0.034811	0.086	0.084287	0.132829	0.086217	0.152399	0.116862
0.243431	0.074386	0.006	0.188103	0.099778	0.00321	0.206973	0.03461	0.086	0.084196	0.132266	0.086179	0.152327	0.116824
0.24283	0.074386	0.011	0.187766	0.099134	0.003174	0.206925	0.03441	0.086	0.084106	0.132196	0.085536	0.151225	0.115233
0.241894	0.074304	0.009	0.187429	0.098651	0.003145	0.206584	0.03421	0.085	0.083272	0.131421	0.084401	0.149032	0.113767
0.241861	0.074236	0.012	0.186923	0.096881	0.00314	0.206437	0.03181	0.085	0.08285	0.13135	0.084174	0.149021	0.113758
0.241702	0.074236	0.048	0.186586	0.096398	0.003131	0.206096	0.031409	0.085	0.082026	0.130505	0.084023	0.148105	0.113488
0.239689	0.074006	0.063	0.186418	0.094306	0.003129	0.205609	0.030609	0.085	0.081945	0.130435	0.084023	0.147672	0.113131
0.237994	0.073355	0.051	0.184732	0.094145	0.003125	0.205511	0.030609	0.084	0.081875	0.130224	0.083909	0.147106	0.112591
0.237426	0.073315	0.047	0.184732	0.093984	0.003093	0.202734	0.030609	0.084	0.081533	0.130224	0.083758	0.146838	0.112099
0.237326	0.073274	0.011	0.183552	0.093662	0.00309	0.202246	0.029609	0.083	0.081443	0.129801	0.083607	0.146643	0.111858
0.236966	0.073044	0.025	0.183552	0.092697	0.003087	0.201564	0.029009	0.083	0.081342	0.129519	0.083077	0.146416	0.110701
0.235688	0.072773	0.011	0.183215	0.091409	0.003053	0.201028	0.028809	0.082	0.081262	0.129308	0.083077	0.146066	0.110672
0.235622	0.071173	0.019	0.182709	0.091248	0.002951	0.200492	0.028409	0.082	0.080699	0.129026	0.082283	0.144532	0.110209
0.235354	0.071146	0.024	0.182372	0.090926	0.002901	0.200492	0.028209	0.082	0.080428	0.128885	0.082093	0.143811	0.110132
0.234686	0.070794	0.041	0.181867	0.090283	0.002892	0.198786	0.027608	0.081	0.079906	0.128533	0.082093	0.143162	0.110055
0.234386	0.070645	0.014	0.181361	0.090122	0.002862	0.19786	0.027208	0.081	0.079644	0.128463	0.081791	0.14311	0.109534
0.233692	0.070604	0.007	0.181361	0.088673	0.002851	0.197714	0.026608	0.08	0.079614	0.128322	0.081639	0.141978	0.109467
0.233183	0.070319	0.026	0.180181	0.088673	0.002845	0.19557	0.026408	0.08	0.079554	0.128181	0.081602	0.139702	0.108078
0.232348	0.07017	0.013	0.17917	0.086742	0.002659	0.194985	0.026408	0.08	0.079373	0.127829	0.081186	0.138806	0.108011
0.23198	0.07017	0.009	0.179001	0.086742	0.002627	0.194156	0.026008	0.08	0.079212	0.126984	0.081186	0.138703	0.107722
0.231729	0.069926	0.011	0.178664	0.08642	0.002626	0.19211	0.025408	0.08	0.079061	0.126068	0.080126	0.138641	0.107191
0.23137	0.06933	0.023	0.178496	0.085777	0.002624	0.188844	0.024407	0.08	0.079021	0.125434	0.080051	0.138291	0.107143
0.230318	0.06933	0.04	0.177653	0.085294	0.002604	0.188747	0.024407	0.08	0.07875	0.125293	0.080013	0.136468	0.106728
0.230293	0.069194	0.008	0.176979	0.084972	0.002574	0.187431	0.024007	0.079	0.078338	0.125153	0.079521	0.135778	0.106593
0.229324	0.068395	0.013	0.17681	0.084489	0.002513	0.187041	0.022207	0.079	0.077755	0.124941	0.07937	0.135768	0.106593
0.229265	0.068259	0.004	0.17563	0.084167	0.002484	0.186554	0.022007	0.079	0.077695	0.124167	0.078916	0.135222	0.106044
0.227236	0.067907	0.011	0.175293	0.083202	0.002477	0.185774	0.022007	0.079	0.077604	0.12311	0.078916	0.134357	0.105996
0.225958	0.067758	0.023	0.175293	0.083041	0.002439	0.184215	0.021807	0.079	0.077373	0.122265	0.078764	0.13411	0.105745
0.225574	0.067581	0.206	0.174619	0.08288	0.002435	0.183484	0.021406	0.078	0.077002	0.122195	0.078424	0.134059	0.105195
0.224354	0.067568	0.052	0.17445	0.082236	0.002435	0.182996	0.021006	0.077	0.076801	0.122054	0.078008	0.132885	0.104376
0.223669	0.067175	0.142	0.17445	0.081271	0.00243	0.182022	0.020806	0.076	0.07674	0.12142	0.078008	0.131927	0.10399
0.223177	0.067066	0.082	0.174282	0.080144	0.002429	0.181924	0.020006	0.076	0.07674	0.121138	0.07797	0.131741	0.103064
0.222584	0.066999	0.006	0.173439	0.079178	0.002429	0.181242	0.020006	0.075	0.076499	0.120927	0.077894	0.131113	0.103035
0.219502	0.066999	0.016	0.173271	0.078696	0.002391	0.179926	0.019206	0.074	0.076308	0.120927	0.077402	0.130773	0.103026
0.219268	0.066958	0.008	0.172428	0.078052	0.002379	0.179439	0.018806	0.074	0.075806	0.120363	0.077024	0.130042	0.102766
0.219209	0.066849	0.008	0.172259	0.075477	0.002377	0.178805	0.018806	0.074	0.075776	0.120223	0.076986	0.129939	0.102592
0.219117	0.066822	0.069	0.171922	0.075477	0.002342	0.177538	0.018806	0.073	0.075605	0.120152	0.076835	0.129754	0.102245
0.218399	0.066809	0.077	0.171248	0.073385	0.002309	0.177441	0.018606	0.072	0.074932	0.1198	0.076419	0.129548	0.102148
0.217773	0.066795	0.204	0.170911	0.072741	0.002272	0.176125	0.018406	0.072	0.074459	0.1198	0.075208	0.129373	0.101792
0.217647	0.06666	0.018	0.170911	0.072741	0.002259	0.176076	0.018406	0.072	0.074359	0.119377	0.07517	0.129363	0.100827
0.217322	0.066321	0.01	0.170237	0.071936	0.00225	0.173688	0.018205	0.072	0.074037	0.119377	0.075057	0.128776	0.100432
0.216177	0.06628	0.028	0.170237	0.071293	0.002227	0.173493	0.017405	0.072	0.073937	0.119377	0.074868	0.128529	0.09969
0.215684	0.066077	0.051	0.169731	0.070971	0.002214	0.172957	0.016805	0.071	0.073635	0.118532	0.074754	0.128065	0.099613
0.214373	0.066063	0.006	0.169562	0.070166	0.002213	0.17247	0.016605	0.071	0.07263	0.117828	0.074716	0.12789	0.09915
0.2116	0.065887	0.091	0.169394	0.069683	0.002174	0.171982	0.016605	0.07	0.072319	0.117687	0.074679	0.12789	0.09887
0.2115	0.065874	0.036	0.169394	0.068074	0.002146	0.171446	0.016005	0.07	0.072178	0.116912	0.074641	0.127612	0.098301
0.211466	0.065779	0.101	0.169225	0.067913	0.002124	0.171398	0.015805	0.07	0.071726	0.116842	0.074111	0.127416	0.097771
0.211341	0.065426	0.068	0.168551	0.066948	0.002117	0.169546	0.015605	0.07	0.071656	0.116138	0.073884	0.127149	0.097366
0.210757	0.065413	0.015	0.168214	0.066948	0.002111	0.169058	0.014804	0.07	0.071636	0.11494	0.073733	0.126675	0.097163
0.210581	0.065291	0.004	0.168045	0.066948	0.002103	0.168474	0.014604	0.069	0.071616	0.114095	0.073619	0.126665	0.096633
0.21018	0.065196	0.008	0.167371	0.066626	0.002094	0.168132	0.014204	0.069	0.071384	0.113109	0.073619	0.125419	0.096546
0.20988	0.065182	0.011	0.166866	0.066304	0.002079	0.167158	0.014004	0.069	0.071183	0.113039	0.073317	0.125295	0.096064
0.209771	0.064681	0.03	0.166866	0.066304	0.002053	0.166768	0.013804	0.068	0.071173	0.112828	0.07309	0.124842	0.095871
0.209729	0.064572	0.016	0.166697	0.06566	0.002005	0.166378	0.013804	0.068	0.071023	0.112616	0.072938	0.124667	0.095833
0.209378	0.064491	0.01	0.16636	0.065499	0.001991	0.165549	0.013804	0.068	0.070792	0.112546	0.072598	0.124636	0.095659
0.209236	0.06422	0.006	0.16636	0.065177	0.001981	0.165111	0.013204	0.068	0.070148	0.111982	0.072333	0.124245	0.095168
0.209195	0.063664	0.009	0.166191	0.065016	0.001971	0.165111	0.013204	0.068	0.069927	0.111842	0.071879	0.122236	0.094531
0.208585	0.063474	0.069	0.166023	0.064534	0.001957	0.165013	0.013204	0.068	0.069797	0.111842	0.071841	0.121752	0.093895
0.208351	0.063312	0.014	0.165854	0.062281	0.00194	0.163941	0.013004	0.068	0.069777	0.11163	0.07169	0.121248	0.093875
0.207716	0.063258	0.015	0.165854	0.061959	0.00189	0.163795	0.012604	0.068	0.069676	0.111349	0.07169	0.12099	0.093499
0.207507	0.063108	0.132	0.165686	0.061798	0.001875	0.163356	0.012404	0.068	0.069556	0.110644	0.071312	0.120506	0.092844
0.207182	0.062607	0.038	0.165686	0.061637	0.001855	0.163356	0.011003	0.068	0.069525	0.110503	0.071312	0.120476	0.091986
0.206948	0.061834	0.087	0.165686	0.061476	0.00185	0.162431	0.010603	0.067	0.069425	0.110503	0.070933	0.120434	0.091079
0.206555	0.06178	0.084	0.165686	0.061476	0.001843	0.162284	0.010603	0.067	0.069154	0.10994	0.070441	0.118086	0.090751
0.206246	0.061563	0.007	0.165517	0.061476	0.001812	0.161943	0.010403	0.067	0.068993	0.109869	0.07029	0.117345	0.090674
0.20572	0.061563	0.01	0.165012	0.061315	0.001804	0.161797	0.010203	0.067	0.068902	0.109799	0.070139	0.117345	0.090636
0.204643	0.061441	0.005	0.164	0.060993	0.001796	0.161602	0.010203	0.067	0.068651	0.109658	0.070139	0.117314	0.090588
0.204517	0.061265	0.005	0.163832	0.060832	0.001768	0.161358	0.010003	0.066	0.068621	0.109376	0.070139	0.117201	0.090568
0.202763	0.06098	0.094	0.163832	0.060671	0.001761	0.161212	0.009803	0.066	0.06835	0.108743	0.070101	0.117108	0.090366
0.202696	0.060736	0.003	0.162652	0.060028	0.001761	0.160627	0.009603	0.065	0.068219	0.108672	0.06995	0.116892	0.090067
0.202605	0.060411	0.009	0.162483	0.059545	0.001756	0.160579	0.009203	0.065	0.067968	0.108602	0.069874	0.116284	0.089913
0.202479	0.060371	0.034	0.162146	0.059062	0.001744	0.160432	0.009003	0.065	0.067787	0.108602	0.069004	0.115934	0.089691
0.202062	0.060249	0.011	0.162146	0.058901	0.00171	0.160286	0.009003	0.065	0.067566	0.10839	0.068777	0.115924	0.089546
0.200049	0.060086	0.007	0.161641	0.05697	0.001684	0.159117	0.008803	0.065	0.067275	0.108179	0.068399	0.115718	0.089141
0.199915	0.059937	0.011	0.160798	0.056487	0.001654	0.158775	0.008403	0.064	0.067194	0.108109	0.068361	0.115697	0.088919
0.199514	0.059774	0.008	0.160292	0.055682	0.001637	0.157996	0.008002	0.064	0.066913	0.107545	0.068285	0.114832	0.0889
0.199472	0.059354	0.018	0.159955	0.055361	0.001636	0.156095	0.007602	0.064	0.066843	0.107334	0.068096	0.114801	0.088756
0.199447	0.058961	0.012	0.159786	0.055361	0.001622	0.155608	0.007602	0.064	0.066692	0.106771	0.068058	0.114503	0.088601
0.199414	0.058812	0.061	0.159618	0.0552	0.001614	0.155462	0.007602	0.064	0.066652	0.10663	0.067869	0.113947	0.088081
0.196516	0.05869	0.006	0.158944	0.054717	0.001599	0.155267	0.006602	0.064	0.066501	0.106418	0.067339	0.113679	0.087811
0.196265	0.058324	0.013	0.158775	0.054717	0.001586	0.155072	0.005802	0.064	0.06641	0.105925	0.066961	0.113638	0.087705
0.196015	0.058039	0.063	0.158269	0.054234	0.001543	0.155072	0.004801	0.064	0.06637	0.105785	0.06681	0.11336	0.087512
0.195873	0.057999	0.013	0.158101	0.05359	0.00154	0.155023	0.004801	0.063	0.06634	0.105714	0.066772	0.112948	0.087145
0.195046	0.057822	0.007	0.157932	0.052947	0.001539	0.154682	0.004601	0.063	0.066149	0.104939	0.066621	0.112917	0.08702
0.194753	0.057687	0.054	0.157595	0.052786	0.001522	0.154487		0.063	0.066059	0.104869	0.066318	0.112886	0.086875
0.193409	0.057673	0.007	0.157258	0.052625	0.001513	0.154389		0.063	0.066039	0.104658	0.066204	0.112618	0.086731
0.192214	0.057592	0.128	0.156753	0.051981	0.001509	0.154389		0.063	0.066039	0.104658	0.065334	0.112217	0.086634
0.192055	0.057443	0.008	0.155573	0.051659	0.001505	0.153951		0.062	0.065958	0.103813	0.065145	0.111321	0.086403
0.19183	0.057389	0.026	0.154056	0.050854	0.001499	0.153853		0.062	0.065285	0.103672	0.064956	0.111249	0.086114
0.191588	0.057239	0.084	0.153887	0.05005	0.00148	0.152781		0.062	0.065235	0.102827	0.064767	0.111053	0.085622
0.191178	0.056846	0.034	0.15355	0.05005	0.001473	0.152538		0.062	0.065094	0.102827	0.064729	0.111012	0.085333

0.190794	0.056711	0.01	0.152707	0.049728	0.001456	0.152489
0.190719	0.056453	0.032	0.152033	0.049406	0.001445	0.151709
0.188856	0.05625	0.048	0.151527	0.048923	0.001444	0.15166
0.18884	0.056223	0.205	0.151359	0.04844	0.001441	0.151465
0.188664	0.056074	0.011	0.151022	0.047797	0.00144	0.151027
0.187311	0.056006	0.006	0.150348	0.047636	0.001412	0.150637
0.187136	0.056006	0.026	0.15001	0.047636	0.00141	0.150296
0.187011	0.055749	0.003	0.149842	0.047475	0.001396	0.150296
0.186083	0.055505	0.055	0.149842	0.047153	0.00136	0.149662
0.185098	0.05545	0.049	0.149673	0.04667	0.001357	0.149419
0.18463	0.055261	0.1	0.149336	0.046187	0.001327	0.148639
0.184371	0.05522	0.041	0.147988	0.046187	0.001327	0.14859
0.184263	0.055193	0.013	0.147988	0.046026	0.0013	0.148298
0.183244	0.055125	0.032	0.147819	0.045705	0.001269	0.147859
0.18306	0.054962	0.02	0.147145	0.045544	0.001267	0.146543
0.182951	0.0548	0.029	0.146808	0.045544	0.001254	0.146543
0.1824	0.054339	0.007	0.144954	0.045383	0.001234	0.146446
0.181991	0.054217	0.013	0.144448	0.045061	0.001232	0.146251
0.181807	0.054108	0.01	0.144111	0.045061	0.00121	0.146007
0.181765	0.053973	0.011	0.143606	0.044578	0.001206	0.145958
0.181473	0.053892	0.152	0.143606	0.044095	0.001198	0.145666
0.181448	0.053797	0.005	0.143437	0.044095	0.001182	0.14552
0.181314	0.053485	0.004	0.142931	0.043773	0.001165	0.14552
0.180997	0.053471	0.084	0.142594	0.042808	0.001155	0.14513
0.17997	0.053241	0.005	0.142257	0.041842	0.001141	0.14357
0.17936	0.053092	0.006	0.142089	0.04152	0.001132	0.143327
0.179268	0.053051	0.02	0.14192	0.040877	0.001127	0.142839
0.1786	0.052997	0.018	0.141751	0.040877	0.001124	0.142498
0.178366	0.052943	0.011	0.141246	0.040877	0.001109	0.142352
0.178291	0.052929	0.003	0.140572	0.040716	0.001099	0.141816
0.177564	0.052875	0.003	0.140403	0.040555	0.001092	0.141426
0.177313	0.052821	0.017	0.140403	0.040072	0.00109	0.140939
0.17728	0.052712	0.048	0.139897	0.039428	0.001053	0.140695
0.177263	0.052414	0.013	0.139392	0.038785	0.001046	0.140646
0.176762	0.052265	0.011	0.138718	0.038785	0.001041	0.140305
0.175125	0.052157	0.003	0.138043	0.038785	0.001041	0.140062
0.17495	0.052143	0.008	0.137538	0.038624	0.001038	0.140013
0.174173	0.051994	0.032	0.137032	0.038141	0.001034	0.139672
0.173805	0.051601	0.004	0.136358	0.03798	0.001019	0.139623
0.173538	0.051506	0.012	0.136358	0.037175	0.00099	0.139477
0.173237	0.051303	0.017	0.135684	0.036692	0.000989	0.139477
0.173095	0.051208	0.01	0.135178	0.036371	0.000989	0.139331
0.172995	0.051127	0.023	0.135178	0.035405	0.000985	0.138015
0.172619	0.051059	0.011	0.135009	0.035083	0.000969	0.138015
0.172035	0.050855	0.067	0.134672	0.035083	0.00096	0.137722
0.17155	0.050611	0.047	0.134504	0.0346	0.00096	0.137527
0.170531	0.050476	0.014	0.134335	0.0346	0.000952	0.137138
0.170281	0.050191	0.003	0.133324	0.034439	0.000936	0.136699
0.169771	0.050191	0.044	0.131976	0.034439	0.000917	0.13665
0.169587	0.050096	0.012	0.131807	0.034118	0.000905	0.136114
0.169521	0.050056	0.005	0.131133	0.033957	0.000904	0.135822
0.167992	0.050015	0.035	0.131133	0.033635	0.000897	0.135432
0.16785	0.049934	0.012	0.131133	0.032508	0.000897	0.134457
0.167299	0.049934	0.003	0.131133	0.032347	0.000878	0.134165
0.167082	0.049812	0.009	0.130964	0.032186	0.000851	0.13319
0.166814	0.049717	0.013	0.130796	0.032025	0.000823	0.133093
0.165837	0.049432	0.025	0.130796	0.031864	0.0008	0.133044
0.165662	0.049364	0.004	0.130459	0.031543	0.000783	0.132605
0.165411	0.049148	0.007	0.130121	0.031221	0.000769	0.132459
0.165086	0.048836	0.018	0.129953	0.03106	0.000759	0.132118
0.165019	0.048809	0.007	0.129616	0.030899	0.000743	0.131923
0.164609	0.048768	0.01	0.12911	0.030899	0.000738	0.131241
0.163991	0.048755	0.007	0.128099	0.030738	0.000728	0.130948
0.163833	0.048402	0.008	0.128099	0.030577	0.000727	0.130851
0.163632	0.048118	0.016	0.12793	0.030577	0.000721	0.130802
0.16344	0.047968	0.028	0.127593	0.030577	0.000718	0.130558
0.163064	0.047955	0.022	0.127593	0.030416	0.000711	0.130266
0.162396	0.047765	0.004	0.127593	0.030094	0.000707	0.12973
0.161937	0.047752	0.018	0.127593	0.029451	0.0007	0.129535
0.161319	0.047589	0.008	0.127088	0.02929	0.000697	0.12934
0.161085	0.047196	0.073	0.126919	0.029129	0.000696	0.128122
0.160634	0.047033	0.022	0.126582	0.028968	0.000694	0.127732
0.160224	0.046979	0.108	0.126245	0.028485	0.000689	0.126562
0.160074	0.046871	0.043	0.125402	0.028324	0.00068	0.126367
0.159832	0.046843	0.016	0.125233	0.028163	0.000675	0.126221
0.159798	0.046816	0.013	0.125233	0.027841	0.000667	0.125977
0.159448	0.046776	0.047	0.124896	0.027519	0.000665	0.125588
0.159314	0.046749	0.017	0.124728	0.027358	0.000656	0.125393
0.159289	0.046708	0.018	0.124559	0.027197	0.000644	0.124808
0.159256	0.046586	0.066	0.124391	0.027197	0.000639	0.124759
0.158771	0.046464	0.078	0.124054	0.027037	0.000637	0.124321
0.158495	0.046396	0.056	0.122874	0.027037	0.000635	0.124028
0.157986	0.046383	0.012	0.122705	0.026554	0.000607	0.123492
0.157978	0.046369	0.005	0.122705	0.026554	0.000607	0.123151
0.157176	0.046369	0.016	0.122368	0.026554	0.000606	0.123151
0.156432	0.046193	0.003	0.122031	0.026554	0.000604	0.122907
0.155915	0.046003	0.064	0.121862	0.026554	0.0006	0.122712
0.155597	0.045949	0.013	0.121694	0.026393	0.000599	0.122225
0.155514	0.045583	0.008	0.121188	0.026232	0.000597	0.122127
0.155363	0.045502	0.011	0.119671	0.026071	0.000592	0.122079
0.155138	0.045447	0.009	0.119166	0.02591	0.000587	0.121445
0.154186	0.045447	0.012	0.118154	0.02591	0.000578	0.121299
0.15406	0.045298	0.019	0.11748	0.02591	0.000578	0.121299
0.153952	0.045217	0.079	0.117143	0.025588	0.000575	0.120519
0.153684	0.045014	0.087	0.117143	0.025427	0.000573	0.120373
0.153041	0.044539	0.011	0.116974	0.025105	0.000566	0.119886
0.152983	0.044363	0.155	0.116974	0.025105	0.000558	0.118814
0.15229	0.044227	0.038	0.1163	0.024944	0.000555	0.118667
0.151989	0.044214	0.005	0.116132	0.024783	0.000554	0.118667
0.151672	0.044133	0.018	0.115963	0.024783	0.000542	0.11779
0.151613	0.044119	0.008	0.115963	0.024462	0.000539	0.117108
0.151613	0.043929	0.011	0.115795	0.024462	0.000539	0.116718
0.15158	0.043889	0.014	0.115458	0.024301	0.000535	0.116523
0.151538	0.043848	0.108	0.115289	0.02414	0.000535	0.116377
0.151346	0.043726	0.01	0.114783	0.023979	0.000529	0.116182
0.151329	0.043712	0.006	0.114783	0.023979	0.000519	0.116036
0.151296	0.043685	0.017	0.114109	0.023979	0.000508	0.115207
0.151296	0.043604	0.011	0.113941	0.023818	0.000508	0.114769
0.151237	0.043563	0.032	0.113435	0.023335	0.000505	0.114671
0.151112	0.043509	0.058	0.113266	0.023174	0.000505	0.114671
0.150711	0.043048	0.033	0.113266	0.023013	0.000504	0.114525
0.150544	0.042953	0.048	0.113098	0.022852	0.000499	0.114476
0.150293	0.042764	0.007	0.111918	0.022691	0.000485	0.114379
0.149968	0.042682	0.004	0.111412	0.02237	0.00047	0.114281

0.062	0.065054	0.102686	0.064578	0.110991	0.084484	
0.061	0.065024	0.102474	0.064502	0.110353	0.084436	
0.061	0.064451	0.102052	0.064426	0.11026	0.084253	
0.061	0.06427	0.101981	0.064426	0.110157	0.084233	
0.06	0.063928	0.101981	0.064351	0.110013	0.084176	
0.06	0.063918	0.10177	0.064275	0.109374	0.084089	
0.06	0.063808	0.1017	0.064162	0.108962	0.083857	
0.06	0.063657	0.1017	0.06401	0.108551	0.083665	
0.06	0.063496	0.101136	0.063821	0.107294	0.083636	
0.06	0.063265	0.101066	0.063745	0.106882	0.083597	
0.06	0.063145	0.100643	0.06367	0.106769	0.083115	
0.06	0.063115	0.100432	0.063632	0.106687	0.082912	
0.06	0.063054	0.099939	0.063556	0.106429	0.082488	
0.06	0.062914	0.099869	0.063518	0.106429	0.082228	
0.059	0.062662	0.099728	0.063481	0.105997	0.08217	
0.059	0.062662	0.099657	0.063405	0.105945	0.081659	
0.059	0.061758	0.099516	0.063216	0.105852	0.081524	
0.059	0.061738	0.099164	0.062837	0.105739	0.081109	
0.059	0.061185	0.098883	0.062837	0.105595	0.080868	
0.058	0.061004	0.098812	0.062497	0.104967	0.080579	
0.058	0.060954	0.09853	0.062383	0.104915	0.080444	
0.057	0.060713	0.09846	0.062119	0.104884	0.080001	
0.056	0.060532	0.09839	0.061929	0.104256	0.079538	
0.056	0.060462	0.098249	0.061854	0.104215	0.079104	
0.056	0.060361	0.098249	0.061665	0.103844	0.078525	
0.056	0.060251	0.097192	0.061665	0.10301	0.077956	
0.056	0.06018	0.096981	0.0614	0.102948	0.077542	
0.056	0.059939	0.09684	0.061324	0.101805	0.077522	
0.056	0.059899	0.096558	0.061211	0.10161	0.077291	
0.056	0.059839	0.096558	0.061059	0.101548	0.076925	
0.056	0.059829	0.095784	0.060946	0.101342	0.076876	
0.055	0.059728	0.095713	0.060795	0.100848	0.076288	
0.055	0.059457	0.09515	0.060757	0.100714	0.076124	
0.055	0.059417	0.095009	0.060416	0.099756	0.076047	
0.054	0.059336	0.094727	0.060341	0.099756	0.075739	
0.054	0.059246	0.094305	0.060227	0.099653	0.075459	
0.054	0.059226	0.094093	0.060151	0.099437	0.075353	
0.054	0.059186	0.093671	0.059811	0.098737	0.075334	
0.054	0.059176	0.093389	0.059773	0.098582	0.075295	
0.054	0.058975	0.092685	0.05947	0.09851	0.07517	
0.054	0.058753	0.092121	0.059395	0.097975	0.075006	
0.054	0.058743	0.091276	0.059206	0.096729	0.074765	
0.054	0.058412	0.090924	0.059092	0.096039	0.074755	
0.054	0.058291	0.090854	0.059016	0.094123	0.074398	
0.054	0.058261	0.090713	0.05879	0.094113	0.074177	
0.053	0.058251	0.090642	0.058752	0.093866	0.073849	
0.053	0.058161	0.090501	0.0586	0.093155	0.073511	
0.053	0.05804	0.09022	0.057995	0.092805	0.073386	
0.053	0.05801	0.090149	0.057882	0.092578	0.07328	
0.053	0.058	0.089586	0.057882	0.092403	0.073251	
0.053	0.05798	0.089515	0.057768	0.092187	0.072325	
0.053	0.05796	0.089445	0.057579	0.092146	0.072152	
0.052	0.05793	0.089163	0.057465	0.091631	0.072046	
0.052	0.057869	0.089093	0.057428	0.090467	0.071776	
0.052	0.057608	0.088811	0.057238	0.090364	0.0714	
0.052	0.057528	0.0886	0.056974	0.090076	0.07138	
0.052	0.057357	0.088529	0.056974	0.08986	0.070947	
0.052	0.057307	0.088318	0.056936	0.089685	0.070918	
0.051	0.057246	0.087966	0.056898	0.08953	0.070686	
0.051	0.057246	0.087966	0.05686	0.089108	0.070571	
0.051	0.057136	0.087332	0.05686	0.088789	0.070551	
0.051	0.056915	0.087191	0.056633	0.088655	0.070513	
0.05	0.056764	0.08698	0.056595	0.088367	0.070349	
0.05	0.056372	0.086839	0.056557	0.088325	0.070262	
0.05	0.056312	0.086698	0.056444	0.087708	0.070185	
0.05	0.056221	0.086276	0.056406	0.087615	0.070185	
0.05	0.05586	0.085501	0.05633	0.087388	0.069963	
0.05	0.055357	0.08536	0.056141	0.08674	0.069818	
0.049	0.055287	0.08529	0.056141	0.086729	0.06952	
0.049	0.054955	0.085219	0.05599	0.086719	0.068883	
0.049	0.054825	0.085219	0.05599	0.086544	0.068555	
0.049	0.054483	0.085149	0.055385	0.086297	0.068083	
0.049	0.054433	0.084938	0.055347	0.086132	0.068073	
0.049	0.054392	0.084867	0.055347	0.085566	0.067919	
0.049	0.054121	0.084726	0.055233	0.085555	0.06788	
0.048	0.05398	0.084515	0.055006	0.084721	0.067784	
0.048	0.05391	0.084445	0.054779	0.084361	0.067138	
0.048	0.05391	0.084163	0.054628	0.083218	0.066926	
0.048	0.053528	0.08374	0.054212	0.08296	0.066907	
0.048	0.053398	0.083599	0.053834	0.082847	0.066849	
0.048	0.053197	0.083247	0.053834	0.082013	0.066781	
0.048	0.052895	0.082754	0.053531	0.082013	0.066704	
0.048	0.052644	0.082684	0.053266	0.08191	0.066444	
0.047	0.052413	0.082684	0.052964	0.081858	0.066261	
0.047	0.052252	0.082402	0.052888	0.081405	0.066019	
0.047	0.052182	0.082332	0.052699	0.081333	0.065672	
0.047	0.052091	0.082261	0.052661	0.081127	0.065123	
0.047	0.052001	0.08212	0.052358	0.080828	0.06493	
0.047	0.051951	0.08205	0.052169	0.080643	0.06492	
0.047	0.05191	0.08198	0.052093	0.080365	0.064911	
0.047	0.05189	0.081909	0.051904	0.080303	0.064872	
0.046	0.05184	0.081839	0.051866	0.080293	0.064592	
0.046	0.05175	0.081627	0.051829	0.079469	0.064486	
0.046	0.05171	0.081487	0.051639	0.079232	0.064072	
0.046	0.051559	0.081346	0.051526	0.078285	0.063975	
0.046	0.051408	0.081346	0.051185	0.076648	0.063946	
0.046	0.051237	0.081205	0.050921	0.076287	0.063628	
0.046	0.051157	0.080782	0.050883	0.076277	0.063619	
0.046	0.051137	0.080782	0.050656	0.075391	0.063484	
0.046	0.050976	0.080712	0.050542	0.075216	0.063223	
0.046	0.050795	0.080641	0.050505	0.075196	0.063088	
0.046	0.050634	0.08043	0.050088	0.075093	0.063069	
0.045	0.050604	0.08036	0.050051	0.074876	0.062442	
0.045	0.050584	0.079726	0.049975	0.074835	0.062375	
0.045	0.049951	0.079515	0.049748	0.074197	0.06222	
0.045	0.049629	0.079233	0.049407	0.073496	0.061652	
0.045	0.049519	0.079092	0.049294	0.072961	0.061015	
0.045	0.049207	0.079092	0.048348	0.07292	0.060822	
0.045	0.048886	0.079022	0.048348	0.072333	0.060745	
0.045	0.048876	0.078599	0.048121	0.071674	0.060726	
0.045	0.048735	0.077965	0.048083	0.071612	0.060707	
0.045	0.048705	0.077895	0.048045	0.069563	0.060687	
0.044	0.048504	0.077472	0.04797	0.069552	0.060543	
0.044	0.048454	0.077402	0.047932	0.069511	0.060176	

0.149784	0.042438	0.066	0.111412	0.022048	0.000466	0.114135
0.149249	0.042249	0.104	0.111244	0.021887	0.000463	0.114038
0.148531	0.042167	0.014	0.110738	0.021726	0.000454	0.113745
0.148397	0.042127	0.046	0.110064	0.021726	0.000443	0.113599
0.148331	0.042113	0.016	0.108715	0.021565	0.000442	0.113502
0.148314	0.042059	0.151	0.108715	0.021404	0.000435	0.113355
0.148172	0.041855	0.013	0.108547	0.021404	0.000434	0.112965
0.14798	0.041774	0.004	0.108378	0.021243	0.000431	0.112624
0.147871	0.041408	0.005	0.10821	0.021243	0.000429	0.112478
0.14742	0.041381	0.042	0.108041	0.021243	0.000429	0.112381
0.146977	0.041137	0.006	0.107873	0.021243	0.000425	0.111893
0.146819	0.040771	0.009	0.107873	0.021082	0.000416	0.111893
0.146535	0.04073	0.084	0.107704	0.020921	0.000411	0.111601
0.146401	0.040676	0.004	0.107536	0.02076	0.000404	0.11126
0.145649	0.040608	0.017	0.107536	0.02076	0.0004	0.110529
0.145524	0.040568	0.007	0.107367	0.02076	0.000391	0.109603
0.145524	0.040541	0.01	0.107367	0.020599	0.000383	0.109603
0.145223	0.040514	0.028	0.107199	0.020599	0.000383	0.109505
0.144714	0.0405	0.02	0.10703	0.020438	0.00038	0.108677
0.144497	0.040337	0.017	0.106861	0.020116	0.000377	0.108628
0.14448	0.040134	0.019	0.106861	0.019956	0.000372	0.107995
0.144054	0.039999	0.002	0.106524	0.019956	0.000365	0.107556
0.143912	0.039971	0.009	0.106019	0.019956	0.00036	0.10741
0.143185	0.039958	0.099	0.105513	0.019956	0.000359	0.107264
0.143069	0.039944	0.011	0.105344	0.019634	0.000358	0.107166
0.142968	0.039755	0.005	0.105007	0.019634	0.000357	0.107069
0.14296	0.039727	0.373	0.104839	0.019634	0.000356	0.106971
0.142584	0.039714	0.012	0.104839	0.019473	0.000349	0.106922
0.142175	0.039687	0.007	0.104165	0.019473	0.000349	0.106825
0.142008	0.03966	0.229	0.104165	0.019312	0.000341	0.105899
0.141841	0.039592	0.008	0.103659	0.01899	0.000327	0.105655
0.141457	0.039511	0.031	0.10349	0.01899	0.000319	0.105607
0.141039	0.039483	0.21	0.103153	0.01899	0.000318	0.105509
0.140412	0.03947	0.006	0.102985	0.018829	0.000318	0.105217
0.139861	0.039375	0.068	0.102985	0.018668	0.000317	0.105022
0.139661	0.039334	0.296	0.102816	0.018668	0.000315	0.104876
0.139586	0.039131	0.224	0.102311	0.018668	0.000311	0.104193
0.139368	0.03909	0.01	0.102311	0.018507	0.00031	0.103706
0.138792	0.038955	0.037	0.101973	0.018346	0.000306	0.103609
0.138759	0.03886	0.037	0.101973	0.018346	0.000304	0.103414
0.138575	0.038819	0.053	0.101636	0.018185	0.000301	0.103365
0.138174	0.038806	0.152	0.101468	0.018185	0.0003	0.102878
0.138141	0.038752	0.044	0.101299	0.018185	0.000298	0.102634
0.138082	0.038697	0.032	0.101299	0.017863	0.000296	0.102147
0.138065	0.038657	0.046	0.101131	0.017863	0.000294	0.102098
0.137756	0.038589	0.016	0.100962	0.017542	0.000293	0.101854
0.137631	0.038521	0.016	0.100625	0.017381	0.000287	0.101659
0.137539	0.038508	0.036	0.100625	0.017381	0.000285	0.100879
0.136545	0.03848	0.006	0.100456	0.017381	0.000284	0.100733
0.13632	0.038372	0.022	0.100119	0.01722	0.000284	0.100684
0.136311	0.03825	0.009	0.099951	0.01722	0.000284	0.100148
0.135702	0.038182	0.124	0.099614	0.016898	0.000281	0.099807
0.135576	0.038169	0.05	0.099445	0.016737	0.000277	0.099759
0.135418	0.037979	0.023	0.099108	0.016737	0.000273	0.099369
0.1351	0.037952	0.033	0.099108	0.016737	0.000267	0.099222
0.134332	0.037884	0.34	0.09894	0.016415	0.000264	0.098686
0.13414	0.037843	0.097	0.098771	0.016415	0.000259	0.098589
0.134073	0.037816	0.019	0.098602	0.016254	0.000256	0.098589
0.133747	0.037803	0.049	0.098602	0.016254	0.000253	0.098491
0.133714	0.037789	0.058	0.097928	0.016254	0.000249	0.097566
0.133689	0.037735	0.006	0.097928	0.015771	0.000243	0.097419
0.133413	0.037694	0.032	0.097591	0.015771	0.000236	0.097224
0.13328	0.037667	0.029	0.097423	0.01561	0.000233	0.097029
0.133271	0.037559	0.061	0.097085	0.01561	0.000232	0.096932
0.133004	0.037545	0.087	0.097085	0.015449	0.000228	0.096883
0.132511	0.03745	0.21	0.097085	0.015449	0.000227	0.096835
0.132394	0.037437	0.02	0.096748	0.015449	0.000223	0.096347
0.132319	0.037247	0.012	0.096411	0.015289	0.000214	0.096298
0.13221	0.037139	0.171	0.096411	0.015289	0.000214	0.096298
0.132202	0.037098	0.014	0.096243	0.015128	0.000212	0.095909
0.132127	0.037071	0.053	0.096074	0.014967	0.00021	0.095324
0.131943	0.037017	0.011	0.095568	0.014806	0.00021	0.095031
0.13186	0.036989	0.011	0.095568	0.014806	0.000208	0.094934
0.131693	0.036922	0.003	0.0954	0.014645	0.000205	0.094836
0.131384	0.036867	0.029	0.095231	0.014484	0.000204	0.094739
0.131242	0.036867	0.024	0.095231	0.014484	0.000196	0.094641
0.131183	0.0368	0.037	0.095231	0.014323	0.000193	0.094641
0.130648	0.036786	0.049	0.094726	0.014323	0.000192	0.094544
0.130548	0.036732	0.053	0.094557	0.014162	0.000182	0.093959
0.130498	0.036664	0.024	0.094389	0.014162	0.000179	0.093862
0.130289	0.036542	0.006	0.094389	0.014162	0.000177	0.093569
0.130248	0.036529	0.007	0.093546	0.014001	0.000177	0.093569
0.130139	0.036434	0.032	0.093546	0.014001	0.000175	0.092936
0.12998	0.036366	0.069	0.093546	0.01384	0.00017	0.092643
0.129262	0.036163	0.003	0.093209	0.013679	0.000162	0.092156
0.128552	0.036163	0.027	0.09304	0.013679	0.000159	0.092059
0.128527	0.036081	0.038	0.092535	0.013518	0.000157	0.09201
0.12846	0.036014	0.007	0.092029	0.013518	0.000155	0.091912
0.128251	0.035946	0.158	0.091692	0.013518	0.000149	0.09123
0.128118	0.035919	0.016	0.091692	0.013357	0.000149	0.090645
0.127992	0.035661	0.03	0.091355	0.013357	0.000146	0.090499
0.127967	0.035634	0.026	0.091355	0.013196	0.000145	0.090255
0.127867	0.035553	0.246	0.091018	0.013035	0.000138	0.090255
0.127224	0.035539	0.048	0.090849	0.013035	0.000136	0.090207
0.126623	0.035417	0.022	0.090849	0.013035	0.000133	0.090158
0.126514	0.035322	0.027	0.090849	0.012875	0.000126	0.090158
0.126088	0.035309	0.241	0.090512	0.012875	0.000124	0.089866
0.125863	0.035282	0.031	0.090512	0.012875	0.000123	0.089817
0.12562	0.035282	0.067	0.089669	0.012875	0.000123	0.089719
0.124635	0.035119	0.012	0.089501	0.012875	0.000122	0.089135
0.124518	0.035024	0.011	0.089501	0.012714	0.000121	0.088696
0.124083	0.034929	0.039	0.089164	0.012553	0.000119	0.08855
0.123908	0.034889	0.021	0.088995	0.012553	0.000117	0.088501
0.123582	0.034807	0.247	0.088995	0.012553	0.000114	0.088501
0.123399	0.034658	0.025	0.088826	0.012392	0.000111	0.088404
0.123365	0.034563	0.004	0.088826	0.012392	0.000109	0.088209
0.123365	0.034536	0.032	0.088658	0.012231	0.000108	0.088111
0.123282	0.034509	0.152	0.087815	0.01207	0.000104	0.088062
0.123073	0.034306	0.131	0.087647	0.01207	0.000104	0.087965
0.123073	0.034211	0.038	0.087478	0.011748	0.000103	0.08777
0.122672	0.034143	0.013	0.087309	0.011587	0.000102	0.087624
0.122597	0.034102	0.085	0.086972	0.011587	0.000101	0.087575
0.12258	0.033994	0.044	0.086804	0.011426	0.0001	0.087331
0.121929	0.033682	0.037	0.086804	0.011426	0.000097	0.087039

0.044	0.048303	0.077331	0.047894	0.069429	0.060138	
0.044	0.048243	0.077331	0.047781	0.068595	0.06008	
0.044	0.048213	0.077261	0.047781	0.06845	0.059906	
0.044	0.048142	0.076909	0.04744	0.068265	0.059906	
0.044	0.047931	0.076838	0.047251	0.06809	0.05981	
0.044	0.047871	0.076768	0.046986	0.067853	0.059752	
0.044	0.047429	0.076768	0.046948	0.067524	0.059019	
0.043	0.047278	0.076275	0.046721	0.067462	0.05899	
0.043	0.047158	0.076204	0.046684	0.067287	0.058981	
0.043	0.047117	0.076063	0.046646	0.06705	0.058798	
0.042	0.046957	0.07557	0.04657	0.066988	0.05872	
0.042	0.046957	0.07557	0.046494	0.066926	0.058643	
0.042	0.046715	0.0755	0.046419	0.066792	0.058595	
0.042	0.046615	0.07543	0.046381	0.066586	0.058518	
0.042	0.046394	0.075148	0.046116	0.066473	0.057997	
0.042	0.046243	0.074937	0.04604	0.06638	0.05792	
0.042	0.045922	0.074937	0.045776	0.066133	0.05791	
0.042	0.045751	0.074866	0.045738	0.065073	0.057824	
0.042	0.04568	0.074796	0.0457	0.06499	0.057679	
0.041	0.045278	0.074655	0.045549	0.064877	0.057467	
0.041	0.045148	0.074655	0.045435	0.064764	0.057457	
0.041	0.044816	0.074584	0.045322	0.063765	0.057264	
0.041	0.044796	0.074232	0.045208	0.063682	0.057264	
0.041	0.044766	0.07388	0.04517	0.063446	0.057081	
0.041	0.044766	0.07381	0.044981	0.063425	0.057033	
0.041	0.044635	0.073739	0.044943	0.063384	0.056966	
0.041	0.044294	0.073739	0.044868	0.063137	0.056686	
0.041	0.044143	0.073598	0.04483	0.063095	0.056368	
0.041	0.044113	0.073528	0.044754	0.06223	0.056021	
0.041	0.043902	0.073458	0.044754	0.06222	0.055818	
0.04	0.043821	0.073387	0.044716	0.06222	0.055288	
0.04	0.043781	0.073317	0.044338	0.062066	0.055095	
0.04	0.043771	0.073105	0.044338	0.06188	0.054921	
0.04	0.04352	0.073035	0.044111	0.061788	0.054555	
0.04	0.04347	0.072965	0.043998	0.061098	0.053986	
0.04	0.043369	0.072965	0.043884	0.061056	0.053764	
0.04	0.043259	0.072965	0.043771	0.060923	0.05362	
0.04	0.043188	0.072824	0.043619	0.06085	0.05361	
0.04	0.043078	0.072753	0.04343	0.060809	0.053485	
0.039	0.042917	0.072612	0.04343	0.060459	0.053369	
0.039	0.042475	0.072331	0.043241	0.060418	0.053205	
0.039	0.042425	0.072331	0.043203	0.060346	0.052983	
0.039	0.042274	0.072331	0.043165	0.060305	0.052916	
0.039	0.042153	0.07226	0.042938	0.059944	0.0528	
0.039	0.042113	0.072119	0.042938	0.059852	0.052771	
0.039	0.042043	0.072119	0.042825	0.059594	0.052752	
0.039	0.041952	0.072049	0.042825	0.059265	0.052617	
0.039	0.041862	0.072049	0.042673	0.059079	0.052578	
0.039	0.041832	0.071908	0.042636	0.058914	0.052549	
0.039	0.041812	0.071838	0.04256	0.058822	0.052453	
0.039	0.041751	0.071556	0.042484	0.058812	0.052308	
0.039	0.041651	0.071345	0.042446	0.058678	0.052231	
0.039	0.041631	0.071204	0.042409	0.058503	0.052222	
0.039	0.041611	0.071204	0.042257	0.058492	0.052173	
0.038	0.041209	0.071133	0.042182	0.058245	0.052164	
0.038	0.041048	0.071133	0.042106	0.058204	0.052106	
0.038	0.040877	0.07064	0.041728	0.057535	0.052009	
0.038	0.040727	0.07064	0.041425	0.057411	0.051846	
0.038	0.040696	0.070359	0.041387	0.057359	0.051826	
0.038	0.040445	0.070359	0.041349	0.057298	0.051778	
0.038	0.040405	0.070288	0.041122	0.057154	0.051556	
0.038	0.040335	0.070147	0.041122	0.057009	0.051527	
0.038	0.040325	0.069936	0.040971	0.056937	0.051527	
0.038	0.040194	0.069795	0.040858	0.056845	0.051479	
0.038	0.040164	0.069795	0.040744	0.056814	0.051479	
0.038	0.039943	0.069795	0.040744	0.056793	0.050949	
0.038	0.039842	0.069725	0.040706	0.055938	0.050525	
0.038	0.039752	0.069584	0.040631	0.055784	0.05037	
0.037	0.039621	0.069584	0.040631	0.055609	0.050149	
0.037	0.039521	0.069584	0.040517	0.055506	0.050139	
0.037	0.03946	0.069021	0.040328	0.055104	0.05012	
0.037	0.03944	0.06895	0.040252	0.055094	0.050023	
0.037	0.03932	0.068809	0.040214	0.055042	0.049965	
0.037	0.03931	0.068809	0.040177	0.054744	0.049908	
0.037	0.03929	0.068739	0.040101	0.054723	0.04985	
0.037	0.039239	0.068528	0.040063	0.054713	0.04984	
0.037	0.039189	0.068387	0.03995	0.054558	0.049763	
0.037	0.039139	0.067964	0.039798	0.054507	0.049618	
0.037	0.039129	0.067964	0.039685	0.054352	0.049618	
0.037	0.039119	0.067894	0.039533	0.054301	0.049541	
0.037	0.039119	0.067823	0.039496	0.053848	0.049541	
0.037	0.038898	0.067682	0.039344	0.053663	0.049531	
0.037	0.038888	0.067682	0.039306	0.053652	0.049503	
0.037	0.038807	0.06726	0.039231	0.052767	0.049233	
0.037	0.038787	0.067049	0.03908	0.052705	0.049059	
0.037	0.038707	0.066978	0.039042	0.052684	0.048857	
0.037	0.038687	0.066696	0.039042	0.052664	0.048635	
0.037	0.038566	0.066696	0.039004	0.052581	0.048606	
0.037	0.038536	0.066626	0.038928	0.052499	0.04848	
0.036	0.038486	0.066415	0.038777	0.052355	0.048432	
0.036	0.038456	0.066415	0.038663	0.052303	0.048326	
0.036	0.038335	0.066274	0.03855	0.052138	0.04822	
0.036	0.038194	0.066274	0.038361	0.052066	0.047979	
0.036	0.038184	0.066203	0.038285	0.052025	0.047902	
0.036	0.037903	0.066133	0.038134	0.051284	0.047854	
0.036	0.037822	0.066133	0.038134	0.05114	0.047709	
0.036	0.037732	0.066063	0.038058	0.051098	0.047642	
0.036	0.03732	0.06564	0.037869	0.051006	0.047574	
0.036	0.03726	0.06557	0.037793	0.050862	0.047555	
0.036	0.037199	0.06557	0.037793	0.05082	0.047497	
0.036	0.037099	0.065499	0.037755	0.050635	0.047468	
0.036	0.036988	0.065499	0.03768	0.050614	0.047381	
0.035	0.036707	0.065288	0.037604	0.050439	0.047343	
0.035	0.036556	0.065288	0.037566	0.050326	0.047025	
0.035	0.036556	0.065147	0.037491	0.050285	0.046976	
0.035	0.036386	0.065077	0.037453	0.050172	0.04688	
0.035	0.036365	0.065006	0.037264	0.050141	0.046832	
0.035	0.036355	0.064936	0.037226	0.050089	0.046764	
0.035	0.036315	0.064724	0.03715	0.050027	0.04662	
0.035	0.036305	0.064654	0.037112	0.049996	0.046427	
0.035	0.036295	0.064584	0.037112	0.049749	0.046427	
0.034	0.036265	0.064443	0.036999	0.049739	0.046272	
0.034	0.035893	0.064372	0.036961	0.049657	0.046263	
0.034	0.035833	0.064372	0.036885	0.049585	0.045954	

0.121361	0.033669	0.013	0.086635	0.011265	0.000097	0.087039
0.121269	0.033655	0.023	0.086467	0.011104	0.000096	0.086893
0.120692	0.033628	0.005	0.086467	0.010782	0.000096	0.086747
0.120442	0.033587	0.009	0.086467	0.010782	0.000091	0.086454
0.119941	0.03352	0.004	0.08613	0.010782	0.00009	0.085967
0.119924	0.033452	0.011	0.08613	0.010782	0.000088	0.085674
0.119782	0.033438	0.07	0.08613	0.010621	0.000082	0.085479
0.119373	0.033343	0.005	0.085793	0.010621	0.00008	0.085041
0.11893	0.033235	0.02	0.085624	0.010461	0.000076	0.085041
0.118629	0.033045	0.022	0.085624	0.010461	0.000073	0.084943
0.118546	0.033005	0.015	0.085455	0.010461	0.000071	0.084846
0.118529	0.032937	0.168	0.085455	0.010461	0.000071	0.084748
0.118212	0.032869	0.004	0.085455	0.0103	0.000066	0.084602
0.117995	0.032828	0.009	0.085287	0.009978	0.000065	0.084602
0.11751	0.032801	0.007	0.085287	0.009978	0.000064	0.084505
0.117151	0.032788	0.015	0.084781	0.009978	0.000063	0.084505
0.117009	0.03272	0.043	0.084781	0.009978	0.000054	0.084456
0.116775	0.03272	0.058	0.084444	0.009978	0.000049	0.084407
0.116575	0.032706	0.012	0.084444	0.009817	0.000046	0.084359
0.116566	0.032679	0.007	0.084276	0.009817	0.000044	0.084212
0.116124	0.032611	0.009	0.084276	0.009817	0.000044	0.084212
0.115623	0.03253	0.07	0.084276	0.009656	0.000043	0.084017
0.115581	0.03253	0.049	0.084107	0.009656	0.000039	0.083823
0.115255	0.03234	0.015	0.083938	0.009495	0.000008	0.083676
0.114887	0.0323	0.01	0.08377	0.009495	0.000002	0.08353
0.114787	0.032273	0.051	0.083601	0.009334	0.000002	0.083384
0.114578	0.032137	0.08	0.083264	0.009173	7.749E-07	0.083384
0.114378	0.031988	0.006	0.083264	0.009173		0.083384
0.114102	0.031974	0.126	0.083096	0.009173		0.083238
0.114027	0.031947	0.083	0.082927	0.009173		0.08314
0.113768	0.03192	0.005	0.082759	0.009012		0.082799
0.113601	0.031893	1.152	0.082759	0.008851		0.082604
0.113275	0.031866	0.008	0.082759	0.00869		0.082312
0.113042	0.031839	0.334	0.08259	0.00869		0.082263
0.11295	0.031825	0.009	0.082421	0.00869		0.081873
0.112941	0.031825	0.026	0.082253	0.00869		0.081435
0.112841	0.031771	0.071	0.081747	0.008529		0.081288
0.112833	0.031771	0.065	0.081747	0.008529		0.081093
0.112816	0.031717	0.01	0.081747	0.008368		0.080898
0.112549	0.03169	0.039	0.081579	0.008368		0.08085
0.112415	0.031636	0.009	0.08141	0.008368		0.080655
0.11214	0.031568	0.005	0.081073	0.008368		0.080655
0.112098	0.031459	0.084	0.081073	0.008368		0.080509
0.111906	0.031419	0.009	0.081073	0.008368		0.080509
0.111772	0.031419	0.212	0.080736	0.008208		0.080411
0.111755	0.031392	0.012	0.080567	0.007886		0.080021
0.111547	0.031351	0.009	0.080399	0.007886		0.079826
0.111271	0.03131	0.019	0.080399	0.007886		0.079778
0.111095	0.031188	0.118	0.080399	0.007886		0.079485
0.111045	0.031053	0.016	0.080399	0.007886		0.079436
0.110895	0.030999	0.018	0.080062	0.007725		0.079388
0.110544	0.030958	0.026	0.080062	0.007725		0.079242
0.110502	0.030931	0.094	0.079893	0.007725		0.078949
0.110419	0.030904	0.018	0.079725	0.007564		0.0789
0.11036	0.030877	0.041	0.079725	0.007564		0.078462
0.110252	0.0307	0.061	0.079556	0.007403		0.078462
0.110218	0.03066	0.008	0.079556	0.007403		0.078413
0.110001	0.030619	0.009	0.079556	0.007403		0.078316
0.109609	0.030605	0.002	0.079388	0.007242		0.078267
0.109225	0.030429	0.042	0.079219	0.007242		0.078169
0.109183	0.030416	0.035	0.079219	0.007081		0.078072
0.109141	0.030416	0.018	0.07905	0.007081		0.077877
0.108949	0.030348	0.012	0.07905	0.007081		0.07778
0.108632	0.030307	0.306	0.078882	0.00692		0.07778
0.108623	0.030294	0.082	0.078713	0.00692		0.077
0.108523	0.030212	0.013	0.078376	0.006598		0.076902
0.108498	0.030158	0.004	0.078376	0.006598		0.076707
0.108306	0.030063	0.013	0.078208	0.006437		0.076659
0.108289	0.030036	0.003	0.078208	0.006437		0.076659
0.108013	0.030036	0.08	0.078039	0.006115		0.07661
0.107988	0.029996	0.037	0.077871	0.005794		0.07661
0.107913	0.029996	0.003	0.077702	0.005794		0.076512
0.107654	0.029968	0.047	0.077534	0.005472		0.076171
0.107521	0.029968	0.032	0.077365	0.005472		0.076171
0.107203	0.029914	0.066	0.077028	0.005472		0.076171
0.107103	0.029914	0.013	0.077028	0.005472		0.075928
0.106978	0.02986	0.175	0.077028	0.005472		0.075879
0.106978	0.029806	0.006	0.077028	0.005311		0.07583
0.106969	0.029724	0.13	0.076859	0.005311		0.07583
0.106861	0.029562	0.282	0.076859	0.004989		0.075733
0.10671	0.029508	0.003	0.076691	0.004828		0.075684
0.10656	0.029467	0.008	0.076691	0.004828		0.075635
0.106518	0.029399	0.022	0.076522	0.004828		0.075538
0.106126	0.029277	0.046	0.076354	0.004828		0.075489
0.106076	0.029196	0.027	0.076354	0.004828		0.075489
0.106059	0.029169	0.071	0.076185	0.004667		0.075489
0.106034	0.029155	0.014	0.076017	0.004667		0.07544
0.106017	0.029114	0.058	0.076017	0.004667		0.07544
0.105466	0.029114	0.053	0.076017	0.004506		0.075343
0.105391	0.029087	0.039	0.075848	0.004506		0.075148
0.105182	0.029074	0.041	0.075679	0.004023		0.074709
0.104823	0.02906	0.026	0.075511	0.003701		0.074709
0.104739	0.02906	0.008	0.075342	0.003701		0.074563
0.104723	0.028938	0.023	0.075174	0.003701		0.074417
0.104338	0.028925	0.056	0.074837	0.003701		0.074417
0.104138	0.028735	0.005	0.074668	0.003701		0.074222
0.103912	0.028681	0.007	0.074668	0.00354		0.074222
0.103879	0.028627	0.039	0.074668	0.003058		0.074173
0.103812	0.028613	0.046	0.0745	0.002897		0.074076
0.103637	0.028518	0.05	0.0745	0.002736		0.073881
0.10362	0.028505	0.009	0.074331	0.002575		0.073832
0.103486	0.028505	0.042	0.073994	0.002414		0.073637
0.103152	0.028437	0.007	0.073825	0.002092		0.073588
0.103077	0.028437	0.014	0.073657			0.073442
0.102776	0.028396	0.057	0.073488			0.073345
0.102509	0.028342	0.131	0.07332			0.073345
0.102342	0.028288	0.038	0.07332			0.073345
0.101824	0.028233	0.022	0.07332			0.073296
0.101691	0.028206	0.162	0.073151			0.072809
0.101607	0.028044	0.015	0.073151			0.072614
0.101549	0.027908	0.198	0.073151			0.072565
0.101474	0.027773	0.074	0.072983			0.072565
0.101448	0.027746	0.027	0.072983			0.072565
0.10139	0.027732	0.014	0.072814			0.072516

0.034	0.035763	0.064091	0.036885	0.049492	0.045752	
0.034	0.035742	0.06402	0.036847	0.049471	0.045106	
0.034	0.035572	0.063809	0.036696	0.04944	0.045086	
0.034	0.035521	0.063598	0.036658	0.049245	0.045067	
0.034	0.03532	0.063598	0.03662	0.049183	0.044874	
0.034	0.03532	0.063386	0.036394	0.04908	0.044518	
0.034	0.034969	0.063245	0.035977	0.048987	0.04445	
0.034	0.034959	0.063034	0.035977	0.048555	0.044354	
0.034	0.034949	0.062964	0.035902	0.048503	0.044248	
0.034	0.034838	0.062893	0.035902	0.048483	0.043968	
0.033	0.034657	0.062823	0.035902	0.048359	0.043881	
0.033	0.034527	0.062823	0.035864	0.048205	0.043765	
0.033	0.034426	0.062752	0.035826	0.048163	0.043669	
0.033	0.034255	0.062752	0.035788	0.048153	0.043563	
0.033	0.034095	0.062682	0.035788	0.048133	0.043544	
0.033	0.034095	0.062682	0.03575	0.047927	0.043438	
0.033	0.034044	0.0624	0.035599	0.047473	0.043409	
0.033	0.033833	0.06233	0.035486	0.047473	0.043332	
0.033	0.033743	0.06233	0.035296	0.047288	0.043303	
0.033	0.033552	0.062189	0.035259	0.047144	0.043062	
0.033	0.033321	0.061978	0.035259	0.046722	0.043042	
0.033	0.033311	0.061696	0.035221	0.04665	0.042869	
0.033	0.03323	0.061626	0.035183	0.046485	0.042734	
0.033	0.03322	0.061485	0.034994	0.046094	0.042493	
0.033	0.03312	0.061273	0.034956	0.045949	0.042396	
0.033	0.033039	0.061273	0.034842	0.045929	0.042136	
0.033	0.032738	0.061062	0.034691	0.04527	0.04202	
0.033	0.032718	0.060992	0.034426	0.045218	0.041702	
0.033	0.032718	0.060921	0.034351	0.045187	0.041702	
0.033	0.032708	0.060851	0.034351	0.045156	0.041702	
0.033	0.032668	0.060851	0.034199	0.044992	0.041692	
0.033	0.032648	0.06071	0.034161	0.044961	0.041654	
0.033	0.032648	0.06064	0.034086	0.044961	0.041586	
0.033	0.032607	0.060569	0.034048	0.044786	0.041577	
0.032	0.032416	0.060569	0.03401	0.044683	0.041538	
0.032	0.032336	0.060358	0.033972	0.044374	0.041374	
0.032	0.032306	0.060358	0.033821	0.044003	0.041336	
0.032	0.032225	0.060287	0.033783	0.043931	0.041287	
0.032	0.031984	0.060217	0.033745	0.043704	0.041259	
0.032	0.031984	0.060147	0.033632	0.043612	0.04122	
0.032	0.031954	0.060076	0.033518	0.043375	0.041046	
0.032	0.031844	0.060006	0.033518	0.043179	0.041027	
0.032	0.031834	0.059865	0.033367	0.043045	0.041027	
0.032	0.031803	0.059865	0.033367	0.042953	0.040699	
0.032	0.031572	0.059724	0.033254	0.042942	0.04067	
0.032	0.031512	0.059513	0.033178	0.042757	0.040593	
0.032	0.031331	0.059513	0.033102	0.042695	0.04042	
0.032	0.03117	0.059372	0.033027	0.042623	0.040371	
0.032	0.03116	0.059372	0.032989	0.042582	0.03988	
0.032	0.03112	0.05916	0.032989	0.042541	0.03987	
0.031	0.03111	0.05902	0.032875	0.04218	0.039677	
0.031	0.03107	0.058949	0.032837	0.04216	0.039369	
0.031	0.03106	0.058949	0.032762	0.041902	0.03934	
0.031	0.031	0.058879	0.03261	0.041841	0.039234	
0.031	0.030959	0.058879	0.032383	0.041707	0.039128	
0.031	0.030919	0.058879	0.03227	0.041665	0.038809	
0.031	0.030899	0.058738	0.032232	0.041583	0.0388	
0.031	0.030899	0.058527	0.032119	0.041254	0.03879	
0.031	0.030879	0.058386	0.032081	0.041202	0.038742	
0.031	0.030869	0.058386	0.032043	0.041192	0.038684	
0.031	0.030758	0.058245	0.032005	0.04112	0.038617	
0.031	0.030608	0.058174	0.031967	0.041089	0.038356	
0.031	0.030557	0.058034	0.031892	0.040687	0.038308	
0.03	0.030527	0.057963	0.031854	0.040419	0.038183	
0.03	0.030447	0.057963	0.031816	0.040244	0.038125	
0.03	0.030387	0.057963	0.03174	0.040162	0.037903	
0.03	0.030377	0.057752	0.031362	0.040121	0.037884	
0.03	0.030266	0.057752	0.031324	0.039688	0.037874	
0.03	0.029944	0.057752	0.031286	0.03939	0.037836	
0.03	0.029944	0.057752	0.031286	0.039215	0.037585	
0.03	0.029854	0.057681	0.031211	0.038823	0.037575	
0.03	0.029643	0.057541	0.031173	0.03871	0.037575	
0.03	0.029613	0.05747	0.031173	0.038607	0.037479	
0.03	0.029532	0.05747	0.031135	0.038463	0.037334	
0.03	0.029532	0.057259	0.031097	0.038411	0.037325	
0.03	0.029472	0.057188	0.031097	0.038411	0.037305	
0.03	0.029442	0.056836	0.031097	0.037866	0.037199	
0.03	0.029422	0.056766	0.030984	0.037824	0.037093	
0.03	0.029402	0.056555	0.030984	0.037804	0.037064	
0.03	0.029281	0.056484	0.030832	0.037608	0.036949	
0.03	0.029231	0.056343	0.030757	0.037248	0.03691	
0.03	0.029141	0.056273	0.030681	0.037176	0.03691	
0.03	0.02903	0.056202	0.030643	0.037103	0.036891	
0.03	0.02901	0.055921	0.030492	0.037011	0.036746	
0.03	0.02893	0.05578	0.030416	0.036867	0.036736	
0.03	0.028658	0.05578	0.030303	0.036867	0.036621	
0.029	0.028608	0.05578	0.030265	0.036815	0.036544	
0.029	0.028598	0.055639	0.030189	0.036743	0.036399	
0.029	0.028558	0.055569	0.030076	0.036712	0.036283	
0.029	0.028508	0.055498	0.030076	0.036599	0.036264	
0.029	0.028487	0.055428	0.03	0.036547	0.036081	
0.029	0.028377	0.055357	0.029962	0.036434	0.036042	
0.029	0.028357	0.055287	0.029887	0.036403	0.035975	
0.029	0.028206	0.055287	0.029811	0.036177	0.035907	
0.029	0.028136	0.055146	0.029773	0.036156	0.035869	
0.029	0.027985	0.055076	0.029773	0.036094	0.035801	
0.029	0.027945	0.054935	0.029735	0.036043	0.035734	
0.029	0.027905	0.054935	0.029622	0.03594	0.035695	
0.029	0.027794	0.054794	0.029622	0.035919	0.035685	
0.029	0.027744	0.054723	0.029622	0.035909	0.035685	
0.029	0.027724	0.054371	0.029584	0.035888	0.035676	
0.028	0.027523	0.05409	0.029584	0.035857	0.035387	
0.028	0.027513	0.053949	0.029546	0.035796	0.034953	
0.028	0.027473	0.053737	0.02947	0.035641	0.034837	
0.028	0.027463	0.053667	0.029433	0.03527	0.034702	
0.028	0.027412	0.053597	0.029433	0.035064	0.034644	
0.028	0.027101	0.053456	0.029395	0.034992	0.034615	
0.028	0.027101	0.053456	0.029281	0.034931	0.034393	
0.028	0.02697	0.053315	0.029092	0.034889	0.034384	
0.028	0.02691	0.053315	0.029092	0.03456	0.034374	
0.028	0.02691	0.053033	0.029016	0.034508	0.034326	
0.028	0.026819	0.052963	0.028979	0.034498	0.034316	
0.028	0.026799	0.052822	0.028941	0.034344	0.034201	
0.028	0.026669	0.052751	0.028941	0.034313	0.034094	

0.101206	0.027705	0.008	0.072646
0.100839	0.027678	0.027	0.072646
0.100563	0.02761	1.857	0.072477
0.100555	0.027596	0.021	0.072477
0.100271	0.027583	0.044	0.07214
0.100129	0.027583	0.009	0.07214
0.09997	0.027556	0.008	0.071971
0.099953	0.027556	0.021	0.071634
0.099728	0.027556	0.008	0.071634
0.099711	0.027529	0.069	0.071634
0.099043	0.027407	0.021	0.071634
0.098976	0.027352	0.013	0.071466
0.098918	0.027095	0.017	0.07096
0.098842	0.027014	0.014	0.07096
0.098826	0.027	0.007	0.07096
0.098642	0.026851	0.08	0.070791
0.098291	0.02681	0.009	0.070623
0.097924	0.026783	0.028	0.070454
0.097723	0.02677	0.018	0.070286
0.097698	0.026756	0.11	0.06978
0.097656	0.026756	0.535	0.06978
0.09759	0.026593	0.029	0.069443
0.097456	0.026485	0.01	0.069275
0.097139	0.026417	0.042	0.069106
0.097105	0.026404	0.081	0.068937
0.097097	0.02639	0.03	0.068769
0.097047	0.026322	0.014	0.0686
0.096905	0.026295	0.045	0.068432
0.096896	0.026282	0.021	0.068432
0.096738	0.026227	0.068	0.068432
0.096629	0.026214	0.027	0.068432
0.096537	0.026065	0.027	0.068263
0.096521	0.026038	0.023	0.068263
0.096512	0.025929	0.037	0.068263
0.096312	0.025861	0.024	0.068095
0.096262	0.025834	0.01	0.067758
0.096161	0.025821	0.019	0.067589
0.096136	0.025753	0.01	0.067589
0.095861	0.025739	0.083	0.067252
0.095852	0.025726	0.089	0.067252
0.095368	0.025712	0.109	0.067083
0.094992	0.025699	0.079	0.067083
0.094984	0.025685	0.004	0.066915
0.094808	0.025685	0.082	0.066915
0.094733	0.025672	0.02	0.066915
0.094683	0.025631	0.154	0.066746
0.094533	0.02559	0.052	0.066746
0.094148	0.025563	0.012	0.066746
0.094115	0.02555	0.028	0.066746
0.09389	0.02555	0.012	0.066241
0.093397	0.025496	0.006	0.066072
0.093305	0.025455	0.017	0.066072
0.09323	0.025455	0.007	0.066072
0.093021	0.025387	0.028	0.065735
0.092937	0.025279	0.01	0.065735
0.092896	0.025211	0.029	0.065735
0.09282	0.025157	0.009	0.065735
0.092687	0.025143	0.012	0.065566
0.092461	0.025008	0.054	0.065566
0.092436	0.024994	0.162	0.065566
0.092161	0.02498	0.045	0.065566
0.092144	0.024967	0.032	0.065229
0.092035	0.024953	0.024	0.065229
0.09191	0.024791	0.19	0.065061
0.091593	0.024736	0.012	0.065061
0.090908	0.024642	0.141	0.064892
0.090749	0.024628	0.065	0.064892
0.090716	0.024628	0.004	0.064892
0.09039	0.024601	0.005	0.064724
0.090331	0.02456	0.096	0.064724
0.090298	0.024492	0.124	0.064555
0.090214	0.024492	0.131	0.064555
0.090189	0.024479	0.087	0.064555
0.090081	0.024452	0.045	0.064387
0.090031	0.024425	0.006	0.064218
0.089655	0.024411	0.008	0.064049
0.089488	0.024235	0.007	0.064049
0.089346	0.024208	0.008	0.064049
0.088937	0.024127	0.005	0.064049
0.08892	0.02395	0.021	0.063881
0.088469	0.02391	0.007	0.063712
0.088318	0.023883	0.009	0.063544
0.088285	0.023869	0.004	0.063038
0.087817	0.023815	0.307	0.063038
0.087709	0.023761	0.005	0.06287
0.087533	0.023761	0.035	0.062532
0.087249	0.023639	0.064	0.062195
0.087157	0.023598	0.023	0.062027
0.086974	0.023571	0.021	0.061858
0.08689	0.02353	0.033	0.06169
0.086848	0.023408	0.025	0.06169
0.086523	0.023367	0.008	0.061521
0.086448	0.023367	0.202	0.061353
0.086439	0.02334	0.085	0.061184
0.086322	0.02334	0.026	0.061184
0.086297	0.023273	0.147	0.061184
0.08628	0.023137	0.062	0.061016
0.08628	0.023042	0.014	0.060847
0.086138	0.02288	0.004	0.06051
0.086088	0.02288	0.148	0.06051
0.085955	0.022785	0.016	0.06051
0.085838	0.022785	0.024	0.060341
0.085821	0.022758	0.023	0.060173
0.085712	0.02273	0.02	0.060173
0.085696	0.022717	0.133	0.060004
0.085687	0.02269	0.062	0.060004
0.085671	0.022622	0.01	0.060004
0.085604	0.022608	0.026	0.060004
0.085579	0.022554	0.03	0.059836
0.08552	0.022432	0.032	0.059836
0.085512	0.022324	0.228	0.059499
0.085445	0.022324	0.026	0.059499
0.085429	0.022324	0.011	0.059499
0.085186	0.022256	0.005	0.05933

0.072467
0.072273
0.072126
0.071298
0.0712
0.070908
0.070421
0.070177
0.070128
0.070128
0.07008
0.070031
0.069982
0.069885
0.069787
0.06969
0.069641
0.069641
0.069202
0.069105
0.069105
0.069105
0.069056
0.068959
0.068812
0.068764
0.068715
0.068715
0.068569
0.068471
0.068471
0.068325
0.068228
0.068179
0.06813
0.068081
0.068033
0.068033
0.067984
0.067935
0.067935
0.06774
0.067643
0.06735
0.067302
0.067253
0.067253
0.067009
0.067009
0.066719
0.066619
0.066571
0.066522
0.066522
0.065986
0.065888
0.065645
0.065645
0.065547
0.065401
0.065255
0.065157
0.065157
0.064865
0.064816
0.064768
0.064621
0.064426
0.064426
0.064378
0.064183
0.064037
0.063939
0.063793
0.063695
0.063695
0.063647
0.063647
0.063549
0.063452
0.063257
0.063208
0.063111
0.062672
0.062428
0.062428
0.06238
0.06238
0.062233
0.062087
0.06199
0.061892
0.061649
0.061454
0.061454
0.061259
0.061161
0.061015
0.060966
0.060869
0.060869
0.060869
0.060771
0.060771
0.060723
0.060674
0.060576
0.060528
0.060479
0.06043
0.060333
0.060235
0.060138
0.060138

0.028	0.026649	0.052681	0.028903	0.034282	0.034046
0.028	0.026528	0.052329	0.028865	0.034179	0.034017
0.028	0.026528	0.052258	0.028714	0.034024	0.033969
0.027	0.026407	0.052258	0.028714	0.033993	0.033931
0.027	0.026377	0.052047	0.0286	0.03388	0.033921
0.027	0.026347	0.051906	0.0286	0.033726	0.033824
0.027	0.026277	0.051836	0.0286	0.033674	0.033786
0.027	0.026257	0.051836	0.028525	0.033561	0.033757
0.027	0.026227	0.051695	0.028487	0.033479	0.03369
0.027	0.026156	0.051625	0.028449	0.033417	0.03367
0.027	0.026146	0.051484	0.028411	0.033407	0.033448
0.027	0.026026	0.051272	0.028335	0.033396	0.033227
0.027	0.026016	0.051202	0.028184	0.033396	0.033121
0.027	0.025905	0.051202	0.028146	0.033365	0.033111
0.027	0.025845	0.051132	0.028108	0.033283	0.032928
0.027	0.025784	0.051132	0.027919	0.033273	0.032889
0.027	0.025684	0.051132	0.027919	0.033118	0.03288
0.027	0.025674	0.051061	0.027919	0.033118	0.032841
0.027	0.025543	0.05085	0.027882	0.033056	0.032793
0.027	0.025473	0.050709	0.027882	0.033036	0.032774
0.027	0.025443	0.050639	0.027882	0.032974	0.032745
0.027	0.025332	0.050568	0.027806	0.032789	0.032667
0.027	0.025232	0.050568	0.027692	0.032562	0.032523
0.027	0.025182	0.050498	0.027655	0.032366	0.032484
0.027	0.025131	0.050498	0.027541	0.032263	0.032378
0.027	0.025021	0.050286	0.02739	0.032191	0.032349
0.027	0.02484	0.050075	0.027352	0.032088	0.032301
0.026	0.02481	0.050005	0.027352	0.031985	0.032195
0.026	0.024759	0.049934	0.027276	0.031954	0.032176
0.026	0.024749	0.049934	0.027163	0.031924	0.032166
0.026	0.024699	0.049864	0.027163	0.03181	0.032147
0.026	0.024659	0.049864	0.027125	0.031718	0.032012
0.026	0.024649	0.049793	0.027087	0.031718	0.031964
0.026	0.024639	0.049723	0.027049	0.031512	0.031751
0.026	0.024579	0.049653	0.027049	0.031378	0.031549
0.026	0.024528	0.049512	0.027011	0.031368	0.031414
0.026	0.024498	0.049441	0.027011	0.031295	0.03124
0.026	0.024398	0.049371	0.026974	0.031295	0.031192
0.026	0.024388	0.049371	0.026822	0.030925	0.031144
0.026	0.024368	0.04923	0.026784	0.030791	0.031134
0.026	0.024136	0.048948	0.026784	0.030739	0.031067
0.026	0.023986	0.048878	0.026747	0.030719	0.030874
0.026	0.023956	0.048807	0.026747	0.030657	0.030537
0.026	0.023946	0.048667	0.026709	0.030636	0.030392
0.026	0.023815	0.048667	0.026709	0.030626	0.030392
0.026	0.023735	0.048596	0.026671	0.0304	0.030373
0.026	0.023654	0.048596	0.026633	0.030297	0.030276
0.026	0.023624	0.048526	0.026444	0.030286	0.030247
0.026	0.023594	0.048526	0.026444	0.030266	0.03016
0.025	0.023483	0.048455	0.026406	0.030194	0.03016
0.025	0.023433	0.048455	0.026406	0.030152	0.030112
0.025	0.023403	0.048385	0.026406	0.030132	0.030016
0.025	0.023363	0.048385	0.026368	0.030091	0.029804
0.025	0.023302	0.048244	0.026293	0.029905	0.029756
0.025	0.023292	0.048244	0.026293	0.029833	0.029746
0.025	0.023262	0.048174	0.026255	0.029802	0.029707
0.025	0.023192	0.048174	0.026141	0.029689	0.029698
0.025	0.023132	0.048103	0.026141	0.029679	0.029678
0.025	0.023091	0.047962	0.026066	0.029668	0.02963
0.025	0.023081	0.047892	0.026066	0.029555	0.029621
0.025	0.023061	0.047892	0.026028	0.029504	0.029601
0.025	0.022951	0.047892	0.026028	0.029411	0.029524
0.025	0.022931	0.047821	0.025952	0.029184	0.029187
0.025	0.02284	0.04761	0.025914	0.029184	0.029148
0.025	0.0228	0.04761	0.025763	0.028886	0.02909
0.025	0.02276	0.04754	0.025725	0.028721	0.028705
0.025	0.02272	0.047399	0.025649	0.028618	0.028695
0.025	0.02272	0.047328	0.025612	0.028422	0.028676
0.025	0.022649	0.047258	0.025536	0.028391	0.02856
0.025	0.022629	0.047188	0.025536	0.028247	0.028531
0.025	0.022428	0.047047	0.025536	0.028144	0.028444
0.025	0.022378	0.046976	0.025498	0.028124	0.028338
0.025	0.022378	0.046976	0.02546	0.028072	0.02829
0.025	0.022288	0.046835	0.025422	0.027918	0.028261
0.025	0.022257	0.046835	0.025385	0.027835	0.028261
0.025	0.022117	0.046835	0.025309	0.027619	0.028242
0.025	0.022066	0.046765	0.025309	0.027609	0.028184
0.025	0.021946	0.046765	0.025309	0.027578	0.028126
0.024	0.021916	0.046765	0.025271	0.027537	0.02801
0.024	0.021916	0.046765	0.02512	0.027485	0.027904
0.024	0.021896	0.046765	0.02512	0.027485	0.027827
0.024	0.021845	0.046624	0.025044	0.027434	0.02775
0.024	0.021845	0.046624	0.025044	0.027403	0.027692
0.024	0.021845	0.046554	0.025044	0.02731	0.027634
0.024	0.021805	0.046554	0.025044	0.027073	0.027596
0.024	0.021725	0.046483	0.025006	0.027032	0.027528
0.024	0.021634	0.046413	0.024931	0.026723	0.027509
0.024	0.021393	0.046342	0.024931	0.026682	0.027364
0.024	0.021363	0.046272	0.024855	0.02663	0.027326
0.024	0.021283	0.046202	0.024855	0.026569	0.027297
0.024	0.021273	0.046131	0.024855	0.026558	0.027287
0.024	0.021253	0.046131	0.024628	0.026208	0.027258
0.024	0.021232	0.046061	0.024628	0.026105	0.027075
0.024	0.021202	0.04599	0.024628	0.025992	0.027075
0.024	0.021142	0.04592	0.02459	0.025982	0.027056
0.024	0.021122	0.045779	0.024552	0.025879	0.027027
0.023	0.021021	0.045709	0.024401	0.025838	0.027008
0.023	0.020981	0.045709	0.024363	0.025642	0.026988
0.023	0.020941	0.045568	0.024288	0.02557	0.026631
0.023	0.020931	0.045497	0.024212	0.025498	0.026583
0.023	0.020901	0.045427	0.024174	0.025456	0.026506
0.023	0.020841	0.045427	0.024098	0.025456	0.026496
0.023	0.02082	0.045356	0.024061	0.025405	0.026458
0.023	0.02073	0.045286	0.023985	0.025354	0.02641
0.023	0.02066	0.045286	0.023947	0.02524	0.026275
0.023	0.02064	0.045286	0.023947	0.02523	0.026217
0.023	0.020609	0.045145	0.023947	0.025209	0.026092
0.023	0.020609	0.044863	0.023909	0.025158	0.026072
0.023	0.020569	0.044863	0.023909	0.024859	0.026053
0.023	0.020549	0.044793	0.023871	0.024839	0.025985
0.023	0.020479	0.044723	0.023796	0.024818	0.025966
0.023	0.020459	0.044723	0.023796	0.024818	0.025966
0.023	0.020439	0.044652	0.023796	0.024808	0.025957
0.023	0.020378	0.044652	0.023796	0.024797	0.025899

0.085153	0.022256	0.028	0.05933
0.085078	0.022215	0.072	0.05933
0.084927	0.022202	0.031	0.059161
0.084852	0.022202	0.049	0.059161
0.084802	0.022175	0.009	0.058993
0.084802	0.022134	0.155	0.058993
0.084777	0.022107	0.19	0.058993
0.084593	0.022107	0.019	0.058487
0.084468	0.022107	0.032	0.058319
0.084334	0.022053	0.245	0.058319
0.084251	0.022039	0.126	0.05815
0.084167	0.022026	0.007	0.05815
0.083925	0.021958	0.007	0.05815
0.083783	0.021931	0.106	0.057982
0.083725	0.021836	0.056	0.057982
0.083407	0.021687	0.044	0.057982
0.083407	0.021646	0.011	0.057644
0.083365	0.021565	0.045	0.057644
0.083207	0.021538	0.087	0.057307
0.083173	0.021511	0.021	0.057307
0.082856	0.021511	0.053	0.057139
0.082756	0.021416	0.308	0.057139
0.082589	0.021402	0.199	0.057139
0.082564	0.021199	0.195	0.05697
0.082472	0.021172	0.041	0.05697
0.082346	0.021145	0.011	0.056802
0.082313	0.021023	0.197	0.056802
0.082313	0.020995	0.024	0.056802
0.082313	0.020982	0.01	0.056802
0.082079	0.020982	0.007	0.056633
0.081954	0.020968	0.008	0.056633
0.081787	0.020955	0.021	0.056633
0.081453	0.020928	0.023	0.056633
0.081411	0.020914	0.025	0.056296
0.081277	0.020901	0.009	0.056296
0.081252	0.020887	0.007	0.056296
0.081102	0.020846	0.025	0.056128
0.080952	0.020792	0.049	0.056128
0.080768	0.020792	0.007	0.056128
0.080659	0.020779	0.035	0.056128
0.080542	0.020752	0.019	0.055959
0.0803	0.020752	0.007	0.05579
0.080275	0.020752	0.009	0.055622
0.080233	0.020738	0.04	0.055622
0.080192	0.020711	0.01	0.055622
0.0801	0.020657	0.025	0.055622
0.080091	0.020657	0.265	0.055453
0.079966	0.020657	0.273	0.055285
0.079857	0.020575	0.058	0.055116
0.079849	0.020575	0.033	0.055116
0.079816	0.020548	0.012	0.055116
0.079715	0.020399	0.009	0.054948
0.079699	0.020196	0.046	0.054948
0.07964	0.020196	0.008	0.054948
0.07949	0.020182	0.025	0.054948
0.079373	0.020128	0.037	0.054779
0.079289	0.020128	0.034	0.054611
0.079281	0.020114	0.012	0.054611
0.079214	0.020114	0.008	0.054611
0.079214	0.020006	0.049	0.054442
0.079206	0.019938	0.003	0.054442
0.07898	0.019938	0.082	0.054442
0.078939	0.019911	0.004	0.054273
0.078897	0.019898	0.014	0.054273
0.078747	0.019884	0.008	0.054105
0.07873	0.019884	0.006	0.054105
0.07868	0.019816	1.078	0.054105
0.078605	0.019816	0.033	0.054105
0.078454	0.019762	0.014	0.054105
0.078387	0.019762	0.008	0.053936
0.078112	0.019572	0.019	0.053936
0.078053	0.019559	0.035	0.053936
0.077828	0.019437	0.019	0.053768
0.077786	0.019315	0.067	0.053599
0.077778	0.019301	0.009	0.053599
0.077677	0.019247	0.441	0.053599
0.077652	0.019247	1.733	0.053431
0.077251	0.01922	0.344	0.053431
0.077084	0.019139	0.024	0.053262
0.076993	0.019071	0.733	0.053262
0.076884	0.018989	0.056	0.053262
0.076867	0.018976	0.079	0.053094
0.076859	0.018949	0.023	0.053094
0.076809	0.0188	0.006	0.052925
0.076792	0.018732	0.003	0.052925
0.076667	0.018718	0.008	0.052925
0.076533	0.018691	0.004	0.052925
0.076508	0.018678	0.01	0.052756
0.076283	0.01861	0.087	0.052756
0.076174	0.018596	0.096	0.052588
0.076065	0.018502	0.039	0.052588
0.075965	0.018488	0.016	0.052251
0.075765	0.018488	0.009	0.052251
0.07574	0.018474	0.138	0.052251
0.07569	0.01842	0.003	0.052251
0.075406	0.018407	0.029	0.052082
0.075389	0.018393	0.011	0.052082
0.075297	0.018393	0.171	0.052082
0.075264	0.018325	0.006	0.052082
0.075247	0.018258	0.004	0.051914
0.075097	0.018258	0.058	0.051914
0.075046	0.018258	0.005	0.051745
0.075038	0.018244	0.006	0.051745
0.074788	0.018244	0.272	0.051577
0.074729	0.01823	0.005	0.051577
0.074487	0.018203	0.044	0.051408
0.074487	0.018163	0.072	0.051408
0.074337	0.018149	0.194	0.05124
0.074278	0.018136	0.026	0.051071
0.07422	0.018122	0.293	0.050902
0.074036	0.018068	0.005	0.050902
0.074027	0.018041	0.015	0.050902
0.073986	0.018027	0.034	0.050734
0.073969	0.018014	0.018	0.050734

0.059894	0.022	0.020358	0.044582	0.02372	0.024664	0.025831
0.059845	0.022	0.020328	0.044582	0.02372	0.024571	0.025764
0.059699	0.022	0.020197	0.044441	0.023682	0.024499	0.025754
0.059504	0.022	0.020197	0.044441	0.023682	0.024499	0.025706
0.059504	0.022	0.020137	0.0443	0.023607	0.024283	0.025609
0.059212	0.022	0.020077	0.044159	0.023531	0.024272	0.02558
0.059114	0.022	0.019996	0.044159	0.023493	0.024231	0.025474
0.059017	0.022	0.019976	0.044089	0.023493	0.02419	0.025446
0.058968	0.022	0.019976	0.044089	0.023455	0.024159	0.025407
0.058968	0.022	0.019966	0.044018	0.023417	0.024077	0.025368
0.058773	0.022	0.019946	0.043807	0.023342	0.024025	0.025359
0.058627	0.022	0.019936	0.043737	0.023342	0.024015	0.025349
0.05853	0.022	0.019926	0.043596	0.023304	0.023881	0.025079
0.05853	0.022	0.019896	0.043525	0.023266	0.023799	0.025041
0.058335	0.022	0.019886	0.043525	0.023266	0.023706	0.024992
0.058335	0.022	0.019866	0.043525	0.023228	0.023572	0.024954
0.057652	0.022	0.019846	0.043314	0.023228	0.02352	0.024954
0.057604	0.022	0.019846	0.043314	0.023153	0.023438	0.024934
0.057555	0.022	0.019846	0.043244	0.023153	0.02315	0.024925
0.057506	0.022	0.019826	0.043244	0.023153	0.023139	0.024896
0.057457	0.022	0.019826	0.043103	0.023077	0.023119	0.024857
0.05736	0.021	0.019816	0.043103	0.023077	0.023067	0.024713
0.05736	0.021	0.019806	0.043103	0.022963	0.022944	0.024703
0.057311	0.021	0.019775	0.042891	0.022926	0.022872	0.024693
0.057214	0.021	0.019755	0.04261	0.022888	0.02282	0.024626
0.057214	0.021	0.019675	0.04261	0.022888	0.022728	0.024616
0.057116	0.021	0.019655	0.042469	0.022888	0.022707	0.024578
0.057019	0.021	0.019635	0.042257	0.02285	0.022666	0.02451
0.056921	0.021	0.019584	0.042257	0.022812	0.022645	0.024472
0.056873	0.021	0.019534	0.042187	0.022774	0.022625	0.024462
0.056824	0.021	0.019434	0.042187	0.022396	0.022614	0.024443
0.056726	0.021	0.019373	0.041905	0.022396	0.022594	0.024395
0.056726	0.021	0.019283	0.041764	0.022358	0.022573	0.024366
0.056678	0.021	0.019283	0.041624	0.02232	0.022522	0.024327
0.056483	0.021	0.019263	0.041624	0.022283	0.022522	0.024231
0.056434	0.021	0.019243	0.041412	0.022207	0.02247	0.024211
0.056385	0.021	0.019213	0.041412	0.022169	0.022429	0.024067
0.056288	0.021	0.019203	0.041342	0.022169	0.022388	0.024047
0.056142	0.021	0.019173	0.041271	0.022131	0.022367	0.024047
0.056142	0.021	0.019162	0.041271	0.022056	0.022326	0.024038
0.056142	0.021	0.019082	0.041271	0.022018	0.02211	0.023961
0.055995	0.021	0.019072	0.041131	0.02198	0.021986	0.023922
0.055995	0.021	0.019072	0.041131	0.021904	0.021749	0.023845
0.055947	0.021	0.019002	0.041131	0.021753	0.021687	0.023787
0.055654	0.021	0.018982	0.041131	0.021715	0.021687	0.0237
0.055411	0.021	0.018972	0.04099	0.021639	0.021677	0.023507
0.055313	0.021	0.018921	0.040919	0.021639	0.02144	0.023411
0.055167	0.021	0.018901	0.040849	0.021639	0.021337	0.023286
0.054972	0.021	0.018851	0.040849	0.021639	0.021276	0.02317
0.054923	0.021	0.018851	0.040778	0.021602	0.021203	0.02317
0.054923	0.021	0.018841	0.040778	0.021602	0.021173	0.023035
0.054875	0.021	0.018841	0.040567	0.021564	0.021173	0.022987
0.054826	0.021	0.018841	0.040426	0.021526	0.021152	0.022929
0.054777	0.021	0.01874	0.040426	0.021526	0.02107	0.0229
0.054728	0.021	0.01871	0.040145	0.021412	0.021059	0.022881
0.054582	0.02	0.01865	0.040145	0.021412	0.021049	0.022861
0.054533	0.02	0.01864	0.040004	0.021375	0.021008	0.022852
0.054387	0.02	0.0186	0.039792	0.021375	0.020977	0.022832
0.054387	0.02	0.018519	0.039652	0.021261	0.020895	0.022813
0.054338	0.02	0.018519	0.039652	0.021223	0.020874	0.022688
0.054241	0.02	0.018459	0.039581	0.021185	0.02075	0.02264
0.054046	0.02	0.018459	0.039581	0.021185	0.020699	0.02262
0.053997	0.02	0.018409	0.039581	0.02111	0.020483	0.02262
0.053949	0.02	0.018399	0.03944	0.021034	0.020483	0.022601
0.053851	0.02	0.018389	0.03937	0.021034	0.020431	0.022601
0.053705	0.02	0.018379	0.03937	0.020996	0.020349	0.022601
0.053705	0.02	0.018379	0.039299	0.020958	0.020328	0.022601
0.053705	0.02	0.018328	0.039299	0.020958	0.020287	0.022591
0.053656	0.02	0.018318	0.039299	0.020958	0.020112	0.022582
0.053412	0.02	0.018268	0.039229	0.020921	0.019762	0.022485
0.053364	0.02	0.018158	0.039088	0.020845	0.019751	0.022476
0.053364	0.02	0.018127	0.038877	0.020845	0.019731	0.022408
0.053364	0.02	0.018107	0.038666	0.020769	0.01971	0.022408
0.053218	0.02	0.018087	0.038595	0.020769	0.019669	0.022379
0.053169	0.02	0.018017	0.038595	0.020769	0.019494	0.02236
0.053071	0.02	0.017987	0.038454	0.02058	0.019412	0.022341
0.053071	0.02	0.017947	0.038384	0.02058	0.019381	0.022331
0.052974	0.02	0.017937	0.038384	0.020504	0.019247	0.022312
0.052974	0.02	0.017876	0.038384	0.020467	0.019226	0.022196
0.052925	0.02	0.017876	0.038384	0.020467	0.019185	0.022177
0.052779	0.02	0.017736	0.038384	0.020353	0.019144	0.022167
0.052681	0.019	0.017695	0.038313	0.02024	0.019123	0.022148
0.052633	0.019	0.017575	0.038102	0.020202	0.019031	0.022129
0.052584	0.019	0.017545	0.038032	0.020164	0.01902	0.022061
0.052535	0.019	0.017535	0.037961	0.020164	0.018907	0.021994
0.052487	0.019	0.017454	0.037961	0.020126	0.018866	0.021965
0.052389	0.019	0.017404	0.037891	0.020126	0.018835	0.021945
0.052389	0.019	0.017394	0.03782	0.020126	0.018825	0.021945
0.052389	0.019	0.017394	0.03775	0.020088	0.018763	0.021916
0.052243	0.019	0.017273	0.03775	0.020088	0.018423	0.021897
0.052243	0.019	0.017253	0.03768	0.02005	0.018413	0.02181
0.052048	0.019	0.017233	0.037609	0.020013	0.018361	0.021743
0.05195	0.019	0.017032	0.037609	0.019975	0.018155	0.021714
0.05195	0.019	0.017022	0.037539	0.019975	0.018145	0.021695
0.051512	0.019	0.016892	0.037539	0.019975	0.018011	0.021685
0.051512	0.019	0.016881	0.037539	0.019861	0.018011	0.021618
0.051463	0.019	0.016801	0.037468	0.019823	0.018011	0.021598
0.051268	0.019	0.016781	0.037398	0.019786	0.017888	0.021502
0.051219	0.019	0.016691	0.037327	0.019786	0.017805	0.021492
0.051122	0.019	0.01666	0.037327	0.019786	0.017743	0.021444
0.051122	0.019	0.01665	0.037187	0.019786	0.017723	0.021348
0.050878	0.019	0.01662	0.037116	0.019748	0.017682	0.021261
0.050683	0.019	0.01656	0.037116	0.019748	0.017682	0.021222
0.050683	0.019	0.01655	0.036905	0.019672	0.01762	0.021213
0.050635	0.019	0.01655	0.036905	0.019672	0.017599	0.021174
0.050635	0.019	0.016299	0.036905	0.019597	0.017568	0.021174
0.050488	0.019	0.016289	0.036834	0.019597	0.017527	0.021155
0.050245	0.019	0.016279	0.036834	0.019559	0.017506	0.021135
0.050147	0.019	0.016228	0.036694	0.019521	0.017496	0.021078
0.050147	0.019	0.016148	0.036694	0.019445	0.017496	0.021058
0.050147	0.019	0.016088	0.036623	0.019407	0.017301	0.021049
0.050001	0.019	0.016057	0.036553	0.01937	0.017177	0.02102
0.049952	0.019	0.016047	0.036553	0.01937	0.017064	0.021
0.049611	0.019	0.015967	0.036482	0.01937	0.017002	0.020943

0.073927	0.017959	0.006	0.050734
0.073911	0.017959	0.031	0.050565
0.073468	0.017932	0.02	0.050397
0.073451	0.017892	0.005	0.050228
0.073384	0.017892	0.106	0.050228
0.073284	0.017878	0.002	0.050228
0.073209	0.01777	0.006	0.050228
0.073109	0.017742	0.01	0.05006
0.073025	0.017702	0.015	0.05006
0.072983	0.017648	1.073	0.05006
0.072975	0.01758	0.007	0.05006
0.072908	0.017539	0.05	0.049723
0.072875	0.017526	0.003	0.049723
0.0728	0.017512	0.035	0.049723
0.072758	0.017485	0.005	0.049385
0.072599	0.017485	0.008	0.049385
0.072557	0.017444	0.004	0.049217
0.072482	0.017404	0.023	0.049217
0.07239	0.017336	0.103	0.049048
0.072365	0.017336	0.042	0.049048
0.07224	0.017295	0.006	0.04888
0.072081	0.017282	0.023	0.04888
0.072065	0.017268	0.005	0.04888
0.071873	0.017255	0.009	0.04888
0.071772	0.017214	0.071	0.048711
0.071589	0.01716	0.006	0.048711
0.071447	0.017146	0.054	0.048711
0.07143	0.017133	0.004	0.048543
0.071388	0.017133	0.009	0.048543
0.071388	0.017038	0.079	0.048543
0.071238	0.016997	0.007	0.048543
0.071213	0.016997	0.033	0.048374
0.071129	0.016983	0.082	0.048374
0.071104	0.016956	0.039	0.048374
0.071037	0.016929	0.017	0.048374
0.070962	0.016929	0.009	0.048374
0.070962	0.016902	0.011	0.048206
0.070937	0.016848	0.333	0.048206
0.070887	0.016848	0.059	0.048206
0.07087	0.016848	0.004	0.048206
0.070812	0.016807	0.184	0.048037
0.070753	0.016767	0.132	0.048037
0.070661	0.016739	0.07	0.048037
0.070603	0.016699	0.021	0.048037
0.070545	0.016672	0.003	0.047869
0.070428	0.016672	0.053	0.0477
0.070336	0.016645	0.029	0.0477
0.070286	0.016645	0.027	0.047531
0.070286	0.016617	0.021	0.047531
0.070269	0.01659	0.018	0.047531
0.07021	0.016523	0.026	0.047531
0.07021	0.016495	0.009	0.047363
0.070185	0.016482	0.016	0.047363
0.07011	0.016468	0.023	0.047194
0.069993	0.016468	0.178	0.047026
0.06986	0.016374	0.015	0.047026
0.069617	0.01636	0.006	0.046857
0.069534	0.016333	0.014	0.04652
0.069484	0.016333	0.006	0.04652
0.069409	0.016319	0.008	0.046352
0.069375	0.016224	0.004	0.046352
0.069242	0.016197	0.004	0.046352
0.069208	0.016197	0.03	0.046352
0.068949	0.01617	0.025	0.046014
0.068932	0.016157	0.005	0.046014
0.068924	0.016143	0.013	0.046014
0.068749	0.01613	0.024	0.046014
0.068632	0.01613	0.006	0.046014
0.068573	0.016116	0.019	0.046014
0.068356	0.016062	0.053	0.046014
0.068339	0.016035	0.057	0.046014
0.068214	0.016008	0.012	0.045846
0.068005	0.015967	0.054	0.045846
0.067989	0.015913	0.005	0.045677
0.067964	0.015845	0.004	0.045509
0.067847	0.015804	0.076	0.045509
0.067813	0.015777	0.014	0.04534
0.06778	0.015601	0.016	0.04534
0.067663	0.015574	0.105	0.045172
0.067579	0.015547	0.013	0.045172
0.067337	0.015533	0.029	0.045172
0.06732	0.015533	0.004	0.045172
0.067262	0.015479	0.015	0.045172
0.067254	0.015479	0.027	0.045172
0.067237	0.015452	0.056	0.045003
0.06717	0.015425	0.002	0.045003
0.066861	0.015384	0.017	0.045003
0.066786	0.015357	0.031	0.045003
0.066786	0.01533	0.01	0.044666
0.066769	0.01533	0.428	0.044666
0.066636	0.015303	0.016	0.044666
0.066519	0.015276	0.037	0.044497
0.06651	0.015262	0.493	0.044497
0.066502	0.015235	0.009	0.044497
0.066452	0.015208	0.003	0.044497
0.066385	0.015208	0.008	0.044497
0.06631	0.015194	0.01	0.044329
0.066151	0.015154	0.038	0.04416
0.066059	0.015113	0.097	0.04416
0.065951	0.015086	0.387	0.04416
0.065834	0.015086	0.003	0.043992
0.065825	0.015086	0.01	0.043823
0.065817	0.015072	0.052	0.043823
0.065483	0.015045	0.053	0.043655
0.065441	0.015032	0.086	0.043655
0.065308	0.015032	0.002	0.043655
0.065291	0.015018	0.717	0.043655
0.065291	0.014991	0.13	0.043655
0.065224	0.014964	0.04	0.043318
0.065074	0.014883	0.118	0.043318
0.065032	0.014855	0.046	0.043149
0.065007	0.014761	0.021	0.043149
0.065007	0.014733	0.021	0.043149
0.064965	0.014706	0.006	0.042981

0.049611
0.049514
0.049465
0.049368
0.049368
0.049368
0.04927
0.049075
0.049026
0.048929
0.04888
0.048783
0.048734
0.048637
0.048637
0.048588
0.048588
0.048539
0.048442
0.048247
0.048052
0.048003
0.047759
0.047662
0.047662
0.047516
0.047516
0.047467
0.047467
0.047272
0.047175
0.047126
0.047126
0.047028
0.046882
0.046882
0.046833
0.046785
0.046736
0.046687
0.046687
0.04659
0.046541
0.046492
0.046395
0.046395
0.046395
0.0462
0.046151
0.046102
0.046054
0.046054
0.045907
0.045859
0.045859
0.045859
0.04581
0.045518
0.045469
0.045469
0.04542
0.045371
0.045274
0.045274
0.045176
0.045176
0.045176
0.045079
0.045079
0.04464
0.044592
0.044543
0.044543
0.044543
0.044494
0.044445
0.044299
0.04425
0.04425
0.04425
0.044153
0.043861
0.043861
0.043812
0.043812
0.043763
0.043714
0.043714
0.043714
0.043617
0.043617
0.043568
0.043568
0.043519
0.043276
0.043276
0.043178
0.043178
0.04313
0.04313
0.043081
0.043032
0.043032
0.042983
0.042837
0.042447
0.04235
0.042204
0.042204
0.042057
0.042057
0.042009
0.04196
0.041911

0.019	0.015887	0.036482	0.019218	0.016981	0.020817
0.019	0.015887	0.036341	0.019218	0.01694	0.020798
0.019	0.015776	0.036341	0.019218	0.01693	0.020769
0.018	0.015585	0.036271	0.01918	0.016889	0.02075
0.018	0.015535	0.036201	0.019143	0.016796	0.02075
0.018	0.015515	0.03613	0.019143	0.016621	0.020692
0.018	0.015515	0.03613	0.019105	0.016538	0.020644
0.018	0.015505	0.03606	0.019105	0.016497	0.020644
0.018	0.015475	0.035989	0.019105	0.016497	0.020538
0.018	0.015424	0.035989	0.019029	0.016425	0.02047
0.018	0.015274	0.035989	0.018953	0.016405	0.020461
0.018	0.015234	0.035989	0.018953	0.016363	0.020461
0.018	0.015213	0.035989	0.018953	0.016322	0.020461
0.018	0.015183	0.035989	0.018916	0.016302	0.020451
0.018	0.015173	0.035919	0.01884	0.01625	0.020441
0.018	0.015143	0.035848	0.018764	0.016219	0.020412
0.018	0.015083	0.035778	0.018726	0.016199	0.020374
0.018	0.015012	0.035778	0.018689	0.016168	0.020306
0.018	0.015002	0.035778	0.018651	0.016127	0.020287
0.018	0.014872	0.035637	0.018651	0.016085	0.020219
0.018	0.014811	0.035637	0.018651	0.016065	0.020094
0.018	0.014811	0.035567	0.018613	0.015952	0.020094
0.018	0.014751	0.035215	0.018537	0.01589	0.020027
0.018	0.014701	0.035215	0.018424	0.015776	0.019863
0.018	0.01459	0.034933	0.018386	0.015735	0.019843
0.018	0.01454	0.034862	0.018272	0.015643	0.019786
0.018	0.01449	0.034792	0.018272	0.015601	0.019737
0.018	0.01449	0.034722	0.018272	0.01554	0.019699
0.018	0.014279	0.034651	0.018235	0.015529	0.019689
0.018	0.014229	0.034651	0.018235	0.015509	0.01967
0.018	0.014188	0.034651	0.018197	0.015467	0.019651
0.018	0.014178	0.034651	0.018197	0.015416	0.019631
0.018	0.014178	0.034651	0.018197	0.015385	0.019545
0.018	0.014158	0.034651	0.018159	0.015323	0.019525
0.018	0.014138	0.034581	0.018159	0.015292	0.019438
0.018	0.014078	0.034581	0.018121	0.015262	0.019429
0.017	0.014068	0.03451	0.018045	0.01522	0.01939
0.017	0.014058	0.03451	0.018008	0.015138	0.019332
0.017	0.013967	0.03451	0.018008	0.015076	0.019275
0.017	0.013967	0.03444	0.01797	0.014644	0.019197
0.017	0.013937	0.03444	0.017894	0.014644	0.01914
0.017	0.013917	0.03444	0.017894	0.014623	0.019111
0.017	0.013897	0.03444	0.017856	0.014582	0.019082
0.017	0.013847	0.034369	0.017856	0.014499	0.019034
0.017	0.013837	0.034369	0.017856	0.014458	0.018985
0.017	0.013827	0.034299	0.017818	0.014397	0.018956
0.017	0.013756	0.034158	0.017781	0.014397	0.01886
0.017	0.013756	0.034088	0.017781	0.014376	0.01885
0.017	0.013736	0.034088	0.017705	0.014314	0.018841
0.017	0.013646	0.034088	0.017705	0.014314	0.018831
0.017	0.013646	0.034017	0.017667	0.01417	0.018821
0.017	0.013616	0.034017	0.017667	0.014005	0.018783
0.017	0.013555	0.033947	0.017629	0.013995	0.018744
0.017	0.013505	0.033806	0.017591	0.013851	0.018735
0.017	0.013485	0.033806	0.017554	0.01383	0.018706
0.017	0.013475	0.033736	0.017554	0.01381	0.018696
0.017	0.013475	0.033736	0.017554	0.013779	0.018686
0.017	0.013475	0.033736	0.017516	0.013707	0.018638
0.017	0.013465	0.033736	0.017516	0.013686	0.018619
0.017	0.013455	0.033665	0.017478	0.013624	0.018609
0.017	0.013445	0.033595	0.01744	0.013521	0.018522
0.017	0.013405	0.033524	0.01744	0.013459	0.018445
0.017	0.013405	0.033454	0.017289	0.013356	0.018397
0.017	0.013385	0.033454	0.017289	0.013326	0.018339
0.017	0.013364	0.033313	0.017251	0.013212	0.01831
0.017	0.013364	0.033313	0.017213	0.013192	0.018195
0.017	0.013364	0.033172	0.017213	0.013161	0.018031
0.017	0.013294	0.033102	0.017213	0.01313	0.017973
0.017	0.013274	0.032961	0.017175	0.013047	0.017944
0.017	0.013254	0.03289	0.017137	0.013027	0.017886
0.017	0.013244	0.03289	0.017137	0.012996	0.017876
0.017	0.013234	0.03289	0.017062	0.012945	0.017838
0.017	0.013224	0.03289	0.016873	0.012914	0.017799
0.017	0.013214	0.03282	0.016873	0.012605	0.017799
0.017	0.013123	0.032679	0.016797	0.012605	0.01778
0.017	0.013073	0.032679	0.016759	0.012584	0.01777
0.017	0.013013	0.032609	0.016759	0.012574	0.017761
0.017	0.012963	0.032609	0.016721	0.012553	0.017761
0.017	0.012942	0.032609	0.016721	0.012193	0.017741
0.017	0.012922	0.032538	0.016684	0.012121	0.017732
0.017	0.012912	0.032538	0.016646	0.0121	0.017722
0.017	0.012912	0.032538	0.016608	0.012079	0.017703
0.017	0.012902	0.032538	0.016608	0.012079	0.017693
0.017	0.012862	0.032468	0.016608	0.012079	0.017626
0.017	0.012832	0.032468	0.01657	0.012069	0.017568
0.017	0.012812	0.032468	0.016532	0.011966	0.017558
0.016	0.012762	0.032397	0.016532	0.011956	0.017529
0.016	0.012762	0.032186	0.016532	0.011832	0.01751
0.016	0.012752	0.032116	0.016494	0.011822	0.017414
0.016	0.012741	0.032045	0.016457	0.011791	0.017404
0.016	0.012661	0.032045	0.016457	0.01174	0.017346
0.016	0.012651	0.032045	0.016381	0.01174	0.017298
0.016	0.012641	0.031975	0.016381	0.011729	0.017269
0.016	0.012621	0.031975	0.016343	0.011719	0.017115
0.016	0.012621	0.031975	0.016343	0.011698	0.017095
0.016	0.012601	0.031904	0.01623	0.011647	0.017095
0.016	0.012601	0.031904	0.01623	0.011637	0.017047
0.016	0.012591	0.031834	0.01623	0.011565	0.017047
0.016	0.012581	0.031693	0.016192	0.011472	0.017028
0.016	0.012571	0.031623	0.016154	0.011348	0.01698
0.016	0.01253	0.031623	0.016116	0.011317	0.016932
0.016	0.01251	0.031552	0.016116	0.011235	0.016883
0.016	0.01249	0.031552	0.016116	0.011153	0.016806
0.016	0.01242	0.031482	0.016078	0.011111	0.016787
0.016	0.01239	0.031411	0.016078	0.01105	0.016748
0.016	0.01238	0.031341	0.01604	0.011019	0.016729
0.016	0.012309	0.031341	0.01604	0.011008	0.016575
0.016	0.012279	0.031271	0.016003	0.011008	0.016575
0.016	0.012209	0.031271	0.015965	0.010998	0.016555
0.016	0.012179	0.0312	0.015965	0.010957	0.016517
0.016	0.012078	0.0312	0.015965	0.010957	0.016488
0.016	0.012058	0.03113	0.015927	0.010854	0.016459
0.016	0.012048	0.03113	0.015927	0.010844	0.016459
0.016	0.012028	0.03113	0.015889	0.010823	0.016459

0.064948	0.014693	0.057	0.042981
0.064823	0.014693	0.335	0.042812
0.064706	0.014679	0.275	0.042812
0.064564	0.014666	0.035	0.042812
0.064489	0.014652	0.006	0.042643
0.064414	0.014639	0.008	0.042643
0.064372	0.014598	0.091	0.042643
0.064297	0.014571	0.024	0.042475
0.06418	0.014557	0.006	0.042475
0.06413	0.01453	0.131	0.042475
0.064122	0.014381	0.059	0.042475
0.064071	0.014367	0.006	0.042475
0.064071	0.01434	0.012	0.042306
0.064063	0.014327	0.005	0.042306
0.063988	0.0143	0.024	0.042306
0.063946	0.014259	0.011	0.042306
0.063921	0.014232	0.008	0.042138
0.063871	0.014178	0.095	0.042138
0.063846	0.014151	0.41	0.041969
0.063662	0.014056	0.01	0.041969
0.063537	0.014015	0.009	0.041801
0.063537	0.014002	0.007	0.041801
0.06352	0.013866	0.015	0.041801
0.063395	0.013866	0.004	0.041632
0.063386	0.013798	0.028	0.041632
0.063378	0.013771	0.199	0.041464
0.063361	0.013758	0.004	0.041464
0.063311	0.013744	0.142	0.041464
0.063278	0.01369	0.032	0.041464
0.063203	0.013595	0.006	0.041464
0.063044	0.0135	0.01	0.041295
0.063027	0.0135	0.014	0.041295
0.062986	0.013459	0.12	0.041126
0.062935	0.013432	0.007	0.041126
0.062877	0.013392	0.077	0.041126
0.062869	0.013351	0.019	0.041126
0.062793	0.013337	0.106	0.040958
0.062793	0.013324	0.025	0.040958
0.062777	0.01331	0.079	0.040958
0.062735	0.013297	0.48	0.040789
0.062677	0.013283	0.007	0.040621
0.062643	0.01327	0.032	0.040621
0.062585	0.01327	0.021	0.040621
0.062342	0.013242	0.022	0.040621
0.062342	0.013202	0.006	0.040452
0.062326	0.013188	0.022	0.040452
0.062317	0.013148	0.26	0.040452
0.062267	0.01312	0.015	0.040452
0.062259	0.013107	0.008	0.040284
0.062092	0.012999	0.007	0.040284
0.062008	0.012971	0.025	0.040284
0.061967	0.012958	0.09	0.040115
0.06185	0.012944	0.377	0.040115
0.06185	0.012822	0.095	0.040115
0.061716	0.012795	0.006	0.040115
0.061616	0.012687	0.013	0.039947
0.061591	0.012687	0.198	0.039947
0.061516	0.012646	0.005	0.039947
0.061424	0.012592	0.084	0.039778
0.061365	0.012538	0.148	0.039778
0.061265	0.012443	0.012	0.039778
0.061106	0.012443	0.132	0.039778
0.061065	0.012429	0.01	0.03961
0.061048	0.012416	0.018	0.03961
0.061006	0.012389	0.006	0.03961
0.060989	0.012375	0.004	0.03961
0.060964	0.012375	0.029	0.03961
0.060864	0.012294	0.006	0.03961
0.060839	0.012253	0.097	0.03961
0.060781	0.012199	0.011	0.039441
0.060764	0.012185	0.014	0.039441
0.060497	0.012172	0.012	0.039272
0.060488	0.012145	0.026	0.039104
0.060413	0.012131	0.005	0.039104
0.060405	0.012131	0.215	0.039104
0.060271	0.012063	0.008	0.038935
0.060096	0.011982	0.009	0.038935
0.060062	0.011968	0.099	0.038767
0.060062	0.011928	0.078	0.038767
0.060062	0.011914	0.015	0.038767
0.059954	0.011914	0.049	0.038598
0.059945	0.011901	0.229	0.038598
0.059912	0.011887	0.011	0.03843
0.05982	0.01186	0.01	0.03843
0.059561	0.011819	0.101	0.038261
0.059494	0.011779	0.03	0.038261
0.059478	0.011779	0.003	0.038261
0.059461	0.011765	0.014	0.038093
0.059369	0.011738	0.078	0.038093
0.05926	0.011724	0.05	0.038093
0.059143	0.011724	0.009	0.037924
0.059135	0.011657	0.019	0.037924
0.059118	0.011616	0.034	0.037755
0.059052	0.011602	0.067	0.037755
0.059018	0.011575	0.023	0.037755
0.059001	0.011535	0.149	0.037587
0.058943	0.011535	0.022	0.037587
0.058851	0.011494	0.041	0.037587
0.058826	0.011426	0.664	0.037587
0.058818	0.011399	0.312	0.037587
0.058818	0.011358	0.057	0.037418
0.058784	0.011345	0.009	0.037418
0.058709	0.011331	0.058	0.037418
0.058667	0.011277	0.01	0.037418
0.058659	0.011264	0.097	0.037418
0.058642	0.01125	0.011	0.037418
0.058634	0.01125	0.02	0.03725
0.058634	0.011223	0.278	0.03725
0.058559	0.011182	0.161	0.03725
0.058534	0.011142	0.005	0.03725
0.0585	0.011128	0.005	0.037081
0.058484	0.011087	0.02	0.037081
0.058484	0.011074	0.079	0.037081
0.058275	0.011074	0.005	0.037081

0.041863			
0.041814			
0.041765			
0.041619			
0.041619			
0.04157			
0.04157			
0.041375			
0.041278			
0.041278			
0.041229			
0.041229			
0.041132			
0.041083			
0.041034			
0.040937			
0.040937			
0.040888			
0.040888			
0.040888			
0.040839			
0.040839			
0.040742			
0.040693			
0.040693			
0.040498			
0.040449			
0.040449			
0.040449			
0.040401			
0.040352			
0.040352			
0.040352			
0.040303			
0.040059			
0.040059			
0.040059			
0.040011			
0.039962			
0.039864			
0.039864			
0.039816			
0.039816			
0.039718			
0.039718			
0.039572			
0.039572			
0.039523			
0.039475			
0.039475			
0.039426			
0.039377			
0.039328			
0.039328			
0.03928			
0.039036			
0.039036			
0.039036			
0.039036			
0.038987			
0.03889			
0.038744			
0.038695			
0.038695			
0.038646			
0.038646			
0.038597			
0.038597			
0.038402			
0.038402			
0.038354			
0.038354			
0.038305			
0.038159			
0.038159			
0.03811			
0.038061			
0.037964			
0.037964			
0.037915			
0.037915			
0.037866			
0.037866			
0.037818			
0.037769			
0.037769			
0.037769			
0.03772			
0.03772			
0.037574			
0.037574			
0.037574			
0.037525			
0.037525			
0.037476			
0.037428			
0.037379			
0.03733			
0.037282			
0.037233			
0.037184			
0.037184			
0.037087			
0.036989			
0.036989			
0.036892			
0.036794			
0.036745			
0.036697			
0.036551			
0.036551			
0.036502			
0.036502			
0.036453			

0.016	0.011958	0.03113	0.015813	0.010782	0.016401
0.016	0.011897	0.03113	0.015813	0.010689	0.016334
0.016	0.011877	0.03113	0.015776	0.010658	0.016314
0.016	0.011867	0.03113	0.015776	0.010638	0.01617
0.016	0.011867	0.03113	0.015738	0.010617	0.016093
0.016	0.011807	0.030989	0.015662	0.010586	0.016083
0.016	0.011757	0.030989	0.015662	0.010463	0.015958
0.016	0.011737	0.030918	0.015586	0.010442	0.015929
0.016	0.011727	0.030848	0.015586	0.010411	0.01589
0.016	0.011717	0.030778	0.015586	0.010339	0.01589
0.016	0.011686	0.030707	0.015586	0.010288	0.01589
0.016	0.011676	0.030707	0.015549	0.010102	0.015881
0.016	0.011656	0.030637	0.015549	0.010061	0.015881
0.016	0.011656	0.030637	0.015511	0.010051	0.015678
0.016	0.011606	0.030566	0.015473	0.01003	0.015668
0.016	0.011596	0.030566	0.015359	0.01001	0.01562
0.016	0.011576	0.030425	0.015359	0.009968	0.015611
0.015	0.011546	0.030425	0.015359	0.009927	0.015601
0.015	0.011506	0.030425	0.015246	0.009917	0.015601
0.015	0.011495	0.030285	0.015246	0.009907	0.015601
0.015	0.011495	0.030214	0.015246	0.009793	0.015591
0.015	0.011455	0.030144	0.015246	0.009773	0.015504
0.015	0.011455	0.030073	0.015246	0.009742	0.015379
0.015	0.011445	0.030073	0.015208	0.009659	0.01537
0.015	0.011345	0.030073	0.01517	0.009639	0.015331
0.015	0.011335	0.030073	0.01517	0.009639	0.015331
0.015	0.011315	0.030073	0.01517	0.009577	0.015292
0.015	0.011294	0.030003	0.01517	0.009567	0.015263
0.015	0.011294	0.029932	0.015132	0.009546	0.015186
0.015	0.011284	0.029932	0.015132	0.009299	0.015157
0.015	0.011274	0.029932	0.015095	0.009237	0.015128
0.015	0.011264	0.029932	0.015095	0.009217	0.0151
0.015	0.011214	0.029862	0.015019	0.009196	0.015061
0.015	0.011194	0.029862	0.014981	0.009124	0.015022
0.015	0.011134	0.029862	0.014943	0.009124	0.014926
0.015	0.011124	0.029792	0.014943	0.009103	0.014887
0.015	0.011114	0.029721	0.014943	0.009062	0.014887
0.015	0.011104	0.029721	0.014905	0.009021	0.014887
0.015	0.011094	0.029651	0.014905	0.009021	0.014752
0.015	0.011094	0.02958	0.014868	0.00899	0.014656
0.015	0.011073	0.02958	0.01483	0.008949	0.01456
0.015	0.011063	0.02958	0.01483	0.008908	0.014511
0.015	0.011033	0.02951	0.01483	0.008908	0.014473
0.015	0.010993	0.02951	0.014754	0.008887	0.014463
0.015	0.010953	0.029439	0.014716	0.008877	0.014463
0.015	0.010943	0.029439	0.014716	0.008856	0.014425
0.015	0.010913	0.029369	0.014716	0.008764	0.014386
0.015	0.010903	0.029299	0.014678	0.008753	0.014357
0.015	0.010862	0.029299	0.014678	0.008743	0.014309
0.015	0.010832	0.029228	0.014565	0.008712	0.01427
0.015	0.010812	0.029158	0.014489	0.008516	0.014232
0.015	0.010812	0.029158	0.014451	0.008506	0.014222
0.015	0.010802	0.029158	0.014451	0.008455	0.014222
0.015	0.010671	0.029158	0.014451	0.008434	0.014184
0.015	0.010641	0.029087	0.014414	0.008341	0.014087
0.015	0.010631	0.029087	0.014376	0.008135	0.013981
0.015	0.010631	0.029087	0.0143	0.008094	0.013942
0.015	0.010611	0.029017	0.0143	0.008053	0.013942
0.015	0.010581	0.029017	0.014262	0.008001	0.013933
0.015	0.010551	0.029017	0.014187	0.007919	0.013923
0.015	0.010511	0.029017	0.014149	0.007888	0.013923
0.015	0.01046	0.028876	0.014149	0.007878	0.013923
0.015	0.01045	0.028876	0.014111	0.007826	0.013875
0.015	0.01045	0.028876	0.014073	0.007816	0.013865
0.015	0.01043	0.028876	0.014073	0.007806	0.013856
0.015	0.01039	0.028735	0.014035	0.007785	0.013856
0.015	0.01037	0.028735	0.014035	0.007754	0.013856
0.015	0.01036	0.028735	0.014035	0.007754	0.013846
0.015	0.01035	0.028665	0.013998	0.007651	0.013846
0.015	0.01034	0.028665	0.01396	0.00762	0.013798
0.015	0.01031	0.028524	0.013922	0.00761	0.013798
0.015	0.0103	0.028524	0.013922	0.007538	0.013788
0.014	0.010239	0.028524	0.013884	0.007528	0.013788
0.014	0.010189	0.028453	0.013846	0.007497	0.01375
0.014	0.010179	0.028383	0.013846	0.007384	0.01373
0.014	0.010169	0.028383	0.013808	0.007312	0.013701
0.014	0.010159	0.028313	0.013771	0.007301	0.013692
0.014	0.010109	0.028313	0.013733	0.007291	0.013682
0.014	0.010099	0.028242	0.013733	0.00725	0.013663
0.014	0.010079	0.028242	0.013695	0.007219	0.013595
0.014	0.010059	0.028242	0.013695	0.007136	0.013586
0.014	0.009988	0.028242	0.013657	0.007075	0.013576
0.014	0.009968	0.028242	0.013619	0.007003	0.013566
0.014	0.009958	0.028172	0.013619	0.006992	0.013557
0.014	0.009958	0.028172	0.013581	0.006961	0.013538
0.014	0.009928	0.028101	0.013581	0.006755	0.013518
0.014	0.009898	0.028101	0.013581	0.006652	0.01348
0.014	0.009878	0.028101	0.013544	0.006622	0.01347
0.014	0.009868	0.028031	0.013468	0.006611	0.01347
0.014	0.009848	0.028031	0.013468	0.00657	0.013451
0.014	0.009837	0.028031	0.013468	0.006539	0.013451
0.014	0.009777	0.028031	0.01343	0.006498	0.013364
0.014	0.009767	0.02796	0.01343	0.006302	0.013354
0.014	0.009677	0.02789	0.013392	0.006282	0.013354
0.014	0.009657	0.02789	0.013392	0.006241	0.013335
0.014	0.009657	0.02782	0.013317	0.00623	0.013296
0.014	0.009616	0.02782	0.013279	0.00622	0.013248
0.014	0.009606	0.02782	0.013279	0.006189	0.013239
0.014	0.009566	0.027749	0.013241	0.006138	0.013219
0.014	0.009516	0.027749	0.013203	0.006096	0.0132
0.014	0.009446	0.027679	0.013203	0.006086	0.013181
0.014	0.009446	0.027679	0.013165	0.006076	0.013171
0.014	0.009395	0.027679	0.013127	0.005777	0.013142
0.014	0.009365	0.027679	0.013127	0.005684	0.013133
0.014	0.009355	0.027679	0.013127	0.005664	0.013104
0.014	0.009315	0.027608	0.01309	0.005561	0.013104
0.014	0.009295	0.027608	0.01309	0.00552	0.013094
0.014	0.009255	0.027608	0.01309	0.00552	0.013075
0.014	0.009144	0.027538	0.013052	0.005334	0.013075
0.014	0.009144	0.027538	0.013052	0.005252	0.013046
0.014	0.009124	0.027538	0.013052	0.005149	0.013046
0.014	0.009124	0.027467	0.013052	0.005139	0.013036
0.014	0.009084	0.027397	0.013052	0.005139	0.013026
0.014	0.009044	0.027397	0.013014	0.005139	0.012998

0.058216	0.01106	0.062	0.036913
0.058216	0.011047	0.005	0.036913
0.058191	0.01102	0.003	0.036913
0.058183	0.011006	0.112	0.036913
0.058041	0.010979	0.089	0.036913
0.057982	0.010938	0.008	0.036913
0.057966	0.010925	0.214	0.036744
0.057941	0.010884	0.04	0.036744
0.057882	0.01087	0.009	0.036744
0.05784	0.010762	0.006	0.036744
0.057799	0.010749	0.039	0.036744
0.05774	0.010694	0.008	0.036744
0.05774	0.010667	0.098	0.036576
0.057673	0.010613	0.06	0.036576
0.057665	0.010572	0.009	0.036407
0.05764	0.010572	0.005	0.036407
0.05759	0.010559	0.035	0.036407
0.057531	0.010518	0.021	0.036238
0.057531	0.010477	0.011	0.036238
0.05744	0.01041	0.094	0.036238
0.05744	0.010396	0.008	0.036238
0.057431	0.010396	0.315	0.03607
0.057406	0.010396	0.012	0.03607
0.057389	0.010396	0.021	0.03607
0.057381	0.010383	0.071	0.03607
0.057222	0.010301	0.011	0.03607
0.057206	0.010288	0.038	0.03607
0.057189	0.010261	0.047	0.03607
0.057139	0.010261	0.013	0.035901
0.057097	0.01022	0.006	0.035733
0.057055	0.01022	0.006	0.035733
0.057055	0.010139	0.018	0.035733
0.056989	0.010044	0.18	0.035564
0.056888	0.010044	0.017	0.035564
0.056771	0.01003	0.016	0.035396
0.056771	0.010003	0.023	0.035396
0.056763	0.009976	0.015	0.035396
0.056755	0.009962	0.011	0.035396
0.05673	0.009949	0.421	0.035396
0.056721	0.009949	0.104	0.035396
0.056713	0.009935	0.141	0.035396
0.056696	0.009935	0.346	0.035227
0.056688	0.009935	0.045	0.035227
0.056654	0.009908	0.015	0.035227
0.056579	0.009895	0.005	0.035059
0.056571	0.009854	0.008	0.035059
0.056387	0.009854	0.005	0.035059
0.056387	0.009854	0.01	0.035059
0.056362	0.00984	0.012	0.035059
0.056362	0.0098	0.036	0.035059
0.056304	0.009786	0.02	0.035059
0.056287	0.009773	0.031	0.03489
0.056095	0.009745	0.122	0.03489
0.056053	0.009718	0.012	0.03489
0.056003	0.009691	0.013	0.03489
0.055995	0.009664	0.104	0.03489
0.055995	0.009637	0.077	0.034722
0.055953	0.009637	0.005	0.034722
0.055936	0.009624	0.01	0.034722
0.055861	0.00961	0.02	0.034553
0.055828	0.009596	0.135	0.034553
0.055802	0.009569	0.146	0.034384
0.055677	0.009529	0.051	0.034384
0.055594	0.009515	0.007	0.034216
0.05556	0.009502	0.004	0.034216
0.055552	0.009488	0.033	0.034047
0.055527	0.009461	0.094	0.034047
0.055377	0.009434	0.041	0.033879
0.055351	0.009407	0.005	0.033879
0.055293	0.009366	0.011	0.033879
0.055285	0.009285	0.169	0.033879
0.05526	0.009258	0.046	0.033879
0.055218	0.00923	0.011	0.033879
0.055184	0.009217	0.108	0.03371
0.055143	0.009203	0.01	0.03371
0.055051	0.009136	0.565	0.03371
0.055051	0.009136	0.106	0.033542
0.055009	0.009081	0.022	0.033542
0.055001	0.009027	0.214	0.033373
0.054834	0.009014	0.326	0.033373
0.054809	0.008986	0.011	0.033373
0.054809	0.008986	0.244	0.033205
0.0548	0.008959	0.004	0.033205
0.054775	0.008864	0.002	0.033205
0.054625	0.008864	0.01	0.033205
0.054591	0.008837	0.065	0.033036
0.054525	0.008783	0.017	0.033036
0.054491	0.008742	0.02	0.032867
0.054466	0.00862	0.026	0.032867
0.054399	0.008593	0.137	0.032867
0.054358	0.00858	0.023	0.032867
0.054332	0.008566	0.018	0.032867
0.054332	0.008512	0.921	0.032867
0.054232	0.008512	0.033	0.032867
0.054165	0.008485	0.03	0.032867
0.054124	0.008431	0.029	0.032867
0.054032	0.00839	0.008	0.032699
0.053756	0.00839	0.039	0.032699
0.053756	0.00839	0.012	0.032699
0.053748	0.00839	0.071	0.032699
0.053681	0.008363	0.017	0.03253
0.053673	0.008322	0.127	0.03253
0.053614	0.008322	0.161	0.03253
0.053589	0.008282	0.026	0.032362
0.053497	0.008268	0.118	0.032362
0.053447	0.008227	0.138	0.032362
0.053347	0.008227	0.075	0.032362
0.053347	0.0082	0.069	0.032193
0.053255	0.008092	0.049	0.032193
0.053138	0.008065	0.348	0.032193
0.053121	0.008038	0.193	0.032193
0.052954	0.008011	0.041	0.032193
0.052913	0.007916	0.043	0.032193
0.052904	0.007902	0.061	0.032025

0.036453
0.036453
0.036356
0.036356
0.036258
0.036209
0.036112
0.036063
0.035917
0.035868
0.03582
0.03582
0.035771
0.035722
0.035722
0.035673
0.035673
0.035673
0.035625
0.035527
0.035381
0.035381
0.035332
0.035283
0.035283
0.035235
0.035235
0.035186
0.035137
0.03504
0.034991
0.034991
0.034942
0.034894
0.034894
0.034845
0.034699
0.034699
0.034699
0.034699
0.03465
0.03465
0.034601
0.034504
0.034504
0.034504
0.034455
0.034455
0.034309
0.03426
0.034211
0.034211
0.034211
0.034163
0.034163
0.034114
0.034114
0.034016
0.033919
0.033919
0.03387
0.033773
0.033626
0.033626
0.033578
0.033529
0.033529
0.033285
0.033285
0.033237
0.033237
0.033188
0.033188
0.033139
0.033139
0.03309
0.03309
0.033042
0.032993
0.032993
0.032944
0.032944
0.032944
0.032895
0.032895
0.032847
0.032798
0.032603
0.032603
0.032554
0.032554
0.032554
0.032554
0.032554
0.032554
0.032506
0.032506
0.032506
0.032457
0.032457
0.032408
0.032408
0.032311
0.032262
0.032262
0.032262
0.032262
0.032164
0.032164
0.032116
0.032018
0.032018
0.032018
0.031921

0.014	0.009044	0.027327	0.013014	0.005128	0.012988
0.014	0.008993	0.027256	0.012976	0.005108	0.012988
0.014	0.008923	0.027256	0.012938	0.005046	0.012969
0.014	0.008873	0.027186	0.012938	0.004953	0.01293
0.014	0.008873	0.027186	0.0129	0.004778	0.012891
0.014	0.008843	0.027186	0.0129	0.004747	0.012853
0.014	0.008823	0.027186	0.012863	0.004696	0.012843
0.014	0.008813	0.027186	0.012863	0.004675	0.012834
0.014	0.008762	0.027186	0.012863	0.004624	0.012834
0.014	0.008752	0.027186	0.012825	0.004583	0.012795
0.014	0.008722	0.027186	0.012825	0.004572	0.012785
0.014	0.008712	0.027115	0.012825	0.004572	0.012756
0.014	0.008692	0.027115	0.012749	0.004541	0.012756
0.013	0.008682	0.027115	0.012711	0.004222	0.012747
0.013	0.008682	0.027045	0.012711	0.004212	0.012737
0.013	0.008622	0.027045	0.012711	0.004212	0.012728
0.013	0.008622	0.027045	0.012711	0.004037	0.012718
0.013	0.008571	0.026974	0.012711	0.004037	0.012718
0.013	0.008561	0.026904	0.012636	0.003924	0.012718
0.013	0.008551	0.026904	0.012636	0.003903	0.012679
0.013	0.008481	0.026834	0.012598	0.003893	0.01266
0.013	0.008461	0.026834	0.01256	0.003831	0.01265
0.013	0.008451	0.026834	0.012484	0.003594	0.01265
0.013	0.008431	0.026834	0.012484	0.003512	0.012631
0.013	0.008431	0.026834	0.012484	0.00346	0.012622
0.013	0.00839	0.026763	0.012446	0.003398	0.012612
0.013	0.00839	0.026693	0.012446	0.003275	0.012602
0.013	0.00837	0.026693	0.012446	0.003254	0.012602
0.013	0.00825	0.026693	0.012446	0.003079	0.012602
0.013	0.00821	0.026622	0.012409	0.002894	0.012602
0.013	0.008179	0.026622	0.012409	0.002894	0.012583
0.013	0.008169	0.026552	0.012409	0.002863	0.012583
0.013	0.008169	0.026552	0.012371	0.002853	0.012573
0.013	0.008169	0.026552	0.012371	0.00275	0.012544
0.013	0.008129	0.026552	0.012333	0.002688	0.012535
0.013	0.008069	0.026552	0.012333	0.002461	0.012525
0.013	0.008049	0.026552	0.012257	0.002276	0.012487
0.013	0.008049	0.026411	0.012257	0.002276	0.012487
0.013	0.008019	0.026411	0.012219	0.00172	0.012477
0.013	0.007989	0.026411	0.012144	0.001689	0.012477
0.013	0.007978	0.026411	0.012144	0.001164	0.012429
0.013	0.007958	0.026411	0.012106	0.000051	0.0124
0.013	0.007928	0.026341	0.012106	0.000021	0.01238
0.013	0.007908	0.026341	0.012106	0.000021	0.012361
0.013	0.007908	0.02627	0.012106	0.00001	0.012352
0.013	0.007898	0.02627	0.012106	0.00001	0.012342
0.013	0.007858	0.0262	0.012068	0.00001	0.012332
0.013	0.007788	0.0262	0.012068	0.00001	0.012332
0.013	0.007767	0.0262	0.01203		0.012323
0.013	0.007747	0.026059	0.01203		0.012303
0.013	0.007717	0.026059	0.01203		0.012274
0.013	0.007697	0.026059	0.011992		0.012245
0.013	0.007657	0.025988	0.011955		0.012236
0.013	0.007627	0.025988	0.011955		0.012197
0.013	0.007627	0.025988	0.011955		0.012188
0.013	0.007526	0.025918	0.011917		0.012178
0.013	0.007426	0.025918	0.011841		0.012149
0.013	0.007416	0.025918	0.011841		0.012139
0.013	0.007315	0.025918	0.011803		0.01211
0.013	0.007305	0.025848	0.011765		0.012091
0.013	0.007275	0.025848	0.011765		0.012072
0.013	0.007235	0.025777	0.011765		0.012072
0.012	0.007205	0.025777	0.011765		0.012053
0.012	0.007054	0.025777	0.011728		0.012024
0.012	0.007034	0.025777	0.01169		0.012004
0.012	0.007024	0.025777	0.011652		0.011975
0.012	0.007024	0.025707	0.011614		0.011956
0.012	0.007014	0.025707	0.011576		0.011927
0.012	0.006964	0.025707	0.011538		0.011927
0.012	0.006954	0.025707	0.011501		0.01184
0.012	0.006863	0.025636	0.011501		0.011831
0.012	0.006853	0.025636	0.011501		0.011821
0.012	0.006843	0.025636	0.011463		0.011812
0.012	0.006833	0.025566	0.011463		0.011783
0.012	0.006803	0.025566	0.011463		0.011715
0.012	0.006793	0.025566	0.011425		0.011706
0.012	0.006773	0.025566	0.011425		0.011706
0.012	0.006763	0.025495	0.011425		0.011648
0.012	0.006753	0.025495	0.011425		0.011638
0.012	0.006743	0.025425	0.011425		0.011628
0.012	0.006712	0.025425	0.011425		0.011619
0.012	0.006702	0.025425	0.011387		0.011609
0.012	0.006672	0.025354	0.011387		0.011599
0.012	0.006662	0.025284	0.011349		0.01158
0.012	0.006662	0.025284	0.011349		0.01158
0.012	0.006662	0.025284	0.011349		0.011571
0.012	0.006652	0.025214	0.011311		0.011532
0.012	0.006632	0.025214	0.011311		0.011493
0.012	0.006612	0.025214	0.011311		0.011474
0.012	0.006602	0.025143	0.011274		0.011445
0.012	0.006602	0.025143	0.011274		0.011426
0.012	0.006582	0.025143	0.011274		0.011378
0.012	0.006572	0.025143	0.011236		0.011358
0.012	0.006562	0.025143	0.011236		0.011349
0.012	0.006411	0.025073	0.011236		0.011349
0.012	0.006401	0.025073	0.011236		0.011329
0.012	0.006381	0.025073	0.011198		0.011329
0.012	0.006371	0.025002	0.011198		0.011291
0.012	0.006361	0.025002	0.01116		0.011262
0.012	0.006361	0.025002	0.01116		0.011252
0.012	0.006341	0.024932	0.01116		0.011252
0.012	0.006331	0.024932	0.01116		0.011243
0.012	0.00629	0.024861	0.011122		0.011233
0.012	0.00626	0.024861	0.011122		0.011223
0.012	0.0062	0.024861	0.011085		0.011223
0.012	0.0062	0.024791	0.011085		0.011214
0.012	0.00619	0.024791	0.011085		0.011185
0.012	0.006099	0.024721	0.011085		0.011175
0.012	0.006069	0.02465	0.011047		0.011098
0.012	0.006069	0.02465	0.011047		0.01104
0.012	0.006059	0.02465	0.011047		0.011021
0.012	0.006039	0.02458	0.011009		0.011002
0.012	0.005999	0.02458	0.011009		0.011002
0.012	0.005949	0.02458	0.010971		0.010982

0.052879	0.007889	0.038	0.032025		0.031921		0.012	0.005919	0.024439	0.010933		0.010982		
0.052829	0.007848	0.109	0.032025		0.031823		0.012	0.005898	0.024298	0.010933		0.010973		
0.052796	0.007848	0.012	0.031856		0.031823		0.012	0.005888	0.024298	0.010933		0.010963		
0.052787	0.007834	0.026	0.031856		0.031823		0.012	0.005868	0.024298	0.010933		0.010934		
0.052729	0.007821	0.025	0.031856		0.031775		0.012	0.005848	0.024298	0.010933		0.010925		
0.052679	0.007739	0.036	0.031688		0.031775		0.012	0.005838	0.024298	0.010858		0.010925		
0.052645	0.007712	0.023	0.031688		0.031775		0.012	0.005828	0.024298	0.010858		0.010925		
0.052612	0.007685	0.01	0.031688		0.031726		0.012	0.005647	0.024228	0.01082		0.010896		
0.05257	0.007672	0.009	0.031688		0.031628		0.012	0.005627	0.024228	0.01082		0.010886		
0.052553	0.007617	0.034	0.031688		0.03158		0.012	0.005627	0.024157	0.010744		0.010876		
0.052528	0.007577	0.007	0.031519		0.031482		0.012	0.005597	0.024157	0.010744		0.010828		
0.05252	0.007563	0.21	0.031519		0.031433		0.011	0.005597	0.024157	0.010744		0.010818		
0.052503	0.007523	0.028	0.031519		0.031433		0.011	0.005537	0.024087	0.010744		0.010809		
0.052462	0.007495	0.037	0.031519		0.031433		0.011	0.005527	0.024087	0.010706		0.01079		
0.05242	0.007455	0.017	0.031351		0.031433		0.011	0.005517	0.024016	0.010706		0.01078		
0.052395	0.007414	0.047	0.031351		0.031385		0.011	0.005446	0.023946	0.010668		0.01077		
0.05237	0.007373	0.004	0.031351		0.031336		0.011	0.005446	0.023946	0.010631		0.010751		
0.05237	0.00736	0.005	0.031351		0.031287		0.011	0.005426	0.023946	0.010631		0.010751		
0.052286	0.00736	0.102	0.031182		0.031287		0.011	0.005406	0.023946	0.010593		0.010751		
0.052186	0.007265	0.724	0.031182		0.031239		0.011	0.005376	0.023805	0.010593		0.010741		
0.052136	0.007197	0.187	0.031182		0.03119		0.011	0.005376	0.023805	0.010555		0.010722		
0.052077	0.007157	0.042	0.031182		0.03119		0.011	0.005316	0.023805	0.010517		0.010703		
0.052052	0.007116	0.097	0.031182		0.031141		0.011	0.005316	0.023805	0.010517		0.010693		
0.052044	0.007062	0.007	0.031013		0.031141		0.011	0.005316	0.023735	0.010479		0.010674		
0.052002	0.007048	0.074	0.031013		0.031141		0.011	0.005306	0.023735	0.010479		0.010664		
0.051927	0.007048	0.024	0.031013		0.031141		0.011	0.005306	0.023735	0.010441		0.010664		
0.051927	0.007048	0.088	0.031013		0.031141		0.011	0.005306	0.023735	0.010404		0.010645		
0.051919	0.006994	0.05	0.031013		0.031092		0.011	0.005286	0.023735	0.010404		0.010626		
0.051877	0.006926	0.023	0.031013		0.031044		0.011	0.005286	0.023664	0.010366		0.010616		
0.051793	0.006926	0.013	0.030845		0.031044		0.011	0.005275	0.023664	0.010366		0.010606		
0.051626	0.006913	0.022	0.030845		0.030995		0.011	0.005265	0.023664	0.010366		0.010606		
0.051568	0.006858	0.073	0.030845		0.030946		0.011	0.005255	0.023664	0.010328		0.010587		
0.051384	0.006845	0.035	0.030845		0.030897		0.011	0.005185	0.023664	0.010328		0.010587		
0.051351	0.006804	0.07	0.030845		0.030849		0.011	0.005175	0.023594	0.01029		0.010577		
0.051351	0.006777	0.193	0.030676		0.0308		0.011	0.005145	0.023594	0.01029		0.010548		
0.051351	0.006777	1.595	0.030508		0.030751		0.011	0.005105	0.023594	0.01029		0.010539		
0.051242	0.006764	0.051	0.030508		0.030702		0.011	0.005074	0.023523	0.01029		0.010539		
0.051209	0.00675	0.254	0.030339		0.030702		0.011	0.005074	0.023523	0.01029		0.01052		
0.051184	0.006696	0.039	0.030339		0.030702		0.011	0.005064	0.023523	0.01029		0.01051		
0.051167	0.006601	0.024	0.030339		0.030702		0.011	0.005024	0.023453	0.010214		0.01051		
0.051133	0.006601	0.025	0.030339		0.030605		0.011	0.005004	0.023453	0.010214		0.0105		
0.05105	0.006547	0.038	0.030339		0.030556		0.011	0.004994	0.023453	0.010214		0.010481		
0.051033	0.006533	0.008	0.030171		0.030556		0.011	0.004924	0.023453	0.010214		0.010471		
0.050983	0.00652	0.012	0.030171		0.030556		0.011	0.004914	0.023382	0.010214		0.010471		
0.050983	0.006506	0.114	0.030002		0.030556		0.011	0.004874	0.023382	0.010177		0.010442		
0.050891	0.006492	0.01	0.030002		0.030459		0.011	0.004823	0.023312	0.010177		0.010433		
0.050858	0.006398	0.008	0.030002		0.030459		0.011	0.004813	0.023312	0.010177		0.010433		
0.050841	0.00637	0.007	0.030002		0.030459		0.011	0.004803	0.023312	0.010139		0.010423		
0.050774	0.006289	0.053	0.030002		0.03041		0.011	0.004713	0.023312	0.010139		0.010394		
0.050724	0.006221	0.005	0.030002		0.03041		0.011	0.004703	0.023312	0.010139		0.010385		
0.050699	0.006208	0.024	0.030002		0.03041		0.011	0.004703	0.023242	0.010139		0.010365		
0.050674	0.006194	0.047	0.029834		0.03041		0.011	0.004673	0.023242	0.010101		0.010365		
0.050591	0.00614	0.015	0.029834		0.03041		0.011	0.004662	0.023171	0.010101		0.010317		
0.050566	0.006113	0.192	0.029834		0.030264		0.011	0.004652	0.023171	0.010101		0.010298		
0.050557	0.006005	0.103	0.029665		0.030215		0.011	0.004632	0.023171	0.010063		0.010288		
0.05054	0.00595	0.016	0.029665		0.030166		0.011	0.004622	0.023171	0.010063		0.010288		
0.050532	0.005896	0.006	0.029665		0.030166		0.011	0.004572	0.023171	0.010063		0.010288		
0.050524	0.005855	0.011	0.029665		0.030166		0.011	0.004572	0.023101	0.010063		0.010259		
0.050474	0.005842	0.008	0.029665		0.030118		0.011	0.004552	0.023101	0.010025		0.01024		
0.050382	0.005652	0.081	0.029496		0.030069		0.011	0.004552	0.023101	0.010025		0.01023		
0.050365	0.005625	0.011	0.029496		0.03002		0.011	0.004542	0.023101	0.009987		0.010221		
0.050332	0.005598	0.023	0.029496		0.03002		0.011	0.004542	0.023101	0.009987		0.010201		
0.050332	0.005584	0.019	0.029496		0.029971		0.011	0.004542	0.023101	0.00995		0.010192		
0.050323	0.005584	0.021	0.029496		0.029923		0.011	0.004532	0.02303	0.009912		0.010134		
0.050307	0.005435	0.013	0.029328		0.029923		0.011	0.004421	0.02303	0.009836		0.010115		
0.050265	0.005367	0.016	0.029328		0.029825		0.011	0.004341	0.02296	0.009836		0.010076		
0.050131	0.005327	0.063	0.029328		0.029728		0.011	0.004311	0.02296	0.009798		0.010066		
0.050106	0.005232	0.032	0.029159		0.029679		0.011	0.004311	0.022889	0.00976		0.010057		
0.050098	0.005191	0.016	0.029159		0.02963		0.011	0.004261	0.022889	0.00976		0.010028		
0.050081	0.005002	0.019	0.028991		0.029533		0.011	0.00415	0.022889	0.009723		0.010018		
0.050073	0.004988	0.031	0.028991		0.029533		0.011	0.00412	0.022889	0.009723		0.010018		
0.050048	0.004961	0.006	0.028991		0.029484		0.011	0.00411	0.022819	0.009723		0.010009		
0.050031	0.004649	0.981	0.028991		0.029338		0.011	0.0041	0.022819	0.009647		0.009989		
0.049998	0.004636	0.062	0.028991		0.029338		0.011	0.0041	0.022749	0.009647		0.009893		
0.049964	0.004568	0.021	0.028991		0.029338		0.011	0.00408	0.022749	0.009571		0.009883		
0.049897	0.004527	0.47	0.028991		0.029289		0.011	0.00406	0.022678	0.009571		0.009854		
0.04978	0.004527	0.007	0.028822		0.029289		0.011	0.004019	0.022678	0.009571		0.009845		
0.049755	0.004419	0.005	0.028822		0.02924		0.011	0.003989	0.022678	0.009533		0.009835		
0.049722	0.004392	0.02	0.028822		0.029143		0.011	0.003919	0.022608	0.009533		0.009816		
0.049705	0.004242	0.013	0.028822		0.029143		0.011	0.003909	0.022608	0.009533		0.009777		
0.049663	0.004175	0.056	0.028822		0.029143		0.011	0.003889	0.022537	0.009496		0.009767		
0.049638	0.00366	0.016	0.028822		0.029143		0.011	0.003839	0.022537	0.009496		0.009767		
0.049496	0.003605	0.021	0.028822		0.029094		0.011	0.003818	0.022467	0.009458		0.009758		
0.04948	0.003511	0.016	0.028822		0.029094		0.011	0.003808	0.022467	0.009458		0.009739		
0.049338	0.003361	1.425	0.028654		0.029045		0.011	0.003798	0.022467	0.009458		0.0097		
0.049338	0.00328	0.116	0.028654		0.028948		0.011	0.003768	0.022467	0.009458		0.009661		
0.049329	0.003145	0.034	0.028654		0.028899		0.011	0.003758	0.022467	0.00942		0.009652		
0.049313	0.002806	0.016	0.028654		0.028802		0.011	0.003738	0.022326	0.00942		0.009623		
0.049221	0.002779	0.082	0.028485		0.028753		0.01	0.003688	0.022256	0.00942		0.009613		
0.049196	0.00244	0.076	0.028485		0.028753		0.01	0.003617	0.022256	0.00942		0.009594		
0.049179	0.00244	0.109	0.028485		0.028704		0.01	0.003517	0.022185	0.009344		0.009594		
0.049137	0.002196	0.011	0.028317		0.028704		0.01	0.003517	0.022185	0.009344		0.009575		
0.049096	0.002033	0.145	0.028317		0.028704		0.01	0.003507	0.022185	0.009344		0.009536		
0.04907	0.001938	0.053	0.028317		0.028656		0.01	0.003386	0.022185	0.009344		0.009526		
0.04907	0.001938	0.06	0.028317		0.028656		0.01	0.003376	0.022115	0.009344		0.009507		
0.04907	0.001748	0.025	0.028317		0.028607		0.01	0.003276	0.022115	0.009306		0.009497		
0.04897	0.001098	0.006	0.028317		0.028607		0.01	0.003125	0.022115	0.009306		0.009497		
0.048945		0.01	0.028317		0.028607		0.01	0.002673	0.021974	0.009306		0.009497		
0.048845		0.026	0.028148		0.028558		0.01	0.002603	0.021974	0.009269		0.009449		
0.048736		0.031	0.028148		0.028509		0.01	0.002572	0.021974	0.009269		0.00944		
0.048711		0.432	0.028148		0.028461		0.01	0.002572	0.021903	0.009231		0.00944		
0.048678		0.039	0.028148		0.028461		0.01	0.002311	0.021903	0.009231		0.00943		
0.048644		0.011	0.028148		0.028461		0.01	0.00216	0.021903	0.009231		0.00943		
0.048569		0.003	0.028148		0.028363		0.01	0.00201	0.021833	0.009193		0.009411		
0.048561		0.006	0.028148		0.028266		0.01	0.001748	0.021833	0.009193		0.009401		
0.048502		0.296	0.028148		0.028217		0.01	0.00006	0.021833	0.009193		0.009334		
0.048444		0.005	0.027979		0.028217		0.01	0.00005	0.021833	0.009193		0.009334		
0.04836		0.011	0.027979		0.028217		0.01	0.00004	0.021763	0.009155		0.009314		
0.048252		0.013	0.027979		0.028168		0.01	0.00003	0.021763	0.009155		0.009314		
0.048193		0.04	0.027811		0.02812		0.01	0.00001	0.021763	0.009155		0.009285		
0.048093		0.002	0.027811		0.02812		0.01	0.00001	0.021692	0.009117		0.009266		
0.048068		0.014	0.027811		0.028022		0.01	0.00001	0.021692	0.009117		0.009266		
0.048043		0.032	0.027642		0.028022		0.01		0.021692	0.009079		0.009237		
0.047851		0.05	0.027642		0.027778		0.01		0.021622	0.009079		0.009227		

0.047826	0.068	0.027642	0.027778	0.01	0.021622	0.009079	0.009208
0.047801	0.01	0.027474	0.02773	0.01	0.021622	0.009042	0.009189
0.047684	0.271	0.027474	0.027681	0.01	0.021551	0.009042	0.009179
0.047609	0.007	0.027474	0.027632	0.01	0.021551	0.009042	0.00915
0.047534	0.031	0.027474	0.027632	0.01	0.021551	0.009042	0.009141
0.047341	0.014	0.027474	0.027632	0.01	0.021551	0.009004	0.009141
0.0473	0.046	0.027474	0.027583	0.01	0.021551	0.008928	0.009141
0.0472	0.019	0.027474	0.027583	0.01	0.021481	0.008928	0.009102
0.047191	0.03	0.027474	0.027535	0.01	0.021481	0.00889	0.009093
0.046966	0.023	0.027474	0.027535	0.01	0.021481	0.00889	0.009093
0.046924	0.007	0.027305	0.027535	0.01	0.021481	0.008852	0.009093
0.04684	0.016	0.027305	0.027535	0.01	0.021481	0.008852	0.009093
0.04679	0.019	0.027305	0.027486	0.01	0.021481	0.008852	0.009093
0.04679	0.045	0.027305	0.027486	0.01	0.02141	0.008815	0.009083
0.046782	0.019	0.027305	0.027486	0.01	0.02134	0.008815	0.009073
0.046757	0.012	0.027305	0.027437	0.01	0.02134	0.008777	0.009064
0.046732	0.003	0.026968	0.027437	0.01	0.02134	0.008777	0.009054
0.046657	0.013	0.026968	0.027437	0.01	0.02134	0.008777	0.009054
0.046456	0.011	0.026968	0.027437	0.01	0.02134	0.008777	0.009035
0.046406	0.032	0.026968	0.027389	0.01	0.02127	0.008739	0.009035
0.046356	0.266	0.026968	0.02734	0.01	0.02127	0.008739	0.009015
0.046323	0.253	0.0268	0.027291	0.01	0.02127	0.008739	0.009006
0.046231	0.037	0.0268	0.027242	0.01	0.02127	0.008701	0.008948
0.046197	0.007	0.0268	0.027242	0.01	0.021199	0.008701	0.008938
0.046189	0.015	0.0268	0.027242	0.01	0.021199	0.008663	0.008929
0.046172	0.026	0.026631	0.027194	0.01	0.021199	0.008663	0.008929
0.046172	0.023	0.026631	0.027096	0.01	0.021199	0.008663	0.008909
0.046164	0.069	0.026631	0.026999	0.01	0.021199	0.008663	0.0089
0.046155	0.08	0.026631	0.02695	0.01	0.021199	0.008625	0.00888
0.046139	0.005	0.026631	0.026901	0.01	0.021199	0.008625	0.008851
0.046122	0.016	0.026631	0.026852	0.01	0.021199	0.008588	0.008842
0.04608	0.013	0.026463	0.026852	0.01	0.021129	0.008588	0.008842
0.045972	0.115	0.026463	0.026755	0.01	0.021129	0.008588	0.008832
0.045963	0.117	0.026294	0.026706	0.01	0.021129	0.00855	0.008823
0.045905	0.018	0.026294	0.026706	0.01	0.021058	0.00855	0.008813
0.045755	0.013	0.026294	0.026706	0.01	0.020988	0.00855	0.008794
0.045713	0.015	0.026294	0.026706	0.01	0.020988	0.008512	0.008794
0.045613	0.025	0.026294	0.026658	0.01	0.020988	0.008474	0.008794
0.045596	0.078	0.026125	0.02656	0.01	0.020917	0.008436	0.008794
0.045587	0.285	0.026125	0.026511	0.01	0.020917	0.008436	0.008726
0.045562	0.018	0.026125	0.026511	0.01	0.020917	0.008361	0.008659
0.045546	0.026	0.026125	0.026511	0.01	0.020847	0.008361	0.008649
0.045529	0.013	0.026125	0.026463	0.01	0.020847	0.008323	0.008649
0.045504	0.047	0.026125	0.026463	0.01	0.020847	0.008323	0.00863
0.045387	0.015	0.025957	0.026463	0.009	0.020777	0.008323	0.00862
0.045379	0.036	0.025957	0.026414	0.009	0.020777	0.008285	0.00862
0.045379	0.016	0.025957	0.026414	0.009	0.020777	0.008247	0.00861
0.045278	0.009	0.025957	0.026414	0.009	0.020777	0.008209	0.008553
0.045245	0.019	0.025957	0.026365	0.009	0.020777	0.008209	0.008553
0.045245	0.016	0.025788	0.026365	0.009	0.020706	0.008209	0.008543
0.045228	0.445	0.02562	0.026316	0.009	0.020706	0.008209	0.008543
0.04522	0.18	0.02562	0.026316	0.009	0.020636	0.008172	0.008533
0.04517	0.068	0.02562	0.026219	0.009	0.020636	0.008172	0.008485
0.045145	0.014	0.02562	0.02617	0.009	0.020636	0.008172	0.008485
0.04512	0.072	0.02562	0.026121	0.009	0.020565	0.008134	0.008466
0.045028	0.049	0.02562	0.026121	0.009	0.020565	0.008134	0.008456
0.044994	0.253	0.02562	0.026073	0.009	0.020565	0.008134	0.008446
0.044936	0.008	0.025451	0.026073	0.009	0.020495	0.008134	0.008437
0.044928	0.007	0.025451	0.026024	0.009	0.020424	0.008096	0.008427
0.044911	0.009	0.025451	0.026024	0.009	0.020424	0.008096	0.008408
0.044903	0.159	0.025451	0.026024	0.009	0.020424	0.008096	0.008408
0.044852	0.073	0.025451	0.025975	0.009	0.020424	0.008058	0.008398
0.044852	0.049	0.025283	0.025927	0.009	0.020424	0.008058	0.008379
0.044802	0.019	0.025283	0.025927	0.009	0.020354	0.008058	0.008369
0.044794	0.134	0.025283	0.025878	0.009	0.020354	0.00802	0.008369
0.04471	0.01	0.025283	0.025829	0.009	0.020284	0.00802	0.00836
0.044577	0.006	0.025283	0.02578	0.009	0.020284	0.007945	0.00834
0.044543	0.131	0.025283	0.02578	0.009	0.020284	0.007945	0.008311
0.044535	0.016	0.025283	0.025683	0.009	0.020284	0.007945	0.008311
0.044527	0.026	0.025283	0.025683	0.009	0.020213	0.007869	0.008311
0.044493	0.026	0.025114	0.025634	0.009	0.020213	0.007869	0.008311
0.04446	0.179	0.025114	0.025585	0.009	0.020213	0.007831	0.008302
0.044443	0.035	0.025114	0.025585	0.009	0.020213	0.007831	0.008302
0.044427	0.011	0.025114	0.025585	0.009	0.020213	0.007793	0.008292
0.044343	0.012	0.024946	0.025585	0.009	0.020213	0.007755	0.008273
0.044293	0.054	0.024946	0.025585	0.009	0.020143	0.007755	0.008254
0.044285	0.006	0.024777	0.025585	0.009	0.020143	0.007755	0.008254
0.044285	0.008	0.024777	0.025537	0.009	0.020143	0.007755	0.008205
0.044176	0.012	0.024777	0.025537	0.009	0.020072	0.007755	0.008196
0.044126	0.026	0.024608	0.025488	0.009	0.020072	0.007718	0.008196
0.044067	0.054	0.024608	0.025488	0.009	0.020072	0.007718	0.008186
0.044026	0.069	0.024608	0.025488	0.009	0.020072	0.007718	0.008177
0.044001	0.093	0.02444	0.025439	0.009	0.020072	0.007718	0.008148
0.043984	0.006	0.02444	0.025342	0.009	0.020072	0.007718	0.008148
0.04395	0.149	0.02444	0.025293	0.009	0.020072	0.007718	0.008138
0.043917	0.006	0.024271	0.025293	0.009	0.020002	0.007642	0.008128
0.043859	0.394	0.024271	0.025293	0.009	0.020002	0.007642	0.008109
0.043783	0.128	0.024271	0.025293	0.009	0.020002	0.007604	0.008099
0.043742	0.012	0.024271	0.025147	0.009	0.020002	0.007604	0.008099
0.043725	0.005	0.024271	0.025147	0.009	0.019931	0.007566	0.008099
0.0437	0.046	0.024271	0.025147	0.009	0.019931	0.007566	0.00809
0.0437	0.011	0.024271	0.025098	0.009	0.019931	0.007528	0.00809
0.043691	0.275	0.024271	0.025098	0.009	0.019861	0.007528	0.00808
0.043691	0.012	0.024103	0.025098	0.009	0.019861	0.007528	0.00807
0.043675	0.067	0.024103	0.025098	0.009	0.019791	0.007491	0.00807
0.043658	0.039	0.024103	0.025049	0.009	0.019791	0.007491	0.008051
0.043608	0.08	0.024103	0.025001	0.009	0.01972	0.007491	0.007974
0.043566	0.038	0.024103	0.025001	0.009	0.01972	0.007453	0.007955
0.043466	0.01	0.024103	0.025001	0.009	0.01965	0.007453	0.007945
0.043408	0.085	0.024103	0.025001	0.009	0.01965	0.007453	0.007945
0.043391	0.006	0.023934	0.024903	0.009	0.01965	0.007453	0.007916
0.043382	0.014	0.023934	0.024903	0.009	0.01965	0.007415	0.007916
0.043366	0.053	0.023934	0.024708	0.009	0.019579	0.007415	0.007907
0.043357	0.007	0.023934	0.024659	0.009	0.019579	0.007377	0.007907
0.043332	0.215	0.023766	0.024659	0.009	0.019579	0.007377	0.007868
0.043324	0.004	0.023766	0.024611	0.009	0.019438	0.007377	0.007858
0.043324	0.016	0.023766	0.024562	0.009	0.019438	0.007377	0.007849
0.043307	0.096	0.023766	0.024513	0.009	0.019368	0.007377	0.007791
0.043282	0.011	0.023766	0.024464	0.009	0.019298	0.007339	0.007781
0.043257	0.037	0.023766	0.024464	0.009	0.019298	0.007339	0.007781
0.04324	0.014	0.023597	0.024416	0.009	0.019298	0.007339	0.007762
0.043007	0.016	0.023597	0.02427	0.009	0.019227	0.007339	0.007762
0.04299	0.005	0.023597	0.02427	0.009	0.019157	0.007301	0.007752
0.042965	0.011	0.023597	0.02427	0.009	0.019157	0.007301	0.007714

0.04294	0.014	0.023597	0.024221	0.009	0.019157	0.007264	0.007714
0.04294	0.024	0.023597	0.024221	0.009	0.019086	0.007226	0.007694
0.042915	0.084	0.023429	0.024172	0.009	0.019086	0.007226	0.007675
0.04284	0.01	0.023429	0.024075	0.009	0.019086	0.007226	0.007646
0.042814	0.014	0.023429	0.024075	0.009	0.019016	0.007188	0.007646
0.042798	0.01	0.023429	0.024026	0.009	0.019016	0.007188	0.007646
0.042789	0.013	0.023429	0.024026	0.009	0.019016	0.007188	0.007646
0.042764	0.003	0.02326	0.024026	0.009	0.018945	0.007188	0.007646
0.042739	0.009	0.02326	0.023977	0.009	0.018945	0.00715	0.007637
0.042739	0.192	0.02326	0.023928	0.008	0.018945	0.00715	0.007637
0.042698	0.017	0.02326	0.023928	0.008	0.018945	0.00715	0.007627
0.042664	0.009	0.02326	0.02388	0.008	0.018945	0.00715	0.007617
0.042606	0.015	0.02326	0.023831	0.008	0.018875	0.007112	0.007598
0.042597	0.025	0.02326	0.023782	0.008	0.018875	0.007112	0.007598
0.042564	0.029	0.02326	0.023782	0.008	0.018875	0.007112	0.007588
0.042531	0.127	0.02326	0.023733	0.008	0.018875	0.007112	0.007579
0.042297	1	0.023092	0.023733	0.008	0.018875	0.007112	0.007569
0.042213	0.016	0.023092	0.023733	0.008	0.018875	0.007112	0.007559
0.04213	0.004	0.023092	0.023685	0.008	0.018875	0.007037	0.00755
0.042121	0.016	0.023092	0.023685	0.008	0.018875	0.007037	0.00754
0.042096	0.014	0.023092	0.023685	0.008	0.018875	0.007037	0.007511
0.042071	0.036	0.023092	0.023685	0.008	0.018875	0.007037	0.007502
0.042029	0.007	0.023092	0.023636	0.008	0.018805	0.006999	0.007502
0.041979	0.012	0.023092	0.023636	0.008	0.018664	0.006999	0.007482
0.041963	0.032	0.022923	0.023636	0.008	0.018523	0.006999	0.007473
0.041937	0.015	0.022923	0.023587	0.008	0.018523	0.006923	0.007463
0.041929	0.016	0.022923	0.02349	0.008	0.018523	0.006923	0.007453
0.041921	0.01	0.022923	0.02349	0.008	0.018452	0.006923	0.007444
0.041921	0.009	0.022923	0.023441	0.008	0.018452	0.006885	0.007434
0.041904	0.007	0.022923	0.023441	0.008	0.018452	0.006885	0.007367
0.041896	0.049	0.022923	0.023441	0.008	0.018382	0.006885	0.007347
0.041871	0.797	0.022586	0.023392	0.008	0.018382	0.006885	0.007328
0.041862	0.008	0.022586	0.023344	0.008	0.018312	0.006885	0.007309
0.041846	0.072	0.022586	0.023149	0.008	0.018312	0.006847	0.007299
0.041779	0.145	0.022586	0.0231	0.008	0.018312	0.006847	0.007289
0.041762	0.005	0.022586	0.0231	0.008	0.018241	0.006847	0.00728
0.041762	0.032	0.022586	0.0231	0.008	0.018241	0.006847	0.007261
0.041745	0.046	0.022586	0.023051	0.008	0.018241	0.006847	0.007241
0.041737	0.031	0.022586	0.023051	0.008	0.018241	0.00681	0.007232
0.041729	0.053	0.022417	0.023051	0.008	0.018241	0.00681	0.007222
0.041704	0.012	0.022417	0.022905	0.008	0.018241	0.00681	0.007193
0.041679	0.026	0.022417	0.022905	0.008	0.018171	0.00681	0.007193
0.041679	0.037	0.022417	0.022905	0.008	0.018171	0.00681	0.007183
0.041645	0.14	0.022417	0.022905	0.008	0.018171	0.006772	0.007183
0.041645	0.107	0.022417	0.022856	0.008	0.0181	0.006772	0.007154
0.041637	0.008	0.022417	0.022856	0.008	0.0181	0.006772	0.007145
0.04162	0.009	0.022417	0.022808	0.008	0.0181	0.006772	0.007097
0.041587	0.005	0.022249	0.022808	0.008	0.0181	0.006772	0.007068
0.041562	0.135	0.022249	0.022759	0.008	0.01803	0.006772	0.007039
0.04152	0.024	0.02208	0.022759	0.008	0.01803	0.006696	0.007039
0.041512	0.01	0.02208	0.02271	0.008	0.01803	0.006696	0.007029
0.04142	0.006	0.02208	0.02271	0.008	0.01803	0.006696	0.007
0.041411	0.025	0.02208	0.022661	0.008	0.01803	0.006658	0.006991
0.041403	0.018	0.02208	0.022661	0.008	0.01803	0.006658	0.006971
0.041395	0.016	0.021912	0.022613	0.008	0.017959	0.00662	0.006971
0.041386	0.03	0.021912	0.022613	0.008	0.017959	0.00662	0.006962
0.041361	0.011	0.021912	0.022564	0.008	0.017889	0.00662	0.006962
0.041319	0.006	0.021912	0.022564	0.008	0.017889	0.00662	0.006962
0.041236	0.08	0.021912	0.022564	0.008	0.017889	0.00662	0.006962
0.041177	0.008	0.021912	0.022564	0.008	0.017889	0.00662	0.006962
0.041152	0.011	0.021743	0.022564	0.008	0.017819	0.006583	0.006952
0.041136	0.008	0.021743	0.022466	0.008	0.017819	0.006583	0.006933
0.041094	0.046	0.021743	0.022466	0.008	0.017819	0.006583	0.006933
0.041002	0.095	0.021743	0.022418	0.008	0.017748	0.006583	0.006894
0.040952	0.025	0.021743	0.022418	0.008	0.017748	0.006583	0.006894
0.040843	0.108	0.021743	0.022418	0.008	0.017748	0.006583	0.006894
0.040818	0.205	0.021743	0.022369	0.008	0.017748	0.006545	0.006894
0.040818	0.185	0.021743	0.022369	0.008	0.017748	0.006507	0.006875
0.040668	0.015	0.021575	0.022369	0.008	0.017678	0.006507	0.006846
0.040584	0.013	0.021575	0.022369	0.008	0.017678	0.006507	0.006836
0.040551	0.034	0.021575	0.02232	0.008	0.017607	0.006507	0.006827
0.040534	0.01	0.021575	0.022271	0.008	0.017607	0.006469	0.006798
0.040459	0.135	0.021575	0.022223	0.008	0.017537	0.006469	0.006798
0.040442	0.015	0.021575	0.022174	0.008	0.017537	0.006469	0.006788
0.040409	0.048	0.021575	0.022125	0.008	0.017537	0.006469	0.006788
0.040392	0.686	0.021406	0.022077	0.008	0.017537	0.006469	0.006788
0.040351	0.586	0.021406	0.022077	0.008	0.017537	0.006431	0.006788
0.040292	0.018	0.021406	0.022077	0.008	0.017537	0.006431	0.006778
0.04025	0.005	0.021406	0.022028	0.008	0.017466	0.006431	0.006759
0.040158	0.011	0.021406	0.022028	0.008	0.017396	0.006393	0.006759
0.040142	0.01	0.021406	0.022028	0.008	0.017396	0.006393	0.00674
0.040133	0.005	0.021237	0.021979	0.008	0.017396	0.006356	0.006701
0.0401	0.026	0.021237	0.021979	0.008	0.017396	0.006356	0.006701
0.040083	0.049	0.021237	0.021979	0.008	0.017326	0.006356	0.006672
0.040083	0.011	0.021237	0.021882	0.008	0.017326	0.006318	0.006634
0.039983	0.043	0.021237	0.021882	0.008	0.017255	0.006318	0.006624
0.039975	0.01	0.021237	0.021882	0.008	0.017255	0.006318	0.006605
0.039975	0.009	0.021069	0.021784	0.008	0.017185	0.006318	0.006595
0.03995	0.009	0.021069	0.021735	0.008	0.017185	0.006318	0.006566
0.039925	1.038	0.021069	0.021735	0.008	0.017185	0.00628	0.006566
0.039916	0.013	0.021069	0.021687	0.008	0.017185	0.00628	0.006557
0.039899	0.005	0.021069	0.021687	0.008	0.017185	0.00628	0.006547
0.039891	0.049	0.021069	0.021687	0.008	0.017185	0.00628	0.006537
0.039866	0.033	0.021069	0.021687	0.008	0.017114	0.00628	0.006537
0.039858	0.033	0.0209	0.021687	0.008	0.017044	0.00628	0.006528
0.039841	0.008	0.0209	0.021687	0.008	0.016973	0.006242	0.006528
0.039808	0.034	0.0209	0.021638	0.008	0.016973	0.006242	0.006518
0.039791	0.137	0.0209	0.021638	0.008	0.016973	0.006242	0.006508
0.039732	0.034	0.0209	0.021589	0.008	0.016973	0.006242	0.006508
0.039716	0.076	0.0209	0.021492	0.008	0.016903	0.006242	0.006508
0.039682	0.011	0.0209	0.021492	0.008	0.016903	0.006204	0.006489
0.039657	0.02	0.020732	0.021492	0.007	0.016903	0.006204	0.006479
0.039649	0.028	0.020732	0.021492	0.007	0.016903	0.006204	0.006479
0.039641	0.007	0.020732	0.021492	0.007	0.016833	0.006204	0.006451
0.039616	0.362	0.020732	0.021443	0.007	0.016833	0.006166	0.006441
0.03959	0.006	0.020732	0.021443	0.007	0.016762	0.006166	0.006441
0.039574	0.033	0.020732	0.021443	0.007	0.016762	0.006166	0.006422
0.039507	0.024	0.020732	0.021443	0.007	0.016762	0.006129	0.006412
0.03944	0.016	0.020732	0.021394	0.007	0.016762	0.006129	0.006412
0.039415	0.014	0.020732	0.021394	0.007	0.016762	0.006129	0.006393
0.039323	0.008	0.020563	0.021297	0.007	0.016762	0.006091	0.006383
0.039164	0.066	0.020563	0.021248	0.007	0.016762	0.006091	0.006364
0.039114	0.047	0.020563	0.021248	0.007	0.016692	0.006091	0.006354
0.039056	0.009	0.020563	0.021199	0.007	0.016692	0.006091	0.006354

0.039014	0.006	0.020563	0.021199	0.007	0.016692	0.006091	0.006345
0.039006	0.005	0.020395	0.021151	0.007	0.016692	0.006091	0.006335
0.038997	0.074	0.020395	0.021151	0.007	0.016692	0.006091	0.006335
0.038981	0.003	0.020395	0.021102	0.007	0.016692	0.006053	0.006335
0.038922	0.443	0.020395	0.021102	0.007	0.016621	0.006053	0.006325
0.038914	0.019	0.020395	0.021102	0.007	0.016621	0.006053	0.006306
0.038906	0.074	0.020395	0.021053	0.007	0.016621	0.006015	0.006287
0.03888	0.022	0.020395	0.020956	0.007	0.016621	0.006015	0.006287
0.038814	0.078	0.020395	0.020956	0.007	0.016551	0.006015	0.006277
0.038814	0.027	0.020395	0.020956	0.007	0.016551	0.006015	0.006277
0.038797	0.094	0.020395	0.020956	0.007	0.016551	0.005977	0.006277
0.038797	0.021	0.020226	0.020956	0.007	0.016551	0.005977	0.006248
0.038772	0.052	0.020226	0.020907	0.007	0.01648	0.005977	0.006238
0.038747	0.02	0.020226	0.020809	0.007	0.01648	0.005977	0.006238
0.038705	0.011	0.020226	0.020809	0.007	0.01648	0.005939	0.006219
0.03868	0.011	0.020226	0.020761	0.007	0.01641	0.005939	0.00621
0.038538	0.005	0.020226	0.020712	0.007	0.01641	0.005902	0.0062
0.03853	0.019	0.020226	0.020712	0.007	0.01641	0.005902	0.006181
0.038505	0.634	0.020058	0.020663	0.007	0.01641	0.005902	0.006171
0.03848	0.029	0.020058	0.020663	0.007	0.01634	0.005864	0.006152
0.038463	0.009	0.020058	0.020663	0.007	0.01634	0.005864	0.006152
0.038446	2.926	0.020058	0.020663	0.007	0.01634	0.005864	0.006142
0.038438	0.01	0.020058	0.020614	0.007	0.01634	0.005864	0.006123
0.038429	0.051	0.020058	0.020614	0.007	0.01634	0.005864	0.006113
0.038421	0.039	0.020058	0.020614	0.007	0.01634	0.005826	0.006103
0.038338	0.079	0.020058	0.020614	0.007	0.01634	0.005826	0.006084
0.038304	0.029	0.020058	0.020614	0.007	0.01634	0.005826	0.006084
0.038287	0.099	0.020058	0.020614	0.007	0.016269	0.005826	0.006084
0.038279	0.419	0.020058	0.020566	0.007	0.016269	0.005826	0.006084
0.038262	0.054	0.020058	0.020566	0.007	0.016269	0.005788	0.006075
0.038237	0.017	0.019889	0.020566	0.007	0.016269	0.005788	0.006075
0.038229	0.011	0.019889	0.020566	0.007	0.016269	0.005788	0.006075
0.038179	0.024	0.019889	0.020517	0.007	0.016269	0.005788	0.006065
0.038129	0.004	0.019889	0.020517	0.007	0.016269	0.00575	0.006055
0.038062	0.101	0.019889	0.020468	0.007	0.016269	0.00575	0.006046
0.038029	0.024	0.019889	0.02042	0.007	0.016269	0.005712	0.006046
0.038029	0.185	0.019889	0.020225	0.007	0.016269	0.005712	0.006017
0.03802	0.172	0.019889	0.020225	0.007	0.016199	0.005675	0.005997
0.037953	0.045	0.01972	0.020176	0.007	0.016199	0.005675	0.005978
0.037912	0.02	0.019552	0.020176	0.007	0.016199	0.005675	0.005959
0.037786	0.15	0.019552	0.020127	0.007	0.016199	0.005637	0.005949
0.037786	0.021	0.019552	0.020078	0.007	0.016199	0.005637	0.005949
0.03777	0.603	0.019552	0.020078	0.007	0.016199	0.005637	0.00594
0.037736	0.035	0.019552	0.020078	0.007	0.016128	0.005637	0.00593
0.037703	0.032	0.019383	0.02003	0.007	0.016128	0.005599	0.00592
0.037694	0.015	0.019383	0.019981	0.007	0.016058	0.005599	0.00592
0.037653	0.053	0.019383	0.019981	0.006	0.016058	0.005599	0.005911
0.037628	0.055	0.019383	0.019932	0.006	0.016058	0.005599	0.005882
0.037578	0.247	0.019383	0.019883	0.006	0.016058	0.005599	0.005882
0.037502	0.032	0.019215	0.019835	0.006	0.016058	0.005561	0.005882
0.037502	0.025	0.019215	0.019786	0.006	0.016058	0.005561	0.005872
0.037461	0.004	0.019215	0.019786	0.006	0.016058	0.005561	0.005872
0.037427	0.063	0.019046	0.019737	0.006	0.016058	0.005561	0.005853
0.03741	0.007	0.019046	0.019689	0.006	0.015987	0.005561	0.005853
0.037402	0.064	0.019046	0.019689	0.006	0.015987	0.005561	0.005833
0.037385	0.099	0.019046	0.019689	0.006	0.015987	0.005523	0.005814
0.037385	0.009	0.019046	0.01964	0.006	0.015987	0.005523	0.005814
0.037344	0.038	0.019046	0.01964	0.006	0.015987	0.005523	0.005785
0.037335	0.011	0.019046	0.019591	0.006	0.015917	0.005523	0.005766
0.037327	0.019	0.019046	0.019591	0.006	0.015917	0.005523	0.005766
0.037302	0.011	0.018878	0.019591	0.006	0.015917	0.005523	0.005756
0.037268	0.008	0.018878	0.019591	0.006	0.015847	0.005486	0.005747
0.037227	0.003	0.018709	0.019591	0.006	0.015847	0.005486	0.005727
0.03721	0.015	0.018709	0.019542	0.006	0.015847	0.005486	0.005727
0.03716	0.27	0.018709	0.019494	0.006	0.015847	0.005448	0.005727
0.037135	0.012	0.018709	0.019445	0.006	0.015847	0.00541	0.005718
0.037135	0.824	0.018709	0.019445	0.006	0.015776	0.00541	0.005718
0.037085	0.125	0.018709	0.019445	0.006	0.015776	0.00541	0.005708
0.03706	0.011	0.018709	0.019396	0.006	0.015776	0.00541	0.005698
0.037035	0.031	0.018709	0.019396	0.006	0.015776	0.00541	0.005698
0.037026	0.04	0.018709	0.019396	0.006	0.015776	0.005372	0.005689
0.036968	0.293	0.018709	0.019396	0.006	0.015776	0.005372	0.00567
0.036959	0.192	0.018709	0.019396	0.006	0.015706	0.005372	0.00567
0.036884	0.156	0.018709	0.019396	0.006	0.015706	0.005372	0.00567
0.036868	0.112	0.018541	0.019347	0.006	0.015706	0.005372	0.00567
0.036868	0.004	0.018541	0.019347	0.006	0.015706	0.005372	0.00566
0.036859	0.025	0.018541	0.019299	0.006	0.015706	0.005372	0.005641
0.036826	0.006	0.018541	0.01925	0.006	0.015706	0.005334	0.005621
0.036809	0.065	0.018541	0.019201	0.006	0.015706	0.005334	0.005592
0.036792	0.546	0.018541	0.019201	0.006	0.015706	0.005296	0.005592
0.036776	0.008	0.018541	0.019201	0.006	0.015635	0.005296	0.005583
0.036759	0.055	0.018372	0.019152	0.006	0.015635	0.005296	0.005583
0.036734	0.005	0.018372	0.019152	0.006	0.015565	0.005296	0.005573
0.036709	0.007	0.018372	0.019152	0.006	0.015565	0.005296	0.005563
0.036642	0.008	0.018372	0.019152	0.006	0.015565	0.005221	0.005554
0.036617	0.012	0.018372	0.019104	0.006	0.015565	0.005221	0.005544
0.036592	0.015	0.018372	0.019055	0.006	0.015565	0.005221	0.005544
0.036542	0.012	0.018372	0.019055	0.006	0.015494	0.005221	0.005544
0.036442	0.031	0.018372	0.019055	0.006	0.015494	0.005183	0.005515
0.036442	0.039	0.018204	0.019055	0.006	0.015494	0.005183	0.005506
0.036375	0.039	0.018204	0.019006	0.006	0.015494	0.005145	0.005496
0.036341	0.04	0.018204	0.019006	0.006	0.015424	0.005145	0.005496
0.036333	0.197	0.018204	0.018958	0.006	0.015424	0.005145	0.005477
0.036275	0.008	0.018204	0.018958	0.006	0.015424	0.005107	0.005477
0.036249	0.006	0.018204	0.018909	0.006	0.015354	0.005107	0.005477
0.036233	0.055	0.018035	0.018909	0.006	0.015354	0.005107	0.005457
0.036183	0.101	0.018035	0.018909	0.006	0.015354	0.005107	0.005448
0.036166	0.02	0.017866	0.01886	0.006	0.015354	0.005107	0.005448
0.036116	0.033	0.017866	0.01886	0.006	0.015354	0.005107	0.005409
0.036099	0.063	0.017866	0.018811	0.006	0.015354	0.005107	0.0054
0.036091	0.002	0.017866	0.018811	0.006	0.015354	0.005069	0.00539
0.035991	0.01	0.017866	0.018763	0.006	0.015283	0.005069	0.00539
0.035991	0.008	0.017866	0.018763	0.006	0.015283	0.005069	0.00539
0.035957	0.029	0.017698	0.018763	0.006	0.015283	0.005069	0.00538
0.035957	0.155	0.017698	0.018714	0.006	0.015283	0.005069	0.00538
0.035949	0.026	0.017698	0.018714	0.006	0.015283	0.005069	0.00538
0.03594	0.163	0.017698	0.018714	0.006	0.015283	0.005032	0.005361
0.035932	0.014	0.017698	0.018714	0.005	0.015283	0.005032	0.005322
0.035915	0.005	0.017698	0.018616	0.005	0.015283	0.005032	0.005294
0.035907	0.01	0.017698	0.018616	0.005	0.015213	0.005032	0.005294
0.035882	0.175	0.017529	0.018568	0.005	0.015213	0.005032	0.005284
0.035874	0.028	0.017529	0.018568	0.005	0.015213	0.004994	0.005265
0.035832	0.006	0.017529	0.018568	0.005	0.015213	0.004994	0.005265
0.035824	0.01	0.017529	0.018519	0.005	0.015213	0.004994	0.005255

0.035824	0.028	0.017529	0.018519	0.005	0.015213	0.004994	0.005255
0.035815	0.004	0.017529	0.018519	0.005	0.015142	0.004994	0.005245
0.035798	0.026	0.017529	0.018519	0.005	0.015142	0.004994	0.005245
0.035757	0.036	0.017361	0.01847	0.005	0.015142	0.004994	0.005245
0.035757	0.013	0.017361	0.01847	0.005	0.015142	0.004956	0.005236
0.035748	0.037	0.017361	0.01847	0.005	0.015142	0.004956	0.005236
0.035707	0.011	0.017361	0.018421	0.005	0.015142	0.004956	0.005226
0.035648	0.017	0.017361	0.018421	0.005	0.015142	0.004956	0.005226
0.03564	0.041	0.017361	0.018421	0.005	0.015072	0.004956	0.005168
0.03564	0.015	0.017361	0.018373	0.005	0.015072	0.004956	0.005168
0.035623	0.07	0.017361	0.018324	0.005	0.015072	0.004956	0.005159
0.035623	0.02	0.017192	0.018275	0.005	0.015072	0.004956	0.005159
0.035606	0.005	0.017192	0.018275	0.005	0.015072	0.004918	0.005139
0.035598	0.009	0.017192	0.018227	0.005	0.015072	0.004918	0.005139
0.035556	0.031	0.017192	0.018178	0.005	0.015072	0.004918	0.005139
0.035556	0.181	0.017192	0.018178	0.005	0.015001	0.004918	0.005139
0.035498	0.065	0.017192	0.018129	0.005	0.015001	0.004918	0.005139
0.035481	0.171	0.017192	0.01808	0.005	0.014931	0.004918	0.005139
0.035473	0.007	0.017024	0.01808	0.005	0.014931	0.004918	0.00512
0.035464	0.009	0.017024	0.018032	0.005	0.014931	0.00488	0.005091
0.035448	0.017	0.017024	0.018032	0.005	0.014931	0.00488	0.005081
0.035448	0.024	0.017024	0.017983	0.005	0.014931	0.00488	0.005052
0.035389	0.045	0.017024	0.017934	0.005	0.014861	0.00488	0.005043
0.035381	0.201	0.017024	0.017885	0.005	0.014861	0.00488	0.005033
0.035381	1.323	0.017024	0.017885	0.005	0.014861	0.004842	0.005014
0.035364	0.011	0.017024	0.017837	0.005	0.014861	0.004842	0.005004
0.035347	0.035	0.016855	0.017837	0.005	0.01479	0.004805	0.005004
0.035347	0.02	0.016855	0.017788	0.005	0.01479	0.004805	0.005004
0.035289	0.009	0.016855	0.017788	0.005	0.01479	0.004805	0.004995
0.035264	0.029	0.016855	0.017739	0.005	0.01479	0.004805	0.004985
0.035239	0.031	0.016855	0.017739	0.005	0.01479	0.004767	0.004985
0.035222	0.112	0.016855	0.01769	0.005	0.01472	0.004767	0.004985
0.035164	0.027	0.016687	0.017642	0.005	0.01472	0.004767	0.004975
0.035164	0.025	0.016687	0.017593	0.005	0.01472	0.004729	0.004975
0.035155	0.156	0.016687	0.017593	0.005	0.01472	0.004729	0.004966
0.035139	0.058	0.016687	0.017593	0.005	0.01472	0.004729	0.004946
0.035105	0.05	0.016687	0.017544	0.005	0.01472	0.004729	0.004946
0.03508	0.314	0.016518	0.017496	0.005	0.01472	0.004691	0.004927
0.03508	0.009	0.016518	0.017496	0.005	0.01472	0.004691	0.004927
0.03508	0.228	0.016518	0.017496	0.005	0.014649	0.004691	0.004927
0.035063	0.004	0.016349	0.017447	0.005	0.014579	0.004691	0.004917
0.035055	0.062	0.016349	0.017447	0.005	0.014579	0.004691	0.004908
0.035047	0.011	0.016349	0.017447	0.005	0.014579	0.004691	0.004908
0.035013	0.17	0.016349	0.017398	0.005	0.014579	0.004653	0.00485
0.035013	0.027	0.016349	0.017398	0.005	0.014508	0.004653	0.00485
0.034955	0.116	0.016349	0.017398	0.005	0.014508	0.004653	0.00484
0.034938	0.011	0.016349	0.017398	0.005	0.014508	0.004653	0.004831
0.03488	0.007	0.016349	0.017301	0.005	0.014508	0.004653	0.004831
0.034871	0.033	0.016181	0.017301	0.005	0.014508	0.004653	0.004831
0.03483	0.036	0.016181	0.017301	0.004	0.014508	0.004653	0.004831
0.034805	0.062	0.016181	0.017252	0.004	0.014508	0.004653	0.004821
0.034805	0.082	0.016181	0.017252	0.004	0.014438	0.004615	0.004811
0.034796	0.013	0.016181	0.017203	0.004	0.014438	0.004615	0.004811
0.034788	0.051	0.016181	0.017203	0.004	0.014438	0.004615	0.004802
0.034771	0.019	0.016181	0.017203	0.004	0.014438	0.004615	0.004802
0.034721	0.062	0.016181	0.017154	0.004	0.014438	0.004578	0.004792
0.034704	0.325	0.016181	0.017154	0.004	0.014438	0.004578	0.004792
0.034621	0.085	0.016181	0.017057	0.004	0.014438	0.004578	0.004782
0.034612	0.021	0.016181	0.017057	0.004	0.014438	0.004578	0.004773
0.034596	0.077	0.016181	0.017008	0.004	0.014368	0.00454	0.004773
0.034596	0.025	0.016181	0.016959	0.004	0.014368	0.004502	0.004754
0.034596	0.11	0.016181	0.016959	0.004	0.014368	0.004502	0.004754
0.034587	0.029	0.016181	0.016959	0.004	0.014368	0.004502	0.004734
0.034571	0.072	0.016012	0.016911	0.004	0.014368	0.004502	0.004725
0.034537	0.008	0.016012	0.016862	0.004	0.014368	0.004502	0.004715
0.034504	0.013	0.016012	0.016862	0.004	0.014368	0.004502	0.004715
0.034487	0.069	0.016012	0.016813	0.004	0.014368	0.004502	0.004715
0.034479	0.006	0.016012	0.016765	0.004	0.014297	0.004502	0.004705
0.03447	0.057	0.016012	0.016716	0.004	0.014297	0.004502	0.004696
0.034437	0.017	0.016012	0.016716	0.004	0.014297	0.004464	0.004676
0.034412	0.136	0.015844	0.016667	0.004	0.014297	0.004464	0.004676
0.034404	0.008	0.015844	0.016667	0.004	0.014227	0.004464	0.004667
0.03437	0.038	0.015844	0.016667	0.004	0.014227	0.004464	0.004657
0.034353	0.267	0.015844	0.016667	0.004	0.014227	0.004426	0.004647
0.034345	0.028	0.015844	0.016618	0.003	0.014156	0.004426	0.004647
0.03432	0.013	0.015844	0.016618	0.003	0.014156	0.004426	0.004647
0.034287	0.011	0.015844	0.016618	0.003	0.014156	0.004426	0.004628
0.034278	0.089	0.015675	0.01657	0.003	0.014156	0.004388	0.004628
0.03427	0.589	0.015675	0.01657	0.003	0.014156	0.004388	0.004609
0.034237	0.006	0.015675	0.01657	0.003	0.014156	0.004388	0.00459
0.034228	0.023	0.015675	0.016521	0.003	0.014156	0.004388	0.00459
0.03422	0.027	0.015675	0.016521	0.003	0.014086	0.004388	0.00459
0.03417	0.062	0.015675	0.016472	0.003	0.014086	0.004388	0.00458
0.034161	0.132	0.015675	0.016472	0.003	0.014086	0.004388	0.00457
0.034161	0.045	0.015507	0.016472	0.003	0.014086	0.004351	0.004551
0.034153	0.023	0.015507	0.016423	0.003	0.014086	0.004351	0.004541
0.034128	0.042	0.015507	0.016375	0.003	0.014015	0.004351	0.004541
0.03412	0.019	0.015507	0.016375	0.003	0.014015	0.004351	0.004541
0.034111	0.02	0.015507	0.016375	0.003	0.014015	0.004313	0.004513
0.034103	0.047	0.015507	0.016375	0.003	0.014015	0.004275	0.004513
0.03407	0.043	0.015507	0.016326	0.003	0.013945	0.004275	0.004503
0.033986	0.255	0.015507	0.016326	0.003	0.013945	0.004275	0.004493
0.033986	0.009	0.015507	0.016326	0.003	0.013945	0.004275	0.004493
0.033969	0.019	0.015507	0.016277	0.003	0.013945	0.004275	0.004455
0.033969	0.025	0.015507	0.016277	0.003	0.013945	0.004275	0.004445
0.033944	0.009	0.015338	0.016228	0.003	0.013875	0.004237	0.004445
0.033928	0.063	0.015338	0.01618	0.003	0.013875	0.004237	0.004435
0.033919	0.037	0.015338	0.016131	0.003	0.013875	0.004237	0.004426
0.033902	0.016	0.015338	0.016131	0.003	0.013875	0.004237	0.004426
0.033852	0.034	0.015338	0.016131	0.003	0.013875	0.004237	0.004416
0.033844	0.023	0.015338	0.016082	0.003	0.013804	0.004199	0.004416
0.033836	0.005	0.015338	0.016033	0.003	0.013804	0.004199	0.004406
0.033811	0.101	0.01517	0.015985	0.003	0.013804	0.004199	0.004397
0.033802	0.257	0.01517	0.015985	0.003	0.013734	0.004161	0.004397
0.033794	0.042	0.01517	0.015985	0.003	0.013734	0.004124	0.004368
0.033794	0.058	0.01517	0.015985	0.002	0.013734	0.004124	0.004358
0.03376	0.031	0.01517	0.015985	0.002	0.013734	0.004124	0.004358
0.033752	0.017	0.015001	0.015985	0.002	0.013734	0.004124	0.004349
0.033735	0.027	0.015001	0.015936	0.002	0.013734	0.004124	0.004349
0.033735	0.029	0.015001	0.015936	0.002	0.013663	0.004124	0.004329
0.033702	0.008	0.015001	0.015936	0.002	0.013663	0.004124	0.004329
0.033669	0.184	0.015001	0.015936	0.002	0.013663	0.004124	0.00431
0.033644	0.41	0.014832	0.015887	0.001	0.013663	0.004086	0.00431
0.033635	0.023	0.014832	0.015839	0.0009424	0.013663	0.004086	0.00431

0.033627	0.032	0.014832	0.015839	0.0003141	0.013593	0.004086	0.004291
0.033602	0.084	0.014832	0.015839	0.0001571	0.013593	0.004048	0.004291
0.033568	0.015	0.014832	0.015839	0.0001571	0.013593	0.004048	0.004291
0.033518	0.062	0.014832	0.015741		0.013593	0.004048	0.004281
0.033443	0.012	0.014832	0.015692		0.013593	0.004048	0.004271
0.033401	0.007	0.014664	0.015692		0.013593	0.004048	0.004262
0.033393	0.182	0.014664	0.015546		0.013522	0.004048	0.004262
0.033376	0.034	0.014664	0.015546		0.013522	0.00401	0.004243
0.033368	1.05	0.014664	0.015546		0.013522	0.00401	0.004233
0.03336	0.042	0.014664	0.015546		0.013522	0.00401	0.004223
0.033351	0.022	0.014664	0.015497		0.013522	0.00401	0.004223
0.033243	0.093	0.014664	0.015449		0.013522	0.003972	0.004223
0.033209	0.039	0.014495	0.015449		0.013522	0.003972	0.004204
0.033151	0.035	0.014495	0.015449		0.013452	0.003934	0.004204
0.033142	0.009	0.014495	0.0154		0.013452	0.003934	0.004204
0.033126	0.03	0.014495	0.0154		0.013452	0.003934	0.004185
0.033109	0.092	0.014495	0.0154		0.013452	0.003934	0.004185
0.033101	0.017	0.014495	0.015351		0.013382	0.003934	0.004185
0.033101	0.035	0.014495	0.015351		0.013382	0.003934	0.004156
0.033042	0.027	0.014495	0.015351		0.013382	0.003934	0.004146
0.033025	0.059	0.014495	0.015302		0.013382	0.003934	0.004136
0.033009	0.006	0.014327	0.015302		0.013311	0.003897	0.004117
0.033	0.134	0.014327	0.015254		0.013311	0.003897	0.004079
0.033	0.053	0.014327	0.015254		0.013311	0.003897	0.004069
0.033	0.021	0.014327	0.015205		0.013311	0.003859	0.004069
0.032975	0.022	0.014327	0.015156		0.013311	0.003859	0.004069
0.032959	0.022	0.014327	0.015156		0.013311	0.003859	0.004059
0.032959	0.045	0.014327	0.014961		0.013311	0.003821	0.004059
0.03295	0.029	0.014327	0.014913		0.013241	0.003821	0.004059
0.032917	0.013	0.014327	0.014913		0.013241	0.003821	0.004059
0.0329	0.044	0.014327	0.014913		0.013241	0.003821	0.00405
0.032883	0.008	0.014327	0.014913		0.013241	0.003821	0.00404
0.032825	0.027	0.014327	0.014864		0.013241	0.003821	0.00403
0.032817	0.033	0.014158	0.014864		0.013241	0.003783	0.004021
0.032817	0.104	0.014158	0.014864		0.013241	0.003745	0.004021
0.032792	0.014	0.014158	0.014864		0.01317	0.003745	0.004001
0.03275	0.208	0.014158	0.014766		0.01317	0.003707	0.004001
0.032741	0.009	0.014158	0.014766		0.01317	0.003707	0.003992
0.032725	0.004	0.014158	0.014718		0.01317	0.003707	0.003982
0.032658	0.019	0.01399	0.014718		0.01317	0.00367	0.003973
0.032641	0.018	0.01399	0.014718		0.01317	0.003632	0.003963
0.032641	0.077	0.01399	0.014718		0.0131	0.003632	0.003953
0.032633	0.011	0.01399	0.014718		0.0131	0.003632	0.003934
0.032599	0.087	0.01399	0.014669		0.0131	0.003632	0.003924
0.032583	0.028	0.01399	0.01462		0.0131	0.003632	0.003915
0.032574	0.067	0.01399	0.01462		0.0131	0.003594	0.003915
0.032549	0.082	0.01399	0.01462		0.013029	0.003594	0.003905
0.032541	0.005	0.01399	0.014523		0.013029	0.003594	0.003905
0.032516	0.103	0.01399	0.014474		0.013029	0.003594	0.003895
0.032466	0.117	0.01399	0.014474		0.013029	0.003594	0.003886
0.032366	0.028	0.01399	0.014377		0.012959	0.003556	0.003886
0.032332	0.095	0.01399	0.014377		0.012959	0.003556	0.003876
0.032324	0.093	0.013821	0.014377		0.012959	0.003556	0.003857
0.032315	0.035	0.013821	0.014328		0.012959	0.003518	0.003857
0.032307	0.026	0.013821	0.014279		0.012959	0.003518	0.003857
0.032299	0.026	0.013821	0.014279		0.012959	0.003518	0.003857
0.03229	0.028	0.013821	0.014279		0.012889	0.003518	0.003847
0.032274	0.007	0.013821	0.01423		0.012889	0.00348	0.003828
0.032265	0.022	0.013821	0.01423		0.012889	0.00348	0.003828
0.03214	0.004	0.013821	0.01423		0.012889	0.00348	0.003818
0.032098	0.04	0.013821	0.014084		0.012818	0.003443	0.003809
0.032065	0.053	0.013821	0.014035		0.012818	0.003443	0.003809
0.032032	0.021	0.013821	0.014035		0.012818	0.003443	0.003799
0.032015	0.251	0.013653	0.014035		0.012818	0.003443	0.003799
0.031973	0.047	0.013653	0.014035		0.012818	0.003443	0.003799
0.031965	0.017	0.013653	0.014035		0.012818	0.003405	0.003799
0.031948	0.082	0.013653	0.013938		0.012748	0.003405	0.003799
0.031948	0.03	0.013653	0.013889		0.012748	0.003405	0.003789
0.031915	0.012	0.013653	0.013889		0.012748	0.003405	0.003789
0.031873	0.006	0.013653	0.013889		0.012677	0.003367	0.003789
0.031864	0.035	0.013484	0.013889		0.012677	0.003367	0.003789
0.031831	0.065	0.013484	0.01384		0.012677	0.003367	0.00378
0.031823	0.023	0.013484	0.01384		0.012677	0.003367	0.00377
0.031781	0.032	0.013484	0.013792		0.012677	0.003367	0.00376
0.031764	0.085	0.013484	0.013792		0.012677	0.003367	0.00376
0.031748	0.044	0.013484	0.013743		0.012607	0.003329	0.003731
0.031731	0.168	0.013484	0.013743		0.012607	0.003329	0.003722
0.031731	0.022	0.013484	0.013694		0.012607	0.003291	0.003722
0.031714	0.024	0.013484	0.013694		0.012607	0.003291	0.003722
0.031706	0.015	0.013484	0.013694		0.012607	0.003291	0.003712
0.031689	0.173	0.013316	0.013646		0.012607	0.003291	0.003703
0.031664	0.16	0.013316	0.013646		0.012536	0.003291	0.003703
0.031647	0.025	0.013316	0.013597		0.012536	0.003291	0.003703
0.031606	0.016	0.013316	0.013451		0.012536	0.003253	0.003693
0.031589	0.048	0.013316	0.013451		0.012536	0.003253	0.003683
0.031572	0.363	0.013316	0.013451		0.012536	0.003253	0.003683
0.031564	0.189	0.013316	0.013451		0.012536	0.003253	0.003664
0.031555	0.29	0.013147	0.013451		0.012536	0.003253	0.003654
0.031555	0.003	0.013147	0.013402		0.012466	0.003253	0.003645
0.03153	0.011	0.013147	0.013402		0.012466	0.003216	0.003645
0.031514	0.066	0.013147	0.013353		0.012466	0.003216	0.003645
0.031505	0.017	0.013147	0.013353		0.012466	0.003216	0.003625
0.031497	0.021	0.013147	0.013353		0.012466	0.003216	0.003616
0.031489	0.326	0.013147	0.013304		0.012396	0.003178	0.003606
0.031472	0.02	0.013147	0.013256		0.012396	0.003178	0.003606
0.031472	0.021	0.012978	0.013207		0.012396	0.003178	0.003606
0.031455	0.076	0.012978	0.013207		0.012396	0.00314	0.003568
0.031455	0.084	0.012978	0.013109		0.012396	0.00314	0.003568
0.031438	0.004	0.012978	0.013109		0.012396	0.003102	0.003558
0.031413	0.02	0.012978	0.013109		0.012396	0.003102	0.003539
0.031405	0.038	0.012978	0.013061		0.012325	0.003102	0.003519
0.031397	0.036	0.012978	0.013061		0.012325	0.003102	0.00351
0.031355	2.526	0.012978	0.012963		0.012255	0.003102	0.00351
0.03133	0.034	0.012978	0.012963		0.012255	0.003064	0.00351
0.03133	0.05	0.012978	0.012915		0.012255	0.003064	0.0035
0.031313	0.029	0.012978	0.012915		0.012255	0.003064	0.0035
0.031313	0.008	0.01281	0.012866		0.012255	0.003064	0.0035
0.031255	0.007	0.01281	0.012817		0.012255	0.003026	0.0035
0.03123	0.268	0.01281	0.012817		0.012184	0.003026	0.00349
0.031213	0.013	0.01281	0.012817		0.012184	0.003026	0.00349
0.031188	0.027	0.01281	0.012817		0.012184	0.003026	0.003481
0.03118	0.02	0.01281	0.012817		0.012184	0.002951	0.003471
0.031155	0.023	0.01281	0.012817		0.012184	0.002951	0.003462
0.031146	0.03	0.012641	0.012817		0.012184	0.002951	0.003452

0.031146	0.006	0.012641	0.012768	0.012114	0.002951	0.003452		
0.031121	0.279	0.012641	0.012768	0.012114	0.002951	0.003452		
0.031088	0.091	0.012641	0.012768	0.012043	0.002951	0.003452		
0.031013	0.029	0.012641	0.01272	0.012043	0.002951	0.003413		
0.030979	0.023	0.012641	0.01272	0.012043	0.002913	0.003413		
0.030971	0.019	0.012641	0.01272	0.012043	0.002913	0.003413		
0.030971	0.02	0.012473	0.012671	0.012043	0.002913	0.003404		
0.030929	0.476	0.012473	0.012671	0.012043	0.002913	0.003404		
0.030904	0.164	0.012473	0.012622	0.012043	0.002875	0.003404		
0.030887	0.043	0.012473	0.012622	0.012043	0.002875	0.003404		
0.030854	0.063	0.012473	0.012622	0.011973	0.002837	0.003394		
0.03082	0.033	0.012473	0.012622	0.011973	0.002837	0.003394		
0.030812	0.057	0.012473	0.012622	0.011973	0.002837	0.003394		
0.030787	0.147	0.012473	0.012573	0.011973	0.0028	0.003384		
0.030787	0.03	0.012473	0.012525	0.011973	0.0028	0.003365		
0.030729	0.063	0.012304	0.012427	0.011973	0.0028	0.003355		
0.030712	0.016	0.012304	0.012427	0.011973	0.0028	0.003346		
0.030687	0.007	0.012304	0.012427	0.011973	0.0028	0.003346		
0.030678	0.031	0.012304	0.012378	0.011973	0.0028	0.003346		
0.030662	0.084	0.012304	0.01233	0.011903	0.0028	0.003346		
0.030662	0.028	0.012304	0.01233	0.011903	0.002724	0.003336		
0.030653	0.012	0.012304	0.012281	0.011903	0.002724	0.003317		
0.030637	0.023	0.012136	0.012232	0.011903	0.002724	0.003317		
0.030495	0.019	0.012136	0.012232	0.011903	0.002724	0.003307		
0.030461	0.147	0.012136	0.012232	0.011903	0.002724	0.003298		
0.030453	0.012	0.012136	0.012184	0.011903	0.002724	0.003298		
0.030445	0.859	0.012136	0.012135	0.011832	0.002686	0.003298		
0.030436	0.07	0.012136	0.012086	0.011832	0.002686	0.003288		
0.03042	0.056	0.012136	0.012086	0.011832	0.002648	0.003278		
0.030403	0.017	0.012136	0.012086	0.011832	0.002648	0.003278		
0.030386	0.012	0.012136	0.011989	0.011832	0.00261	0.003269		
0.030386	0.017	0.011967	0.011891	0.011832	0.002573	0.003269		
0.030378	0.043	0.011967	0.011891	0.011832	0.002573	0.00324		
0.030378	1.726	0.011967	0.011842	0.011762	0.002573	0.003211		
0.030378	0.082	0.011967	0.011842	0.011762	0.002573	0.003201		
0.030336	0.162	0.011967	0.011842	0.011762	0.002573	0.003201		
0.030328	0.039	0.011967	0.011794	0.011762	0.002535	0.003192		
0.030319	0.012	0.011967	0.011696	0.011691	0.002535	0.003192		
0.030286	0.026	0.011967	0.011696	0.011691	0.002535	0.003182		
0.030278	0.023	0.011967	0.011647	0.011691	0.002535	0.003182		
0.030261	0.026	0.011799	0.011647	0.011691	0.002535	0.003182		
0.030252	0.076	0.011799	0.011599	0.011691	0.002535	0.003182		
0.030244	0.212	0.011799	0.011599	0.011621	0.002497	0.003182		
0.030211	0.05	0.011799	0.01155	0.011621	0.002497	0.003172		
0.030202	0.008	0.011799	0.01155	0.011621	0.002497	0.003172		
0.030194	0.022	0.011799	0.01155	0.011621	0.002497	0.003172		
0.030177	0.04	0.011799	0.011501	0.011621	0.002459	0.003143		
0.030177	0.05	0.011799	0.011452	0.01155	0.002421	0.003143		
0.030169	0.025	0.011799	0.011404	0.01155	0.002421	0.003134		
0.030161	0.014	0.01163	0.011404	0.01155	0.002383	0.003124		
0.030161	0.025	0.01163	0.011404	0.01155	0.002383	0.003114		
0.030119	0.065	0.01163	0.011404	0.01155	0.002346	0.003085		
0.030102	0.013	0.01163	0.011355	0.01155	0.002308	0.003076		
0.030085	0.009	0.01163	0.011355	0.01155	0.002308	0.003066		
0.030077	0.015	0.01163	0.011258	0.01155	0.002308	0.003057		
0.030044	0.046	0.011461	0.011258	0.01155	0.00227	0.003008		
0.029985	0.007	0.011461	0.011209	0.01148	0.00227	0.003008		
0.02996	0.097	0.011461	0.011209	0.01148	0.00227	0.002999		
0.02996	0.087	0.011461	0.011111	0.01148	0.00227	0.002989		
0.029952	0.289	0.011461	0.011111	0.01148	0.00227	0.002979		
0.029943	0.298	0.011461	0.011111	0.01148	0.002194	0.00295		
0.029935	0.008	0.011293	0.011063	0.01148	0.002194	0.002941		
0.029927	0.059	0.011293	0.011014	0.01148	0.002194	0.002931		
0.02991	0.741	0.011293	0.010965	0.01141	0.002194	0.002912		
0.02991	0.035	0.011293	0.010965	0.01141	0.002194	0.002912		
0.029868	0.045	0.011293	0.010916	0.01141	0.002156	0.002893		
0.029852	0.013	0.011293	0.010916	0.01141	0.002156	0.002893		
0.029826	0.042	0.011293	0.010868	0.01141	0.002156	0.002883		
0.029818	0.203	0.011293	0.01077	0.01141	0.002156	0.002873		
0.029818	0.021	0.011293	0.01077	0.011339	0.002119	0.002864		
0.029801	0.2	0.011293	0.01077	0.011339	0.002119	0.002864		
0.029801	0.052	0.011293	0.010673	0.011339	0.002119	0.002854		
0.029793	0.164	0.011293	0.010673	0.011339	0.002081	0.002844		
0.029785	0.017	0.011124	0.010575	0.011339	0.002081	0.002835		
0.029785	0.04	0.011124	0.010575	0.011339	0.002081	0.002825		
0.029768	0.006	0.011124	0.010527	0.011339	0.002043	0.002815		
0.029751	0.067	0.011124	0.010478	0.011339	0.002005	0.002815		
0.029735	0.094	0.011124	0.010429	0.011269	0.001967	0.002806		
0.029693	0.177	0.011124	0.01038	0.011269	0.001967	0.002806		
0.029684	0.042	0.010956	0.010283	0.011269	0.001967	0.002796		
0.029676	0.007	0.010956	0.010234	0.011269	0.001929	0.002777		
0.029651	0.025	0.010956	0.010234	0.011269	0.001892	0.002738		
0.029626	0.042	0.010956	0.010234	0.011269	0.00174	0.002738		
0.029542	0.02	0.010956	0.010137	0.011269	0.001702	0.002738		
0.029534	0.023	0.010956	0.010137	0.011198	0.001702	0.002709		
0.029526	0.329	0.010956	0.010137	0.011198	0.001702	0.002709		
0.029517	0.013	0.010956	0.010088	0.011198	0.001627	0.002709		
0.029459	0.04	0.010956	0.010039	0.011198	0.001513	0.0027		
0.029451	0.015	0.010956	0.010039	0.011198	0.001513	0.002681		
0.029434	0.115	0.010956	0.00999	0.011198	0.001438	0.002671		
0.029401	0.012	0.010956	0.00999	0.011198	0.001362	0.002661		
0.029375	0.008	0.010956	0.009942	0.011128	0.001324	0.002661		
0.029375	0.036	0.010787	0.009942	0.011128	0.001324	0.002642		
0.029367	0.005	0.010787	0.009942	0.011128	0.001248	0.002603		
0.029359	0.03	0.010787	0.009942	0.011128	0.001211	0.002594		
0.029334	0.012	0.010787	0.009942	0.011128	0.001135	0.002594		
0.0293	0.029	0.010787	0.009893	0.011128	0.000984	0.002584		
0.029275	0.01	0.010787	0.009893	0.011128		0.002584		
0.029267	0.544	0.010787	0.009893	0.011128		0.002574		
0.029225	0.014	0.010787	0.009844	0.011128		0.002565		
0.029217	0.04	0.010787	0.009844	0.011128		0.002565		
0.029192	0.016	0.010787	0.009796	0.011057		0.002546		
0.029183	0.015	0.010787	0.009796	0.011057		0.002536		
0.02915	0.08	0.010619	0.009796	0.011057		0.002536		
0.02915	0.363	0.010619	0.009747	0.011057		0.002526		
0.029108	0.033	0.010619	0.009747	0.011057		0.002517		
0.029091	0.086	0.010619	0.009747	0.011057		0.002497		
0.029008	0.075	0.010619	0.009698	0.010987		0.002497		
0.029	0.011	0.010619	0.009698	0.010987		0.002488		
0.029	0.005	0.010619	0.009698	0.010987		0.002488		
0.028975	0.01	0.010619	0.009698	0.010987		0.002468		
0.028975	0.23	0.01045	0.009649	0.010987		0.002468		
0.028975	0.26	0.01045	0.009649	0.010987		0.002449		
0.028958	0.015	0.01045	0.009649	0.010987		0.002449		

0.028908		0.019	0.01045			0.009649				0.010917			0.002439						
0.028891		0.123	0.01045			0.009649				0.010917			0.002439						
0.028858		0.076	0.01045			0.009649				0.010917			0.00242						
0.028841		0.011	0.01045			0.009649				0.010917			0.00242						
0.028833		0.01	0.01045			0.009601				0.010846			0.00242						
0.028816		0.33	0.010282			0.009552				0.010846			0.002401						
0.028749		0.072	0.010282			0.009552				0.010846			0.002391						
0.028741		0.087	0.010282			0.009552				0.010846			0.002382						
0.028707		0.629	0.010282			0.009503				0.010846			0.002372						
0.028657		0.008	0.010282			0.009454				0.010846			0.002343						
0.028649		0.049	0.010282			0.009406				0.010846			0.002343						
0.028632		0.007	0.010282			0.009406				0.010846			0.002343						
0.028624		0.095	0.010282			0.009357				0.010776			0.002333						
0.028624		0.013	0.010282			0.009357				0.010776			0.002324						
0.028599		0.018	0.010282			0.009357				0.010776			0.002314						
0.028582		0.039	0.010113			0.009357				0.010776			0.002295						
0.028574		0.009	0.010113			0.009308				0.010776			0.002256						
0.028557		0.171	0.010113			0.009308				0.010776			0.002247						
0.02854		0.005	0.010113			0.009259				0.010776			0.002247						
0.028524		0.009	0.010113			0.009259				0.010705			0.002237						
0.028473		0.027	0.010113			0.009211				0.010705			0.002218						
0.02844		0.275	0.010113			0.009211				0.010705			0.002208						
0.028398		0.014	0.010113			0.009211				0.010705			0.002189						
0.028382		0.005	0.010113			0.009211				0.010705			0.002189						
0.028373		0.006	0.009945			0.009162				0.010705			0.002179						
0.028331		0.031	0.009945			0.009113				0.010705			0.002169						
0.028315		0.007	0.009945			0.009065				0.010635			0.00216						
0.02829		0.043	0.009945			0.009065				0.010635			0.002141						
0.028281		0.014	0.009945			0.009065				0.010635			0.002141						
0.028281		0.036	0.009945			0.009016				0.010564			0.002141						
0.028273		0.077	0.009945			0.008967				0.010564			0.002131						
0.028265		0.011	0.009945			0.008967				0.010564			0.002102						
0.028265		0.032	0.009945			0.008918				0.010564			0.002092						
0.028265		0.882	0.009945			0.00887				0.010564			0.002063						
0.02824		0.025	0.009945			0.00887				0.010564			0.002054						
0.028223		0.021	0.009945			0.008821				0.010564			0.002034						
0.028223		0.006	0.009945			0.008821				0.010564			0.002034						
0.028148		0.024	0.009945			0.008821				0.010564			0.002034						
0.028148		0.026	0.009776			0.008772				0.010494			0.002025						
0.028139		0.016	0.009776			0.008723				0.010494			0.002025						
0.028123		0.029	0.009776			0.008626				0.010494			0.002015						
0.028114		0.019	0.009776			0.008626				0.010494			0.001996						
0.028047		0.023	0.009776			0.008577				0.010494			0.001996						
0.028031		0.132	0.009776			0.008577				0.010424			0.001986						
0.027947		0.04	0.009776			0.008528				0.010424			0.001957						
0.02793		0.497	0.009776			0.008528				0.010424			0.00189						
0.027889		0.071	0.009776			0.00848				0.010424			0.001851						
0.02788		0.093	0.009776			0.00848				0.010424			0.001842						
0.027864		0.1	0.009776			0.00848				0.010424			0.001832						
0.027855		0.007	0.009776			0.008431				0.010424			0.001832						
0.027847		0.021	0.009776			0.008431				0.010353			0.001813						
0.027847		0.02	0.009776			0.008334				0.010353			0.001813						
0.027822		0.041	0.009776			0.008285				0.010353			0.001784						
0.027822		1.577	0.009776			0.008285				0.010353			0.001774						
0.027788		0.055	0.009776			0.008236				0.010353			0.001765						
0.02773		0.02	0.009607			0.008236				0.010353			0.001678						
0.027722		0.055	0.009607			0.008236				0.010283			0.001649						
0.027688		0.02	0.009607			0.008236				0.010283			0.00163						
0.02768		0.022	0.009607			0.008187				0.010283			0.00162						
0.027655		0.134	0.009607			0.008187				0.010283			0.001601						
0.027638		0.02	0.009607			0.008139				0.010283			0.001591						
0.027638		0.027	0.009607			0.008139				0.010283			0.001591						
0.027605		0.874	0.009607			0.00809				0.010283			0.001591						
0.027588		0.02	0.009439			0.00809				0.010283			0.001581						
0.02758		0.005	0.009439			0.00809				0.010212			0.001572						
0.02758		0.005	0.009439			0.00809				0.010212			0.001552						
0.027488		0.003	0.009439			0.00809				0.010212			0.001523						
0.027488		0.007	0.009439			0.008041				0.010212			0.001417						
0.027471		0.007	0.009439			0.008041				0.010212			0.001417						
0.027454		0.005	0.009439			0.007895				0.010212			0.001417						
0.027454		0.006	0.009439			0.007895				0.010212			0.000829						
0.027446		0.015	0.009439			0.007797				0.010212									
0.027446		0.015	0.009439			0.007797				0.010212									
0.027429		0.285	0.00927			0.007797				0.010142									
0.027421		0.039	0.00927			0.007797				0.010142									
0.027413		0.106	0.00927			0.007749				0.010142									
0.027413		0.01	0.00927			0.007749				0.010142									
0.027363		0.007	0.00927			0.007651				0.010142									
0.027354		0.132	0.00927			0.007651				0.010142									
0.027346		0.056	0.00927			0.007554				0.010142									
0.027346		0.007	0.00927			0.007505				0.010142									
0.027337		0.007	0.009102			0.007505				0.010142									
0.027296		0.074	0.009102			0.007456				0.010071									
0.027262		0.009	0.009102			0.007456				0.010071									
0.027262		0.116	0.009102			0.007408				0.010071									
0.027246		0.31	0.009102			0.007408				0.010071									
0.027237		0.028	0.009102			0.007408				0.010071									
0.027229		0.029	0.009102			0.007359				0.010071									
0.027187		0.014	0.008933			0.007359				0.010071									
0.027187		0.159	0.008933			0.007359				0.010001									
0.027145		0.008	0.008933			0.00731				0.010001									
0.027137		0.03	0.008933			0.007261				0.010001									
0.027137		0.009	0.008933			0.007261				0.010001									
0.027129		0.013	0.008933			0.007261				0.010001									
0.02712		0.072	0.008765			0.007261				0.010001									
0.027104		0.027	0.008765			0.007261				0.010001									
0.027095		0.012	0.008765			0.007213				0.009931									
0.027079		0.015	0.008765			0.007164				0.009931									
0.027079		0.031	0.008765			0.007066				0.009931									
0.027062		0.155	0.008765			0.007066				0.009931									
0.027053		0.222	0.008765			0.007018				0.00986									
0.027037		0.023	0.008765			0.006969				0.00986									
0.02702		0.065	0.008596			0.00692				0.00986									
0.026987		0.231	0.008596			0.00692				0.00986									
0.026962		0.133	0.008596			0.006871				0.00986									
0.026937		0.026	0.008596			0.006774				0.00986									
0.02692		0.248	0.008596			0.006774				0.00986									
0.02692		0.126	0.008596			0.006774				0.00986									
0.026911		0.035	0.008596			0.006774				0.00979									
0.026903		0.011	0.008596			0.006725				0.00979									
0.026895		0.16	0.008428			0.006725				0.00979									
0.026886		0.02	0.008428			0.006677				0.00979									
0.026861		0.153	0.008428			0.006677				0.00979									
0.026861		0.04	0.008428			0.006677				0.00979									

| | | |

0.024899	0.044	0.006236						0.008663			
0.024899	0.09	0.006236						0.008663			
0.024899	0.054	0.006236						0.008663			
0.02489	1.425	0.006236						0.008663			
0.02489	0.009	0.006236						0.008663			
0.024865	0.113	0.006236						0.008592			
0.024865	0.018	0.006236						0.008592			
0.024848	0.035	0.006236						0.008592			
0.024848	0.038	0.006068						0.008592			
0.024815	0.346	0.006068						0.008522			
0.024815	0.017	0.006068						0.008522			
0.02474	0.009	0.006068						0.008522			
0.024706	0.793	0.006068						0.008522			
0.024698	0.011	0.006068						0.008522			
0.024698	0.05	0.006068						0.008451			
0.02469	0.053	0.006068						0.008451			
0.024681	0.065	0.006068						0.008451			
0.024673	0.014	0.005899						0.008451			
0.024648	0.056	0.005899						0.008451			
0.024623	5.912	0.005899						0.008451			
0.024615	0.064	0.005899						0.008381			
0.024615	0.038	0.005899						0.008381			
0.024606	0.012	0.005899						0.008381			
0.024606	0.017	0.005899						0.008381			
0.024598	0.094	0.005731						0.008381			
0.024598	0.16	0.005731						0.008381			
0.024556	0.11	0.005731						0.008381			
0.024531	0.023	0.005731						0.008381			
0.024506	0.101	0.005731						0.008381			
0.024498	0.047	0.005731						0.008381			
0.024481	0.012	0.005731						0.008311			
0.024473	0.043	0.005731						0.008311			
0.024464	0.047	0.005731						0.008311			
0.024448	0.019	0.005562						0.008311			
0.024448	0.086	0.005562						0.008311			
0.024422	0.025	0.005562						0.008311			
0.024397	0.057	0.005562						0.008311			
0.024389	0.038	0.005562						0.008311			
0.024356	0.018	0.005562						0.008311			
0.024306	0.007	0.005562						0.008311			
0.024306	0.183	0.005562						0.00824			
0.024297	0.012	0.005562						0.00824			
0.024289	0.011	0.005562						0.00824			
0.024164	0.711	0.005562						0.00824			
0.024155	0.006	0.005394						0.00824			
0.024138	0.021	0.005394						0.00824			
0.02413	0.019	0.005394						0.00824			
0.024105	0.006	0.005394						0.00824			
0.024105	0.022	0.005394						0.00817			
0.024097	0.017	0.005394						0.00817			
0.024072	0.681	0.005394						0.00817			
0.024072	0.056	0.005394						0.00817			
0.024063	0.02	0.005394						0.00817			
0.024047	0.008	0.005394						0.00817			
0.023996	0.089	0.005394						0.00817			
0.02398	0.029	0.005225						0.00817			
0.023971	0.019	0.005225						0.00817			
0.023913	0.04	0.005225						0.00817			
0.023905	0.298	0.005225						0.00817			
0.023896	0.286	0.005225						0.008099			
0.02388	0.051	0.005225						0.008099			
0.023871	0.163	0.005225						0.008099			
0.023871	0.007	0.005225						0.008099			
0.023871	0.072	0.005225						0.008099			
0.023846	0.019	0.005225						0.008099			
0.023846	0.026	0.005057						0.008099			
0.023838	0.015	0.005057						0.008029			
0.023838	0.013	0.005057						0.008029			
0.023838	0.086	0.005057						0.008029			
0.023838	0.008	0.005057						0.008029			
0.023821	0.014	0.005057						0.008029			
0.023821	0.106	0.005057						0.008029			
0.023813	0.015	0.004888						0.008029			
0.023813	1.1	0.004888						0.008029			
0.023788	0.097	0.004888						0.008029			
0.023788	0.152	0.004888						0.008029			
0.023779	0.021	0.004888						0.008029			
0.023754	0.012	0.004888						0.008029			
0.023746	0.037	0.004888						0.008029			
0.023738	0.27	0.004719						0.007958			
0.023729	0.64	0.004719						0.007958			
0.023729	0.026	0.004719						0.007958			
0.023729	0.008	0.004719						0.007958			
0.023729	0.024	0.004719						0.007958			
0.023721	0.014	0.004719						0.007958			
0.023713	0.01	0.004719						0.007958			
0.023704	0.061	0.004551						0.007958			
0.023679	0.013	0.004551						0.007888			
0.023679	0.062	0.004551						0.007888			
0.023679	0.024	0.004551						0.007888			
0.023679	0.396	0.004551						0.007888			
0.023646	1.695	0.004551						0.007888			
0.023646	0.015	0.004551						0.007888			
0.023579	0.009	0.004551						0.007888			
0.023562	0.698	0.004551						0.007888			
0.023554	0.009	0.004551						0.007888			
0.023545	0.118	0.004551						0.007888			
0.023537	0.007	0.004382						0.007818			
0.023512	0.162	0.004382						0.007818			
0.02347	5.131	0.004382						0.007818			
0.023462	0.034	0.004382						0.007818			
0.023462	0.469	0.004382						0.007818			
0.023454	0.005	0.004214						0.007818			
0.023445	0.005	0.004214						0.007818			
0.023378	0.135	0.004214						0.007818			
0.023362	0.03	0.004214						0.007818			
0.02332	0.014	0.004214						0.007818			
0.023312	0.071	0.004214						0.007747			
0.023312	0.004	0.004214						0.007747			
0.023303	0.018	0.004214						0.007747			
0.023295	0.026	0.004214						0.007747			
0.023287	0.058	0.004214						0.007747			
0.023278	0.117	0.004214						0.007677			
0.02327	0.051	0.004214						0.007677			

0.023261	0.154	0.004214						0.007677				
0.023211	0.008	0.004214						0.007677				
0.023203	0.068	0.004045						0.007677				
0.023203	0.05	0.004045						0.007677				
0.023195	0.025	0.004045						0.007677				
0.023186	0.012	0.004045						0.007677				
0.02317	0.122	0.004045						0.007677				
0.023161	0.011	0.004045						0.007677				
0.023136	0.02	0.004045						0.007606				
0.023128	0.381	0.004045						0.007606				
0.023128	0.014	0.004045						0.007606				
0.023119	0.01	0.004045						0.007606				
0.023119	0.007	0.004045						0.007606				
0.023119	0.171	0.004045						0.007606				
0.023069	0.009	0.003877						0.007606				
0.022986	0.044	0.003877						0.007606				
0.022952	0.068	0.003877						0.007606				
0.022936	0.018	0.003877						0.007606				
0.022936	0.04	0.003877						0.007606				
0.022919	0.213	0.003877						0.007606				
0.022877	0.076	0.003877						0.007536				
0.022836	0.039	0.003708						0.007536				
0.02281	0.193	0.003708						0.007536				
0.02281	0.101	0.003708						0.007536				
0.022777	0.005	0.003708						0.007536				
0.022777	0.038	0.00354						0.007536				
0.02276	0.007	0.00354						0.007536				
0.022744	0.072	0.00354						0.007536				
0.022744	0.007	0.00354						0.007536				
0.022719	0.058	0.00354						0.007536				
0.02271	0.099	0.00354						0.007536				
0.02271	0.023	0.00354						0.007536				
0.022685	0.032	0.00354						0.007536				
0.022677	0.015	0.00354						0.007536				
0.022668	0.062	0.003371						0.007536				
0.02266	0.785	0.003371						0.007465				
0.022627	0.017	0.003202						0.007465				
0.022577	0.076	0.003202						0.007465				
0.022568	0.048	0.003202						0.007465				
0.022552	0.707	0.003202						0.007465				
0.022535	0.427	0.003202						0.007465				
0.022535	0.394	0.003202						0.007465				
0.022535	0.005	0.003034						0.007465				
0.022518	0.025	0.003034						0.007465				
0.02251	0.013	0.003034						0.007395				
0.02251	0.018	0.003034						0.007395				
0.022493	0.043	0.003034						0.007395				
0.022485	0.018	0.003034						0.007395				
0.022476	1.021	0.002865						0.007395				
0.022451	0.013	0.002865						0.007395				
0.022443	0.01	0.002865						0.007395				
0.022426	0.02	0.002865						0.007325				
0.022426	0.341	0.002865						0.007325				
0.022401	0.007	0.002865						0.007325				
0.022393	0.157	0.002865						0.007325				
0.022384	0.016	0.002865						0.007254				
0.022376	0.011	0.002697						0.007254				
0.022368	0.021	0.002697						0.007254				
0.022343	0.063	0.002697						0.007254				
0.022343	0.025	0.002697						0.007254				
0.022334	0.028	0.002528						0.007254				
0.022326	0.006	0.002528						0.007254				
0.022326	0.161	0.002528						0.007254				
0.022318	0.135	0.002528						0.007254				
0.022318	0.01	0.002528						0.007184				
0.022301	0.036	0.00236						0.007184				
0.022284	0.023	0.00236						0.007184				
0.022259	0.016	0.00236						0.007184				
0.022259	0.027	0.00236						0.007184				
0.022226	0.006	0.00236						0.007184				
0.022209	0.066	0.00236						0.007184				
0.022142	0.021	0.00236						0.007184				
0.022117	0.015	0.00236						0.007184				
0.022092	0.048	0.002191						0.007184				
0.022067	0.009	0.002191						0.007184				
0.022067	0.014	0.002191						0.007184				
0.022059	0.809	0.002191						0.007184				
0.022025	0.026	0.002191						0.007113				
0.022025	0.888	0.002191						0.007113				
0.022025	0.007	0.002191						0.007113				
0.022017	0.241	0.002023						0.007113				
0.022009	0.069	0.002023						0.007113				
0.022	0.013	0.002023						0.007113				
0.021984	0.012	0.001854						0.007113				
0.02195	0.011	0.001854						0.007113				
0.021925	0.031	0.001854						0.007043				
0.021917	0.315	0.001686						0.007043				
0.021917	0.041	0.001686						0.007043				
0.021875	0.564	0.001686						0.007043				
0.021875	0.033	0.001686						0.007043				
0.021858	0.084	0.001517						0.007043				
0.021825	0.009	0.001517						0.007043				
0.021791	0.087	0.001517						0.007043				
0.021783	0.06	0.001517						0.006972				
0.021766	0.738	0.001348						0.006972				
0.02175	0.626	0.001348						0.006972				
0.021741	0.968	0.001348						0.006972				
0.021733	0.016	0.001348						0.006902				
0.021725	0.119	0.001348						0.006902				
0.021725	0.037	0.00118						0.006902				
0.021725	0.542	0.00118						0.006902				
0.021725	0.009	0.00118						0.006902				
0.021708	0.032	0.00118						0.006902				
0.021708	0.01	0.00118						0.006902				
0.0217	0.013	0.00118						0.006832				
0.0217	0.154	0.001011						0.006832				
0.021658	0.014	0.001011						0.006832				
0.021649	0.03	0.001011						0.006832				
0.021641	0.023	0.001011						0.006832				
0.021633	0.01	0.001011						0.006832				
0.021616	0.029	0.001011						0.006832				
0.021608	0.056	0.000843						0.006832				
0.021599	0.016	0.000337						0.006832				
0.021558	0.055							0.006761				

0.021533	0.186							0.006761				
0.021507	0.101							0.006761				
0.021499	0.207							0.006761				
0.021482	0.005							0.006761				
0.021466	0.202							0.006761				
0.021441	0.005							0.006761				
0.021441	0.046							0.006761				
0.021424	0.094							0.006761				
0.021416	0.087							0.006691				
0.021391	0.168							0.006691				
0.021382	0.016							0.006691				
0.021365	0.043							0.006691				
0.021357	0.558							0.006691				
0.02134	0.048							0.006691				
0.021315	0.005							0.006691				
0.021307	0.106							0.006691				
0.021299	0.084							0.006691				
0.02129	0.056							0.00662				
0.02129	0.074							0.00662				
0.02129	0.01							0.00662				
0.02129	0.016							0.00662				
0.021257	0.086							0.00662				
0.021257	0.055							0.00662				
0.021249	0.034							0.00655				
0.021232	0.08							0.00655				
0.021215	0.042							0.00655				
0.021165	0.065							0.00655				
0.021123	0.021							0.00655				
0.021123	0.138							0.00655				
0.021107	0.022							0.00655				
0.021107	0.012							0.00655				
0.021107	0.559							0.00655				
0.021107	0.014							0.006479				
0.021107	0.015							0.006479				
0.021081	0.051							0.006479				
0.021073	0.213							0.006479				
0.021048	0.091							0.006479				
0.021048	0.011							0.006479				
0.021031	0.181							0.006479				
0.021031	0.014							0.006479				
0.021023	0.293							0.006479				
0.021015	0.016							0.006409				
0.021006	0.048							0.006409				
0.021006	0.01							0.006409				
0.020973	0.043							0.006409				
0.020956	0.029							0.006409				
0.02094	0.027							0.006409				
0.020931	0.005							0.006409				
0.020906	0.03							0.006409				
0.020898	0.044							0.006409				
0.020873	0.012							0.006409				
0.020873	0.023							0.006339				
0.020856	0.431							0.006339				
0.020848	0.132							0.006339				
0.020831	0.019							0.006339				
0.020823	0.019							0.006339				
0.020814	0.012							0.006339				
0.020798	0.372							0.006339				
0.020756	0.017							0.006339				
0.020747	0.036							0.006339				
0.020739	1.361							0.006268				
0.020722	0.009							0.006268				
0.020689	0.625							0.006268				
0.020689	0.086							0.006268				
0.020672	0.04							0.006268				
0.020664	0.021							0.006268				
0.020656	0.155							0.006268				
0.020622	0.015							0.006268				
0.020605	0.023							0.006268				
0.020589	0.009							0.006268				
0.02058	0.013							0.006268				
0.020555	0.029							0.006198				
0.020555	0.398							0.006198				
0.020547	0.012							0.006198				
0.020539	0.01							0.006198				
0.020522	0.432							0.006198				
0.020497	0.093							0.006198				
0.020497	0.212							0.006127				
0.020405	0.205							0.006127				
0.020397	0.006							0.006127				
0.02038	0.007							0.006127				
0.020372	0.011							0.006127				
0.020346	0.01							0.006057				
0.02033	0.017							0.006057				
0.020321	0.047							0.006057				
0.020313	0.027							0.006057				
0.020305	0.035							0.006057				
0.020305	0.226							0.006057				
0.020296	0.587							0.006057				
0.020296	0.024							0.006057				
0.020288	0.02							0.006057				
0.02028	0.015							0.005986				
0.02028	0.112							0.005986				
0.020271	0.048							0.005986				
0.020271	0.005							0.005986				
0.020263	0.285							0.005986				
0.020255	0.043							0.005986				
0.020255	0.036							0.005986				
0.020246	0.223							0.005986				
0.020221	0.107							0.005916				
0.020213	0.037							0.005916				
0.020163	0.03							0.005916				
0.020163	0.009							0.005916				
0.020154	0.006							0.005916				
0.020146	0.05							0.005916				
0.020129	0.046							0.005916				
0.020113	0.015							0.005916				
0.020104	0.301							0.005916				
0.020096	0.021							0.005916				
0.020096	0.026							0.005916				
0.020088	0.501							0.005916				
0.020071	0.053							0.005916				
0.020071	0.119							0.005916				
0.020063	0.015							0.005916				

0.020063	0.005							0.005916			
0.020012	0.027							0.005916			
0.020012	0.023							0.005916			
0.020012	0.019							0.005846			
0.020004	0.017							0.005846			
0.020004	0.141							0.005846			
0.019962	0.212							0.005846			
0.019954	0.015							0.005846			
0.019954	0.015							0.005846			
0.019954	0.027							0.005846			
0.019937	0.091							0.005846			
0.019929	0.145							0.005775			
0.019929	0.042							0.005775			
0.019904	0.055							0.005775			
0.019895	0.055							0.005775			
0.019895	0.046							0.005775			
0.019895	0.014							0.005775			
0.019895	0.1							0.005775			
0.019887	0.014							0.005775			
0.019879	0.018							0.005775			
0.019837	0.303							0.005775			
0.019812	0.226							0.005775			
0.019787	0.424							0.005775			
0.019787	0.011							0.005705			
0.019787	0.009							0.005705			
0.019779	0.12							0.005705			
0.019762	0.011							0.005705			
0.019737	0.008							0.005705			
0.01972	0.07							0.005705			
0.019662	0.254							0.005705			
0.019662	0.156							0.005705			
0.019645	0.048							0.005705			
0.019637	0.006							0.005705			
0.019628	0.015							0.005705			
0.019628	0.035							0.005634			
0.01962	0.086							0.005634			
0.019545	0.012							0.005634			
0.019536	0.155							0.005634			
0.019503	0.022							0.005634			
0.019478	0.057							0.005634			
0.019453	0.033							0.005634			
0.019444	0.011							0.005634			
0.019444	0.037							0.005634			
0.019436	3.184							0.005634			
0.019428	0.024							0.005634			
0.019428	0.061							0.005634			
0.019419	0.006							0.005564			
0.019419	0.106							0.005564			
0.019411	0.022							0.005564			
0.019403	0.017							0.005564			
0.019386	0.533							0.005564			
0.019369	0.016							0.005564			
0.019369	0.158							0.005564			
0.019361	0.026							0.005564			
0.019336	0.025							0.005493			
0.019336	0.068							0.005493			
0.019327	0.894							0.005493			
0.019319	0.211							0.005493			
0.019311	0.015							0.005493			
0.019302	0.243							0.005493			
0.019277	0.182							0.005493			
0.019269	0.009							0.005493			
0.019269	0.131							0.005493			
0.019261	0.051							0.005493			
0.019252	0.016							0.005493			
0.019244	0.017							0.005493			
0.019236	0.02							0.005493			
0.019211	0.018							0.005423			
0.019211	0.172							0.005423			
0.019194	0.059							0.005423			
0.019194	0.141							0.005423			
0.019177	0.056							0.005423			
0.01916	0.014							0.005353			
0.019127	0.216							0.005353			
0.019127	0.017							0.005353			
0.019119	0.03							0.005282			
0.019094	0.073							0.005282			
0.019094	0.145							0.005282			
0.019085	0.011							0.005282			
0.019069	0.037							0.005282			
0.019052	0.007							0.005282			
0.019044	0.026							0.005282			
0.01901	0.063							0.005282			
0.018985	0.018							0.005212			
0.018977	0.636							0.005212			
0.018977	0.011							0.005212			
0.018918	0.018							0.005212			
0.018876	0.071							0.005212			
0.018868	0.05							0.005212			
0.018851	0.008							0.005212			
0.018851	0.079							0.005212			
0.018826	0.056							0.005212			
0.018818	0.148							0.005212			
0.01881	0.013							0.005212			
0.018785	0.014							0.005141			
0.018785	0.37							0.005141			
0.01876	0.071							0.005141			
0.018751	0.028							0.005141			
0.018726	0.17							0.005141			
0.018693	0.038							0.005141			
0.018693	0.03							0.005141			
0.018693	0.085							0.005141			
0.018651	0.084							0.005071			
0.018651	0.061							0.005071			
0.018643	0.027							0.005071			
0.018643	0.005							0.005071			
0.018643	0.018							0.005071			
0.018618	0.053							0.005071			
0.018592	0.077							0.005071			
0.018592	0.298							0.005071			
0.018584	0.025							0.005071			
0.018576	0.013							0.005071			
0.018559	0.039							0.005071			
0.018526	0.016							0.005			

0.018526	0.099							0.005			
0.018509	0.011							0.005			
0.018501	0.031							0.005			
0.018501	0.012							0.005			
0.018467	0.022							0.005			
0.018459	0.024							0.005			
0.018459	0.208							0.005			
0.01845	0.061							0.005			
0.018434	0.298							0.00493			
0.018434	0.005							0.00493			
0.018434	0.146							0.00493			
0.018425	0.045							0.00493			
0.018417	0.016							0.00493			
0.018392	0.113							0.00493			
0.018392	0.032							0.00493			
0.018384	0.055							0.00493			
0.018375	0.031							0.00486			
0.018342	0.004							0.00486			
0.018342	0.028							0.00486			
0.018342	0.326							0.004789			
0.018325	0.018							0.004789			
0.018325	0.006							0.004789			
0.018325	0.081							0.004789			
0.018325	0.008							0.004789			
0.018317	0.125							0.004789			
0.018308	0.018							0.004789			
0.018308	0.01							0.004789			
0.018308	0.187							0.004789			
0.0183	0.02							0.004719			
0.018292	0.427							0.004719			
0.018258	0.013							0.004719			
0.018225	0.105							0.004719			
0.018217	0.013							0.004719			
0.018208	0.021							0.004719			
0.018208	0.044							0.004719			
0.0182	0.023							0.004719			
0.0182	0.039							0.004719			
0.018192	0.007							0.004719			
0.018192	0.052							0.004719			
0.018192	0.021							0.004648			
0.018175	0.025							0.004648			
0.018175	0.032							0.004648			
0.018167	0.008							0.004648			
0.018158	0.011							0.004578			
0.018158	0.127							0.004578			
0.018125	0.03							0.004578			
0.018058	0.234							0.004578			
0.01805	0.039							0.004578			
0.01805	0.026							0.004507			
0.018033	0.09							0.004507			
0.018033	0.047							0.004507			
0.018033	0.017							0.004507			
0.018016	0.019							0.004507			
0.017974	0.071							0.004507			
0.017941	0.025							0.004507			
0.017924	0.02							0.004507			
0.017924	0.016							0.004507			
0.017924	0.021							0.004507			
0.017916	0.246							0.004507			
0.017916	0.504							0.004437			
0.017899	0.015							0.004437			
0.017891	0.015							0.004437			
0.017874	0.04							0.004437			
0.017874	0.017							0.004437			
0.017857	0.02							0.004437			
0.017857	0.135							0.004437			
0.017849	0.04							0.004437			
0.017832	0.028							0.004367			
0.017816	0.017							0.004367			
0.017816	0.335							0.004367			
0.017799	0.213							0.004367			
0.017782	0.004							0.004367			
0.017774	0.081							0.004367			
0.017766	0.007							0.004367			
0.017757	0.018							0.004296			
0.017757	0.042							0.004296			
0.017749	0.042							0.004296			
0.017732	0.019							0.004296			
0.017732	0.026							0.004296			
0.017707	0.047							0.004296			
0.017699	0.032							0.004296			
0.01769	0.005							0.004296			
0.017665	0.191							0.004296			
0.017665	0.134							0.004226			
0.017649	0.01							0.004226			
0.017632	0.277							0.004226			
0.017624	0.026							0.004226			
0.017615	0.022							0.004226			
0.017599	0.009							0.004155			
0.017582	0.009							0.004155			
0.017548	0.02							0.004155			
0.017515	0.023							0.004155			
0.017507	0.189							0.004155			
0.017507	0.079							0.004155			
0.017507	0.027							0.004155			
0.017507	0.073							0.004085			
0.017498	0.035							0.004085			
0.017498	0.154							0.004085			
0.01749	0.011							0.004085			
0.017482	0.021							0.004085			
0.017465	0.119							0.004085			
0.017465	0.015							0.004085			
0.017457	0.094							0.004014			
0.017448	0.044							0.004014			
0.017431	0.264							0.004014			
0.017348	0.132							0.004014			
0.017331	0.031							0.004014			
0.017315	0.109							0.004014			
0.017315	0.068							0.004014			
0.017315	0.011							0.004014			
0.017273	0.207							0.004014			
0.017248	0.037							0.004014			
0.017231	0.099							0.003944			
0.017223	0.013							0.003944			

0.017206	0.05							0.003944			
0.017206	0.351							0.003944			
0.017198	0.006							0.003874			
0.017173	0.031							0.003874			
0.017164	0.022							0.003874			
0.017156	0.071							0.003874			
0.017139	0.36							0.003874			
0.017131	0.037							0.003874			
0.017122	0.004							0.003874			
0.017122	0.035							0.003803			
0.017114	0.006							0.003803			
0.017081	0.058							0.003803			
0.017056	0.009							0.003803			
0.017056	0.088							0.003803			
0.017056	0.027							0.003803			
0.017031	0.015							0.003803			
0.017006	0.026							0.003803			
0.017006	0.008							0.003803			
0.016997	0.083							0.003803			
0.016955	0.009							0.003733			
0.016947	0.047							0.003733			
0.01693	0.213							0.003733			
0.01693	0.039							0.003733			
0.016914	0.011							0.003733			
0.016914	0.016							0.003733			
0.016905	0.008							0.003733			
0.016889	0.045							0.003733			
0.01688	0.037							0.003733			
0.01688	0.042							0.003733			
0.016872	0.011							0.003733			
0.016872	0.022							0.003662			
0.016872	0.017							0.003662			
0.016847	0.16							0.003662			
0.016847	0.075							0.003662			
0.016838	0.007							0.003662			
0.016822	0.162							0.003592			
0.016813	0.008							0.003592			
0.016797	0.082							0.003592			
0.016755	0.096							0.003592			
0.016755	0.032							0.003592			
0.016747	0.02							0.003592			
0.016722	0.03							0.003592			
0.016713	0.039							0.003592			
0.016696	0.047							0.003521			
0.016696	0.286							0.003521			
0.016696	0.127							0.003521			
0.016696	0.04							0.003521			
0.016696	0.002							0.003521			
0.016688	0.02							0.003521			
0.016688	0.032							0.003521			
0.01668	0.043							0.003521			
0.01668	0.006							0.003521			
0.01668	0.008							0.003521			
0.016646	0.052							0.003451			
0.016638	0.006							0.003451			
0.01663	0.023							0.003451			
0.01663	0.023							0.003451			
0.01663	0.048							0.003451			
0.016621	0.346							0.003451			
0.016613	0.11							0.003451			
0.01658	0.011							0.003451			
0.01658	0.052							0.003381			
0.016571	1.772							0.003381			
0.016571	0.013							0.003381			
0.016554	0.56							0.003381			
0.016554	0.007							0.003381			
0.016538	0.053							0.003381			
0.016529	0.495							0.003381			
0.016521	0.424							0.003381			
0.016513	0.009							0.003381			
0.016504	0.008							0.003381			
0.016471	0.004							0.003381			
0.016463	0.056							0.003381			
0.016463	0.211							0.003381			
0.016454	0.015							0.00331			
0.016446	0.217							0.00331			
0.016404	0.033							0.00331			
0.016404	0.151							0.00331			
0.016396	0.056							0.00324			
0.016379	0.013							0.00324			
0.016379	0.026							0.00324			
0.016379	0.063							0.00324			
0.016371	0.013							0.00324			
0.016362	0.014							0.00324			
0.016362	0.021							0.003169			
0.016346	0.006							0.003169			
0.016337	0.106							0.003169			
0.016321	0.123							0.003169			
0.016312	0.062							0.003169			
0.016304	0.19							0.003169			
0.016304	0.106							0.003169			
0.016304	0.338							0.003169			
0.016304	0.009							0.003099			
0.016304	0.048							0.003099			
0.016304	0.01							0.003099			
0.016296	0.024							0.003099			
0.016262	0.007							0.003099			
0.016262	0.097							0.003099			
0.016262	0.011							0.003099			
0.016245	0.058							0.003028			
0.016245	0.111							0.003028			
0.016237	0.045							0.003028			
0.016237	0.011							0.003028			
0.016229	0.014							0.003028			
0.01622	0.156							0.002958			
0.016212	0.029							0.002958			
0.016212	0.033							0.002958			
0.016204	0.04							0.002958			
0.016179	0.021							0.002888			
0.016145	0.036							0.002888			
0.016129	0.009							0.002888			
0.016112	0.009							0.002817			
0.016112	0.647							0.002817			
0.016112	0.034							0.002747			

0.016103	0.005							0.002747			
0.016087	0.912							0.002747			
0.016087	0.047							0.002747			
0.016062	0.116							0.002747			
0.016037	0.015							0.002747			
0.016003	0.014							0.002747			
0.015978	0.03							0.002676			
0.01597	0.185							0.002676			
0.01597	0.087							0.002676			
0.015911	0.013							0.002676			
0.015886	0.103							0.002606			
0.015886	0.004							0.002606			
0.01587	0.176							0.002606			
0.015861	0.061							0.002606			
0.015828	0.024							0.002606			
0.015811	0.064							0.002606			
0.015794	0.042							0.002606			
0.015778	0.081							0.002606			
0.015761	0.476							0.002606			
0.015753	0.044							0.002535			
0.015753	0.005							0.002535			
0.015736	0.036							0.002535			
0.015736	0.034							0.002535			
0.015711	0.004							0.002535			
0.015703	0.322							0.002535			
0.015703	0.005							0.002535			
0.015669	0.008							0.002535			
0.015669	0.007							0.002535			
0.015661	0.095							0.002535			
0.015636	0.063							0.002535			
0.015627	0.013							0.002465			
0.015627	0.019							0.002465			
0.015627	0.009							0.002465			
0.015619	0.075							0.002465			
0.015611	0.022							0.002395			
0.015602	0.015							0.002395			
0.015594	0.018							0.002395			
0.015586	0.042							0.002395			
0.015577	0.037							0.002395			
0.015577	0.013							0.002395			
0.015561	0.872							0.002395			
0.015561	0.063							0.002395			
0.015552	0.088							0.002395			
0.015552	0.005							0.002324			
0.015544	0.072							0.002324			
0.015527	0.012							0.002324			
0.015485	0.016							0.002324			
0.015485	0.035							0.002324			
0.015469	0.015							0.002183			
0.01546	0.244							0.002183			
0.015435	0.026							0.002183			
0.015435	0.024							0.002183			
0.015435	0.039							0.002183			
0.015427	0.013							0.002183			
0.015427	0.042							0.002183			
0.015419	0.011							0.002042			
0.01541	0.033							0.002042			
0.015402	1.001							0.002042			
0.015402	0.111							0.002042			
0.015385	0.031							0.001972			
0.015385	0.042							0.001972			
0.015385	0.061							0.001972			
0.015385	0.018							0.001972			
0.015377	0.042							0.001902			
0.015343	0.007							0.001902			
0.015335	0.019							0.001902			
0.015327	0.283							0.001902			
0.015318	0.17							0.001902			
0.015302	1.791							0.001902			
0.015302	0.014							0.001831			
0.015293	0.04							0.001831			
0.015293	0.012							0.001761			
0.015293	0.028							0.001761			
0.01526	0.211							0.001761			
0.01526	0.043							0.001761			
0.015252	0.003							0.001761			
0.015235	0.097							0.001761			
0.015226	0.026							0.00169			
0.015218	0.019							0.00169			
0.015218	0.007							0.00169			
0.015218	0.018							0.00169			
0.015218	0.207							0.00169			
0.01521	0.197							0.00162			
0.01521	0.025							0.00162			
0.015201	0.039							0.00162			
0.015193	0.024							0.00162			
0.015185	0.014							0.00162			
0.015185	0.018							0.001549			
0.015185	0.01							0.001549			
0.015176	0.143							0.001549			
0.015168	0.16							0.001549			
0.015168	0.013							0.001549			
0.015168	0.029							0.001549			
0.015168	0.015							0.001549			
0.01516	0.049							0.001549			
0.015143	0.026							0.001479			
0.015143	0.015							0.001479			
0.015135	0.022							0.001479			
0.015135	0.102							0.001479			
0.015126	0.011							0.001479			
0.015126	0.033							0.001479			
0.015118	0.049							0.001409			
0.015101	0.008							0.001409			
0.015068	0.024							0.001409			
0.015043	0.02							0.001338			
0.015034	0.724							0.001338			
0.015001	0.057							0.001268			
0.014993	0.032							0.001268			
0.014993	0.04							0.001268			
0.014959	0.019							0.001268			
0.014942	0.131							0.001268			
0.014942	0.042							0.001197			
0.014934	0.022							0.001197			
0.014926	0.011							0.001197			

0.014917	0.006								0.001127			
0.014917	0.034								0.001127			
0.014909	0.102								0.001127			
0.014901	0.277								0.001127			
0.014884	0.062								0.001056			
0.014884	0.127								0.000986			
0.014884	0.012								0.000916			
0.014876	0.026								0.000916			
0.014867	0.012								0.000845			
0.014859	0.036								0.000845			
0.014851	0.019								0.000775			
0.014834	0.01								0.000775			
0.014826	0.053								0.000775			
0.0148	0.154								0.000775			
0.0148	0.069								0.000775			
0.014792	0.148								0.000775			
0.014792	0.039								0.000704			
0.014784	0.143								0.000704			
0.014775	0.021								0.000704			
0.014759	0.029								0.000704			
0.01475	0.033								0.000634			
0.014742	0.09								0.000563			
0.014692	0.043								0.000563			
0.014684	0.047								0.000563			
0.014667	0.008								0.000563			
0.01465	0.208								0.000493			
0.014642	0.01								0.000493			
0.014633	0.332								0.000493			
0.014625	0.024								0.000423			
0.0146	0.017								0.000423			
0.014592	0.013								0.000282			
0.014583	0.153								0.000282			
0.014575	0.006								0.000211			
0.014567	0.033								0.000211			
0.014558	0.156											
0.014558	0.033											
0.014558	0.021											
0.014558	0.008											
0.014558	0.012											
0.014542	0.052											
0.014525	0.089											
0.014525	0.017											
0.014516	0.015											
0.014516	0.204											
0.014508	0.115											
0.0145	0.016											
0.014491	0.08											
0.014491	0.036											
0.014483	0.019											
0.014483	0.006											
0.014475	0.006											
0.014475	0.004											
0.014475	0.051											
0.014475	0.027											
0.014466	0.122											
0.014466	0.074											
0.014458	0.047											
0.014458	0.102											
0.014458	0.012											
0.014458	0.095											
0.014458	0.124											
0.014425	0.017											
0.014425	0.029											
0.014391	0.532											
0.014375	0.013											
0.014375	0.002											
0.014366	0.096											
0.014358	0.317											
0.014358	0.016											
0.014358	0.007											
0.014349	0.03											
0.014349	0.035											
0.014341	0.014											
0.014341	0.013											
0.014341	0.02											
0.014333	0.438											
0.014324	0.028											
0.014316	0.044											
0.014274	0.057											
0.014274	0.02											
0.014266	0.018											
0.014249	0.926											
0.014241	0.055											
0.014241	0.011											
0.014233	0.017											
0.014224	0.073											
0.014224	0.046											
0.014216	0.102											
0.014207	0.012											
0.014199	0.065											
0.014191	0.056											
0.014182	0.022											
0.014182	0.074											
0.014182	0.07											
0.014182	0.014											
0.014141	0.014											
0.014141	0.314											
0.014141	0.004											
0.014141	0.068											
0.014116	0.225											
0.014116	0.019											
0.014099	0.179											
0.014099	0.01											
0.014099	0.026											
0.014065	0.049											
0.014057	0.044											
0.014057	0.063											
0.014049	0.006											
0.014015	0.03											
0.014015	0.014											
0.014007	0.012											
0.014007	0.071											
0.013999	0.017											
0.013999	0.095											

0.013999	0.083
0.013999	0.012
0.013999	0.027
0.013974	0.015
0.013957	0.061
0.013957	0.02
0.013957	0.022
0.01394	0.004
0.01394	0.09
0.013932	0.109
0.013932	0.017
0.013932	0.091
0.013932	0.02
0.013923	0.02
0.013915	0.031
0.013907	0.004
0.013882	0.005
0.013882	0.136
0.013873	0.049
0.013865	0.005
0.013857	0.021
0.013848	0.174
0.01384	0.085
0.013832	0.065
0.013815	0.09
0.013807	0.06
0.013807	0.074
0.013798	0.013
0.013765	0.026
0.013765	0.007
0.01374	0.009
0.01374	0.047
0.01374	0.149
0.013731	0.063
0.013731	0.015
0.013723	0.018
0.013715	0.112
0.013706	0.019
0.013706	0.011
0.01369	0.043
0.013681	0.009
0.013673	0.034
0.013673	0.011
0.013665	0.003
0.013665	0.013
0.013656	0.019
0.013648	0.034
0.013639	0.023
0.013631	0.027
0.013623	0.011
0.013623	0.013
0.013606	0.061
0.013598	0.089
0.013598	0.088
0.013581	0.198
0.013573	0.004
0.013573	0.015
0.013556	0.217
0.013531	0.007
0.013523	0.014
0.013523	0.016
0.013514	0.024
0.013506	0.038
0.013489	0.061
0.013481	0.017
0.013464	0.101
0.013447	0.164
0.013447	0.032
0.013422	0.026
0.013406	0.041
0.013381	0.022
0.013364	0.044
0.013364	0.14
0.013364	0.055
0.013339	0.013
0.013339	0.008
0.013339	0.028
0.013314	0.034
0.013305	0.127
0.013297	0.128
0.013272	0.075
0.013264	0.037
0.013264	0.012
0.013255	0.029
0.01323	0.015
0.013222	0.006
0.013222	0.13
0.013205	0.036
0.013205	0.099
0.013197	0.004
0.013188	0.02
0.013188	0.232
0.01318	0.227
0.013172	0.004
0.013163	0.075
0.013155	0.023
0.013155	0.007
0.013147	0.013
0.013138	0.031
0.013138	0.007
0.01313	1.333
0.01313	0.988
0.013105	0.015
0.013105	0.008
0.013097	0.004
0.013088	0.091
0.01308	0.036
0.01308	0.01
0.013072	0.026
0.013063	0.032
0.013055	0.077
0.013055	0.157
0.013046	0.014
0.013038	0.017

0.012996	0.034
0.012996	1.031
0.012988	0.009
0.012971	0.102
0.012971	0.007
0.012963	0.034
0.012963	0.03
0.012963	0.116
0.012955	0.03
0.012955	0.023
0.012938	0.025
0.012938	0.017
0.012904	0.039
0.012904	0.018
0.012896	0.06
0.012888	0.018
0.012879	0.005
0.012871	0.021
0.012863	0.018
0.012854	0.026
0.012829	0.012
0.012829	0.089
0.012829	0.01
0.012813	0.011
0.012813	0.006
0.012788	0.034
0.012771	0.08
0.012762	0.171
0.012762	0.101
0.012754	0.056
0.012746	0.036
0.012729	0.041
0.012712	0.011
0.012696	0.049
0.012696	0.009
0.012687	0.025
0.012662	0.073
0.012662	0.069
0.012637	0.032
0.012637	0.012
0.012604	0.042
0.012595	0.026
0.012587	0.05
0.012579	0.035
0.012554	0.392
0.012554	0.008
0.012545	0.013
0.012545	0.022
0.012545	0.008
0.012537	0.004
0.012529	0.014
0.012529	0.067
0.01252	0.018
0.012504	0.015
0.012504	0.005
0.012504	0.107
0.012487	0.008
0.012487	0.017
0.012462	0.028
0.012453	0.061
0.012453	0.01
0.012445	0.07
0.012445	0.014
0.012437	0.02
0.012437	0.03
0.01242	0.008
0.01242	0.174
0.012412	0.017
0.012387	0.005
0.012362	0.199
0.012328	0.121
0.012295	0.036
0.012295	0.021
0.012295	0.019
0.012295	0.005
0.01227	0.02
0.012261	0.051
0.012253	0.154
0.012253	0.013
0.012253	0.009
0.012245	0.005
0.012236	0.031
0.01222	0.052
0.01222	0.026
0.012211	0.039
0.012211	0.004
0.012203	0.199
0.012195	0.015
0.012195	0.195
0.012178	0.016
0.012178	0.004
0.012161	0.009
0.012153	0.206
0.012153	0.08
0.012144	0.012
0.012136	0.009
0.012119	0.124
0.012119	0.121
0.012119	0.037
0.012119	0.02
0.012111	0.116
0.012103	0.021
0.012094	0.014
0.012094	0.211
0.012086	0.003
0.012086	0.11
0.012086	0.023
0.012078	0.04
0.012061	0.024
0.012061	0.017
0.012036	0.083
0.012027	0.172
0.012027	0.461
0.012027	0.037

0.012019	0.025
0.011986	0.036
0.011986	0.007
0.011977	0.266
0.011952	0.12
0.011952	0.033
0.011944	0.007
0.011919	0.017
0.011902	0.005
0.011902	0.004
0.011902	0.02
0.011894	0.009
0.01186	0.191
0.01186	0.029
0.011852	0.009
0.011844	0.106
0.011844	0.024
0.011844	0.029
0.011844	0.01
0.011827	0.035
0.011827	0.026
0.011827	0.233
0.011827	0.175
0.011827	0.23
0.011827	0.02
0.011819	0.039
0.011819	0.065
0.01181	0.012
0.011802	0.004
0.011802	0.01
0.011802	0.185
0.011794	0.035
0.011785	0.076
0.011785	0.012
0.011769	0.02
0.011769	0.018
0.01176	0.006
0.011752	0.006
0.011743	0.051
0.011743	0.045
0.011727	0.019
0.011727	0.005
0.011718	0.03
0.011718	0.29
0.01171	0.012
0.01171	0.029
0.011702	0.01
0.011702	0.006
0.011702	0.004
0.011693	0.053
0.011693	0.02
0.011685	0.172
0.011685	0.013
0.011685	0.127
0.011677	0.012
0.011652	0.021
0.011643	0.021
0.011643	0.028
0.011643	0.074
0.011635	0.413
0.011627	0.008
0.011627	0.034
0.011618	0.012
0.011618	0.014
0.01161	0.006
0.01161	0.005
0.011602	0.098
0.011602	0.12
0.011593	0.094
0.011593	0.059
0.011585	0.107
0.011576	0.033
0.011568	0.058
0.011551	0.627
0.011551	0.005
0.011551	0.006
0.011543	0.042
0.011543	0.011
0.011535	0.015
0.011535	0.004
0.011535	0.067
0.011535	0.155
0.011535	0.012
0.011526	0.022
0.011526	0.193
0.011526	0.011
0.011518	0.013
0.011518	0.015
0.011518	0.027
0.01151	0.036
0.01151	0.105
0.011501	0.019
0.011501	0.095
0.011493	0.028
0.011485	0.013
0.011476	0.005
0.011476	0.003
0.01146	0.014
0.011451	0.005
0.011434	0.025
0.011434	0.362
0.011426	0.056
0.011426	0.039
0.011426	0.03
0.011426	0.903
0.011418	0.004
0.011409	0.027
0.011401	0.896
0.011401	0.021
0.011401	0.181
0.011401	0.037
0.011393	0.007
0.011376	0.012
0.011376	0.05

0.011376	0.01
0.011376	0.07
0.011368	0.052
0.011359	0.164
0.011359	0.077
0.011359	0.018
0.011351	0.016
0.011334	0.004
0.011326	0.009
0.011318	0.374
0.011309	0.721
0.011301	0.089
0.011292	0.071
0.011284	0.103
0.011284	0.157
0.011284	0.045
0.011276	0.051
0.011276	0.083
0.011259	0.012
0.011251	0.039
0.011251	0.027
0.011251	0.03
0.011234	1.655
0.011226	0.009
0.011226	0.007
0.011201	0.019
0.011184	0.032
0.011176	0.007
0.011167	0.052
0.011167	0.007
0.011159	0.047
0.01115	0.068
0.011134	0.043
0.011125	0.008
0.011117	0.003
0.011117	0.014
0.0111	0.135
0.0111	0.052
0.011084	0.057
0.011084	0.015
0.011075	0.008
0.011067	0.067
0.011067	0.048
0.011067	0.005
0.01105	0.572
0.01105	0.043
0.011034	0.049
0.011034	0.01
0.011025	0.024
0.011025	0.024
0.011017	0.186
0.011017	0.028
0.011017	0.007
0.011017	0.014
0.011008	0.034
0.011	0.077
0.011	0.006
0.011	0.028
0.010992	0.022
0.010983	0.028
0.010975	0.012
0.010967	0.053
0.01095	0.095
0.01095	0.313
0.010942	0.031
0.010933	0.005
0.010933	0.005
0.010917	0.023
0.010908	0.082
0.010908	0.018
0.010892	0.012
0.010866	0.329
0.010866	0.02
0.010858	0.03
0.01085	0.023
0.010833	0.011
0.010816	0.024
0.010816	0.033
0.010808	0.016
0.010808	0.044
0.010808	0.013
0.010808	0.05
0.0108	0.019
0.010791	0.327
0.010791	0.084
0.010791	0.034
0.010791	0.015
0.010783	0.006
0.010775	0.01
0.010766	0.065
0.010758	0.032
0.010758	0.055
0.010733	0.09
0.010716	0.018
0.010708	0.015
0.010699	0.076
0.010691	0.122
0.010674	0.03
0.010658	0.006
0.010641	0.012
0.010624	0.061
0.010624	0.015
0.010624	0.007
0.010616	0.017
0.010616	0.079
0.010608	0.003
0.010591	0.194
0.010591	0.105
0.010583	0.155
0.010583	0.01
0.010566	0.031
0.010566	0.007
0.010557	0.011
0.010557	0.617

0.010557	0.003
0.010549	0.296
0.010549	0.013
0.010541	0.058
0.010532	0.004
0.010532	0.015
0.010524	0.06
0.010524	0.039
0.010524	0.229
0.010516	0.019
0.010507	0.022
0.010507	0.027
0.010499	0.04
0.010482	0.069
0.010482	0.056
0.010482	0.028
0.010474	0.028
0.010457	0.094
0.010441	0.014
0.010424	0.086
0.010424	0.023
0.010407	0.027
0.010399	0.1
0.010399	0.01
0.010374	0.047
0.010374	0.018
0.010374	0.016
0.010374	0.054
0.010357	0.169
0.010357	0.696
0.010357	0.195
0.010332	0.011
0.010332	0.004
0.010324	0.011
0.010315	0.207
0.010307	0.029
0.010299	0.011
0.01029	0.01
0.010282	0.023
0.010273	0.081
0.010273	0.106
0.010265	0.007
0.010257	0.12
0.010257	0.021
0.010248	0.008
0.010248	0.011
0.010232	0.022
0.010223	0.011
0.010223	0.017
0.010198	0.109
0.010198	0.008
0.01019	0.115
0.01019	0.023
0.010182	0.01
0.010157	0.012
0.010157	0.142
0.010148	0.042
0.01014	0.143
0.010131	0.015
0.010115	0.133
0.010115	0.009
0.010098	0.009
0.010098	0.016
0.010073	0.019
0.010073	0.045
0.010065	0.007
0.010065	0.021
0.010056	0.017
0.010048	0.009
0.010048	0.016
0.010023	0.031
0.010015	0.003
0.010006	0.012
0.009989	0.115
0.009981	0.08
0.009981	0.036
0.009964	0.011
0.009956	0.016
0.009956	0.042
0.009939	0.041
0.009931	0.043
0.009923	0.022
0.009914	0.083
0.009914	0.043
0.009906	0.02
0.009906	0.048
0.009898	0.08
0.009889	0.235
0.009889	0.015
0.009881	0.016
0.009881	0.007
0.009873	0.109
0.009864	0.487
0.009864	0.099
0.009856	11.152
0.009856	0.021
0.009847	0.068
0.009831	0.014
0.009831	0.042
0.009831	0.023
0.009822	0.121
0.009822	0.038
0.009822	0.002
0.009814	0.007
0.009806	0.029
0.009806	0.032
0.009797	0.028
0.009797	0.017
0.009789	0.117
0.009781	0.01
0.009772	0.025
0.009764	0.299
0.009764	0.031
0.009764	0.019

0.009764	0.031
0.009747	0.024
0.009747	0.047
0.009739	0.012
0.009739	0.023
0.009731	0.015
0.009731	0.007
0.009706	0.022
0.009697	0.012
0.009672	0.117
0.009672	0.009
0.009664	0.032
0.009664	0.117
0.009655	0.061
0.009647	0.032
0.009639	0.013
0.009639	0.008
0.009639	0.08
0.009639	0.042
0.00963	0.03
0.00963	0.005
0.009622	5.665
0.009614	0.026
0.009605	0.01
0.009597	0.018
0.009597	0.06
0.009589	0.01
0.009589	0.021
0.009589	0.039
0.00958	0.009
0.009572	0.011
0.009572	0.006
0.009555	0.058
0.009547	0.028
0.009547	0.059
0.009547	0.026
0.009547	0.008
0.00953	0.01
0.00953	0.101
0.00953	0.027
0.009522	0.055
0.009522	0.012
0.009513	0.007
0.009505	0.086
0.009505	0.029
0.009497	0.018
0.009488	0.04
0.009488	0.036
0.00948	0.006
0.009463	0.02
0.009447	0.11
0.009438	0.021
0.00943	0.017
0.00943	0.034
0.009422	0.016
0.009413	0.03
0.009396	0.125
0.00938	0.009
0.009371	0.004
0.009371	0.003
0.009371	0.011
0.009363	0.197
0.009363	0.028
0.009363	0.046
0.009363	0.098
0.009355	0.013
0.009346	0.008
0.009346	0.007
0.009338	0.004
0.009338	0.015
0.009338	0.015
0.00933	0.015
0.009321	0.125
0.009321	0.007
0.009313	0.004
0.009296	0.008
0.009296	0.102
0.009288	0.019
0.009288	0.02
0.009288	0.04
0.00928	0.034
0.009271	0.04
0.009263	0.026
0.009254	0.009
0.009246	0.018
0.009246	0.091
0.009213	0.027
0.009213	0.021
0.009213	0.021
0.009204	0.383
0.009179	0.038
0.009179	0.031
0.009171	0.127
0.009163	0.007
0.009163	0.043
0.009154	0.054
0.009154	0.011
0.009146	0.026
0.009146	0.118
0.009138	0.017
0.009129	0.01
0.009129	0.005
0.009129	0.007
0.009129	0.034
0.009121	0.098
0.009112	0.048
0.009104	0.133
0.009104	0.631
0.009096	0.073
0.009096	0.07
0.009087	0.123
0.009087	0.008
0.009079	0.23
0.009079	0.022

0.009079	0.034
0.009071	0.005
0.009062	0.02
0.009046	0.016
0.009037	0.034
0.009037	0.017
0.009037	0.009
0.009029	0.006
0.009021	0.027
0.009021	0.005
0.009021	0.071
0.009012	0.009
0.009012	0.042
0.009004	0.023
0.009004	0.087
0.008996	0.047
0.008996	0.114
0.008987	0.009
0.008987	0.018
0.008979	0.026
0.008979	0.074
0.008979	0.105
0.00897	0.03
0.00897	0.004
0.008954	0.029
0.008954	0.029
0.008954	0.009
0.008945	0.01
0.008945	0.029
0.008937	0.025
0.008929	0.013
0.008929	0.014
0.00892	0.009
0.008895	0.13
0.008895	0.029
0.008887	0.043
0.008879	0.01
0.008879	0.209
0.00887	0.009
0.00887	0.016
0.00887	0.022
0.00887	0.005
0.00887	0.032
0.008854	0.023
0.008854	0.021
0.008845	0.006
0.008845	0.006
0.008837	0.008
0.008829	0.037
0.00882	0.061
0.00882	0.004
0.008812	0.01
0.008812	0.241
0.008795	0.043
0.008787	0.006
0.008778	0.011
0.00877	0.16
0.008745	0.123
0.008745	0.01
0.008737	0.011
0.008737	0.008
0.008737	0.071
0.008728	0.042
0.008728	0.018
0.008712	0.048
0.008695	0.41
0.008695	0.014
0.008687	0.045
0.008687	0.012
0.008678	0.12
0.00867	0.03
0.008661	0.032
0.008653	0.02
0.008653	0.029
0.008653	0.01
0.008645	0.016
0.008636	0.056
0.008628	0.006
0.008628	0.042
0.00862	0.053
0.00862	3.076
0.008611	0.073
0.008603	0.046
0.008603	0.008
0.008595	0.022
0.008595	0.023
0.008586	0.017
0.008586	0.081
0.008586	0.309
0.00857	0.009
0.00857	0.14
0.008561	0.073
0.008553	0.011
0.008553	0.052
0.008553	0.019
0.008519	0.021
0.008511	0.01
0.008494	0.04
0.008494	0.035
0.008478	0.012
0.008478	0.025
0.008478	0.02
0.008478	0.02
0.008478	0.022
0.008469	0.086
0.008461	0.014
0.008461	0.027
0.008453	0.003
0.008453	0.136
0.008453	0.022
0.008444	0.013
0.008444	0.01
0.008444	0.013
0.008444	0.022

0.008444	0.251
0.008444	0.027
0.008436	0.011
0.008436	0.01
0.008436	0.025
0.008436	0.207
0.008428	0.143
0.008428	0.013
0.008419	0.059
0.008419	0.017
0.008411	0.032
0.008411	0.015
0.008403	0.361
0.008403	0.014
0.008386	0.012
0.008377	0.017
0.008377	0.027
0.008369	0.009
0.008369	0.197
0.008361	0.017
0.008361	0.035
0.008361	0.041
0.008344	0.101
0.008336	0.03
0.008327	0.056
0.008319	0.032
0.008311	0.067
0.008311	0.015
0.008302	0.006
0.008294	0.015
0.008294	0.09
0.008286	0.011
0.008269	0.022
0.008261	0.017
0.008261	0.085
0.008261	0.07
0.008252	0.269
0.008252	0.024
0.008252	0.033
0.008252	0.009
0.008244	0.097
0.008227	0.051
0.008219	0.003
0.008219	0.035
0.008219	0.022
0.008219	0.169
0.008219	0.022
0.00821	0.214
0.008202	0.005
0.008202	0.028
0.008194	0.028
0.008194	0.045
0.008194	0.124
0.008194	0.008
0.008177	0.016
0.008169	0.141
0.008169	0.025
0.008152	0.006
0.008152	0.013
0.008144	0.034
0.008144	0.063
0.008135	0.015
0.008135	0.013
0.008135	0.024
0.008127	0.063
0.008127	0.009
0.008119	0.076
0.00811	0.095
0.00811	0.016
0.00811	0.022
0.008102	0.161
0.008102	0.009
0.008093	0.026
0.008085	0.071
0.008085	0.214
0.008085	0.021
0.008077	0.012
0.008077	0.05
0.008068	0.015
0.008068	0.007
0.008052	0.015
0.008052	0.005
0.008052	0.006
0.008043	0.117
0.008035	0.014
0.008035	0.044
0.008027	0.009
0.008002	0.016
0.008002	0.097
0.007993	0.317
0.007993	0.009
0.007977	0.452
0.007977	0.022
0.007977	0.005
0.007968	0.262
0.007952	0.04
0.007952	0.006
0.007935	0.005
0.007935	0.003
0.007935	0.021
0.007935	0.045
0.007935	0.015
0.007926	0.027
0.007926	0.089
0.007926	0.008
0.007918	0.018
0.007918	0.077
0.00791	0.097
0.00791	0.019
0.00791	0.023
0.00791	0.012
0.007901	0.004
0.007901	0.015
0.007893	0.087

0.007893	0.082
0.007893	0.03
0.007893	0.013
0.007893	0.01
0.007885	0.004
0.007885	3.029
0.007876	0.04
0.00786	0.054
0.00786	0.159
0.00786	0.041
0.007843	0.055
0.007843	0.065
0.007818	0.034
0.00781	0.061
0.00781	0.01
0.007793	0.014
0.007776	0.019
0.007776	0.006
0.007768	0.025
0.007768	0.108
0.007759	0.034
0.007751	0.013
0.007751	0.01
0.007743	0.027
0.007734	0.011
0.007726	0.016
0.007709	0.009
0.007693	0.017
0.007684	0.007
0.007676	0.01
0.007676	0.003
0.007668	0.04
0.007659	0.004
0.007651	0.061
0.007642	0.024
0.007642	0.032
0.007642	0.163
0.007642	0.006
0.007626	0.016
0.007617	0.06
0.007609	0.041
0.007609	0.009
0.007609	0.013
0.007601	0.113
0.007601	0.028
0.007601	0.039
0.007601	0.038
0.007592	0.053
0.007592	0.135
0.007592	0.061
0.007576	0.01
0.007567	0.016
0.007567	0.054
0.007559	0.145
0.007551	0.029
0.007551	0.013
0.007542	0.013
0.007542	0.01
0.007534	0.037
0.007526	0.049
0.007517	0.013
0.007517	0.007
0.0075	0.06
0.0075	0.018
0.0075	0.076
0.007492	0.014
0.007484	0.017
0.007484	0.133
0.007459	0.007
0.00745	0.007
0.00745	0.028
0.007442	0.023
0.007442	0.048
0.007442	0.017
0.007442	0.03
0.007434	0.013
0.007434	0.004
0.007434	0.009
0.007409	0.041
0.007409	0.004
0.007409	0.021
0.0074	0.058
0.0074	0.521
0.007384	0.017
0.007384	0.029
0.007384	0.031
0.007384	0.027
0.007375	0.003
0.007375	0.078
0.007358	0.033
0.00735	0.088
0.00735	0.013
0.007342	0.006
0.007342	0.053
0.007333	0.207
0.007333	0.022
0.007325	0.04
0.007317	0.02
0.0073	0.011
0.007292	0.012
0.007283	0.016
0.007283	0.006
0.007275	0.018
0.007275	0.155
0.007267	0.008
0.007242	0.008
0.007242	0.018
0.007233	0.167
0.007233	0.02
0.007225	0.01
0.007225	0.022
0.007216	0.004
0.007216	0.01
0.007208	0.042

0.0072	0.016
0.0072	0.021
0.007175	0.008
0.007141	0.033
0.007133	0.039
0.007133	0.176
0.007125	0.03
0.007125	0.023
0.007116	0.065
0.007116	
0.007116	
0.0071	
0.0071	
0.0071	
0.007091	
0.007091	
0.007091	
0.007091	
0.007083	
0.007083	
0.007083	
0.007083	
0.007074	
0.007066	
0.007066	
0.007066	
0.007066	
0.007066	
0.007058	
0.007049	
0.007049	
0.007049	
0.007033	
0.007024	
0.007008	
0.007008	
0.006999	
0.006999	
0.006991	
0.006991	
0.006983	
0.006983	
0.006974	
0.006966	
0.006966	
0.006966	
0.006949	
0.006949	
0.006949	
0.006933	
0.006933	
0.006924	
0.006924	
0.006916	
0.006899	
0.006899	
0.006899	
0.006891	
0.006874	
0.006866	
0.006857	
0.006857	
0.006841	
0.006832	
0.006824	
0.006824	
0.006816	
0.006816	
0.006791	
0.006791	
0.006791	
0.006791	
0.006782	
0.006782	
0.006774	
0.006774	
0.006774	
0.006765	
0.006757	
0.006757	
0.006749	
0.006749	
0.006749	
0.00674	
0.006732	
0.006732	
0.006732	
0.006732	
0.006724	
0.006715	
0.006715	
0.006715	
0.006715	
0.006707	
0.006707	
0.006699	
0.006699	
0.00669	
0.00669	
0.006674	
0.006674	
0.006674	
0.006665	
0.006657	
0.006657	
0.006649	
0.006649	
0.00664	
0.006632	
0.006632	
0.006632	
0.006607	
0.006598	
0.00659	

0.00659
0.006582
0.006582
0.006573
0.006573
0.006565
0.006548
0.006548
0.00654
0.00654
0.006532
0.006523
0.006523
0.006507
0.006507
0.006498
0.006498
0.006498
0.00649
0.00649
0.00649
0.006481
0.006481
0.006473
0.006456
0.006456
0.006448
0.00644
0.00644
0.006423
0.006415
0.006415
0.006406
0.006398
0.00639
0.006381
0.006381
0.006365
0.006348
0.006331
0.006323
0.006314
0.006314
0.006306
0.006306
0.006298
0.006289
0.006273
0.006273
0.006273
0.006273
0.006273
0.006264
0.006264
0.006264
0.006256
0.006256
0.006248
0.006248
0.006239
0.006239
0.006239
0.006239
0.006223
0.006223
0.006223
0.006223
0.006214
0.006214
0.006214
0.006206
0.006206
0.006206
0.006197
0.006197
0.006197
0.006189
0.006189
0.006189
0.006189
0.006181
0.006172
0.006156
0.006156
0.006156
0.006156
0.006156
0.006139
0.006139
0.006139
0.006131
0.006131
0.006131
0.006106
0.006106
0.006097
0.006097
0.006097
0.006089
0.006089
0.006081
0.006072
0.006064
0.006056
0.006056
0.006056
0.006047
0.006047
0.006047
0.006039
0.006039
0.006039
0.006039
0.006039

0.00603
0.00603
0.00603
0.006022
0.006014
0.006014
0.006014
0.006005
0.006005
0.006005
0.005997
0.005997
0.005997
0.005989
0.005989
0.005989
0.005989
0.00598
0.00598
0.00598
0.00598
0.005972
0.005964
0.005964
0.005955
0.005955
0.005955
0.005947
0.005939
0.005939
0.005922
0.005922
0.005922
0.005922
0.005914
0.005914
0.005914
0.005914
0.005914
0.005905
0.005888
0.005888
0.005872
0.005863
0.005863
0.005863
0.005863
0.005855
0.005855
0.005855
0.005847
0.005847
0.005847
0.005838
0.00583
0.00583
0.00583
0.00583
0.005813
0.005813
0.005813
0.005805
0.005805
0.005797
0.005797
0.005797
0.00578
0.00578
0.00578
0.00578
0.005772
0.005772
0.005763
0.005763
0.005755
0.005755
0.005755
0.005755
0.005755
0.005746
0.005746
0.005738
0.005738
0.00573
0.005721
0.005721
0.005713
0.005713
0.005696
0.005696
0.005696
0.005696
0.005696
0.005688
0.005663
0.005655
0.005655
0.005646
0.005646
0.005638
0.005638
0.005638
0.005638
0.00563
0.005621
0.005621
0.005604
0.005604
0.005604
0.005596
0.005596
0.005588
0.005588
0.005579

0.005571
0.005563
0.005563
0.005563
0.005563
0.005563
0.005554
0.005554
0.005554
0.005546
0.005538
0.005538
0.005529
0.005521
0.005521
0.005513
0.005513
0.005513
0.005504
0.005504
0.005504
0.005496
0.005496
0.005496
0.005479
0.005479
0.005471
0.005471
0.005462
0.005454
0.005454
0.005454
0.005454
0.005446
0.005437
0.005429
0.005429
0.005429
0.005429
0.005412
0.005412
0.005412
0.005404
0.005404
0.005404
0.005404
0.005396
0.005387
0.005387
0.005387
0.005387
0.005379
0.005371
0.005362
0.005354
0.005354
0.005346
0.005337
0.005329
0.00532
0.00532
0.00532
0.00532
0.005312
0.005312
0.005312
0.005304
0.005304
0.005295
0.005295
0.005287
0.005287
0.005287
0.005279
0.005279
0.00527
0.00527
0.00527
0.00527
0.00527
0.00527
0.005262
0.005262
0.005262
0.005262
0.005254
0.005254
0.005254
0.005245
0.005245
0.005245
0.005237
0.005229
0.00522
0.00522
0.00522
0.005212
0.005212
0.005195
0.005187
0.005187
0.005187
0.005187
0.005178
0.00517
0.005153
0.005153
0.005153
0.005153
0.005153
0.005145
0.005145
0.005145
0.005128

0.00512
0.00512
0.00512
0.005112
0.005112
0.005112
0.005103
0.005087
0.005078
0.005078
0.00507
0.00507
0.005062
0.005062
0.005053
0.005053
0.005053
0.005045
0.005045
0.005037
0.005028
0.005028
0.00502
0.00502
0.005011
0.005003
0.005003
0.005003
0.005003
0.004995
0.004995
0.004986
0.004986
0.004986
0.004978
0.004978
0.00497
0.004961
0.004953
0.004953
0.004945
0.004936
0.004928
0.004928
0.004928
0.004928
0.00492
0.00492
0.004911
0.004911
0.004911
0.004903
0.004903
0.004903
0.004895
0.004895
0.004886
0.004878
0.004869
0.004869
0.004869
0.004861
0.004861
0.004853
0.004853
0.004853
0.004853
0.004844
0.004844
0.004836
0.004836
0.004836
0.004828
0.004828
0.004828
0.004819
0.004819
0.004819
0.004819
0.004819
0.004819
0.004811
0.004811
0.004803
0.004803
0.004794
0.004786
0.004786
0.004778
0.004778
0.004761
0.004761
0.004761
0.004761
0.004761
0.004753
0.004753
0.004744
0.004744
0.004736
0.004736
0.004736
0.004727
0.004727
0.004719
0.004719
0.004711
0.004711
0.004694
0.004686
0.004686
0.004677
0.004669
0.004669

0.004669
0.004661
0.004652
0.004652
0.004652
0.004644
0.004644
0.004644
0.004644
0.004636
0.004636
0.004627
0.004619
0.004611
0.004602
0.004594
0.004594
0.004585
0.004577
0.004577
0.004577
0.00456
0.00456
0.004552
0.004544
0.004544
0.004535
0.004535
0.004535
0.004535
0.004519
0.004519
0.004519
0.00451
0.00451
0.00451
0.00451
0.00451
0.004502
0.004502
0.004502
0.004502
0.004502
0.004494
0.004494
0.004494
0.004494
0.004485
0.004477
0.004477
0.004477
0.004477
0.004469
0.00446
0.00446
0.00446
0.00446
0.004452
0.004452
0.004452
0.004443
0.004443
0.004443
0.004443
0.004435
0.004435
0.004435
0.004427
0.004418
0.00441
0.004402
0.004402
0.004393
0.004393
0.004385
0.004377
0.004377
0.004368
0.00436
0.004352
0.004343
0.004343
0.004327
0.004318
0.004318
0.004293
0.004293
0.004293
0.004293
0.004293
0.004285
0.004285
0.004285
0.004285
0.004276
0.004276
0.004276
0.004268
0.004268
0.00426
0.004251
0.004251
0.004251
0.004251
0.004243
0.004235
0.004235
0.004226
0.004226
0.004226
0.004226
0.004218
0.004218
0.00421

0.00421
0.00421
0.00421
0.00421
0.004201
0.004201
0.004193
0.004193
0.004185
0.004185
0.004176
0.004168
0.00416
0.00416
0.00416
0.004143
0.004126
0.004126
0.004126
0.004126
0.004126
0.004126
0.004118
0.004118
0.004118
0.004109
0.004109
0.004109
0.004101
0.004101
0.004101
0.004093
0.004093
0.004084
0.004076
0.004068
0.004068
0.004059
0.004059
0.004059
0.004051
0.004051
0.004043
0.004043
0.004034
0.004034
0.004026
0.004018
0.004009
0.004009
0.004009
0.004001
0.004001
0.004001
0.003984
0.003984
0.003984
0.003976
0.003976
0.003976
0.003967
0.003959
0.003959
0.003959
0.003959
0.003959
0.003959
0.003951
0.003951
0.003951
0.003951
0.003951
0.003951
0.003942
0.003942
0.003934
0.003934
0.003934
0.003934
0.003934
0.003934
0.003926
0.003926
0.003917
0.003917
0.003917
0.003909
0.003901
0.003901
0.003901
0.003892
0.003892
0.003884
0.003884
0.003876
0.003876
0.003876
0.003867
0.003867
0.003867
0.003867
0.003867
0.003859
0.00385
0.00385
0.003842
0.003834
0.003834
0.003825
0.003825
0.003825
0.003809
0.003809
0.003792
0.003792
0.003792

0.003784
0.003784
0.003759
0.003759
0.003759
0.003759
0.003759
0.00375
0.003742
0.003742
0.003734
0.003725
0.003725
0.003708
0.003708
0.003708
0.003708
0.0037
0.003683
0.003683
0.003683
0.003683
0.003683
0.003675
0.003675
0.003675
0.003658
0.003658
0.003658
0.003658
0.003658
0.00365
0.00365
0.003642
0.003642
0.003633
0.003633
0.003633
0.003625
0.003625
0.003625
0.003625
0.003625
0.003617
0.003617
0.003617
0.003608
0.003608
0.0036
0.0036
0.003592
0.003592
0.003583
0.003583
0.003583
0.003575
0.003575
0.003566
0.003558
0.003558
0.003558
0.003541
0.003533
0.003533
0.003533
0.003533
0.003525
0.003516
0.003516
0.003508
0.003508
0.0035
0.0035
0.0035
0.0035
0.003491
0.003491
0.003491
0.003491
0.003491
0.003483
0.003483
0.003483
0.003483
0.003483
0.003483
0.003483
0.003475
0.003466
0.003466
0.003458
0.00345
0.00345
0.003441
0.003441
0.003441
0.003433
0.003433
0.003424
0.003416
0.003416
0.003408
0.003383
0.003383
0.003383
0.003383
0.003383
0.003366
0.003358
0.003358
0.003349
0.003341
0.003333
0.003333
0.003333

0.003333
0.003333
0.003316
0.003316
0.003316
0.003308
0.003308
0.003308
0.003308
0.003299
0.003299
0.003299
0.003291
0.003291
0.003291
0.003291
0.003282
0.003282
0.003257
0.003257
0.003249
0.003249
0.003249
0.003241
0.003241
0.003241
0.003241
0.003241
0.003232
0.003224
0.003216
0.003216
0.003216
0.003216
0.003207
0.003207
0.003207
0.003207
0.003207
0.003199
0.003191
0.003191
0.003182
0.003166
0.003166
0.003166
0.003166
0.003166
0.003157
0.003157
0.003157
0.003157
0.003157
0.003149
0.003149
0.003141
0.003141
0.003141
0.003132
0.003124
0.003115
0.003115
0.003107
0.003107
0.003107
0.003107
0.00309
0.00309
0.00309
0.003082
0.003082
0.003082
0.003082
0.003074
0.003065
0.003065
0.003049
0.00304
0.00304
0.00304
0.003032
0.003032
0.003024
0.003024
0.003024
0.003024
0.003015
0.003015
0.003015
0.003007
0.002999
0.00299
0.002982
0.002982
0.002973
0.002973
0.002965
0.002965
0.002965
0.002965
0.002965
0.002957
0.002957
0.002957
0.002957
0.002948
0.002948
0.002948
0.002948
0.002948
0.00294
0.00294
0.00294
0.00294

0.002932
0.002923
0.002923
0.002923
0.002923
0.002923
0.002923
0.002923
0.002907
0.002907
0.002898
0.002898
0.002898
0.002898
0.002898
0.002898
0.002898
0.00289
0.00289
0.00289
0.00289
0.002882
0.002882
0.002882
0.002873
0.002873
0.002865
0.002865
0.002865
0.002857
0.002857
0.002848
0.002848
0.00284
0.002831
0.002831
0.002831
0.002823
0.002823
0.002823
0.002798
0.002798
0.002798
0.002773
0.002773
0.002773
0.002765
0.002765
0.002765
0.002765
0.002756
0.002748
0.002748
0.00274
0.002731
0.002731
0.002731
0.002723
0.002723
0.002715
0.002715
0.002715
0.002706
0.002706
0.002706
0.002706
0.002698
0.002698
0.002698
0.002689
0.002689
0.002681
0.002681
0.002681
0.002673
0.002673
0.002673
0.002673
0.002664
0.002664
0.002664
0.002664
0.002656
0.002656
0.002656
0.002639
0.002639
0.002639
0.002631
0.002631
0.002631
0.002631
0.002623
0.002614
0.002614
0.002614
0.002614
0.002606
0.002606
0.002606
0.002606
0.002606
0.002606
0.002606
0.002598
0.002598
0.002598
0.002598
0.002581
0.002581
0.002573
0.002564
0.002564
0.002564
0.002556
0.002556

0.002556
0.002556
0.002539
0.002531
0.002531
0.002522
0.002514
0.002514
0.002514
0.002514
0.002514
0.002506
0.002497
0.002497
0.002489
0.002481
0.002481
0.002481
0.002472
0.002464
0.002464
0.002464
0.002447
0.002439
0.002439
0.002439
0.002439
0.002439
0.002439
0.002439
0.002431
0.002431
0.002431
0.002431
0.002422
0.002422
0.002422
0.002414
0.002414
0.002414
0.002414
0.002414
0.002414
0.002405
0.002405
0.002405
0.002405
0.002397
0.002397
0.002397
0.002389
0.002389
0.002389
0.00238
0.00238
0.002372
0.002364
0.002364
0.002364
0.002339
0.002339
0.00233
0.00233
0.00233
0.002322
0.002314
0.002314
0.002305
0.002305
0.002305
0.002289
0.002272
0.002264
0.002264
0.002255
0.002255
0.002255
0.002247
0.002247
0.002238
0.002238
0.002238
0.002238
0.00223
0.00223
0.002222
0.002213
0.002213
0.002213
0.002213
0.002213
0.002213
0.002213
0.002205
0.002205
0.002205
0.002197
0.002197
0.002197
0.002197
0.002197
0.002188
0.002188
0.002188
0.002188
0.00218
0.00218
0.00218
0.00218
0.002172
0.002172
0.002163
0.002163
0.002163
0.002155
0.002147
0.002147

0.002147
0.002147
0.002147
0.002138
0.002138
0.00213
0.00213
0.00213
0.00213
0.00213
0.002122
0.002122
0.002122
0.002113
0.002113
0.002113
0.002113
0.002105
0.002096
0.002096
0.002088
0.002088
0.00208
0.00208
0.00208
0.002071
0.002063
0.002063
0.002055
0.002055
0.002055
0.002046
0.002046
0.002038
0.002038
0.002038
0.002038
0.002021
0.002021
0.002005
0.002005
0.001996
0.001988
0.00198
0.001971
0.001971
0.001963
0.001963
0.001963
0.001954
0.001938
0.001938
0.001938
0.001938
0.001929
0.001929
0.001929
0.001929
0.001929
0.001921
0.001913
0.001913
0.001913
0.001904
0.001904
0.001896
0.001896
0.001888
0.001888
0.001888
0.001888
0.001879
0.001871
0.001871
0.001871
0.001863
0.001854
0.001846
0.001846
0.001846
0.001829
0.001821
0.001804
0.001804
0.001804
0.001796
0.001796
0.001796
0.001796
0.001787
0.001787
0.001771
0.001754
0.001754
0.001737
0.001737
0.001737
0.001729
0.001729
0.001729
0.001729
0.001721
0.001721
0.001712
0.001704
0.001704
0.001704
0.001696
0.001696
0.001687
0.001687
0.001679
0.00167
0.001662

0.001645													
0.001637													
0.001637													
0.001629													
0.00162													
0.001612													
0.001604													
0.001604													
0.001595													
0.001587													
0.001579													
0.00157													
0.001562													
0.001545													
0.001537													
0.001537													
0.001537													
0.001537													
0.001537													
0.001528													
0.001528													
0.00152													
0.001512													
0.001495													
0.001495													
0.001478													
0.00147													
0.00147													
0.00147													
0.001462													
0.001462													
0.001453													
0.001453													
0.001445													
0.001437													
0.00142													
0.001412													
0.001412													
0.001403													
0.001395													
0.001387													
0.001387													
0.00137													
0.001361													
0.001353													
0.001353													
0.001345													
0.001336													
0.001311													
0.001295													
0.001286													
0.001278													
0.001278													
0.001253													
0.001253													
0.001211													
0.001203													
0.001203													
0.001203													
0.001186													
0.001169													
0.001161													
0.001119													
0.001119													
0.001052													
0.001036													
0.001027													
0.000994													
0.000994													
0.000961													
0.000952													
0.000944													
0.000894													
0.00086													
0.000852													
0.000819													
0.00081													
0.00081													
0.000626													
0.000543													
0.000451													
0.000426													

All raw bubble area data (mm^2) from the image analysis of the SEM binary images. Values correspond to the binary images presented in Appendix D.

Primary				Late-stage					Secondary				
4A	4Q	8B	8Ei	1A q	1C q	5K	1D q	6A q	12B q	12G	12H	12Ni	15Mii q
1.304379	2.344316	0.91626	1.280465	0.742662	2.033119	2.724232	2.366875	0.455626	2.396724	0.526168	1.433331	12.130259	4.087366
1.236818	1.36214	0.498768	0.730704	0.717036	1.83414	1.562905	0.226737	0.239258	2.14456	0.399813	0.442341	2.554212	1.146484
0.745999	0.869778	0.345834	0.647797	0.499082	0.829208	1.555853	0.124969	0.166101	0.661534	0.254472	0.414149	2.2132	0.442597
0.489435	0.779686	0.261305	0.58907	0.369652	0.673278	1.188262	0.096579	0.163316	0.625746	0.221052	0.397429	1.124889	0.261139
0.352723	0.743402	0.191119	0.577252	0.314167	0.649806	0.952631	0.08063	0.124924	0.413635	0.215591	0.381765	0.696575	0.21575
0.295456	0.527078	0.142861	0.492058	0.297274	0.607075	0.739882	0.04879	0.123506	0.392396	0.177967	0.372156	0.691974	0.199355
0.250124	0.490685	0.14226	0.428139	0.20562	0.597536	0.599806	0.045582	0.114709	0.386256	0.177016	0.256253	0.655965	0.186663
0.197918	0.411717	0.137216	0.409761	0.202373	0.562789	0.562135	0.026737	0.110128	0.356171	0.165131	0.234091	0.553003	0.161976
0.191348	0.383235	0.134307	0.374971	0.176231	0.512249	0.509584	0.021034	0.10495	0.337598	0.158862	0.204614	0.474404	0.156277
0.185486	0.365676	0.103216	0.354887	0.127518	0.48385	0.481528	0.01205	0.092129	0.32904	0.146799	0.196413	0.467611	0.122643
0.167378	0.344124	0.08434	0.305267	0.092448	0.469957	0.426279	0.006965	0.082151	0.32393	0.142368	0.192918	0.445598	0.116918
0.162192	0.316082	0.077046	0.290981	0.092137	0.394766	0.418592	0.005012	0.081566	0.300672	0.13351	0.186472	0.442093	0.114331
0.145976	0.310077	0.074952	0.251655	0.086099	0.389474	0.38361	0.00167	0.079646	0.282514	0.123949	0.173951	0.390475	0.105694
0.142906	0.302847	0.072991	0.247057	0.083958	0.340088	0.319913	0.00149	0.076888	0.197156	0.121513	0.142858	0.366717	0.103117
0.137501	0.288388	0.069045	0.234665	0.081563	0.330921	0.315718	0.001482	0.071138	0.189726	0.120896	0.13467	0.361232	0.096429
0.131023	0.23225	0.065785	0.232319	0.06654	0.253909	0.294101	0.001287	0.061902	0.178001	0.118446	0.131333	0.343414	0.087862
0.130843	0.219238	0.062514	0.225494	0.064173	0.252178	0.293821	0.001072	0.059186	0.173864	0.112118	0.130176	0.330189	0.081663
0.126754	0.219027	0.060157	0.224934	0.05851	0.241867	0.289283	0.000852	0.059093	0.167981	0.110142	0.129802	0.288632	0.073961
0.117522	0.215612	0.060101	0.21858	0.056792	0.232356	0.289019	0.000645	0.054421	0.164724	0.108253	0.129226	0.28824	0.069035
0.117397	0.18075	0.056524	0.201927	0.047411	0.213764	0.280261	0.00063	0.050316	0.152987	0.096693	0.124156	0.280946	0.068982
0.11236	0.180718	0.055565	0.201368	0.039152	0.209285	0.244233	0.000627	0.049067	0.148797	0.09552	0.120001	0.280794	0.067688
0.110206	0.152403	0.055418	0.18586	0.03897	0.206386	0.23771	0.000581	0.048901	0.145592	0.095195	0.114229	0.279935	0.067657
0.10974	0.146842	0.054438	0.18489	0.037079	0.200081	0.208046	0.000564	0.044444	0.143621	0.09347	0.113308	0.276356	0.063492
0.100134	0.131257	0.053489	0.184737	0.029816	0.193316	0.192994	0.000552	0.042285	0.140313	0.091447	0.113106	0.253217	0.058643
0.099584	0.127221	0.050969	0.16673	0.025212	0.191203	0.189835	0.000541	0.039788	0.136742	0.08719	0.110287	0.233789	0.058234
0.093544	0.12372	0.050539	0.166386	0.024959	0.186161	0.184901	0.000509	0.039671	0.129992	0.086105	0.108023	0.231941	0.055896
0.090037	0.121829	0.050516	0.164416	0.023178	0.173646	0.179455	0.000501	0.038687	0.128523	0.085347	0.105153	0.22845	0.054632
0.089338	0.116058	0.047346	0.156625	0.022365	0.170888	0.166863	0.000479	0.034154	0.12151	0.083703	0.102857	0.202248	0.051066
0.084265	0.115954	0.044789	0.153075	0.019506	0.169753	0.154308	0.000476	0.034055	0.118601	0.082283	0.100094	0.20202	0.049575
0.08232	0.112585	0.043	0.152667	0.019154	0.166069	0.150077	0.000473	0.031584	0.113886	0.080634	0.098149	0.193252	0.049206
0.081912	0.11217	0.042984	0.147383	0.018107	0.152621	0.148925	0.000431	0.031176	0.109428	0.074911	0.096701	0.183496	0.046833
0.081499	0.110079	0.042886	0.14491	0.015664	0.133138	0.141698	0.000404	0.030817	0.108507	0.074048	0.096402	0.173637	0.046429
0.080311	0.107706	0.041577	0.139805	0.01467	0.124596	0.141124	0.000398	0.030564	0.10745	0.073214	0.089861	0.167872	0.038631
0.077278	0.107094	0.040714	0.138883	0.010779	0.116454	0.138835	0.000391	0.030114	0.105919	0.072742	0.089789	0.16481	0.038531
0.077023	0.104276	0.039468	0.137313	0.009962	0.103716	0.134266	0.000378	0.029079	0.104146	0.072661	0.089205	0.13988	0.036852
0.076768	0.103977	0.039089	0.135274	0.009796	0.101451	0.131863	0.000346	0.028948	0.101436	0.07243	0.085809	0.13914	0.036766
0.075437	0.101433	0.038773	0.134666	0.00863	0.099077	0.13149	0.000334	0.028755	0.092106	0.070743	0.081051	0.138391	0.035181
0.07413	0.101311	0.038536	0.133772	0.008142	0.093163	0.12873	0.000308	0.027924	0.090109	0.069036	0.080325	0.134061	0.033134
0.073295	0.098868	0.038373	0.130977	0.006962	0.091459	0.128224	0.00024	0.027924	0.088166	0.067728	0.079471	0.126915	0.030714
0.07162	0.097674	0.037742	0.128583	0.005913	0.091419	0.124302	0.000207	0.027873	0.086851	0.065624	0.079265	0.121602	0.030229
0.070919	0.093484	0.036274	0.122381	0.005573	0.085339	0.117191	0.000202	0.027745	0.07933	0.064396	0.077962	0.121356	0.028313
0.07058	0.09268	0.036101	0.117651	0.005373	0.084412	0.112027	0.000167	0.027029	0.077673	0.063882	0.077429	0.11904	0.027574
0.070059	0.091477	0.0349	0.117002	0.004021	0.082087	0.109321	0.000158	0.026833	0.075631	0.061393	0.071693	0.113379	0.027291
0.065155	0.088049	0.033041	0.112918	0.003821	0.081252	0.109137	0.000141	0.025999	0.075375	0.061254	0.068802	0.111681	0.027272
0.064886	0.085324	0.032966	0.106496	0.003577	0.078297	0.108256	7.406E-07	0.025924	0.072074	0.060518	0.066835	0.109569	0.026757
0.064124	0.082219	0.031238	0.105495	0.002354	0.078193	0.107766	7.406E-07	0.025847	0.071147	0.059054	0.063532	0.107247	0.02671
0.063	0.081174	0.030945	0.104816	0.001861	0.077456	0.107058	7.406E-07	0.025187	0.069212	0.057333	0.062521	0.095143	0.024513
0.062719	0.080193	0.030409	0.102151	0.001665	0.072249	0.103876		0.024661	0.06816	0.057238	0.062341	0.089101	0.023425
0.062553	0.077968	0.029942	0.101711	0.001162	0.070056	0.101992		0.021664	0.066602	0.056297	0.062008	0.085282	0.023036
0.061815	0.077146	0.029871	0.101135	0.000714	0.067886	0.095665		0.020923	0.064088	0.05532	0.06162	0.079424	0.021933
0.060354	0.076142	0.029431	0.100905	0.000418	0.064602	0.095387		0.02063	0.062745	0.054275	0.061544	0.072775	0.021832
0.05875	0.075567	0.028905	0.100889		0.061675	0.095261		0.020223	0.061497	0.053103	0.060004	0.07139	0.021744
0.05356	0.073881	0.028577	0.100523		0.060496	0.093969		0.020121	0.061324	0.050708	0.059978	0.070704	0.021095
0.052495	0.07028	0.028434	0.096446		0.060352	0.09182		0.018835	0.061102	0.049659	0.059929	0.065622	0.019195
0.052036	0.068964	0.02752	0.096322		0.058543	0.090974		0.018796	0.058459	0.049428	0.059403	0.064193	0.017985
0.051362	0.068747	0.027485	0.094544		0.057775	0.087463		0.018775	0.056179	0.049244	0.058698	0.059761	0.0178
0.050805	0.067607	0.02735	0.090001		0.057775	0.087301		0.018648	0.052374	0.049035	0.058477	0.059225	0.017555
0.050034	0.066856	0.027134	0.089255		0.057621	0.085686		0.018571	0.05101	0.048851	0.057631	0.05899	0.017172
0.048744	0.06624	0.026744	0.085193		0.057127	0.081861		0.018449	0.050439	0.048639	0.057384	0.058439	0.016761
0.048742	0.065992	0.025908	0.083287		0.056587	0.078984		0.017992	0.047411	0.047987	0.055182	0.057315	0.016256
0.04781	0.065944	0.02581	0.078777		0.054329	0.078495		0.017471	0.045218	0.046758	0.054711	0.054615	0.015431
0.047105	0.065661	0.024472	0.078767		0.05141	0.078246		0.017357	0.04341	0.046706	0.054616	0.054304	0.01525
0.046498	0.06542	0.024215	0.0747		0.051338	0.077333		0.017216	0.042513	0.045333	0.05449	0.052767	0.015062
0.046267	0.065393	0.023962	0.072187		0.049635	0.074866		0.016904	0.041667	0.044997	0.054439	0.050609	0.014736
0.046242	0.063594	0.023388	0.070648		0.049001	0.074108		0.016731	0.038574	0.044954	0.054398	0.049855	0.01466
0.046183	0.063158	0.023162	0.064961		0.048024	0.073341		0.015825	0.038358	0.044827	0.054348	0.04946	0.014288
0.042946	0.063143	0.022858	0.063593		0.046863	0.072989		0.015716	0.037867	0.044528	0.053229	0.047079	0.014156
0.042898	0.062007	0.022117	0.061115		0.045027	0.07205		0.015404	0.037489	0.043943	0.053055	0.046788	0.013286
0.04245	0.061986	0.022037	0.061039		0.042136	0.070852		0.015386	0.036288	0.043622	0.052188	0.045743	0.012502
0.041533	0.06002	0.02071	0.060744		0.042048	0.067045		0.015353	0.035179	0.041433	0.05204	0.042777	0.012267
0.040128	0.059914	0.0204	0.060564		0.040366	0.065856		0.014425	0.035054	0.040738	0.050591	0.042681	0.012101
0.040043	0.05964	0.019879	0.059421		0.040161	0.065523		0.013611	0.034894	0.040709	0.050506	0.041339	0.012079
0.038429	0.057507	0.019295	0.058468		0.039455	0.064557		0.013345	0.03438	0.040702	0.04979	0.040921	0.011346
0.038094	0.056365	0.019141	0.057476		0.036359	0.06394		0.012866	0.033956	0.039992	0.049576	0.040596	0.011151
0.038052	0.055723	0.019047	0.057279		0.03477	0.062879		0.012821	0.033921	0.039474	0.049011	0.040268	0.010997
0.037634	0.055507	0.018808	0.055355		0.034413	0.062679		0.012273	0.033825	0.038918	0.049002	0.039975	0.010453
0.036895	0.05495	0.018686	0.054564		0.034327	0.061278		0.012103	0.033653	0.036335	0.0479	0.039822	0.010408
0.036861	0.054787	0.018638	0.051188		0.033936	0.060989		0.011743	0.033129	0.03613	0.047895	0.039624	0.009805
0.036758	0.054404	0.018398	0.050912		0.032609	0.060421		0.011692	0.033074	0.03538	0.047464	0.039494	0.009733
0.0364	0.053574	0.018132	0.050821		0.032271	0.058625		0.011288	0.032091	0.034726	0.046789	0.038579	0.009452
0.036356	0.053035	0.017547	0.049585		0.031578	0.058169		0.011175	0.031125	0.034228	0.045832	0.036932	0.00941
0.036309	0.052779	0.017261	0.048004		0.03132	0.057899		0.010985	0.030555	0.033644	0.045483	0.035817	0.009347
0.036275	0.052325	0.017193	0.04672		0.031169	0.057564		0.010729	0.030389	0.032884	0.044377	0.035534	0.009154
0.036152	0.052155	0.017138	0.046145		0.031087	0.057378		0.010708	0.029398	0.032281	0.043378	0.0353	0.009103
0.036082	0.051889	0.017058	0.045818		0.030159	0.055049		0.010686	0.029123	0.032014	0.043327	0.033916	0.00903
0.035329	0.051538	0.016721	0.045723		0.030077	0.054673		0.010225	0.028243	0.031931	0.043161	0.03276	0.009027
0.03494	0.050684	0.016226	0.045436		0.029722	0.054042		0.010224	0.027707	0.03192	0.04261	0.032532	0.008911
0.034889	0.050239	0.016083	0.045285		0.027575	0.053799		0.009876	0.027443	0.031827	0.042587	0.031681	0.008749
0.03477	0.049651	0.015954	0.045191		0.027442	0.053284		0.009869	0.026587	0.030825	0.04245	0.031633	0.008585
0.034263	0.049633	0.015848	0.044126		0.027018	0.052616		0.009797	0.026339	0.030656	0.04214	0.030797	0.008542
0.033619	0.049556	0.015751	0.043383		0.026857	0.052268		0.009792	0.026191	0.030245	0.042132	0.030374	0.008534
0.0336	0.048651	0.01559	0.042652		0.026301	0.052209		0.009709	0.025644	0.029851	0.040966	0.02967	0.008465
0.032857	0.04832	0.015558	0.042282		0.026236	0.051717		0.009649	0.025444	0.029104	0.0409	0.029136	0.00837
0.032555	0.048032	0.015305	0.041189		0.025414	0.050195		0.009641	0.025388	0.028675	0.04049	0.028665	0.007708
0.031673	0.047836	0.014893	0.040799		0.024062	0.049887		0.009637	0.024583	0.028353	0.038859	0.025752	0.007667
0.031631	0.047341	0.014354	0.040783		0.023728	0.049266		0.009626	0.024153	0.027962	0.038812	0.025394	0.007646
0.031544	0.046807	0.014053	0.039292		0.023633	0.049244		0.009587	0.023841	0.027832	0.038557	0.025139	0.007282
0.03119	0.046797	0.014027	0.03922		0.023569	0.049126		0.009507	0.023576	0.027155	0.037931	0.025103	0.007187
0.030802	0.046463	0.013539	0.03889		0.022787	0.048241		0.008909	0.022972	0.026897	0.03769	0.02506	0.007184
0.030366	0.046253	0.013456	0.038494		0.022047	0.047904		0.008898	0.021798	0.02675	0.036613	0.024993	0.006713
0.030295	0.045811	0.013195	0.037923		0.021621	0.047752		0.008838	0.021535	0.026074	0.036437	0.024603	0.006618
0.030192	0.045668	0.013183	0.037809		0.021563	0.047724		0.008736	0.021174	0.025953	0.035415	0.024473	0.006599
0.030095	0.045496	0.013148	0.036672		0.021525	0.047375		0.008505	0.020382	0.025821	0.035198	0.024015	0.00658
0.03007	0.045491	0.012959	0.036247		0.021493	0.047227		0.008461	0.020265	0.025786	0.033077	0.023945	0.006472
0.029677	0.045311	0.012895	0.03573		0.02139	0.046913		0.008234	0.020043	0.025742	0.032879	0.022973	0.006431
0.02937	0.04421	0.012881	0.035468		0.021049	0.046895		0.008128	0.019684	0.025741	0.032829	0.022563	0.006424
0.029186	0.042204	0.012793	0.034584		0.019691	0.046098		0.007931	0.019608	0.025131	0.032439	0.022433	0.006396
0.028941	0.042032	0.012536	0.034165		0.019592	0.045934		0.007547	0.019442	0.025105	0.032347	0.021448	0.00639
0.028563	0.041578	0.012536	0.033831		0.019447	0.045177		0.007491	0.019436	0.024988	0.032244	0.021391	0.006354
0.028487	0.041197	0.012374	0.033809		0.01895	0.044823		0.007406	0.019214	0.024897	0.032231	0.021168	0.006047

0.028039	0.041012	0.012374	0.033257		0.018907	0.044646		0.007063	0.019203	0.024659	0.03103	0.020953	0.005985
0.027431	0.040965	0.012335	0.032573		0.018838	0.044613		0.006942	0.019151	0.024153	0.030768	0.020775	0.005909
0.027168	0.040849	0.011977	0.031223		0.018665	0.044375		0.006922	0.018328	0.024105	0.030637	0.020693	0.005643
0.026872	0.040391	0.011914	0.031074		0.018481	0.043735		0.006913	0.017274	0.023906	0.030341	0.020549	0.005492
0.026676	0.040111	0.011836	0.030739		0.017654	0.042888		0.006816	0.01685	0.023407	0.030327	0.020516	0.00549
0.025057	0.039902	0.011788	0.030513		0.017093	0.042763		0.00679	0.016797	0.023274	0.029256	0.01888	0.005337
0.024803	0.039305	0.011453	0.030245		0.017074	0.042362		0.006686	0.016753	0.0231	0.027956	0.018716	0.005328
0.023745	0.039214	0.011365	0.030141		0.016955	0.041731		0.006514	0.016547	0.023081	0.027488	0.018629	0.005275
0.023721	0.039121	0.01126	0.028354		0.016883	0.041613		0.006398	0.016464	0.022731	0.02746	0.017824	0.005274
0.02367	0.037794	0.011153	0.027644		0.016485	0.041579		0.006354	0.016321	0.022549	0.027227	0.017804	0.005099
0.023621	0.037702	0.011027	0.027234		0.016339	0.04073		0.006351	0.015994	0.022518	0.027063	0.017572	0.005024
0.023593	0.037243	0.010948	0.026856		0.016241	0.040442		0.006342	0.015965	0.021742	0.027039	0.017428	0.005002
0.023494	0.03724	0.010805	0.026582		0.015706	0.039945		0.006184	0.015869	0.021679	0.026952	0.017202	0.004959
0.022882	0.036958	0.010538	0.026539		0.015403	0.03909		0.006142	0.015831	0.021504	0.026926	0.017168	0.004927
0.022533	0.036932	0.010484	0.026028		0.015248	0.038689		0.006142	0.015408	0.02111	0.026807	0.01673	0.004818
0.022502	0.036318	0.010475	0.02592		0.015227	0.038457		0.006114	0.015331	0.020872	0.025938	0.016459	0.004769
0.022311	0.036227	0.010419	0.025906		0.015151	0.038307		0.006011	0.015211	0.02021	0.025767	0.016118	0.00476
0.022223	0.036124	0.010403	0.025586		0.014783	0.038117		0.005967	0.015151	0.019661	0.025563	0.016055	0.004681
0.022041	0.035531	0.010361	0.025137		0.01471	0.037886		0.005896	0.014738	0.019594	0.025545	0.015897	0.00454
0.021923	0.035349	0.010354	0.025017		0.014674	0.037595		0.005775	0.014006	0.019007	0.025485	0.014397	0.004533
0.021805	0.035312	0.010305	0.024679		0.01448	0.037113		0.005615	0.01372	0.018908	0.025421	0.014369	0.00442
0.021567	0.035286	0.009929	0.024478		0.013869	0.036681		0.005544	0.013693	0.01873	0.025298	0.01418	0.004243
0.021566	0.0352	0.009928	0.024101		0.013854	0.036405		0.005515	0.013638	0.018689	0.025045	0.013976	0.004116
0.021504	0.035124	0.009886	0.024083		0.013187	0.036387		0.005459	0.013582	0.018647	0.024974	0.013527	0.003962
0.02147	0.035074	0.009805	0.023996		0.012962	0.036067		0.005436	0.013451	0.018392	0.024942	0.013488	0.003906
0.021062	0.034936	0.009782	0.023687		0.0127	0.035628		0.005376	0.013371	0.017716	0.024813	0.013231	0.003901
0.020796	0.034794	0.009612	0.023576		0.012537	0.035135		0.005303	0.012104	0.017635	0.024799	0.013177	0.003808
0.020723	0.034659	0.009462	0.023062		0.012399	0.0351		0.00528	0.01133	0.017581	0.024701	0.013036	0.003704
0.020586	0.03451	0.009404	0.023032		0.012348	0.03495		0.005109	0.011316	0.01742	0.024657	0.012474	0.003694
0.020327	0.034064	0.009391	0.022471		0.012049	0.034395		0.004897	0.011262	0.017221	0.024373	0.012451	0.003657
0.020256	0.03398	0.009242	0.021769		0.011788	0.034241		0.004875	0.010781	0.017199	0.024205	0.012332	0.003613
0.019948	0.033931	0.009079	0.021718		0.011418	0.034112		0.004796	0.010748	0.017169	0.024085	0.012047	0.003594
0.019895	0.033835	0.008999	0.020634		0.011311	0.033873		0.004696	0.010047	0.017102	0.023967	0.011327	0.003589
0.019847	0.033354	0.008844	0.020509		0.010962	0.03295		0.004651	0.010029	0.016981	0.023833	0.011321	0.003536
0.019668	0.033041	0.008836	0.019829		0.010948	0.032842		0.004648	0.009521	0.016847	0.023735	0.010906	0.003377
0.019339	0.031864	0.008815	0.019642		0.010786	0.032467		0.004275	0.009453	0.016696	0.023724	0.010872	0.003252
0.019331	0.03185	0.008494	0.019621		0.010596	0.032258		0.004197	0.00943	0.01652	0.023657	0.010827	0.00323
0.019049	0.031198	0.008447	0.019216		0.01057	0.032244		0.004034	0.009362	0.016391	0.023339	0.009982	0.003139
0.018556	0.030782	0.008411	0.019174		0.010452	0.031919		0.003913	0.009361	0.016303	0.023327	0.009943	0.003084
0.018236	0.030652	0.008399	0.019165		0.010401	0.03184		0.003796	0.009253	0.016165	0.02306	0.009835	0.002996
0.018095	0.030399	0.008373	0.019125		0.010329	0.031633		0.003761	0.009251	0.016057	0.023002	0.009773	0.002987
0.018021	0.030241	0.008297	0.018989		0.010315	0.031476		0.003675	0.009246	0.016053	0.022804	0.009398	0.002981
0.018012	0.030205	0.008295	0.018889		0.010036	0.031317		0.003645	0.009235	0.015522	0.022704	0.009217	0.002943
0.017889	0.030158	0.008199	0.018879		0.009966	0.031166		0.003639	0.009213	0.015198	0.021223	0.009183	0.002722
0.017745	0.030152	0.008143	0.018678		0.009866	0.031121		0.003594	0.009097	0.015144	0.021184	0.009084	0.002709
0.017742	0.029985	0.008121	0.01785		0.00979	0.03088		0.003567	0.008862	0.015047	0.021079	0.008957	0.002636
0.01759	0.029871	0.008068	0.01715		0.009598	0.030865		0.003563	0.008629	0.014832	0.020988	0.008799	0.002635
0.017439	0.029868	0.008017	0.017123		0.009589	0.030684		0.00353	0.008447	0.01469	0.02095	0.008734	0.002613
0.017409	0.02983	0.007992	0.017006		0.009502	0.029823		0.003284	0.008374	0.014465	0.020851	0.008711	0.002593
0.017307	0.029616	0.007931	0.016926		0.009488	0.029261		0.003122	0.008337	0.014306	0.020709	0.008285	0.002491
0.017274	0.029471	0.007884	0.016542		0.009361	0.028994		0.003114	0.008245	0.014212	0.02046	0.008248	0.002425
0.017013	0.029363	0.007651	0.015267		0.009353	0.02816		0.003042	0.008205	0.014084	0.019928	0.008214	0.002369
0.016881	0.029317	0.007593	0.014943		0.009322	0.027963		0.002972	0.008188	0.013658	0.019882	0.007833	0.002026
0.016809	0.029236	0.007448	0.014914		0.008611	0.027786		0.002892	0.007883	0.013578	0.019718	0.007403	0.002018
0.016741	0.028803	0.007441	0.014643		0.008288	0.027742		0.002881	0.007883	0.013575	0.019655	0.007381	0.002
0.016528	0.028514	0.00742	0.014603		0.008169	0.027407		0.002878	0.007577	0.01338	0.019236	0.007299	0.001996
0.016148	0.028221	0.007165	0.014409		0.00807	0.027244		0.002866	0.007327	0.013302	0.018967	0.007214	0.001956
0.016034	0.028202	0.007133	0.014194		0.008016	0.027206		0.002841	0.007269	0.013185	0.018862	0.006991	0.001917
0.015917	0.027925	0.006858	0.014162		0.007981	0.027149		0.002811	0.00713	0.013127	0.018849	0.006943	0.00182
0.015827	0.027477	0.006717	0.014145		0.007913	0.026496		0.002721	0.00705	0.013039	0.018752	0.006565	0.001697
0.015577	0.027469	0.006667	0.014131		0.007889	0.026065		0.002707	0.006657	0.013019	0.018578	0.006449	0.001677
0.015551	0.027376	0.006661	0.014016		0.007876	0.024737		0.002579	0.006489	0.012865	0.018482	0.006429	0.001588
0.015488	0.027154	0.006545	0.013964		0.007747	0.02468		0.00251	0.006486	0.012613	0.018402	0.006395	0.001387
0.015468	0.026986	0.006533	0.013758		0.007565	0.024582		0.002359	0.006441	0.012594	0.018337	0.006259	0.001385
0.015149	0.026916	0.006511	0.01371		0.007463	0.023869		0.002339	0.006265	0.012556	0.018233	0.006194	0.001309
0.015085	0.026906	0.006507	0.013698		0.007246	0.02368		0.002269	0.005937	0.012456	0.018075	0.006113	0.001272
0.014955	0.026592	0.006419	0.013571		0.006965	0.023677		0.00224	0.00575	0.012366	0.017823	0.005898	0.001204
0.014908	0.026389	0.006418	0.013365		0.006818	0.023635		0.002221	0.005742	0.012303	0.017785	0.005875	0.001194
0.014883	0.026206	0.006376	0.013117		0.006773	0.023437		0.002209	0.005578	0.012254	0.017743	0.005822	0.001067
0.014734	0.026038	0.006359	0.012993		0.00674	0.023405		0.002191	0.005455	0.012221	0.017462	0.005717	0.001058
0.014539	0.025919	0.006321	0.012989		0.006473	0.023318		0.002187	0.005344	0.011877	0.017198	0.005607	0.001044
0.014438	0.025212	0.00632	0.012482		0.006411	0.023193		0.002168	0.005271	0.011791	0.017146	0.005579	0.001003
0.014182	0.025033	0.006309	0.012003		0.00641	0.023095		0.002048	0.005174	0.011661	0.017057	0.00535	0.000989
0.014131	0.025029	0.006297	0.011975		0.006363	0.022958		0.002043	0.005072	0.011654	0.016973	0.005324	0.000986
0.014074	0.024987	0.006286	0.011947		0.006305	0.022415		0.002037	0.004994	0.011588	0.016871	0.005124	0.000983
0.014062	0.024845	0.006263	0.011862		0.00628	0.022036		0.001999	0.004967	0.011566	0.016664	0.005118	0.000982
0.013937	0.024444	0.006219	0.011834		0.005944	0.021898		0.001934	0.004952	0.011513	0.016482	0.005008	0.000981
0.013865	0.024375	0.006207	0.011616		0.005814	0.02181		0.001927	0.004881	0.011499	0.016409	0.004938	0.000926
0.013858	0.024089	0.006188	0.011049		0.005687	0.021715		0.001901	0.004609	0.011284	0.016357	0.004938	0.000871
0.013748	0.023948	0.006164	0.010852		0.005678	0.021606		0.001846	0.004469	0.011267	0.016073	0.004909	0.000813
0.013503	0.023651	0.00616	0.0107		0.005629	0.021572		0.001781	0.004362	0.011226	0.015676	0.004892	0.000776
0.013436	0.023468	0.006101	0.010633		0.005542	0.021521		0.001752	0.004268	0.011121	0.015659	0.004593	0.000739
0.013333	0.023272	0.006093	0.010531		0.005502	0.021305		0.001676	0.00406	0.01112	0.015584	0.004522	0.000709
0.013229	0.023034	0.006043	0.010452		0.005483	0.020861		0.001668	0.003896	0.011071	0.015561	0.004293	0.000664
0.013024	0.023003	0.005986	0.009868		0.005452	0.020795		0.001655	0.003455	0.01096	0.015371	0.0041	0.000651
0.013005	0.022846	0.00591	0.009766		0.005379	0.020784		0.001608	0.00344	0.010795	0.015044	0.003813	0.00065
0.012973	0.022805	0.005839	0.009698		0.005372	0.0204		0.001593	0.003436	0.010681	0.015041	0.003342	0.000614
0.012934	0.022497	0.005828	0.00941		0.005268	0.019095		0.001579	0.003144	0.01054	0.014888	0.002802	0.000553
0.012852	0.022292	0.005753	0.009135		0.005255	0.018869		0.001569	0.003064	0.010524	0.014755	0.002658	0.000553
0.012823	0.02224	0.005691	0.00909		0.005251	0.018754		0.001537	0.00272	0.010471	0.014667	0.002573	0.000542
0.012805	0.022143	0.005678	0.008991		0.005213	0.018018		0.001515	0.002563	0.010441	0.014622	0.002257	0.000525
0.012781	0.022087	0.005661	0.008838		0.005188	0.01772		0.001514	0.00256	0.010423	0.014595	0.002167	0.000503
0.01272	0.022003	0.005644	0.008808		0.00515	0.017625		0.001498	0.002496	0.010406	0.014503	0.002093	0.000478
0.012653	0.021948	0.005625	0.008271		0.005121	0.017612		0.001495	0.002452	0.010233	0.014302	0.001926	0.000478
0.012638	0.021933	0.005533	0.00822		0.005107	0.017551		0.001377	0.002204	0.010233	0.014224	0.001771	0.000475
0.012554	0.021931	0.005517	0.008206		0.004985	0.017207		0.001372	0.00214	0.00999	0.014174	0.001438	0.000473
0.012475	0.021829	0.005499	0.008064		0.004969	0.016622		0.001286	0.002081	0.0098	0.013858	0.001254	0.000468
0.012473	0.021818	0.005483	0.007941		0.004954	0.016545		0.001282	0.002065	0.009618	0.013848	0.001215	0.000468
0.01247	0.021815	0.005468	0.007838		0.004897	0.016279		0.00126	0.002016	0.009502	0.013844	0.001189	0.000434
0.012391	0.021779	0.00546	0.007714		0.004834	0.016041		0.001219	0.00201	0.00947	0.013775	0.001028	0.000417
0.012261	0.021572	0.005447	0.007625		0.004801	0.015613		0.001076	0.001959	0.00937	0.013674	0.001003	0.000365
0.012013	0.021543	0.005421	0.007573		0.004722	0.015537		0.001049	0.00188	0.009275	0.013592	0.001003	0.000344
0.011962	0.02151	0.005359	0.00756		0.004704	0.015223		0.001036	0.001745	0.009246	0.013317	0.000958	0.000332
0.011936	0.02145	0.005353	0.007175		0.004657	0.015137		0.000981	0.001723	0.009176	0.013111	0.000828	0.000332
0.0116	0.021329	0.005327	0.007095		0.004569	0.015027		0.000969	0.001606	0.009167	0.013095	0.000774	0.000326
0.011476	0.02119	0.005287	0.007029		0.004511	0.014838		0.000895	0.001562	0.009121	0.013027	0.000751	0.000322
0.011476	0.021185	0.005285	0.006913		0.004463	0.014813		0.000891	0.001462	0.008979	0.01302	0.00074	0.00031
0.011258	0.02118	0.00522	0.006697		0.004386	0.014065		0.000853	0.001453	0.008943	0.012678	0.00074	0.00026
0.011231	0.0211	0.005211	0.006696		0.004339	0.013933		0.000847	0.00144	0.008921	0.012535	0.000726	0.000244
0.011139	0.020866	0.005209	0.006654		0.004333	0.013814		0.000838	0.001411	0.008697	0.012379	0.000675	0.000232
0.01106	0.020062	0.005158	0.006593		0.004309	0.013275		0.000825	0.001381	0.008671	0.012061	0.000658	0.000182
0.010532	0.019434	0.005116	0.006563		0.004282	0.013235		0.000805	0.001356	0.008589	0.012045	0.000652	0.000174
0.010409	0.019308	0.005049	0.006509		0.004276	0.012993		0.000799	0.001225	0.008535	0.012035	0.000636	0.000156
0.010392	0.019216	0.005042	0.006428		0.004263	0.01298		0.000748	0.001179	0.008469	0.01192	0.00063	0.000152

0.010354	0.019148	0.005027	0.00634	0.00423	0.012909	0.000747	0.001142	0.008378	0.011459	0.000627	0.000152
0.010289	0.01908	0.004859	0.006335	0.004205	0.012859	0.000718	0.001101	0.008172	0.011397	0.000621	0.000151
0.010215	0.019029	0.004742	0.006207	0.00417	0.012661	0.000678	0.001004	0.008093	0.011394	0.000573	0.000136
0.010178	0.01898	0.004694	0.006163	0.004085	0.0126	0.000643	0.001001	0.008003	0.011181	0.000559	0.000127
0.010148	0.018946	0.004685	0.006047	0.004074	0.012516	0.000636	0.000974	0.008002	0.01102	0.000548	0.000122
0.010026	0.018939	0.004652	0.006042	0.004059	0.012504	0.000628	0.000859	0.007962	0.010968	0.000534	0.00012
0.009978	0.018937	0.004637	0.006032	0.004015	0.012293	0.00062	0.000844	0.007922	0.010765	0.000523	0.000115
0.00993	0.018911	0.004637	0.00596	0.00401	0.012254	0.000556	0.000843	0.007858	0.010526	0.000523	0.000094
0.009922	0.01889	0.004631	0.005541	0.003929	0.01194	0.000553	0.000791	0.007721	0.010496	0.00052	0.000066
0.00982	0.018789	0.004574	0.005408	0.003901	0.011746	0.000548	0.000772	0.007676	0.010462	0.000517	0.000049
0.00982	0.018444	0.004573	0.0052	0.003866	0.011651	0.000544	0.000717	0.007644	0.010375	0.000511	0.000033
0.009817	0.018375	0.004508	0.005086	0.003809	0.011405	0.000543	0.000711	0.00745	0.010322	0.000486	0.000006
0.009803	0.018329	0.004449	0.005077	0.003765	0.011368	0.000533	0.000696	0.007316	0.01032	0.000486	0.000002
0.009776	0.018251	0.004447	0.005037	0.003716	0.011349	0.000518	0.000694	0.007224	0.010167	0.000486	0.000001
0.009638	0.018229	0.00438	0.004871	0.003708	0.011133	0.000503	0.000674	0.007201	0.010108	0.000475	0.000001
0.00963	0.017485	0.004309	0.004777	0.003626	0.011078	0.000502	0.000665	0.007191	0.010085	0.000466	0.000001
0.009628	0.017126	0.004283	0.004738	0.00362	0.010856	0.0005	0.000624	0.007055	0.009701	0.000432	7.085E-07
0.009537	0.017015	0.004278	0.004732	0.003599	0.010661	0.000493	0.000613	0.007029	0.009617	0.000415	7.085E-07
0.009392	0.016667	0.004276	0.004731	0.003466	0.010424	0.000487	0.000609	0.006853	0.009443	0.000412	7.085E-07
0.00938	0.016544	0.00425	0.004714	0.003424	0.010112	0.000484	0.000607	0.006796	0.009402	0.000407	7.085E-07
0.00915	0.016205	0.004194	0.004714	0.003365	0.00974	0.000483	0.000593	0.006695	0.009253	0.000381	7.085E-07
0.009141	0.016144	0.004145	0.004669	0.003313	0.009706	0.000475	0.000592	0.006682	0.009007	0.000319	
0.009129	0.016142	0.004121	0.004586	0.003245	0.009668	0.00047	0.000583	0.006565	0.009002	0.000311	
0.009118	0.015995	0.004102	0.004544	0.003213	0.009592	0.000453	0.000583	0.006501	0.008998	0.000311	
0.009006	0.015961	0.004099	0.004424	0.00321	0.009284	0.000423	0.000558	0.006405	0.00896	0.000294	
0.008984	0.015794	0.004089	0.00437	0.003174	0.009262	0.00042	0.000548	0.006256	0.008867	0.000288	
0.008913	0.015747	0.004074	0.004296	0.003145	0.008923	0.000415	0.000544	0.006064	0.00884	0.000268	
0.008862	0.01569	0.004038	0.004268	0.00314	0.008743	0.000412	0.000537	0.00605	0.008675	0.000263	
0.008749	0.015572	0.004014	0.004263	0.003131	0.008665	0.000412	0.000523	0.005985	0.008664	0.000257	
0.008676	0.015482	0.004014	0.004261	0.003129	0.008471	0.000408	0.000491	0.005985	0.008566	0.000237	
0.008624	0.015443	0.003932	0.004241	0.003125	0.008336	0.000408	0.000488	0.005873	0.00852	0.000226	
0.00857	0.015342	0.003893	0.004147	0.003093	0.00807	0.000407	0.000469	0.005832	0.008439	0.000195	
0.008556	0.015281	0.003865	0.004136	0.00309	0.008057	0.000389	0.000469	0.005814	0.00843	0.000195	
0.008488	0.01528	0.003813	0.004116	0.003087	0.007931	0.000366	0.000452	0.005764	0.008413	0.000186	
0.008422	0.015176	0.003704	0.004059	0.003053	0.007926	0.000366	0.000439	0.005727	0.00831	0.000175	
0.008415	0.015006	0.003582	0.003998	0.002951	0.0079	0.000352	0.000424	0.005646	0.008258	0.000161	
0.008402	0.014894	0.003574	0.003982	0.002901	0.007715	0.000339	0.000417	0.005644	0.008175	0.000161	
0.008348	0.014726	0.00357	0.003954	0.002892	0.007625	0.000333	0.000416	0.005593	0.00816	0.000158	
0.008309	0.014682	0.003557	0.003947	0.002862	0.007514	0.00032	0.000413	0.005566	0.007812	0.000153	
0.008223	0.014658	0.003538	0.003753	0.002851	0.00744	0.000312	0.000412	0.005564	0.0076	0.000147	
0.008084	0.01441	0.003483	0.003692	0.002845	0.007292	0.000303	0.000407	0.005542	0.007567	0.000127	
0.008075	0.013997	0.003477	0.003565	0.002659	0.0071	0.000288	0.000405	0.005367	0.007556	0.000121	
0.008026	0.013996	0.003433	0.00336	0.002627	0.006664	0.000281	0.000386	0.005267	0.007528	0.000113	
0.007953	0.013991	0.003411	0.003325	0.002626	0.006416	0.000279	0.000375	0.005239	0.007471	0.00011	
0.007931	0.013924	0.003397	0.003322	0.002624	0.006294	0.000273	0.000369	0.005218	0.007459	0.000088	
0.007882	0.013908	0.003272	0.003317	0.002604	0.006264	0.000271	0.000363	0.004978	0.00743	0.000079	
0.007639	0.013843	0.003144	0.003313	0.002574	0.005969	0.000264	0.000362	0.00497	0.007368	0.000076	
0.007559	0.013803	0.003022	0.003295	0.002513	0.004868	0.00025	0.000361	0.004927	0.007333	0.000073	
0.007481	0.013764	0.002992	0.003273	0.002484	0.004863	0.000227	0.000343	0.004878	0.007149	0.000065	
0.007452	0.013632	0.002989	0.003231	0.002477	0.004862	0.000225	0.000343	0.004817	0.007106	0.000062	
0.007406	0.013578	0.002922	0.003224	0.002439	0.004559	0.000225	0.000336	0.00481	0.007056	0.000059	
0.007348	0.01355	0.002913	0.00322	0.002435	0.004405	0.000217	0.000335	0.004803	0.007021	0.000059	
0.007324	0.01349	0.00288	0.003179	0.002435	0.004404	0.0002	0.000323	0.004667	0.006968	0.000059	
0.007263	0.013472	0.002844	0.00314	0.00243	0.004294	0.000193	0.000316	0.004641	0.006924	0.000059	
0.007238	0.01327	0.002838	0.00313	0.002429	0.004253	0.000188	0.000313	0.004552	0.006914	0.000054	
0.007176	0.012952	0.002776	0.003118	0.002429	0.004217	0.000188	0.000311	0.004504	0.006865	0.00004	
0.006992	0.012944	0.00276	0.003106	0.002391	0.003626	0.000181	0.000311	0.004434	0.00685	0.000031	
0.00696	0.012849	0.002756	0.003071	0.002379	0.003401	0.000176	0.000305	0.004425	0.006788	0.000003	
0.006959	0.012847	0.002747	0.00292	0.002377	0.003145	0.000176	0.000296	0.00441	0.006745		
0.006886	0.012599	0.002737	0.00287	0.002342	0.002889	0.000175	0.000296	0.004403	0.006704		
0.006861	0.012493	0.002728	0.002853	0.002309	0.002881	0.000172	0.000296	0.004166	0.006489		
0.006852	0.012403	0.002697	0.002826	0.002272	0.002878	0.000167	0.000296	0.004156	0.006483		
0.006821	0.012382	0.002653	0.00268	0.002259	0.002721	0.000166	0.000295	0.004085	0.006436		
0.006794	0.012361	0.002644	0.002664	0.00225	0.002512	0.000162	0.000295	0.00403	0.006432		
0.00679	0.012315	0.002636	0.002661	0.002227	0.002509	0.000159	0.000293	0.004027	0.006293		
0.006715	0.012243	0.002592	0.002654	0.002214	0.002306	0.000159	0.000291	0.003874	0.006257		
0.006609	0.012069	0.002587	0.002642	0.002213	0.002225	0.000157	0.000288	0.003823	0.006233		
0.006471	0.012057	0.00257	0.002627	0.002174	0.001995	0.000155	0.000284	0.003742	0.006231		
0.006432	0.011978	0.002512	0.002594	0.002146	0.001927	0.000154	0.000284	0.003725	0.006225		
0.006429	0.011847	0.002468	0.002554	0.002124	0.001422	0.000151	0.000278	0.003667	0.00622		
0.006365	0.01179	0.002441	0.002545	0.002117	0.001122	0.000141	0.000277	0.003523	0.00621		
0.006168	0.011746	0.002404	0.002534	0.002111	0.001117	0.000133	0.000271	0.003503	0.006167		
0.006064	0.011565	0.0024	0.002527	0.002103	0.00106	0.000129	0.000267	0.003297	0.006132		
0.006049	0.011554	0.002389	0.002526	0.002094	0.001005	0.000128	0.000265	0.00326	0.005992		
0.006044	0.011465	0.002349	0.002522	0.002079	0.001002	0.000125	0.00026	0.003198	0.005933		
0.005954	0.01143	0.002331	0.002436	0.002053	0.000964	0.000119	0.000254	0.003104	0.005925		
0.005934	0.011333	0.002325	0.002429	0.002005	0.000953	0.000116	0.000252	0.002991	0.005828		
0.005923	0.011189	0.002214	0.002411	0.001991	0.000944	0.000113	0.000251	0.002991	0.005622		
0.005891	0.01115	0.00219	0.002386	0.001981	0.000852	0.000111	0.000244	0.002901	0.00562		
0.005811	0.011148	0.00214	0.00235	0.001971	0.000838	0.000106	0.000238	0.002837	0.005606		
0.005794	0.011064	0.002136	0.002343	0.001957	0.000755	0.000102	0.000235	0.002743	0.0056		
0.005765	0.011054	0.002133	0.002342	0.00194	0.000733	0.0001	0.000232	0.002663	0.005457		
0.005746	0.010904	0.002117	0.00233	0.00189	0.000727	0.000096	0.000228	0.002598	0.005446		
0.005554	0.010749	0.0021	0.00233	0.001875	0.000717	0.000094	0.000223	0.002589	0.005412		
0.005451	0.010728	0.00208	0.002309	0.001855	0.000675	0.000093	0.000218	0.002573	0.005393		
0.005413	0.010654	0.002076	0.002262	0.00185	0.000634	0.000091	0.000218	0.002544	0.005389		
0.00529	0.010613	0.00201	0.002257	0.001843	0.000634	0.000091	0.000216	0.002488	0.005363		
0.005239	0.010581	0.002006	0.002218	0.001812	0.000626	0.00009	0.000214	0.002402	0.005292		
0.005182	0.010523	0.001995	0.002215	0.001804	0.000609	0.000086	0.000213	0.002396	0.005289		
0.00517	0.010509	0.001981	0.002213	0.001796	0.000598	0.000083	0.000212	0.002294	0.005271		
0.00514	0.010501	0.001973	0.00213	0.001768	0.000597	0.000078	0.000211	0.002205	0.005237		
0.005094	0.010422	0.001968	0.002123	0.001761	0.000596	0.000075	0.00021	0.002077	0.005236		
0.005063	0.010337	0.001946	0.002114	0.001761	0.000587	0.000074	0.000202	0.00206	0.005173		
0.005052	0.010325	0.001945	0.002109	0.001756	0.000573	0.000072	0.000199	0.002039	0.005125		
0.004977	0.010309	0.001929	0.002077	0.001744	0.000572	0.00007	0.000195	0.002034	0.004986		
0.004718	0.010296	0.001926	0.002066	0.00171	0.000565	0.000065	0.000194	0.002	0.004941		
0.004712	0.010126	0.001911	0.002036	0.001684	0.000563	0.000065	0.000194	0.00199	0.004891		
0.004707	0.010122	0.001897	0.002033	0.001654	0.000508	0.000062	0.000193	0.001939	0.004878		
0.004628	0.010012	0.001894	0.002007	0.001637	0.000504	0.00006	0.000191	0.001876	0.004841		
0.004581	0.010012	0.001875	0.002004	0.001636	0.000486	0.000055	0.00019	0.001831	0.004801		
0.004528	0.009831	0.001866	0.001957	0.001622	0.000484	0.000049	0.000183	0.001829	0.004796		
0.004501	0.009781	0.001807	0.001922	0.001614	0.000483	0.000041	0.000182	0.001827	0.004741		
0.004501	0.009755	0.001781	0.001917	0.001599	0.000474	0.000035	0.000179	0.001822	0.0047		
0.004493	0.009648	0.001772	0.0019	0.001586	0.000452	0.000034	0.000177	0.001725	0.004695		
0.004492	0.009635	0.001772	0.001899	0.001543	0.000435	0.000034	0.000171	0.001647	0.00469		
0.004461	0.009608	0.001707	0.00188	0.00154	0.000399	0.000031	0.00017	0.001583	0.004676		
0.004413	0.009531	0.001687	0.001863	0.001539	0.000388	0.000031	0.000168	0.001484	0.004632		
0.00436	0.00928	0.00162	0.001843	0.001522	0.000372	0.000028	0.000168	0.001463	0.004494		
0.004326	0.009265	0.001609	0.001828	0.001513	0.000371	0.000026	0.000163	0.001416	0.004462		
0.004317	0.009251	0.001602	0.001815	0.001509	0.000354	0.000019	0.000163	0.001377	0.004442		
0.004253	0.009227	0.0016	0.00181	0.001505	0.000352	0.000019	0.00016	0.001295	0.004409		
0.004207	0.009153	0.001585	0.001794	0.001499	0.000349	0.000018	0.000158	0.00129	0.004406		
0.004176	0.009115	0.001574	0.001783	0.00148	0.00034	7.085E-07	0.000157	0.00127	0.00433		
0.004163	0.009114	0.001566	0.001778	0.001473	0.000329		0.000149	0.001248	0.004312		

0.004086	0.009093	0.001543	0.001773		0.001456	0.000325			0.000149	0.001197	0.004309		
0.004053	0.009074	0.001534	0.001759		0.001445	0.000322			0.000149	0.001149	0.00423		
0.004042	0.009069	0.00153	0.001757		0.001444	0.000312			0.000146	0.00111	0.0042		
0.003999	0.008944	0.001528	0.001749		0.001441	0.000307			0.000145	0.001051	0.00415		
0.003986	0.008923	0.001508	0.00174		0.00144	0.000304			0.000144	0.001026	0.004135		
0.003961	0.008812	0.00149	0.001736		0.001412	0.000303			0.000144	0.000996	0.004107		
0.003896	0.008811	0.001474	0.001715		0.00141	0.000303			0.000143	0.000986	0.004081		
0.003887	0.008678	0.001453	0.001701		0.001396	0.000279			0.00014	0.00091	0.00407		
0.003863	0.008451	0.001405	0.001688		0.00136	0.000264			0.000137	0.000903	0.004052		
0.003838	0.00836	0.001392	0.001684		0.001357	0.000259			0.000135	0.000852	0.004013		
0.003828	0.008341	0.00139	0.001683		0.001327	0.000254			0.000133	0.00083	0.003963		
0.003808	0.008294	0.001385	0.001675		0.001327	0.000248			0.000132	0.000824	0.003904		
0.003806	0.008199	0.001368	0.001671		0.0013	0.000239			0.000132	0.000817	0.003884		
0.003799	0.008168	0.001362	0.00167		0.001269	0.000236			0.000129	0.000816	0.00385		
0.003761	0.008156	0.001305	0.001659		0.001267	0.00023			0.000124	0.000799	0.003838		
0.003651	0.008147	0.001299	0.001656		0.001254	0.000221			0.000119	0.000794	0.003773		
0.00358	0.008073	0.001291	0.001645		0.001234	0.000185			0.000116	0.000755	0.003765		
0.003556	0.008035	0.001281	0.00164		0.001232	0.000183			0.000112	0.000752	0.00374		
0.003525	0.008021	0.001268	0.001631		0.00121	0.000157			0.000111	0.000736	0.003648		
0.003482	0.007987	0.001229	0.001623		0.001206	0.000154			0.000111	0.000705	0.003608		
0.003401	0.007892	0.001226	0.001579		0.001198	0.000149			0.00011	0.000701	0.003578		
0.00337	0.007822	0.001211	0.001549		0.001182	0.00014			0.000109	0.000628	0.003544		
0.003359	0.007784	0.001197	0.001547		0.001165	0.000139			0.000108	0.000624	0.003529		
0.003349	0.007576	0.001192	0.001541		0.001155	0.000135			0.000106	0.000606	0.003505		
0.003341	0.007506	0.001182	0.001518		0.001141	0.000123			0.000105	0.000601	0.003471		
0.003281	0.007485	0.001151	0.001516		0.001132	0.00012			0.000101	0.000594	0.00342		
0.00327	0.007468	0.001125	0.001494		0.001127	0.000108			0.000099	0.000594	0.003416		
0.003244	0.007466	0.001116	0.001477		0.001124	0.000099			0.000099	0.000577	0.003412		
0.00324	0.007455	0.001102	0.001463		0.001109	0.000095			0.000098	0.000573	0.003369		
0.003225	0.007422	0.0011	0.00145		0.001099	0.000094			0.000098	0.000568	0.003367		
0.003159	0.007355	0.001094	0.001449		0.001092	0.000092			0.000096	0.000563	0.003341		
0.003091	0.00734	0.001086	0.001445		0.00109	0.000088			0.000096	0.000543	0.003288		
0.003053	0.00734	0.00107	0.001436		0.001053	0.000077			0.000096	0.000531	0.003255		
0.003029	0.007316	0.001023	0.001429		0.001046	0.000074			0.000095	0.000524	0.003202		
0.002962	0.007285	0.001013	0.001419		0.001041	0.00007			0.000093	0.00052	0.003173		
0.002955	0.007161	0.001002	0.001414		0.001041	0.000066			0.000091	0.000499	0.003169		
0.002905	0.007066	0.000956	0.001414		0.001038	0.000064			0.000091	0.000487	0.003162		
0.002899	0.007056	0.000949	0.001407		0.001034	0.000062			0.00009	0.000473	0.003048		
0.002874	0.007017	0.000943	0.001396		0.001019	0.000054			0.000089	0.000468	0.003033		
0.002765	0.006995	0.000942	0.001382		0.00099	0.00005			0.000087	0.000436	0.003027		
0.002688	0.006944	0.000941	0.001338		0.000989	0.000047			0.000085	0.000436	0.003		
0.002595	0.006932	0.000937	0.001335		0.000989	0.000045			0.000085	0.000436	0.002927		
0.00259	0.006921	0.000921	0.001326		0.000985	0.000043			0.000082	0.000431	0.002881		
0.002566	0.006901	0.000894	0.001325		0.000969	0.000038			0.00008	0.000427	0.002842		
0.002547	0.006786	0.000877	0.001318		0.00096	0.000038			0.000078	0.000419	0.002835		
0.00253	0.006781	0.00085	0.001313		0.00096	0.000033			0.000078	0.000412	0.002824		
0.002527	0.006741	0.000847	0.001312		0.000952	0.000033			0.000072	0.000397	0.002812		
0.002522	0.006724	0.000825	0.001309		0.000936	0.00003			0.000071	0.000388	0.002768		
0.002474	0.006671	0.000815	0.001282		0.000917	0.000025			0.00007	0.000368	0.002766		
0.002469	0.006596	0.000808	0.001275		0.000905	0.000012			0.000068	0.000368	0.002761		
0.002294	0.006546	0.000802	0.001261		0.000904	0.000006			0.000066	0.000363	0.002731		
0.002274	0.006509	0.00077	0.001253		0.000897	0.000004			0.000065	0.00036	0.002697		
0.002273	0.006504	0.000764	0.001251		0.000897	0.000003			0.000065	0.000335	0.002683		
0.002192	0.006504	0.000757	0.001248		0.000878	0.000003			0.000062	0.000332	0.002666		
0.002134	0.00649	0.000732	0.001248		0.000851	0.000001			0.000061	0.000328	0.002533		
0.002123	0.00642	0.000725	0.001248		0.000823	7.085E-07			0.000057	0.000326	0.002527		
0.002115	0.006201	0.000721	0.001245		0.0008	7.085E-07			0.000057	0.000325	0.002501		
0.002068	0.00615	0.000706	0.001244		0.000783	7.085E-07			0.000056	0.000324	0.002464		
0.002026	0.006141	0.000695	0.001225		0.000769	7.085E-07			0.000055	0.000319	0.002435		
0.00201	0.006025	0.000694	0.001211		0.000759	7.085E-07			0.000054	0.000316	0.002425		
0.0019	0.005962	0.000692	0.00121		0.000743	7.085E-07			0.000051	0.000314	0.002411		
0.001888	0.005941	0.000687	0.001147		0.000738	7.085E-07			0.00005	0.000312	0.00241		
0.001862	0.005912	0.000677	0.001146		0.000728				0.000048	0.000275	0.002307		
0.001853	0.005885	0.000668	0.001139		0.000727				0.000045	0.000264	0.002299		
0.001851	0.005881	0.000613	0.001137		0.000721				0.000043	0.000261	0.002298		
0.001823	0.005838	0.00061	0.001133		0.000718				0.00004	0.000247	0.002284		
0.001811	0.005811	0.000609	0.001116		0.000711				0.000027	0.000242	0.002273		
0.001756	0.005787	0.000588	0.0011		0.000707				0.000023	0.000237	0.002246		
0.001751	0.005649	0.00058	0.001088		0.0007				0.000021	0.000237	0.002243		
0.001727	0.005588	0.00058	0.001048		0.000697				0.000016	0.000233	0.002213		
0.001698	0.00558	0.000572	0.001038		0.000696				0.000016	0.000223	0.002193		
0.001672	0.005549	0.000552	0.001037		0.000694				0.000016	0.000222	0.002154		
0.00166	0.005472	0.00054	0.00102		0.000689				0.000015	0.000222	0.002105		
0.001652	0.005416	0.000528	0.001009		0.00068				0.000007	0.000222	0.002099		
0.001649	0.005401	0.000491	0.001009		0.000675				0.000004	0.00022	0.002093		
0.001636	0.005332	0.000489	0.001002		0.000667				0.000004	0.000217	0.002092		
0.001632	0.005312	0.000486	0.000988		0.000665				0.000004	0.000215	0.002076		
0.001631	0.005269	0.000482	0.000985		0.000656				0.000002	0.000208	0.00202		
0.001606	0.005267	0.000466	0.000971		0.000644				0.000002	0.000206	0.002019		
0.00159	0.005263	0.000466	0.000962		0.000639				0.000002	0.000201	0.001989		
0.001564	0.005248	0.000462	0.000961		0.000637				0.000001	0.000198	0.001954		
0.001517	0.0052	0.000444	0.000959		0.000635				0.000001	0.000197	0.001902		
0.001517	0.005133	0.000441	0.000954		0.000607				0.000001	0.000191	0.001897		
0.001477	0.005119	0.00043	0.000947		0.000607				0.000001	0.000188	0.001891		
0.001432	0.005108	0.000429	0.000946		0.000606				7.355E-07	0.000186	0.001846		
0.001419	0.004923	0.000422	0.000936		0.000604				7.355E-07	0.000185	0.001834		
0.001418	0.004913	0.000412	0.000933		0.0006					0.000181	0.001769		
0.001416	0.004904	0.000399	0.000915		0.000599					0.000179	0.001759		
0.001399	0.004888	0.00039	0.000909		0.000597					0.000174	0.001751		
0.001399	0.004877	0.000389	0.000901		0.000592					0.000171	0.001721		
0.001396	0.004854	0.000386	0.000896		0.000587					0.000167	0.001603		
0.00136	0.004779	0.000385	0.000895		0.000578					0.000164	0.001602		
0.001357	0.004747	0.000385	0.000889		0.000578					0.000164	0.001592		
0.001333	0.004707	0.000378	0.000872		0.000575					0.000162	0.001571		
0.001286	0.00469	0.000373	0.000861		0.000573					0.00016	0.001549		
0.001274	0.004559	0.00037	0.000858		0.000566					0.000157	0.001538		
0.001251	0.004558	0.00037	0.000857		0.000558					0.000154	0.0015		
0.001235	0.004533	0.000369	0.000851		0.000555					0.000147	0.001449		
0.001226	0.004484	0.000362	0.000842		0.000554					0.000142	0.001446		
0.001219	0.004461	0.00035	0.000838		0.000542					0.000142	0.001402		
0.001213	0.004416	0.000349	0.000828		0.000539					0.000141	0.001395		
0.001161	0.004395	0.000344	0.000825		0.000539					0.000135	0.001358		
0.001132	0.00435	0.000336	0.000823		0.000535					0.000135	0.001325		
0.001117	0.004331	0.000335	0.000804		0.000535					0.000133	0.001272		
0.001085	0.004295	0.000331	0.000794		0.000529					0.000121	0.001255		
0.001062	0.004285	0.000326	0.000793		0.000519					0.00012	0.00123		
0.001019	0.004277	0.000324	0.000786		0.000508					0.000118	0.001216		
0.001008	0.004225	0.000324	0.000785		0.000508					0.000118	0.0012		
0.000968	0.004217	0.000319	0.000785		0.000505					0.000115	0.001171		
0.000966	0.004158	0.000313	0.000779		0.000505					0.000115	0.001148		
0.000949	0.004151	0.000288	0.000776		0.000504					0.000114	0.001141		
0.000935	0.004117	0.000286	0.000771		0.000499					0.000113	0.001114		
0.000933	0.004021	0.000278	0.000765		0.000485					0.000108	0.001112		
0.000897	0.004021	0.000276	0.00076		0.00047					0.000104	0.001056		

0.000897	0.003925	0.000273	0.000758	0.000466					0.000104	0.000984
0.000894	0.003915	0.000268	0.000753	0.000463					0.000102	0.000972
0.000872	0.003888	0.000265	0.000752	0.000454					0.000101	0.000946
0.000862	0.003876	0.00026	0.000735	0.000443					0.000099	0.000937
0.000855	0.003812	0.00026	0.000733	0.000442					0.000099	0.000917
0.000853	0.00376	0.000249	0.000725	0.000435					0.000098	0.000911
0.000844	0.003743	0.000243	0.000723	0.000434					0.000098	0.000834
0.000835	0.003696	0.00023	0.000722	0.000431					0.000097	0.000834
0.00083	0.003694	0.000224	0.000716	0.000429					0.000094	0.00083
0.000828	0.003677	0.000221	0.000712	0.000429					0.000094	0.000827
0.000806	0.003599	0.000221	0.000704	0.000425					0.000091	0.000826
0.000801	0.003597	0.00022	0.000702	0.000416					0.000088	0.000801
0.000793	0.003561	0.000213	0.00068	0.000411					0.000081	0.000797
0.00079	0.003539	0.000213	0.000677	0.000404					0.000079	0.000793
0.000765	0.003491	0.000211	0.000673	0.0004					0.000078	0.000776
0.000761	0.003474	0.00021	0.00067	0.000391					0.000073	0.000769
0.000752	0.003468	0.000201	0.000669	0.000383					0.000073	0.00076
0.00075	0.003436	0.000197	0.000666	0.000383					0.000073	0.000758
0.000748	0.003429	0.000195	0.000665	0.00038					0.000072	0.000752
0.000743	0.003407	0.000195	0.000664	0.000377					0.000069	0.000743
0.000731	0.003302	0.000194	0.000658	0.000372					0.000067	0.000712
0.000726	0.003298	0.000189	0.000649	0.000365					0.000067	0.000712
0.000726	0.003285	0.000188	0.000644	0.00036					0.000062	0.000699
0.000718	0.003228	0.000186	0.000643	0.000359					0.000057	0.000661
0.000714	0.003199	0.000183	0.00064	0.000358					0.000055	0.000655
0.000692	0.003176	0.000182	0.000632	0.000357					0.000055	0.000654
0.000687	0.003067	0.000177	0.000629	0.000356					0.000053	0.000653
0.000678	0.003059	0.000172	0.000616	0.000349					0.000049	0.000651
0.000675	0.003024	0.000165	0.000616	0.000349					0.000048	0.000625
0.000671	0.002988	0.000164	0.000609	0.000341					0.000047	0.000625
0.000668	0.002957	0.000164	0.000604	0.000327					0.000045	0.000623
0.000658	0.002875	0.000163	0.000603	0.000319					0.000045	0.000612
0.000641	0.002785	0.000162	0.000601	0.000318					0.000042	0.000606
0.00064	0.00278	0.000159	0.000591	0.000318					0.000039	0.000599
0.000638	0.002776	0.000156	0.000575	0.000317					0.000032	0.000584
0.000637	0.002759	0.000153	0.000571	0.000315					0.000026	0.000569
0.000636	0.002732	0.00015	0.00057	0.000311					0.000025	0.000567
0.000635	0.002703	0.000148	0.00057	0.00031					0.000023	0.000559
0.000631	0.00269	0.000147	0.000569	0.000306					0.000011	0.000553
0.00063	0.002683	0.000145	0.000562	0.000304					0.000009	0.000534
0.000626	0.00265	0.000144	0.000543	0.000301					0.000008	0.000533
0.000614	0.002628	0.000138	0.000541	0.0003					0.000006	0.00053
0.000614	0.002598	0.000138	0.000535	0.000298					0.000006	0.000521
0.000611	0.002594	0.000137	0.000528	0.000296					0.000006	0.000519
0.000608	0.002557	0.000137	0.000526	0.000294					0.000001	0.000517
0.000598	0.002534	0.000136	0.000524	0.000293					0.000001	0.000517
0.000596	0.00251	0.000135	0.00052	0.000287					7.085E-07	0.000513
0.000595	0.002496	0.000135	0.000516	0.000285					7.085E-07	0.000504
0.000593	0.002493	0.000131	0.000507	0.000284					7.085E-07	0.000498
0.000584	0.002486	0.000129	0.000505	0.000284					7.085E-07	0.000496
0.000573	0.002463	0.000126	0.000504	0.000284						0.000494
0.000566	0.002447	0.000125	0.0005	0.000281						0.000492
0.000547	0.002443	0.000123	0.000495	0.000277						0.000489
0.000543	0.002407	0.000122	0.000493	0.000273						0.000489
0.000538	0.002308	0.000121	0.000492	0.000267						0.000488
0.000536	0.002291	0.00012	0.000487	0.000264						0.000488
0.000533	0.002287	0.000119	0.000485	0.000259						0.000477
0.000531	0.002272	0.000118	0.00048	0.000256						0.000468
0.00053	0.00226	0.000112	0.000478	0.000253						0.000467
0.000525	0.002252	0.000112	0.000476	0.000249						0.000443
0.000525	0.002196	0.00011	0.000468	0.000243						0.000443
0.000519	0.002195	0.00011	0.00046	0.000236						0.000426
0.000518	0.002189	0.000109	0.000455	0.000233						0.000422
0.000512	0.002146	0.000108	0.000452	0.000232						0.000415
0.000502	0.002131	0.000106	0.000445	0.000228						0.000413
0.0005	0.002125	0.000105	0.000444	0.000227						0.000403
0.000492	0.00212	0.000102	0.000442	0.000223						0.000403
0.00049	0.002107	0.000099	0.000442	0.000214						0.000396
0.000483	0.001995	0.000095	0.00044	0.000214						0.000392
0.000478	0.001969	0.000094	0.000439	0.000212						0.000385
0.000475	0.001956	0.000094	0.000429	0.00021						0.000385
0.000472	0.001877	0.000093	0.000429	0.00021						0.000382
0.00047	0.001861	0.000092	0.000429	0.000208						0.00038
0.000465	0.001859	0.000092	0.00041	0.000205						0.000377
0.000461	0.001852	0.000092	0.00041	0.000204						0.000372
0.000453	0.0018	0.000091	0.000401	0.000196						0.000369
0.000453	0.001745	0.000091	0.000399	0.000193						0.000368
0.000444	0.001727	0.000091	0.000391	0.000192						0.000362
0.000443	0.001709	0.000088	0.000389	0.000182						0.000348
0.00044	0.001708	0.000088	0.000386	0.000179						0.000342
0.000435	0.001685	0.000088	0.000385	0.000177						0.000333
0.000425	0.001674	0.000086	0.000384	0.000177						0.000316
0.000419	0.00163	0.000086	0.000383	0.000175						0.000315
0.00041	0.001613	0.000084	0.00038	0.00017						0.000298
0.000407	0.001596	0.000083	0.000373	0.000162						0.000298
0.000404	0.001595	0.000083	0.00036	0.000159						0.000283
0.000396	0.001593	0.000083	0.000353	0.000157						0.000258
0.000394	0.001585	0.000083	0.000353	0.000155						0.000257
0.000385	0.00156	0.000079	0.000352	0.000149						0.000245
0.000377	0.00156	0.000079	0.000349	0.000149						0.000242
0.000376	0.001557	0.000079	0.000344	0.000146						0.000228
0.000373	0.00153	0.000079	0.000339	0.000145						0.000214
0.000373	0.001511	0.000079	0.000337	0.000138						0.00021
0.000365	0.001491	0.000078	0.000333	0.000136						0.000199
0.000363	0.00148	0.000077	0.000332	0.000133						0.00019
0.000359	0.001443	0.000077	0.000332	0.000126						0.000186
0.000354	0.001441	0.000077	0.000332	0.000124						0.000168
0.000352	0.001437	0.000077	0.000329	0.000123						0.000165
0.000352	0.001406	0.000076	0.000329	0.000123						0.000163
0.000348	0.001406	0.000075	0.000328	0.000122						0.000162
0.000347	0.001404	0.000074	0.000322	0.000121						0.000146
0.000346	0.001395	0.000073	0.000322	0.000119						0.000143
0.000338	0.001365	0.000073	0.000319	0.000117						0.00013
0.000332	0.001354	0.000071	0.000317	0.000114						0.000125
0.000331	0.001331	0.000071	0.000313	0.000111						0.000118
0.000323	0.001324	0.00007	0.000312	0.000109						0.000108
0.000323	0.001312	0.000068	0.000309	0.000108						0.000107
0.000322	0.00131	0.000067	0.000307	0.000104						0.000107
0.000317	0.001291	0.000067	0.000307	0.000104						0.0001
0.000312	0.00127	0.000066	0.000305	0.000103						0.000092
0.000309	0.001177	0.000065	0.000303	0.000102						0.000084
0.000307	0.00117	0.000065	0.000303	0.000101						0.000083
0.000302	0.001138	0.000063	0.0003	0.0001						0.000067
0.000296	0.001137	0.000063	0.0003	0.000097						0.000048

0.000295	0.001132	0.000061	0.000296	0.000097						0.000046			
0.000294	0.001129	0.000058	0.00029	0.000096						0.000045			
0.000293	0.001112	0.000057	0.000284	0.000096						0.000044			
0.000293	0.001105	0.000057	0.000281	0.000091						0.000015			
0.000289	0.001104	0.000056	0.000281	0.00009						0.00001			
0.000288	0.001097	0.000053	0.000278	0.000088						0.00001			
0.000288	0.001093	0.00005	0.000277	0.000082						0.000009			
0.000287	0.001068	0.000049	0.000275	0.00008						0.000008			
0.000287	0.001056	0.000047	0.000273	0.000076						0.000006			
0.00028	0.001046	0.000047	0.000269	0.000073						0.000006			
0.00027	0.001029	0.000046	0.000269	0.000071						0.000004			
0.00027	0.001013	0.000046	0.000269	0.000071						0.000004			
0.000269	0.000999	0.000046	0.000259	0.000066						0.000003			
0.000264	0.000991	0.000045	0.000255	0.000065						0.000003			
0.00026	0.000953	0.000045	0.000254	0.000064						0.000003			
0.000255	0.000931	0.000045	0.000254	0.000063						0.000002			
0.000253	0.000904	0.000044	0.000254	0.000054						0.000002			
0.000252	0.00089	0.000044	0.000254	0.000049						0.000002			
0.000252	0.000889	0.000044	0.000252	0.000046						0.000002			
0.000252	0.000874	0.000043	0.000249	0.000044						0.000002			
0.000251	0.000868	0.000043	0.000249	0.000044						0.000001			
0.000249	0.000859	0.000043	0.000247	0.000043						0.000001			
0.000249	0.000811	0.000042	0.000244	0.000039						0.000001			
0.000249	0.000788	0.000041	0.000244	0.000008						0.000001			
0.000249	0.000785	0.000041	0.000243	0.000002						0.000001			
0.000248	0.000782	0.00004	0.000242	0.000002						0.000001			
0.000242	0.000777	0.00004	0.000235	7.749E-07						0.000001			
0.000241	0.000777	0.00004	0.000235							0.000001			
0.000239	0.000777	0.000039	0.000234							9.434E-07			
0.000239	0.00077	0.000039	0.000225							9.434E-07			
0.000237	0.000757	0.000038	0.00022							9.434E-07			
0.000235	0.000755	0.000036	0.000219							9.434E-07			
0.000235	0.00075	0.000036	0.000217							9.434E-07			
0.000235	0.000745	0.000036	0.000217							9.057E-07			
0.00023	0.000739	0.000035	0.000215							4.717E-07			
0.000229	0.000735	0.000035	0.000205							4.717E-07			
0.000229	0.000731	0.000035	0.000204							4.717E-07			
0.000228	0.000726	0.000034	0.000201							4.717E-07			
0.000227	0.000726	0.000034	0.000201							4.717E-07			
0.000225	0.000718	0.000032	0.000198							4.717E-07			
0.000224	0.000706	0.000032	0.000198							4.717E-07			
0.000224	0.000699	0.000031	0.000198							4.717E-07			
0.000217	0.000694	0.000031	0.000193							4.717E-07			
0.000216	0.000682	0.000031	0.000191							4.553E-07			
0.000216	0.000667	0.00003	0.000184							4.553E-07			
0.000213	0.000665	0.000029	0.000184							4.553E-07			
0.000209	0.000662	0.000028	0.000184							4.553E-07			
0.000209	0.000657	0.000027	0.00018							4.553E-07			
0.000208	0.000645	0.000026	0.000179							4.529E-07			
0.000208	0.000645	0.000025	0.000179							4.529E-07			
0.000201	0.00062	0.000025	0.000177							4.529E-07			
0.000201	0.000611	0.000023	0.000176							4.529E-07			
0.000195	0.000602	0.000022	0.000175										
0.000191	0.000602	0.00002	0.000171										
0.000191	0.000595	0.00002	0.000171										
0.000187	0.000593	0.000019	0.000171										
0.000187	0.000589	0.000018	0.000169										
0.000186	0.000587	0.000017	0.000169										
0.000186	0.000585	0.000017	0.000167										
0.000185	0.000585	0.000017	0.000166										
0.000184	0.000566	0.000017	0.000162										
0.000182	0.000561	0.000016	0.000159										
0.000179	0.000554	0.000016	0.000157										
0.000179	0.000554	0.000016	0.000156										
0.000179	0.000553	0.000016	0.000155										
0.000177	0.000541	0.000016	0.000154										
0.000175	0.000536	0.000015	0.000152										
0.000174	0.000536	0.000013	0.00015										
0.000174	0.000531	0.000013	0.000147										
0.000173	0.000529	0.000013	0.000147										
0.00017	0.000526	0.000012	0.000147										
0.000169	0.000521	0.000011	0.000145										
0.000169	0.000521	0.000011	0.000145										
0.000164	0.000521	0.000011	0.000142										
0.000161	0.00051	0.000011	0.000141										
0.00016	0.000509	0.000011	0.000141										
0.000159	0.000505	0.00001	0.000141										
0.000159	0.000503	0.00001	0.00014										
0.000159	0.000502	0.000009	0.00014										
0.000156	0.000501	0.000008	0.000139										
0.000153	0.000498	0.000008	0.000139										
0.000152	0.000489	0.000007	0.000137										
0.000152	0.000486	0.000007	0.000135										
0.00015	0.000482	0.000007	0.000132										
0.00015	0.000476	0.000007	0.000132										
0.000149	0.000474	0.000003	0.000131										
0.000146	0.000465	9.504E-07	0.00013										
0.000145	0.000463	9.504E-07	0.00013										
0.000142	0.000463	6.336E-07	0.00013										
0.000142	0.00046	3.168E-07	0.000129										
0.000139	0.00046	3.168E-07	0.000128										
0.000138	0.000459	3.168E-07	0.000126										
0.000137	0.000459	3.168E-07	0.000125										
0.000137	0.000453	3.168E-07	0.000124										
0.000136	0.000451	3.168E-07	0.000123										
0.000135	0.000447	3.168E-07	0.000123										
0.000135	0.000432	3.168E-07	0.000123										
0.000132	0.00043	3.168E-07	0.00012										
0.00013	0.000429	3.534106	0.000118										
0.000129	0.000429	1.896705	0.000118										
0.000128	0.000429	1.033169	0.000114										
0.000128	0.000427	0.468747	0.000113										
0.000128	0.000425	0.153786	0.000111										
0.000126	0.000422	0.123708	0.00011										
0.000122	0.000418	0.118964	0.00011										
0.000121	0.000415	0.115988	0.000109										
0.000121	0.00041	0.108903	0.000108										
0.000117	0.000402	0.108259	0.000108										
0.000115	0.000402	0.090401	0.000108										
0.000115	0.000393	0.08191	0.000107										
0.000114	0.000392	0.081446	0.000106										
0.000114	0.00039	0.080571	0.000105										
0.000114	0.000385	0.079532	0.000101										
0.000113	0.000383	0.079115	0.0001										

0.000112	0.00038	0.074167	0.0001
0.000112	0.000377	0.071039	0.000099
0.000111	0.000368	0.067329	0.000096
0.000109	0.000366	0.06481	0.000094
0.000108	0.000364	0.062479	0.000091
0.000107	0.000349	0.054478	0.000091
0.000105	0.000344	0.05254	0.000089
0.000104	0.000344	0.051337	0.000089
0.000104	0.000342	0.050947	0.000086
0.000103	0.000339	0.050055	0.000086
0.000103	0.000337	0.045532	0.000084
0.000103	0.000337	0.042575	0.000084
0.000103	0.000336	0.04115	0.000084
0.000103	0.000335	0.040366	0.000081
0.000101	0.000335	0.040225	0.000079
0.000101	0.000333	0.039119	0.000079
0.000098	0.000333	0.038855	0.000078
0.000098	0.000332	0.038752	0.000077
0.000098	0.000332	0.038549	0.000077
0.000097	0.000332	0.03754	0.000074
0.000095	0.000327	0.036948	0.000074
0.000094	0.000322	0.035642	0.000074
0.000093	0.00032	0.035373	0.000074
0.000092	0.00032	0.034109	0.00007
0.00009	0.00032	0.033191	0.000069
0.000088	0.000316	0.033012	0.000069
0.000084	0.000316	0.03286	0.000065
0.000081	0.000305	0.032219	0.000064
0.000081	0.000305	0.031833	0.000062
0.00008	0.000305	0.031726	0.000062
0.000079	0.000299	0.030214	0.00006
0.000079	0.000298	0.03003	0.00006
0.000076	0.000298	0.029935	0.000058
0.000075	0.000296	0.029862	0.000055
0.000075	0.000295	0.029534	0.000054
0.000074	0.000295	0.029383	0.000044
0.000074	0.000293	0.028513	0.000035
0.000074	0.000288	0.028512	0.000033
0.000072	0.000286	0.027632	0.000028
0.000071	0.000283	0.026567	0.000026
0.00007	0.000276	0.026191	0.000018
0.000068	0.000273	0.026138	0.000005
0.000068	0.000271	0.025921	0.000004
0.000067	0.000269	0.025662	0.000004
0.000067	0.000266	0.024651	0.000002
0.000067	0.000266	0.022988	0.000002
0.000066	0.000252	0.022497	0.000002
0.000065	0.000251	0.02202	0.000002
0.000065	0.000248	0.021904	0.000001
0.000064	0.000245	0.021262	0.000001
0.000063	0.000244	0.021065	0.000001
0.000063	0.000243	0.020613	0.000001
0.000063	0.00024	0.019473	0.000001
0.000061	0.000239	0.019342	0.000001
0.000058	0.000237	0.018951	0.000001
0.000058	0.000233	0.01893	7.085E-07
0.000057	0.000232	0.018762	7.085E-07
0.000056	0.000231	0.018667	7.085E-07
0.000055	0.000229	0.018474	7.085E-07
0.000055	0.000224	0.018202	7.085E-07
0.000055	0.000222	0.017709	7.085E-07
0.000055	0.00022	0.017239	7.085E-07
0.000055	0.000213	0.017212	7.085E-07
0.000052	0.00021	0.016944	7.085E-07
0.000052	0.00021	0.016829	7.085E-07
0.00005	0.000208	0.0167	7.085E-07
0.00005	0.000203	0.016554	7.085E-07
0.00005	0.0002	0.01609	
0.000049	0.000198	0.015663	
0.000049	0.000196	0.015624	
0.000047	0.000193	0.015605	
0.000047	0.000193	0.015268	
0.000046	0.000191	0.015108	
0.000045	0.000191	0.014799	
0.000045	0.000191	0.014646	
0.000042	0.000185	0.014251	
0.000042	0.000184	0.014191	
0.00004	0.000181	0.01393	
0.000037	0.000179	0.013424	
0.000037	0.000177	0.013393	
0.000035	0.000174	0.013354	
0.000033	0.000169	0.012777	
0.000033	0.000165	0.012712	
0.000031	0.000163	0.012385	
0.000028	0.000162	0.012246	
0.000027	0.00016	0.012232	
0.000023	0.000145	0.012124	
0.000018	0.000141	0.012047	
0.000018	0.00014	0.011844	
0.000017	0.00014	0.011785	
0.000014	0.000138	0.011751	
0.000013	0.000137	0.01175	
0.000013	0.000136	0.011598	
0.000009	0.000136	0.011101	
0.000006	0.00013	0.011051	
0.000006	0.000129	0.010903	
0.000004	0.000125	0.010869	
0.000003	0.000118	0.010805	
0.000001	0.000111	0.010704	
0.000001	0.000106	0.01065	
0.000001	0.000101	0.010643	
7.085E-07	0.000094	0.010628	
7.085E-07	0.000093	0.010621	
7.085E-07	0.000085	0.010412	
7.085E-07	0.000084	0.010331	
7.085E-07	0.000082	0.010311	
7.085E-07	0.000072	0.010128	
7.085E-07	0.000036	0.010069	
	0.000036	0.00987	
	0.000034	0.009842	
	0.000025	0.009832	
	0.000022	0.009803	
	0.000009	0.009764	
	0.000009	0.009434	

	0.000006	0.009417												
	0.000004	0.009342												
	0.000004	0.009144												
	0.000004	0.009137												
	0.000002	0.009011												
	0.000002	0.008809												
	0.000002	0.008745												
	0.000002	0.008672												
	0.000002	0.008567												
	0.000002	0.008503												
	0.000002	0.008475												
	0.000001	0.008446												
	0.000001	0.008393												
	0.000001	0.008181												
	0.000001	0.008077												
	0.000001	0.007929												
	0.000001	0.007755												
	0.000001	0.007718												
	7.085E-07	0.007718												
	7.085E-07	0.007635												
	7.085E-07	0.00763												
	7.085E-07	0.007603												
	7.085E-07	0.007586												
	7.085E-07	0.007548												
	7.085E-07	0.007544												
	7.085E-07	0.007541												
	7.085E-07	0.007367												
	7.085E-07	0.007353												
	7.085E-07	0.007307												
		0.007285												
		0.007282												
		0.007268												
		0.007235												
		0.00723												
		0.007228												
		0.007197												
		0.007176												
		0.007135												
		0.007046												
		0.006981												
		0.00696												
		0.006909												
		0.00681												
		0.006788												
		0.006755												
		0.006753												
		0.006601												
		0.006543												
		0.006533												
		0.006489												
		0.006462												
		0.006319												
		0.006247												
		0.00622												
		0.006178												
		0.006132												
		0.006014												
		0.006011												
		0.006009												
		0.005993												
		0.005828												
		0.00575												
		0.005725												
		0.005631												
		0.005456												
		0.005438												
		0.005429												
		0.005379												
		0.005368												
		0.005318												
		0.005182												
		0.005149												
		0.005023												
		0.00498												
		0.004962												
		0.004947												
		0.004947												
		0.004862												
		0.004832												
		0.00474												
		0.004718												
		0.004689												
		0.004621												
		0.004604												
		0.004568												
		0.004552												
		0.004545												
		0.004523												
		0.004498												
		0.004474												
		0.004406												
		0.0044												
		0.004389												
		0.004348												
		0.004325												
		0.00431												
		0.004308												
		0.004299												
		0.004279												
		0.004208												
		0.004206												
		0.004108												
		0.003992												
		0.003957												
		0.003945												
		0.003931												
		0.003918												
		0.003905												
		0.003891												
		0.003849												
		0.003814												
		0.003794												
		0.003757												
		0.003697												

0.00368
0.003664
0.003636
0.003624
0.00358
0.00356
0.00353
0.003526
0.003521
0.003504
0.003459
0.003441
0.00329
0.00327
0.003236
0.003234
0.00323
0.003171
0.003151
0.003144
0.00312
0.00312
0.003082
0.003069
0.003006
0.002992
0.00297
0.002953
0.002952
0.002927
0.002903
0.002871
0.002863
0.002833
0.002829
0.002825
0.002821
0.002792
0.002774
0.00277
0.002755
0.002728
0.002726
0.002708
0.002705
0.00269
0.002675
0.002668
0.002664
0.002659
0.002623
0.002574
0.002569
0.002556
0.002531
0.002502
0.002465
0.002443
0.002439
0.002412
0.002407
0.00236
0.00236
0.002324
0.002308
0.002294
0.002278
0.002278
0.002273
0.002271
0.002246
0.002191
0.002181
0.00217
0.002169
0.002168
0.00216
0.002156
0.002143
0.002137
0.002129
0.002122
0.002089
0.002061
0.002052
0.00204
0.00203
0.002025
0.002023
0.00201
0.001998
0.001957
0.001957
0.001939
0.001932
0.001931
0.00193
0.00192
0.001919
0.001912
0.001907
0.001897
0.001887
0.001875
0.001846
0.001814
0.001809
0.001798
0.001769
0.001767
0.001761
0.001757
0.001755
0.001749

		0.001745												
		0.001714												
		0.001707												
		0.001701												
		0.001694												
		0.001681												
		0.00167												
		0.001662												
		0.001656												
		0.001649												
		0.001642												
		0.001639												
		0.001634												
		0.001632												
		0.00162												
		0.001614												
		0.001608												
		0.001597												
		0.001595												
		0.001593												
		0.001585												
		0.00155												
		0.001546												
		0.001531												
		0.001515												
		0.001514												
		0.001512												
		0.001495												
		0.001489												
		0.001472												
		0.001471												
		0.001471												
		0.001443												
		0.001436												
		0.00143												
		0.00142												
		0.001418												
		0.001415												
		0.001415												
		0.00141												
		0.001406												
		0.001405												
		0.001405												
		0.001384												
		0.001379												
		0.001375												
		0.001371												
		0.001365												
		0.001362												
		0.001362												
		0.001359												
		0.001348												
		0.00134												
		0.001339												
		0.001325												
		0.001315												
		0.001311												
		0.0013												
		0.001296												
		0.001289												
		0.001287												
		0.001286												
		0.001281												
		0.00127												
		0.001265												
		0.001264												
		0.001254												
		0.001237												
		0.001233												
		0.001224												
		0.001219												
		0.001218												
		0.00121												
		0.001205												
		0.001185												
		0.001184												
		0.001177												
		0.001173												
		0.001168												
		0.001157												
		0.001149												
		0.001144												
		0.001144												
		0.001131												
		0.001127												
		0.001121												
		0.00112												
		0.001119												
		0.001118												
		0.001114												
		0.001102												
		0.001097												
		0.001093												
		0.001082												
		0.001077												
		0.001076												
		0.001073												
		0.00107												
		0.001064												
		0.001028												
		0.001014												
		0.001004												
		0.001002												
		0.001												
		0.000998												
		0.000995												
		0.000987												
		0.000987												
		0.000987												
		0.000985												
		0.000981												
		0.000975												
		0.000971												
		0.000969												

		0.000956											
		0.000952											
		0.00095											
		0.000941											
		0.000939											
		0.000935											
		0.000934											
		0.000928											
		0.000925											
		0.000915											
		0.000907											
		0.000907											
		0.000906											
		0.000899											
		0.000879											
		0.000877											
		0.000875											
		0.000873											
		0.000873											
		0.00087											
		0.000868											
		0.000862											
		0.000861											
		0.000857											
		0.000854											
		0.000851											
		0.000849											
		0.000846											
		0.000845											
		0.000841											
		0.000839											
		0.000834											
		0.000828											
		0.000828											
		0.00081											
		0.000798											
		0.000792											
		0.000791											
		0.000791											
		0.000787											
		0.000785											
		0.000782											
		0.000776											
		0.000776											
		0.000775											
		0.000765											
		0.000765											
		0.000763											
		0.000762											
		0.00076											
		0.000755											
		0.000753											
		0.000749											
		0.000741											
		0.00074											
		0.000735											
		0.000706											
		0.000706											
		0.000704											
		0.000704											
		0.000699											
		0.000695											
		0.000693											
		0.000692											
		0.000692											
		0.000691											
		0.000682											
		0.000681											
		0.000681											
		0.000678											
		0.000676											
		0.000671											
		0.000669											
		0.000667											
		0.00066											
		0.000649											
		0.000641											
		0.000634											
		0.000623											
		0.000616											
		0.000613											
		0.00061											
		0.000599											
		0.00059											
		0.000577											
		0.000573											
		0.00057											
		0.000569											
		0.000567											
		0.000566											
		0.00056											
		0.000558											
		0.000555											
		0.000549											
		0.000548											
		0.000547											
		0.000542											
		0.000542											
		0.00054											
		0.000538											
		0.000536											
		0.000533											
		0.000528											
		0.000526											
		0.000523											
		0.000522											
		0.000517											
		0.000515											
		0.000506											
		0.000504											
		0.000503											
		0.000496											
		0.000495											
		0.000494											

		0.00049
		0.000474
		0.000467
		0.000466
		0.000461
		0.000458
		0.000458
		0.000454
		0.000453
		0.000453
		0.000452
		0.00045
		0.000448
		0.000445
		0.000444
		0.000442
		0.000438
		0.000438
		0.000437
		0.000435
		0.000433
		0.000431
		0.000427
		0.000424
		0.000419
		0.000419
		0.000415
		0.000414
		0.000412
		0.000411
		0.000411
		0.00041
		0.00041
		0.000408
		0.000407
		0.000406
		0.000405
		0.000402
		0.000401
		0.000401
		0.000399
		0.000399
		0.000398
		0.000397
		0.000394
		0.00038
		0.000379
		0.000377
		0.000376
		0.000375
		0.000372
		0.000369
		0.000367
		0.000362
		0.000361
		0.000358
		0.000351
		0.000347
		0.000341
		0.000339
		0.00033
		0.00033
		0.000329
		0.000329
		0.000328
		0.000326
		0.000321
		0.00032
		0.000318
		0.000314
		0.000314
		0.000314
		0.000313
		0.000311
		0.000303
		0.000303
		0.000301
		0.000297
		0.000294
		0.000294
		0.000293
		0.000291
		0.000291
		0.000286
		0.000285
		0.000283
		0.000279
		0.000279
		0.000279
		0.000276
		0.000276
		0.000274
		0.000274
		0.000273
		0.000271
		0.000271
		0.000269
		0.000266
		0.000265
		0.000265
		0.000262
		0.00026
		0.00026
		0.000259
		0.000259
		0.000258
		0.000254
		0.000252
		0.000252
		0.000248
		0.000247
		0.000247
		0.000246
		0.00024

		0.00024
		0.000236
		0.000234
		0.000234
		0.000234
		0.000227
		0.000226
		0.000224
		0.000224
		0.000223
		0.000221
		0.00022
		0.00022
		0.000217
		0.000217
		0.000216
		0.000215
		0.000214
		0.000214
		0.000209
		0.000208
		0.000206
		0.000205
		0.000202
		0.000202
		0.000201
		0.000198
		0.000195
		0.000194
		0.000193
		0.000193
		0.000193
		0.000192
		0.000191
		0.000187
		0.000187
		0.000186
		0.000185
		0.000183
		0.000182
		0.000181
		0.000181
		0.000178
		0.000176
		0.000176
		0.000176
		0.000172
		0.00017
		0.00017
		0.000169
		0.000167
		0.000166
		0.000166
		0.000165
		0.000165
		0.000164
		0.000163
		0.000162
		0.00016
		0.00016
		0.000158
		0.000158
		0.000158
		0.000158
		0.000156
		0.000156
		0.000156
		0.000155
		0.000153
		0.00015
		0.00015
		0.000147
		0.000147
		0.000147
		0.000144
		0.000144
		0.000143
		0.000143
		0.000143
		0.000142
		0.000141
		0.000141
		0.000136
		0.000132
		0.000129
		0.000128
		0.000126
		0.000126
		0.000126
		0.000123
		0.000122
		0.000122
		0.000121
		0.000116
		0.000116
		0.000115
		0.000115
		0.000115
		0.000114
		0.000112
		0.000112
		0.000111
		0.00011
		0.000109
		0.000108
		0.000106
		0.000105
		0.000104
		0.000104
		0.000102
		0.000101
		0.0001
		0.0001
		0.0001

0.0001
0.000099
0.000099
0.000098
0.000097
0.000097
0.000096
0.000095
0.000095
0.000093
0.000093
0.000093
0.000092
0.000092
0.000091
0.000091
0.000089
0.000085
0.000082
0.000082
0.000081
0.000081
0.000079
0.000079
0.000078
0.000073
0.000073
0.000071
0.000071
0.000071
0.00007
0.000069
0.000069
0.000067
0.000067
0.000067
0.000067
0.000066
0.000065
0.000065
0.000065
0.000064
0.000063
0.000062
0.000062
0.000062
0.000061
0.00006
0.000059
0.000058
0.000057
0.000057
0.000057
0.000056
0.000056
0.000055
0.000053
0.000052
0.000051
0.000051
0.00005
0.000049
0.000048
0.000048
0.000047
0.000045
0.000045
0.000045
0.000045
0.000044
0.000044
0.000044
0.000044
0.000044
0.000043
0.000043
0.000043
0.000042
0.00004
0.00004
0.00004
0.000039
0.000039
0.000038
0.000037
0.000037
0.000036
0.000036
0.000036
0.000035
0.000035
0.000035
0.000035
0.000034
0.000034
0.000033
0.000033
0.000033
0.000033
0.000033
0.000033
0.000032
0.000031
0.000031
0.000031
0.000031
0.000031
0.000031
0.00003
0.00003
0.00003
0.000029
0.000029
0.000029

		0.000029											
		0.000029											
		0.000028											
		0.000028											
		0.000028											
		0.000027											
		0.000027											
		0.000027											
		0.000027											
		0.000027											
		0.000026											
		0.000026											
		0.000025											
		0.000025											
		0.000024											
		0.000024											
		0.000023											
		0.000023											
		0.000022											
		0.000022											
		0.000021											
		0.000021											
		0.000021											
		0.00002											
		0.00002											
		0.00002											
		0.00002											
		0.00002											
		0.00002											
		0.00002											
		0.00002											
		0.000019											
		0.000019											
		0.000018											
		0.000018											
		0.000018											
		0.000018											
		0.000017											
		0.000017											
		0.000017											
		0.000017											
		0.000017											
		0.000017											
		0.000016											
		0.000016											
		0.000016											
		0.000015											
		0.000015											
		0.000015											
		0.000014											
		0.000014											
		0.000014											
		0.000014											
		0.000014											
		0.000013											
		0.000013											
		0.000012											
		0.000012											
		0.000011											
		0.000011											
		0.000011											
		0.000011											
		0.00001											
		0.000009											
		0.000009											
		0.000008											
		0.000008											
		0.000008											
		0.000008											
		0.000007											
		0.000007											
		0.000006											
		0.000006											
		0.000005											
		0.000005											
		0.000004											
		0.000003											
		0.000002											
		0.000002											
		0.000002											
		0.000001											
		9.504E-07											
		9.504E-07											
		6.336E-07											
		6.336E-07											
		6.336E-07											
		3.168E-07											
		3.168E-07											
		3.168E-07											
		3.168E-07											

Appendix E

Binary images from Chapter 5

This appendix contains the manually traced fluid areas from images taken during the exchange flow experiments (Chapter 5). In all cases the upwelling low viscosity, low density fluid is traced in black. Traces are all above the initial interface line marked at t_0 and are within the viewing window.

280616a (cPGS-air):

28.96 s into the experiment:

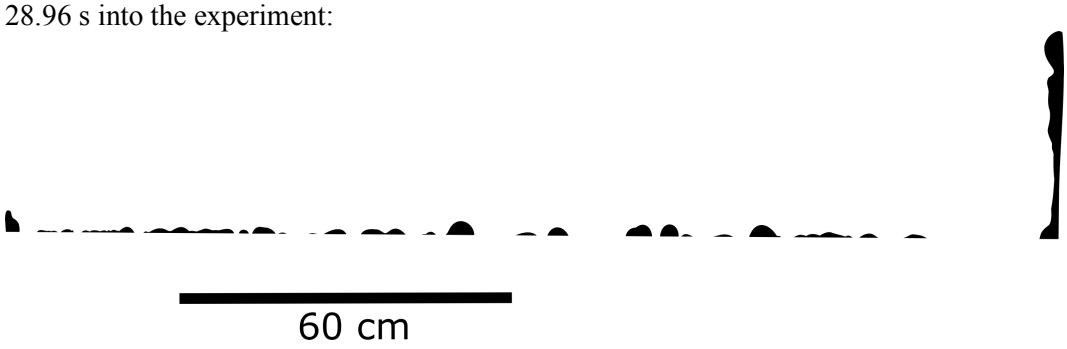

30.97 s into the experiment:

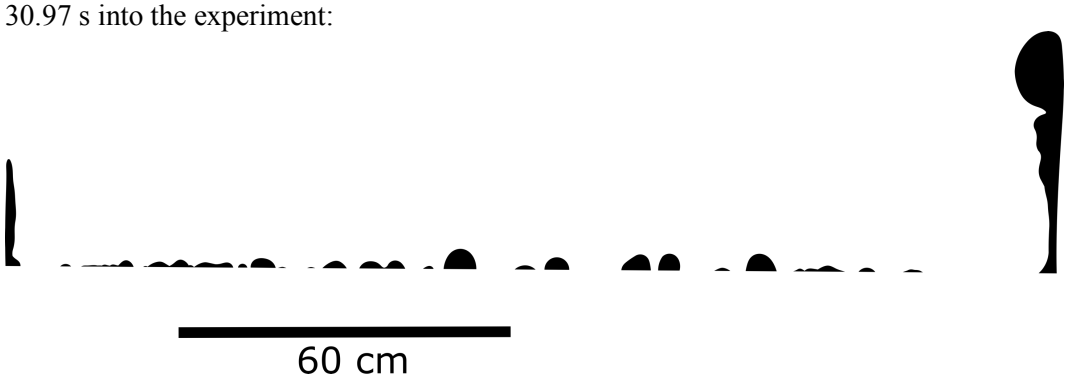

34.34 s into the experiment:

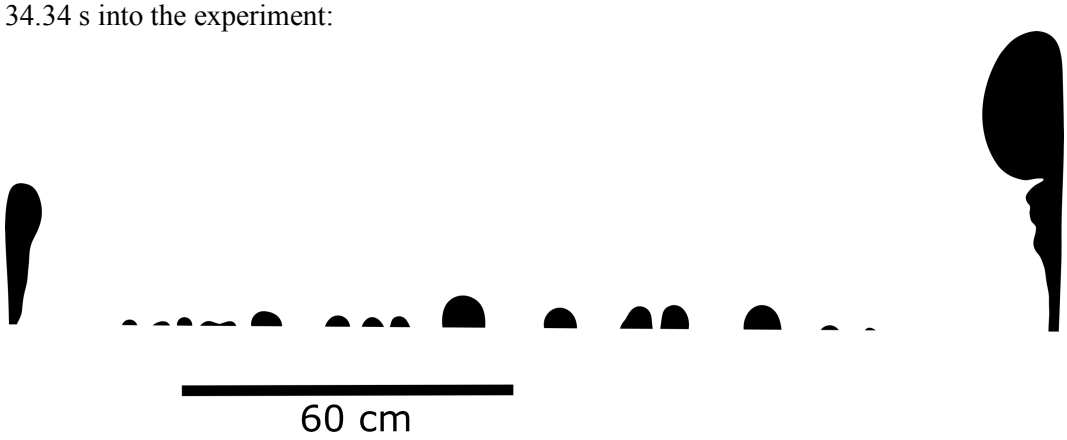

47.98 s into the experiment:

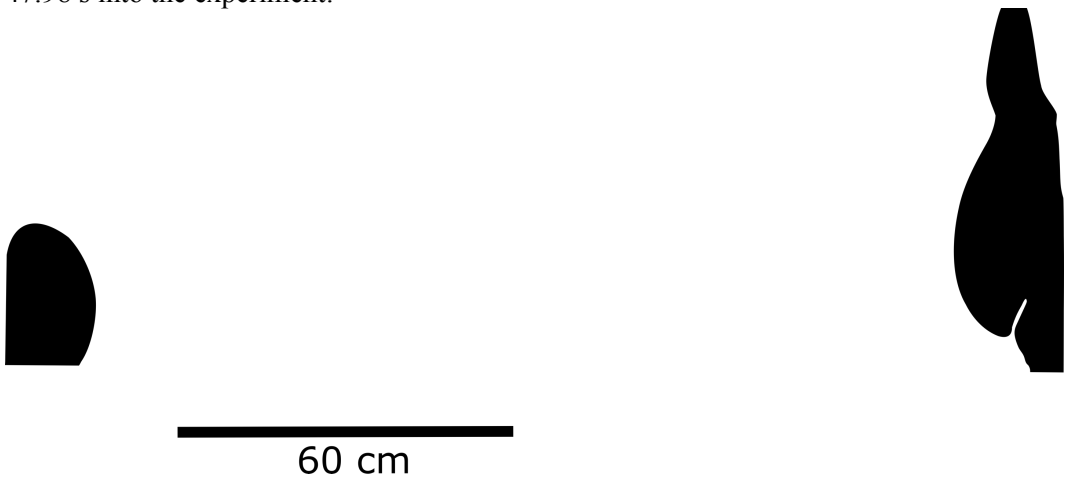

62.99 s into the experiment:

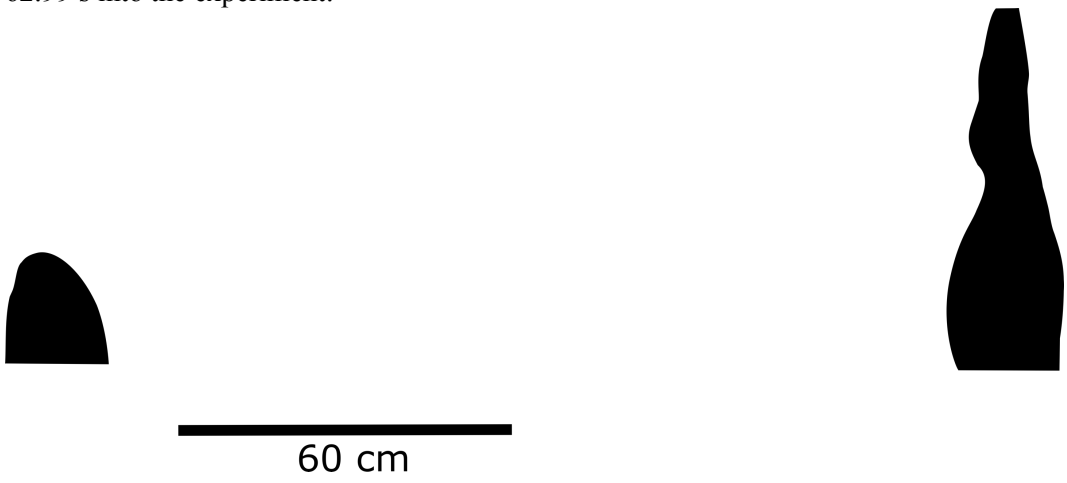

77.95 s into the experiment:

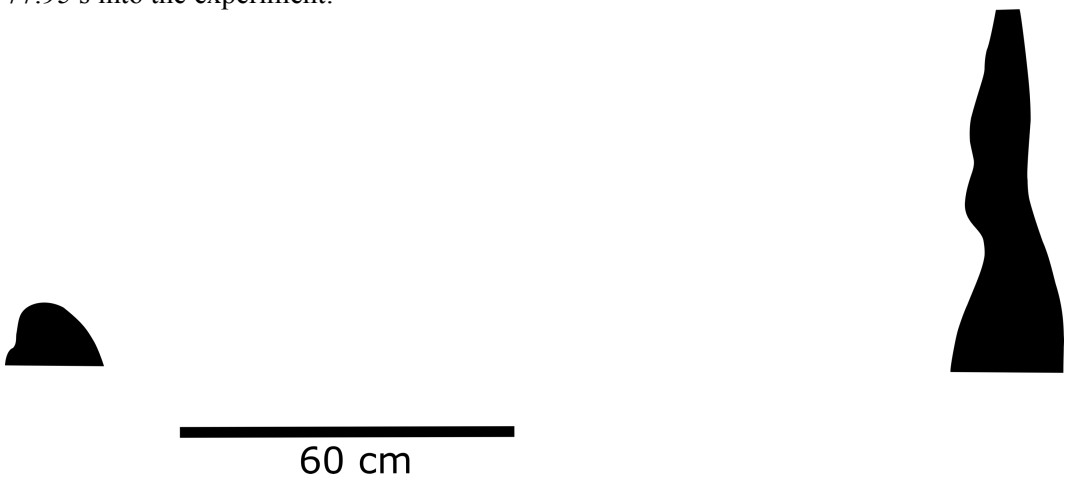

93.04 s into the experiment:

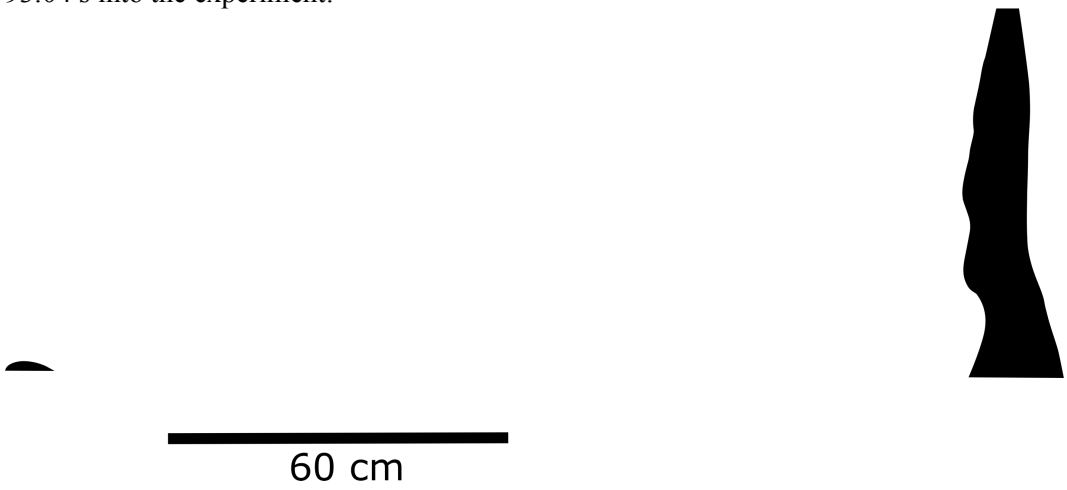

107.97 s into the experiment:

280616b (cPGS-air):

27.08 s into the experiment:

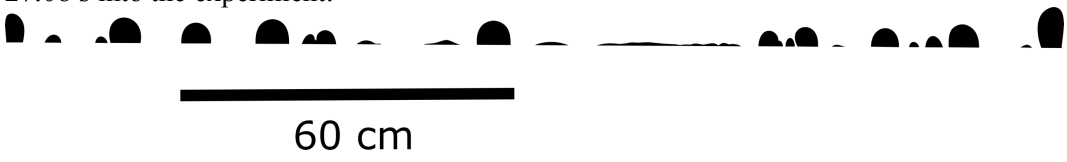

34.78 s into the experiment:

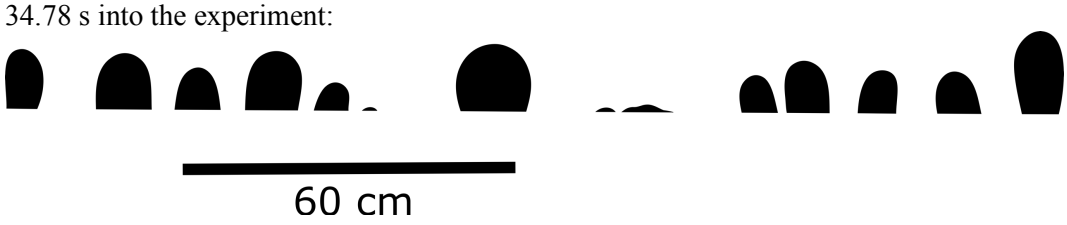

44.81 s into the experiment:

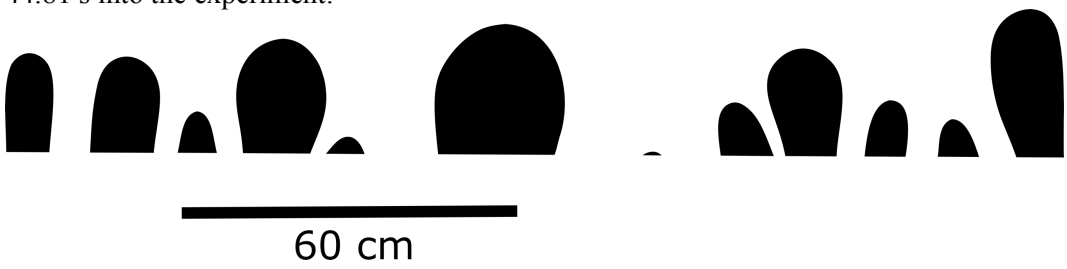

54.68 s into the experiment:

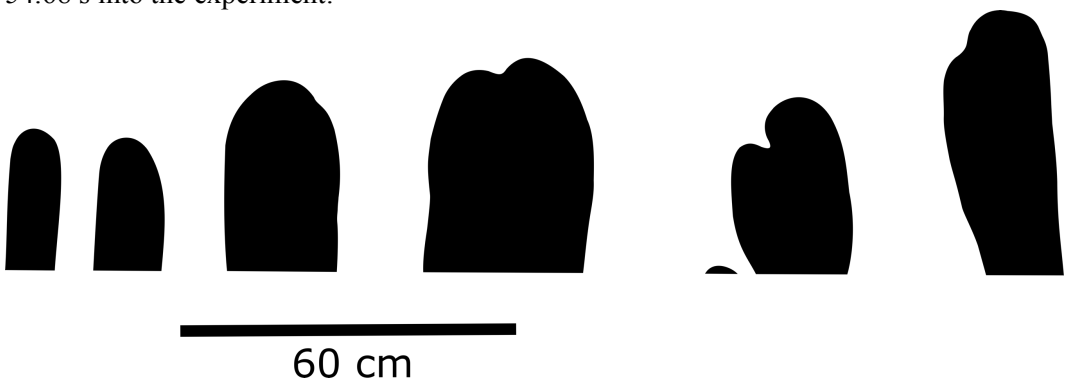

60.73 s into the experiment:

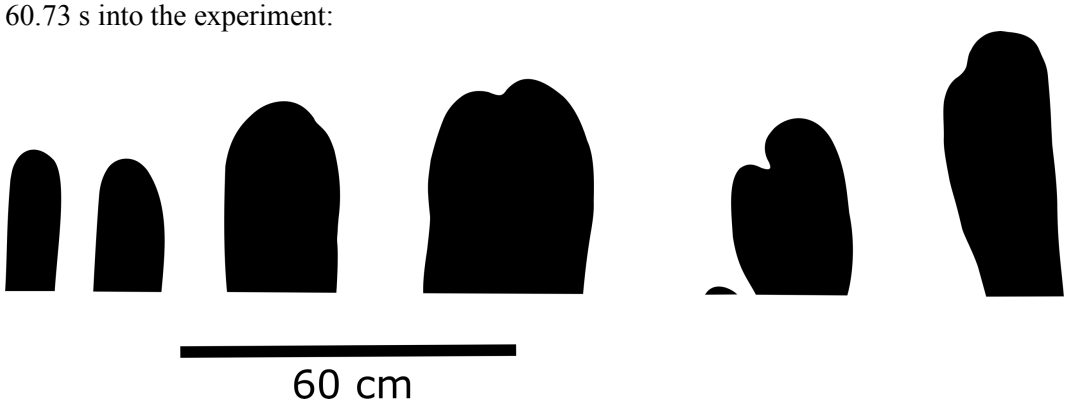

65.04 s into the experiment:

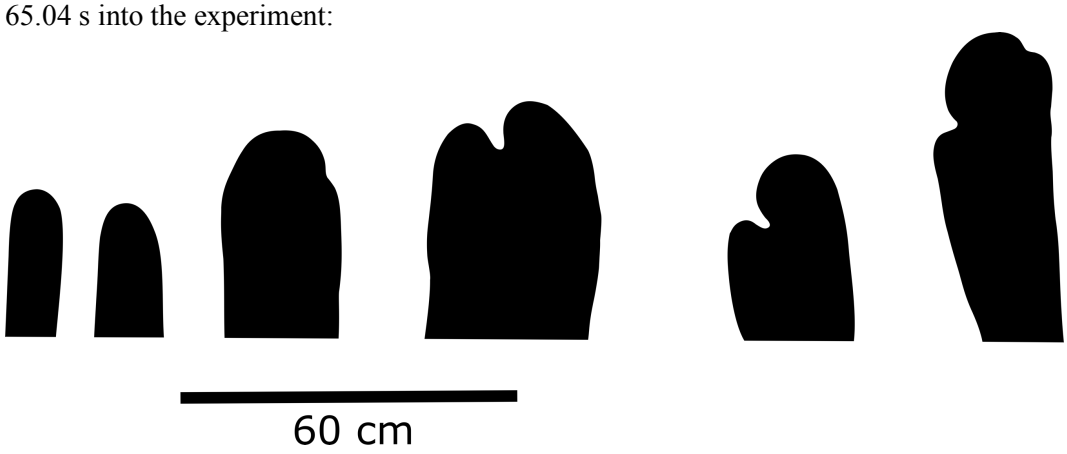

80.02 s into the experiment:

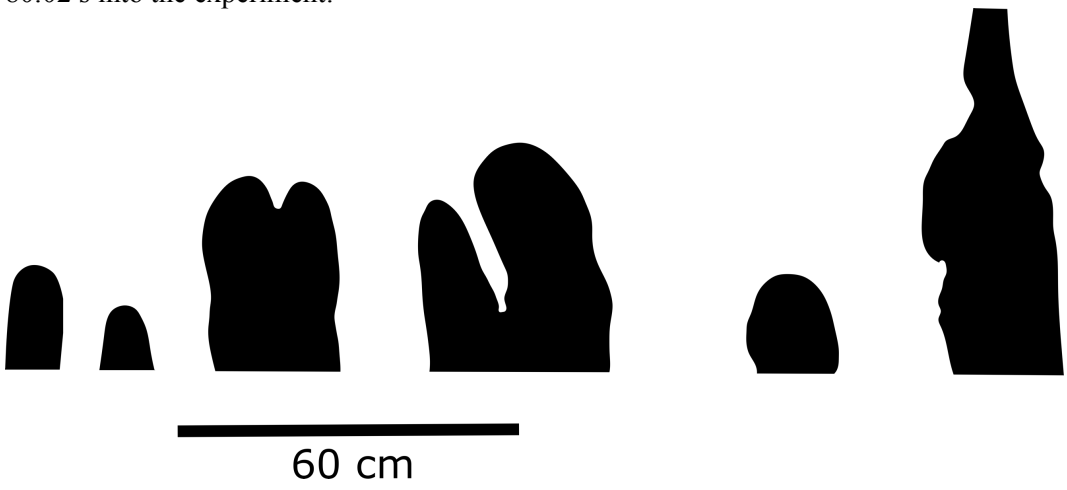

94.06 s into the experiment:

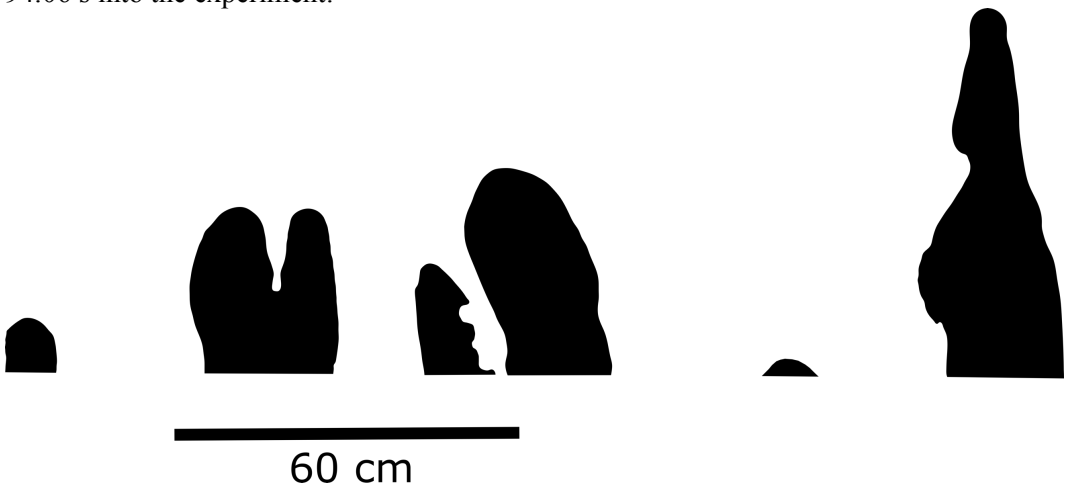

108.8 s into the experiment:

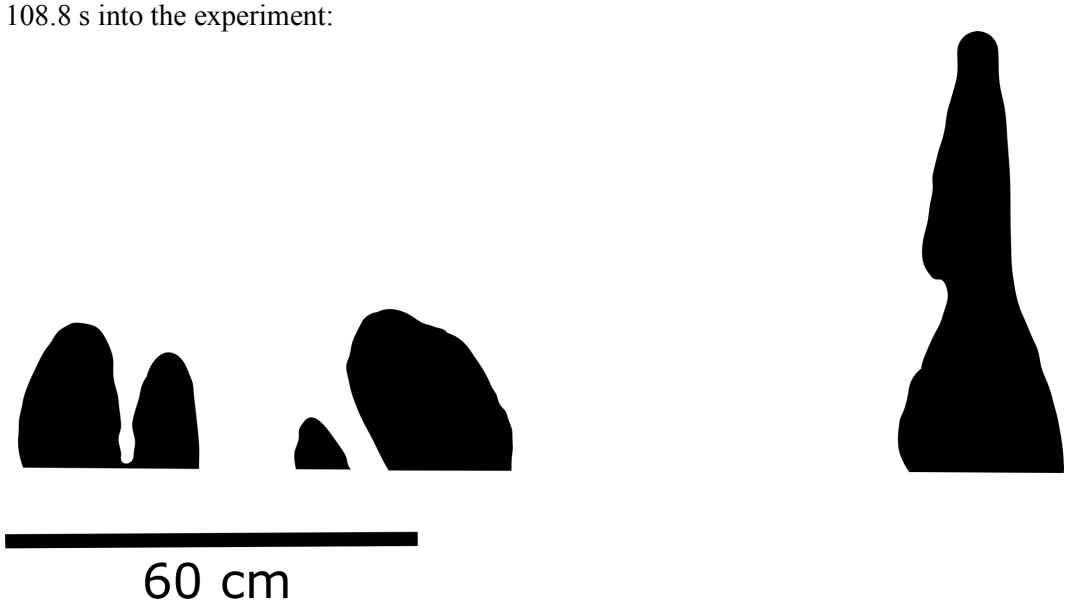

119.06 s into the experiment:

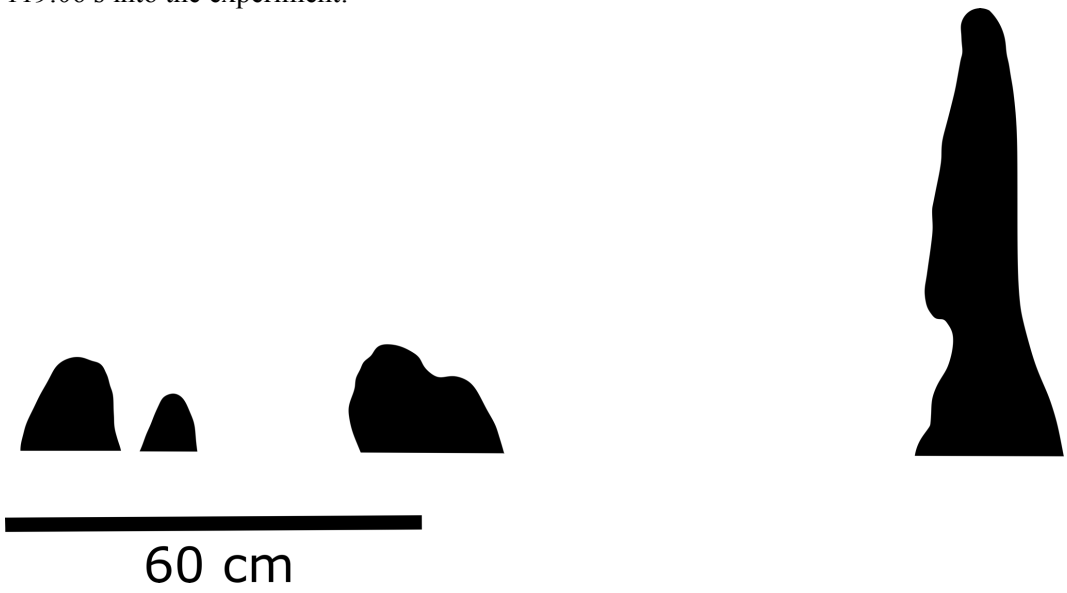

130.68 s into the experiment:

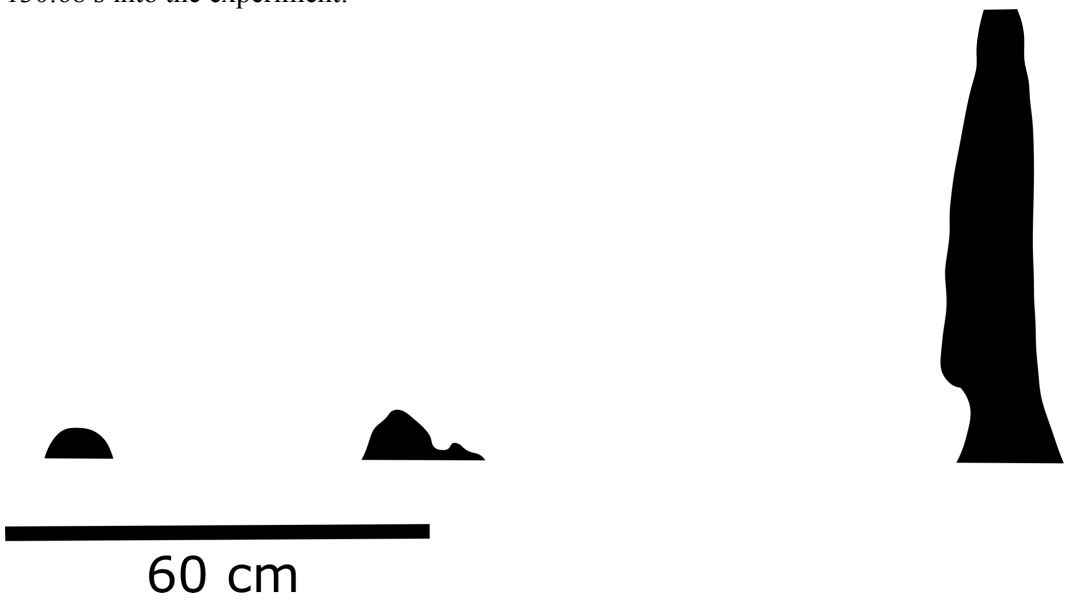

<u>280616c (cPGS-air):</u>

36.71 s into the experiment:

41.41 s into the experiment:

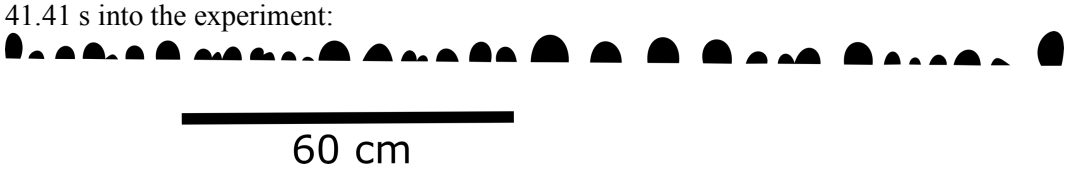

44.41 s into the experiment:

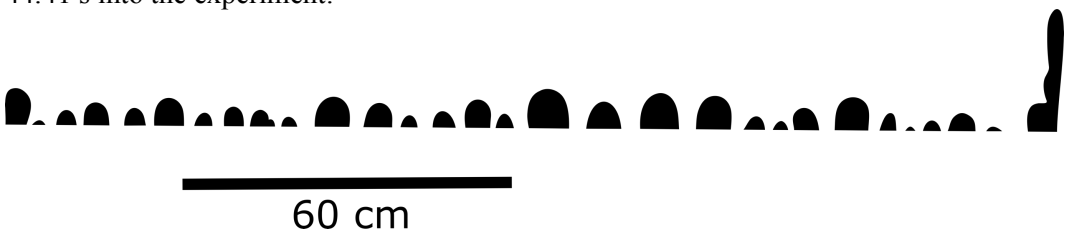

49.42 s into the experiment:

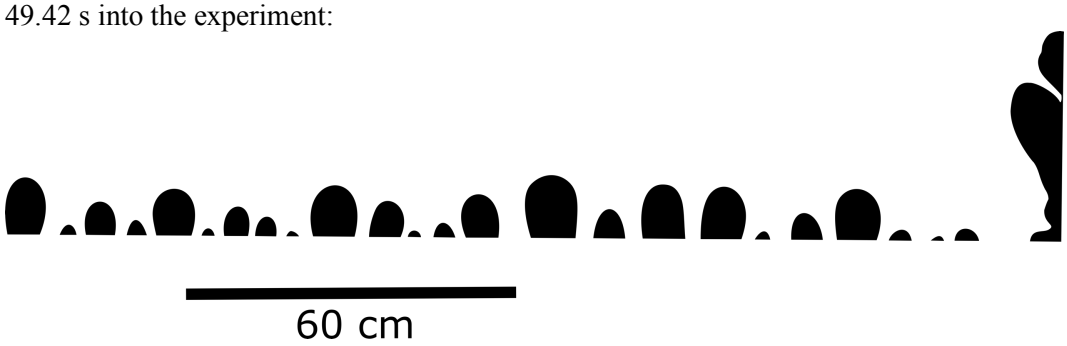

57.77 s into the experiment:

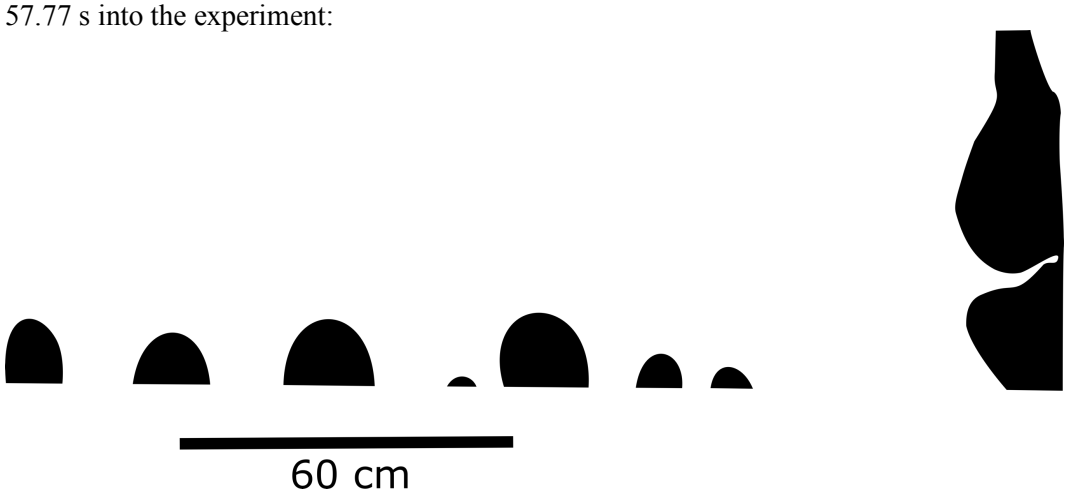

010716a (PGS-air):

9.00 s into the experiment:

13.67 s into the experiment:

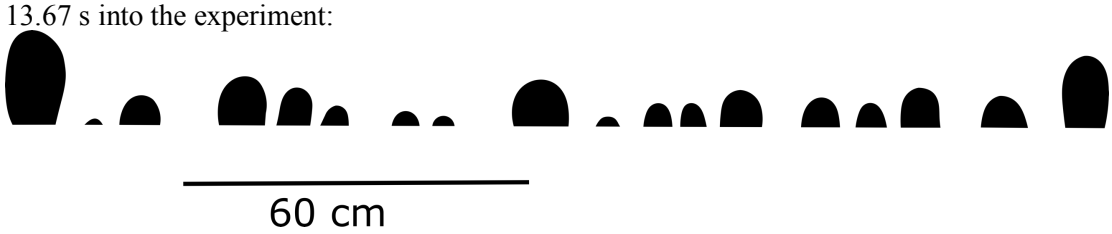

21.00 s into the experiment:

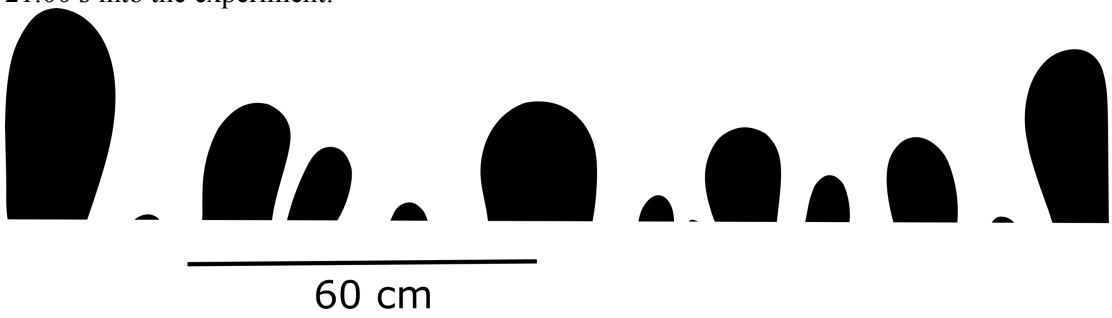

24.71 s into the experiment:

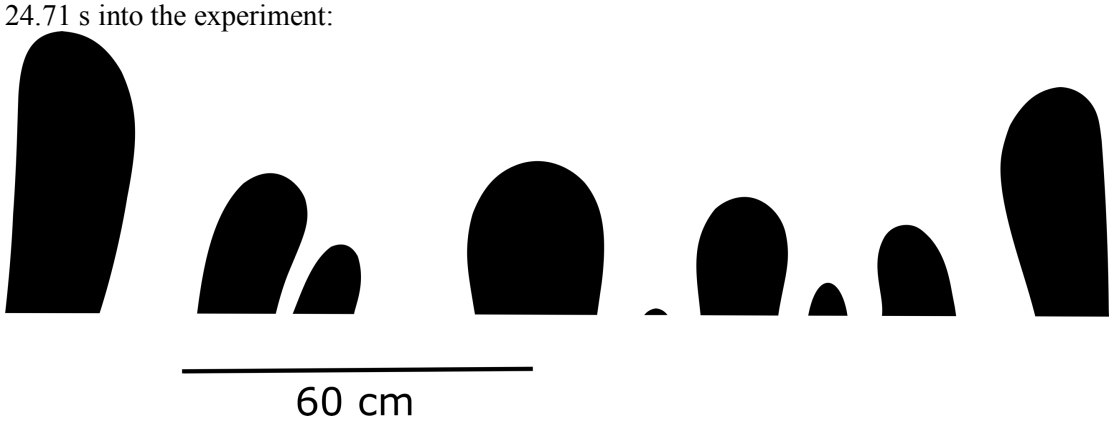

28.03 s into the experiment:

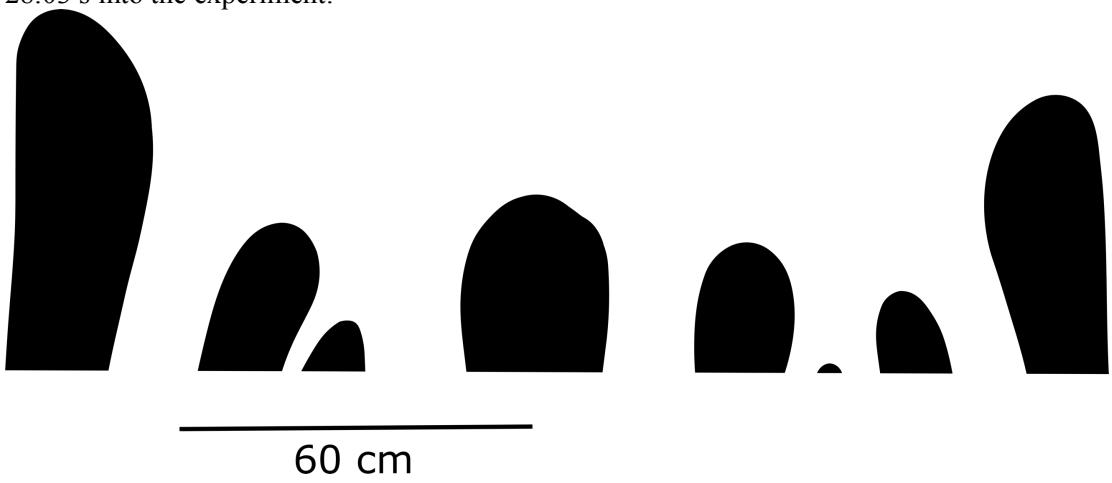

43.73 s into the experiment:

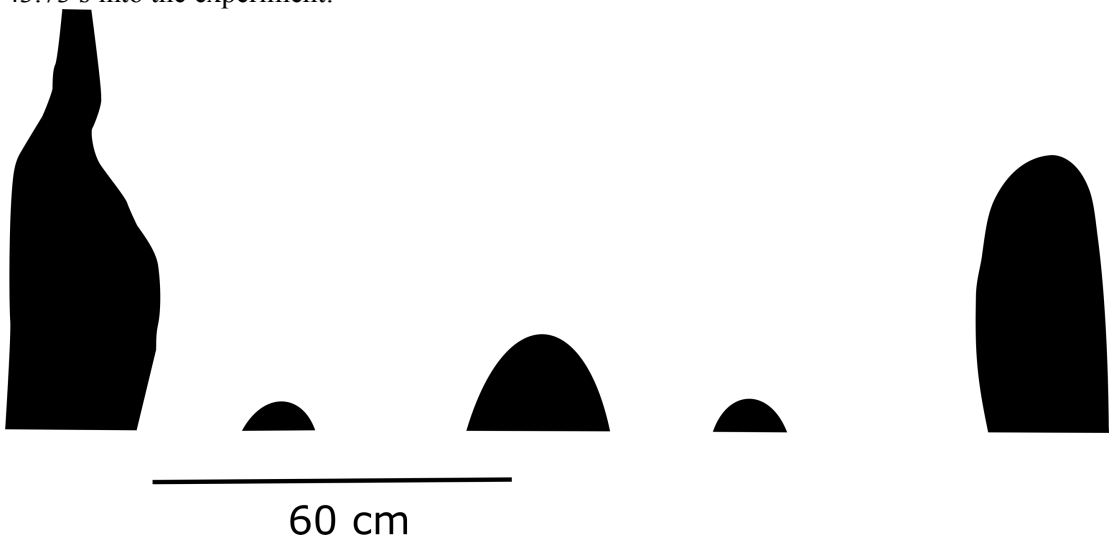

53.69 s into the experiment:

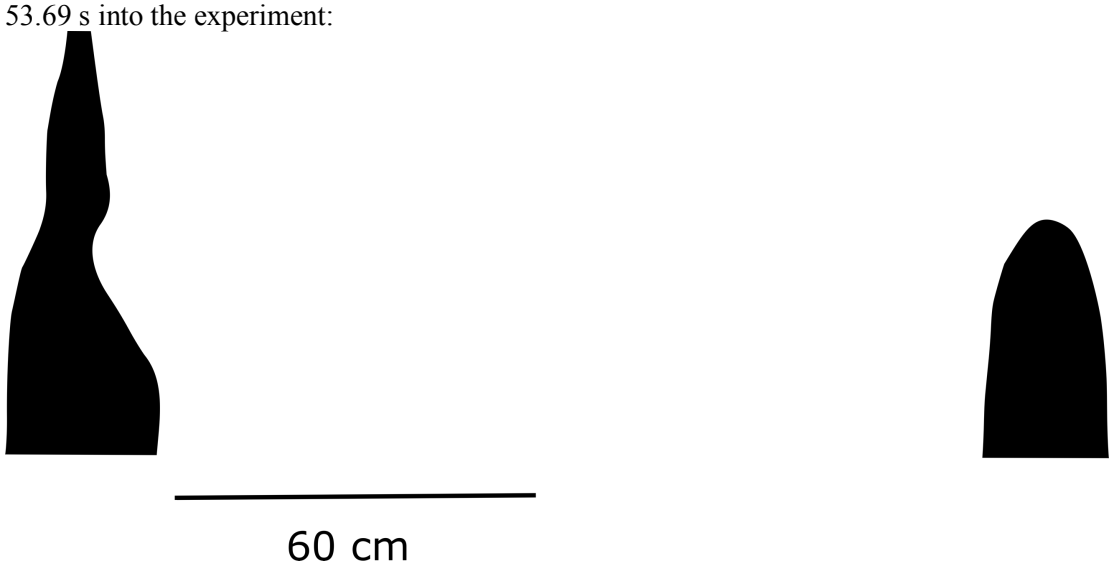

62.07 s into the experiment:

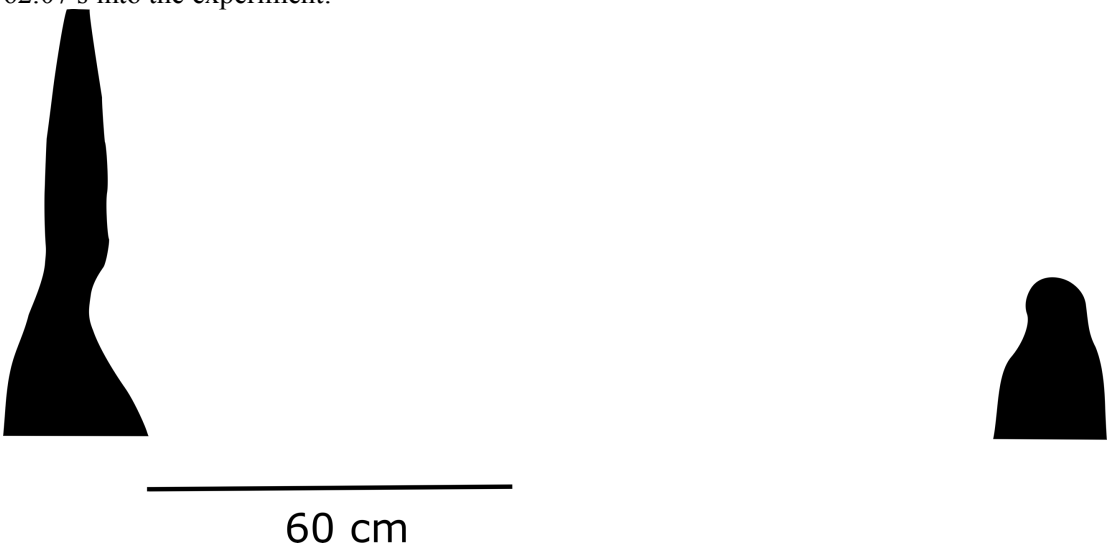

70.74 s into the experiment:

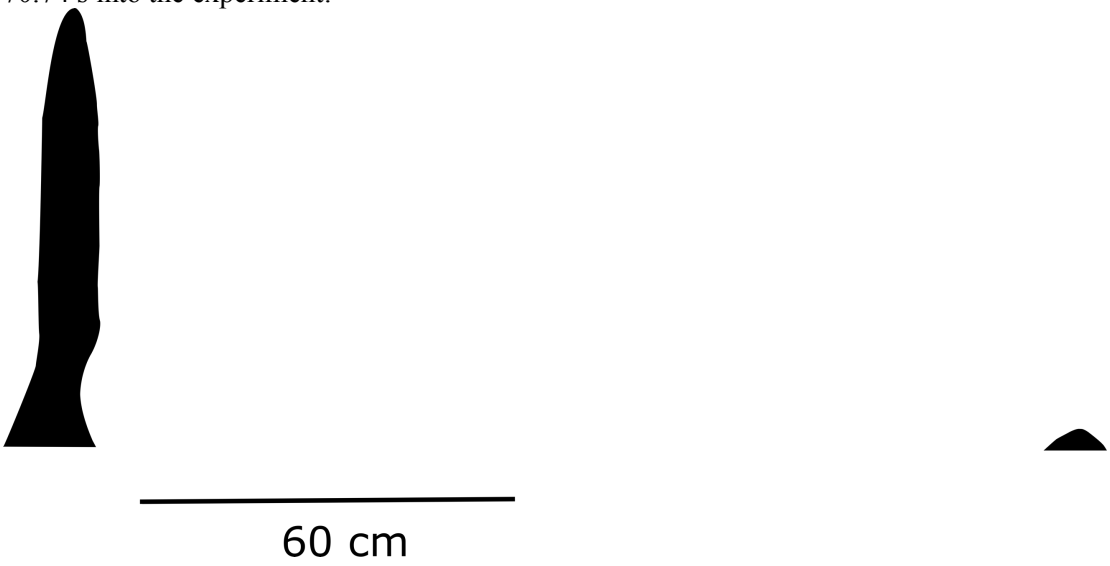

81.11 s into the experiment:

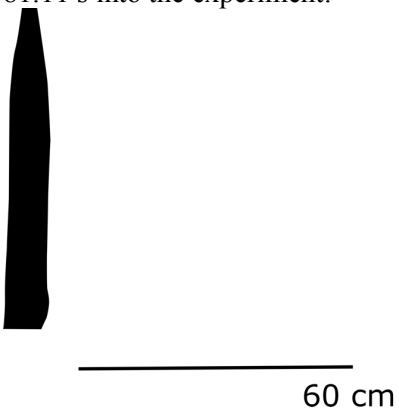

040716a (PGS-air):

9.70 s into the experiment:

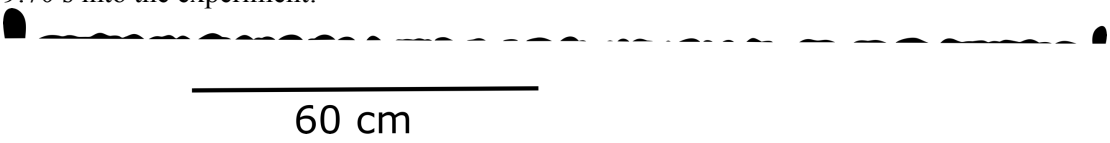

14.6 s into the experiment:

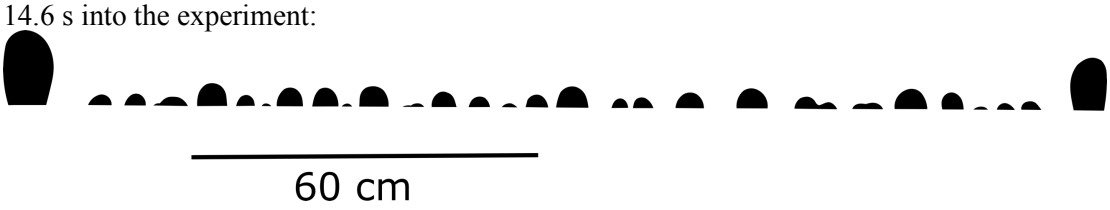

21.97 s into the experiment:

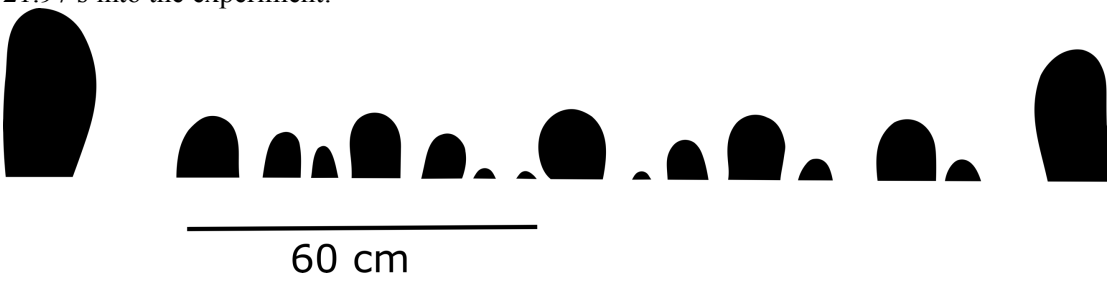

28.64 s into the experiment:

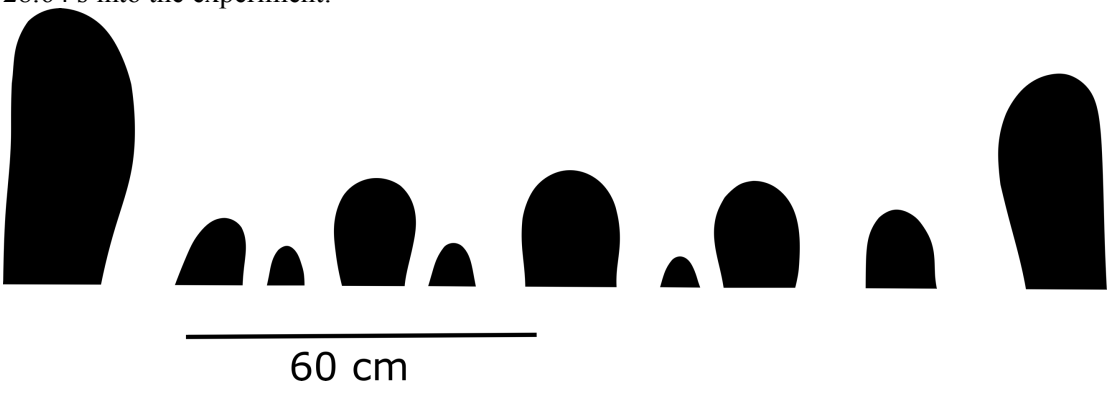

30.00 s into the experiment:

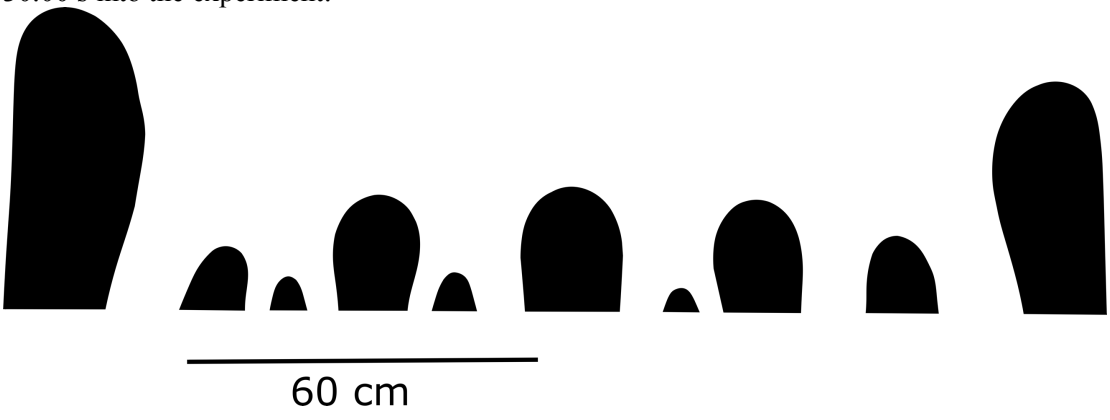

32.68 s into the experiment:

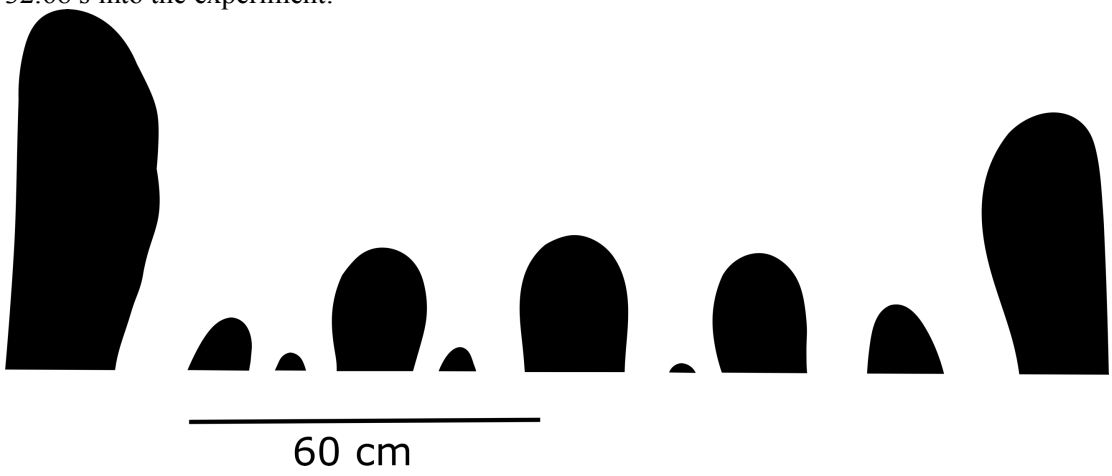

41.68 s into the experiment:

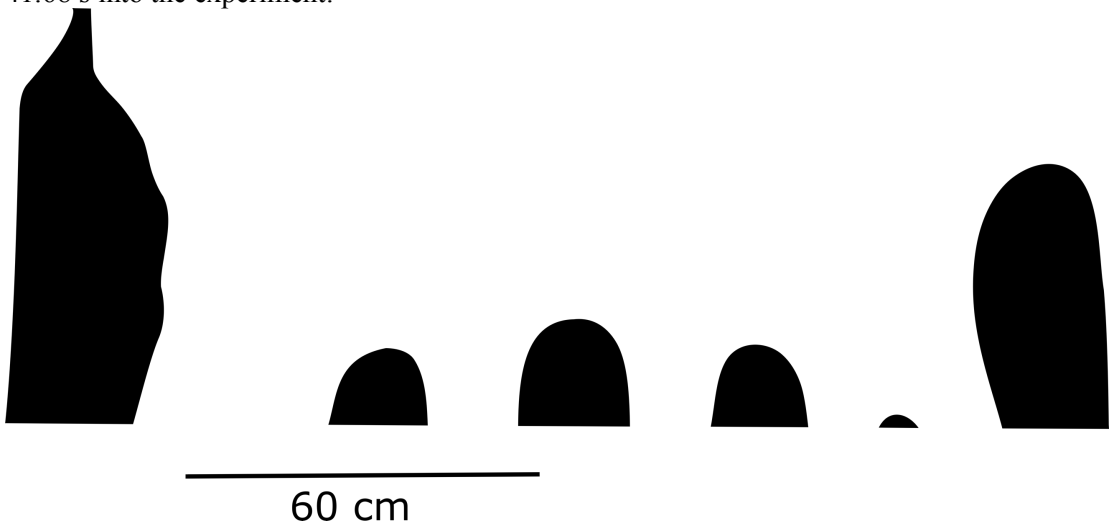

50.69 s into the experiment:

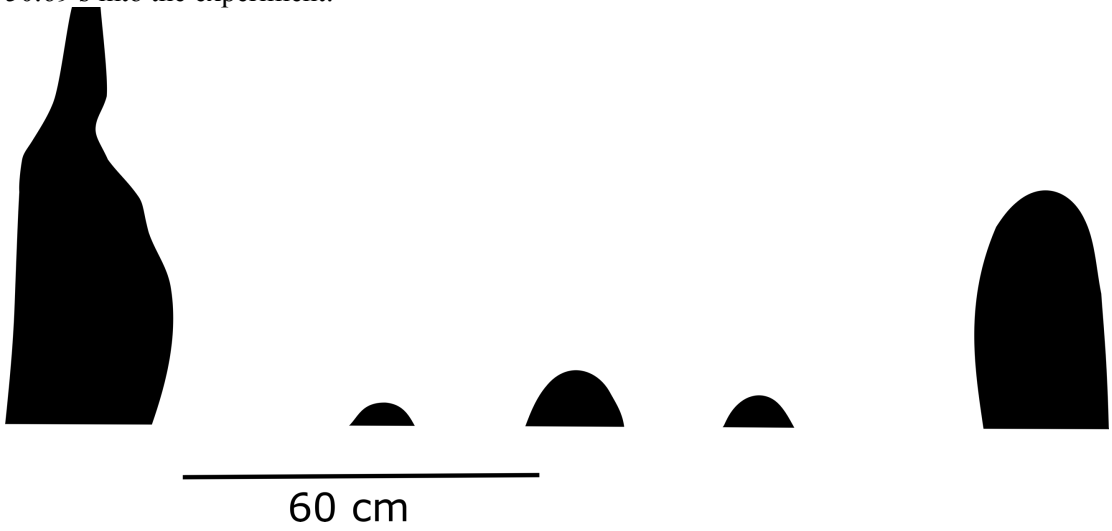

59.72 s into the experiment:

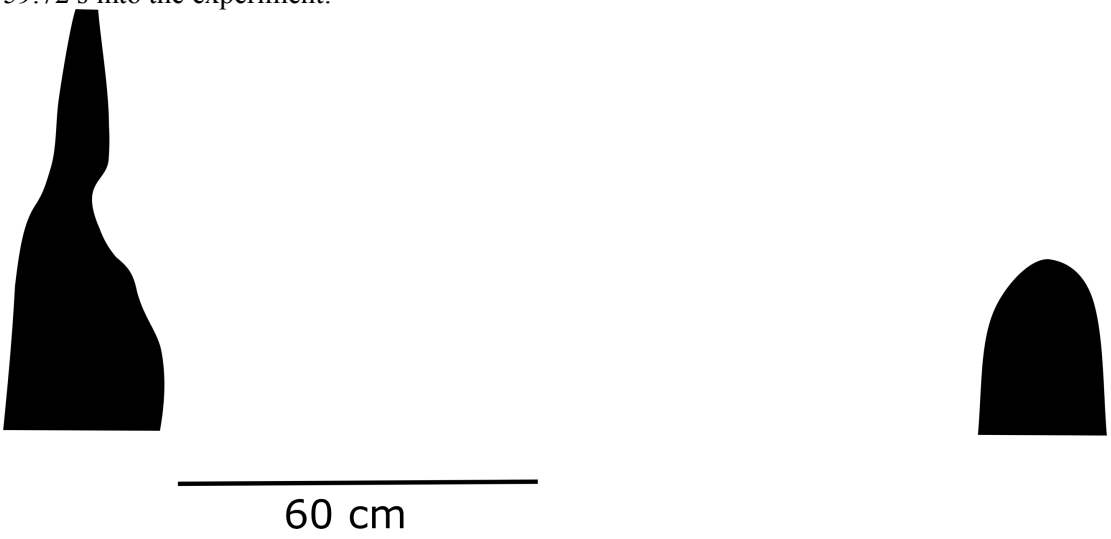

68.72 s into the experiment:

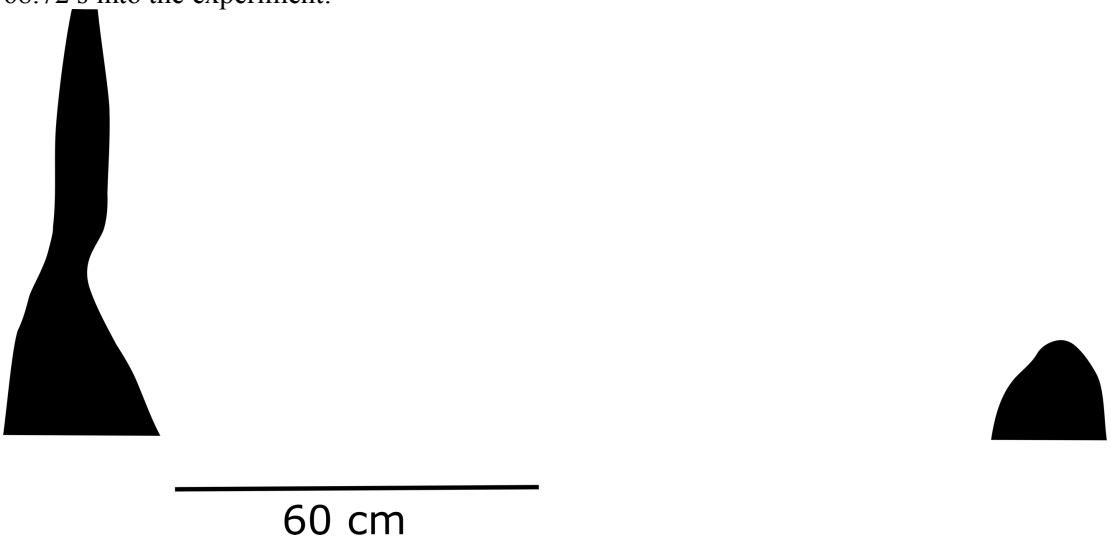

77.61 s into the experiment:

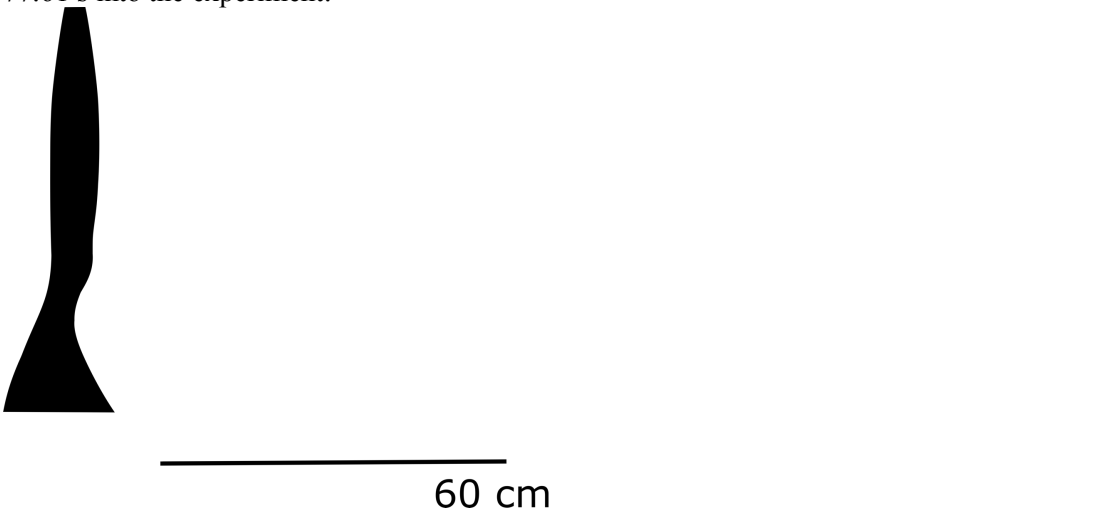

040716d (PGS-air):

4.66 s into the experiment:

6.99 s into the experiment:

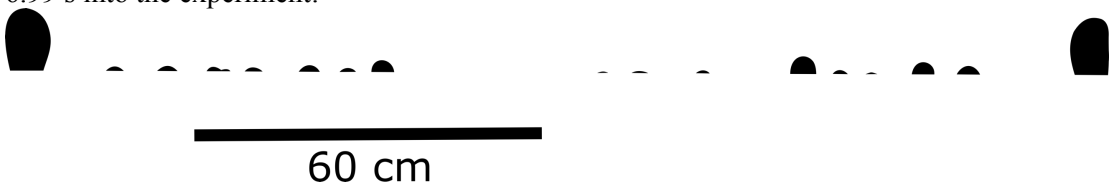

12.03 s into the experiment:

17.03 s into the experiment:

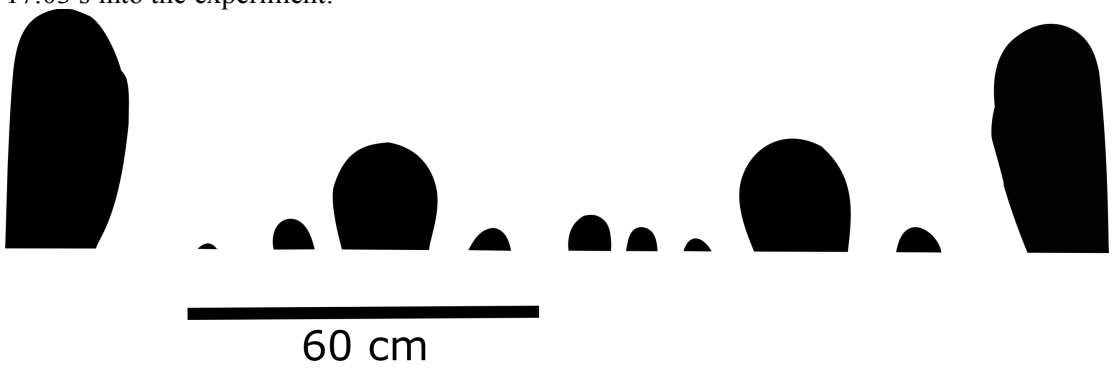

20.43 s into the experiment:

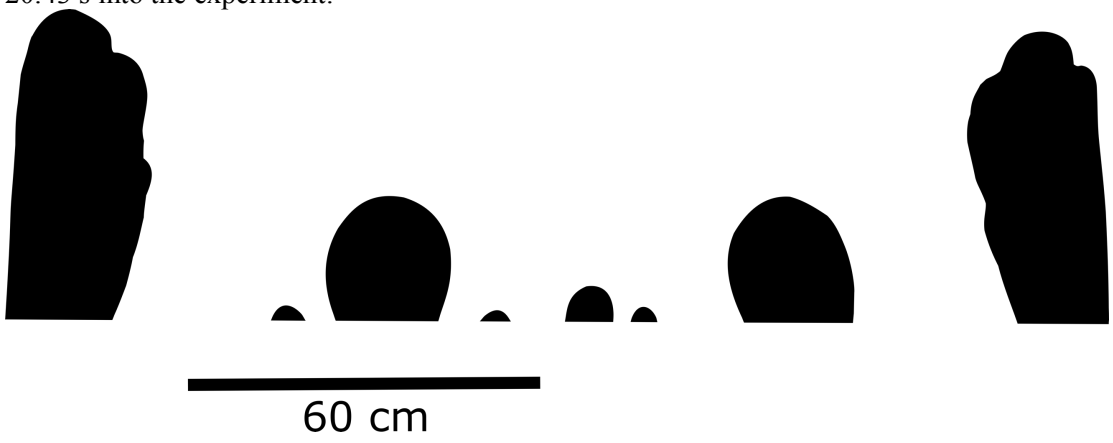

40.97 s into the experiment:

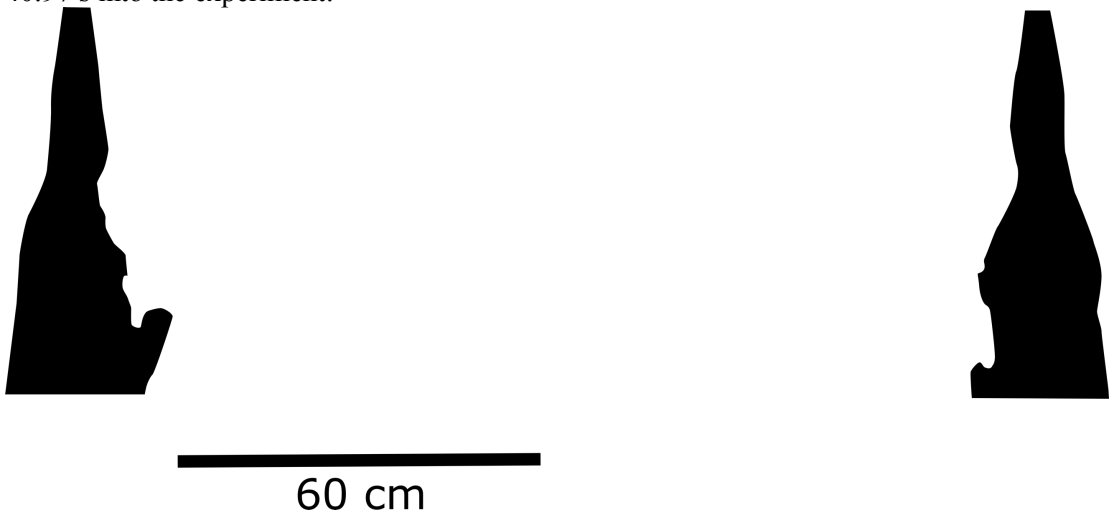

50.63 s into the experiment:

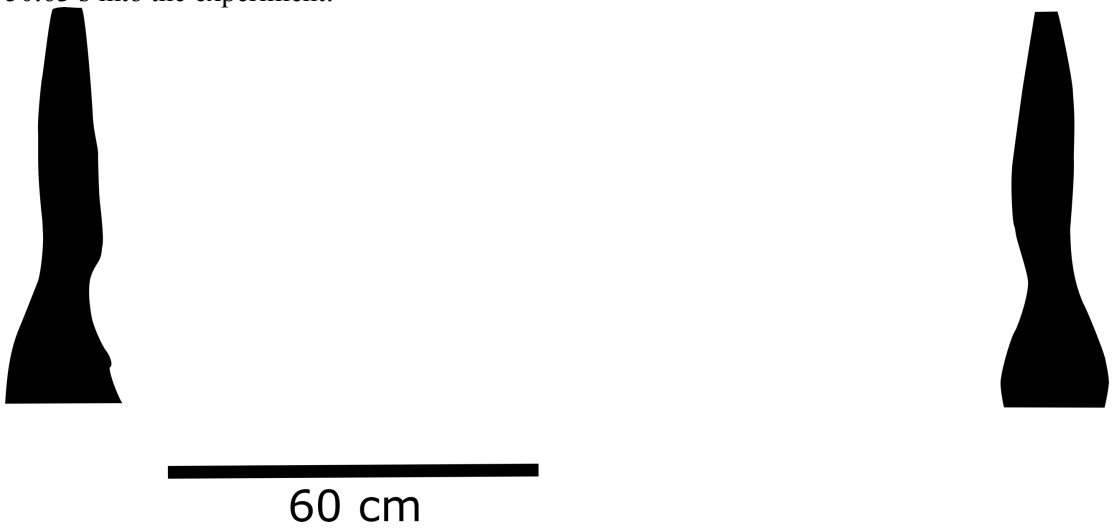

57.97 s into the experiment:

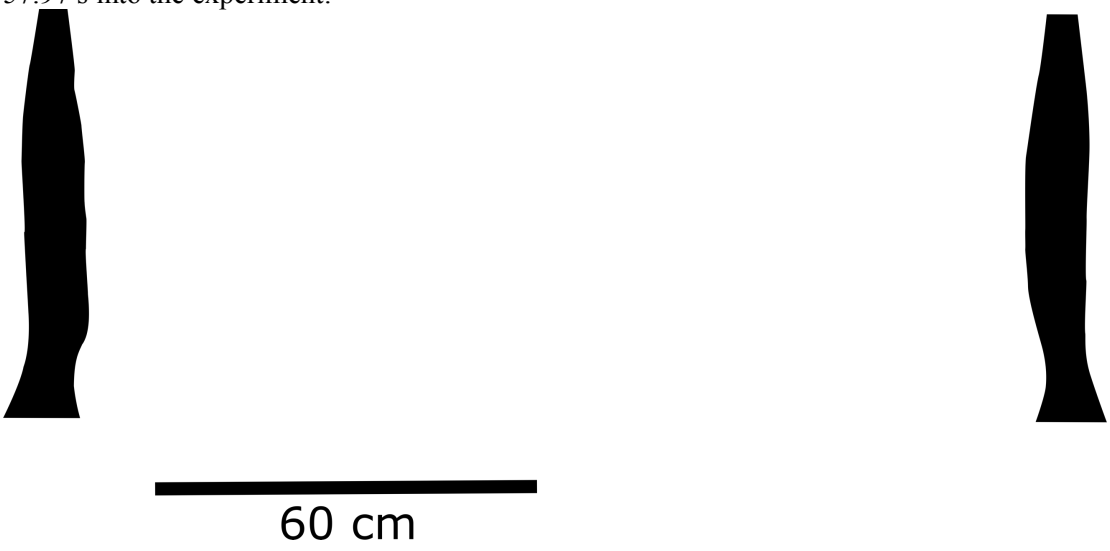

63.63 s into the experiment:

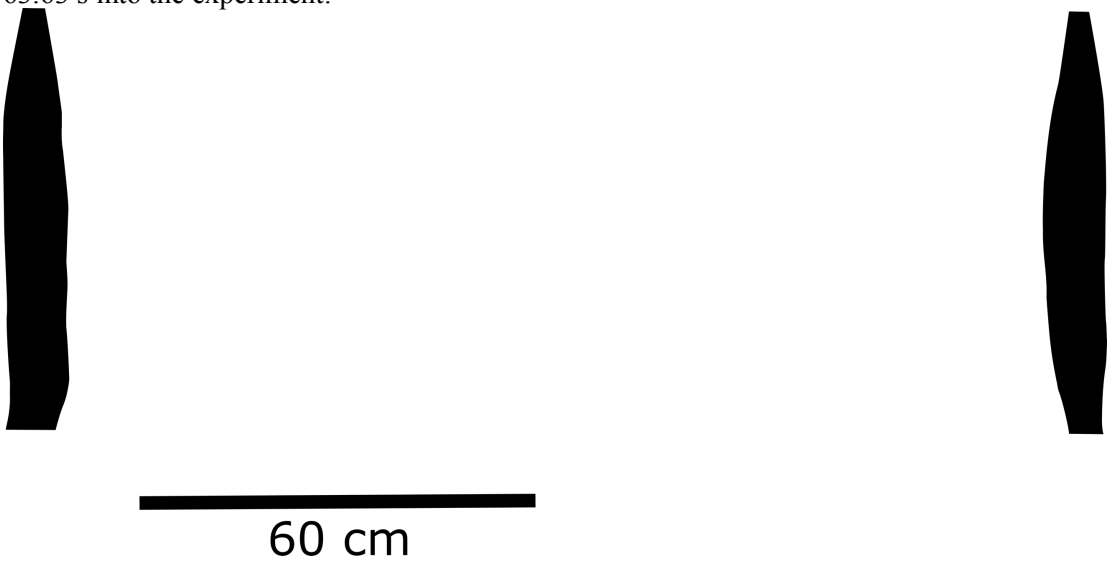

71.96 s into the experiment:

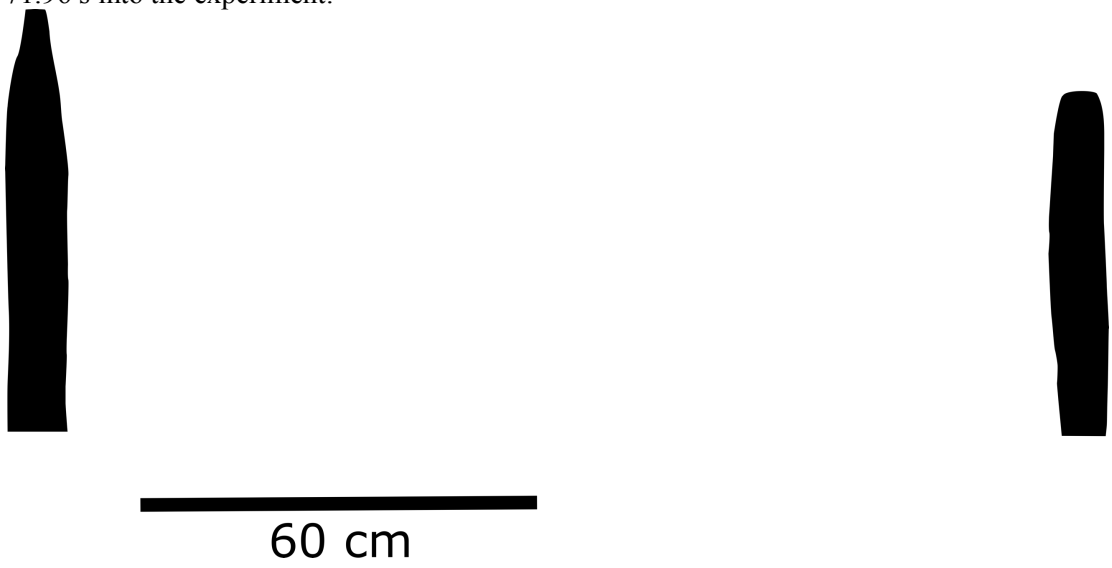

130716b (PGS-oil):

11.69 s into the experiment:

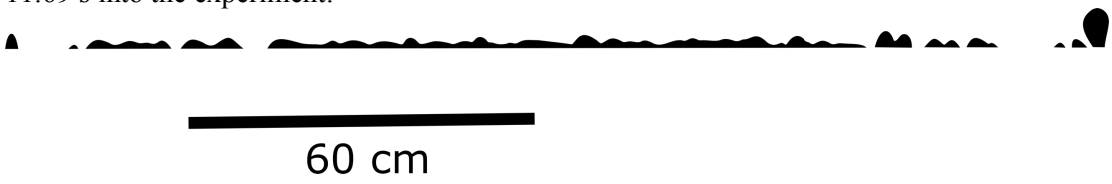

20.02 s into the experiment:

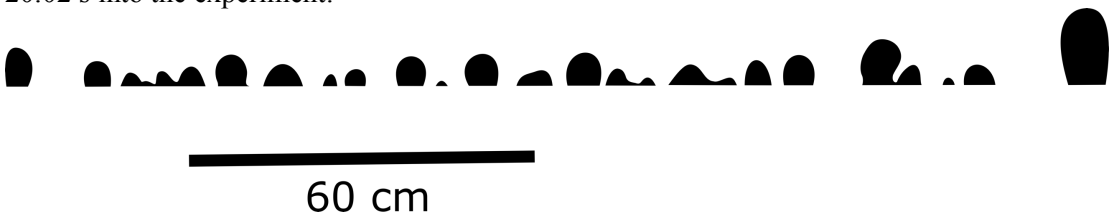

27.21 s into the experiment:

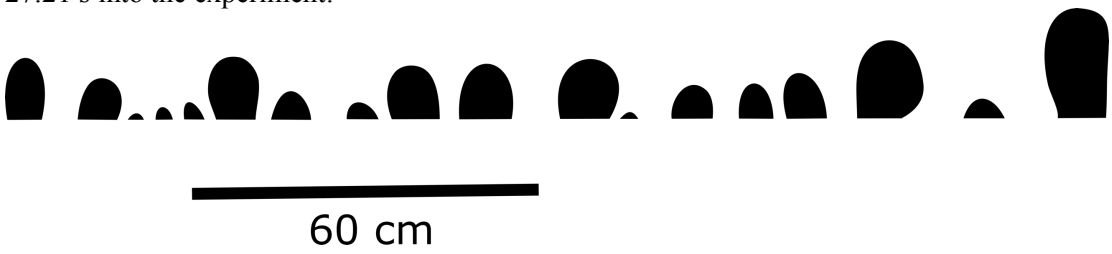

33.59 s into the experiment:

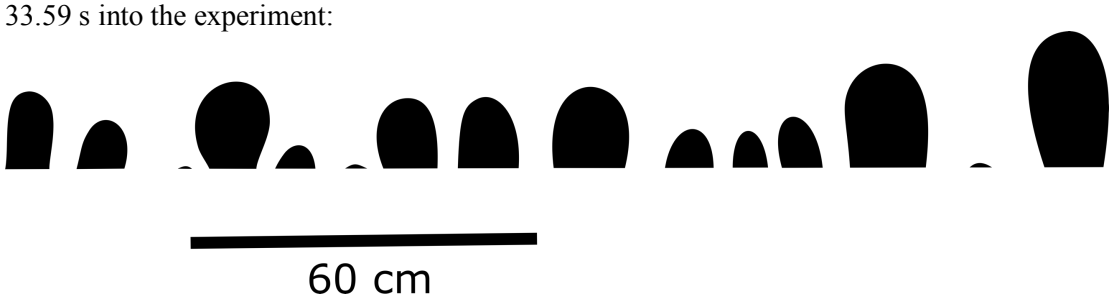

41.67 s into the experiment:

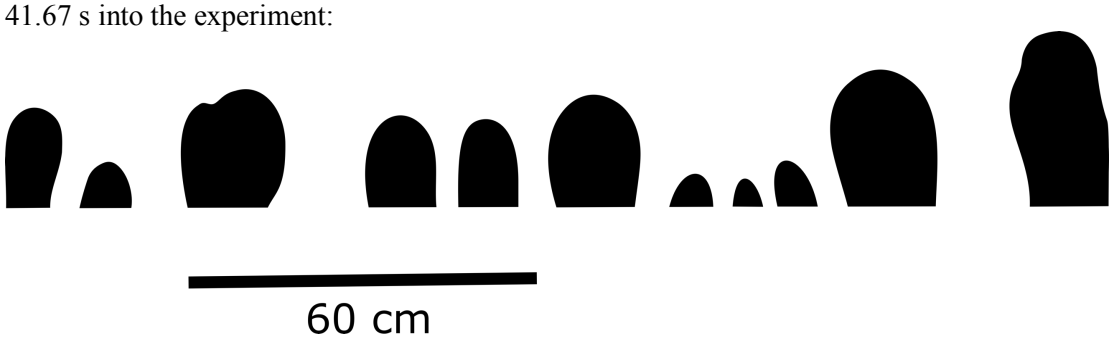

53.64 s into the experiment:

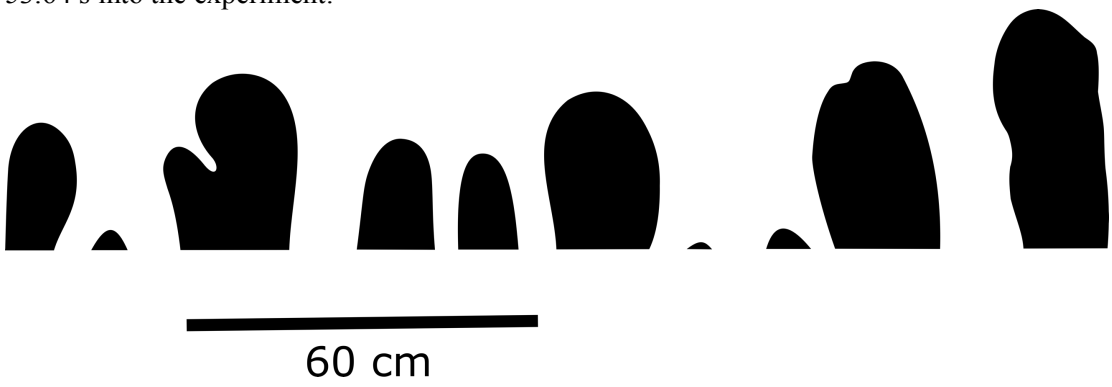

61.68 s into the experiment:

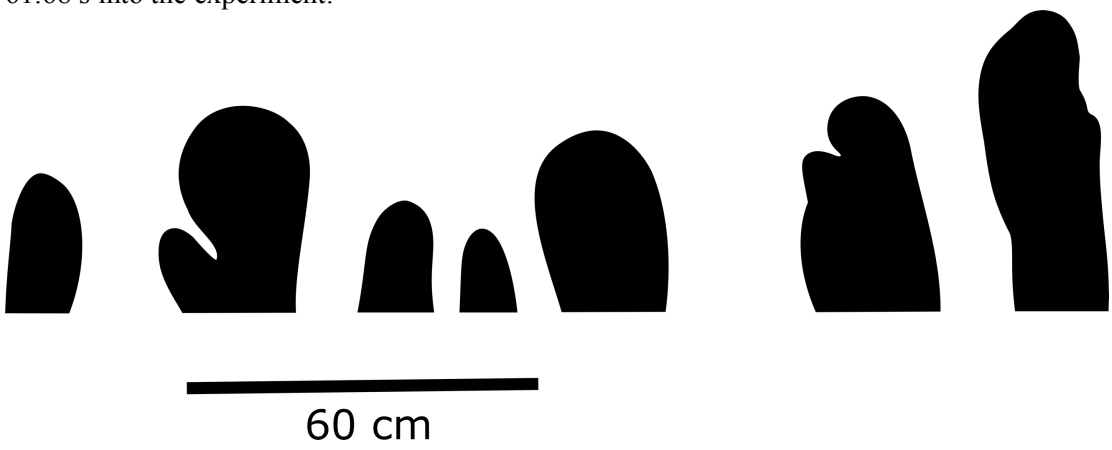

107.73 s into the experiment:

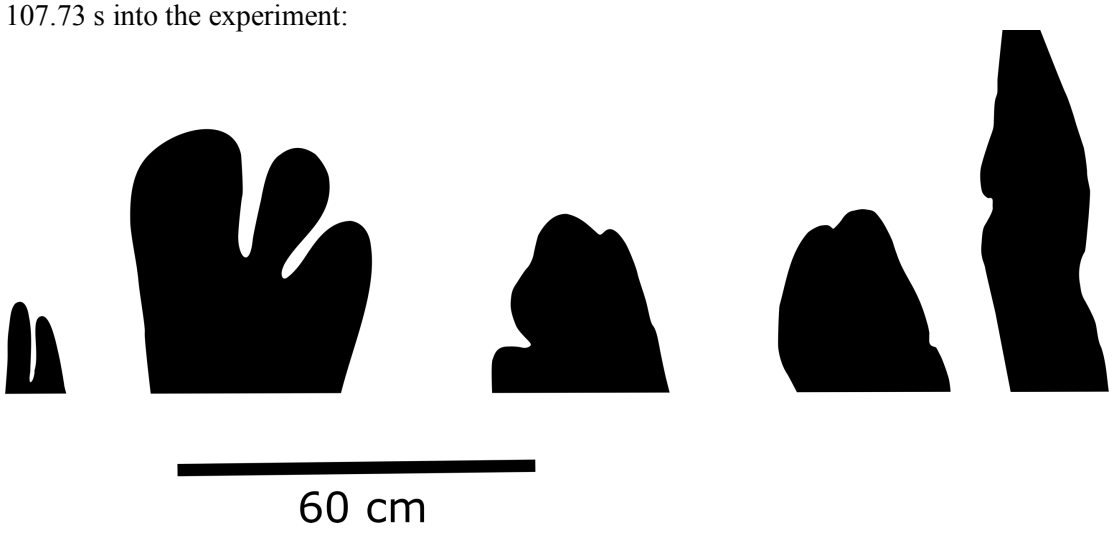

117.71 s into the experiment:

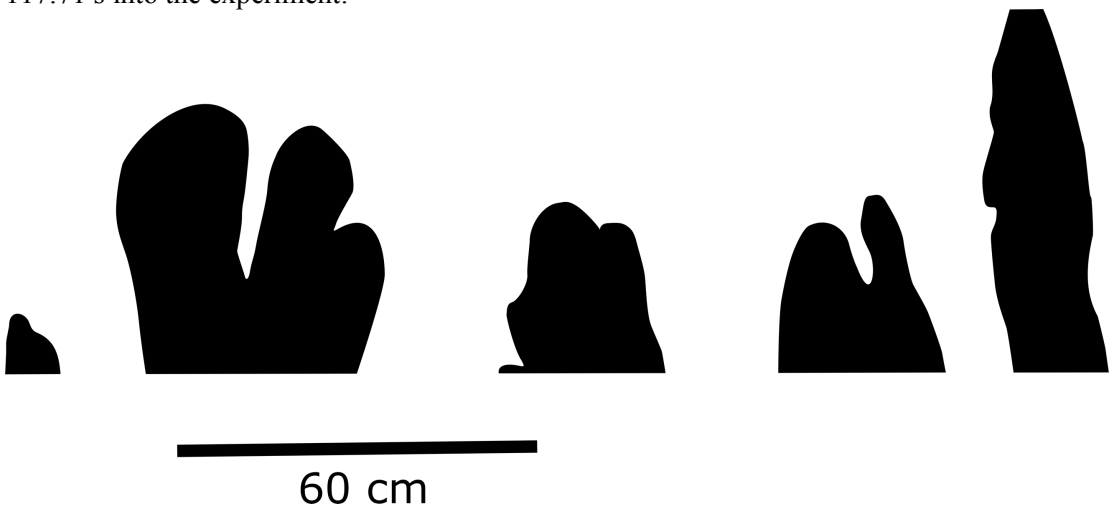

135.00 s into the experiment:

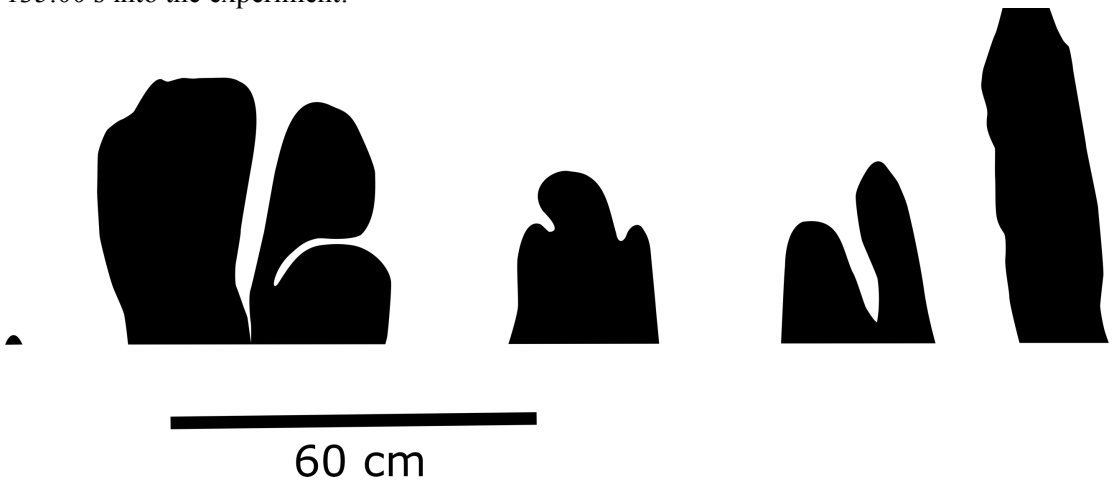

148.99 s into the experiment:

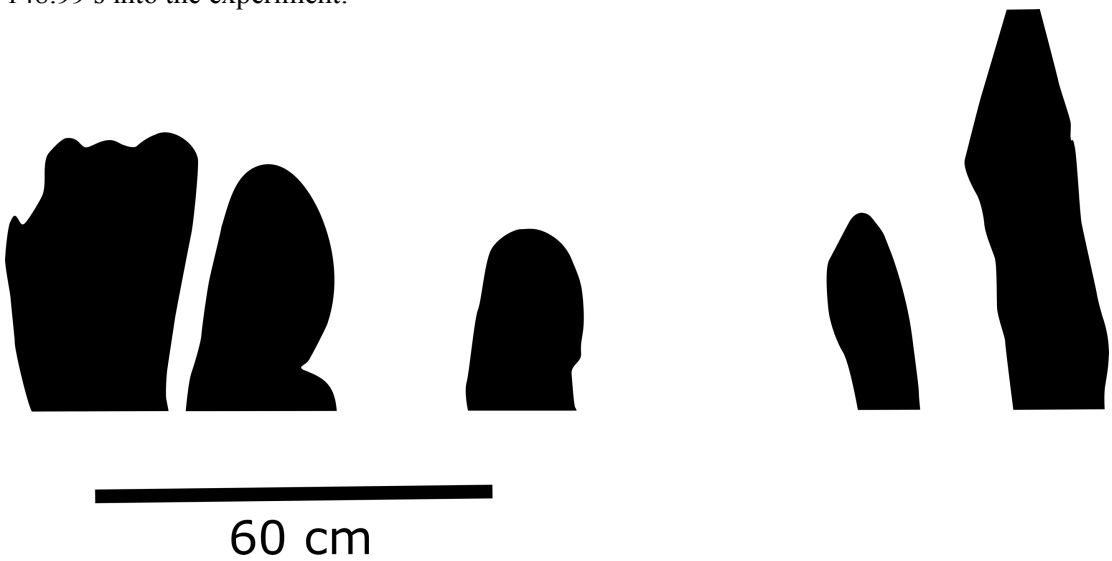

162.71 s into the experiment:

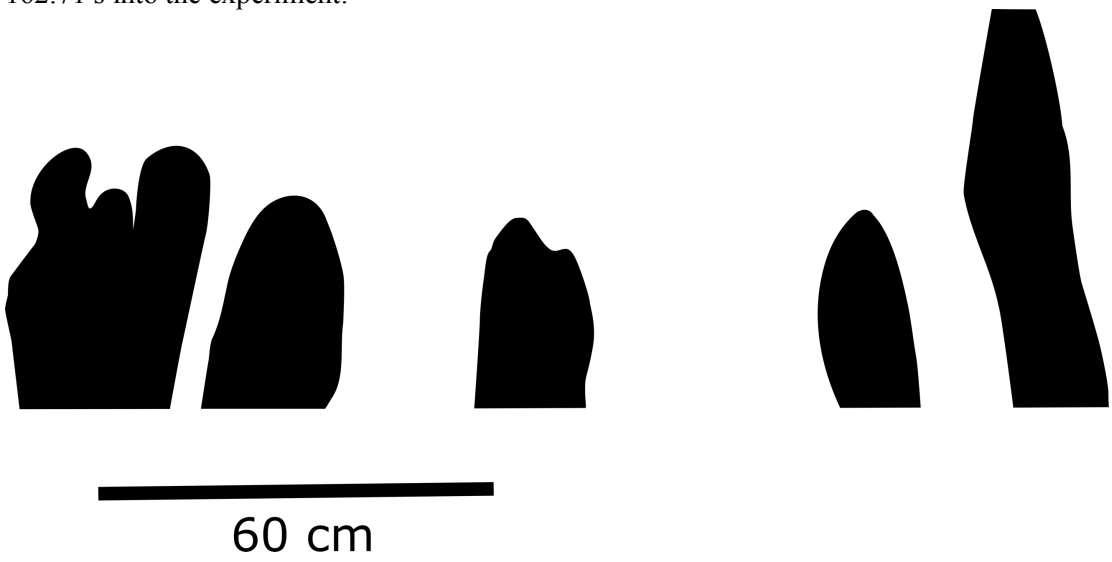

<u>140716b (PGS-oil):</u>

10.64 s into the experiment:

16.7 s into the experiment:

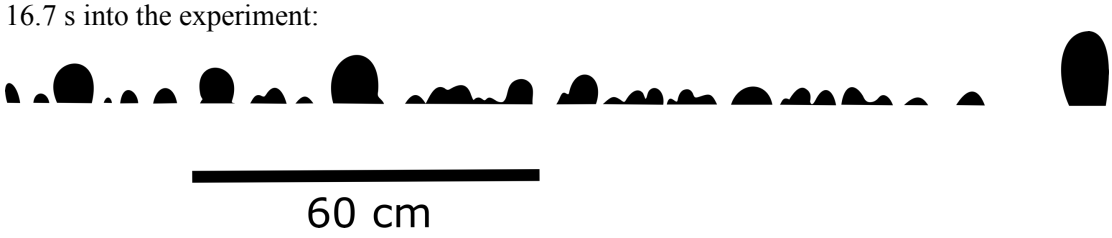

28.68 s into the experiment:

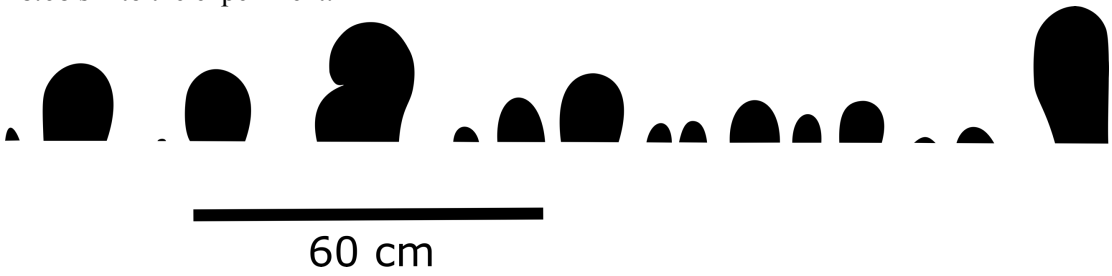

34.01 s into the experiment:

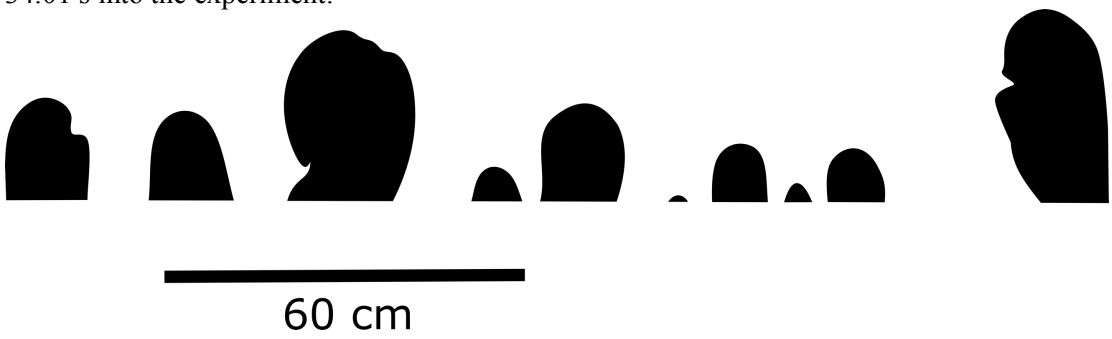

41.67 s into the experiment:

46.67 s into the experiment:

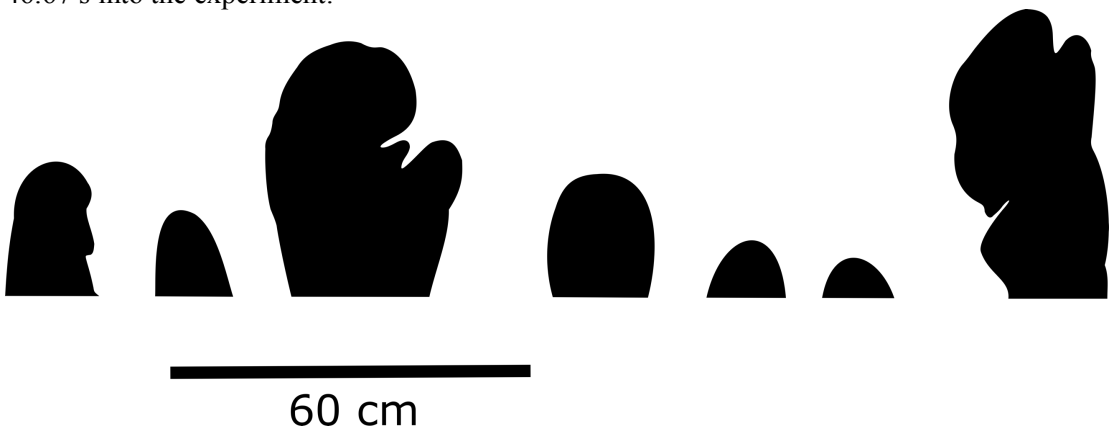

48.68 s into the experiment:

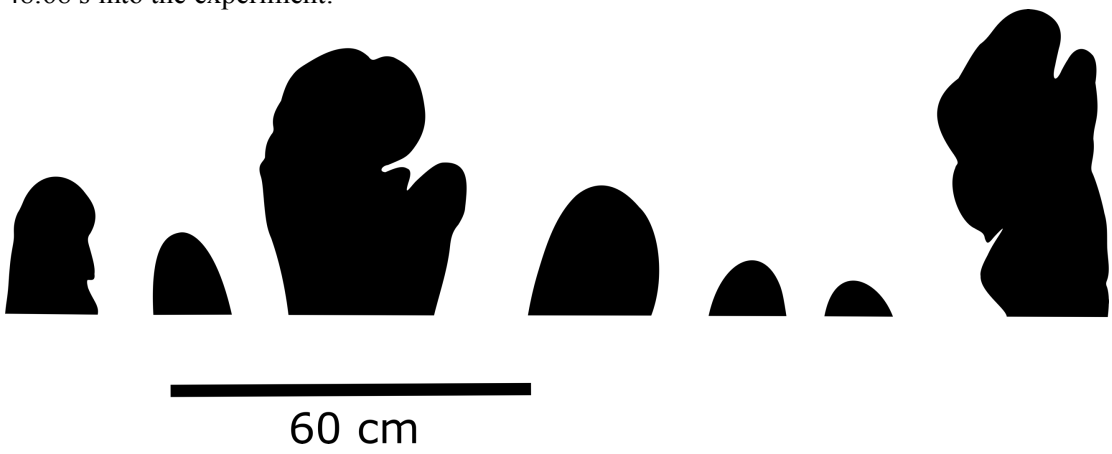

102.08 s into the experiment:

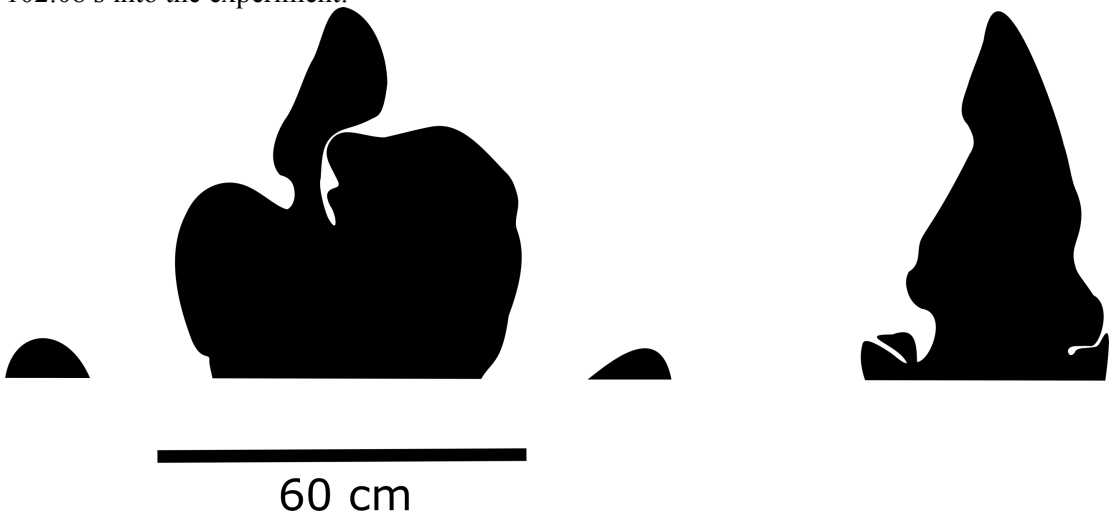

115.62 s into the experiment:

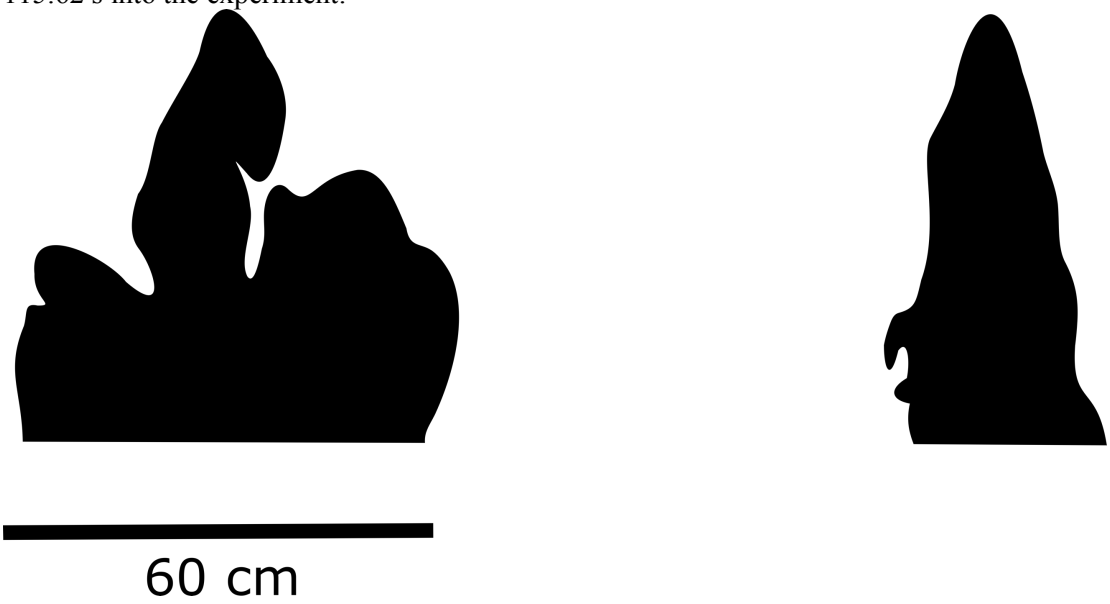

134.66 s into the experiment:

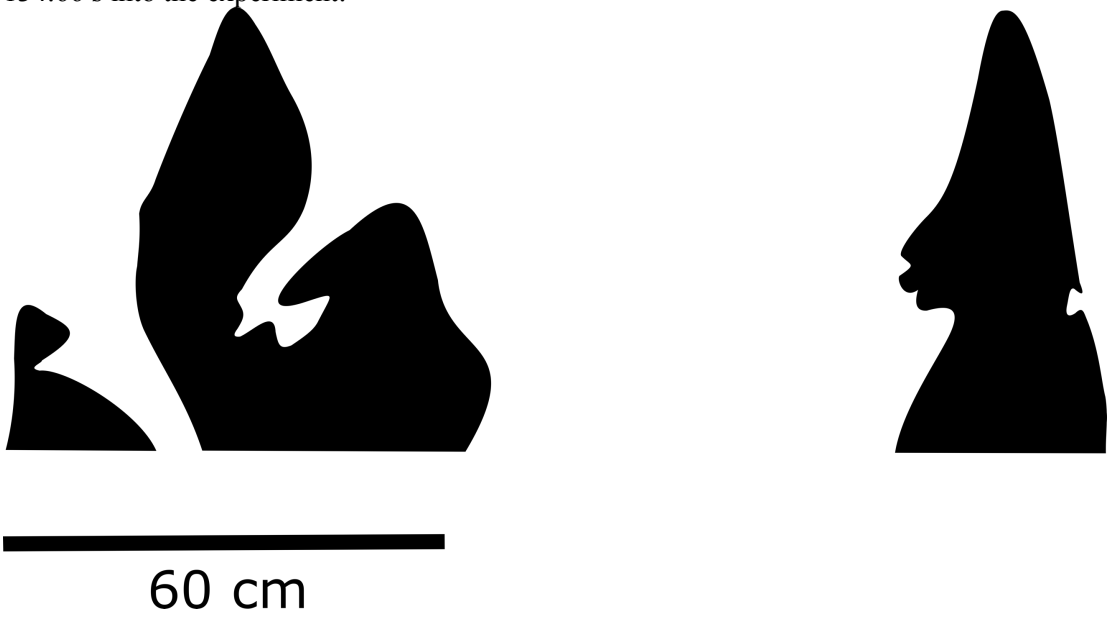

152.64 s into the experiment:

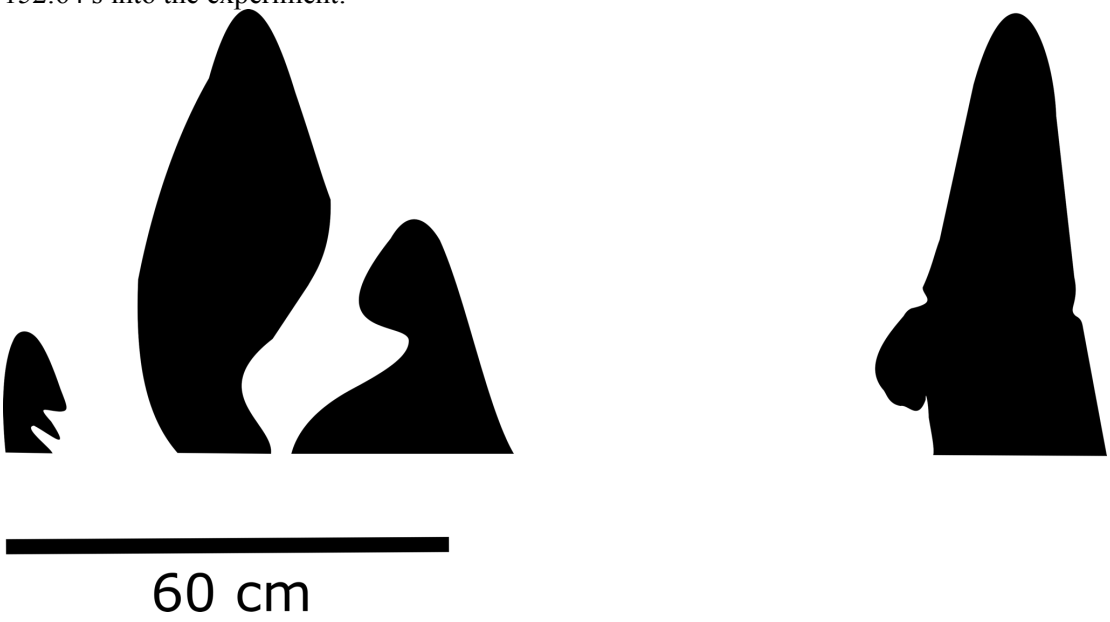

172.04 s into the experiment:

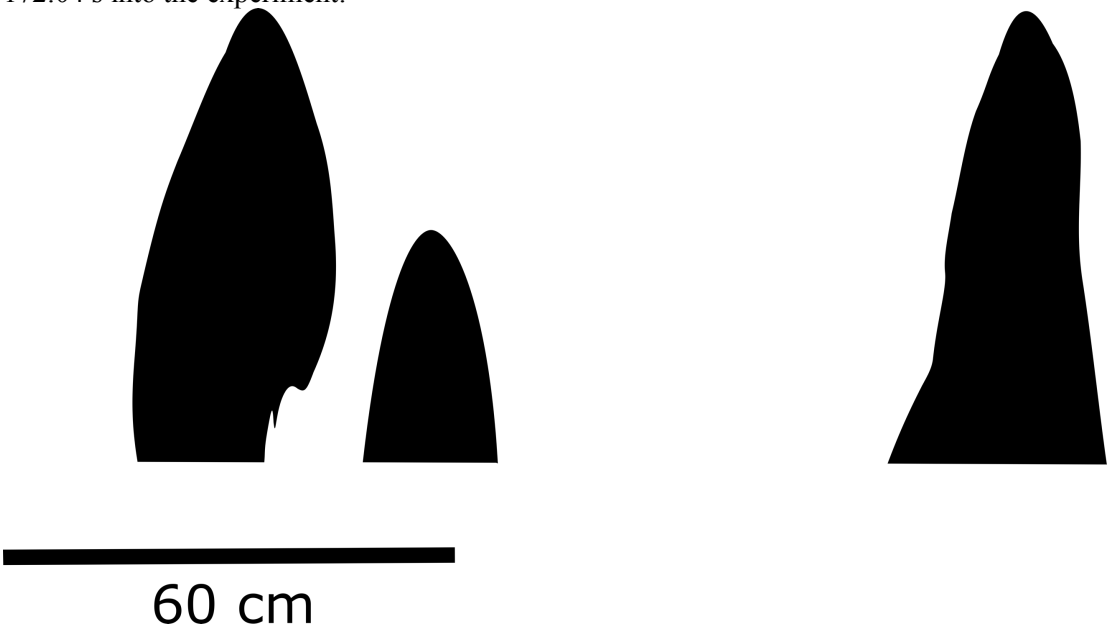

184.08 s into the experiment:

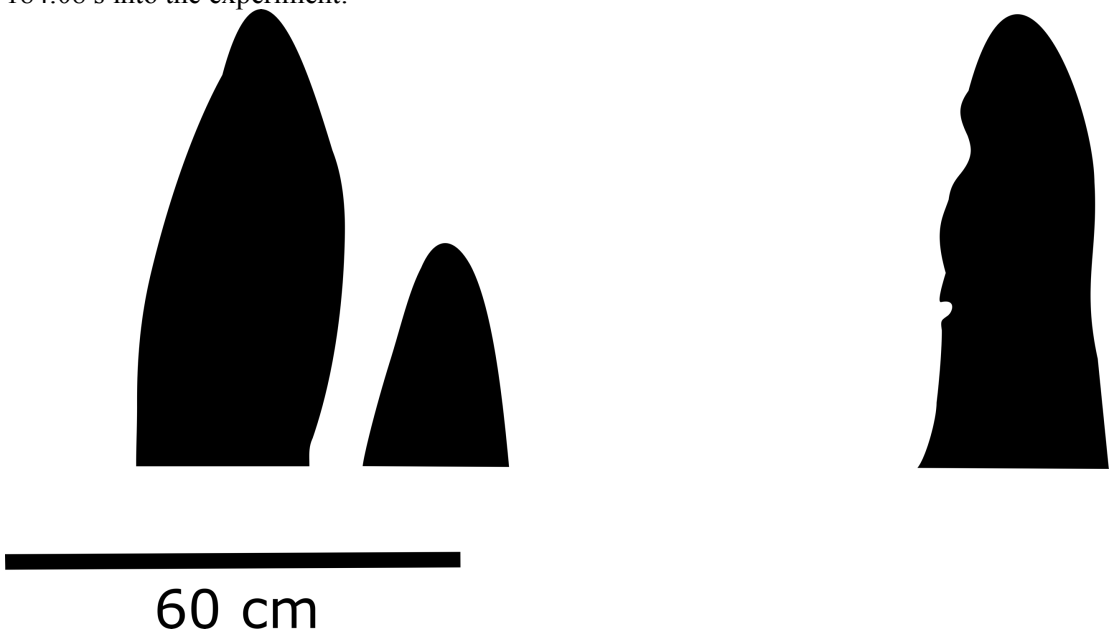

180716a (PGS-oil):

8.37 s into the experiment:

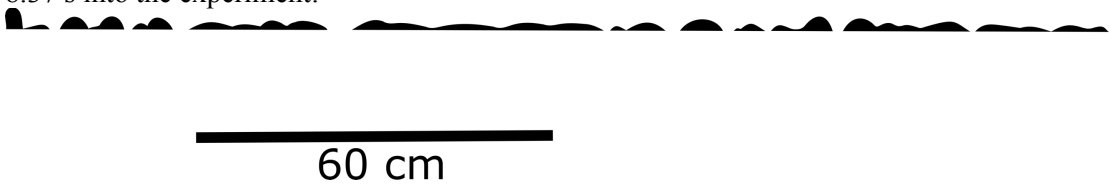

12.32 s into the experiment:

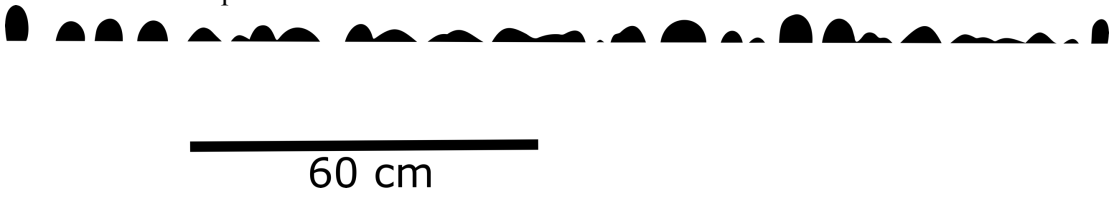

17.34 s into the experiment:

27.35 s into the experiment:

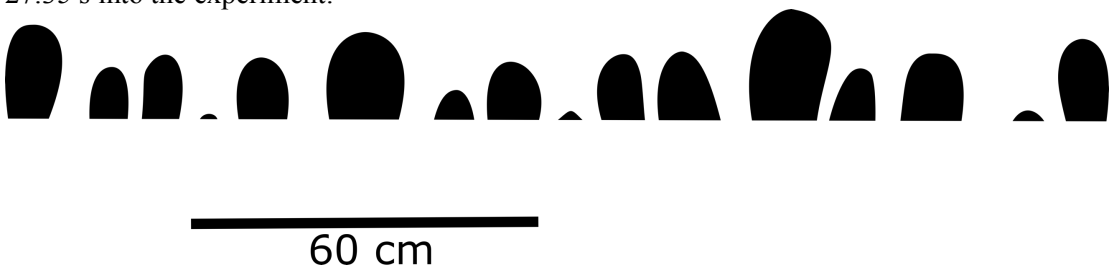

41.41 s into the experiment:

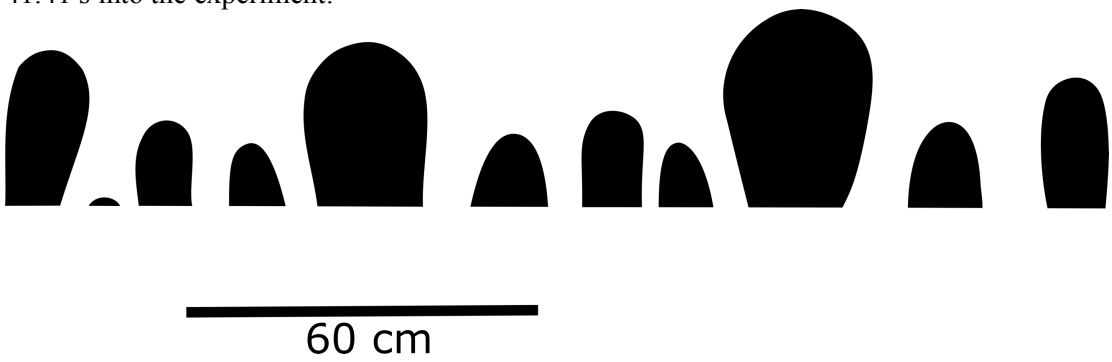

52.32 s into the experiment:

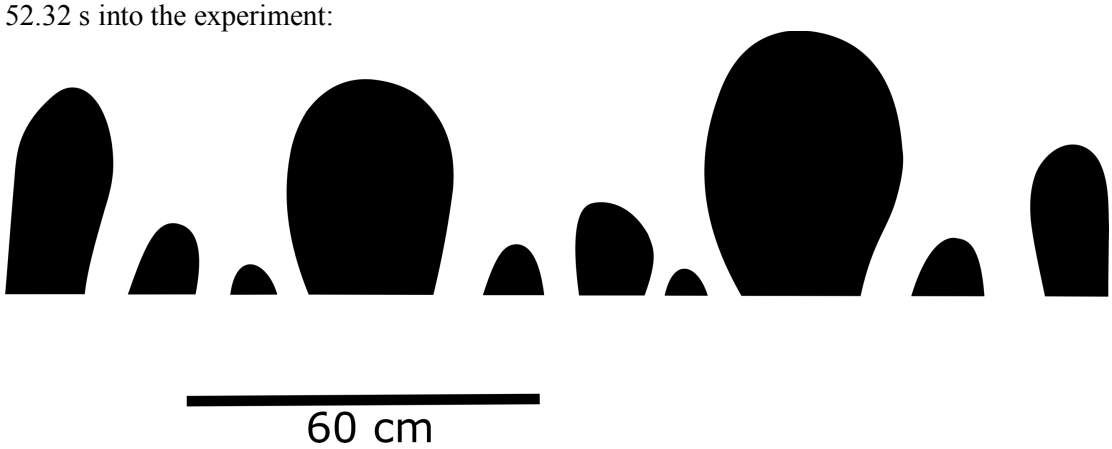

59.94 s into the experiment:

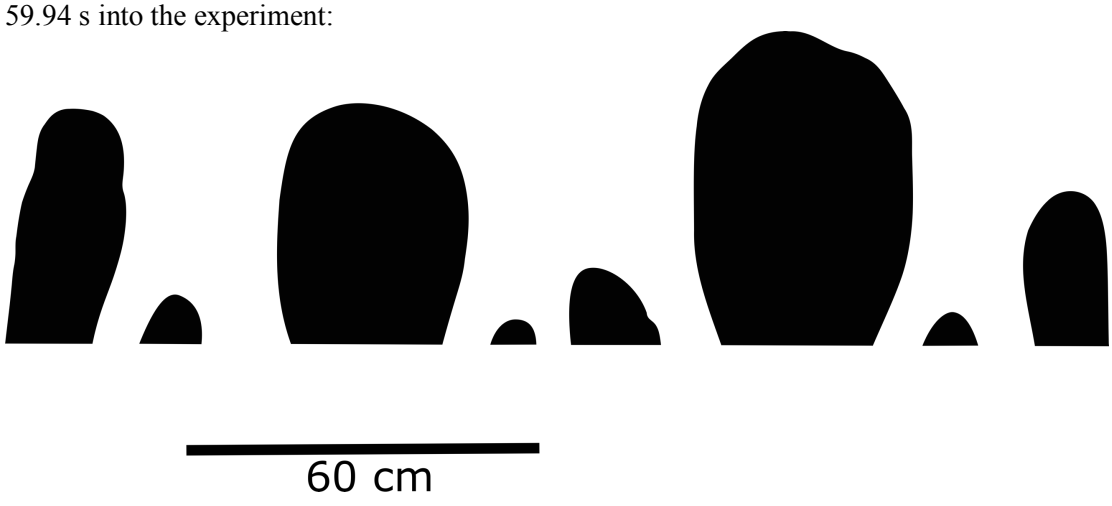

92.32 s into the experiment:

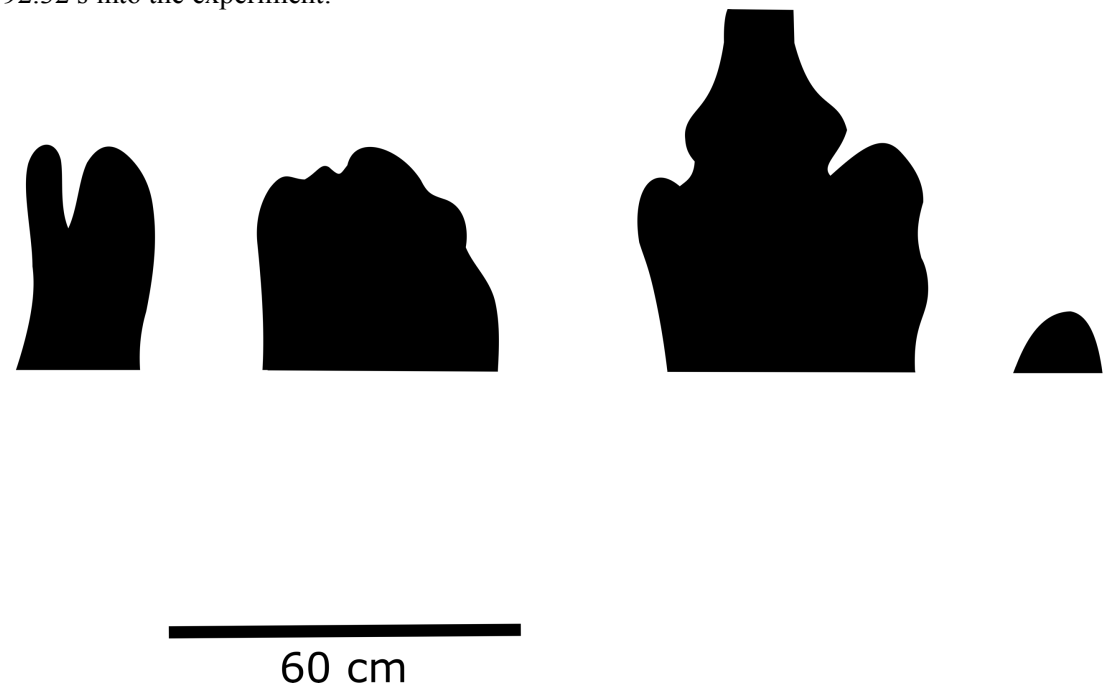

120.05 s into the experiment:

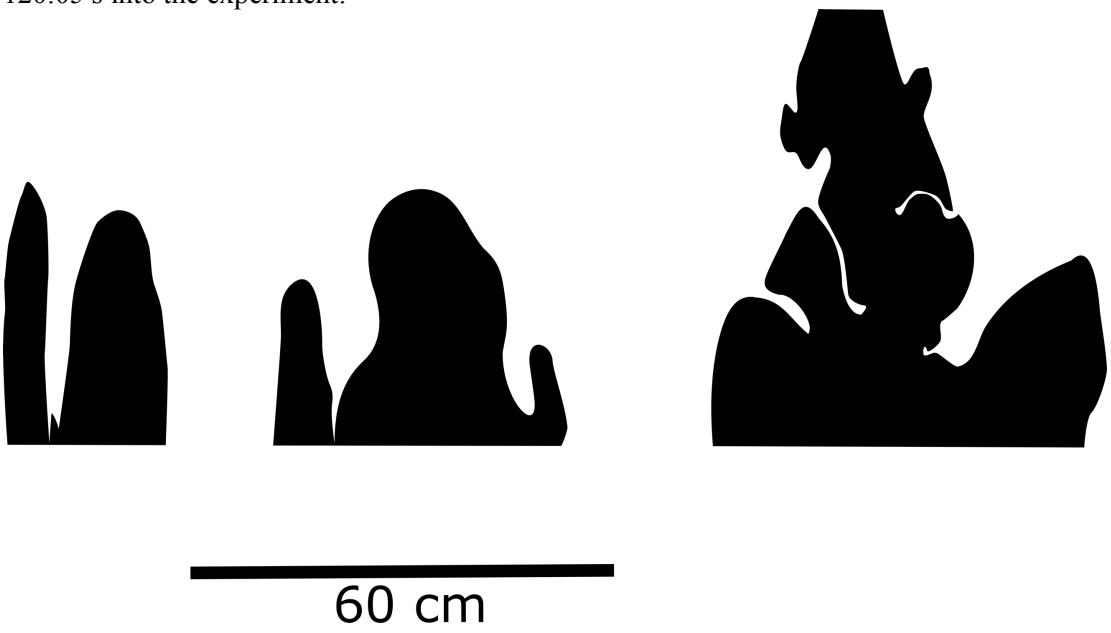

132.4 s into the experiment:

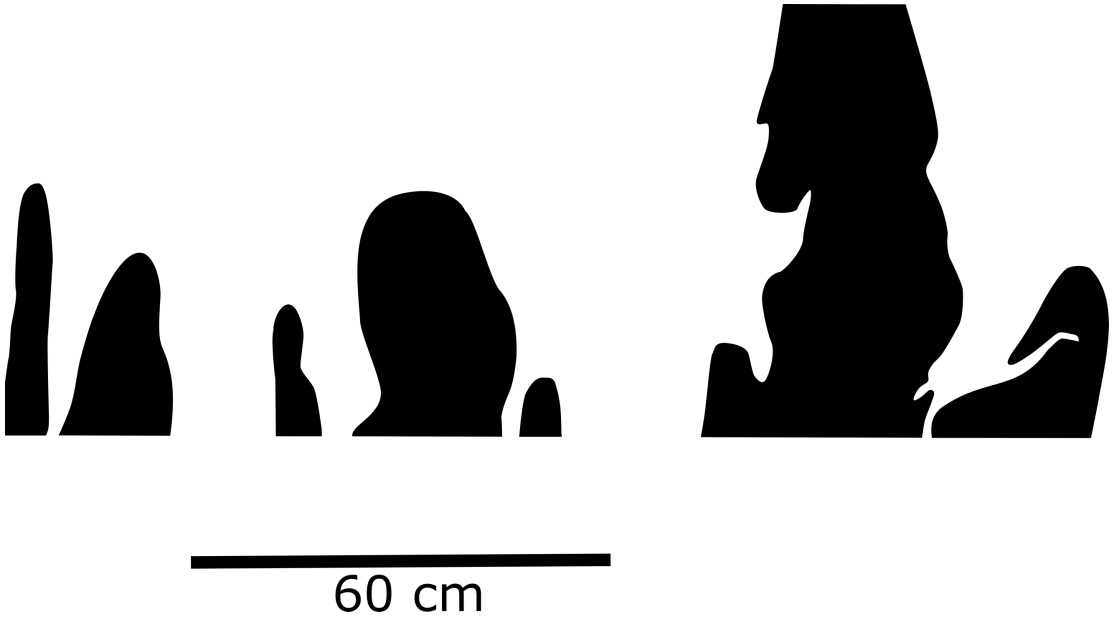

144.98 s into the experiment:

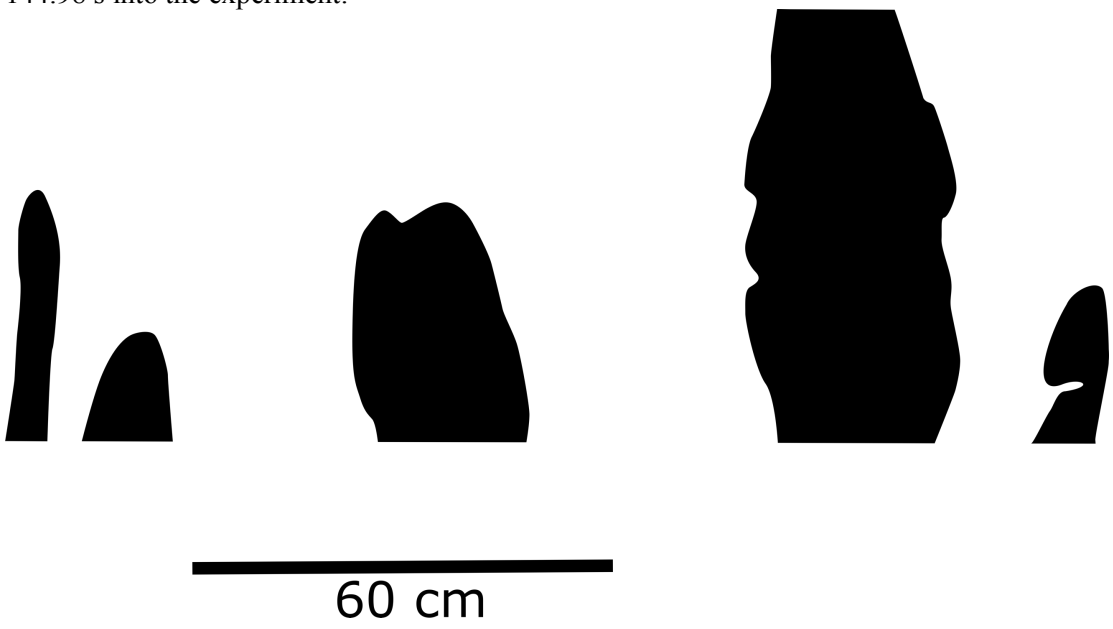

159.94 s into the experiment:

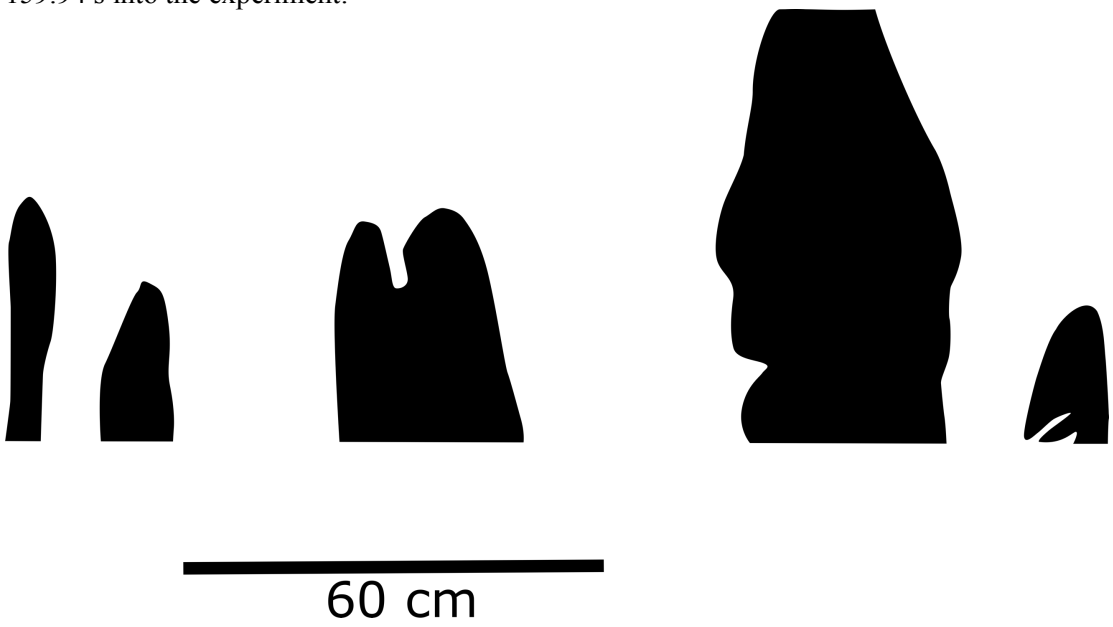

175.03 s into the experiment:

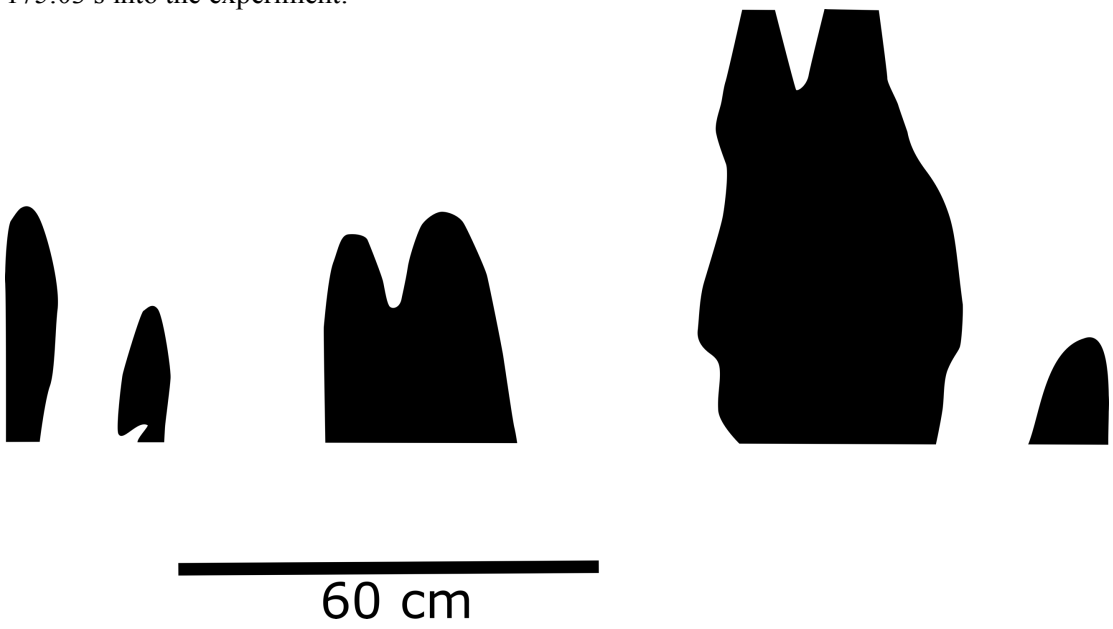

200716b (DGS-oil):

2.96 s into the experiment:

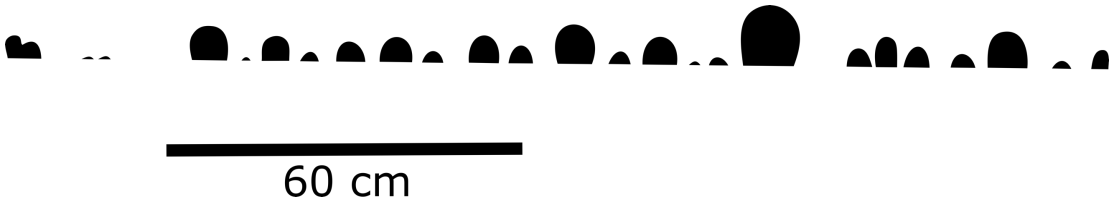

5.97 s into the experiment:

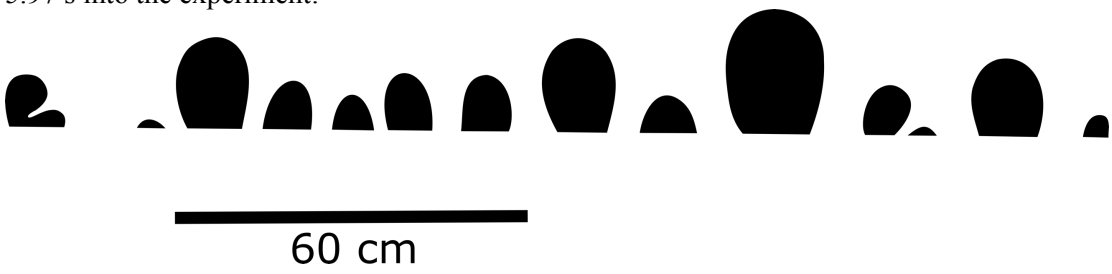

8.30 s into the experiment:

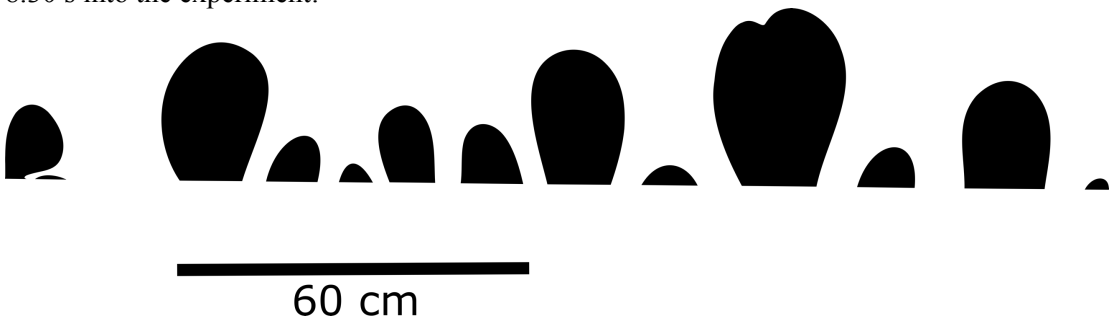

10.30 s into the experiment:

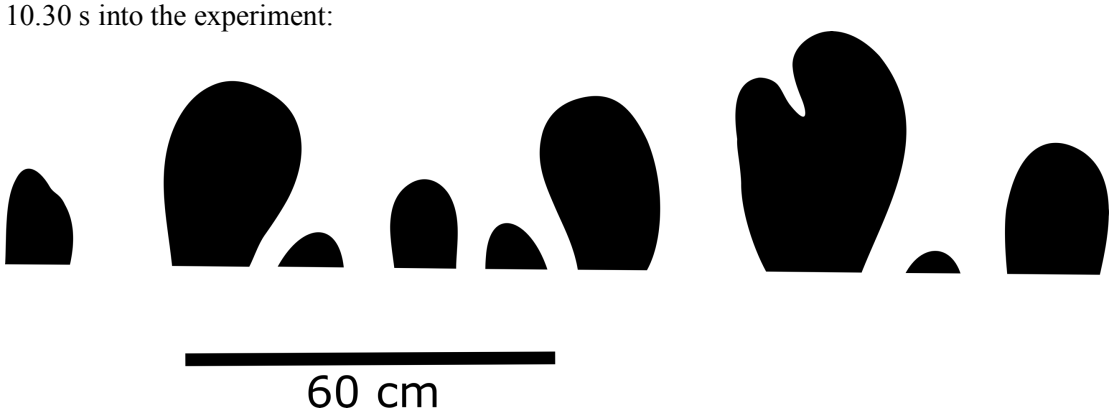

12.34 s into the experiment:

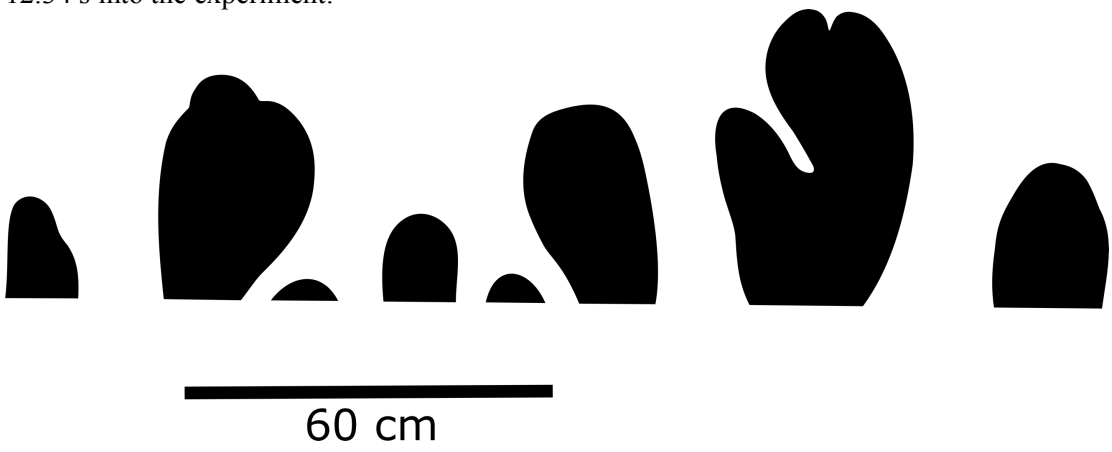

62.28 s into the experiment:

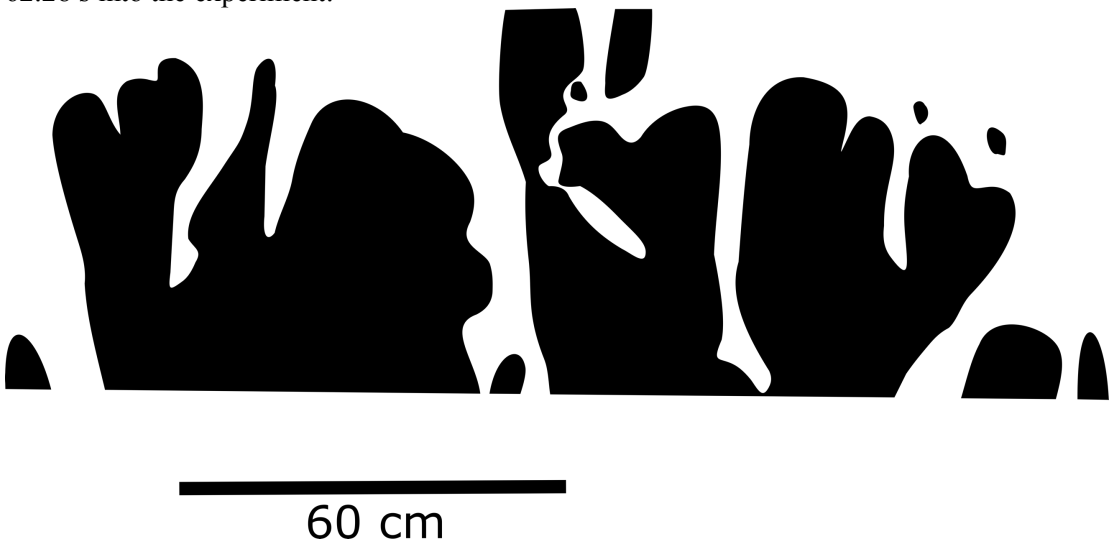

66.95 s into the experiment:

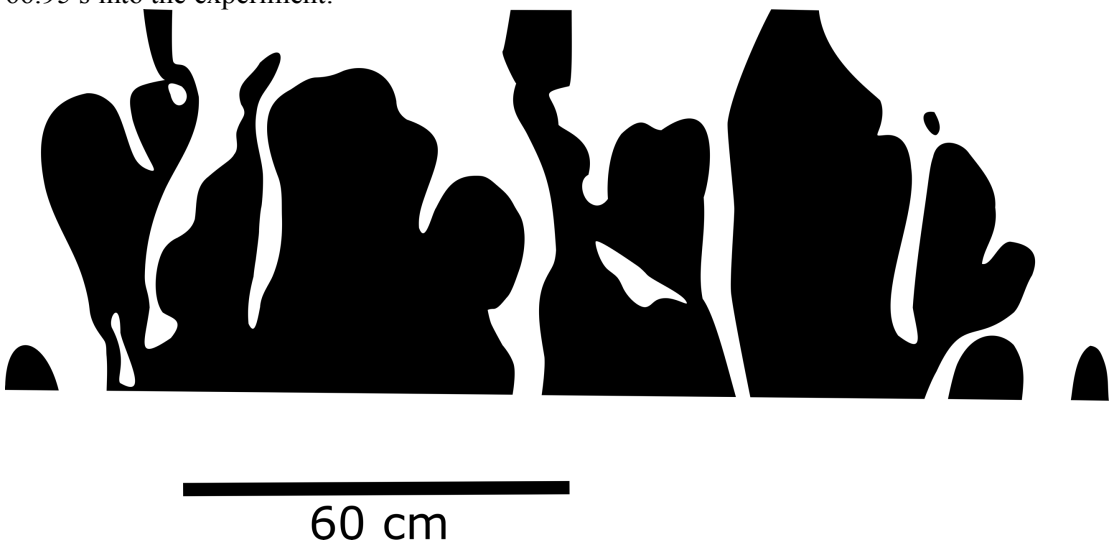

69.98 s into the experiment:

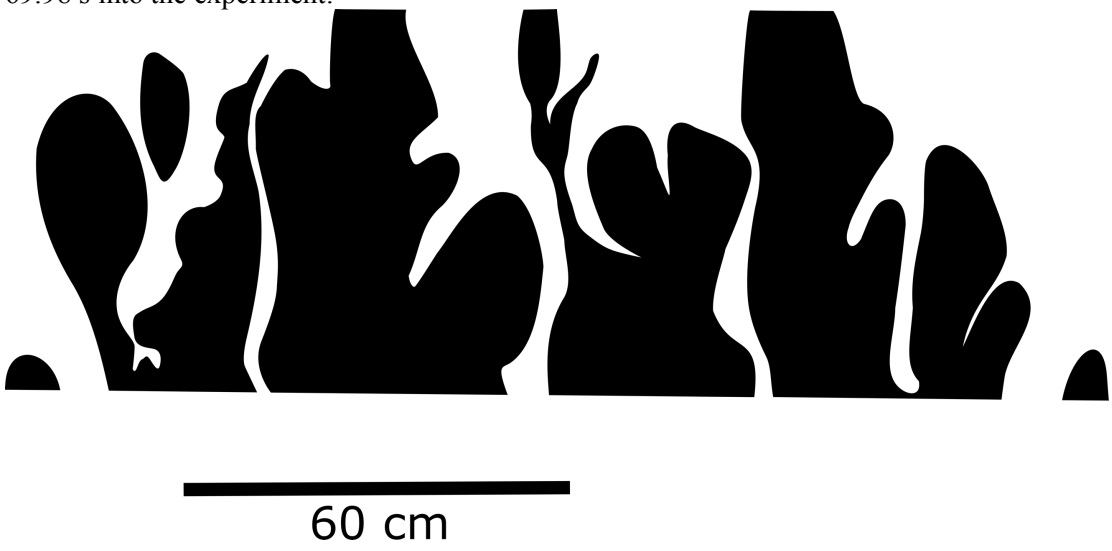

72.97 s into the experiment:

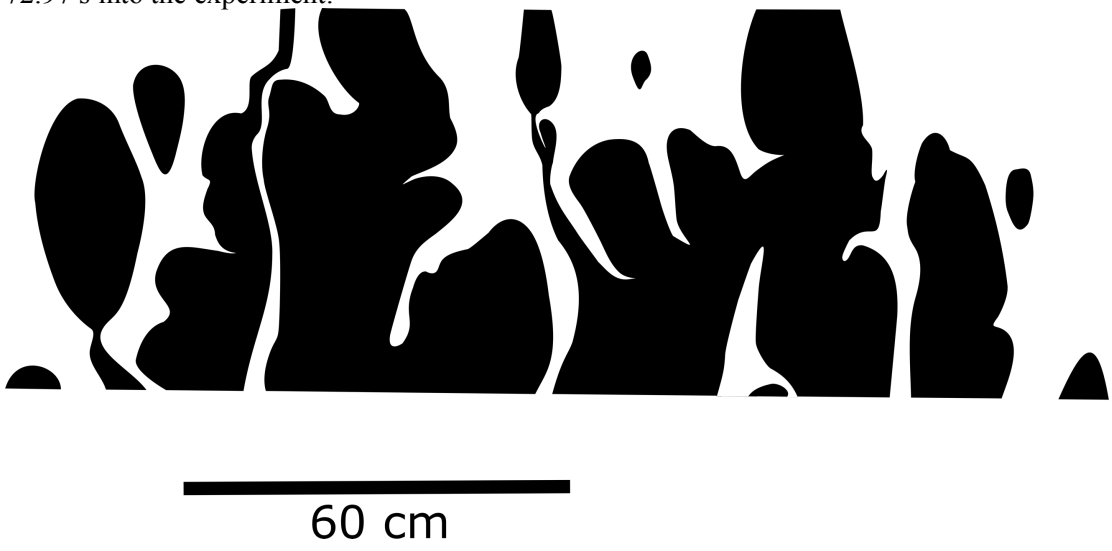

2110716a (DGS-oil):

1.36 s into the experiment:

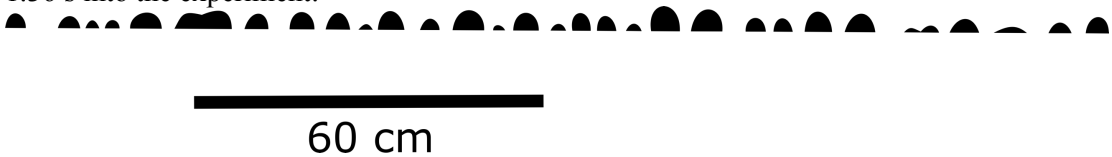

4.04 s into the experiment:

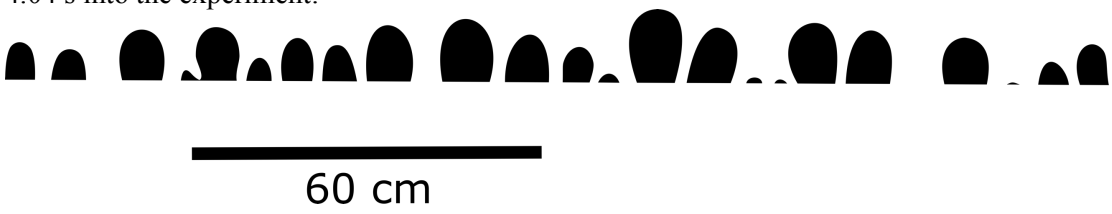

6.40 s into the experiment:

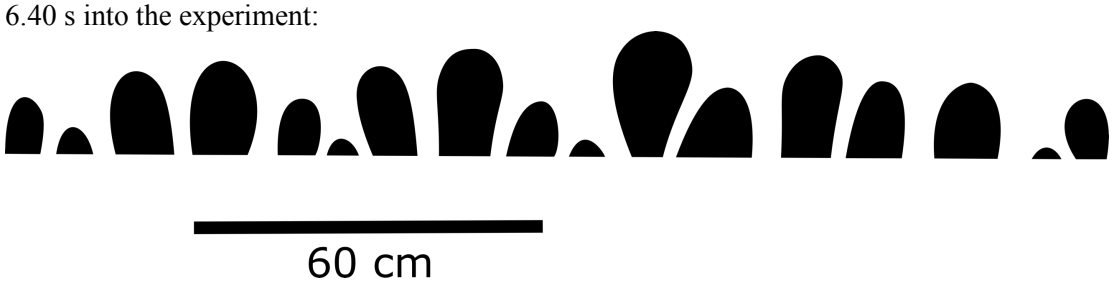

9.03 s into the experiment:

12.39 s into the experiment:

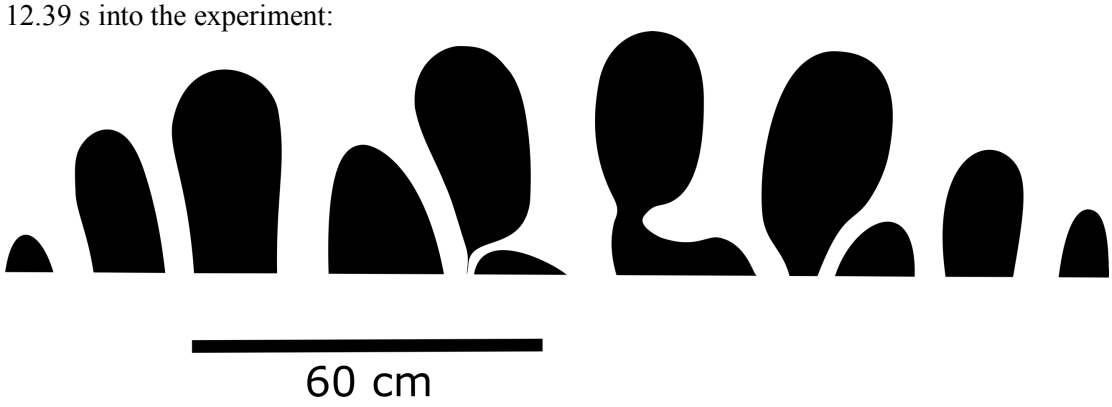

15.40 s into the experiment:

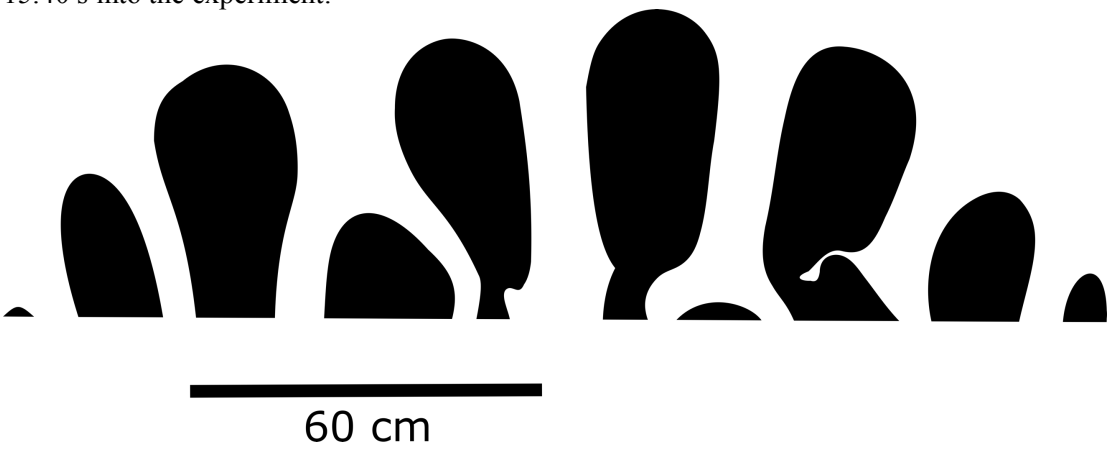

27.38 s into the experiment:

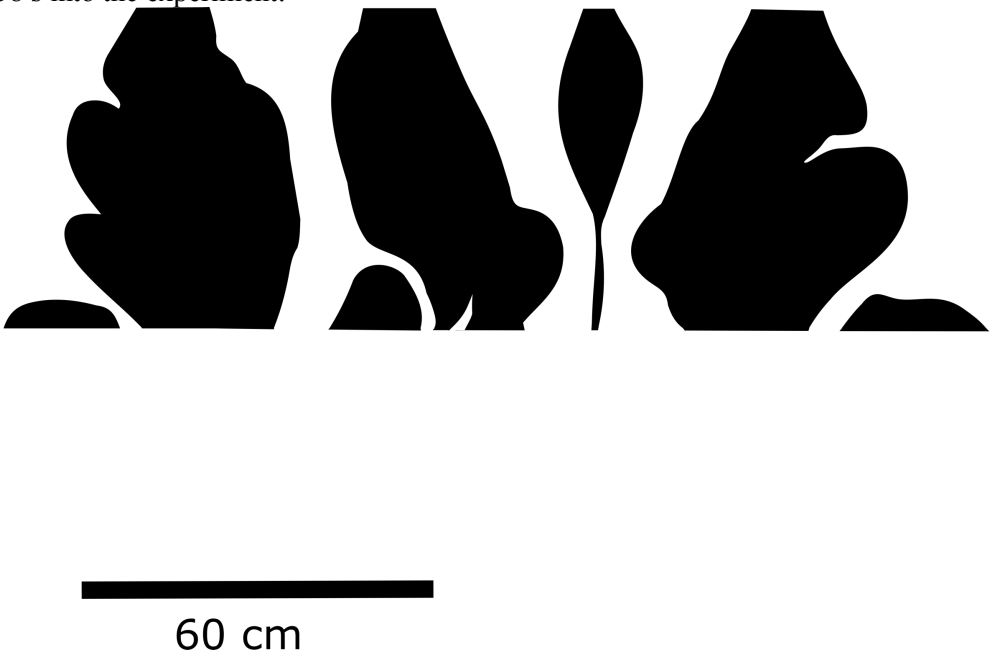

39.39 s into the experiment:

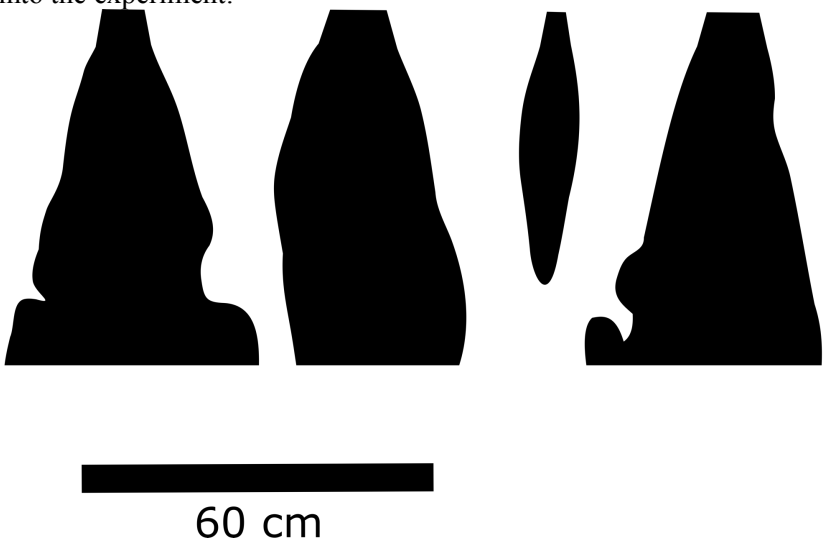

48.07 s into the experiment:

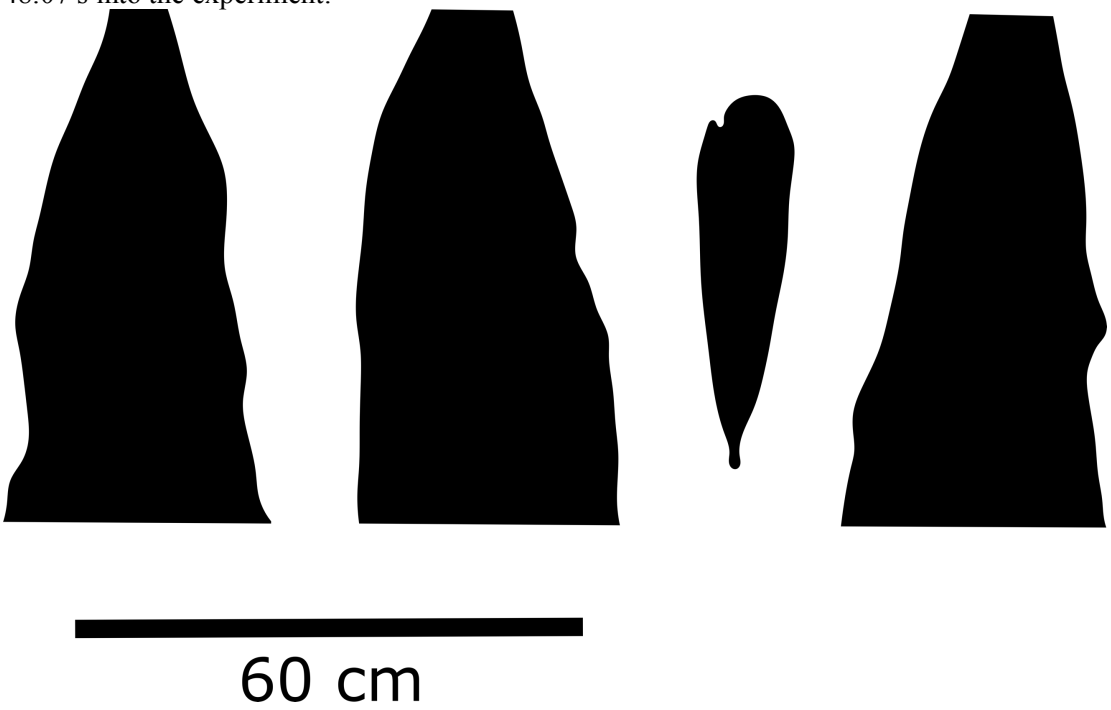

51.43 s into the experiment:

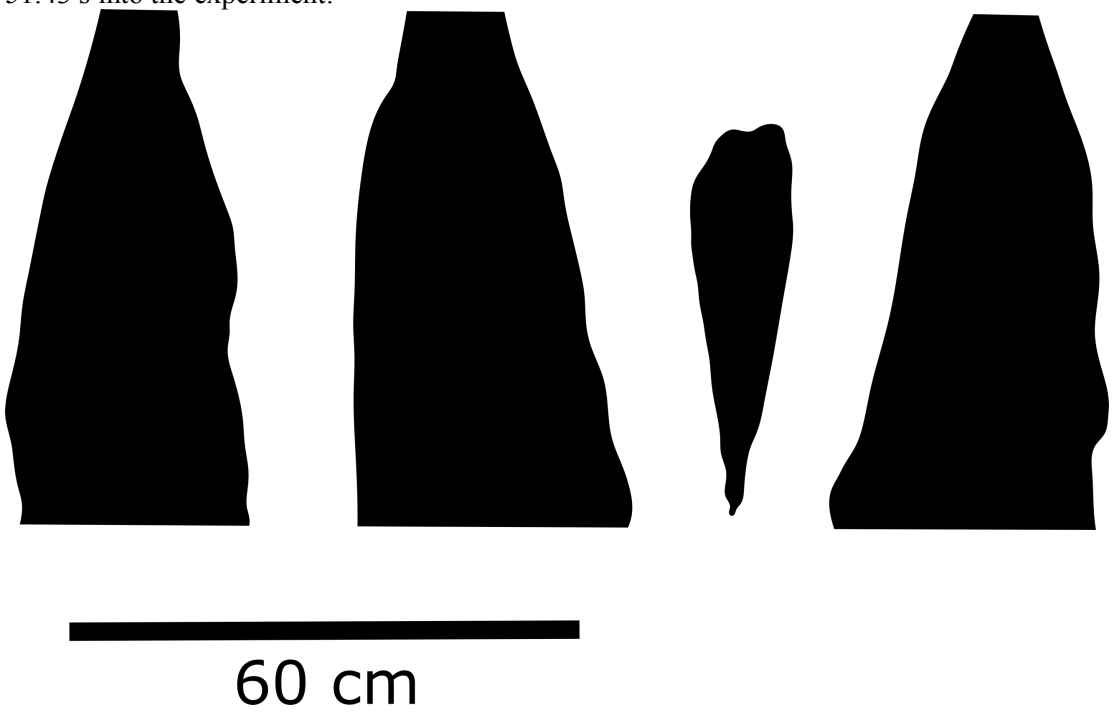

56.43 s into the experiment:

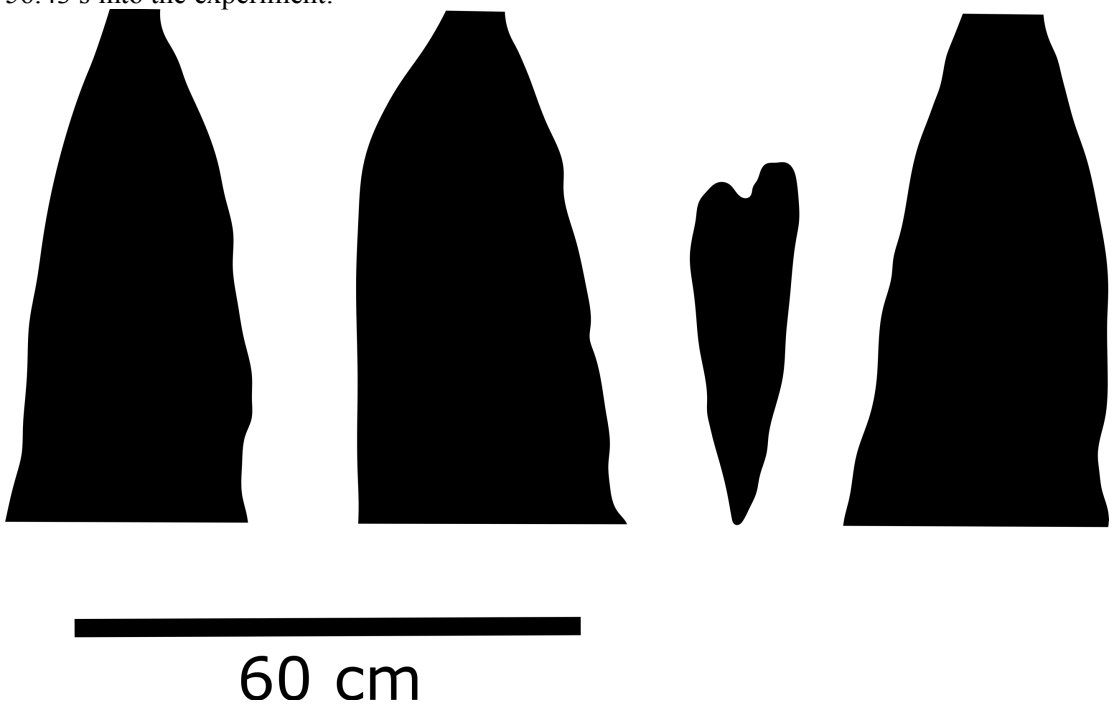

63.40 s into the experiment:

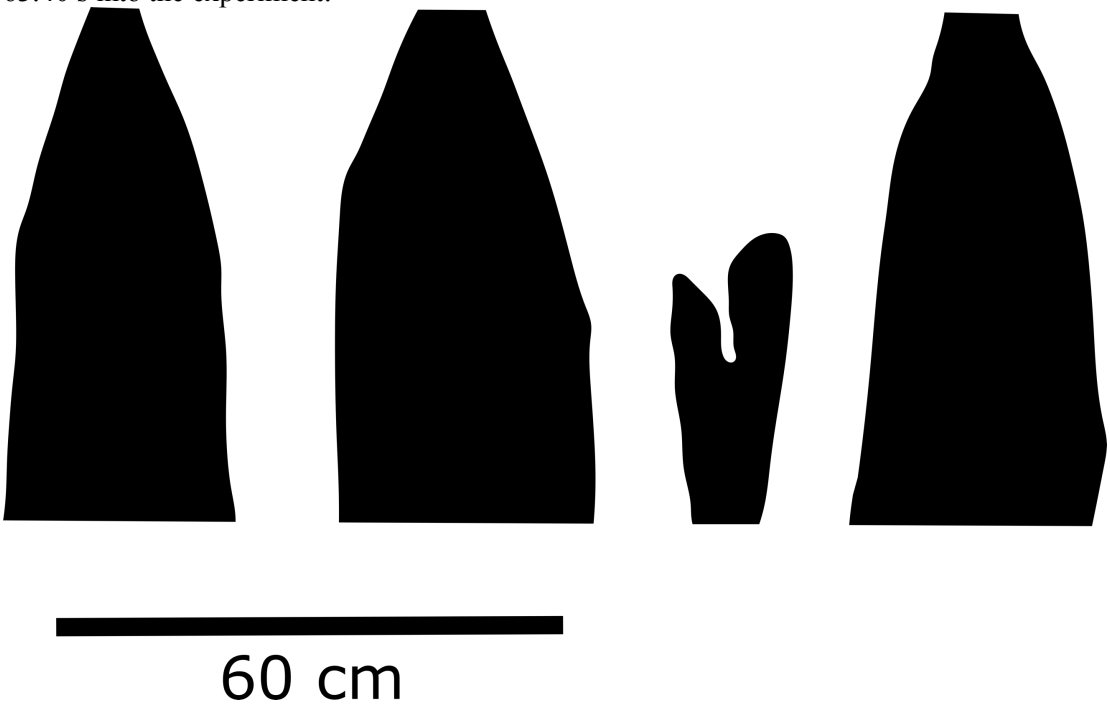

2110716c (DGS-oil):

1.69 s into the experiment:

4.99 s into the experiment:

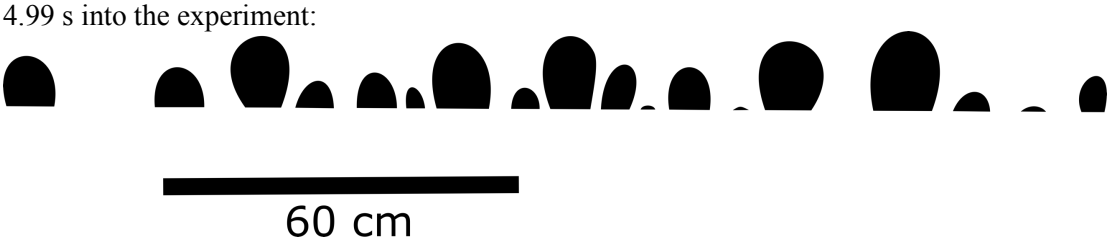

7.67 s into the experiment:

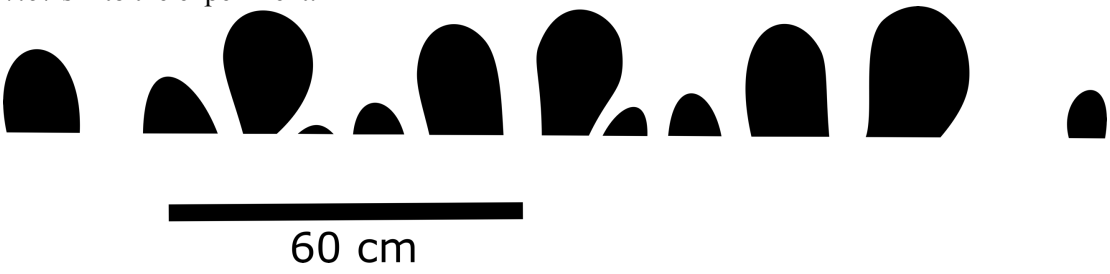

11.04 s into the experiment:

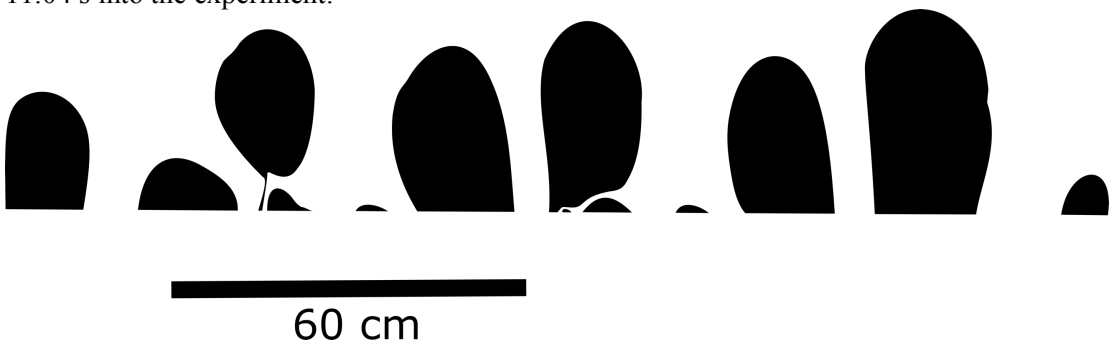

13.06 s into the experiment:

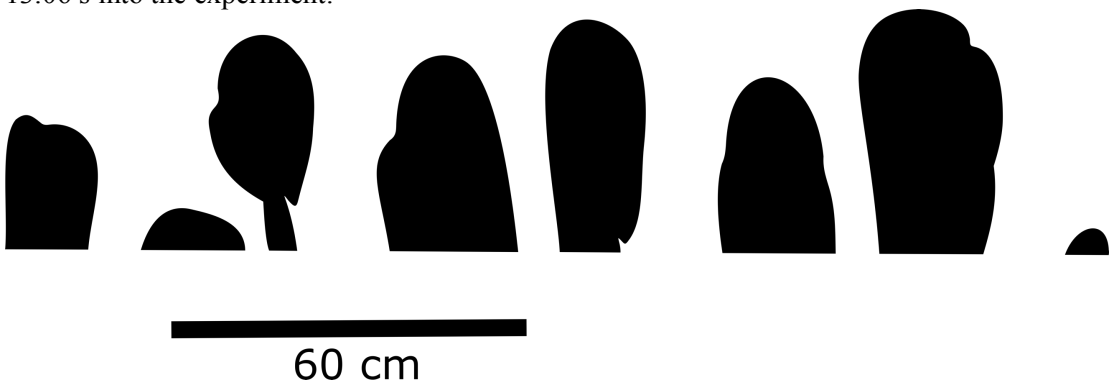

16.02 s into the experiment:

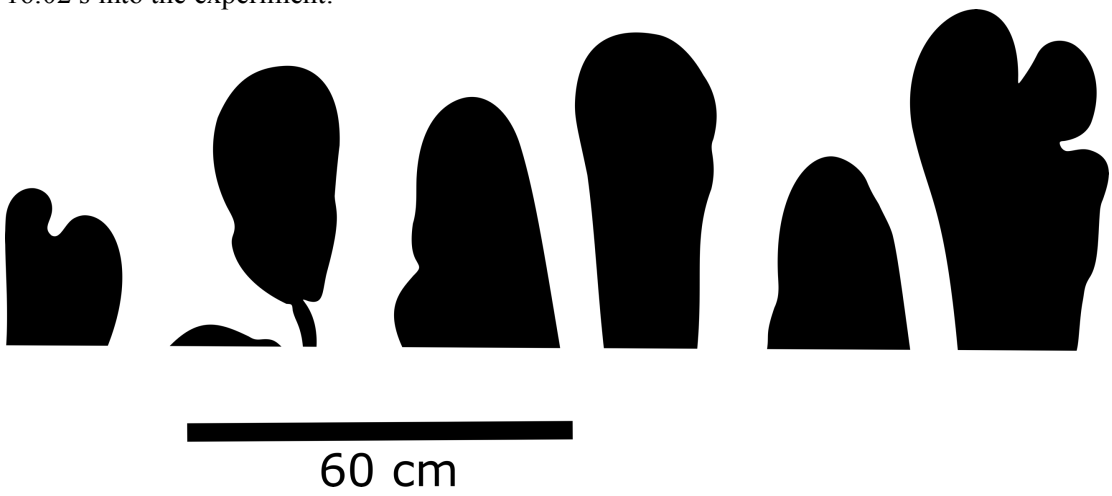

56.95 s into the experiment:

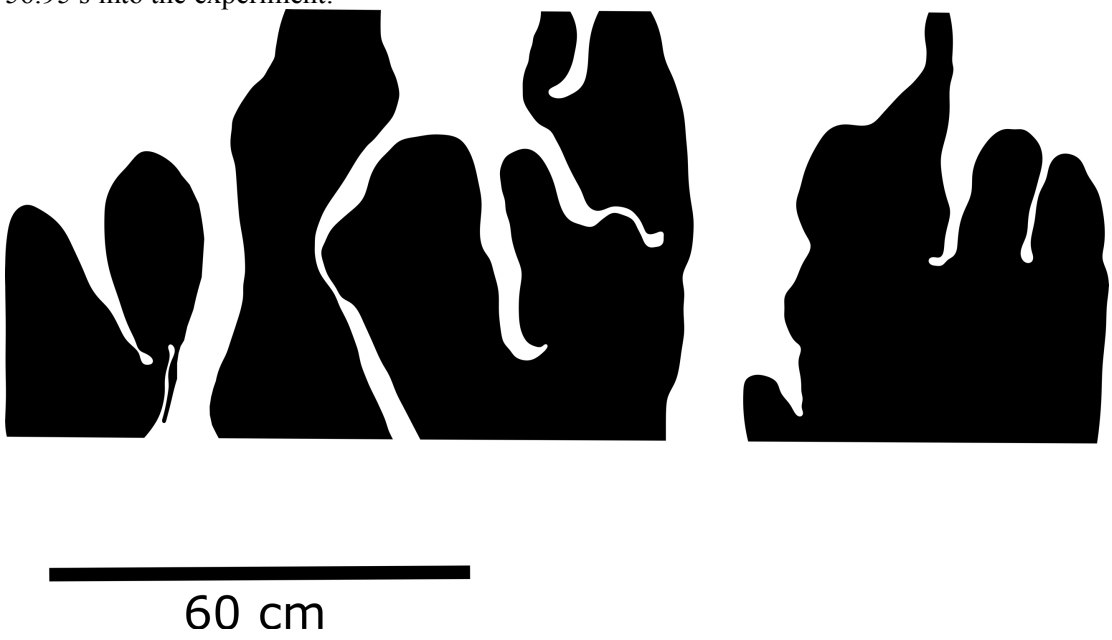

62.66 s into the experiment (red = low viscosity fluid):

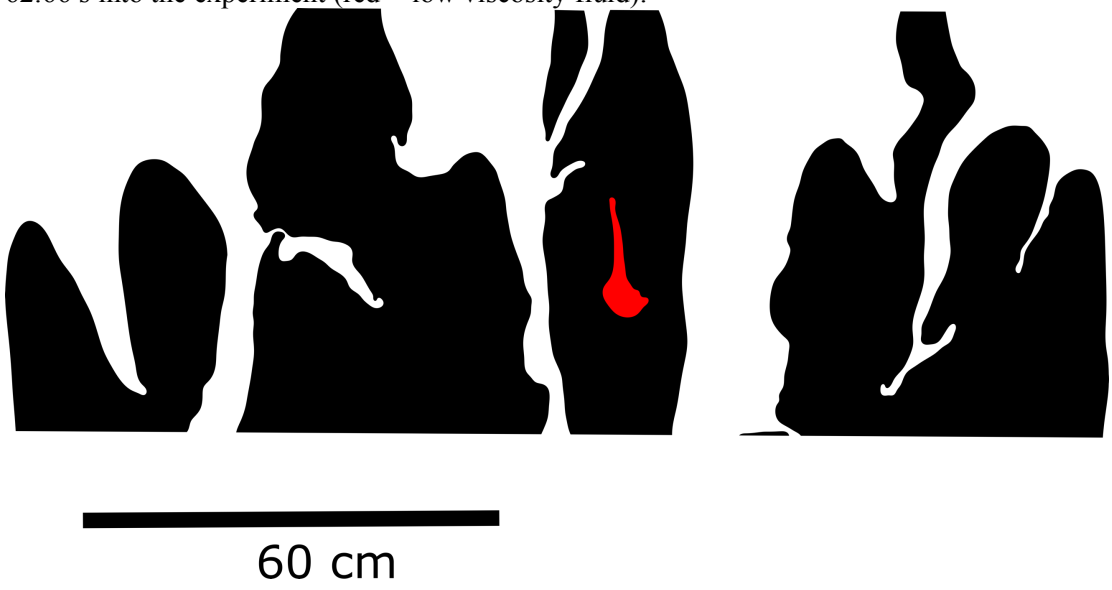

68.99 s into the experiment:

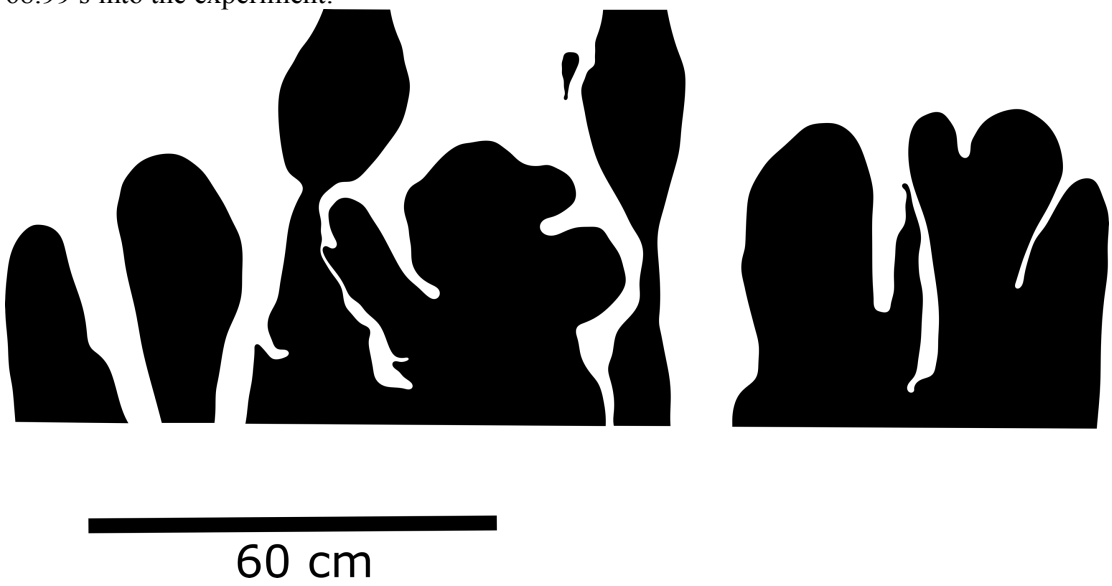

77.68 s into the experiment:

060916d (Gly-oil):

1.63 s into the experiment:

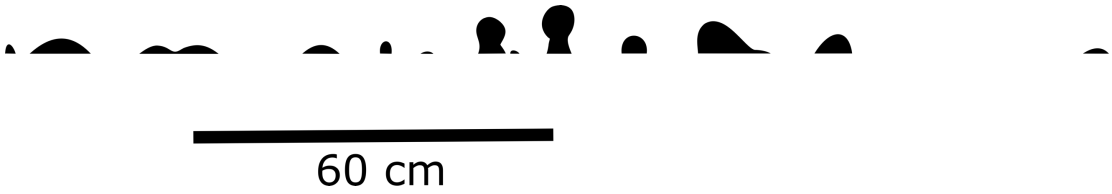

2.28 s into the experiment:

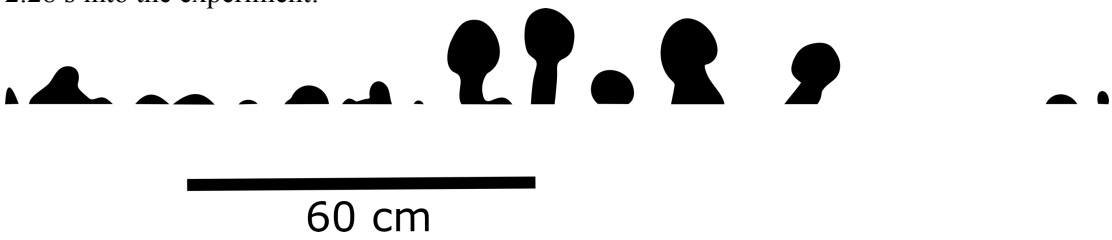

2.96 s into the experiment:

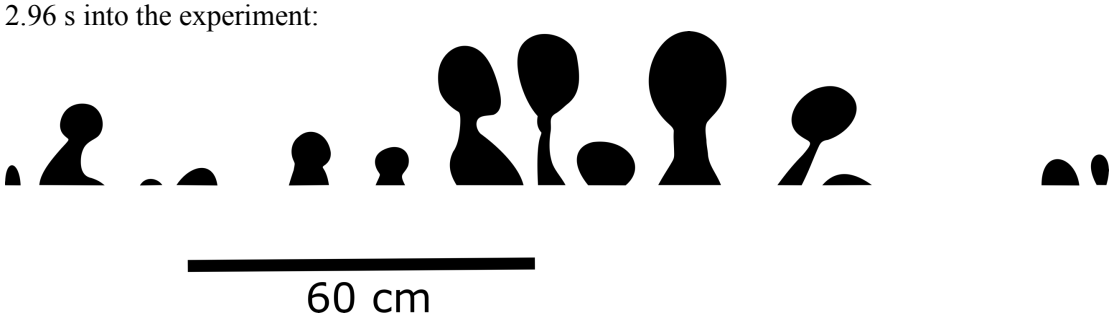

3.62 s into the experiment:

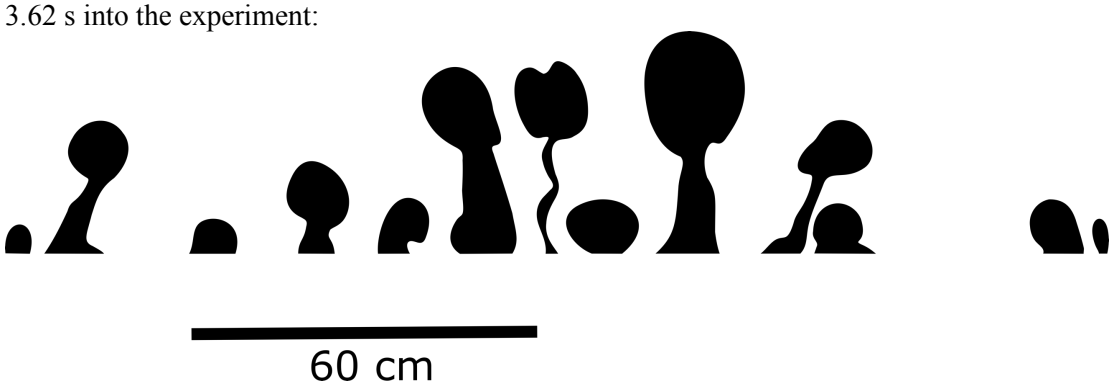

4.48 s into the experiment:

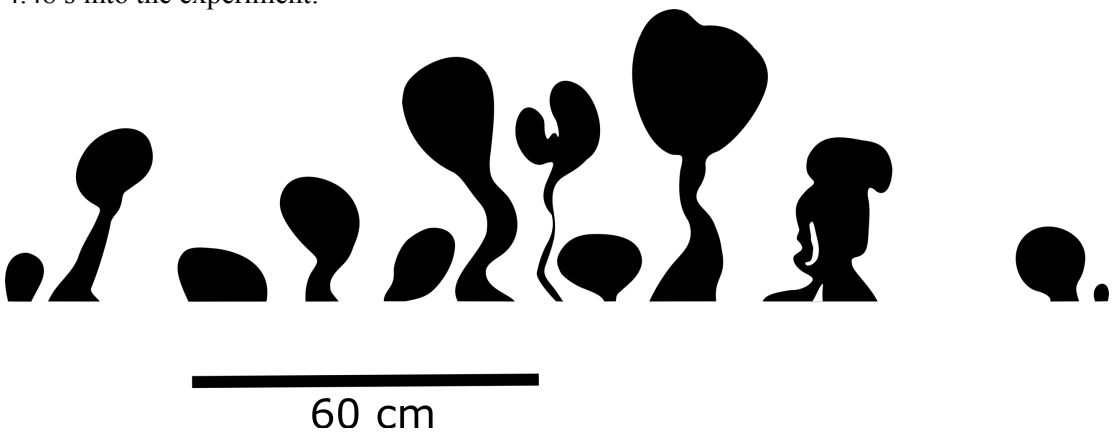

10.41 s into the experiment:

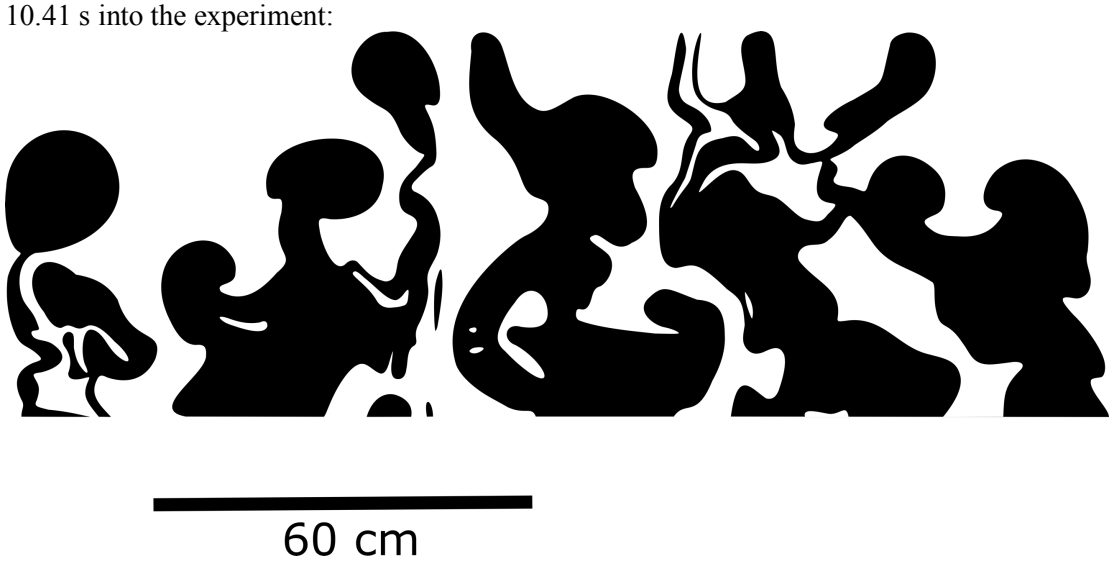

17.00 s into the experiment:

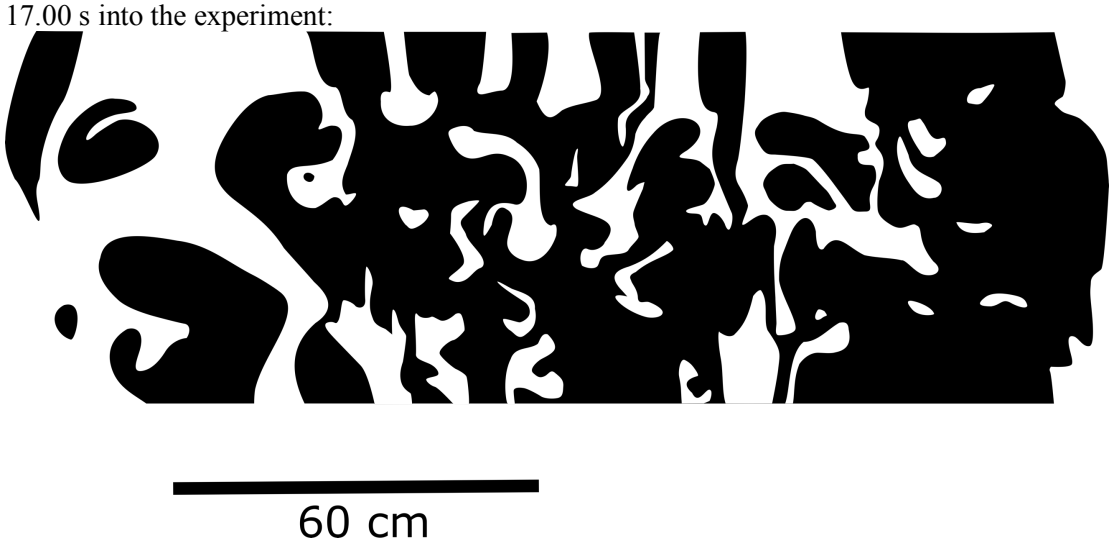

27.70 s into the experiment:

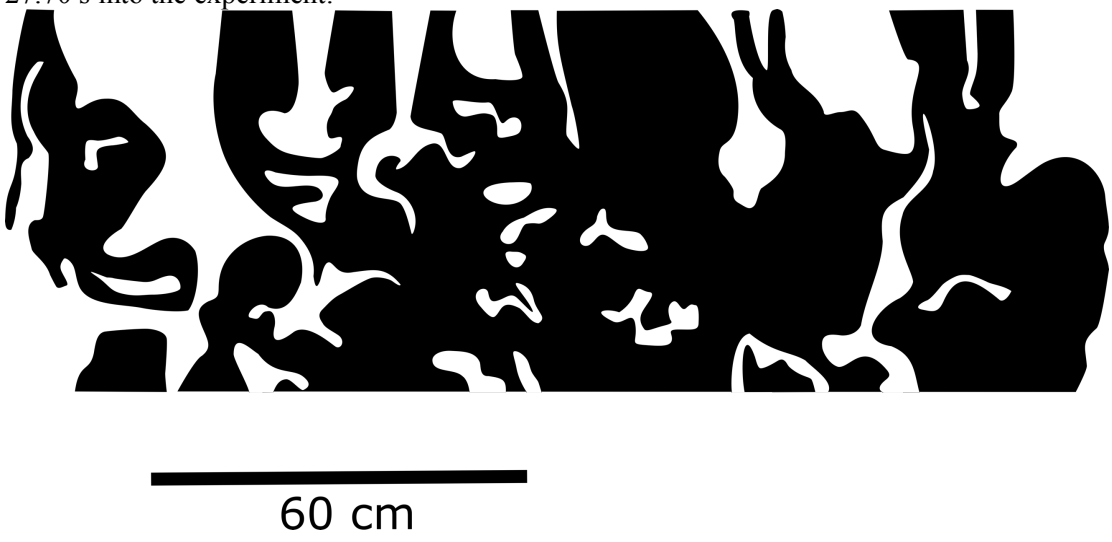

28.60 s into the experiment:

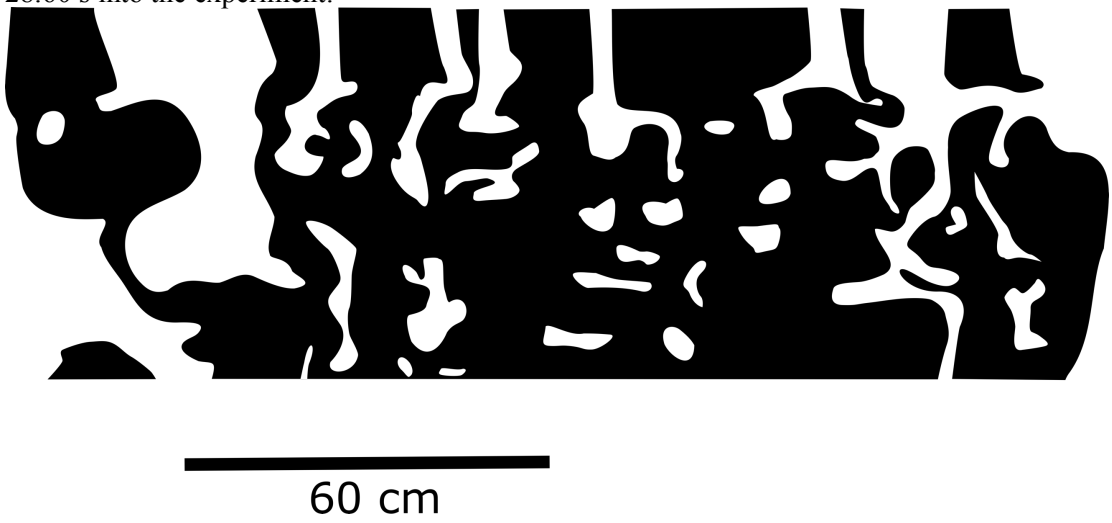

35.03 s into the experiment:

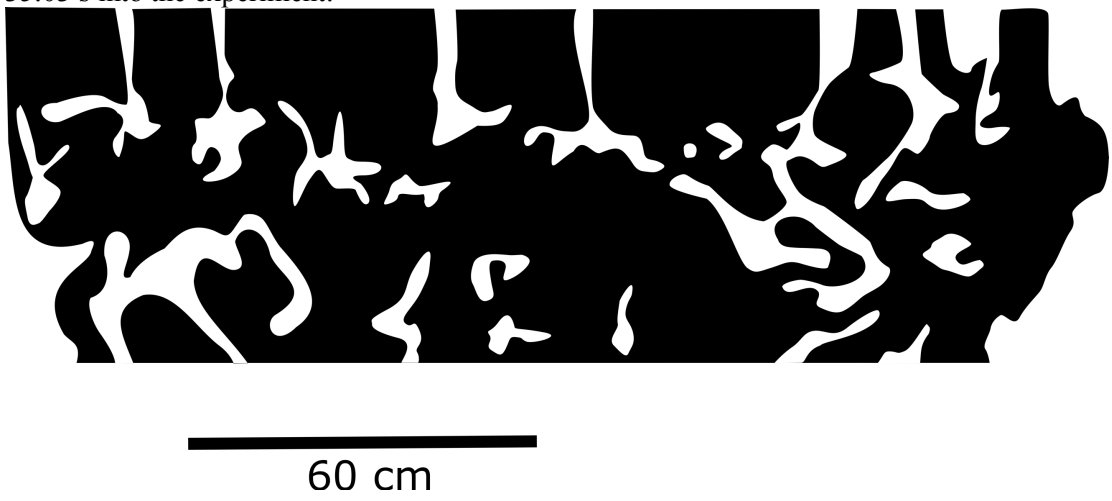

070916a (Gly-oil):

0.99 s into the experiment:

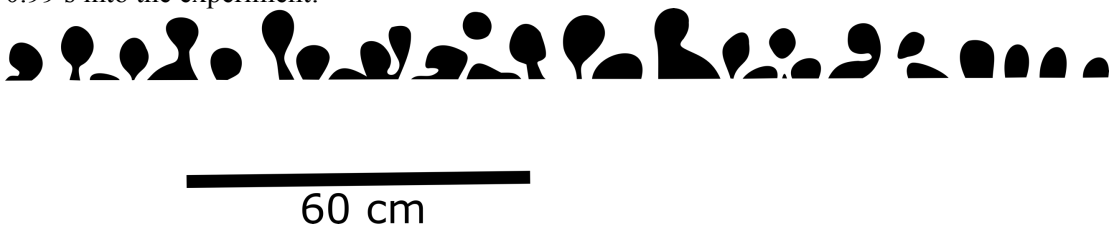

1.68 s into the experiment:

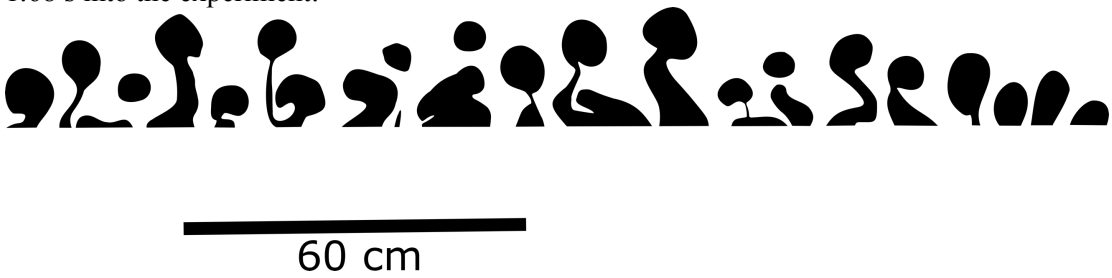

2.68 s into the experiment:

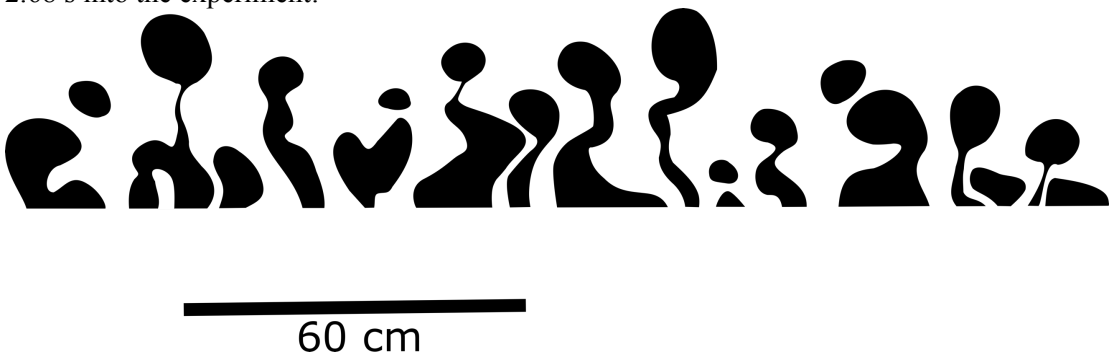

3.67 s into the experiment:

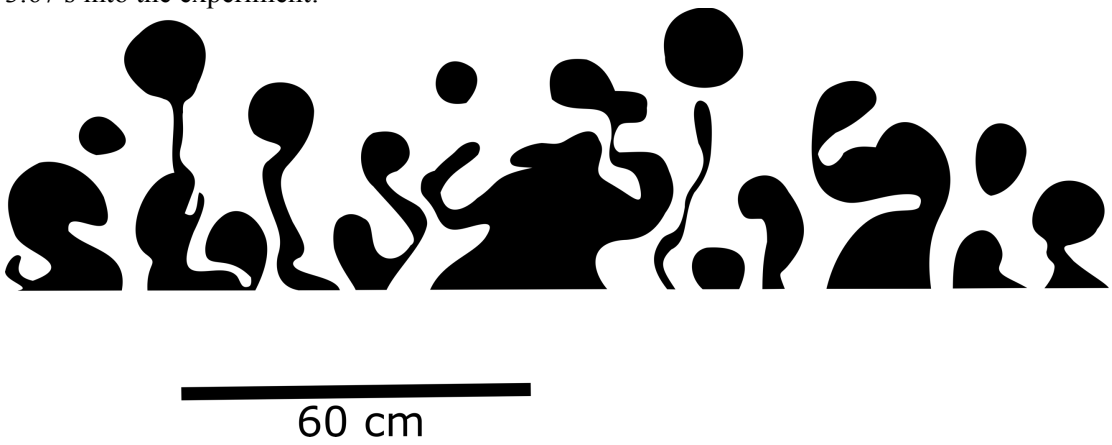

6.68 s into the experiment:

13.02 s into the experiment:

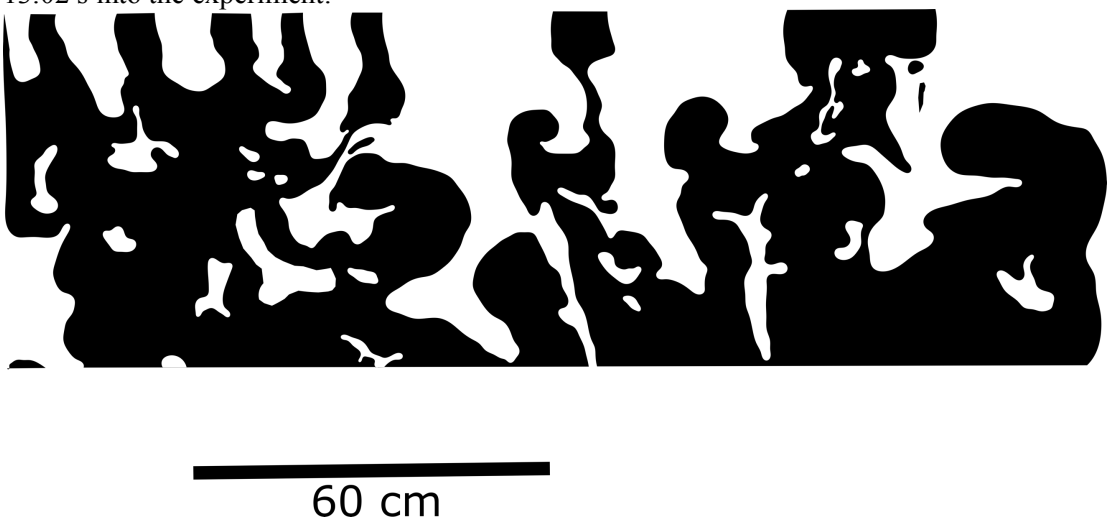

19.32 s into the experiment:

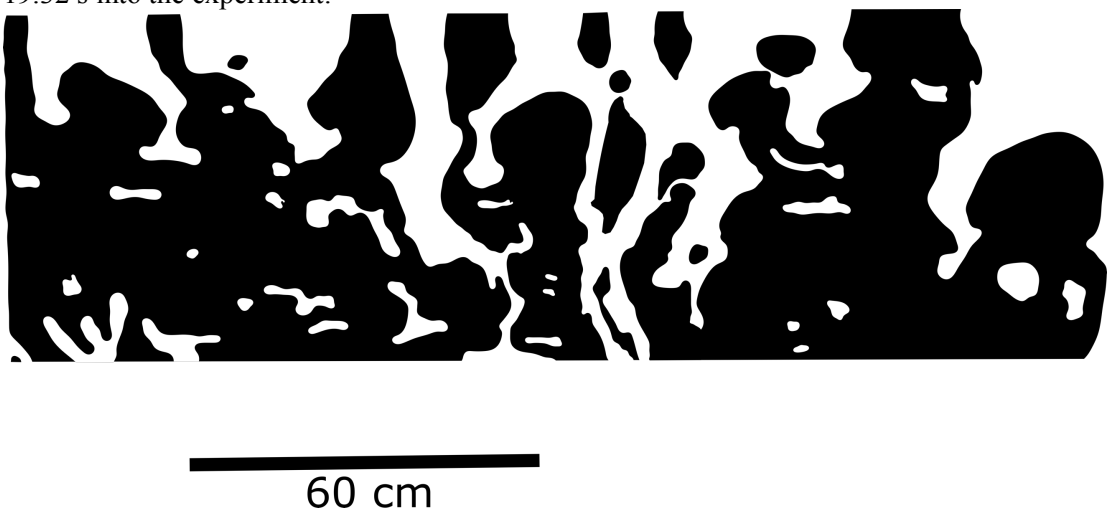

25.02 s into the experiment:

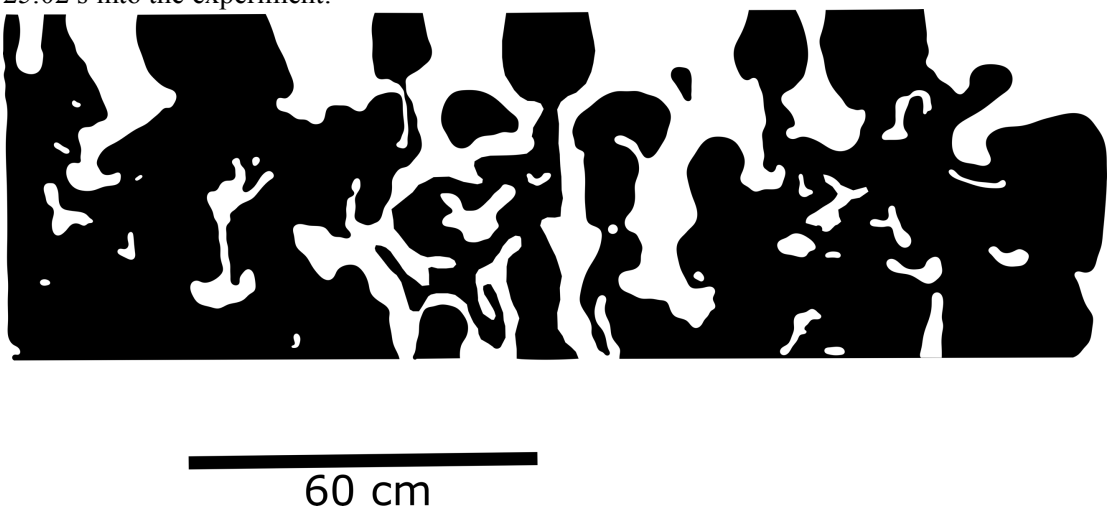

<u>080916a (Gly-oil):</u>

0.14 s into the experiment:

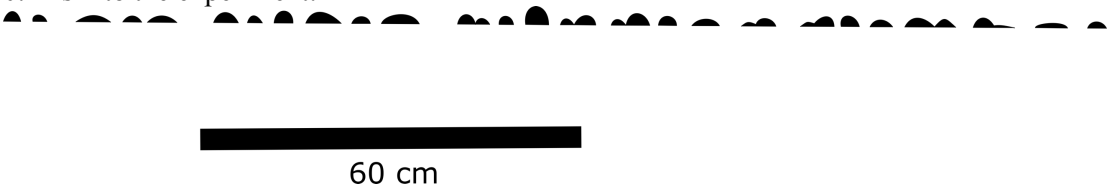

0.37 s into the experiment:

1.04 s into the experiment:

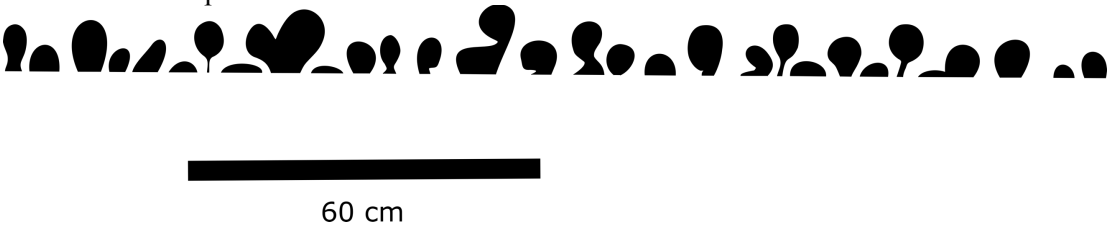

1.47 s into the experiment:

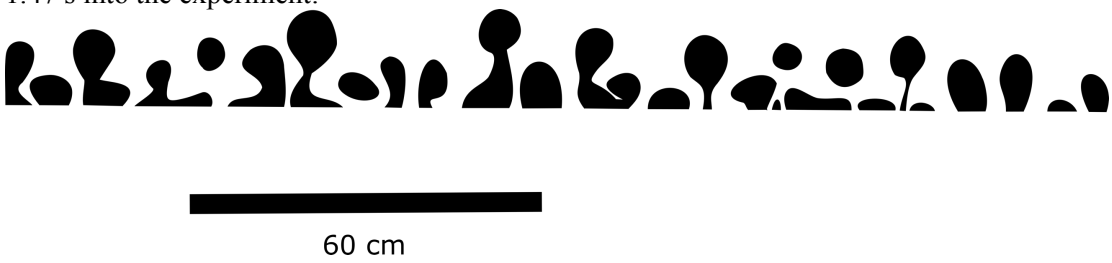

2.70 s into the experiment:

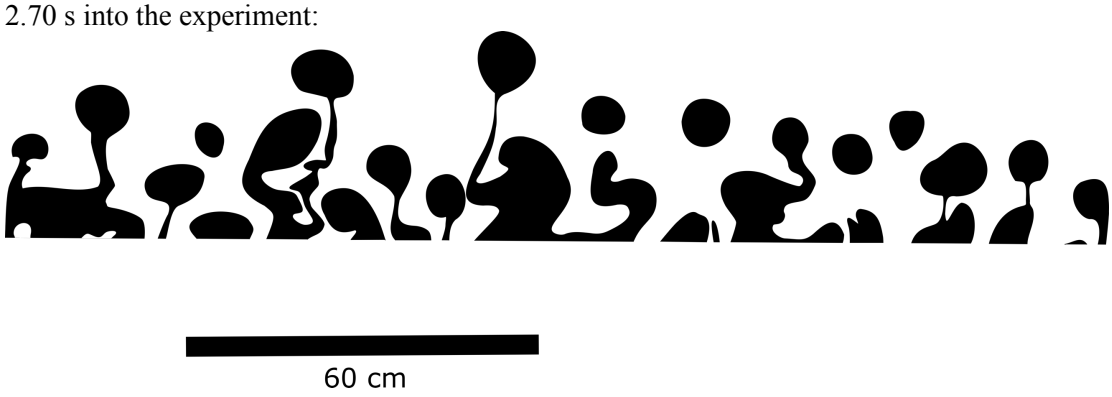

3.71 s into the experiment:

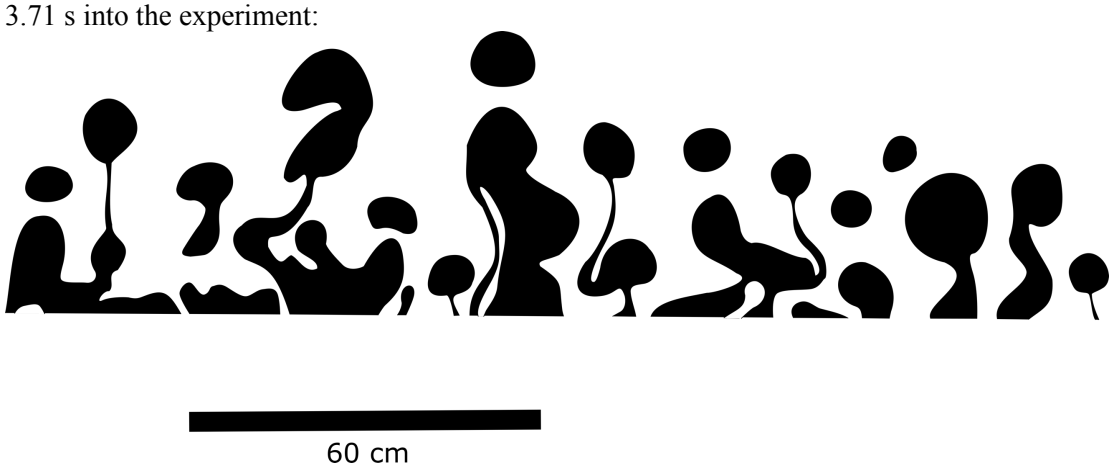

7.31 s into the experiment:

13.15 s into the experiment:

18.99 s into the experiment:

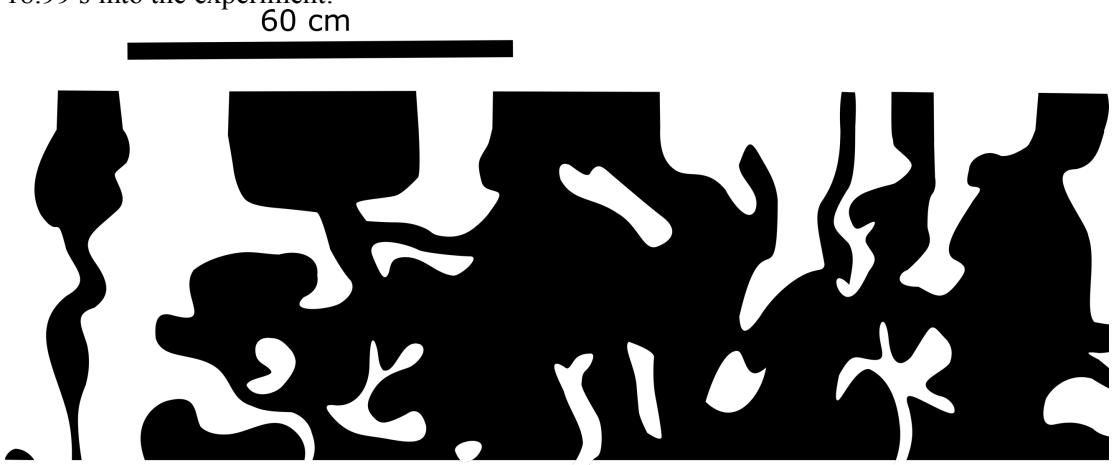

24.83 s into the experiment:

28.06 s into the experiment: